Sustainable Construction Materials 2012

Edited by
Shaopeng Wu
Liantong Mo
Baoshan Huang
Benjamin F. Bowers

ASCE

CONSTRUCTION INSTITUTE

SUSTAINABLE CONSTRUCTION MATERIALS 2012

PROCEEDINGS OF THE SECOND INTERNATIONAL CONFERENCE ON SUSTAINABLE CONSTRUCTION MATERIALS—DESIGN, PERFORMANCE, AND APPLICATION

October 18–22, 2012
Wuhan, China

SPONSORED BY
Wuhan University of Technology, China
Delft University of Technology, The Netherlands
Eindhoven University of Technology, The Netherlands
Southeast University, China
Arizona State University, USA
International Society for Concrete Pavements (ISCP)
The Construction Institute of the American Society of Civil Engineers
The University of Tennessee, USA

EDITED BY
Shaopeng Wu
Liantong Mo
Baoshan Huang
Benjamin F. Bowers

ASCE

CONSTRUCTION INSTITUTE

Published by the American Society of Civil Engineers

Cataloging-in-Publication Data on file with the Library of Congress.

American Society of Civil Engineers
1801 Alexander Bell Drive
Reston, Virginia, 20191-4400

www.pubs.asce.org

ISBN 978-0-7844-1267-1
Manufactured in the United States of America.

Preface

Sustainable Construction Materials 2012 selects 37 papers that represent the latest developments in construction materials that support sustainable development for infrastructures.

Many of the selected papers were presented at the Second International Conference on Sustainable Construction Materials: Design, Performance and Application which occurred from October 18 – 22, 2012 in Wuhan, Hubei Province of China. The conference was hosted by the Wuhan University of Technology in collaboration with the Delft University of Technology in Netherland, Eindhoven University of Technology in Netherland, Southeast University in China, Arizona State University in USA, International Society for Concrete Pavements (ISCP), the American Society of Civil Engineers (ASCE), and the University of Tennessee, Knoxville in USA.

The papers presented within the *Sustainable Construction Materials 2012* Special Technical Publication are divided into two groups. The first group contains 20 papers which examine sustainable application of cementitious materials. Within this group a global perspective is provided on sustainable construction practices in a developing country. Additionally, more fundamental research is explored through the study of rheological behavior of fresh cement mortar and the examination of the effects of small recycled aggregate fractions in concrete production. The use of recycled materials such as waste tire rubber and rubber powder is also studied. The second group of papers contains 17 papers focused on bituminous material. A focus is placed on the use of waste material in asphalt cement such as reclaimed asphalt pavement (RAP), crumb rubber, and coal tar pitch. Studies were conducted to evaluate behavior of SBS and PE modified asphalt cement during the asphalt aging process. Pavement life, an important factor of sustainability, is presented with respect to fatigue life and a study of a new maintenance solution for porous asphalt cement pavements. Furthermore a study which examines different conditions in which volatile organic compound emission is influenced in asphalt cement is provided.

Two or more reviewers along with the editors evaluated each paper published in this ASCE Special Technical Publication (STP). All published papers are eligible for discussion in the *Journal of Materials in Civil Engineering*, and are eligible for ASCE awards.

We would like to acknowledge the great support from Laura Ciampa and Marvin Oey from the ASCE Construction Institute (CI) that makes it possible for this high quality peer reviewed Special Technical Publication. Most importantly, we would like to thank the peer reviewers who spent their time and efforts in ensuring the exceptional

quality of the papers presented within this STP. Without their contributions this publication would not be possible.

Cong Peiliang, Chang'an University
Guiming Wang, Wuhan University of Technology
Han Jun, Zhejiang University
Husken Gotz, Bundesanstalt für Materialforschung und -prüfung
Lambert J.M. Houben, Delft University of Technology
Limbachiya Mukesh, Kingston University
Lin Juntao, Wuhan University of Technology
Liu Gang, Delft University of Technology
Liu Honghai, Chang'an University
Liu Quantao, Delft University of Technology
Liu Xiaoming, Central South University
Ma Tao, Southeast University
Mo Liantong, Wuhan University of Technology
Pradena Mauricio, Delft University of Technology
Qian Shunzhi, Southeast University
Ren Dongya, Delft University of Technology
Rudman Chantal, University of Stellenbosch
Wang Dapeng, Highway Research Institute, MOC, Beijing
Wang Hainian, Chang'an University
Wang Ji, Wuhan University of Technology
Wang Jingang, University of Stellenbosch
Wei Chen, Wuhan University of Technology
Xiao Yue, Delft University of Technology
Yan Shilin, Wuhan University of Technology
Ye Guang, Delft University of Technology
Ye Qunshan, Changsha University of Science and Technology
Yu Zhuqing, Delft University of Technology
Zheng Chen, Xi'an University of Architecture & Technology
Zhang Henglong, Wuhan University of Technology
Zhao Qinglin, Wuhan University of Technology
Zhang Yuan, Delft University of Technology
Zhou Jian, Sinoma Research Institute, Beijing, P R China
Zuo Junqing, Tongji University

Authors List

Contents

Cementitious Material

This page intentionally left blank

Sustainable Road Construction Practice in a Developing Country: a South African perspective

C.E. Rudman[1] and K.J. Jenkins[2]

[1]Lecturer,Department of Civil Engineering, Section Geotechnical & Transport Engineering, Stellenbosch University, Stellenbosch, 8000, South Africa; email: rudman@sun.ac.za
[2]Sanral Chair, Department of Civil Engineering, Section Geotechnical & Transport Engineering, Stellenbosch University, Stellenbosch, 8000, South Africa; email: kjenkins@sun.ac.za

ABSTRACT: The South African government plans to create a low carbon industry whilst simultaneously creating new jobs through industrial development. These plans coincide with the released UN publication: "Towards a Green Economy: Pathways to Sustainable Development and Poverty Eradication". National policies are underway to ensure execution of these environmental and social objectives within the industry. The industry consists of many disciplines of which the road pavement sector is a major role player. The aim of this paper is to establish whether the road construction industry is equipped to implement such proposed policies. The institutional obstacles are reviewed in order to identify key issues that are prevalent in developing countries. The sustainability of some current road construction practices are assessed with regard to climate change mitigation. In addition the importance of the implementation of strategic objectives and the formulation of clear goals are investigated. This paper will show the necessity of a paradigm shift by role players and stakeholders in order for the country to reach long term sustainable goals.

INTRODUCTION

South Africa contributes on average to 1.4% of the total world's carbon emissions. This seems very low, especially compared to China and the USA who contributes 20.2% and 19.1%, respectively (Baer *et al*, 2007). Moreover, South Africa is still developing and striving to alleviate its domestic poverty with almost half of South Africa's population still under the official poverty line.

The released UN publication: "Towards a Green Economy: Pathways to Sustainable Development and Poverty Eradication" elaborates on the participation of developing countries in contributing to these mitigation options. The publication takes note of the greater responsibility of industrialized countries to that of developing countries in protecting the environment, as they are putting much larger strain on natural resources and the environment.

High income countries consist of one sixth of the world population, but is responsible for two thirds of the world's GHG (Green House Gas) emissions into the atmosphere, but it is developing countries that will suffer the most from the effects of weather extremes (World Bank, 2010). These indicators question South Africa's responsibility with regard to sustainable development and in lieu of this, the crux of sustainable development is questioned: which should come first, growth or green development? However, recent studies raise critical questions about the mutual exclusivity of ecological sustainability and poverty alleviation. The above-mentioned publication and further work of Burgess *et al* (1997), also highlights this point by addressing social consequences and poverty eradication within the framework of sustainability.

Extensive international literature elaborates on the need and importance of sustainability, but as reported by Swilling (2006), various social movements within the country are also evident and contribute to the current greening of national policies. The further pressure received from international stakeholders also promotes this issue.

Regarding the above-mentioned reference, the question should be asked: not if sustainable development is applicable, but if the industry is equipped to implement policies with regard to sustainable development. Within this questioning framework it is highlighted that, globally, the transportation sector is estimated to contribute to about 25% of carbon dioxide (CO_2) emissions whilst as part of this sector, road transport contributes 80% (WRI, 2007).

This paper will focus specifically on identified key issues within the road construction industry, explore some policies and regulations within this framework and question if stakeholders are equipped to meet the demands as identified by the key issues. A case study is developed that will serve as a reference measurement of current construction practices in terms of energy consumed as well as CO_2 emissions. By evaluating these results and identifying key issues, this can be compared to the current status quo, plans, regulations, policies and initiatives in order to identify if stakeholders should alternate its primary focus in order to work towards sustainable development within the road construction industry. With further reference to this paper, the concept of sustainable road construction practice implies the reduction of the environmental impacts within the system, through mitigation of energy consumption and emissions.

A REVIEW ON CURRENT CONSTRUCTION EMISSIONS AND ENERGY CONSUMPTION

Case study approach

In lieu of identifying the current practice and key environmental issues pertaining to sustainable road construction, a reference case study was identified for measurement of CO_2 emissions and energy consumption within the road construction industry. The systematic approach included the calculation of these emissions and energy consumption for standard designs at different traffic intensities in the construction and the use phase.

In recent years many methods have been developed and used within South Africa

for the design of road pavement layers and subsequent construction. In this paper the approach as stipulated in the South African Guidelines for the Design of Flexible Pavements for Interurban and Rural Roads (TRH 4, 1996), Catalogue method was used which ultimately allows the user to choose a pavement layer system from a "catalogue". In South Africa, typical design fundamentals include the "upside down" pavement composition, which is based on a structurally balanced approach. The concept behind the design includes that each of the pavement layers are stressed to the same level of its maximum design and that the bearing capacity of a structurally well balanced pavement structure increases evenly with increasing depth. In principle, the more the bearing capacity of the lower layers has to carry within the structure the deeper the lower layers will have to be. The standard design usually includes a thin asphalt layer, base from crushed stone and a cemented subbase. This design is based on the concept that the neutral axis sit well below the crushed stone base and it is then possible for the base layer to resist very high loads.

The catalogue is subdivided into a matrix which subdivides the road pavement types into different road categories, as well as number of heavy vehicles (in millions) , measured in standard 80kN axle loads, over the design life time of the pavement. Some inherent assumptions are included within this empirical design method and it can be argued that the catalogue choices should be refined. However, for the purpose of this paper it is considered acceptable to use these suggested pavement layers for measuring the emissions and energy consumption for the construction phase as well as the user phase. In order to establish a comparable unit value the road was taken as 10.0m wide and 1.0km long.

Pavement layer construction - pavement types analysed for case study:

Tables 1 and 2 show the choice of traffic parameters chosen and the subsequent Catalogue pavement design for each of these parameters. The traffic class indication in the table relates to the number of standard 80kN axle loads applied over the design life of the pavement measured in millions. Each pavement design includes 3 layers namely the wearing coarse, base and subbase. Associated with each layer is the type of material used and thickness of each layer. A name is identified for each pavement type. By using the example pavement titled: GD ǀ A ǀ ES0.3.; the parts of the name is explained: The first part relates to the identification of the base layer i.e GD (Granular Dry), GW (Granular Wet), HMA (Hot mix asphalt) and CB (Cemented Base). The second part of the title is associated with the road category. The category is related to certain design reliabilities.

A road with a higher level of service is related to higher reliability against failure. The design reliability is defined as: "The length of the road that will not exceed the

specified terminal functional performance criteria at the end of the Structural Design Period". Within the context of this paper the categories are defined as follow:

1.) Category A – 95%, 2.) Category B - 90%, 3.) Category C-80% design reliability.

The last part of the pavement type name is associated with the allowable number of standard 80kN axles (measured in millions) associated with the pavement type.

Table 1. Catalogue designs used for analysis of emissions and energy consumption (Category A and B)

Traffic class						
ES0.1	ES0.3	ES1	ES3	ES10	ES30	ES100
No Catalogue Design	No Catalogue Design	No Catalogue Design	A[0.04] G2[0.125] C3[0.15] GD|A|ES03	A[0.04] G2[0.15] C3[0.25] GD|A|ES10	A[0.05] G1[0.15] C3[0.25] GD|A|ES30	A[0.05] G1[0.15] C3[0.3] GD|A|ES100
			A[0.04] G2[0.15] G5[0.15] GD|A|ES03			
			A[0.03] G1[0.15] C3[0.2] GW|A|ES03	A[0.04] G1[0.15] C3[0.3] GW|A|ES10	A[0.05] G1[0.15] C3[0.4] GW|A|ES30	A[0.05] G1[0.15] C3[0.3] GW|A|ES100
			A[0.04] HMA[0.08] C3[0.25] HMA|A|ES3	A[0.04] HMA[0.09] C3[0.3] HMA|A|ES10	A[0.04] HMA[0.12] C3[0.4] HMA|A|ES30	A[0.05] HMA[0.18] C3[0.45] HMA|A|ES100
			A[0.03] C3[0.15] C4[0.2] CB|A|ES3			
No Catalogue Design	No Catalogue Design	S[1] G4[0.125] C4[0.15] GD|B|ES1	A[0.03] G3[0.15] C4[0.15] GD|B|ES3	A[0.04] G2[0.15] C4[0.2] GD|B|ES10	No Catalogue Design	No Catalogue Design
		S[1] G4[0.15] G5[0.15] GD|B|ES1	A[0.03] G3[0.15] G5[0.15] GD|B|ES3	A[0.03] G2[0.15] G5[0.2] GD|B|ES10		
		S[1] G2[0.15] C4[0.15] GW|B|ES1	A[0.03] G1[0.15] C4[0.2] GW|B|ES3	A[0.04] G1[0.15] C4[0.3] GW|B|ES10		
		S[1] G2[0.15] G5[0.2] GW|B|ES1				
			A[0.03] HMA[0.08] C4[0.2] HMA|B|ES3	A[0.03] HMA[0.08] C3[0.3] HMA|B|ES10		
		S[1] C3[0.125] C4[0.15] CB|B|ES1	S[1] C3[0.125] C4[0.2] CB|B|ES3	A[0.03] C3[0.15] C4[0.3] CB|B|ES10		

Legend:
S[1] -Single Seal
A - Asphalt Surfacing
G1to4 - Granular Materials
C1to4 - Cemented Materials

Table 2. Catalogue designs used for analysis of emissions and energy consumption (Category C)

Traffic class						
ES0.1	ES0.3	ES1	ES3	ES10	ES30	ES100
S[1] G5[0.1] C4[0.125] GD|C|ES0.1	S[1] G5[0.125] C4[0.125] GD|C|ES0.3	S[1] G4[0.125] C4[0.125] GD|C|ES1	S[1] G3[0.15] C4[0.15] GD|C|ES3	No Catologue Design	No Catologue Design	No Catologue Design
S[1] G4[0.125] G6[0.125] GD|C|ES0.1	S[1] G4[0.125] G6[0.15] GD|C|ES0.3	S[1] G4[0.125] G5[0.15] GD|C|ES1	S[1] G3[0.15] G5[0.15] GD|C|ES3			
S[1] G5[0.1] C4[0.125] GW|C|ES0.1	S[1] G5[0.125] C4[0.125] GW|C|ES0.3	S[1] G2[0.125] C4[0.15] GW|C|ES1	S[1] G2[0.15] C4[0.2] GW|C|ES3			
S[1] G4[0.125] G6[0.125] GW|C|ES0.1	S[1] G4[0.15] G6[0.15] GW|C|ES0.3	S[1] G2[0.15] G5[0.15] GW|C|ES1	S[1] G2[0.15] G4[0.15] GW|C|ES3	**Legend:** S[1] -Single Seal A - Asphalt Surfacing G1to4 - Granular Materials C1to4 - Cemented Materials		
S[1] C4[0.1] G6[0.1] CB|C|ES0.1	S[1] C4[0.125] G6[0.125] CB|C|ES0.3	S[1] C3[0.125] C4[0.125] CB|C|ES1	S[1] C3[0.15] C4[0.15] CB|C|ES3			

Measurement of emissions and energy consumption of pavement construction

Many studies have been carried out to evaluate the energy emissions and consumption in the production of construction materials (such as bitumen, cement aggregates) as well as various construction activities such as excavating, transporting, asphalting and paving. The research of interest to this paper is work done by Patrick *et al*. (2010), Chappat and Bilal (2003), Meil (2006) and Chehovits *et al*. (2010). These research values were used to determine and evaluate the various construction activities of a typical catalogue design.

A systematic approach was applied by obtaining the emission and energy consumption factors for each of the individual materials used within the pavement. These values obtained from Chappat and Bilal (2003) is shown in the first part of Table 2. Values were used by the authors to calculate the consumption and emissions, as a total of the final product (a mixture of the individual ingredients) to be placed within the layer.

Note that these values only show the contribution of each individual ingredient as a resource and does not include the manufacturing intensity values of the final product i.e Hot Mix Asphalt (HMA), C3 (Cemented Material) or C4 (Cemented material).

Further calculations by the authors include the contribution of the manufacturing process of the mixed product, transport to site and laying of the product. The following assumptions with regard to the various processes are made:

Table 3. Values of individual and mixed products, after Chappat and Bilal (2003)

	Energy Consumption (MJ/ton)	Emmisions (CO_2 kg/t)	Source
Crushed Aggregates	40	10	Chappat and Bilal (2003)
Borrow-pit aggregates	30	2.5	
Cement	4976	980	
Bitumen	4900	285	
Emulsion (60%)	3490	221	
Water	10	0.3	
G1-G3 (Graded Crushed Stone)	40	10.00	See discussion[a]
G4 (Crushed or Natural Gravel)	35	6.25	
G5-G7 (Natural Gravel)	30	2.50	
C3-C4 (Cemented crushed stone or gravel)	129.42	22.07	
Hot Mix Asphalt	258.7	639.71	
Double Seal*	11.27	0.91	

*Energy Consumption and emmisions is measured in MJ/m^2 and kg/m^2 is measured in

[a]Calculated byauthors using typical mix values i.e in the case of hot mix asphalt 4.5% binder 95% graded crushed stone by weight.

Transport of material from manufacturing site:

In South Africa the use of borrow pits are prevalent and a high probability of locating a borrow pit within a 30km range exists. However, a 200% increase is assumed for crushed aggregates i.e 60km. In addition, these higher haulage values will be applied for any of the manufactured products. To determine the transport to site from the manufacturing plant, the vehicles suggested are 20 ton for cement, hot mix asphalt and crushed aggregate. A wide range of values exist for each decision of truck type, these decisions are usually based on local manufacturer's availability and preference. Energy values are based on values as stipulated by Patrick *et al*. (2010), which included fuel consumption values for full, fuel empty, laden, partly laden and empty trucks. Values of 1825/kJ/ton/km and 1403kJ/ton/km for a 14 ton and 20 ton truck were used respectively, assuming a fully laden truck to the site and empty on the return trip. It should be noted that there is not a linear relationship between the truck and fuel consumption as the efficiency kJ/ton/km increases with larger trucks. No values were given for emissions of these trucks and an adjustment factor was assumed by using the equivalent 900kJ/ton/km used by Chappat and Bilal (2003), energy consumed and 0.06kg/ton/km of emissions. i.e. doubling this value for emissions of the 14 ton truck (0.12 CO_2 kg/ton/km) and multiplying the value with 1.5 (0.09 CO_2 kg/ton/km) for a 20 ton truck.

Graded crushed stone and gravel:

No manufacturing values are stipulated for crushed aggregate as this has already

been included in the manufacturing of the individual product as obtained from Chappat and Bilal (2003). The proposed value of 30 and 40 MJ/ton for natural and crushed aggregate respectively, seems low in comparison with the values proposed by Patrick *et al*. (2003), however, Chappat and Bilal (2003) includes emissions as well as energy consumed, similarly values for laying have been applied.

Table 4. Total Energy and emissions contribution for each type of pavement layer

	Energy Consumption(MJ / ton mixed material)					Emmisions (CO_2 kg/t)				
	Ingredient contribution	Manufacture of total product	Transport (per tonne for total distance)	Laying	Total	Ingredient contribution	Manufacture of total product	Transport (per tonne for total distance)	Laying	Total
G1-G3 (Graded Crushed Stone)	40.0	0.0	84.2	6.0	130.2	10.0	0.0	5.4	0.4	15.8
G4 (Crushed or Natural Gravel)	35.0	0.0	69.5	6.0	110.5	6.3	0.0	4.5	0.4	11.2
G5-G7 (Natural Gravel)	30.0	0.0	54.8	6.0	90.8	2.5	0.0	3.6	0.4	6.5
C3-C4 (Cemented crushed stone or	129.4	14.0	55.3	6.0	204.8	22.1	1.0	3.6	0.4	27.1
Hot Mix Asphalt	258.7	275.0	84.2	9.0	626.9	639.7	22.0	5.4	0.6	50.4
Double Seal*	11.3	0.0	1.9	1.0	14.2	0.9	0.0	0.4	0.3	1.6

*Energy Consumption and emmisions is measured in MJ/m^2 and kg/m^2 is measured in

Cemented materials and hot mix asphalt:

The cumulative manufacture and laying values was taken for cemented materials as reported by Chappat and Bilal (2003). Similarly Chappat and Bilal's values were used for hot mix asphalt.

Double seals:

A typical double seal is included for the catalogue suggestions including seal layers. A chip spreading rate of 20 kg/m^2, a cold binder application rate of $3.0l/m^2$ and a fog spray of 60% emulsion at an application rate of 1.0 ℓ/m^2 is assumed (Note that there are varying factors that would change these values). In the case of laying, a value of 1 MJ/m^2 for energy consumption and a value of 0.3 kg CO_2/ m^2 is assumed with no further investigation.

The energy and emissions contribution for each type of pavement layer is shown in Table 4.The total value of 14.2 MJ/ton and 1.5 kg CO_2/ton, calculated by the authors, compares to values reported by Chehovits *et al.* (2010), which calculated a value of 8.9MJ/ m^2 and 0.5kg/ m^2 for energy consumption and emissions, respectively.

Measurement of emissions and energy consumption of surface maintenance

Surfacing and structural maintenance is dependent on the amount as well as type of traffic associated with the road, and the necessity of surfacing a road. For the purpose of measurement it will be assumed the road must be surface maintained twice within in the structural design period (First 20 years).

For the purpose of surface maintenance a seal similar to the original construction is assumed for all cases. The average results in choice of seal are considered consistent and acceptable. A value of 14.2MJ/m^2 and 1.6 kg CO_2/m2 was used for calculation and results in a value of 142061MJ/1km and 15726.8 kg CO_2/1km of 10.0m width road is used for each application of seal for energy and consumption use, respectively.

Measurement of emissions and energy consumption for road use vehicles on category roads

To calculate the amount of energy consumed the number of vehicles passing over the road was taken as suggested by the South African Guidelines for the Design of Flexible Pavements for Interurban and Rural Roads (TRH 4, 1996) for each vehicle class (See Table 5). Emissions and energy consumption unit values for light and commercial vehicles were taken as shown in Table 6. It is emphasized that these values are taken as an average. The authors believe that for South Africa these values are conservative, giving smaller energy consumption emissions. For calculation the road was taken as 10.0m wide and was assumed that the road would have 4 lanes.

Table 5. Vehicles/day/lane as suggested emission by TRH 4 (1996)

Vehicle class	Vehicles per day /per lane	
	Lower Limit	Upper Limit
ES0.1	20	75
ES0.3	75	220
ES1	220	700
ES3	770	2200
ES10	770	2200
ES30	2200	6500
ES100	6500	40000

Table 6. Energy consumption and values for light and heavy vehicles (Chappat and Bilal, 2003)

Energy consumed heavy vehicles	10.8	MJ/km
Energy consumed light vehicles and light commercial vehicles	2.59	MJ/km
Emmisions heavy vehicles	2.41	$CO_{2\ kg}$/km
Emmisions light vehicles and light commercial vehicles	0.57	$CO_{2\ kg}$/km

To determine the number of vehicles per pavement class an average was taken

between the upper and lower limit of vehicles/lane/day. The TRH 4 categorizes the roads within the number of ESAL's which relates to the number of standard axles. This makes it impossible to define the percentage of heavies related to the amount of light vehicles. To evaluate the influence of the number of heavies a variance in the % heavies was applied and will be reported in the results.

Results of emissions and energy consumption of the construction and use phase

Figs. 1 and 2 show the total amount of energy and emissions to construct a 1 km of road, 10.0m wide. Results indicate an expected upward trend (due to the increase in use of materials) in energy use and emissions as the traffic class is increased. This is especially evident in pavements using cemented materials as part of the ingredients.

In comparing the values of cemented or granular layers it can be seen that the use of cemented materials is at least double the energy and emission intensity of granular materials. Pavements consisting out of a HMA base and typical cemented base show the largest energy consumption and energy emissions within the range of pavements. Within the context the results, bitumen or cement contributes largely to emission and energy consumption results. However, looking at typical material volumes, the influence of materials used within the base or subbase has a much larger influence on the total values and should be prioritised for consideration.

In addition, the values for the construction of the surfacing layers for each of the respective pavements show the beneficial application of seals with results less than half the energy outputs measured on the asphalt surfacing.

Figs. 3-4 and 5-6 show the total amount of energy required and the amount of emissions for the use of the roads in comparison to the construction and surface maintenance of the road with regard to energy consumption and emissions.

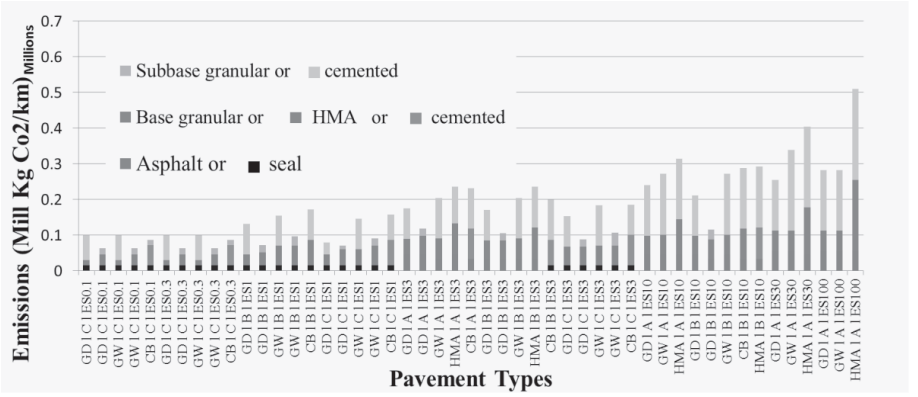

FIG. 1. Emissions in the construction phase for different pavement types.

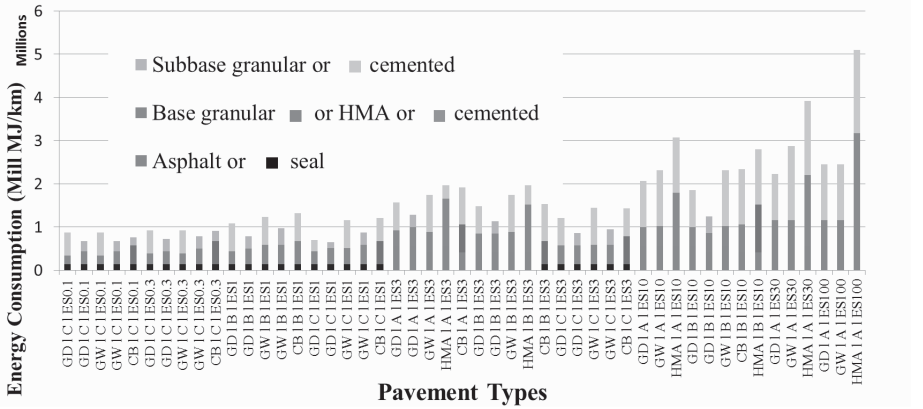

FIG. 2. Energy consumption in the construction phase for different pavement types .

The percentage light and heavy vehicles were alternated within this comparison as no prediction could be made with regard to this ratio. It should be noted that the vertical scale is in log units and could be deceiving in terms of the true difference between the construction and user phase.

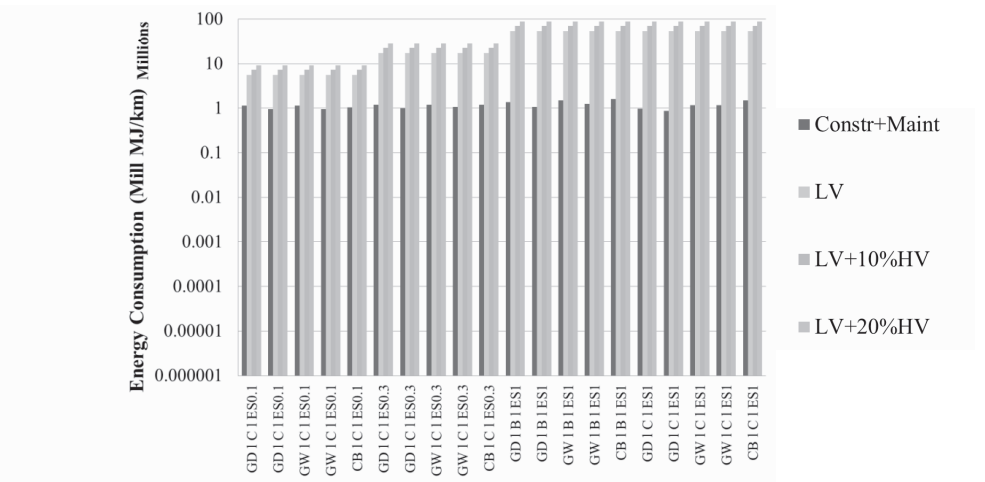

FIG. 3. Energy consumption-Construction vs traffic (ES0.1 to ES1) .

The results for the energy consumption and emissions show that the pavement construction phase results in much lower results than the user phase. Values for

energy consumption are in the range of 10 times more for the ES0.3 roads and 5000 times more for ES100 roads. Similar trends are prevalent for GHG emissions.
The variance in results between the choices in different % heavies is minimal in terms of the order size of the results. It should be noted that only energy emission values for ES3 and 10 has been shown but a linear increase results between ES0.1 and ES100.

These results show that by making a small change in the distribution of type of vehicle, far outweighs the mitigation options of that in the construction phase.

The energy consumption and emission results presented in this section provide a foundation to identify and evaluate opportunities for reducing these values within the pavement industry.

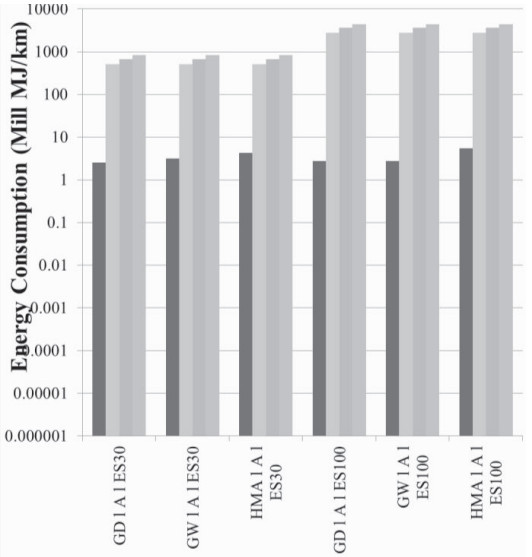

Fig. 4. Energy consumption - Construction vs traffic (ES10 to ES100).

Identification of the key issues influencing sustainability in road construction

Within the construction phase it is shown that the use of cement within the cemented base and subbase is not beneficial in energy terms. Opportunities for alternatives are available and should be explored. One such material is construction demolition waste. This might prove a suitable alternative to cemented materials or reduce the amount, especially due to its cementing properties. Comprehensive work on the a material performance of construction demolition waste can be found on work done by Van Niekerk (2002).The use of secondary materials within the road construction environment is scarce and encouragement due to a lack of understanding and the red tape surrounding regulations hinders the use of such

material. The acts and regulations with regard to this will be discussed in a subsequent section. The use of bitumen within the construction phase does not result in the critical mass, due to the volumes used. It should be noted that indicators used for calculation did not account for the importing of bitumen from other countries, which is the present status quo for South Africa. Transport has a big influence on the energy consumption and emissions of such a material will adversely affect results.

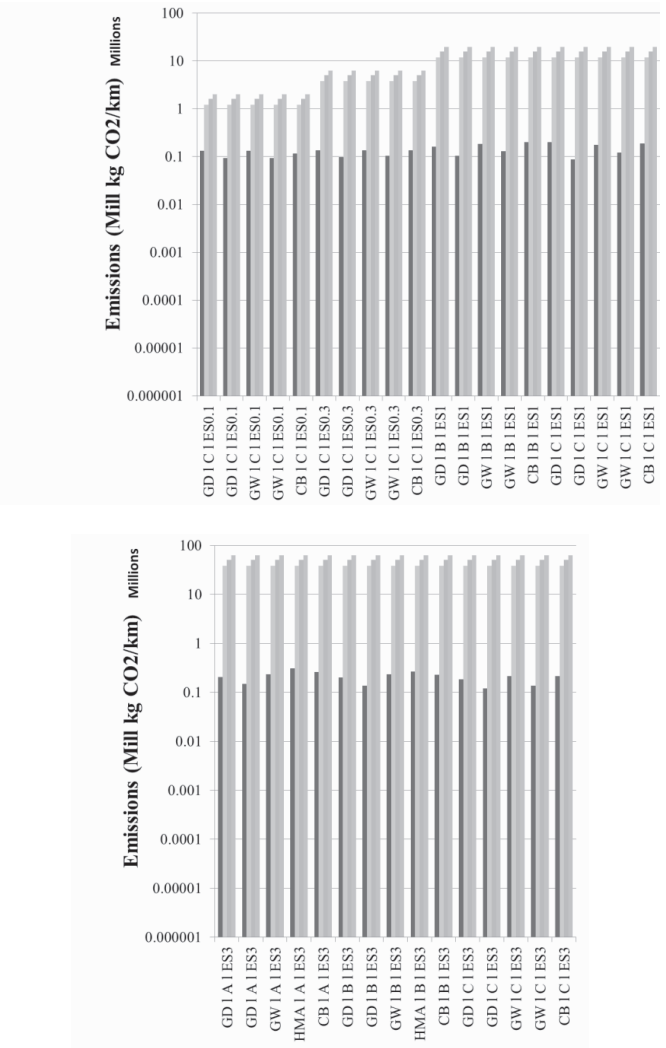

FIG. 5. Energy consumption-Construction vs traffic (ES10 to ES100).

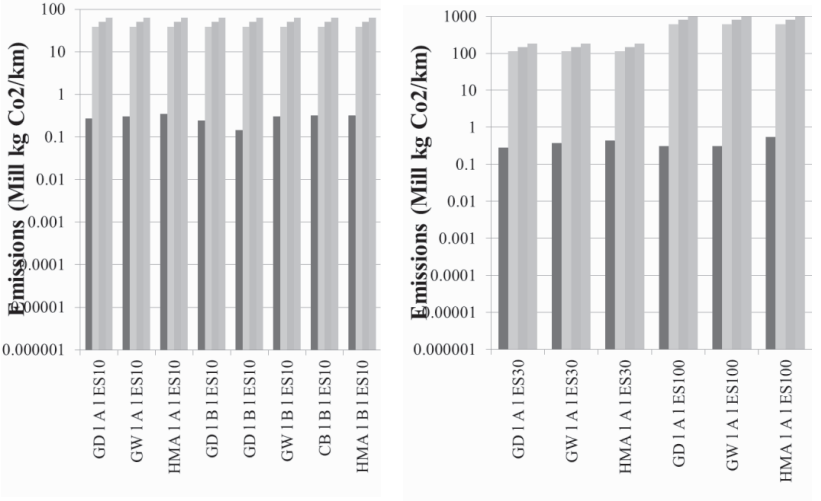

FIG. 6. Emissions-Construction vs traffic (ES3 to ES10).

The most important key issue identified is the emissions and energy consumption within the use phase. Decisions with regard to environmental issues should be guided by these findings in terms of prioritising. One such consideration includes the regular maintenance of roads, which will affect the riding quality and ultimately influence the fuel usage. A 1% saving in fuel will far outweigh the benefits that can be achieved through solutions within the pavement construction phase.

CURRENT POLICIES WITH REGARD TO SUSTAINABILITY APPLICABLE TO THE ROAD CONSTRUCTION INDUSTRY

The question remains if policies, strategies and current status quo within the industry are aligned with the key issues identified within the preceding section. A summary of some main strategic plans, policies, laws and status quo "aligned" with these key issues are discussed in order to determine if the industry is moving towards sustainable construction.

Macro level

National Development Plan:

By far the most comprehensive application to sustainability is the National Development Plan –Vision 2030 (NPC, 2012) developed for South Africa by the National Planning Commission. In this plan, reference is made to the transition to a low carbon economy. The points of interest in this paper include the aim to reach maximum output and decline trajectory of GHG emissions by the year 2025.

Some actions are proposed but no part of this low carbon strategic plan directly relates to the road construction industry. In summarising, the authors cannot identify

the direct contribution of the National Development Plan to the key issues identified.

Emission policies

In addressing the large variance of the emissions between road construction and road use it is important to mention the implementation of emission controls within the country.

The South African government has implemented a strategy for the control of exhaust emissions from road-going vehicles as reported in the government gazetted in 2003 (SA, 2003). The overall approach used in this strategy was based on the example of the European standards for vehicle exhaust emissions and fuel specifications and stated that in January 2006 all newly manufactured vehicles sold in South Africa are required to conform to Euro 2 and Euro 3 emission standards. This directly addresses the emissions of vehicles but, changes to vehicle technology alone cannot reduce emissions. The average vehicle on the road in South Africa is 13 years and does not address the issue on the short-term. This solution this is not obsolete and the critical issue of reducing the emissions of vehicles which do not fall within this category is eminent. In December 2010, the "Discussion Paper for Public Comment- Reducing Greenhouse Gas Emissions: The Carbon Tax Option", was released. In this paper the various implementation measures are explored. No clear concise method is prevalent. At present it does not directly address the key issues identified within this paper, and behavioral change on the micro level might not be influenced by the incorporation of carbon tax.

Micro level

Basic assesments or EIA (Environemental Impact Assessment)

With focus on micro level application of laws and regulations, the most applicable is the National Environmental Management Act 107 of 1998 and the subsequent EIA regulations (Government Notices 543-546, June 2010 as amended) promulgated in terms of the Act. These Regulations and Acts govern the execution of an Environmental Basic Assessment or Scoping-Environmental Impact Assessment process in order to identify potential impacts on the environment and to suggest mitigation measures. However, these reports typically focus on the construction phase with less emphasis being placed on the operational phase and/or the responsibility in this phase being shifted to the applicant, which is not held liable.

Other acts pertaining to beneficial use of secondary material

Results for the reference case study show the beneficial use of construction demolition waste as a road construction material. Within this context it is necessary to address the policies guiding the use of a waste material in a second stream. Waste in South Africa should be managed according to the: Minimum Requirements for the Handling, Classification and Disposal of Hazardous Waste, (Second Edition), 1998- Department of Water Affairs, the Environmental Conservation Act no. 73 of 1989, National Environmental Management Act no. 107 of 1998, the Health Act no. 63 of 1977 and the National Water Act no. 36 of 1998. At present these acts and regulations do not adress the key issues associated with a secondary waste stream,

mostly due to industry's lack of knowledge with regard to these materials. In order for users to freely use these materials, a significant improvement on the acts and regulation's with regard to implementation protocol should be revised.

The procurement of bitumen for the road industry

The present status quo which includes extensive measures to obtain bitumen within the country has a large influence within the pavement construction sector. Some SA refineries' continous insistence on exporting when there is a dire need within the country is questioned. This highlights the role of government within the road construction industry. Until date no regulatory institutions have positively attributed to this lack of road construction resource by securing future supply.

The green roads rating system initiave

By far the most applicable association with the movement towards sustainable construction is the current development of the Green roads rating system, an initiative driven and supported mainly by some industry partners and road authority clients within the industry. The Green roads rating system includes the rating of sustainability in projects through best practices. However, this can only be successful if developed to a true industry standard. However, only involvement of all stakeholders including governmental authorities will make this initiative a success.

INSTITUTIONAL OBSTACLES PERTAINING TO THE STATUS QUO

With reference to the identification of the key sustainable issues and the subsequent acts, policies and status quo, some of the more prevalent institutional obstacles with regards to these issues are summarised.

Lack of applicable road construction policy and identifying the key issues relevant to sustainable construction

The discussion on policies and current status quo in the road engineering industry show that a lack of understanding the key issues identified by the reference example are prevalent within the industry. The lack of knowledge of risks and effects of unsustainable road construction and the paired consequences make addressing of associated sustainable issues difficult. The economic advantages are shown for long term investment, however, the initial capital costs are much higher and greatly influences the mind-set and decision making process and emphasis are always on the short term which stunts economic growth. In a developing country such as South Africa, the disassociation of environmental sustainability and poverty is not possible.

As shown by the reference example the institutional obstacles associated with these policies and status quo is two-fold: 1.) Policies guiding the re-use of materials are currently insufficient and at best ambiguous. (2) The large variance between energy consumption and emissions between the construction phase as well as the use phase show that maintenance within the road sector is of utmost importance, as the riding quality of the road is directly related to the fuel use. Although carbon tax is applied as a whole to newly acquired vehicles, it is believed that this will not address the real issue.

Lack of efficiency to manage growing demands and political will

It is necessary to align as well as coordinate existing policies and regulations. At present, the state's ability to lead is greatly influenced by lack of coordination between governments. Various degree of institutional inadequacy and loosely defined polices are spread through different levels of government and municipalities. The responsibility of each governing authority is not clearly defined as the lack of governance is associated with clear undefined policies. Responsible parties are not kept publicly accountable. No institutional framework with the inclusion of monitoring is currently in place. This should be implemented after key issues have been identified.

CONCLUSION

The neccesity to reasses, identify and prioritise key issues affecting sustainable road construction are highlighted within this paper. A paradigm shift by all stakeholders within the pavement environment with regard to the real issues and areas to adress should be undertaken. This paper shows the necessity of an institutional framework to evaluate,monitor and mitigate environmental issues. This can only be achieved if clear and conscise goals are set through these strategic objectives.

Policy and regulations should adress these key issues, not only on a macro level, but also on a identifiable and pragmatical micro level. By exploring some issues associated with sustainable construction within the road construction, it is concluded that a substantial amount of fundamental work must still be done before the industry is equipped to meet the demands associated with sustainable construction within the road sector.

REFERENCES

Baer, P., Athanasiou, T., Kartha, S., and Kemp-Benedict, E. (2008). *The Greenhouse Development Rights Framework – The Right to Development in a Climate Constrained World. 2nd Edition,* Heinrich Böll Foundation, Christian Aid, EcoEquity and the Stockholm Environmental Institute, Berlin.

Burgess, R., Carmona, M. and Kolstee, T. (1997). *The Challenge of Sustainable Cities*, London, Zed.

Chappat, M. and Bilal, J. (2003). *The Environmental Road of the Future*. Colas Group, France.

Chehovits,J. and Galehouse, L., 2010. "Energy Usage and Greenhouse Gas Emissions of Pavement Preservation Processes for Asphalt Concrete Pavements". *Compendium of Papers from the First International Conference on Pavement Preservation*. Chapter 1: Paper 65 pg 27-41.

Committee of Land Transport Officials. (1996). "Structural Design of Flexible Pavements and Rural roads". *Technical Recommendations for Highways*, COLTO.

Department of Water Affairs and Forestry. (1998). *Minimum Requirements for the handling, Classification and Disposal of Hazardous Waste, Second Edition*,

Republic of South Africa.
Department of National Treasury. (2010). "Reducing Greenhouse Gas Emissions: The Carbon Tax Option". *Discussion Paper for Public Commen,.* Department National Treasury, Pretoria, South Africa.
Department of Environmental Affairs and Tourism. (2010). "National Waste Management Strategy". *First Draft for public comment*. South Africa.
Haw, M., and Hughes, A. (2007)."Clean energy and development for South Africa: Background data. Report 1(3)". *Energy Research Centre*, Cape Town, South Africa. http://www.erc.uct.ac.za/Research/publications/07Haw-Hughes%20Clean%20energy%20&%20development%20-%201.pdf (Accessed 29 March 2012)
http://www.mrmca.com/paving/athena.pdf (Accessed 12 February 2012)
National Planning Commission (NPC), 2011 National Development Plan-Vision 2030. Report No 270/2011. National Planning Commission, South Africa.
http://www.npconline.co.za/medialib/downloads (Accessed 28 February 2012)

Meil, J. (2006). *A Life Cycle Perspective on Concrete and Asphalt Roadways: Embodied Primary Energy and Global Warming Potential*. Athena institute, Canada.
Patrick, J. and Arampamoorth, H. (2010). "Quantifying the Benefits of Waste Minimisation in Road Construction". *NZ Transport Agency research report 406*, NZ Transport Agency, Opus International Consultants, New Zealand.
South African National Roads Agency, TRH3 (2007). "Design and construction of surfacing seals". *Technical Recommendations for Highways*, South Africa.
South Africa (SA). (2003). "Final Draft: Joint Implementation Strategy for the Control of Exhaust Emissions from Road-going Vehicles in the Republic South Africa. (Notice 3324 of 2003)". *Government Gazette 25741: 12 December 2003*, Republic of South Africa.
Swilling, M. (2006). "Rethinking the Sustainability of the South African City". *Sustainability Institute School of Public Management and Planning*, University of Stellenbosch, Stellenbosch, South Africa.
UNEP. (2011). "Towards a Green Economy: Pathways to Sustainable Development and Poverty Eradication". www.unep.org/greeneconomy (Accessed 22 February 2012)
World Bank. (2010). "Development and Climate Change". *World Development Report*, Washington DC:World Bank.
World Resources Institute (WRI). (2007). *Climate Analysis Indicators Tool (CAIT)*, Washington, DC.

The use of South African Fe-Mn, Si-Mn, Pt-converter and matte-smelting furnace slags in composite Portland cement – first results

Sabine M.C. Verryn[1], Herbert Pöllmann[2*], Elsabé Kearsley[3]

[1]Department of Material Science and Metallurgical Engineering, University of Pretoria, Pretoria, 0002 South Africa, email: sabine.verryn@xrd.ac.za

[2]Martin-Luther-University Halle-Wittenberg, Geological Institute, Halle/Saale, Germany

[3]Department of Civil Engineering, University of Pretoria, Pretoria, 0002 South Africa

[*] corresponding author

ABSTRACT: In this paper the use of slags from ferro- and silicomanganese alloy production as well as from the production of Pt-group element concentrates, in blended cements is discussed. The properties of the mixtures depend on the cement type, the mixtures, and the different manufacturers. Some cement performs better than others. The results are promising, but show variable behavior depending on slag and cement composition. Compressive strength tests as well as heat flow curves showing the hydration behaviour, indicate that 10-20 % addition of these slags to ordinary Portland cement is possible.These slags can be used as additions to cements to produce composite cements fulfilling the requirements up to 42.5N MPa class. By the addition of slag the amount of calcium carbonate, necessary for clinker production is reduced and therefore CO_2 emissions are decreased. Also large slag stock piles can be avoided.

INTRODUCTION

The South African Mining industry produces large amounts of slag in various ore-beneficiation processes. Examples are ferro- and silico manganese alloy production in submerged arc-furnaces as well as the production of Pt-group element concentrates, where large amounts of matte-smelting converter- and furnace slag is produced. Although a portion of the slag is used in the civil and road building industry, storage of the slag is becoming an increasing problem. As slag originating from the production of iron in a blast furnace, has been used in blended cements since before 1900, this study was initiated to utilize the various slag types in blended Portland cement.

In South Africa over 9.1 million tons of cement were sold in 2003 (CCI, 2004). Cement is divided into different classes or types, each with a specific notation, e.g.

"CEM I" contains only Portland cement with 0-5 % minor additinal constituents. CEM II A-S and CEM II B-S (Portland-slag cement) contains between 6 and 35 % granulated blast furnace slag (GBS), CEM III (Blastfurnace cement) contains between 36 and 95 % GBS, CEM V (Composite cement) contains between 18 and 50 % GBS, other CEM II types may also contain GBS. Nearly 7 million tons of cement types CEM II (6million tons), CEM III & V (0.7 Million tons) have been sold in 2003 (CCI, 2003). Frias (2006) have also recently shown that recycling of Spanish silicomanganese slag as pozzolanic material is possible. Rai (2002) has shown that some metallurgical slags from ferromanganese and ferromanganese-silicon alloy plants in India can be used for non-structural concrete.

Substitution of cement clinker with slag is investigated, which will deplete the large slag stockpiles as well as reduce CO_2 emissions during cement clinker production. Any addition of slag to clinker will reduce the amount of clinker in finished cement and with that the amount of calcium carbonate needed in the initial raw meal.

RAW MATERIALS

Manganese slag

In South Africa manganese ore is converted into alloys at a plant in Meyerton in the Gauteng Province. In the production of ferromanganese alloy in a submerged arc-furnace large amounts (approximately 140 000t) of air-cooled slag are produced yearly. Silicomanganese alloy production results in approximately 33 000t of slag.

Mineralogically the phases in the ferromanganese slag are glaucochroite (Ca-Mn-Silicate), some bustamite (Ca-Mn-Di-Silicate), gehlenite (Ca-Al-Silicate), quartz and minor silicate glass phases. The Silico-manganese slag is composed mainly of glaucochroite, bustamite, manganosite (Mn-oxide), gehlenite, quartz, calcite and glass. A reflected light photomicrograph of this slag showing crystalline and amorphous parts is shown in Fig. 1.

Due to the mineralogical phase composition these slags are potentially latent hydraulic materials and can participate in the hydration process of the composite cement after the hydration reaction being initiated. Non reactive parts can act as an inert filler. The slags were ground to a fineness similar to the used cements. Macroscopic view of the ferromanganese and silicomanganese material is given in Fig. 1.

Slag from the Pt-industry

Large amounts of slag result from the production of Pt-group element concentrates. The main producers are the source of approximately 1 million tons of furnace slag and 250 000 tons of converter slag.

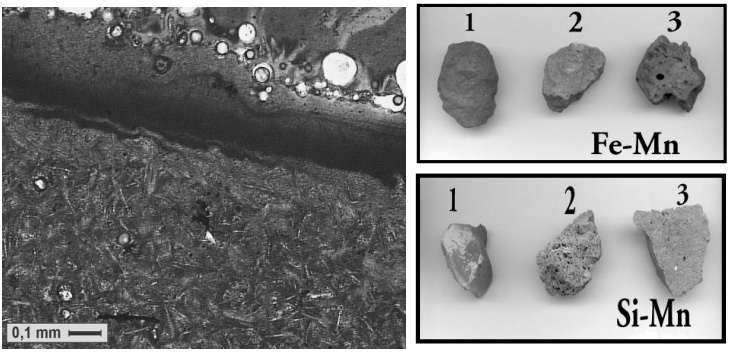

FIG. 1. Photomicrograph (reflected light) of Silico-manganese slag, showing contact of glassy and crystalline parts (letft), **Ferromanganese slag (right-upper) and Silicomanganese slag(right-below).**

Table 1. Chemical composition of used slags

Oxide	FeMn slag	SiMn slag	Pt-furnace slag	Pt-converter slag
SiO_2	29-34	40-42	41	26
Al_2O_3	6	6	5	1
CaO	19-30	15-21	16	1
MgO	7	7	19	2
Na_2O	<1	<1	<1	<1
K_2O	n.d	<1	<1	<1
MnO	18-23	15	<1	<1
FeO	2	1	15	64
Cr_2O_3	<1	<1	2	1.5
NiO	<1	<1	<1	1.5
SO_3	1	1	<1	1

Mineralogically the furnace slag is composed mainly of a glass with traces of crystalline olivine (Mg-Fe-Silicate) and magnetite (FeII+-FeIII+- Oxide).

The Pt-converter slag contains glass, olivine, magnetite, quartz and a Ca-Al-Mg silicate. Based on the mineralogical composition of Pt-industry slags are potentially less reactive. The mineralogical composition of all the slags was determined by X-Ray Powder Diffraction using a Siemens D500 Diffractometer and EVA treatment software.

Approximate chemical compositions (in weight percent) analyzed by X-Ray fluorescence spectrometry using an ARL9400XP+ spectrometer of the above slags are given in Table 1.

Granulated blast furnace slag from the steel industry using the Corex process (Alexander, 2003), which is widely used in South African cements and performing very well, was used for additional comparison in the blends prepared with the cement milled in a ball grinding mill.

Cements

The South African ordinary Portland cements used and listed below are Type CEM I with 42.5 MPa strength.

- Ordinary Portland Cement (CEM): This cement is milled in a laboratory sized ball grinding mill at the University of Pretoria from cement clinker adding 3.5% gypsum.
- Commercially available Ordinary Portland Cement from PPC (Pretoria Portland Cement).
- Commercially available Portland cement from Lafarge South Africa was used for additional comparison in the compressive strength tests.

Addionally European Portland cements Type CEM I with 32.5, 42.5 and 52.5 MPa strength from different manufacturers were used in some tests.

The selected 5 cements are conformal to normal Portland cements consisting of the main phases Tricalciumsilicate, Dicalciumsilicate, Tricalciumaluminate and Tetracalciumaluminateferrite. During the hydration of these cements the newly formed Portlandite ($Ca(OH)_2$) is necessary to initiate the reactions of the latent hydraulic slags. The different specific surfaces of these Portland cements Type CEM I (32.5, 42.5, 52.5 Mpa) are producing different final strengths. The different reaction behaviour by addition of slag was tested.Abbreviations used in the text, diagrams and tables are shown in Table 2:

Table 2. Abbreviations of used materials

Slag/Cement	Abbreviation
Ferro-Manganese Slag	FeMn
Silico-Manganese Slag	SiMn
Converter Slag from Pt-industry	PtC
Furnace Slag from Pt-Industry	PtF
Granulated Blast Furnace Slag from Corex process, South Africa	Cor(ex)
Ordinary Portland Cement milled from clinker at University of Pretoria	CEM
Pretoria Portland Cement 42.5 R CEM1	PPC

EXPERIMENTAL

Mixtures

The various slags were blended with the raw Portland cement clinker as well as the commercially available cements from South Africa and Europe in various cement / slag ratios, ranging from 10 to 50 percent slag additions as are indicated in the results below.

Testing

The chemical composition of slag was determined by XRF (ARL9400XP) spectrometer. The chemical composition of the cements were used as available from supplier.The strength development was measured at 2, 7 and 28 days using the SANS 50196 compressive strength test method on 40x40x160 mm blocks. 450g cementitious material, 225g water and 1350g standard sand were used in each test, which were carried out in duplicate an average values are used here.

All results were compared to 100% percent cement mixtures and for data evaluation also to a widely used blast furnace slag as described before.

The course of hydration was determined by isoperibolic heat-flow calorimetry (Pöllmann *et al*.). The hydration studies were performed with a w/s ratio of 0.5 using 1ml of water with 2g cement/slag mixture at controlled constant temperature of 25^{o}C. All data were collected relative to an inert standard to avoid influence from surrounding.

For comparison purposes the calorimetric curves of the pure cements are given in all the given figures.

RESULTS

The heat calorimetry was used to test the potential use of latent hydraulic slag materials in combination with cements to determine the limits of addition without loosing properties not conformal to specifications. The consumption of $Ca(OH)_2$ coming from the hydration of the cement part because of the participation of the slags in the hydration was obtained by the varying heat flow curves. Therefore a comparison to 100% cement was used. In case that the addition exceeds the acceptable lower limit the hydration change and therefore the shape of the heat flow curves also. This is used as an indication that the addition of slag must be reduced.

In the following Figs. 2-4 the evolution of different cement slag mixtures are shown.

Fig. 2 shows the heat evolvement of the mixtures of cements PPC, CEM with addition of manganese slag, displaying the curves for pure cement for comparison.

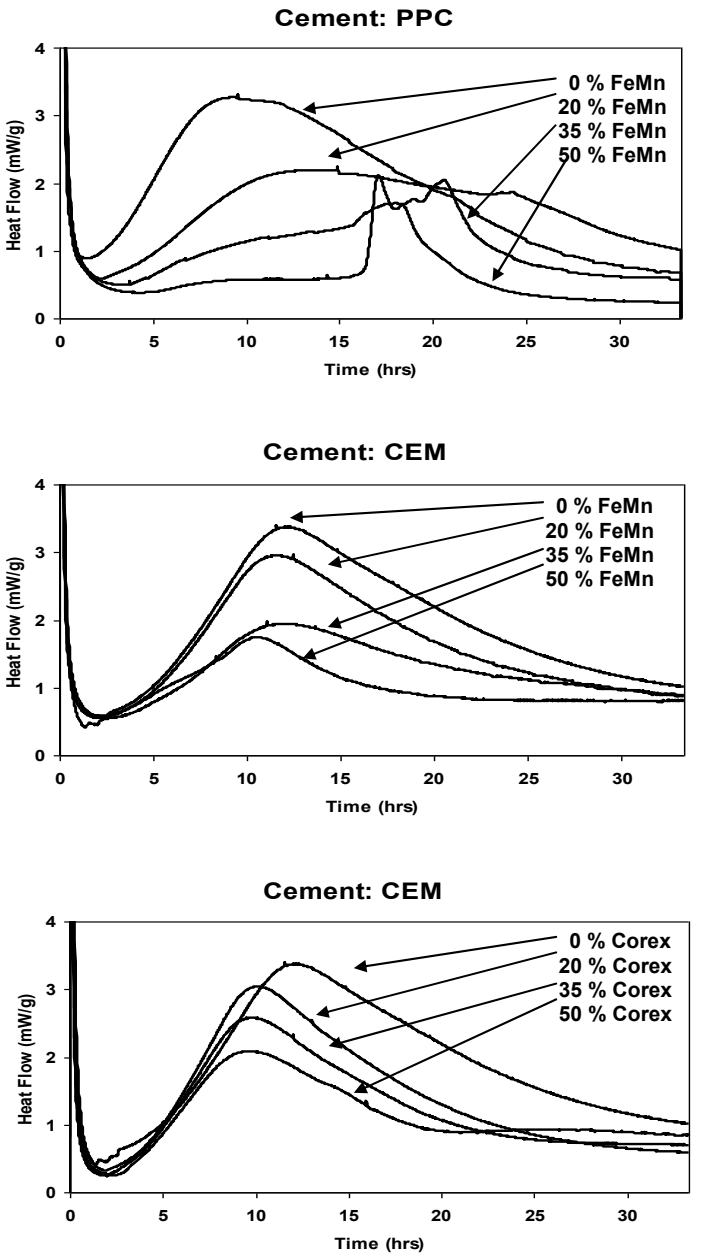

FIG. 2. Heat flow curves for South African cement (upper), Ferro Manganese-Slag mixtures (middle) and Addition of blast furnace slag COREX (bottom).

The cement type is indicated at the top of each diagram and the amount of slag in the legend.

In the blends using PPC cement maximum hydration occurs later with increasing slag concentration with exception of the blends with 50% addition of slag. Here the maximum occurs earlier than that for the 35% addition of slag. The shape of the curves show up to 35% of addition still the main broad heat flow decreasing with increasing slag contents. Starting with 35 % of slag also different curve shapes occur due to the formation of other hydration products. The behaviour of the CEM cement is slightly different, but also the heat evolution drops with increasing amounts of added slag. For both cements the addition of 20% of slag addition appears to be the maximum.

For comparison the use of a typical iron blast furnace slag COREX is shown in Fig. 2. In this case it can be shown that more than 35% of addition is favourable. The potential use of Si-Mn slag was investigated using European cements with 32.5, 42.5 and 52.5 MPa in Fig. 3.

In all 3 cases the use of up to 20% is possible. The shape of heat flow in comparison of all 3 types of European cements shows the influence of reactive surface, because it can be shown, that the drastic change in heat evolution at higher slag additions does not occur. The heat flow curves of the 52.5 cement do have similar shape but less heat is evolved. The influence on heat evolution on the cements 32.5 and 42.5 at higher additions of slag lead to different hydration behaviour.

Fig. 4 describes the heat evolution for cements with addition of slag from the Pt industry. Heat flow curves of CEM and PPC cements with addition of PtF slag show a decrease in heat flow with increasing addition of slag, which is more pronounced when using the CEM cement milled from clinker. In both cases the maximum hydration occurs earlier than that of the pure cement. The addition of Pt-slag shows that due to the composition the slag does only slightly participate in the reaction behaviour but still can be used in low amounts up to 20 % depending on the type of cement. The heat flow curves differ from typical latent hydraulic material addition curves and more inert material in slag is involved.

Addition of 35 % PtC slag to CEM shows very little heat evolvement and the curves for the 10 and 20 % additions show less heat flow than that of the pure CEM cement. Addition of 10 % PtC slag to PPC cement results in slightly earlier hydration maxima than that of pure PPC cement and those with 20 and 35% addition show even earlier maxima (Fig. 4).

Higher additions of slag can lead to some abnormal heat flow curves due to varying hydration reactions.

Results of the compressive strength tests are presented in Fig. 5 for cement - FeMn slag mixtures and in Fig. 6 for cement-Pt-slag mixtures. SiMn slag – European cement mixtures were not tested at this stage.

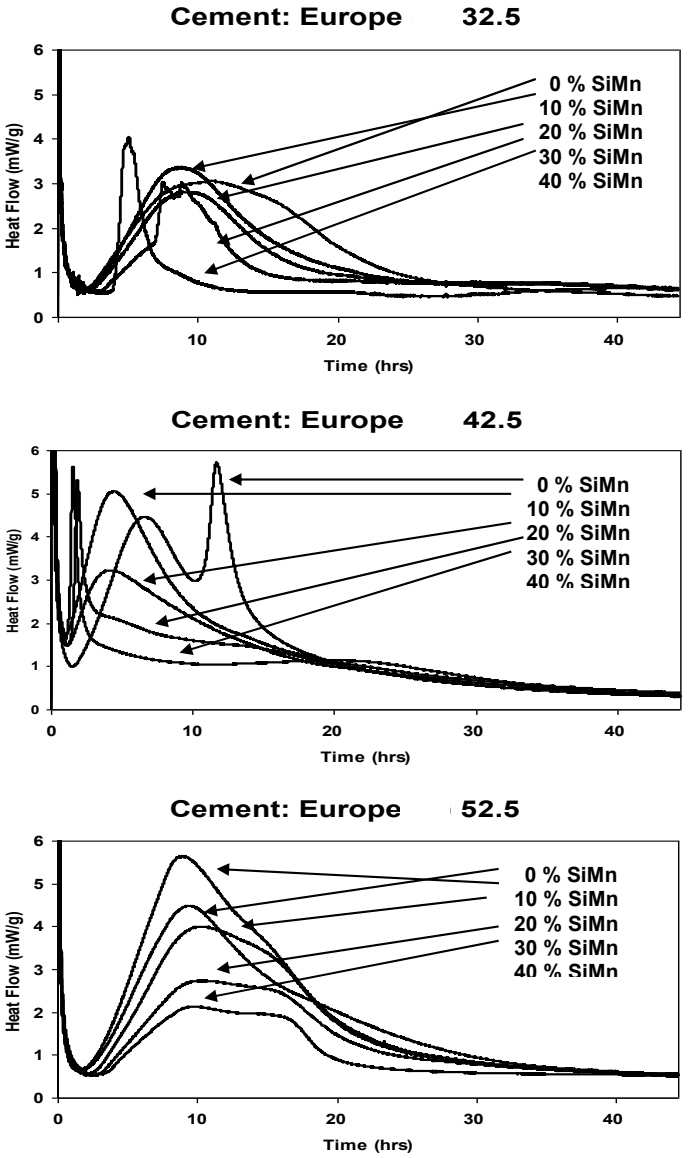

FIG. 3. Heat flow curves for European cement (upper), Silico Manganese (middle), Slag mixtures (bottom). The cement type is indicated at the top of each diagram and the amount of slag in the legend.

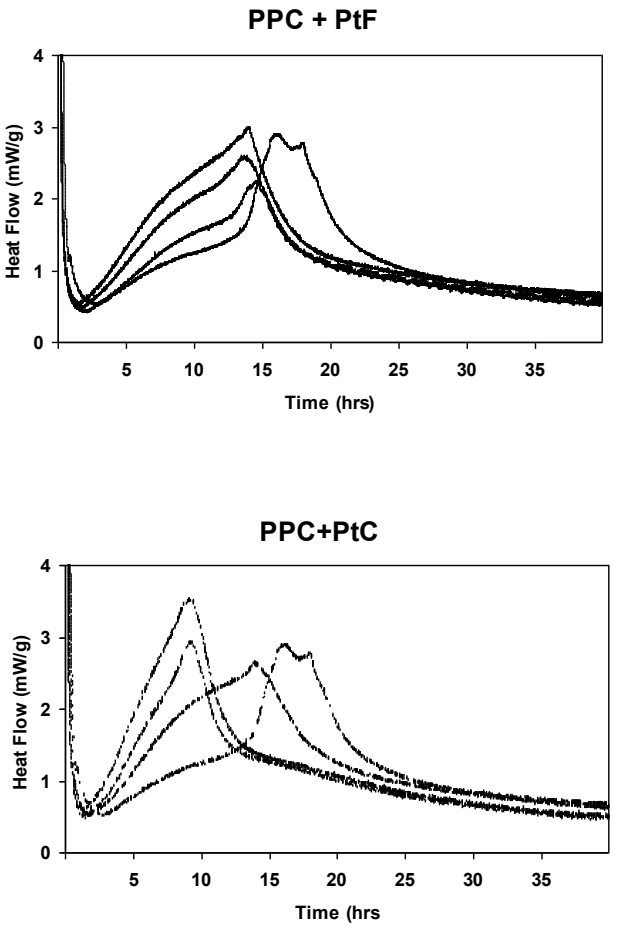

FIG. 4. Heat flow curves for South African cement – furnace slag from the Platinum industry (PtF) (upper) and converter slag from the Platinum industry (PtC) (bottom).The cement and slag type is indicated at the top of each diagram and the amount of slag added is shown in the legend.

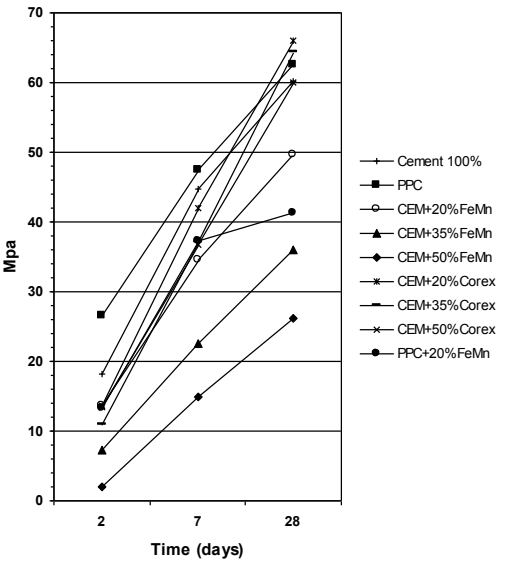

FIG. 5. Compressive strength at 2, 7 and 28 days of cement – slag blends as indicated in the legend.

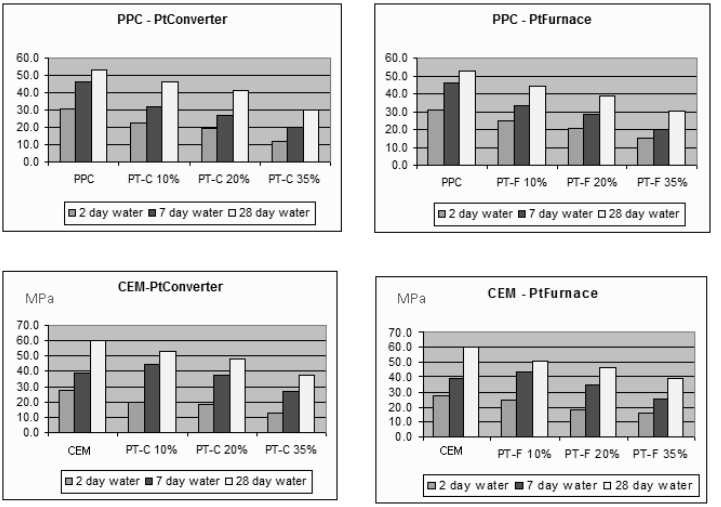

FIG. 6. Compressive strength at 2, 7 and 28 days for cements and Pt-industry-slag mixtures as indicated in the legends.

Results compare well with the results obtained from the heat flow curves. The compressive strength of the cement – FeMn slag mixtures is lower than that of the respective cement-Corex slag mixtures.

The compressive strength of the cements with addition of Pt slag is lower than that of the pure cements for each time period. The performance of the cements with added PtC slag is marginally better than those with addition of PtF slag.

SUMMARY AND DISCUSSION

The results of the Mn-slag blends indicate that the amount of heat developed increases with increasing cement content within each sample group. Comparison of each ratio shows that the FeMn slag containing composite cements show less heat evolvement than the respective composite blast-furnace (corex) slag cement of the same ratio. Compressive strength of the cement – Mn slag mixtures is lower than that of the respective cement-Corex blast furnace slag mixtures.

Test results for the Pt-industry slag – cement blends show similar trends, with the PtC slag – cements blends showing higher strength than that of their respective PtFslag – cement mixtures.

Comparing the results with the compressive strength requirements of SANS 5019, as well as BS12:1996, show that on the basis of the strength requirements the Cement (CEM) with 50% FeMn slag addition falls outside the requirements for all cement classes, the 35% FeMn slag addition blend as well as the PPC cement with 20% FeMn slag addition fall within the limits for class 32.5N and the 20 % FeMn slag mixtures fall into the 42.5N class.

All tested cements with 10% Pt-slag addition as well as the CEM cement with 20 % Pt slag addition fall inside the strength requirements of the 42.5MPa class. The PPC cement with 20% Pt slag additions fall into the 32.5 N class. Higher amounts of added Pt-slag are not favourable, because of low reactivity in hydration reactions.

In comparison of addition of different amounts of slags it could be shown that the amounts of Fe-Mn slag should be less than 20 %, because otherwise the hydration behaviour is strongly influenced and also the existing norms are not fulfilled. Although the widely used COREX iron blast furnace slag shows better performance, it could be shown, that the Fe-Mn and Si-Mn slags can be utilized in adequate additions due to their enlowered latent hydraulicity. The Pt-industry slags do not perform as well and are more resembling a filling material.

The properties of these mixtures depend on the cement type, the mixtures, and the different manufacturers. Some cement performs better than others. The results are promising, but show variable behavior depending on slag and cement composition. There is a large potential to use these slags in cement mixtures and this study can be used to develop cements that will positively influence CO_2 emissions and help to reduce large slag stock piles.

The expected hydration products of these additions are mainly unknown yet (incorporation of manganese in cement hydration products).

This preliminary study is going on to optimize the additions to cements and also to understand the formation of different hydration products containing manganese.

From the present stage it can be said, that also manganese And Pt-slags can be used similarly to iron blast furnace slags, but lower amounts are only be usable at the present state.

In case that also the quality of slag can be improved for cement use probably higher amounts can be added.

ACKNOWLEDGEMENTS

The authors would like to thank Prof. JPR de Villiers (University of Pretoria) and Dr Stefan Stöber (Martin-Luther-University Halle-Wittenberg) for fruitful discussions and Mr. HF Mostert for the compressive strength tests. The financial assistance provided by the National Research Foundation of South Africa and the Forschungsgemeinschaft Jülich in Germany is greatly appreciated.

REFERENCES

Alexander M.G., Jaufeerally, H., Machechnie, J.R.(2003). "Structural and durability properties of concrete made with Corex Slag". *Research Monograph No 6*, Departments of Civil Engineering, University of Cape Town and of the Witwatersrand,.

Bye, GC. (1999). *Portland Cement 2nd ed.* London: Thomas Telford Publishing,

Cement & Concrete Institute, (CCI). (2004). *Cement and Concrete Review 2003*, Halfway House, South Africa.

Cement & Concrete Institute, (CCI). (2000). Cementitious *Materials for Concrete: Standards, selection and properties*, Halfway House , South Africa.

Frias, M., Sánchez, M.I., Santamaría, J. and Rodríguez, C. (2006). "Recycling of silicomanganese slag as pozzolanic material in Portland cements: Basic and engineering properties". *Cement and Concrete Research,* 36 (3): 487-491

Pöllmann, H., Kuzel, H.J., Meyer H. (1991). "Heat flow calorimetry in cement chemistry". *Proc. 13th Int. Conf. Cem. Micr.*, Tampa, 254-272

Rai, A., Prabakar, J., Raju, C.B. and Morchalle, R.K. (2002). "Metallurgical slag as a component in blended cement". *Construction and Building Materials*, 16: 489-494.

SANS 5019. (2006). *Cement Part 1: Composition, specifications and conformity criteria for common cements*, Pretoria: South African Bureau of Standards.

Monitoring Early-age Cracking of Continuously Reinforced Concrete Pavements on the E17 at Ghent (Belgium)

Dongya Ren[1], Lambert J.M. Houben[2] and Luc Rens[3]

[1]PhD candidate, Faculty of Civil Engineering and Geosciences, Delft University of Technology, 2600 GA Delft, the Netherlands; email: d.ren@tudelft.nl
[2]Associate Professor, Faculty of Civil Engineering and Geosciences, Delft University of Technology, 2600 GA Delft, the Netherlands; email: L.J.M.Houben@tudelft.nl
[3]Engineering Consultant, Depart of Road and Infrastructure, Federation of the Belgian Cement Industry, 1170 Brussels, Belgium; email: l.rens@febelcem.be

ABSTRACT: Continuously reinforced concrete pavements (CRCP) are frequently applied on motorways and also on other heavily trafficked roads in Belgium, mainly because of the confidence in its durability. An exposed aggregate surface is used to reduce the traffic noise. The durability, the sustainability, the low maintenance and the low traffic noise production of CRCP lead to long lasting applications in Belgium. This paper presents the observations and findings from the monitoring of three CRCP test sections constructed on the motorway E17 near the city of Ghent, Belgium in August 2011. The three test sections have a reinforcement rate of 0.75%, 0.70% and 0.65% + 20 kg/m^3 steel fibers, respectively. Right from the moment of construction, the behavior of the pavements was monitored for the concrete temperature, the crack spacing and the crack width, and the development of the crack pattern in time. The temperatures within the concrete were evaluated using thermocouples. The crack spacings were measured with a distance measuring wheel. The width of a number of cracks was measured with a microscope and the movements within the CRCP were also measured with a linear variable differential transformer (LVDT) across a number of cracks. Major observations and findings from the monitoring of the CRCP test sections include: the effect of longitudinal reinforcement on the early-age cracking; the effect of time of construction during the day on the early-age cracking; the effect of curing time of concrete on the early-age cracking.

INTRODUCTION

Continuously reinforced concrete pavements (CRCP) are applied in Belgium for more than 60 years. In 1950, the first CRCP test section was constructed in Belgium (Verhoeven,K.,1993). Forty percent of the motorways in Belgium are concrete

pavements, and CRCP is nowadays frequently applied on these motorways (Hall, K. et al., 2007). The durability, the sustainability, low maintenance and low noise production of CRCP lead to long lasting applications (Rens, L., 2010). However, the early age behavior after the placement which is considered as a key factor for the long term performance of CRCP has not been fully investigated. In this study, right from the moment of construction, the early age behavior was investigated on three actual test sections at the E17 motorway near the city of Ghent. This paper presents the preliminary measurement results with particular focus on the evolution of the crack pattern during the very early age of the CRCP pavements.

DEVELOPMENT OF CRCP IN BELGIUM

Table 1 shows a summary of design concepts and performance of CRCP in Belgium since 1970 (Rens, L., 2010).

Table 1. Summary of design concepts and performance of CRCP in Belgium

	Concept 1	Concept 2	Concept 3
Period	1970-1981	1981-1995	1995-
Longitudinal reinforcement	0.85% Φ18@150	0.67% Φ16@150	0.75% Φ20@180
Depth Concrete Cover	60 mm	90 mm	80 mm
Slab thickness	200 mm	200 mm	230 mm
Interlayer	asphalt interlayer	no asphalt interlayer, directly on lean concrete base	asphalt interlayer
Air-entraining agent	no	no	yes
Surface treatment	transversely grooved	transversely grooved or exposed aggregate	exposed aggregate
Performance	Average crack spacing: 0.4 to 0.6 m about 18 years after construction. Many clusters of closely spaced cracks	Average crack spacing: 1.4 to 2.4 m about 18 years after construction. About 70 % of the crack spacings within 0.8~3 m	Average crack spacing about 1.0 m after 2 years with clusters of closely spaced cracks (few data available)

Due to economic reasons, concept 2 was introduced in the early eighties. The most important changes were the reduction of the percentage of longitudinal reinforcement from 0.85% to 0.67% and omitting the asphalt interlayer between CRCP and the cement-bound base. The distribution of cracks was much more regular than with concept 1. However, it was found that CRCPs constructed according to concept 1 with an apparently very unfavorable crack pattern with many clusters of closely spaced cracks, still behave perfectly after 40 years of service. By contrast, concept 2 CRCPs rapidly exhibited punchout problems due to erosion of the base layer. Because of the failure of concept 2 and in view of the ever increasing traffic loads, the standard structure for main roads in CRCP was adapted in the nineties by introducing the current concept 3.

TEST SECTIONS

The test sections described in this paper are a part of an 11 km long stretch of the motorway E17 that was reconstructed in mid-2011. Within this stretch, over a length of 9.9 km CRCP (250 mm thick) was applied upon an asphalt interlayer (50 mm), a roller compacted concrete base layer (150 mm) and a sub-base of unbound aggregates coming from crushed lean concrete (Fig 1). The old jointed plain concrete pavement was recycled into the new base and sub-base of the CRCP. The details of the test sections and the concrete mix composition are shown in table 2 and table 3, respectively.

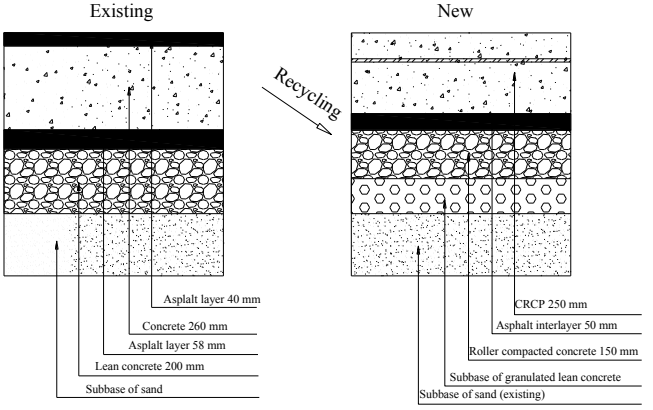

FIG. 1. The existing jointed plain concrete pavement (left) and new CRCP (right) .

Table 2. CRCP test sections design details

Test section	Location (km)	Subsection (km)	Slab thickness (mm)	Longitudinal reinforcement	Depth concrete cover (mm)	Asphalt interlayer (mm)
1	44.7-45.2	45.0-45.1	250	0.75%	80	50
2	45.2-46.2	46.0-46.1	250	0.70%	80	50
3	46.2-46.7	46.4-46.5	250	0.65% + 20 kg/m^3 steel fibers	80	50

Table 3. Concrete mixture per m^3

Cement type	Cement (kg)	Water (kg)	W/C	Air content
CEM III/A 42,5 N LA	400	172	0.43	3%
Coarse aggregate type	Maximum aggregate size (mm)	Coarse Aggregate (kg)	Fine aggregate (kg)	Admixture (kg)
Porphyry	20	1331	474	1.6

TEST METHODS

Temperature

At two locations (km 45.780 and km 45.790) a set of three thermocouples have been installed to measure the concrete temperature at different depths within the concrete slab, the upper one 30 mm below the pavement surface, the middle one at the height of the reinforcement and the bottom one 30 mm above the asphalt interlayer as shown in Fig 2.

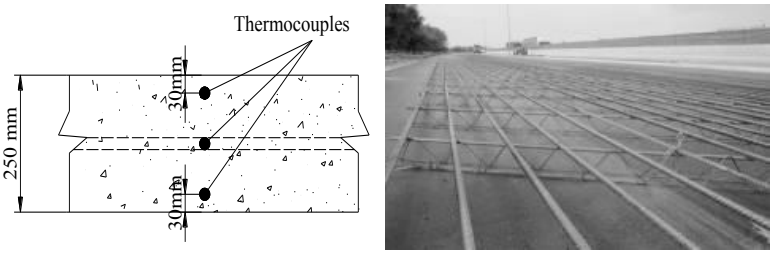

FIG. 2. Installation layout of thermocouples.

The time of concrete placement at the location of the thermocouples was at 10 PM on 18th August, 2011. Subsequently, the temperatures were collected every 30 minutes during the first 24 hours after concrete placement, and afterwards every 2 hours until 2 PM on 22th August, 2011.

Crack spacing

The crack spacing survey was conducted by slowly walking along the edge of the pavement. The length of each section for the crack spacing survey is 500 m, 1000 m and 500 m, respectively (see table 2). Within each of the 3 sections more detailed crack surveys were done in a 100 m long subsection (see table 2). Each transverse crack within the subsection was identified by the time of occurrence, location, absolute crack width and length. The occurrence time, location and length were recorded as detailed as possible on the crack detail map.

Crack width

In order to obtain the horizontal crack width variation due to concrete shrinkage and environmental effects, temperature variation and moisture changes, close to the surface and at the depth of the steel reinforcement, a procedure was adopted to accurately measure the horizontal crack width change by a LVDT. The measurement concerns the distance between two fixed points, as shown in Fig 3.

FIG. 3. Crack width measurement by LVDT (left) and Microscope (right)

Two sets of studs were attached to both sides of the selected cracks within the subsections on the edge of the pavement. The distance between two studs is 100 mm and the upper set of studs is 30 mm below the pavement surface and the bottom set of studs is at the depth of the longitudinal steel reinforcement. An external LVDT was used to measure the horizontal crack width movements at each selected crack one by one. This method thus provides only information to determine changes in crack width due to environmental effects. These measurements could only be done a few times because on 22th August, 2011 all the studs were buried into a gutter that was constructed alongside the emergency lane. A microscope was used to give the absolute crack width on the surface of the pavement of the selected cracks within the 3 subsections (Fig 3).

MESUREMENT RESULTS

Ambient temperature and concrete temperature

The time histories of the air temperature, the concrete temperatures at the pavement surface, top, middle and bottom of the concrete slab are shown in Fig 4. As shown in Fig 4, the concrete temperature in the first 90 hours is always higher than the air temperature. The largest difference between concrete temperature and air temperature occurred on the first day due to the large amount of heat of hydration. Subsequently the difference decreased in the following three days even though the air temperature variation became larger. The maximum concrete temperature variations at top and bottom during the first night after construction were 14.2°C and 7.1°C, respectively.

The typical daily cycle of the temperature profile through the depth of the concrete slab is shown in Fig 5. The results shown in the Fig illustrate the variation of the temperature profile through the slab depth for 24 hours on the second day after concrete placement. The maximum temperature gradient (0.030°C/mm) on the second day after concrete placement occurred at 3 PM and the minimum temperature gradient (-0.024°C/mm) occurred at 7 AM. The maximum and minimum temperature gradient during the four days after concrete placement was about 0.033°C/mm and -0.029°C/mm, respectively. A large temperature variation at the concrete surface compared to that at the bottom could be one the major causes for cracking at the very early ages. Consideration of the effect of the nonlinear temperature variation, and the

effect of their nonlinearity with respect to time, is critical to understand the pavement behavior in the first few days after construction.

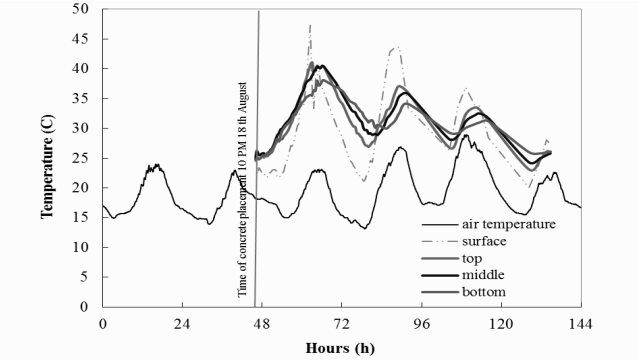

FIG. 4. Air Temperature and concrete temperature

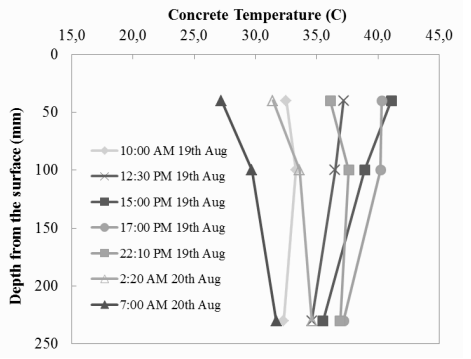

FIG. 5. Daily cycle of concrete temperature profile through the slab depth

Crack spacing

The average crack spacing and other crack spacing statistics of the 3 sections are presented in table 4.

In the first 100 m long subsection (table 2) no cracks were observed the first day after construction. Two days after construction 12 cracks had occurred due to substantial temperature drop and shrinkage, 2 additional cracks were observed on the third day after construction and no additional cracks were observed on the fourth day after construction (Fig 6). In the second 100 m long subsection 29 cracks were observed after the first night after construction. 3 and 5 additional cracks were observed on the subsequent two days, respectively. In the third 100 m long

subsection there are 12, 19 and 27 cracks after the first three nights respectively.

Table 4. Crack spacing statistics of the sections

Date	4 days			60 days		
Test Section	0.75%	0.70%	0.65% + fibers	0.75%	0.70%	0.65% + fibers
Length of test section (m)	500	1000	500	500	1000	500
Number of cracks	87	259	151	260	515	315
Mean crack spacing (m)	5.7	3.9	3.3	1.93	1.95	1.59
Maximum crack spacing (m)	24.8	17.7	15.4	8.2	7.8	5.8
Minimum crack spacing (m)	0.2	0.1	0.1	0.1	0.1	0.1
Standard deviation (m)	4.46	2.49	2.84	1.92	1.54	1.27

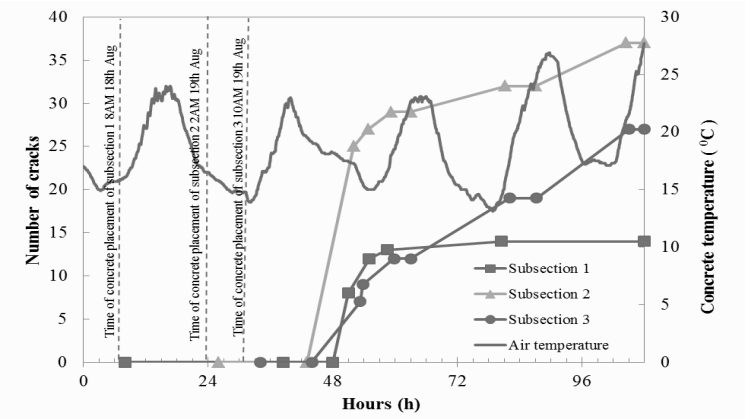

FIG. 6. Number of cracks as a function of the concrete age

Effect of longitudinal reinforcement content

It is a generally accepted theory among previous researchers that the higher the percentage of longitudinal reinforcement in CRCP, the larger the number of cracks, a result of the bond between concrete and steel reinforcement restricting concrete movements (Suh, Y.C.,1992; Zollinger, D.G.,1998; Kohler, E.R.,2006). Fig 8 shows the distribution of crack spacings for the test sections at two ages, 4 days (red color) and 60 days (blue color) after construction, respectively. In all the sections, in time there is a shift towards more cracks, so towards smaller crack spacings.

However, the crack pattern in the three sections at 4 days and 60 days after construction is not as expected and is quite contrary to the generally accepted theory, as can be seen in the Fig 7 and table 4. The first section has the highest longitudinal reinforcement content (0.75%) while the average crack spacing is the largest compared to the other two sections. However, the growth rate of the number of

cracks in section 1 is faster than in the other two sections. One of the major reasons could be related to the curing time. The other possible reason may be related to the time of concrete placement on the day. It is too early to draw a conclusion about the effect of the longitudinal reinforcement percentage on the crack spacing only based on the results of the (very) early age surveys.

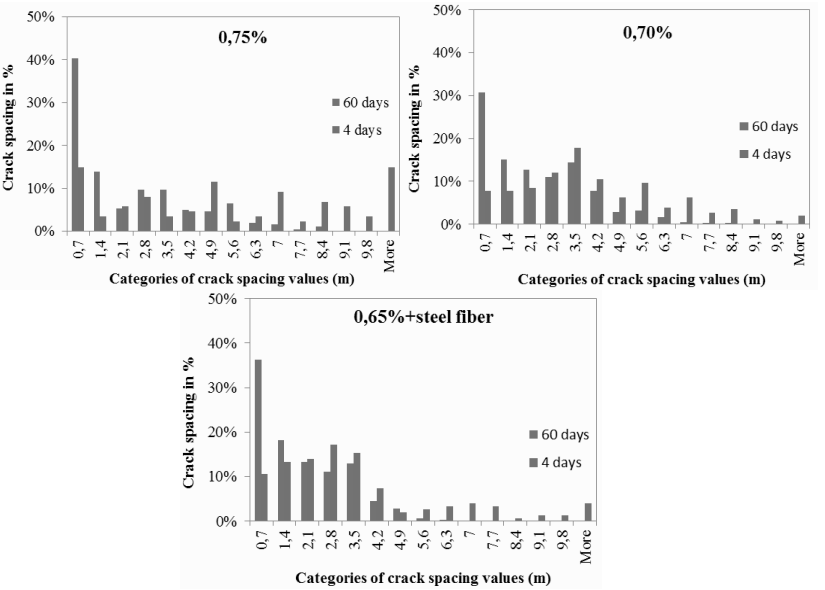

FIG. 7. Crack spacing distribution on the three test sections

Effect of placement time on the day and curing time

As can be seen in the Fig 8, the first subsection was placed at 8 AM at 18th August, 2011, and the plastic sheet was removed at 4 PM 19th August, 2011. However, the third subsection with steel fibers was placed at 10 AM 19th August, 2011 and the plastic sheet was removed at 8 PM the same day. The initial curing time of the first subsection is about 32 hours while the initial curing time of the third subsection is only 10 hours. After 4 days 26 cracks were observed in the third subsection and only 13 cracks in the first subsection (see Fig 6). The third subsection might not have gained sufficient strength due to the very short initial curing period to resist the stresses caused by the huge temperature drop and shrinkage during the night following the construction day.

As already shown in Fig 6, in the first subsection no cracks were observed during the night following the construction day even though the concrete temperature drop was at its maximum, up to 10°C. The plastic sheet was removed at 4 PM, 32 hours after construction. Then 12 cracks were observed after the second night after

construction. During both of the subsequent two nights only one new crack occurred within the 100 m subsection. The subsections 2 and 3 were constructed at 2 AM and 10 AM, on 19th August, 2011, respectively. The initial curing time for those two subsections was 15 hours and 10 hours, respectively. After the night following the construction day, 29 cracks were found in subsection 2 and 12 cracks in subsection 3. After the subsequent two nights 3 and 4 new cracks were observed in the second subsection and 7 and 8 new cracks occurred in the third subsection.

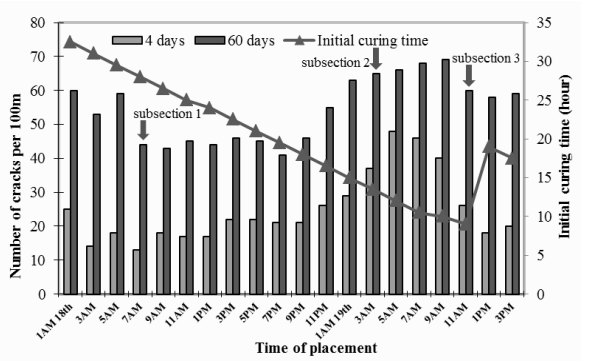

FIG. 8. The effect of the time of placement during the day and the initial curing time on cracking

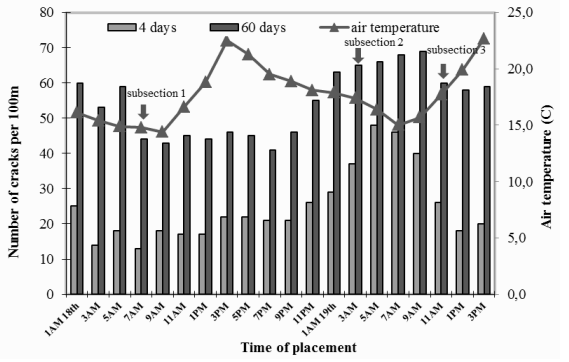

FIG. 9. The effect the time of placement during the day and the air temperature on cracking

As seen in Fig 8 and 9, the number of cracks at a specific time after construction seems to be larger if the curing period was shorter and the air temperature during construction was lower.

Crack width measurement results

Table 5 shows the crack width on the pavement surface measured by Microscope during the first three days after construction.

Table 5. Measured crack widths on surface by Microscope

Section	Length of the subsection (m)	Number of cracks measured	Temperature (°C)	Crack width (mm)			
				Average	Min	Max	Stdv
0.75%	100	7	22.1	0.37	0.21	0.56	0.09
		8	30.3	0.17	0.10	0.20	0.04
		8	22.8	0.32	0.24	0.40	0.05
0.70%	100	7	31.5	0.24	0.13	0.40	0.06
		9	31.4	0.21	0.08	0.35	0.07
		9	20.9	0.35	0.18	0.56	0.10
0.65%+steel fiber	100	8	34.0	0.25	0.14	0.35	0.06
		12	30.6	0.29	0.16	0.43	0.07
		12	24.7	0.33	0.20	0.61	0.07

As can be seen in table 5 the mean crack width for subsection 1 around 30 °C is 0.17 mm while the value for subsection 3 is 0.29 mm. However, when the concrete surface temperature is around 20 °C, there is no significant difference of mean crack width on the pavement surface. The first possible reason may be that the mean crack spacing is different for the three subsections. As can be seen in table 4, the mean crack spacing for the three subsections is 5.7 m, 3.9 m, and 3.3 m, respectively, the crack patterns are still under full development. Another possible reason is that the crack width measurement by the microscope is not reliable. The crack width does not only vary along the depth of the concrete slab but also along the transverse direction. In addition, the use of microscopes is limited by the subjectivity of the operator (which was the same person for all the measurements). The difficulty of placing the microscope at exactly the same place from one measurement to another one presents a serious difficulty for long term studies of changes in crack width.

Table 6 presents the mean crack width of 7 different transverse cracks in each subsection, measured for three locations (surface, top, and the location of the longitudinal steel reinforcement) at two temperature conditions. The results obtained by LVDT, are indicating that the change of the crack width decreases along the depth of the slab. It can also be observed that the magnitude of crack width change due to temperature variation is quite large. For instance, in subsection 1, the value of crack width change is up to 0.172 mm and 0.140 mm on the top and middle of the slab, respectively, when the temperature difference is 8.2 ℃. The change of the crack width on the surface measured by microscope doesn't match well with the values measured by the LVDT on the edge which indicates the crack width measured by the microscope is less reliable than LVDT. The crack width measurement using LVDT are more precise and reliable than the measurements by microscope. However, after the construction of the concrete gutter along with the CRCP structure, all studs were lost and the edge of the CRCP slab was no longer available for more LVDT measurements

Table 6. Comparison of the change of crack width between LVDT and Microscope

Crack width change(mm)	Sub-section	Temperature change	Crack number							Average
			1	2	3	4	5	6	7	
△W1	1	22.0→30.2 ℃	0.132	0.202	0.328	0.182	0.190	0.170	0.206	0.201
△W2			0.136	0.212	0.222	0.195	0.154	0.127	0.158	0.172
△W3			0.131	0.178	0.192	0.161	0.133	0.084	0.102	0.140
△W1	2	20.9→31.5 ℃	0.070	0.058	0.260	0.142	0.240	0.180	0.078	0.147
△W2			0.169	0.093	0.205	0.149	0.243	0.190	0.163	0.173
△W3			0.155	0.088	0.143	0.110	0.211	0.188	0.105	0.143
△W1	3	24.7→34.0 ℃	0.084	0.048	0.064	0.098	0.070	0.132	0.066	0.080
△W2			0.263	0.230	0.159	0.121	0.113	0.179	0.186	0.179
△W3			0.241	0.197	0.136	0.113	0.104	0.145	0.171	0.158

*: △W1 represents the crack width change on the surface measured by Microscope; △W2 represents the crack width change at a location 30 mm beneath the pavement surface measured by LVDT; △W3 represents the crack width change at the location of the longitudinal reinforcement steel bars by LVDT.

CONCLUSIONS

In this study, the early age behavior of three CRCP test sections on the motorway E17 near the city of Ghent, Belgium was investigated right from the construction. From this short-term monitoring, the following conclusions can be drawn:

- The temperature variation within the concrete slab is a dominant factor in the occurrence of cracking in the very early age. Consideration of the effect of their nonlinearity with respect to time is critical to understand the pavement behavior in the first few days after construction. Sufficient curing time should be guaranteed to avoid the phenomenon of an undesirable crack pattern and wide cracks.
- The effect of the percentage of longitudinal reinforcement on crack spacing and crack width is not significant in the very early ages after construction. It is too early to draw a conclusion about the effect of the percentage of longitudinal reinforcement and steel fibers on the crack pattern only based on the results of the (very) early age surveys. Long term monitoring of the effect of these factors should be continued in the future.

ACKNOWLEDGMENTS

The assistance received from Federation of the Belgian Cement Industry (FEBELCEM) and Flemish Ministry for Mobility and Public Works is greatly appreciated.

REFERENCES

Hall, K. et al. (2007).“Long Life Concrete Pavements in Europe and Canada.”*Report*

No. FWHA-PL-07-027, American Trade Initiatives.

Kohler, E.R. and Roesler,J.R. (2006). "Crack Spacing and Crack Width Investigation from Experimental CRCP Sections." *International Journal of Pavement Engineering*, 7(4).

Nam, J.H. (2010). "Early Age Behavior of CRCP and its Implications for Long-term Performance." Doctoral dissertation, the University of Texas at Austin, 2005.

Rens, L. (2010). "Continuously Reinforced Concrete-State-of-the-art in Belgium", *11th International Symposium on Concrete Roads*, Seville, Spain.

Rens, L. and Beeldens, A. (2010). "The behavior of CRCP in Belgium: Observation and Measurement of Crack Pattern, Bond and Thermal Movement." *Proceedings 7th International DUT-Workshop on Design and Performance of Sustainable and Durable Concrete Pavements*, Carmona, Spain.

Suh, Y.C., Hankins, K. and McCullough, B.F. (1992) "Early-age behavior of continuously reinforced concrete pavement and calibration of the Failure prediction model in the CRCP–7 program." *Research Report 1244–3, Center for Transportation Research*, The University of Texas at Austin, Austin, TX.

Verhoeven, K. and Van Audenhove, P. (1993). "Cracking and corrosion in continuously reinforced concrete pavements." *Proceedings 5th International Conference on Concrete Pavement Design and Rehabilitation*, Purdue University, Indiana.

Winne, P., Poupeleer, A., Rens, L. and Feys, F. (2010)."Crack Behavior of Continuously Reinforced Concrete Pavements." *Proceedings 11th International Symposium on Concrete Roads*, Seville, Spain.

Zollinger, D.G., Buch, N., Xin, D. and Soares, J. (1998). "Performance of CRCP Volume 6 - CRCP Design, Construction, and Performance."*Report No.FHWA-RD-97-151, U.S. Department of Transportation*, Washington, DC.

New Model for Longitudinal Tracking in Non-jointed Plain Concrete Pavements

Mauricio Pradena[1] and Lambert Houben[2].

[1]Assistant Professor, Civil Engineering Department, University of Concepcion, Chile; PhD Candidate, Section Road and Railway Engineering, Delft University of Technology, P.O. Box 5048, 2600 GA, Delft, the Netherlands; email: m.a.pradenamiquel@tudelft.nl
[2]Associate Professor, Section Road and Railway Engineering, Delft University of Technology, P.O. Box 5048, 2600 GA, Delft, the Netherlands; email: L.J.M.Houben@tudelft.nl

ABSTRACT: Houben has developed a model concerning the transversal cracking in non-jointed plain concrete pavements using equations from the standard Eurocode 2 for the time-dependent concrete properties and shrinkage. For properties that are not available in standards, Houben made assumptions based on engineering judgment. After that, Pradena and Houben studied those assumptions more in depth, including the maturity method. The results were compared with field measurements and a new equation for the relaxation factor was proposed. The objective of the present paper is to apply those findings for analysis of the longitudinal cracking process in non-jointed plain concrete pavements taking into account different conditions. The calculation results include the time of occurrence of longitudinal crack(s), if any, the variation of the crack widths and the maximum pavement width that can be constructed without any longitudinal joint. In the cases that a longitudinal crack occurs, it is always only one crack which occurs at early age. Because differences in the relaxation at this age are fundamental, future analyses need to concentrate at early age. The new approach confirms the complexity of this kind of modelling, improves the analysis from a theoretical point of view and yields new insights for future investigations.

INTRODUCTION

Houben has published a model for the transversal and longitudinal cracking in non-jointed plain concrete pavements (Houben, 2010; Houben 2011) using equations from the standard Eurocode 2 (2005) for the time-dependent concrete properties and the drying and autogenous shrinkage. For properties that are not available in standards, Houben made assumptions based on engineering judgment. After that, Pradena and Houben made an analysis of the models of the transverse cracking process in Jointed Plain Concrete Pavements (JPCP) where those assumptions were

studied more in depth and compared with preliminary field measurements in Belgium and Chile. They introduced the maturity method in the calculations and a new equation for the stress relaxation was proposed (Pradena, 2012).

Because the possibilities to perform field measurements for the longitudinal cracking process in non-jointed plain concrete pavements are highly improbable, the findings of Pradena and Houben for the transverse cracking process in JPCP now are applied for the longitudinal cracking process in non-jointed plain concrete pavements.

MODELS FOR THE LONGITUDINAL CRACKING PROCESS IN NON-JOINTED PLAIN CONCRETE PAVEMENTS

Models for the Time Dependent Concrete Properties and Shrinkage

Houben modelled the time dependent concrete properties and the drying and the autogenous shrinkage according to the standard Eurocode 2 (2005). A better theoretical modelling of the development of the concrete elastic modulus and strength at early age is obtained when the concept of degree of hydration or the maturity method is applied. Pradena and Houben introduced the maturity method for the calculation of the tensile strength and the modulus of elasticity (Pradena, 2012), resulting in an improvement of the theoretical background of the modeling but it does not produce significant changes in the results.

Model for the Thermal deformation

In the standard Eurocode 2 (2005) a Coefficient of Thermal Expansion (CTE) $1*10^{-5}$ is advised for concrete. However, the CTE is not constant in fresh concrete, it is high in the first hours and it drops rapidly to a minimum value at t_0 = 12-14 hours after mixing. Beyond this minimum point the CTE increases gradually. The assumption made by Houben follows this trend (Pradena, 2012).

Model for the relaxation factor

Pradena and Houben analyzed different expressions for the relaxation and found significant differences in the results of those expressions, when they were applied to real JPCPs. The expression proposed by Houben was the only one with realistic results, but according to preliminary field measurements in Belgium and Chile the calculated crack widths are smaller than the ones observed in practice. For that reason Pradena and Houben proposed the Eq. 1 for the relaxation factor as a function of the time (Pradena, 2012).

$$R = 0.8265 * e^{-8*10^{-5}*t} \quad (1)$$

Although this equation needs to be validated with more field measurements and laboratory tests, it is possible and useful to apply this equation to the case of the

longitudinal cracking process in non-jointed plain concrete pavements, especially because performing field measurements in this case is highly improbable.

Model for the development of the temperature

Houben modeled the climate-dependent temperature as a sine function, taking into account the yearly temperature amplitude ($T_{ampyear}$) and the daily temperature amplitude (T_{ampday}). The heat of hydration was assumed to be a function of time (Houben, 2010).

Pradena and Houben made a comparison of Houben's assumption with respect to the increase of the temperature as a function of the hydration heat released, and the hydration temperature calculated using the *HYMOSTRUC* software (Van Breugel, 1991). This analysis showed that the Houben model yields the most unfavourable condition, because his equation yields a lower temperature of the concrete, i.e. more contraction of the pavement. In fact, according to preliminary field measurements on JPCPs, the crack width calculated according to the Houben model for the hydration temperature seem to be low. The calculated crack widths are smaller when the temperature product of the hydration heat released is applied (Pradena, 2012).

Model for the friction with the underlying base layer

In the transverse direction of the concrete pavement the tensile stresses build up over the so-called breathing length. In case of indefinite width of the concrete pavement the breathing length $L_{a1\infty}$ is expressed in Eq. 2 (Houben, 2011).

$$L_{a1\infty} = ABS\left(\frac{E_{cm}(t) * \varepsilon(t)}{\gamma * f}\right) \quad \text{(m)} \tag{2}$$

where:
$E_{cm}(t)$ = the average modulus of elasticity (MPa) of the plain concrete pavement at the moment of the primary cracks.
$\varepsilon(t)$ = the maximum total obstructed deformation of the plain concrete pavement
γ = the volume weight of the plain concrete pavement (kN/m^3)
f = the coefficient of friction between the plain concrete pavement and the underlying base
ABS = absolute value

Modeling the Development of the Longitudinal Cracking Process

In this section only a summary of the model for the development of the cracking process is presented for the case that 1 longitudinal crack develops. The detailed model can be found in (Houben, 2011).

The initial width w_i of the longitudinal crack is expressed by Eq. 3.

$$w_i = 1000000 * \frac{E_{cm}(t) * \varepsilon_{cr}(t)^2}{\gamma * f} \quad \text{(mm)} \tag{3}$$

where:
$\varepsilon_{cr}(t)$ = the total obstructed transverse deformation (tensile strain) of the plain concrete pavement at the moment of the crack(s)

In the transverse direction of the concrete pavement the breathing length is limited to half of the width between the pavement edge and the longitudinal crack according to Eq. 4.

$$L_{aW} = MIN(L_{aW\infty}, W/4) \quad \text{(m)} \tag{4}$$

where:
W = total concrete pavement width (m)
MIN = minimum value

The change of the crack width $\Delta w(t)$ in time is calculated by means of the Eq. 5.

$$\Delta w(t) = 1000000 * \frac{E_{cm}(t) * \varepsilon(t)^2}{\gamma * f} * (\frac{L_{aw}}{W/4})^2 \quad \text{(mm)} \tag{5}$$

The Eq. 6 shows the development of the width w(t) of the longitudinal crack.

$$w(t) = w_i + \Delta w(t) \quad \text{(mm)} \tag{6}$$

EVALUATION OF THE LONGITUDINAL CRACKING PROCESS IN NON-JOINTED PLAIN CONCRETE PAVEMENTS

Analysis of the Longitudinal Cracking Process at Different Scenarios

Houben made calculations of the longitudinal cracking process in non-jointed plain concrete pavements for different times of construction (DayConstr), different pavement temperature conditions ($T_{ampyear}$; T_{ampday}), two concrete grades, different friction values between the concrete pavement and the underlying base (f), and different pavement widths (W). Houben developed regression models for the maximum value of the ratio of the transverse tensile stress and the tensile strength as a function of the above-mentioned variables. For instance, Eq. 7 is the model for concrete grade C28/35 and hour of construction 10 am (Houben, 2011).

$$MaxRatio = 0.0007 * (T_{ampyear} + 1)^{-0.016} * (T_{ampday} + 7.784)^{1.615} * f^{0.640} * DayConstr^{0.012} * W^{0.637} \tag{7}$$

Houben found that, besides the time of construction during the day, the daily

temperature amplitude T_{ampday} has the largest effect on the maximum stress ratio. The friction f between the pavement and the base as well as the pavement width W give second order effects on the maximum stress ratio (Houben, 2011).

Scenarios of Evaluation

According to the Houben findings, the evaluation of the different models and the proposed equation for the relaxation factor (Eq. 1) is made for all the possible combinations shown in the scenarios of evaluation of Table 1.

The month refers to the northern hemisphere. August 1 is assumed to be the hottest day of the year and therefore is the most unfavourable condition. At 10 am the average pavement temperature on a day occurs and at 4 pm the pavement temperature on a day is maximum.

Table 1. Parameters of the Scenarios of Evaluation

Parameter	Data
Period of evaluation	8640 hours (≈ 1 year)
Concrete grade	C28/35
Yearly temperature amplitude	10°C
Daily temperature amplitude	5°C - 10°C
Time of construction	August 1st 10 am - August 1st 4 pm
Pavement width	3 m – 6 m – 9 m
Friction	1 – 5 – 10

RESULTS OF THE MODELING PROCESS

Occurrence of Cracks

Tables 2 and 3 show all the scenarios in which a longitudinal crack occurs, and the time of occurrence of the cracks. In the cases that the Houben model yields cracks, the maximum ratio between the tensile stress and the tensile strength according to the Pradena and Houben model is shown.

It can be seen in Tables 2 and 3 that the results of the two models are very similar, and in the cases that the Houben model yields cracks, the maximum ratio according to the Pradena and Houben model is close to 1. In fact, if the variability of the parameters is taken into account, and a Security Factor (SF) of 1.25 or 1.50 is applied, the maximum ratio is equal or bigger than 1, and potentially a crack occurs.

Tables 2 and 3 also show that construction of the concrete pavement in the afternoon in a period with high daily temperature amplitudes is most critical.

Table 2. Time of Occurrence of Cracks and Maximum Ratio for C28/35 - $T_{ampyear}$ 10°C - T_{ampday} 5°C

Time of construction	Friction	Pavement width (m)	Houben	Pradena and Houben		
				SF 1.00	SF 1.25	SF 1.50
4 pm	5	3	-	-	-	-
		6	-	-	-	-
		9	11	12/0.80	12/1.00	12/1.20
	10	3	-	-	-	-
		6	11	12	12	12
		9	11	12	12	12

Table 3. Time of Occurrence of Cracks and Maximum Ratio for C28/35 - $T_{ampyear}$ 10°C – T_{ampday} 10°C

Time of construction	Friction	Pavement width (m)	Houben	Pradena and Houben		
				SF 1.00	SF 1.25	SF 1.50
10 am	10	3	-	-	-	-
		6	16	16/0.85	16/1.06	16/1.27
		9	16	16	16	16
4 pm	5	3	-	-	-	-
		6	6	7/0.97	7/1.21	7/1.45
		9	6	7	7	7
	10	3	6	7/0.97	7/1.21	7/1.45
		6	6	7	7	7
		9	6	7	7	7

Practical Approach to the Maximum Pavement Width without Cracks

The trends for the maximum concrete pavement width that can be constructed without the risk for any longitudinal crack are shown in the Fig. 1 for a concrete pavement, grade C28/35, constructed at 10 am while the temperature amplitudes are $T_{ampyear}$ = 10°C and T_{ampday} = 10°C. Because of the practical approach, this Figure only includes the pavement widths from the scenarios of evaluation (Table 1) with the addition of the widths 1.5, 4.5, 7.5 and 10.5 m.

Variation of the Crack Width

For the analyzed pavement widths of 3 to 9 m, in all the cases only 1 longitudinal crack occurs, if any (see Tables 2 and 3), and the crack width never exceeds 0.3 mm. From the point of view of the Load Transfer Efficiency (LTE) of longitudinal joints, with this magnitude of crack width a good behavior may be expected, especially if tie bars are used.

As an example, for a period of 1 year Fig. 2 shows the development of the width

of the longitudinal crack for a concrete pavement, grade C28/35, constructed at 10 am while the temperature amplitudes are $T_{ampyear}$ = 10°C and T_{ampday} = 10°C; the friction value is 10.

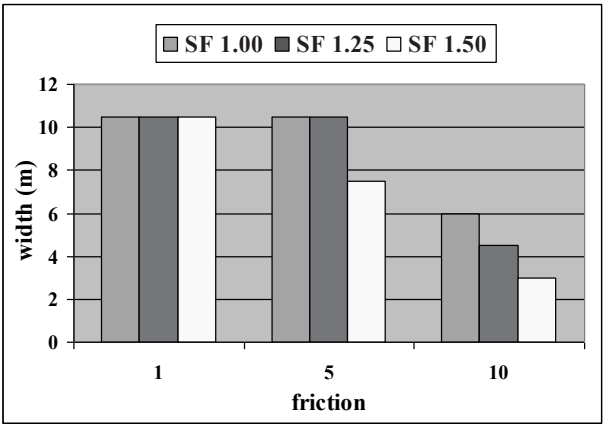

FIG. 1. Trends of maximum concrete pavement widths for C28/35 - $T_{ampyear}$ 10°C –10 am.

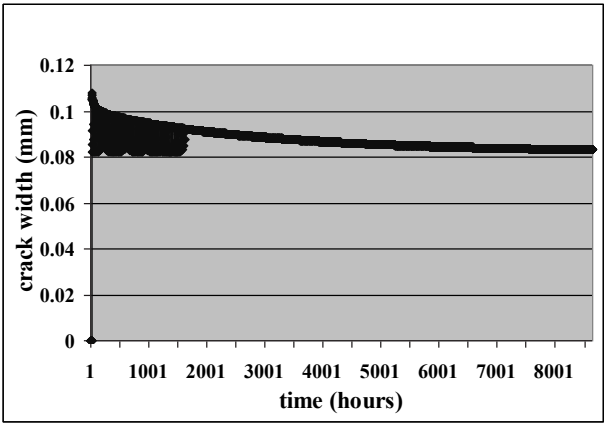

FIG. 2. Development of the crack width for C28/35 - $T_{ampyear}$ 10°C – T_{ampday} 10°C – f10 – 10 am.

DISCUSSION

The Effect of the Relaxation Factor on the Occurrence of Cracks

Fig. 3 shows the development of the tensile strength and the maximum tensile stresses for the Houben model and the Pradena and Houben model. Both models follow the curve of their respectively relaxation factors and it can be seen that both curves of the occurring tensile stresses are very close to the tensile strength in early age. Hence, Fig. 4 shows the same information but focusing on the early age.

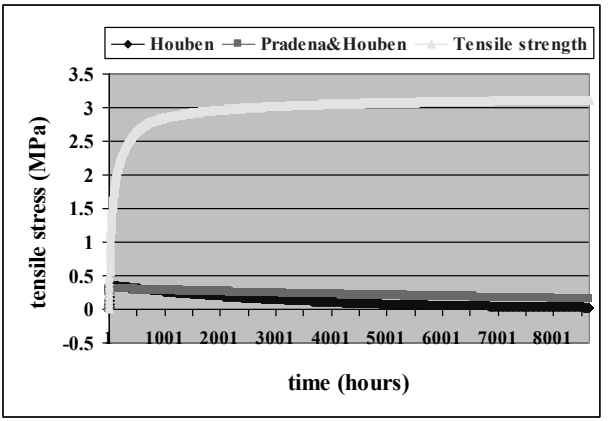

FIG. 3. Development of maximum tensile stress and tensile strength for 1 year for C28/35 – $T_{ampyear}$ 10°C – T_{ampday} 10°C – f5 – 4 pm.

In the Fig. 4 it can be observed that the Pradena and Houben model does not yield a longitudinal crack, but it is very close to do it. In fact, when a very reasonable security factor of 1.25 is applied the crack occurs (Table 3). Even when the Pradena and Houben model follows, at early age, the trends of different relaxation models proposed by various authors (big relaxation at the beginning) and that the Pradena and Houben model seems to be more in agreement with the reality of JPCP, it is necessary to continue the analysis, perform laboratory tests and field measurements. It is necessary because at early age differences in the stress relaxation are fundamental to the longitudinal cracking process of non-jointed plain concrete pavements. In fact, in all the analyzed cases, when the pavement is cracked, only 1 longitudinal crack occurs and always at early age. Hence, future analyses need to be concentrated on this part of the evaluation period.

Practical Insights from the Modeling Process

One of the most important issues of the construction of a JPCP is the saw-cutting of the joints. In fact, the pavement needs to be cut before the cracks occur but not so early that it can produce raveling (Fig. 5). To know the risk of cracks is very important to the construction process, taking into account that in concrete pavements there is only one chance to obtain a good construction result, in particular without uncontrolled ‘wild’ cracks.

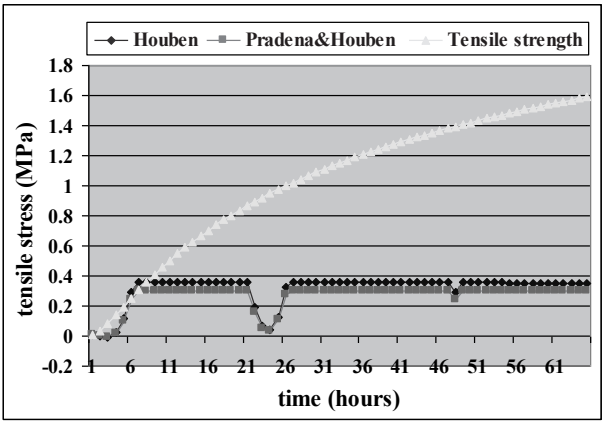

FIG. 4. Development of maximum tensile stress and tensile strength for the early age for C28/35 – $T_{ampyear}$ 10°C – T_{ampday} 10°C – f5 – 4 pm.

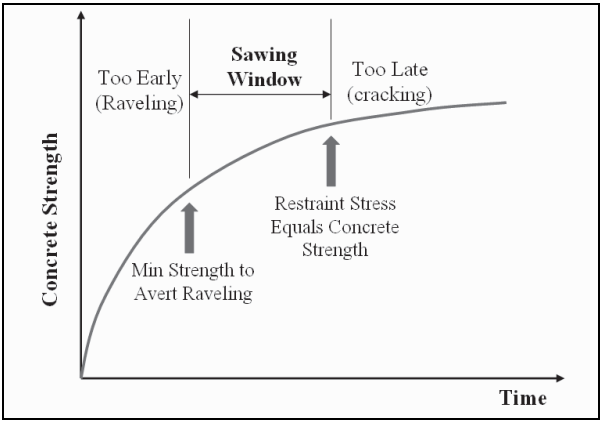

FIG. 5. Sawing window (Okamoto, 1994).

The type of information shown in the Fig. 1 is useful for knowing the maximum width of a concrete pavement that can be constructed in one gang (as is shown in Fig. 6) without risk of longitudinal cracks at the first hours. This knowledge is very important because it can help to distribute the construction resources in an efficient way, putting the attention to the critical points, as the saw-cutting of the transverse joints.

That was the situation of the project of Fig. 6 in Chile. It is a JPCP with short slabs, this means 3 longitudinal joints equally divided over the width of the

pavement, which is constructed in one gang by the slipformer paver shown in Fig. 6. The average daily production is 700 m of pavement, i.e. over 400 potential cuts for the transverse joints. In this case efficiency of the resources for the saw-cutting of the joints is absolutely necessary. In particular, in this project during the first hours the attention was put in saw-cutting the transverse joints, but not in the longitudinal joints because it was assumed that there is no risk of longitudinal cracks. Then, after having excluded the risk of 'wild' transverse cracking, the longitudinal joints were made. The final result of this saw-cutting regime was that no 'wild' cracking occurred at all.

FIG. 6. Paving in one gang with slipformer in Chilean project.

FIG. 7. JPCP with short slabs in the Andes Mountains, Chile.

Tables 2 and 3 show the big effect of the friction, the daily temperature amplitude and the time of construction on the occurrence of longitudinal cracks. Fig. 7 shows a project in the Chilean Andes Mountains where the daily air temperature difference between day and night is around 20°C, hence T_{ampday} = 10°C in the sine function that describes the variation of the temperature during a day. In these climatic conditions the time of construction has a big influence on the occurrence of longitudinal cracks.

Table 4 shows, with an X, the decisive influence of the parameters daily temperature amplitude and friction in different concrete paving solutions. The bonded overlays and the JPCPs with short slabs are thin solutions, hence the T_{ampday} is more influential.

Table 4. Influence of the T_{ampday} and Friction in Different Concrete Paving Solutions

Concrete Pavement/Overlay	T_{ampday}	Friction
Bonded overlay over asphalt	X	X
Bonded overlay over concrete	X	X
JPCP over cement stabilized base	-	X
JPCP over asphalt base	-	X
Unbonded overlay over asphalt	-	X
Unbonded overlay over concrete	-	X
JPCP (short slabs) over granular base	X	x
JPCP (short slabs) over cement stabilized base	X	X

CONCLUSIONS

For the scenarios of evaluation analyzed in this paper, if any, only one longitudinal crack occurs and always at early age. Therefore the development of the stress relaxation at early age is fundamental.

Taking into account the disparity between the results from different relaxation models found previously by Pradena and Houben, the results of the occurrence of cracks from the models under comparison in this paper confirm the complexity of the modeling of the longitudinal cracking process in non-jointed plain concrete pavements, and in particular of the relaxation factor. Hence, it is necessary to continue the analysis supported by laboratory tests and field measurements. The analysis needs to be concentrated especially at early age and the field measurements on JPCPs need to continue because direct measurements of the longitudinal cracking process in non-jointed plain concrete pavements are highly improbable.

The modeling of the longitudinal cracking process in non-jointed plain concrete

pavements has important practical insights that can help to take decisions in the construction process dependent on the type of the concrete paving solution, the local climatic conditions and the hour of construction during the day.

ACKNOWLEDGEMENTS

Authors appreciate all the support of the National Highway Laboratory of Chile to enable the technical visits of the concrete pavements projects in Chile.

REFERENCES

Eurocode 2. (2005). "Design and Calculation of concrete structures." Part 1-1: General rules and rules for buildings (in Dutch). Netherlands standard NEN-EN 1992-1-1 (en), NNI, Delft.

Houben, L.J.M. (2010). "Model for transversal cracking in non-jointed plain concrete pavements as a function of the temperature variations and the time of construction". *Proc., 7th Int. DUT-Workshop on Design and Performance of Sustainable and Durable Concrete Pavements,* Carmona, Spain.

Houben, L.J.M. (2011). "Model for longitudinal cracking in non-jointed plain concrete pavements". *Proc., 2nd Int. Conf. on Best Practices for Concrete Pavements,* IBRACON, Florianopolis, Brazil.

Okamoto, P. A. et al. (1994). "Guidelines for Timing Contraction Joint Sawing and Earliest Loading for Concrete Pavements", Vol. I: Final Report. FHWA-RD-91-079. Federal Highway Administration, U.S. Department of Transportation, VA.

Pradena M. and Houben, L.J.M. (2012). "Early age deformation and internal stresses in jointed plain concrete pavements for Dutch conditions". *Proc., 2nd Int. Conf. on Microstructural Related Durabilty of Cementitious Composites*, RILEM, Amsterdam, the Netherlands.

Van Breugel, K. (1991). "Simulation of hydration and formation of structure in hardening cement-based material." Doctoral Thesis, Delft University of Technology, Delft, the Netherlands.

Rheological Behavior of Fresh Cement Asphalt Mortar

Zhifei Liu[1] , Jinxiang Hong [2] and Jiaping Liu [3]

[1] State Key Laboratory of High Performance Civil Engineering Materials (Jiangsu Research Institute of Building Science), Nanjing 210008, China; Jiangsu Bote New Material Co., Ltd, Nanjing 210008, China; email: liuzhifei@cnjsjk.cn
[2] State Key Laboratory of High Performance Civil Engineering Materials (Jiangsu Research Institute of Building Science), Nanjing 210008, China; Jiangsu Bote New Material Co., Ltd, Nanjing 210008, China; email: hongjinxiang@cnjsjk.cn
[3] State Key Laboratory of High Performance Civil Engineering Materials (Jiangsu Research Institute of Building Science), Nanjing 210008, China; Jiangsu Bote New Material Co., Ltd, Nanjing 210008, China; email: liujiaping@cnjsjk.cn

ABSTRACT: Cement asphalt mortar (CA mortar) is the key component in the structure of Shinkansen slab track and serves as the elastic shock-absorber. CA mortar is a composite material with cement and asphalt emulsion and acts as a cushion layer in the structure of slab track. The workability and homogeneity quality of fresh CA mortar is governed by its rheological behavior. Influences of cement type, emulsified asphalt type and superplasticizer dosages on the rheological parameters were analyzed by means of a rheometer. The rheological model was also explored. The results show that the CA mortar is a non Newtonian fluid and it shows thixotropic flow behaviour. The fresh CA mortar behavior is better described by the Herschel-Bulkley model. From the point of thixotropic behavior, the cement C-3 and emulsion A-1 may be beneficial for higher static and dynamic segregation resistance.

INTRODUCTION

Ballastless slab track is one of the main track structures, which is widely applied in high speed railways in China (Zhong Cao, 2011). As an elastic shock-absorber，the cement asphalt (CA) mortar is composed of cement, asphalt emulsion, sand, water and several chemical admixtures, which is the key component in the slab track structure (Jin Shouhua, 2006). CA mortar is a semirigid high-performance composite with the combined merits of cement paste with high-strength and asphalt materials with good elasticity, so it can be used to adjust distance between concrete roadbed and track slabs, and supply a certain elastic and strength (Harada Y, 1983).

CA mortar has been used in Japan and Germany for a long time (Takai H, 2007). During the past several years, some research work has been done in China on the

relationship between the composition and properties of CA mortar. Cement setting process of CA mortar has been studied (Fazhou Wang, 2008&2009). The hydration and hardening mechanism of cement asphalt binder (CAB) was studied (Yang Jinbo, 2010; Rong Chen, 2011). The uniformity of CA mortar was improved by increasing the volume of fibre (Zhu Xiaobin, 2010). The presence of cement accelerated the breaking of asphalt emulsion in CA mortar (Hu Shuguang, 2008). There are few publications focusing on its rheological behavior.

During in situ construction, CA mortar is injected into a 645×255×30mm narrow space without external pressure, so is characterized by ultrahigh flowability, which necessitates exorbitant water content. In order to keep a balance between the groutability and segregation resistance, the rheological behavior of CA mortar should be studied.

Avoiding segregation is a matter of CA mortar rheology. The CA mortar has to be sufficiently fluid to ensure the fluidity sufficient. To make them flow, sufficiently strong shearing forces are necessary to break the bonds between grains that are the cause of an initial yield value.

The two main goals of the current study are: first, to analyze rheological model and parameters of CA mortars; second, to evaluate the effect of cement and superplasticizers on the segregation based on rheological behavior. To accomplish this, seven CA mortars (corresponding to three different cement types, and three different asphalt types, and three different superplasticizer dosages) were characterized at the same flowability (flow time of 110s).

EXPERIMENTAL

Three types of cements (C1, C2, C3) were used, all of which were 52.5 P.II from different companies. The chemical compositions are shown in Table 1. Three types of anionic asphalt emulsions (A-1, A-2, A-3) had a solid content of 60%. Superplasticizer (SP) was supplied by Jiangsu Bote New Material Co., Ltd (Nanjing, China) with 40% mass content. The fine aggregates (S) were river sand with maximum size of 1.18mm. Antifoaming agent (AFA) was Organic silicon. All the water (W) used was drinking water.

Table 1. Chemical Compositions of Cement (wt%)

Type	CaO	SiO_2	Al_2O_3	Fe_2O_3	SO_3	MgO	K_2O	LOI
C-1	65.09	20.53	4.50	3.47	2.19	0.96	0.62	1.74
C-2	66.40	19.60	4.73	3.45	3.12	1.32	0.82	1.23
C-3	68.10	18.00	4.29	3.94	1.95	1.55	0.67	1.11

In order to match with construction, the flow time of all CA mortars are adjusted at the value of 110±2s, which should be controlled in the range of 80s to 120s in construction. The dosages of water are adjusted to meet the fluidity. A total of seven

mixes were used in the experiment and the mix proportions of CA mortar were listed in Table 2. NO.1, NO.2 and NO.3 are changed by cement type. NO.1, NO.4 and NO.5 are changed by asphalt type. NO.1, NO.6 and NO.7 are changed by superplasticizers dosages.

Table 2. Mixing Proportions and Materials Type of CA Mortar (kg/m3)

NO.	A	C	W	S	SP	AFA
1	240(A-1)	600(C-1)	165	900	0.8	0.075
2	240(A-1)	600(C-2)	175	900	0.8	0.075
3	240(A-1)	600(C-3)	154	900	0.8	0.075
4	240(A-2)	600(C-1)	143	900	0.8	0.075
5	240(A-3)	600(C-1)	145	900	0.8	0.075
6	240(A-1)	600(C-1)	173	900	0.5	0.075
7	240(A-1)	600(C-1)	165	900	1.1	0.075

The rheological behavior of CA mortar was measured immediately using a Rheometer (R/S) equipped with coaxial cylinder measurement geometry in controlled shear rate mode at a constant temperature of 20^{o}C. The measuring device was the CC25 spindle coaxial system. For all mortar samples, the rheological test consists of the following steps: (1) pre shearing with 200 s-1 for all the mortars during 60 s after mixing, (2) a linear decreasing shear rate from 200 to 0 s-1 for 10 s; (3) the shear rate kept at 0 s-1 for 60 s, the pre shearing action was intended to cause structural breakdown of the CA mortar sample and create uniform conditions before testing; (4) a linear increasing shear rate from 0 to 200 s-1 within 60 s to produce the up-curve of the flow test; (5) Then, the shear rate was ramped down from 200 to 0 s-1 within 60 s to produce the down-curve. Time, shear stress and shear rate were recorded and data were analyzed using Rheo2000 software for plotting of the flow curves. The up-curve and down-curve were used to calculate various rheological properties.

Flow time tests were measured according to the tentative specification of cement asphalt mortar of CRTS Ⅱ ballastless slab track. Flow time of CA mortar was indicated by pouring the grout into a funnel and measuring the flowing time until the grout drained away. Workable time was defined as the interval time during which the fluidity of grout was between 80s and 120s.

The test procedure of separation rate was as follows: pour the CA mortar into Φ50×50 mm cylindrical mould; after hardening, demould the specimen and cut it into halves and measure the density of each half. The separation rate is determined by the difference in density between top and bottom halves, which is given in Eq. 1.

$$\text{Separation rate} = \frac{\rho_1 - \rho_2}{\rho_1 + \rho_2} \quad (1)$$

Where: ρ1—density of bottom half, ρ2—density of top half.

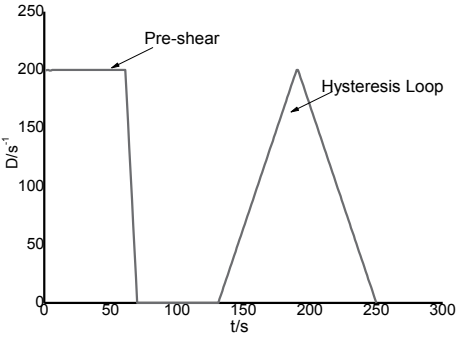

FIG. 1. Test program of rheological behavior.

RESULTS AND DISCUSSION

Rheological Model

The rheometer test was performed on all of the mortars that were made. The software of rheometer AR2000 enabled us to identify the rheological behavior of these mortars.

In general, the Bingham model is used to estimate the rheological model of cement-based materials. For each rheometer test, a linear regression analysis was performed on the values of the data in order to deduce the Bingham parameters, the yield stress and plastic viscosity.

The rheological data were analyzed by running a regression analysis to determine the rheological model relationship parameters in Formula 2.

$$\tau = \tau_0 + \eta_p \gamma \quad (2)$$

Where τ is shear stress (Pa); τ_0 is yield stress (Pa); η_p is plastic viscosity (Pa·s); γ is shear rate (s^{-1}).

Regression parameters for Eq. (2) are shown in Table 3. It shows that all of the yield stress values are zero, and there can be identified as Newton model in this case. The high water consumption causes the mortar to become self-leveling (very low yield stress) because it leads to a high flowability.

Indeed, the flow curves were not linear and thus the mortars were not plastic in their

behaviour since they often exhibited shear thinning or shear thickening behaviour. Therefore, we conclude that the rheological behavior of the mixtures that were studied is nonlinear.

Table 3. The Regression Results of the Bingham Model

NO.	Yield stress (Pa)	Regression equation	R^2	Standard deviation
1	0	$\tau=0+1.0707\gamma$	0.98945	6.87
2	0	$\tau=0+1.3942\gamma$	0.99186	7.60
3	0	$\tau=0+0.47232\gamma$	0.99492	2.06
4	0	$\tau=0+0.87074\gamma$	0.99709	3.13
5	0	$\tau=0+0.92695\gamma$	0.99850	2.14
6	0	$\tau=0+0.6943\gamma$	0.99686	2.35
7	0	$\tau=0+0.7805\gamma$	0.97402	8.25

All flows have been modelled by Herschel-Bulkley Formula 3 for describing the rheological behaviour of different CA mortars.

$$\tau = \tau_0 + \eta_p \gamma^{n} \tag{3}$$

Where τ_0 is the shear yield stress, η_p is the plastic viscosity; the exponent n characterizes the behavior of the mortars: shear thinning for n<1 and shear thickening for n>1.

Regression parameters for Formula 3 are shown in Table 4. The Herschel-Bulkley model for CA mortars has high coefficient of multiple determination above 0.999. The shear thinning or shear thickening behavior of CA mortars could be best described by the Herschel-Bulkley model. The behavior of all CA mortars is well fitted to a Herschel-Bulkley law, so the fresh CA mortar behavior is better described by the Herschel-Bulkley model.

Table 4 The regression results of the Herschel-Bulkley model

NO.	Yield stress (Pa)	Regression equation	R^2	Standard deviation
1	9.7315	$\tau=9.7315+0.24135\gamma^{1.283}$	0.99900	2.210
2	20.715	$\tau=20.715+0.27518\gamma^{1.3011}$	0.99900	2.620
3	4.1159	$\tau=4.1159+0.354\gamma^{1.1584}$	0.99951	1.090
4	10.155	$\tau=10.155+1.6529\gamma^{0.90161}$	0.99950	1.260
5	10.811	$\tau=10.811+1.0746\gamma^{0.97144}$	0.99939	1.340
6	5.9786	$\tau=5.9786+0.27798\gamma^{1.1698}$	0.99960	0.828
7	5.6725	$\tau=5.6725+0.096232\gamma^{1.405}$	0.99908	1.540

Effect of Cement Type on the Rheological Behavior of the CA Mortars

All the CA mortar studied exhibited a rheological behaviour which can be defined as being of thixotropic type. According to the experimental procedure applied, the cycle is schematically shown in Fig. 2. The up-curve lies on the lower torque side of the down-curve: this means that structure breaks down during the test and the material shows thixotropic flow behaviour. The result of C-3 shows the highest value of 2349.1 Pa/s. C-1 and C-2 exhibits poor thixotropic behaviour with values of 1713.8 Pa/s and 1213.8 Pa/s, respectively. The higher thixotropy associated with C-3 may be beneficial for higher static and dynamic segregation resistance and reduced leakage of CA mortar during construction. This can be proved by the separation rate test.

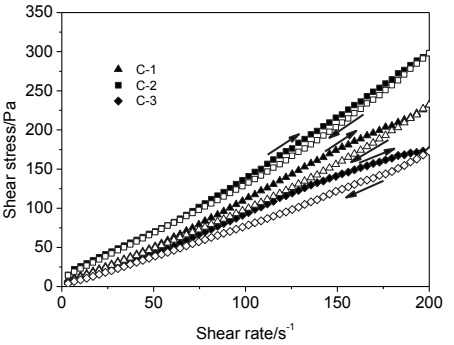

FIG. 2. The thixotropic behaviour of CA mortar with different cement types.

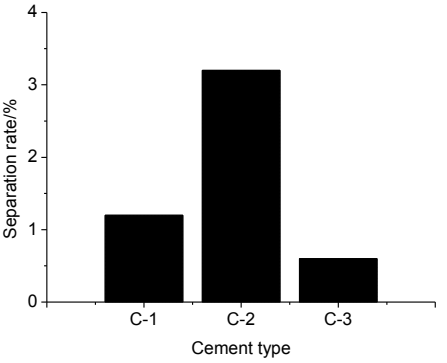

FIG. 3. The separation rate of CA mortar with different cement types.

In Fig. 3, separation rate test carried out with different cements is compared. In the results, CA mortar with cement C-3 showed a separation rate of 0.6%. The separation rate for the CA mortars with cement C-1 and C-2 showed separation rate of about 1.2% and 3.2%, respectively. From this, it is thought that the CA mortar with C-3 cement shows the best separation resistance.

Effect of Emulsion Type on the Rheological Behavior of the CA Mortars

According to the experimental procedure applied, the thixotropic behaviour of CA mortar with different asphalt emulsion types was show in Fig.4. The result of A-1 shows the highest value of 1713.8 Pa/s. A-2 and A-3 exhibits poor thixotropic behaviour with values of 669.9 Pa/s and 1038.9 Pa/s, respectively. The higher thixotropy associated with A-1 may be beneficial for higher static and dynamic segregation resistance and reduced leakage of CA mortar during construction. This can be proved by Fig. 5.

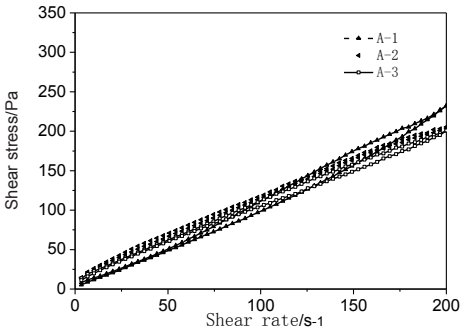

FIG. 4. The thixotropic behaviour of CA mortar with different emulsion types.

Fig. 5 shows the results from the separation rate test, where CA mortar with emulsion A-1 showed a separation rate of 1.2%. The other two mortars (A-2 and A-3) had separation rate of 3.1% and 2.5%, respectively. Considering the figure, the A-1 emulsion has the best separation resistance property and the A-2 the worst.

Effect of Superplasticizer on the Rheological Behavior of the CA Mortars

For shear stress as function of shear rates, the samples show very similar shapes each other, and for all CA mortar with different SP dosage, shear stresses decrease with the increasing of SP dosage (Fig. 6). So the SP improves the CA mortar flowability, especially the dossages of 1.1kg/m³.

Fig. 7 represents the evaluation of CA mortar viscosity for different dosages of SP as function as shear rate. It can be observed that all the mortars prepared with different SP

dosages exhibit a shear thinning behavior till a certain limit of shear rate because of the viscosity decreasing, except at high shear rates where Newtonian behavior is evident. At low shear rates, the inter-particle forces are predominant over the hydrodynamic ones, leading to the formation of flocs. With increasing shear rate, the hydrodynamic forces become stronger and stronger, so flocs are broken down into smaller and smaller flow units and the liquid immersed within them is gradually released. This results in a decrease of the viscosity. At high shear rates, the viscosity increases with increasing of shear rate (shear thickening) due to some sedimentation of the fine aggregates and data became unreliable.

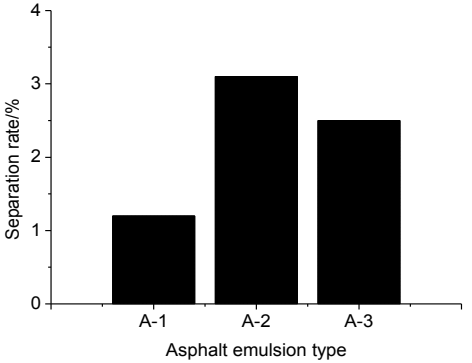

FIG. 5. The separation rate of CA mortar with different cement types.

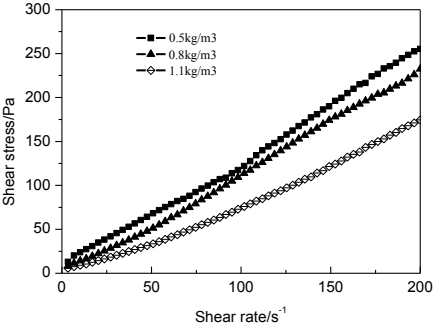

FIG. 6. Flow curves of CA mortar for different proportion of SP.

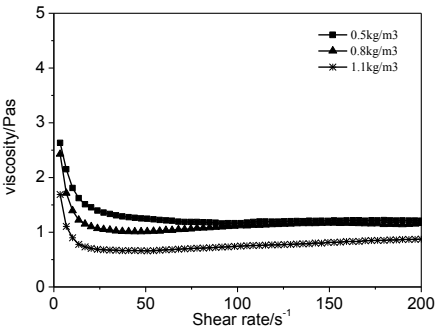

FIG. 7. Evaluation of viscosity of CA mortar for different proportion of SP.

CONCLUSIONS

The following conclusions were determined based upon the limited experimental data presented in this research project:

(1) The CA mortar is a non Newtonian fluid and it shows thixotropic flow behaviour. The fresh CA mortar behavior is better described by the Herschel-Bulkley model.

(2) From the point of thixotropic behavior, the cement C-3 and emulsion A-1 may be beneficial for higher static and dynamic segregation resistance.

(3) Superplasticizers can improve the flowability (viscosity, shear stress, and yield stress) of CA mortars

ACKNOWLEDGMENTS

This study is financially supported by National Basic Research Program of China (973 Program) (Grant No.2012CB724600) and the railway ministry science and technology research and development program (2008G031-F).

REFERENCES

Fazhou Wang, Zhichao Liu and Tao Wang. (2008). "A novel method to evaluate the setting process of cement and asphalt emulsion in CA mortar." *Materials and Structures*, 41 (4): 643-647.

Harada Y, Tottori S and Itai N. (1983). "Development of cement asphalt mortar for slab tracks in cold climate". Quarterly Report of RTRI (Railway Technical Research Institute), 15 (1): 62-67.

Hu Shuguang, Wang Tao and Wang Fazhou, et al. (2008). "Adsorption behavior between cement and asphalt emulsion in CA mortar." *Advances in Cement Research*, 20 (1): 1-4.

Jin Shouhua, Chen Xiufang and Yang Jun. (2006). "Key technologies of CA mortar for slab track. " *China Railway Science*, 27 (2): 20-25.

Rong Chen, Ping Wang and Zhe Liu. (2011). "Influences of CA Mortar Elastic Modulus on Stress and Deformation of Slab Track in High Speed Railway." *Advanced Materials Research*, 197-198: 1480-1485.

Takai H. (2007). "40 years experiences of the slab track on Japanese high speed lines." *1st International Conferences organized by Euskal Trenbide Sarea.*

Wang Fazhou, Zhang Yunhua and Liu Zhichao. (2009). "Preliminary Study on Asphalt Emulsion Used in Cement Asphalt Mortar." *Journal of Testing and Evaluation*, 37 (5): 14-17.

Yang Jinbo, Yan Peiyu and Kong Xiangming. (2010). "Study on the hardening mechanism of cement asphalt binder. " *Science China*, 53 (5):1406–1412.

Zhong Cao, Xueqiang Cao and Lixian Sun. (2011). "Research and Progress on CA Mortar Emulsifying Asphalt of Ballast-Less Slab Track." *Advanced Materials Research.*, 239-242: 2399-2402.

Zhu Xiaobin, Hong Jinxiang and Xu Jing. (2010). "Influence of fiber on the performances of CA mortar mixture." *Journal of Southeast University*, 40 (s2): 79-83.

Effect of Hydrated Lime on Behavior of Expansive Soil as Subgrade of Flexible Pavement Structural System

A. A. M. Adam [1] I.A. Ibrahim [2] A.J. Alhardllo [3] A.M. Hadi [4] and M.Y. Ibrahim [5]

[1] Gazera University, College of Engineering and Technology, WadMadani, P. O. Box 20, Sudan; email: abdallaadam45@yahoo.com
[2] Gazera University, College of Engineering and Technology, WadMadani, P. O. Box 20, Sudan
[3] Gazera University, College of Engineering and Technology, WadMadani, P. O. Box 20, Sudan
[4] Gazera University, College of Engineering and Technology, WadMadani, P. O. Box 20, Sudan
[5] Gazera University, College of Engineering and Technology, WadMadani, P. O. Box 20, Sudan

ABSTRACT: The main objective of this paper presents a study of the effect of engineering properties of expansive soil as subgrade when stabilized by using different percentage of hydrated lime on thickness of pavement structural system. A series of Physical tests in term of sieve analysis, liquid limit, plastic limit and plasticity index as well as dry density, moisture content relationship also mechanical tests in term of and CBR test was conducted before and after adding three percentages of lime (2%, 4% and 6%) by weight of expansive soil with curing time of 24 hour to evaluate the effect of hydrated lime on behavior of expansive soil as subgrade on thickness of flexible pavement structural system. The results shows that the lime provides better physical properties in term of liquid limit, plastic limit and plasticity index and shows that the lime increase the CBR value to 52%, 27% and 44% when adding 2%, 4% and 6% percentages of lime respectively for untreated soil (CBR=1%), also the lime decrease swelling from 4% in untreated soil to 1.20%, 0.01% and 0.20% when adding 2%, 4% and 6% lime percentages respectively. The design of Pavement thickness shows that the adding of lime decrease the thickness from 92.5 cm when using untreated expansive soil as subgrade to 45cm ,35cm and 35 cm when using 2%, 4% and 6% percentages of lime respectively in stabilization of expansive soil as subgrade. The results suggest that the lime content 6% is optimum percentage were that given a highly strength, lowest swelling and small thickness of pavement.

INTRODUCTION

Flexible pavements are layered systems with better materials on top where the intensity of stress is high and inferior materials at the bottom where the intensity is low. These types of pavements are called flexible since the total pavement structure bends or deflect due to traffic loads. Atypical flexible pavement consists of surface, base course, and subbase course built over compacted subgrade (natural soil). Each layer receives the load from the above layer, spreads them out, and then passes on these loads to the next layer below. In some cases, the subbase layer is not used, whereas in small number of cases both base and subbase are omitted. The material for the base course is typically unstabilized aggregates. The aggregate base could also be stabilized with asphalt, Portland cement, or anther stabilizing agent. The subbase is mostly a local aggregate material. Also the top of subgrade is some time stabilized with either cement or lime. The objective of pavement design is to provide a structural and economical Combination of materials to carry traffic in a given climate over the existing soil (subgrade) conditions for a specified time interval. (Yang, 2004)

Flexible Pavement design methods

Methods of flexible pavement design can be classified into five categories: empirical method with or without a soil strength test, limiting shear failure method, limiting deflection method, regression method based on pavement performance or road test, and mechanistic–empirical method (Yang, 2004). Several design methods can be use in design the flexible pavement thickness which are depend on some factor include the traffic loading, environmental and subgrade soil (Ali, A. M., 2001). Shallal (2010) reported in Sudan some designers use the design catalogue of the Road Note No.31 and other similar design catalogue by determining the strength from the soil testing and estimating the traffic loading category.

Sub-grade

Sub-grade soil is an integral part of the pavement structure as it provides the support to the pavement from beneath. The sub-grade soil and its properties are important in the design of pavement structure. The main function of the sub-grade is to give adequate support to the pavement and for this the sub-grade should possess sufficient stability under adverse climate and loading condition. (Khanna and Justo, 1990). In Sudan the main subgrade soil types are identified as expansive soils, red sand ironstone soils, and laterite and lateritic soils. These soil types is shown in Fig.1

Expansive soil

Expansive soil also known as "black cotton soil" is derived from the soil's dark or black color and the fact that it was originally used for growing cotton. In general, black

cotton soils are formed in areas where the parent material is a basic such as basalt. The black cotton's structure allows water molecules to enter between the layers causing expansion or shrinkage and that cause damage take place in many infrastructures also the expansive soil capable to cause deformations in roads, building and pipe lines. In Sudan, black cotton soil is formed by one of the following processes: to the east of the Blue Nile black cotton is a residual soil derived from its parent basalt rock. Between the two Niles (the Gezria clay plain) the black cotton soil is a transported alluvial deposit from the Ethiopian mountains to the east. To the south and south-west, black cotton soils occurs as a transported soil derived from the volcanic tuffs (Adam and.Agib.2001), Expansive soils have caused significant damage to irrigation system, water line, sewers, buildings, roads and other structures located in Sudan. Over one-third of Sudan's 2.6 million square kilometers may have expansive soil. Unfortunately, this area includes most of nation's population centers and development projects. The frequent failure to recognize the potential problem has resulted in extensive damages. In some cases, the cost of repairs to or replacement of irreparably damaged structures has exceeded the structure's initial value. Nationwide, the estimate cost of damage currently exceeds five million Sudanese pounds (six million U.S dollars) annually (Osman and charlis 1983), Sudan has tropical continental climate over most of the country. The climate merges into a desert climate to the north, with a short, unreliable rainy season during the month of July, august and September. The daytime temperatures from February to November are hot, frequently exceeding 40oc, and dust storms are common. The central area has a variable rainy season of medium rainfall. The climate merges into an equatorial rainy zone to the south having a short dry season in the month of December and January. (Nelson, et al. 1973)

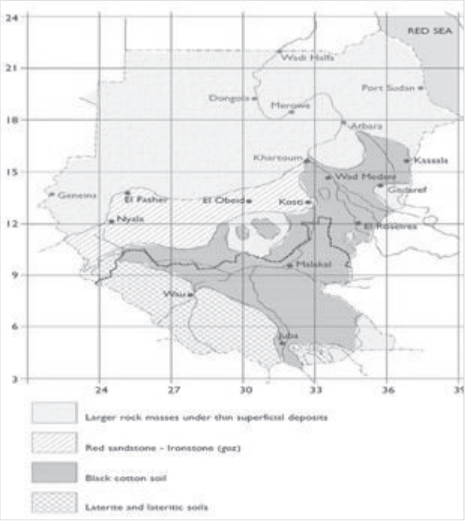

FIG.1. Distribution of Main Soil Types a crosses Sudan.

Stabilization

Stabilization is the process of blending and mixing materials with a soil to improve properties of the soil. The process may include the blending of soils to achieve a desired gradation or the mixing of commercially available additives that may alter the gradation, texture or plasticity, or act as a binder for cementation of the soil. Mechanical stabilization is accomplished by mixing or blending soils of two or more gradations to obtain a material meeting the required specification. The additive stabilization is achieved by the addition of proper percentages of cement, lime, fly ash, suitable grouts, bitumen, or combinations of these materials to the soil stabilized. (Washington Technical Manual 1994)

Lime stabilization

Lime is one of the several products that can be successfully used in the improvement of the engineering characteristics of soils. Depending on the characteristics of the lime-treated soils and service requirements, lime stabilized soils have been utilized as modified sub-grades, subbase and base course of pavement construction. When lime is added to a fine-grained soil, several reactions are initiated. Those reactions that occur soon after the lime and soil have been intimately mixed are action exchange and flocculation – agglomeration. A lime-soil pozzolinc reaction may occur resulting in the formation of various types of hydrated calcium silicate and aluminates cementing agents. The pozzolinc reaction is time and temperature dependent and the reaction and the reaction may continue for several years. Improvement in soil plasticity, workability, swell properties, water resistance, shear strength and stiffness are effect by the action exchange and flocculation –agglomeration reactions. Strength, stiffness and durability properties are further improved as a result of cementing materials formed in the lime-soil pozzolnic reaction. The degree of improvement effected by pozzolnic reaction is controlled by the extent of formation of various cementing agent (El-Rayes and Ahmed 1974).

Hydrated Lime

Lime as stabilizer is manufactured in various forms; the most typically used in soil stabilization are high quality hydrated lime Ca (OH) 2, monohydrated dolomitic lime [Ca (OH) 2. Mg (OH) 2], quick lime CaO and dolomitic quick lime [CaO.MgO]. Hydrated Lime is preferred as it comes in powder form, consumes no additional water for hydration and provides more free calcium for stabilization

Traffic loading

The consideration traffic should include both the loading magnitude and configuration and the number of load repetitions. There are three different procedures for considering vehicular and traffic effects in pavement design: fixed traffic, fixed vehicle, and variable traffic and vehicle. (Yang, 2004), In Sudan, road traffic is growing rapidly in volume, size and Wight of the vehicles using the roads. As a consequence, highway engineers concerned with designing new road or strengthen of existing roads require

reliable information about the distribution of axle loads for existing traffic as well as information on national or regional axle load trends. This information is required so that accurate forecasts can be made of axle loads that a road will have to carry over its design life (Shallal. 2010).To calculate the damage factor for any truck type, the information about axle loading is the most essential one to obtain the truck damage factors. There are only two ways to get this information; the first is to have portable weighbridges to be used through the traffic survey to each axle for the selected truck samples and the second way is to use legal axle load limits for the whole country determined by the National Highway Authority. The point is that till this date no portable weight bridges have been used in Sudan by consultants or government authorities in traffic surveys for new roads design.

EXPERIMENTAL

Materials

***Expansive Soil*:** The soil used in this study was obtained from highway project site near wad- madani city in the south of Khartoum. Previous soil investigations carried out at the site indicated the presence of clays**.** These soft clays were encountered at a depth of about 0.5m to 1.0m. The disturbed soil was excavated, placed in plastic bags, and transported to the laboratory for preparation and testing**.**

***Stabilizer Product (Lime)*:** The stabilizer materials used in this study were Lime .The lime stone used was obtained from ksala state then crushed and heating it to a high temperature at 900 C^o Intel become fine and easy to pass Sieve No 200

***Water*:** Distilled water was used for mixing soil and lime in all classification and strength tests

Sample preparation: The preparation of treated expansive soil were conducted in the laboratory by mixed a known percentage of hydrated lime 2%, 4% and 6% respectively of the total weight of expansive soil, then added initial water to occur reaction between clay and lime for 24 hours. A sample test should be blocked carefully even don't occurs evaporation for water by putting the samples in a plastic bags.

Table 1. Chemical Analysis of Hydrated Lime used

Test	Results% by mass		Requirement (ASTM-Part- 9)
	Sample (1)	Sample (2)	
Calcium Oxide (CaO)	72.7	73.0	72.0% min
Calcium Hydroxide Ca $(OH)_2$	96.02	96.5	95.0% min
Magnesium oxide MgO	0.5	0.4	0.5% min
Silica as SiO_2	0.62	0.58	0.7% min
Aluminum Oxide (Al_2O_3)	0.5	0.6	0.15% min
Ferric Oxide (Fe_2O_3)	0.05	0.03	0.08% min
Sulphur trioxide (SO_3)	-	-	0.10% min
Moisture	0.1	0.2	0.75% min

Test method

The purposes of this paper study the effect of hydrated lime on behavior of expansive soil as subgrade of flexible pavement structural system. A series of laboratory experiments have been conducted for treated and untreated samples. These experiments are to measure the engineering properties of the soil as follow:

- Physical Properties (Grain Size Distribution ,Consistency Limits and Swelling)
- Compaction Characterization
- California Bearing Ratio

DESIGN PROCEDUERS

The outcomes of the experimental works done on the untreated and treated subgrade were used to design the thickness of flexible pavement. The design passed on Overseas Road Note No.31 catalogue. The design procedures are based on cumulative expected 18-kip (80-kN) equivalent single-axle load (ESAL) and strength of subgrade soil (CBR).

RESULTS AND DISCUSSION

Three different percentage of Hydrated Lime; 2%, 4% and 6% were evaluated by six tests; sieve analysis, liquid limit, plastic limit, plasticity index, moisture content with dry density relationship and CBR. The effect of lime percentages on the liquid limit, plastic limit, plasticity index, moisture content, dry density and CBR are presented in table 2 and shown in paragraphs below

Table 2. Results of Treated and Untreated Expansive Soil

Lime %	LL%	PL%	PI %	MMD gm/cc	OMC %	CBR %	Swell %	AASHTO Classification	USCS Classification
0	40.50	20.30	20.00	1.64	19.00	1	4.36	A-7-5	CL
2	44.10	31.67	12.43	1.66	19.80	52	1.20	A-7-5	ML
4	40.25	30.88	9.370	1.66	19.50	27	0.18	A-4	ML
6	0.000	0.000	0.000	1.64	20.50	44	0.01	A-4	ML

Grain Size Distribution

The effect of lime in the grain size of expansive soil is presented in Fig.2. Fig.2 shows that there is a decrease of finer particles in the gradation of treated expansive soil when mixed with lime.

Consistency Limits

The Atterberg limits for the untreated and treated soils were determined. The treated soil samples were allowed to cure for one day before testing but were not compacted. The results are presented in Table 2 and plotted in Fig.3, 4 and 5. Fig.3 shows the effect of Lime on Liquid limit, Fig.4 shows effect of Lime on Plastic limit and Fig.5 shows the effect of Lime on Plastic index.

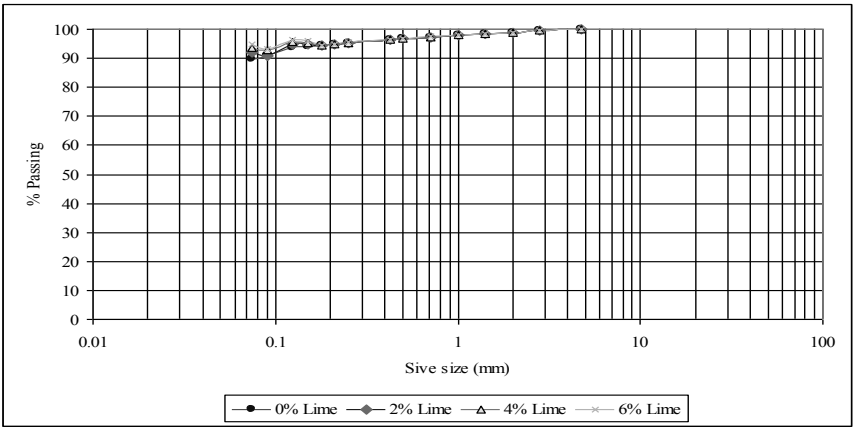

FIG.2. Effect of Lime in Grain Size Distribution

Effect of Lime Percentages on Liquid limit

Fig.3 shows the variation of results of liquid limit by using different hydrated lime percentages modified expansive soil; general trend shows that the liquid limit increases when adding 2% and 4% lime by weight of expansive soil and then the soil become non liquid when adding 6% of lime. The decreasing in liquid limit may be attributed to the increasing in the fine particles. The maximum liquid limit (44.1%) was reported for soil modified with 2% lime. Generally, the liquid limit of treated expansive soil and regardless of the lime percentage is higher than the liquid limit of untreated soil except the result of the percentage lime (higher than 5%). Therefore the minimum liquid limit was reported in 6% of lime.

Effect of Lime on Plastic limit

Fig.4 shows the variation of results of plastic limit by using different hydrated lime percentages modified expansive soil, general trend shows that the plastic limit increases according to adding 2% and 4% lime, and then decrease by using 6% lime. The maximum plastic limit (31.67%) was reported for 2% lime and minimum plastic limit (0%) was reported for those modified with %6 lime.

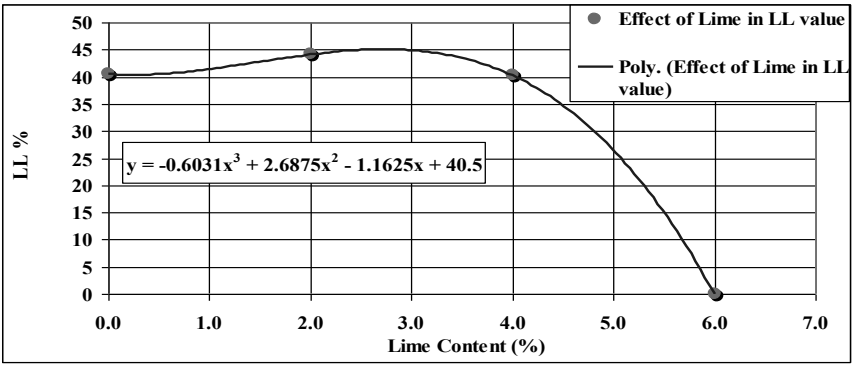

FIG.3. Effect of Lime on liquid limit.

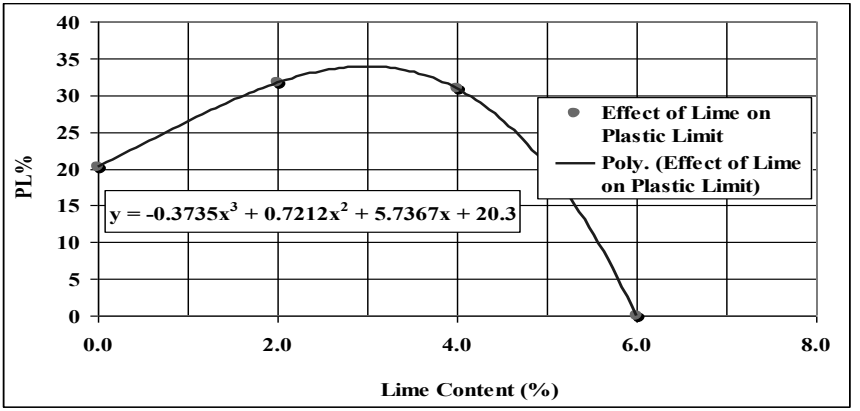

FIG.4. Effect of Lime on Plastic Limit.

Effect of Lime on Plasticity Index

Fig.5 shows the variation of results by using different hydrated lime percentages modified expansive soil; general trend shows that the plasticity index decreases as the lime percentage increases. Generally, the plasticity index of the expansive soil and regardless of the lime percentage is lower than the plasticity index of untreated soil. The maximum plasticity index (20%) was reported for untreated expansive soil and the minimum plasticity index (0%) was reported for expansive soil treated by using 6% of lime. The decrease in plasticity index for (2% &4%) of lime may be attributed to the increasing in the plastic limit is more than increasing in liquid limit.

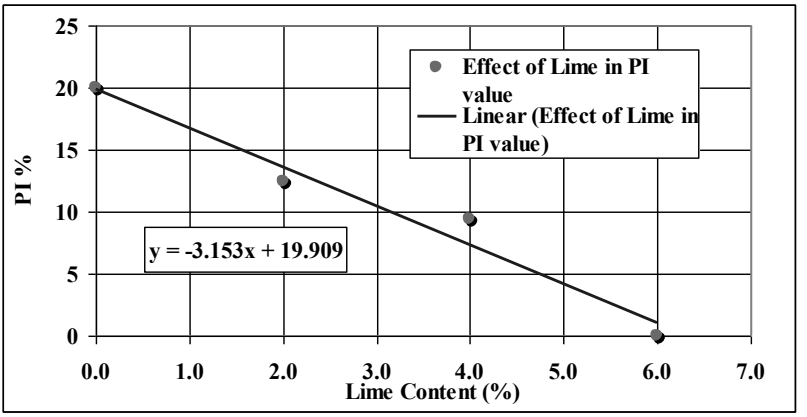

FIG.5. Effect of Lime on Plasticity Index.

Moisture Content - Dry Density Relationship

Moisture-unit weight curves for all treated and untreated soils were determined using a proctor compaction effort. This established OMC for preparing all of the compacted soil specimens for subsequent swell and CBR testing. In Figs.6 and 7, influence of lime on Maximum Dry Density (M.D.D) and optimum moisture content (O.M.C) of expansive soil is presented. Fig.6 represents that Maximum Dry Density (M.D.D) increase by increasing lime content until 4% and then decreases in 6% lime. M.D.D tends to increase and also O.M.C increases.

Effect of Lime on Moisture Content and Dry Density

Compaction characterization of expansive soil with Blended by lime is plotted in Figs.6 and 7; Fig.6 shows that the M.D.D reported of untreated expansive soil is less than M.D.D of treated expansive soil. Fig.7 shows increasing in optimum moisture content as the lime percentages increases. The lime flocculates the clay partials of the soil and makes the soil fluffy. The higher maximum dry density reported in lime 2% & 4% (1.65 and 1.66 g/cc), and higher optimum moisture content reported for 6% lime (20.5%).

Lime Percentages - CBR Relationship

Results of California Bearing Ration of soil with blended by lime are presented in table 3 and Fig.8.Fig.8 shows the variation of subgrade strength (CBR) by using different hydrated lime percentages modified expansive soil; generally, the strength of the treated expansive soil and regardless of the lime percentages is greater than the strength of untreated expansive soil - no modifier. Fig.8 shows the highest CBR (52%) was reported for the soil treated with 2% lime by weight of soil which is higher than CBR of soil

treated with the 4% & 6%. The decreases in CBR while increasing lime percentage may be attributed to the increasing in O.M.C and decreases in the M.D.D.

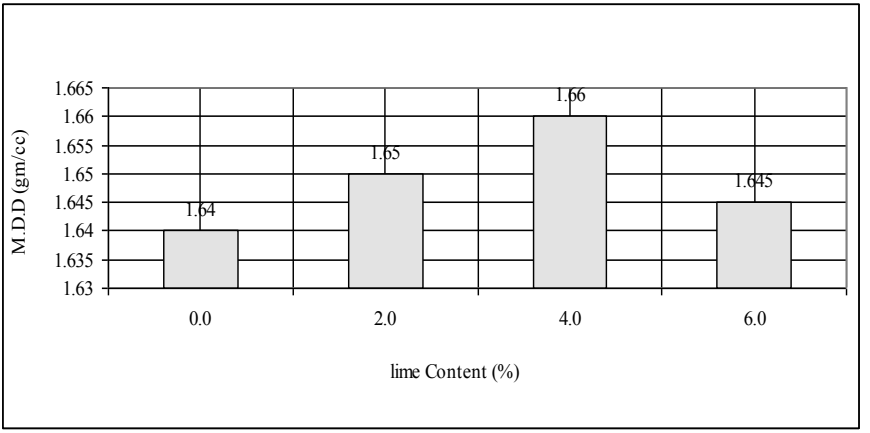

FIG.6. Effect of Lime on M.D.D.

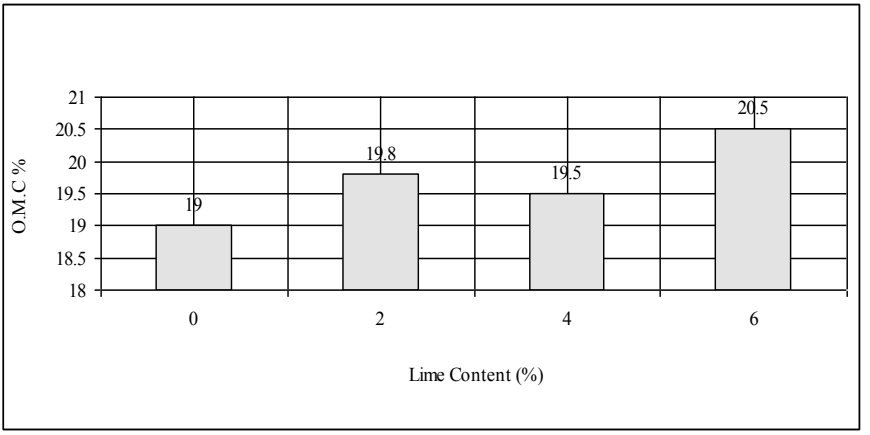

FIG.7. Effect of Lime on O.M.C %.

Effect of Lime on Swelling

Fig.9 shows the effect of different percentages of lime in swelling. At 2% of lime the swelling decrease to acceptable percentage (swelling value about 1.2%) where the lime percent increase to 4% the swelling decrease to 0.20%. The lowest swelling percentage was reported in 6% of lime which give 0.01% of swelling. The swelling of treated

expansive soil and regardless of lime percentage is lower than the no modified expansive soil

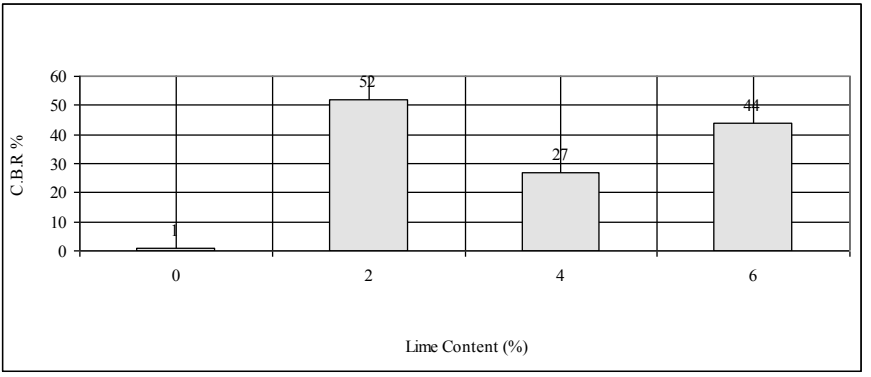

FIG.8. Effect of Lime on CBR%.

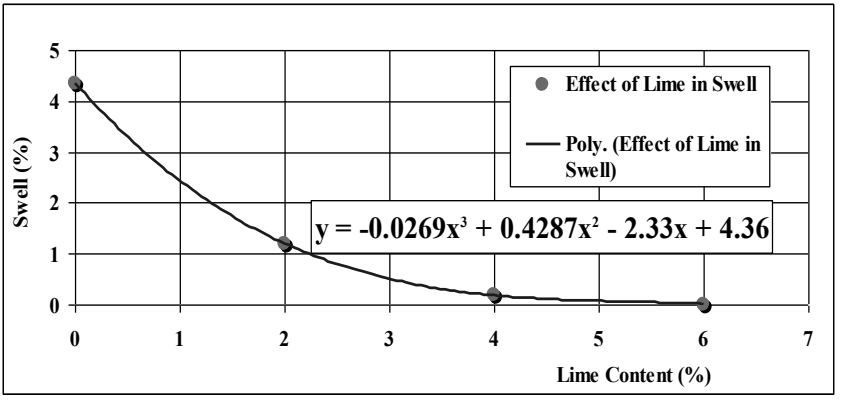

FIG.9. Effect of Lime on Swell %

Lime Percentages – Pavement Thickness Relationship

Results of design of pavement thickness are presented in Fig.10. Fig.10 shows that the lime decrease the thickness of pavement from 92.5 cm when using untreated expansive soil as subgrade to 45cm, 35cm and 35 cm when using 4% and 2% and 6% lime percentages respectively in stabilization of expansive soil as subgrade of flexible pavement structural system

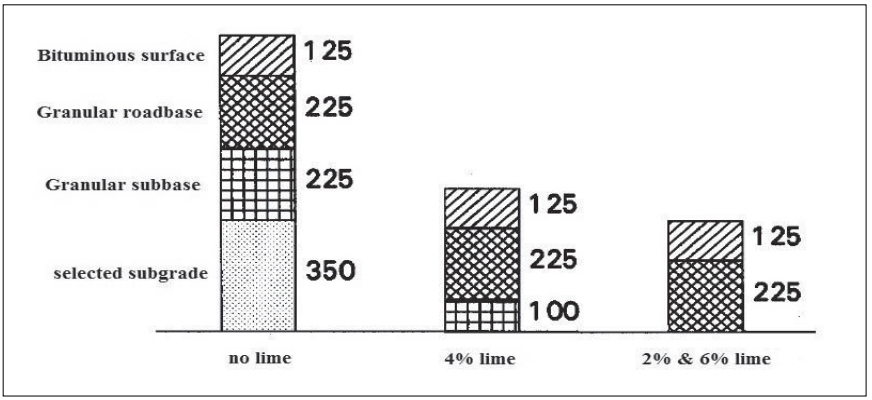

FIG.10. Effect of Lime on Pavement Thickness

CONCLUSIONS

The expansive soil one of the real problem should be considered as the damage it can made, one of the best solution for this problem adding some additive to expansive soil. In this paper the lime is good enough to treat the soil, so a different percentage of hydrated lime 2%, 4% and 6% by weight of soil samples were added with curing time of 24 hour, then the change in the physical and mechanical properties was easy to recognize on those different percentages. The laboratory test was conducted to determine the different properties of the samples before and after adding the lime; liquid limit, plastic limit, plasticity index, moisture content and dry density relationship and CBR, also the effect of using the lime as stabilizer on the thickness of pavement was studied. The result of study indicated that the treated soils have better physical properties, lowest swelling, and high strength. Better properties were found would positively influence in the reducing the thickness of pavement. Therefore, it can be concluded that lime can improve the engineering properties of expansive soils. Practically, the effective lime content should be blended in the 6 percentage which provides high strength, decrease swelling to lowest percentage and provides small thickness of pavement

ACKNOWLEDGMENT

The authors' wishes to thank the Building and Road research Institute, Khartoum University for offer the chance to conduct the experimental works of this paper. The authors also thankful especially to Adiel Ahmed Mohammed Alhassan Ph.D Student, Building and Road research Institute, Khartoum University and Dr. Ahemd Mohammed Elsharif head of Building and Road research Institute for continuous encouragement and assistance during study time

REFERENCES

Adam, E.A. and A.R.A.Agib. (2001). Compressed Stabilised Earth Block Manufacture in Sudan. United Nations Educational, Scientific and Cultural Organization (UNESCO).

Ali, A. M. (2001). "Deformation Characteristics of soils in Sudan impact on structural Design of highway." *first Engineering conference of road in Sudan*, Sudan Engineering Society.

American Society for Testing and Materials "Standard Test Methods for Laboratory Compaction Characteristics of Soil Using Standard Effort." ASTM D 698.

El-Rayes,M.K. and Ahmed .A.E (1974) "Lime Soil Stabilization." *Sudan Engineering Society Journal* 21:13-17.

Khanna,S.K. and Justo,C.E.G.(1990)."Highway engineering." *6th ed. Nem chand and bros*, roorkee.

Nelson H.D., et al. (1973). "Area Handbook for the Democratic Republic of Sudan. 2nd Edition". U.S Gov't .Printing Office, Washington, D.C. U.S.A.

Osman,M.A and charlis.W.A. (1983) "Expansive soil in Sudan". BRRI CURR.ENT PAPER.

Overseas Road Note. 31. (1993) "A guide to the Structural Design of Bitumen Surfaced Road in Tropical and Sub-Tropical Countries." Transport Research Laboratory, London, UK.

Overseas Road Note 40. (2004)."A guide to axle load surveys and traffic counts for determining traffic loading on pavement." Transport Research Laboratory, London, UK.

Shallal, M. M.. (2010)."Traffic Loading for Pavement Design in Sudan." *Journal of Building and Road Research*, U of K Sudan.

Washington Technical Manual (1994) "Soil Stabilization for Pavement."Departments of the Army and Air Force, USA, TM 5-822-14/AFMAN 32-8010.

Yang, H. (2004)."Pavement analysis and Design."2nd Edition.

Yoder,E.J. and Witczak,M.W.(1975). "Principles of Pavement Design."2nd Edition, John Wiley & Sons, Inc., USA.

Improvement on Recognition Method of Void beneath Slab Based on Nondestructive Testing Technologies

Xue Yanqing[1], Huang Xiaoming[2], Zhou Wei[3] and Qian Shunzhi[4]

[1]Ph.D. Candidate, School of Transportation, Southeast University, Nanjing, 210096, China; email: 494961575@qq.com.
[2] Professor, School of Transportation, Southeast University, Nanjing, 210096, China; email: huangxm@seu.edu.cn.
[3]Ph.D. Candidate, Born in 1985, Sipailou 2#, School of Transportation, Southeast University, Nanjing, 210096, China; email: lygzhouw@126.com.
[4] Professor, School of Transportation, Southeast University, Nanjing, 210096, China; email: sqian@seu.edu.cn.

ABSTRACT: In preventative maintenance, it is very significant to accurately recognize the void beneath the cement concrete pavement. However, there are quite a few defects in the current NDT technologies of void recognition. Based on ground penetrating radar (GPR), the void investigation is carried out on several typical highway sections in Anhui Province. Then, the reflected wave profile is obtained by "Reflex-Win" so as to ascertain whether there is void at the bottom of these pavement slabs. Next, falling weight deflectometer (FWD) is utilized to carry out multi-level load deflection test. So, the "load-deflection" regression models can be established by the test results. Additionally, extension evaluation is adopted to recognize the void and its index system comprises the regression model's slope, intercept as well as the maximum deflection. Finally, comparing to the detection results of GPR, by way of adjusting the section domains of these indexes, the classical domains of different void status and their weight coefficients scientifically, relatively higher recognition ratio and relatively lower misjudgment ratio can be acquired. The study shows that under this improved method, the void ratio of the typical highway sections is 33%, approximately to the result of GPR (35%). Moreover, this method's recognition ratio is 88.6% and its misjudgment ratio is merely 6.1%. The superior accuracy of void recognition shows that the improved method is able to satisfy the demands of engineering detection, recognition and structural evaluation.

INTRODUCTION

As one of the structural damages of cement concrete pavement, the void beneath slab is meanwhile a significant hidden trouble of some potential more severe structural damages of cement concrete pavement. Studies have shown that the void beneath slab will bring about adverse effects on the performance, durability and service life of cement concrete pavement. Especially, the pavement fracture is practically interrelated to the void (Tan Zhiming, 2010; Zhou Yumin, 2010). For the pavement structure with void beneath slab, it is necessary to take measures of the preventative maintenance. For instance, grouting technology is usually used in plugging the void so as to postpone the pavement fracture. Therefore, it is very important to accurately recognize the void beneath slab for the pavement's preventative maintenance (Liang Xinzheng, 2008). Since the 1980s, the researches about nondestructive testing (NDT) technology in the detection of highway engineering have been carried out abroad. According to the technical criterions of NDT technology jointly put forward by ASTM, ISO and BSI, the current technologies of NDT in void recognition of cement concrete pavement mainly include the detection technology by ground penetrating radar (GPR) and the multi-level load detection technology by falling weight deflectometer (FWD) (Geng Yuling, 2007). However, there are quite a few defects in the current NDT technologies of void recognition.

DEFECT ANALYSES OF THE CURRENT NDT TECHNOLOGIES IN VOID RECOGNITION

As an efficient NDT technology in void recognition, the detection technology of GPR can realize the rapid continuous testing. Additionally, it can quantify the void status beneath slab. However, because of the expensive detection costs, the professional post-processing analysis, and the complex recognition procedures, the application of the detection technology of GPR is undoubtedly subject to the restriction to a certain degree. So nowadays, as everyone knows, the most widely used NDT technology in void recognition is still the multi-level load detection technology by FWD. Besides, for grouting operations, although the detection technology of GPR can quantify the void status beneath slab, it is only necessary to find out whether there is void at the bottom of the pavement slab. That is to say, it is not concerned about the specific status of the void beneath slab (Imad L. Al-Qadi, 2005; Z. Leng, 2009; Desh Raj Sonyok, 2008). For FWD, the resolution of its deflection sensor can approach 1μm and its systematic error can be no more than 2%. Therefore, the multi-level load detection technology by FWD is adopted in the specifications of AASHTO and the current specifications of China also recommend recognizing the void beneath slab by taking advantage of this technology.

Nevertheless, under the multi-level load detection technology by FWD, the void's criterion and its value depend on experience totally, so the recognition results may be different from the actual situation. In other words, the void's recognition ratio and its misjudgment ratio could be unsatisfactory.

Based on the multi-level load deflection test by FWD, according to NCHRP, the intercept of the regression model of "load-deflection" on its deflection axis and the model's slope are made use of as the void's criterion respectively. For the current specifications of China, the maximum deflection at the slab corner is made use of as the void's criterion. NCHRP suggests when the intercept is no less than 50μm, it can be recognized that there is void at the bottom of the pavement slab. Also, when the slope is no less than 4μm/kN, it can be recognized that there is void at the bottom of the pavement slab. The current specifications of China reckon when the maximum deflection at the slab corner is no less than 200μm, it can be recognized that there is void at the bottom of the pavement slab. Obviously, under load actions, the void beneath slab will mapped to the response indexes mentioned above. However, the value of each void's criterion is merely a definite empirical value. Surely, it can not take a good many factors into account, such as the technical class of highway, the structural composition of pavement, the engineering hydrogeology, the traffic as well as the environment. For this method of single index, because of the error or the human factors, there will inevitably be misjudgment in the final recognition results.

METHOD IMPROVEMENT IDEAS AND EXTENSION EVALUATION

For the purpose of enhancing the recognition ratio and reducing the misjudgment ratio of the void beneath slab, the improvement ideas of the method of void recognition is determined as follows. Relying on several typical highway sections of Anhui, the GPR recognition results of the void beneath slab are utilized as the basis and extension evaluation is adopted to analyze the acquired data of the multi-level load deflection test by FWD. By way of creating comprehensive index system of the evaluation method, setting void classification scientifically and determining the indexes' classical domains, section domains as well as weight coefficients properly, an improved method of void recognition based on comprehensive NDT technologies can be formed finally.

The theoretical base of extension evaluation is extension theory and the logical cell of extension theory is called matter-element. The matter-element can simultaneously describe the characteristics and the values of an object. Name, characteristic and value of an object are called the three factors of this object's matter-element. The procedure of extension evaluation is as follows: ① Establishing the matter-elements of the classical domains and the section domains; ② Ascertaining the matter-elements of the object to be evaluated; ③ Calculating the values of the correlation functions; ④ Determining the weight coefficients and

calculating the correlation degrees; ⑤ Ascertaining the grade of the object on specific level (Ling Jianming, 2008; Qiang Li, 2008).

Within this procedure of extension evaluation, the form of the correlation function is the key. A simple whilst widely used function form is as follows:

$$K_j(v_i)=\begin{cases}\dfrac{-\rho(v_i,v_{0ji})}{\left|v_{0ji}\right|}, & v_i \in v_{0ji}\\ \dfrac{\rho(v_i,v_{0ji})}{\rho(v_i,v_{Pi})-\rho(v_i,v_{0ji})}, & v_i \notin v_{0ji}\end{cases} \tag{1}$$

In Eq.(1), the computing equations of the distance between the point and the interval are:

$$\rho(v_i,v_{0ji})=abs(v_i-\frac{a_{0ji}+b_{0ji}}{2})-\frac{b_{0ji}-a_{0ji}}{2} \qquad i=1,2,\cdots,n \tag{2}$$

$$\rho(v_i,v_{Pi})=abs(v_i-\frac{a_{Pi}+b_{Pi}}{2})-\frac{b_{Pi}-a_{Pi}}{2} \qquad i=1,2,\cdots,n \tag{3}$$

Let the weight coefficients of the indexes in extension evaluation be λ_1, λ_2… λ_n. Apparently, $\sum_{i=1}^{n}\lambda_i=1$. Than, by $K_j(p)=\sum_{i=1}^{n}\lambda_i K_j(v_i)$, the correlation degree about the grade of the object on specific level to be evaluated can be calculated. If $K_j(p)=\max_{j\in\{1,2,\cdots,m\}}K_j(p)$, it means that the object to be evaluated belongs to P_{0j}.

Setting $\overline{K}_j(p)=\dfrac{K_j(p)-\min\limits_j K_j(p)}{\max\limits_j K_j(p)-\min\limits_j K_j(p)}$, $j^*=\dfrac{\sum_{j=1}^{m} j\times\overline{K}_j(p)}{\sum_{j=1}^{m}\overline{K}_j(p)}$. Here, j^* is called level variable eigenvalue.

THE INVESTIGATION OF THE VOID BENEATH SLAB BASED ON GPR TECHNOLOGY

Taking several technical factors into account, such as Anhui's overall situation, the province's physical geography characteristics, its climatic environment and the highway department's recommendations of the province, several highway sections of cement concrete pavement of different regions distributing in Anhui are selected to

carry out the investigation of the void beneath slab based on GPR technology. The selected highway sections are respectively located at the arterial highways such as Provincial Highway S103 (Huangshan), National Highway G206 (Tongcheng), Provincial Highway S202 (Fuyang) and National Highway G104 (the boundary of Mingguang and Wuhe). These highway sections cover the vast majority of the administrative levels, the technical grades, the pavement structural compositions, the geographic regions and the climatic environments of the arterial highways in Anhui. So, they are also called the typical highway sections. Considering the requirements of the investigation and the existing equipments of Anhui Testing Center for Highway Engineering, one GPR system of the model of RAMAC is equipped. Besides, the shielded antenna of ground-coupled is applied in this GPR system and its center frequency can be set as 800MHz in terms of several technical literatures. From the typical highway sections of cement concrete pavement, one hundred slabs are randomly chosen as the testing samples.

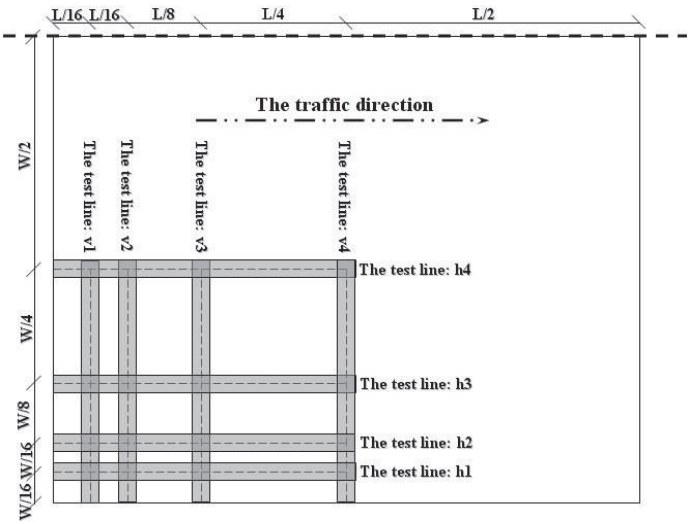

FIG.1.The testing lines of GPR investigation.

Now, the investigation of the void beneath these slabs and the corresponding post-processing analysis can be carried out. The mesh lines along or vertical with the traffic direction are respectively drew on each 1/4 slab (Fig.1). The mesh lines are also the testing lines of GPR. The serial numbers of the testing lines along the traffic direction is h1, h2, h3 and h4 from the slab edge to the slab middle. The serial numbers of the testing lines vertical with the traffic direction is v1, v2, v3 and v4 from the slab edge to the slab middle. So, there are eight testing lines for each pavement slab of cement concrete and totally, there are eight hundred testing lines to

be detected by GPR. Along these GPR testing lines, the investigation of the void beneath the pavement slabs can be carried out. The typical testing sites are shown in Fig.2. After the GPR investigation of each testing line, one rd3 format file can be obtained. The file includes the original data for the post-processing analysis. The post-processing analysis is carried out so as to reduce the interference of the clutter and recognize the void effectively. The adopted software for the post-processing analysis is Reflex Win. By this software, the reflected wave profile can be obtained easily. And then, whether there is void at the bottom of these slabs can be determined scientifically.

FIG.2. The testing sites based on GPR technology (left: the test along the traffic direction; Right: the test vertical with the traffic direction).

For Reflex Win, there are six main steps when carrying out the post-processing analysis: ① Subtracting DC shift; ② Moving start time; ③ The energy decay; ④ Subtracting average; ⑤ Wave filtering by the band pass of Butterworth; ⑥ Running average. Among the steps, the third step is to amplify the signal of the deep, the fourth step is to remove the horizontal portion in the image and the sixth step is to suppress the noise as well as make the image smoother (Jiang Hong, 2010). After accomplishing these six steps of the original data's post-processing analysis, the reflected wave profile of a testing line can be acquired (Fig.3). In Fig.3, the horizontal coordinate is the detection distance and its unit is "m". The vertical coordinate is the highway structure depth and its unit is "ns". In Fig.3, it can be seen that there is an obvious disorder of the reflected wave at 8ns of the vertical coordinate and 0~0.7m of the horizontal coordinate. Therefore, it can be empirically recognized that there is void at the bottom of this slab.

According to the same procedure, the post-processing analyses of the original data corresponding to the eight hundred testing lines are carried out. Therefore, for the one hundred slabs mentioned above, the void recognition results of the investigation based on GPR technology can be acquired. The void recognition results are shown in Table 1. Table 1 shows that the void ratio of the typical highway sections is 35%.

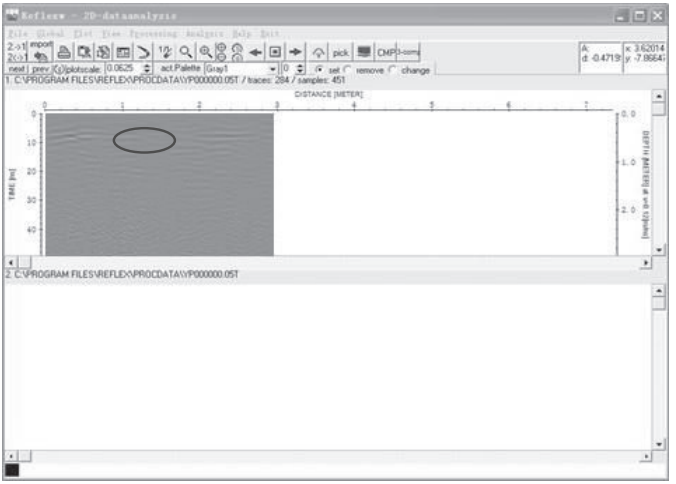

FIG.3.The reflected wave profile acquired by the post-processed analysis

Table 1.The void recognition results of the investigation based on GPR technology

Number	1	2	3	4	5	6	7	8	9	10	11	12	13	14	15	16	17	18	19	20
Result	Y	Y	N	N	N	N	N	N	N	N	N	N	N	N	N	N	N	N	N	N
Number	21	22	23	24	25	26	27	28	29	30	31	32	33	34	35	36	37	38	39	40
Result	N	N	N	N	N	N	N	Y	Y	N	N	N	N	N	N	Y	N	N	N	Y
Number	41	42	43	44	45	46	47	48	49	50	51	52	53	54	55	56	57	58	59	60
Result	Y	Y	Y	Y	Y	Y	Y	Y	N	N	N	N	N	N	N	N	N	Y	N	N
Number	61	62	63	64	65	66	67	68	69	70	71	72	73	74	75	76	77	78	79	80
Result	Y	N	N	N	N	N	N	N	Y	N	Y	Y	N	N	Y	Y	Y	Y	Y	Y
Number	81	82	83	84	85	86	87	88	89	90	91	92	93	94	95	96	97	98	99	100
Result	N	Y	N	N	Y	N	N	N	N	Y	Y	Y	Y	N	Y	Y	Y	Y	N	N

IMPROVEMENT OF THE VOID RECOGNITION METHOD

According to the recommendation of China's current specifications, the multi-level load deflection test should be carried out by FWD at the corner of the pavement slab. Then, the curve of the "load-deflection" relationship can be drawn easily based on the test results. Furthermore, taking the response indexes such as the maximum deflection at the slab corner into account, extension evaluation can be

adopted to recognize the void status beneath the pavement slab comprehensively. The loads of FWD are set three levels and their values are taken as 46kN, 50kN, 80kN. In the deflection test, the pavement slabs are exactly the same as Table 1. The regression analysis results of the test data are displayed in Table 2. In Table 2, A is the serial number of the test, B is the maximum deflection at the slab corner, C is the relationship curve's slope and D is its intercept.

Table 2.The regression analysis results of the test data based on FWD

A	B	C	D	A	B	C	D	A	B	C	D	A	B	C	D
1	277.7	4.87	33.0	**26**	54.1	0.97	7.4	**51**	131.6	2.60	0.8	**76**	273.0	5.11	17.4
2	276.9	5.26	15.5	**27**	62.9	1.14	6.5	**52**	195.0	3.51	18.0	**77**	293.3	4.52	66.5
3	214.5	4.08	9.9	**28**	183.4	3.35	18.9	**53**	154.2	2.93	5.0	**78**	382.2	5.88	83.8
4	164.2	2.97	17.4	**29**	296.1	4.15	88.5	**54**	109.5	2.13	2.5	**79**	283.4	4.26	69.3
5	159.9	2.87	18.9	**30**	75.1	1.31	10.2	**55**	67.0	1.44	0.0	**80**	384.9	5.30	116.5
6	185.3	3.35	19.9	**31**	140.5	2.85	0.0	**56**	49.1	1.11	0.0	**81**	151.7	2.87	8.6
7	193.1	3.66	12.0	**32**	209.4	4.09	5.6	**57**	79.2	1.68	0.0	**82**	353.6	4.99	99.2
8	203.7	4.02	1.7	**33**	97.6	2.08	0.0	**58**	254.8	4.07	50.7	**83**	219.8	3.95	20.7
9	140.0	2.59	12.4	**34**	96.9	2.03	0.0	**59**	159.0	3.00	8.5	**84**	264.9	4.83	20.4
10	115.2	2.24	5.4	**35**	126.9	2.58	0.0	**60**	237.0	4.38	15.9	**85**	282.4	4.48	57.5
11	129.6	2.42	10.3	**36**	297.4	5.41	23.4	**61**	280.8	4.69	50.4	**86**	236.7	4.02	33.7
12	134.7	2.46	11.4	**37**	203.5	3.13	45.1	**62**	237.8	4.50	10.3	**87**	197.0	3.07	42.0
13	174.7	3.04	23.8	**38**	60.6	1.32	0.0	**63**	149.0	2.98	0.3	**88**	279.6	4.51	53.9
14	225.8	4.60	0.0	**39**	55.6	1.06	3.3	**64**	122.6	2.21	12.7	**89**	210.0	4.02	8.5
1	221.	4.0	20.	**4**	174.	2.2	59.0	**6**	176.	3.0	23.	**90**	359.	5.9	58.8

5	8	3	1	**0**	7	8		**5**	4	7	1		7	3	
16	160.0	3.05	10.4	**41**	444.6	5.06	185.0	**66**	125.7	2.39	8.5	**91**	293.3	4.52	66.5
17	155.5	2.85	10.9	**42**	168.4	1.68	84.1	**67**	125.6	2.30	11.1	**92**	382.2	5.88	83.8
18	140.3	2.60	10.2	**43**	341.8	4.18	130.3	**68**	157.3	3.03	5.6	**93**	318.2	5.26	51.7
19	113.2	1.60	35.7	**44**	138.5	1.66	56.3	**69**	331.0	4.89	79.2	**94**	238.6	4.20	24.8
20	91.0	1.59	12.0	**45**	257.4	2.00	157.9	**70**	219.8	3.78	29.3	**95**	345.5	5.57	65.7
21	56.6	1.01	6.7	**46**	233.4	3.59	50.3	**71**	290.3	4.56	59.9	**96**	279.6	4.51	53.9
22	91.0	1.37	24.1	**47**	276.0	4.95	26.0	**72**	267.9	4.63	34.1	**97**	289.3	4.70	50.2
23	66.7	1.32	0.7	**48**	319.7	6.43	0.0	**73**	154.1	3.37	0.0	**98**	289.3	4.70	50.2
24	64.6	1.17	6.9	**49**	140.8	2.72	5.3	**74**	187.1	2.87	45.9	**99**	200.1	3.52	24.5
25	69.2	1.31	4.8	**50**	192.3	3.73	5.5	**75**	334.1	6.18	21.1	**100**	210.0	4.02	8.5

The testing sites of the multi-level load deflection test are shown in Fig.4 and Fig.5.

FIG.4.The testing site of the deflection test.

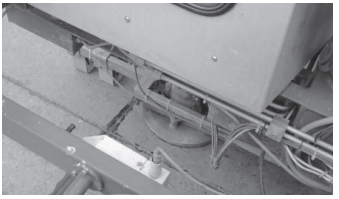

FIG.5.The partial enlargement of the testing site.

Several years ago, extension evaluation was introduced into the application of recognizing the void beneath the pavement slab by Guangdong Province. Four technical indexes such as the maximum deflection at the slab corner, the slope of the relationship curve, the curve's intercept and the coefficient of load transfer at the slab joint are all adopted during the practical recognition process. However, in the practice of Guangdong Province, there are several severe problems as follows. Firstly, it is wrong to recognize there is void or not by the load transfer coefficient's value. Numerous domestic and foreign studies show that there is no simple monotonic decreasing relationship between the void and the coefficient of load transfer at the slab joint. As a matter of fact, with the development of the void size, the coefficient of load transfer at the slab joint will initially diminish and then increase under some certain conditions, even monotonically increase. Secondly, the section domains and the classical domains of the four technical indexes in the practice are all determined empirically, lack of the necessary theory and data support. Thirdly, the recognition accuracy of the void beneath slab in the practice lacks the necessary scientific verification. Based on the main purpose of overcoming the three problems of Guangdong's practice, the improved recognition method of the void beneath slab will be developed.

Above all, only three technical indexes, the maximum deflection at the slab corner, the slope of the relationship curve and the curve's intercept are selected into the index system of the improved method.

And then, during the void recognition process, the status of "ambiguous void" is introduced temporarily. In the calculation of extension evaluation, according to the sequence of "no void" status, the "ambiguous void" status and the "definite void" status, "1", "2" and "3" are assigned respectively. The greater the calculated level variable eigenvalue (j^*) is, the more obvious the void beneath the slab is. "2" (the status of "ambiguous void") is utilized as the boundary of the recognition results. When j^* is less than "2", the recognition result is "no void" status. When j^* is more than "2", the recognition result is the "definite void" status. With regard to the ambiguous void status's classical domains, for the maximum deflection at the slab corner, it can be set as 200μm in advance, for the slope of the relationship curve, it can be set as 4μm/kN in advance, and for the curve's intercept, it can be set as 50μm in advance. Then, based on these pre-set values, the values of the three technical indexes can be varied. According to Table 2, the void recognition ratios and its misjudgment ratios corresponding to the different values of the three technical indexes can be calculated, taking advantage of these values as the void criterions respectively. The void recognition ratios and its misjudgment ratios are shown in Table 3.

Table 3.The recognition ratios and the misjudgment ratios of the three technical

indexes

Technical index	The maximum deflection at the slab corner / μm					The slope of the relationship curve / μm/kN						
Value	160	180	200	220	240	3.6	3.8	3.9	4	4.1	4.2	4.4
Recognition ratio / %	97.1	91.4	82.9	77.1	74.3	74.3	71.4	71.4	71.4	71.4	68.6	62.9
Misjudgment ratio / %	43.3	41.8	39.6	30.8	18.8	44.7	41.9	41.9	32.4	26.5	25.0	24.1

Technical index	The curve's intercept / μm							
Value	38	40	42	44	46	48	50	52
Recognition ratio / %	74.3	74.3	74.3	71.4	65.7	65.7	65.7	54.3
Misjudgment ratio / %	13.3	13.3	13.3	13.8	14.8	14.8	14.8	9.5

Table 3 shows that the recognition ratio increases from 82.9% to 97.1% during the criterion value of the maximum deflection at the slab corner diminishes from 200μm to 160μm. Meanwhile, the misjudgment ratio merely increases form 39.6% to 43.3%, much less than the increment of the recognition ratio. When its criterion value increases from 200μm to 240μm, the misjudgment ratio sharply decreases to 18.8% and the recognition ratio only diminishes to 74.3%. Considering the change laws of the recognition ratio and the misjudgment ratio, the ambiguous void status's classical domain of the maximum deflection at the slab corner can be set as 160~240μm. During the criterion value of the slope of the relationship curve diminishes from 4μm/kN to 3.6μm/kN, the recognition ratio merely grows from 71.4% to 74.3% whilst the misjudgment ratio increases from 32.4% to 44.7% significantly. When its criterion value increases from 4μm/kN to 4.2μm/kN, the recognition ratio only slightly reduces to 68.6% and the misjudgment ratio drops to 25.0% rapidly. When its criterion value goes on increasing from 4.2μm/kN to 4.4μm/kN, although the misjudgment ratio reduces by 0.9%, the recognition ratio falls by 5.7%. Considering the change laws of the recognition ratio and the misjudgment ratio, the ambiguous void status's classical domain of the slope of the relationship curve can be set as 4~4.2μm/kN. During the criterion value of the curve's intercept decreases from 50μm to 42μm, the recognition ratio increases from 65.7% to 74.3% rapidly whilst the misjudgment ratio descends from 14.8% to 13.3%. When its criterion value goes on descending from 42μm to 38μm, there are not any change in the misjudgment ratio and the recognition ratio. During its criterion value increases from 50μm to 52μm, although the misjudgment ratio reduces from 14.8% to 9.5%, the recognition ratio sharply decreases from 65.7% to 54.3%. Considering the change laws of the recognition ratio and the misjudgment ratio, the ambiguous void status's classical domain of the curve's intercept can be set as 42~50μm.

Table 4. The section domains and the classical domains of the improved recognition method

Technical index	The classical domain		The section domain
The maximum deflection at the slab corner / μm	No void	60~160	60~350
	Ambiguous void	160~240	
	Definite void	240~350	
The slope of the relationship curve / μm/kN	No void	1.2~4	1.2~5.6
	Ambiguous void	4~4.2	
	Definite void	4.2~5.6	
The curve's intercept / μm	No void	0~42	0~100
	Ambiguous void	42~50	
	Definite void	50~100	

Finally, with regard to the section domains, for the maximum deflection at the slab corner, the section domain is recommended as 60~350μm, for the slope of the relationship curve, the section domain is recommended as 1.2~5.6μm/kN, and for the curve's intercept, the section domain is recommended as 0~100μm. The section domain of each technical index can cover 90% of the corresponding testing data in Table 2. By now, the section domains of the three technical indexes and the classical domains of different void statuses of the improved void recognition method in this paper can all be determined, shown in Table 4.

According to Table 4, the matter-elements of the classical domains about the status of "no void", "ambiguous void" and "definite void" can be established respectively as follows:

$$R_{01}=\begin{bmatrix} P_{01} & c_1 & <60,160> \\ & c_2 & <1.2,4> \\ & c_3 & <0,42> \end{bmatrix}, \quad R_{02}=\begin{bmatrix} P_{02} & c_1 & <160,240> \\ & c_2 & <4,4.2> \\ & c_3 & <42,50> \end{bmatrix},$$

$$R_{03}=\begin{bmatrix} P_{03} & c_1 & <240,350> \\ & c_2 & <4.2,5.6> \\ & c_3 & <50,100> \end{bmatrix}.$$

So, the matter-element of the section domains can be established, $R_P=\begin{bmatrix} P & c_1 & <60,350> \\ & c_2 & <1.2,5.6> \\ & c_3 & <0,100> \end{bmatrix}$.

THE APPLICATION OF THE IMPROVED VOID RECOGNITION METHOD

Utilizing the void recognition results based on GPR technology (Table 1) as the basis, the weight coefficients of the three technical indexes (the maximum deflection at the slab corner, the slope of the relationship curve, the curve's intercept) can be determined by pilot calculation. The calculated weight coefficients are 0.35, 0.3, and 0.35 respectively. Then, the first slab is taken for instance to illustrate the application of the improved method. First of all, the matter-element of the slab is established, $R = \begin{vmatrix} p & c_1 & 277.7 \\ & c_2 & 4.87 \\ & c_3 & 33.0 \end{vmatrix}$. Then, the values of the correlation functions can be calculated by Eq.(1) ~ Eq.(3). Ultimately, the correlation degrees would be calculated easily. By calculation, $K_3(p) = \max_{j\in\{1,2,3\}} K_j(p)$, so it can be ascertained that "p", the slab, belongs to P_{03} (the definite void status). In addition, by calculation, the level variable eigenvalue (j^*) is 2.87. This datum further demonstrates that there is void at the bottom of this pavement slab and the void degree is relatively serious. For the remaining pavement slabs, according to Table 4 and the same procedure mentioned above, the void recognition results can all be obtained, shown in Table 5. From Table 5, the void ratio of the typical highway sections mentioned above is ascertained of 33%, approximately to the GPR investigation result (35%).

Furthermore, to verify the void recognition accuracy of the improved method, the recognition results of GPR are utilized as the basis. It is counted that the void recognition ratio of this method is 88.6% and the corresponding misjudgment ratio is merely 6.1%. No matter from the void ratio, or specifically in terms of the recognition ratio and the misjudgment ratio, the superior recognition accuracy about void beneath slab shows that the improved method is able to satisfy the demands of engineering detection, recognition and structural evaluation.

Table 5.The void recognition results acquired by the improved method

Number	Result (j^*)	Number	Result (j^*)	Number	Result (j^*)	Number	Result (j^*)	Number	Result (j^*)
1	Y(2.87)	**21**	N(1.01)	**41**	Y(2.99)	**61**	Y(2.80)	**81**	N(1.17)
2	Y(2.36)	**22**	N(1.07)	**42**	N(1.87)	**62**	N(1.74)	**82**	Y(2.98)
3	N(1.50)	**23**	N(1.01)	**43**	Y(2.91)	**63**	N(1.16)	**83**	N(1.35)
4	N(1.21)	**24**	N(1.02)	**44**	N(1.08)	**64**	N(1.11)	**84**	Y(2.30)
5	N(1.20)	**25**	N(1.02)	**45**	Y(2.44)	**65**	N(1.27)	**85**	Y(2.80)
6	N(1.31)	**26**	N(1.01)	**46**	Y(2.32)	**66**	N(1.10)	**86**	N(1.62)
7	N(1.36)	**27**	N(1.01)	**47**	Y(2.53)	**67**	N(1.11)	**87**	N(1.53)
8	N(1.44)	**28**	N(1.30)	**48**	Y(2.36)	**68**	N(1.19)	**88**	Y(2.78)

9	N(1.14)	**29**	Y(2.81)	**49**	N(1.14)	**69**	Y(2.94)	**89**	N(1.43)
10	N(1.09)	**30**	N(1.04)	**50**	N(1.36)	**70**	N(1.43)	**90**	Y(2.95)
11	N(1.12)	**31**	N(1.14)	**51**	N(1.11)	**71**	Y(2.84)	**91**	Y(2.86)
12	N(1.13)	**32**	N(1.52)	**52**	N(1.35)	**72**	Y(2.99)	**92**	Y(2.98)
13	N(1.27)	**33**	N(1.06)	**53**	N(1.17)	**73**	N(1.19)	**93**	Y(2.89)
14	N(1.69)	**34**	N(1.06)	**54**	N(1.07)	**74**	N(1.59)	**94**	N(1.25)
15	N(1.40)	**35**	N(1.10)	**55**	N(1.01)	**75**	Y(2.31)	**95**	Y(2.96)
16	N(1.20)	**36**	Y(2.45)	**56**	N(1.00)	**76**	Y(2.35)	**96**	Y(2.78)
17	N(1.18)	**37**	N(1.67)	**57**	N(1.03)	**77**	Y(2.86)	**97**	Y(2.82)
18	N(1.14)	**38**	N(1.00)	**58**	Y(2.48)	**78**	Y(2.98)	**98**	Y(2.82)
19	N(1.13)	**39**	N(1.00)	**59**	N(1.19)	**79**	Y(2.82)	**99**	N(1.40)
20	N(1.06)	**40**	N(1.24)	**60**	N(1.34)	**80**	Y(2.99)	**100**	N(1.43)

CONCLUSIONS

Relying on several Anhui's typical highway sections of cement concrete pavement, the GPR investigation results of the void beneath these pavement slabs are utilized as the basis and extension evaluation is adopted to process the test data of FWD multi-level load deflection test. By building the comprehensive index system, setting the void classification scientifically and determining the indexes' classical domains, section domains as well as weight coefficients properly, an improved void recognition method can be established scientifically. The main conclusions are as follows:

(1) Three technical indexes, the maximum deflection at the slab corner, the slope of the relationship curve and the curve's intercept, are selected into the index system of the improved method. Calculated by this improved method, the void ratio of the typical highway sections is 33%, approximately to the detection result of GPR (35%).

(2) In the improved method, under the status of "ambiguous void", the classical domain of the maximum deflection at the slab corner is 160~240μm, the classical domain of the slope of the relationship curve is 4~4.2μm/kN, and the classical domain of the curve's intercept is 42~50μm; meanwhile, the section domain of the maximum deflection at the slab corner is 60~350μm, the section domain of the slope of the relationship curve is 1.2~5.6μm/kN, and the section domain of the curve's intercept is 0~100μm. The weight coefficients of these three technical indexes are 0.35, 0.3, and 0.35 respectively.

(3) Comparing to the investigation results of GPR, this method's recognition ratio is 88.6% and the corresponding misjudgment ratio is 6.1%. The superior accuracy of void recognition shows that the improved method is able to satisfy the demands of

engineering detection, recognition and structural evaluation.

REFERENCES

Desh Raj Sonyok, Jie Zhang (2008). "Ground Penetration Radar for Highway Infrastructure Condition Diagnostics: Overview of Current Applications and Future Development." *Proceedings of TRB 2008 Annual Meeting*. TRB, National Research Council, Washington D.C., USA, 2008.1.

Geng Yuling, Jia Xuemin (2007). "Research on ground penetrating radar technology in nondestructive testing of highway pavement." *Beijing*: *Earthquake Press*.

Imad, L., Al-Qadi, Samer Lahouar, Kun Jiang, Kevin, M. McGhee, and David Mokarem (2005). "Validation of Ground Penetration Radar Accuracy for Estimating Pavement Layer Thicknesses." *Proceedings of TRB 2005 Annual Meeting*. TRB, National Research Council, Washington D.C., USA, 2005.1.

Jiang Hong and Wang Xuancang (2010). "Signal analysis and processing for detecting void phenomenon under concrete pavement by using ground penetrating radar." *Journal of Highway and Transportation Research and Development*, 27(1): 22-27.

Leng, Z., I.L., Al-Qadi, J. Baek, and S. Lahouar (2009). "Selection of Antenna Type and Frequency for Pavement Surveys Using Ground Penetrating Radar." *Proceedings of TRB 2009 Annual Meeting*. TRB, National Research Council, Washington D.C., USA, 2009.1.

Liang Xinzheng (2008). "Study on identification of void beneath cement concrete slab and its engineering application." *Modern Transportation Technology*, 5(3): 1-4.

Ling Jianming, Hao Hangcheng, Lv Lixuan (2008). "Extension assessment method applying to pavement performance." *Journal of Tongji University*, 36(1): 32-36.

Qiang Li, Kelvin,C.P. Wang (2008). "Pavement performance evaluation and prediction based on extension theory." *Proceedings of TRB 2008 Annual Meeting*. TRB, National Research Council, Washington D.C., USA, 2008.1.

Tan Zhiming, Zhou Yumin (2010). "Mechanistic model of double-layered concrete pavement structures with unequal planar dimensions." *Engineering Mechanics*, Vol. 27(3): 132-137.

Zhou Yumin, Tan Zhiming (2010). "Analysis of near-corner stresses in concrete pavement structure." *Engineering Mechanics*, 27(3): 105-110.

Self-Compacting Concrete Reinforced by Waste Tyre Rubber Particle and Emulsified Asphalt

Guangcheng Long[1], Kunlin Ma[2], Zhe Li[3] and Youjun Xie[4]

[1]Professor, School of Civil Engineering, Central South University, Changsha 410075, China; email: scc2005@csu.edu.cn
[2]Lecturer, School of Civil Engineering, Central South University, Changsha 410075,China; email: mark-mkl@163.com;
[3]Assistant researcher, School of Civil Engineering, Central South University, Changsha 410075, China;
[4]Professor, School of Civil Engineering, Central South University, Changsha 410075, China; email: yjxie2007@163.com.

ABSTRACT: For the sake of developing new cementitious materials with high toughness and excellent workability, an extensive research programme was set up to investigate the properties of self-compacting concrete(SCC) with waste tyre rubber particles and emulsified asphalt in fresh state and hardened state. The effects of rubber particles and emulsified asphalt on strength, dynamic elastic modulus, stress-strain response and impact toughness of hardened SCC were analyzed in detail. Results indicate that rubber particle and emulsified asphalt remarkably influence mechanical properties of SCC. Incorporating rubber particles together with emulsified asphalt is conducive to improve self-compactability of fresh SCC. The strain capability and toughness of SCC can be greatly enhanced by addition of rubber particle and emulsified asphalt. A combination of rubber particles and emulsified asphalt is an effective way to prepare new self-compacting concrete with excellent dynamic mechanical properties.

INTRODUCTION

It is well known that traditional cement concrete show poor dynamic mechanical properties especially bad toughness, which hinders its application in bending structural element or dynamic loading domain in practice. For the sake of overcoming the shortage of high brittleness of traditional concrete and further satisfying the requirements of actual engineering structures, a considerable amount of research work have been devoted over the last several decades to make concrete more robust in toughness and resistance to cracking. Some new type concretes with more higher toughness compared

to traditional concrete, such as fiber reinforced concrete and polymer modified concrete, were developed(Bentur, 2008; Xu, 2008; Joshua, 1997). In recent decades, extensive research projects were carried out on rubberized concrete by use of massive stockpile waste tyre rubber particles to improve some certain properties of traditional concrete and self-compacting concrete(Najim, 2010; Bignozzi, 2006; Turatsinze,2008; Topcu,2009). Waste tyre rubber particles can stably exist in alkaline environment of cement paste and has positive effect in improving the deformation capability, damping and toughness of concrete as well as the resistance to cracking (Aiello, 2010; Segre, 2000; Liu, 2009; Najim, 2012; Reda Taha, 2008; Turatsinze, 2008; zheng, 2008). Due to the hydrophobic property and large deformation characteristics of waste tyre rubber particle, the interfacial transition zone microstructure between paste and rubber particle is poor(Turki, 2009). And the compressive strength of concrete significantly decreases with the increasing amount of rubber(Aiello, 2010; Liu, 2009; Reda Taha, 2008). Huang et al. gave some interesting suggestions for improving strength of rubberized concrete by using a modifying composite materials model and finite element analysis method(Huang, 2004). Li reported that rubberized self-compacting concrete has a higher compressive strength, compared to rubberized traditional vibrated concrete, resulting from a better interface microstructure between rubber aggregate and hardened paste owing to the reduction of local liquidisation by eliminating vibrating (Li, 2012). Rubberized self-compacting concrete appears very attractive potential in civil engineering (Najim, 2010; Bignozzi, 2006)

In order to expand the current research knowledge-based on enhancing mechanical properties of concrete by use of waste tyre rubber particles, in present paper an extensive research programme was designed to investigate the effect of a combination of waste tyre rubber particle and emulsified asphalt on properties of self-compacting concrete(SCC) in fresh state and hardened state.

EXPERIMENTAL

Raw Materials

In present experimental program, raw materials used include ordinary Portland cement, fly ash, silica fume, aggregates and etc. The ordinary Portland cement (C) is similar to ASTM Type I cement. The cement satisfies the Chinese Standards (GB175-1999) and was manufactured by Ningxiang Cement Plant, Hunan Province, China. Class F fly ash (FA) employed in this experiment was produced by Xiangtan Power Plant of Hunan Province. Silica fume (SF) is the product of Shanghai Elkem Company. Table 1 listed the chemical compositions, Blain finenesses, and density for the C, FA and SF.

Crushed limestone (CS) and natural river sand(S) were used as coarse and fine aggregates, respectively. Maximum aggregate size of coarse aggregate is 16mm, and its crushed index is 7.8%. The fine aggregates with a fineness modulus of 2.51 came from the Xiangjiang River. Waste tyre rubber particle(R) was produced by Wuhan Hedeli Company. The size of rubber particle is 5~8 mesh and its apparent density of rubber

particle is 1.03g/cm^3. Emulsified asphalt (EA) was provided by Guangdong Nanyue Logistics Group and its basic properties were shown in Table 2.

An polyocarboxy acid superplasticizer(SP) with a water-reducing ratio of 30% was produced by Wuhan Ge-ruilin Building Materials Technology Ltd. The SP complies with the Chinese National Standard-Concrete admixtures(GB8076-2008) (Chinese National Standard, 2008). The drinkable tap water was used as mixing water (W).

Table 1. Chemical and physical properties of cement, fly ash and silica fume

Compositions / Items	SiO_2	Al_2O_3	Fe_2O_3	CaO	MgO	SO_3	IL	Blain fineness (m^2/kg)	Density (kg/m^3)
Cement(C)	24.6	7.3	4.0	60.7	3.8	2.5	2.2	350	3100
Fly ash (FA)	52.7	25.8	9.7	3.7	1.2	0.2	3.0	460	2350
Silica fume(SF)	90.6	0.6	1.5	0.3	0.6	1.3	1.8	17800	2120

Table 2. Properties of emulsified asphalt

EN Viscosity at 25^0C	Residual/% by mass	Pin-penetration depth at 25^0C (100g)	Softening point (ring method)	Stability for storage (1-day, 25^0C)
6	60.5	68	56^0C	0.6

Mixing, Curing and Preparation of Specimens

For the sake of obtaining good workability in fresh state, fly ash and silica fume as well as an polyocarboxy acid superplasticizers were used to prepare SCC. The effect of replacement volume of sand by rubber particle on properties of SCC as well as the combination of rubber particles and emulsified asphalt was investigated in this experiment. Nine concrete mixtures, with the mixing proportions shown in Table 3, were designed.

Each mixture was mixed by a forced mixer with 60l volume. After mixing, the workability of fresh self-compacting concrete including slump flow (*sf*), T_{50} time and visual stability index was evaluated. The slump flow and T_{50} for all mixtures keeps within a range of 650±30mm and 3~5s, respectively. The tested value of slump flow, T_{50} time and visual stability index of fresh concrete were shown in Table 3. Concrete specimen with sizes of 150mm×150mm×150mm for compressive strength test, 100mm×100mm×300mm for stress-strain curve test and Φ150mm×65mm for impact test were moulded. And then, the specimen were demould at 1-day after casting and were cured in fog room with a temperature of (20±2)℃ and more than 90% relative

humidity until 28-day age.

Table 3. Mixing proportions of SCC samples and corresponding workability

Serials	Raw materials / kg/m^3									workability		
	C	FA	SF	W	SP	CS	S	R	EA	*sf* /mm	T_{50} /s	Stability index
SCCR-0	386	134	16	200	4.3	795	795	0	0	630	3.75	0
SCCR-5	386	134	16	200	4.3	795	756	15	0	640	4.06	0
SCCR-10	386	134	16	200	4.3	795	716	30	0	625	4.30	0
SCCR-15	386	134	16	200	4.3	795	676	45	0	620	4.55	0
SCCR-20	386	134	16	200	4.7	795	636	60	0	655	3.29	1
SCCR-25	386	134	16	200	4.7	795	597	75	0	645	3.81	1
SCCR-15-EA1	386	134	16	194	4.3	795	676	45	16.1	630	3.95	0
SCCR-15-EA2	386	134	16	189	4.3	795	676	45	26.8	635	3.80	0
SCCR-15-EA3	386	134	16	177	4.3	795	676	45	53.6	660	3.84	1

Testing Methods

The workability parameters including slump flow, T_{50} time and visual stability index of fresh SCC was measured according to *Standard Test Method for Slump Flow of Self-Consolidating Concrete* (ASTM C1611/C1611M, including appendix). The mechanical strength and stress-strain curve of SCC samples was tested according to *Chinese standard for experimental method of mechanical properties of ordinary concrete* (GB/T50081-2002) by use of MTS experimental system. The ultrasonic wave velocity and dynamic elastic modulus of concrete sample were obtained by use of ultrasonic method. And the dynamic elastic modulus can be calculated in light of equation (1) as following:

$$E_d = \rho V^2 \frac{(1+\upsilon)(1-2\upsilon)}{(1-\upsilon)} \qquad (1)$$

Where: ρ——apparent density of concrete, kg/m^3;

V——ultrasonic wave velocity, m/s;

υ——Possion ratio, it was assumed to 0.2 in this study. Slight variation of Poisson's ratio of concrete sample was neglected.

Impact toughness of concrete was measured by use of drop hammer method according to American Concrete Institute standard (ACI-544).The detailed impact experimental method of concrete was shown in Fig. 1. The impact numbers were recorded when sample occurred first crack (denoted as initial crack) and failure (named

as final crack), respectively. The impact energy of sample can be obtained according to equation (2). The average of results of six samples was taken as the final result.

$$w=n\times mgh \quad (2)$$

Where, w — impact energy, J;
n — impact number;
h — the height hammer drops , 457mm;
g — accelerating velocity, 9.81m/s^2;
m — weight of hammer, 4.5kg .

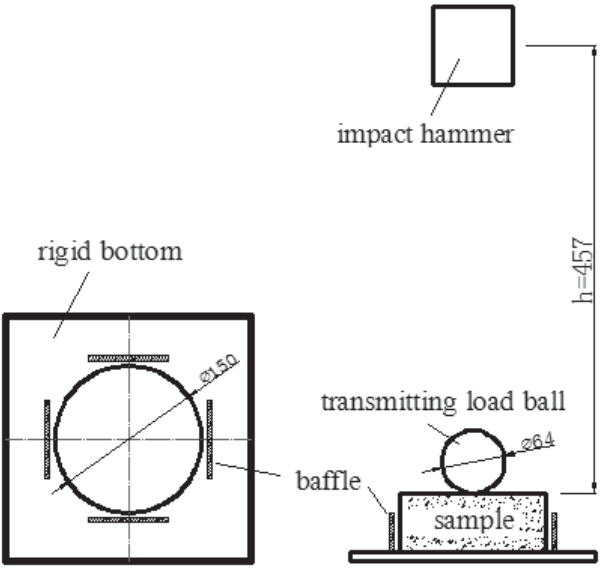

Fig.1.Schematic diagram of concrete impact experimental setup.

RESULTS AND DISCUSSION

Workability of Fresh SCC

Fresh SCC requires enough flowability and high viscosity, which is essential to ensure good filling ability and excellent stability in formwork during placing process. It can be found that, from the result shown in Table3, SCC with rubber particle and/or EA has good workability. And the visual stability for each fresh SCC mixture was observed very well. At relatively low replacement level of rubber particle, the workability of fresh self-compacting concrete almost keeps constant. And when the replacement of sand by

rubber particle is up to 60kg/m^3 (see serial SCCR-20) or more, a slightly more superplasticizer (about 10%) is needed to keep the similar workability, compared to self-compacting concrete without rubber particle. However, the fresh SCC with a combination of rubber particle and EA shows an excellent flowability and a good stability.

Compressive Strength of Hardened SCC

The compressive strength of hardened SCC with different contents of rubber particles and emulsified asphalt were shown in Fig.2. From the results shown in Fig.2, one can find that the compressive strength of SCC decreases with the increasing content of rubber particle. The compressive strength of SCC decreases by 5% to 26% when sand of 5% to 25% volume was replaced by rubber particle, compared to SCC without rubber particle. And there is a close linear relationship between the replacement volume of rubber particle and the variation of compressive strength of SCC. As for the samples with 45kg/m^3 rubber particle and 16.1kg/m^3 up to 56.3kg/m^3 EA, one can also find that the compressive strength of SCC reduces slightly with the increasing content of EA. Results indicate that the addition of rubber particles and EA both decrease the compressive strength of SCC sample. The rubber particle has high deformation like as "soft inclusion"(Reda Taha, 2008) which is responsible for the reduction of compressive strength of SCC. However, in this investigated area, the reduction of compressive strength of sample is not remarkable. When the replacement level of sand by rubber particle is no more than 10% in volume, the reduction in compressive strength of SCC samples is less 15%.

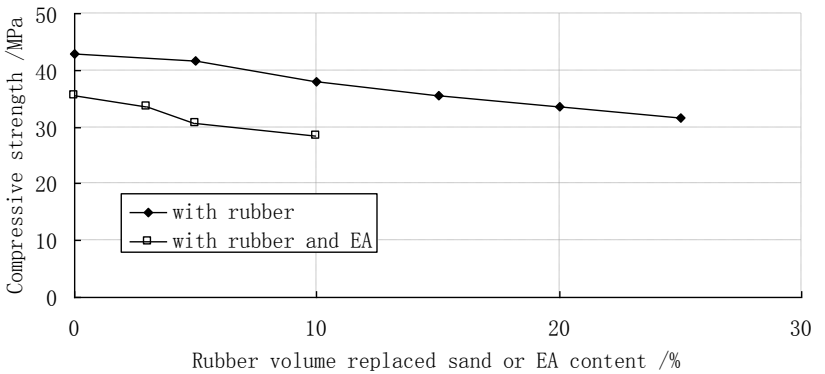

Fig. 2.Compressive strength of hardened SCCs with rubber particles and EA at 28-

day age.

Ultrasonic Velosity and Dynamic Elastic Modulus of Hardened SCC

The values of ultrasonic velocity and dynamic modulus of elasticity for SCC with rubber particle and/or EA were given in Fig.3 and Fig.4, respectively. The dynamic elastic modulus of SCC was determined by ultrasonic wave method. Each point on the graph was the average of at least three replicate specimens.

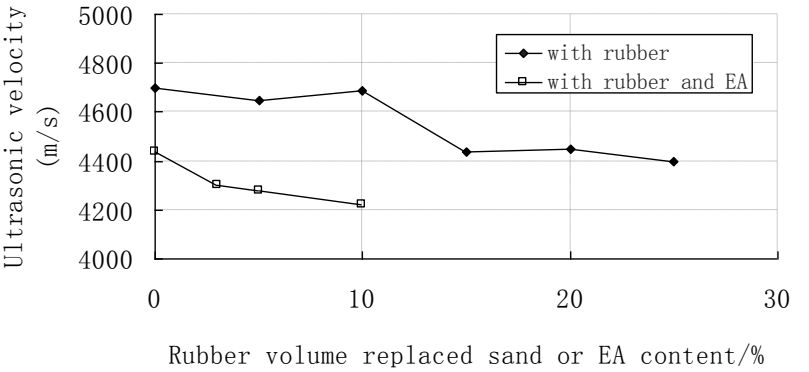

Fig. 3.Ultrasonic velocity of SCCs with rubber particles and EA at 28-day age.

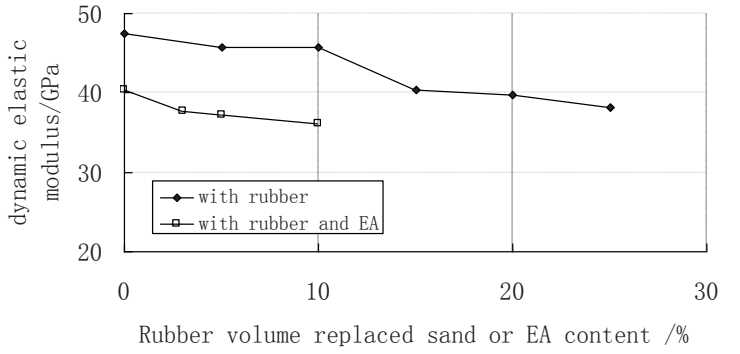

Fig. 4.Dynamic elastic modulus of SCCs with rubber particles and EA at 28-day age.

From the result given in Fig.3, it can be found that the ultrasonic velocity of SCC

samples decreases with the increasing replacement volume of rubber and EA content. This means that the ability of absorbing energy of SCC was enhanced by adding the rubber and EA. As demonstrated in Fig.4, the value of dynamic elastic modulus of the rubberized SCC decreases gradually with the increase of rubber content. For the concrete only with rubber particle the decrease in dynamic elastic modulus is from 3.8% to 19.5% as the replacement volume of sand by rubber particle increased from 5% to 25%, compared to SCC without rubber. Similar result was reported by Turatsinze et al. (Turatsinze, 2008). Meanwhile, SCC both with rubber particle and EA has lower dynamic elastic modulus compared to samples only with rubber particle. The dynamic elastic modulus for SCC with 45kg/m^3 rubber and 16.1 kg/m^3 or 26.8kg/m^3 EA is lower than that of SCC with 60 kg/m^3 or 75kg/m^3 rubber, respectively. The low elastic modulus of rubber particle and asphalt polymer film layer formed in hardened matrix is responsible for the reduction of the dynamic elastic modulus of SCC incorporating with rubber and EA.

Stress-Strain Response of Hardened SCC

The uniaxial comression test was carried out to obtain the stress-strain curves of different SCCs with tire rubber particles and/or EA. During the test process, it can be observed that the failure model of SCC with rubber particle and EA is obviously different from SCC specimen without rubber or EA. SCC with rubber and EA shows an obviously high ductility.

The stress–strain curves of different SCCs in the investigated area were shown in Fig. 5. The stress-strain curves tested indicate that the behavior of SCC with rubber particle and/or EA is more nonlinear compared to that of SCC without rubber, implying a different failure type for SCC with waste tire rubber and/or EA. The stress-strain curves of rubberized SCCs show two distinct regions: a linear region up to 40% of the fracture load followed by a nonlinear ascending region up to the peak. The nonlinear descending portion of the stress-strain curve is observed in SCC specimens with relative high rubber particles and/or EA content. After the peak load, the deformations of these specimens are significantly larger than that of SCC without rubber particles or with less rubber. Moreover, one can also find that the peak strain corresponding to peak stress of SCC with rubber and/or EA is much larger compared to SCC without rubber. The presence of rubber particle was expected to act like a hole at the crack tip and thus to decrease the tip sharpness of the first micro-crack, resulting in stress relaxation and ultimately slowing down the kinetics of the first micro-crack's propagation. Such a mechanism is expected to delay micro-crack coalescence and the resulting macro-crack localization and to increase the deformation where the stress-strain curve begins to fall in the post peak zone(Turatsinze, 2008; Reda Taha,2008).

In order to further analyze the effect of rubber particles and EA on toughness of SCC, mathematical method was employed to establish stress-strain constitutive relationship for different SCCs with rubber particles and/or EA based on Guo model (Guo, 1997). The corresponding fitting parameters were shown in Table 4 for each SCC

sample, including peak stress σ_c and peak strain ε_c , residual stress σ_3 and strain ε_3 ($\varepsilon_3=3\varepsilon_c$), residual stress to peak stress ratio σ_3/σ_c and compression toughness index *a* and *p*.

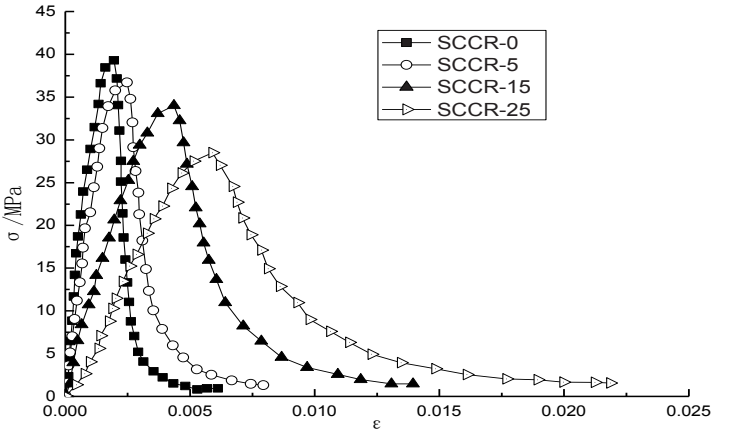

(a) samples with rubber

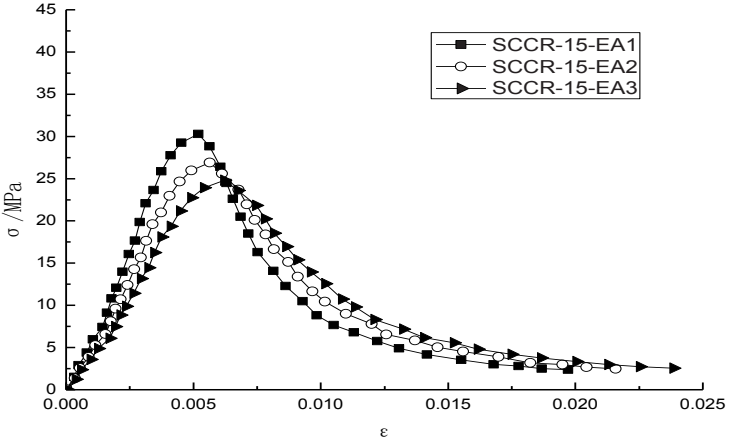

(b) samples with rubber and EA

Fig.5.Stress-strain curve of SCCs with rubber particles and EA at 28-day age.

Table 4. Fitting parameters of stress-strain curves for different SCCs

serials	σ_c/MPa	ε_c	a	p	σ_3/MPa	σ_3/σ_c
SCCR-0	39.3	0.00195	2.001782	32.62385	0.95	0.02417
SCCR-5	36.7	0.00248	1.731645	17.85374	1.47	0.04005
SCCR-15	34.0	0.00436	1.205043	12.36517	1.48	0.05181
SCCR-25	28.5	0.00590	0.817167	8.54813	2.05	0.07193
SCCR-15-EA1	30.3	0.00519	0.703172	5.39802	3.54	0.11683
SCCR-15-EA2	26.9	0.00564	0.657265	4.27374	3.90	0.14498
SCCR-15-EA3	24.8	0.00622	0.628039	4.02731	3.76	0.15161

From the results shown in Table 4, it can be quantitatively found that the characteristic parameters of stress-strain curve of SCC with rubbers and/or EA are different from each other. The peak stress of curve decreases with the increasing rubber content while its peak strain and residual stress remarkably increase with the increasing rubber content. At the same time, one can further see that the compression toughness index *p* of SCC obviously decreases with the increasing rubber particle, especially after incorporating EA. That is to say the toughness of SCC can be significantly improved by adding rubber particles or EA. It is worth noting that a combination of rubber particle and EA will further greatly increase the peak strain, residual stress and toughness of SCC.

Impact Toughness of SCC

Fig. 6 gave the effect of different replacement levels of waste tire rubber particles and EA on the impact energy at initial crack (the first crack occurrence) and final crack (failure state) of samples measured through the impact test discussed above, respectively. It can be observed that, from the result shown in Fig.6, increasing the replacement level of sand with rubber particles noticeably improves the impact strength of the SCC in investigated area. This pattern of energy absorption in relation to the tire rubber particles content indicates the energy absorption of concrete matrix and rubber particle. The low stiffness of the tire particles allowed the rubber-cement composite to have a relatively high flexibility and thus absorb a considerable amount of energy higher than that absorbed by normal concrete without rubber or EA. Meanwhile, it is worth noting that at each replacement level of rubber, the impact energy of SCC at final crack is slightly higher than that of at initial crack. Similar behavior was observed for SCC incorporating 45kg/m^3 tire rubber particles and different contents of EA. Moreover, the impact resistance of SCC with rubber particle and EA is higher compared to SCC only with rubber particle. The ability of the tire rubber particles and EA to enhance the ductility and strain capacity of concrete is as indicators of energy absorption of SCC.

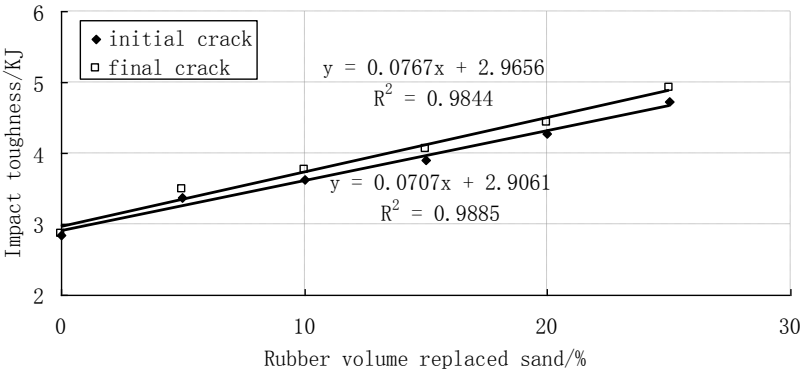

(a) samples with rubber

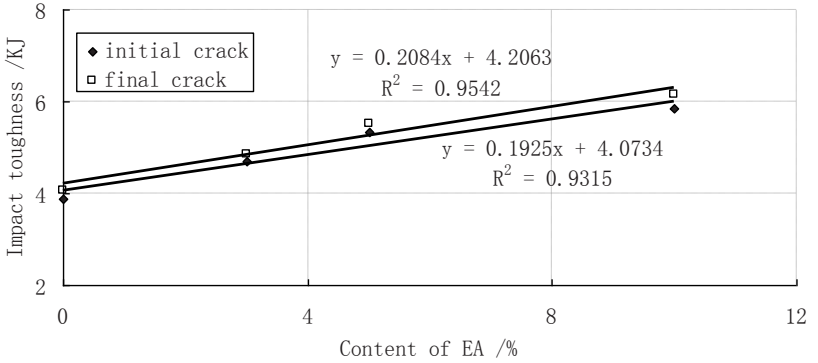

(b) samples with rubber and EA

Fig. 6 Impact toughness of SCCs with rubber particle or EA at 28-day age.

CONCLUSIONS

The use of tire rubber particles as aggregate in cement concrete not only could release the increasingly serious environmental problems presented by waste tires, but

also shows promising results in producing a new type of concrete by using the high deformation of rubber particle. This study has exclusively focused on self-compacting concrete reinforced by rubber particles and emulsified asphalt. Based on above studies, the following conclusions can be drawn:

(1) Fresh self-compacting concrete with a combination of rubber particle and EA has high flowability and good viscosity when the dosage of superplasticizer and unit water content is similar to that of control self-compacting concrete without rubber or EA.

(2) The compressive strength of SCC decreases with the increasing replacement volume of sand by rubber particle or with the increasing EA content. The compressive strength of SCC with rubber and EA is almost similar to that of SCC only with rubber of the same amount as former (including rubber and EA).

(3) The ultrasonic velocity and dynamic elastic modulus of SCC decreases with the increase of rubber or EA content in mixture. However, Adding rubber together with EA will cause more reduction in ultrasonic velocity and dynamic property of SCC than only adding rubber of same amount as former.

(4) The peak strain and toughness (including impact toughness) of SCC noticeably increases by using rubber replaced sand. Compared to sample only with rubber, SCC with rubber and EA has larger peak strain and higher toughness. A combination of rubber particle and EA will further greatly increase the deformation capability and toughness of SCC.

Further research is needed to address the interaction between rubber particle and EA in mixture and the corresponding effect on SCC by the microstructure investigation.

ACKNOWLEDGMENTS

Authors appreciate the financial support from National Science Fund Committee (51178467) and Ministry of Education of China(NCET-10-0839).

REFERENCES

Aiello, M.A. and Leuzzi, F. (2010). “Waste tyre rubberized concrete: Properties at fresh and hardened state”. *Waste Management*, Vol.30(8-9): 1696–1704.

Bentur Arnon and Mindess Sidey(2007). “Fiber reinforced cementitious composites.”(I) (second edition). London: Taylor & Francis Group, 2007, pp1-10.

Bignozzi, M.C. and Sandrolini, F. (2006). “Tyre rubber waste recycling in self-compacting concrete.”*Cement and Concrete Research* , Vol. 36(4): 735−739.

Chinese National Standard (2008) *Concrete admixtures* (GB8076-2008).

Guo Zhenhai. (1997). “Concrete strength and deformation—experimental basis and constitute relationship.” Beijing: Tsinghua University press *(Chinese)*.

Huang Baoshan, Li Guoqiang, Pang Su-Seng, et al. (2004). “Investigation into waste tire rubber filled concrete”. *Journal of Materials in Civil Engineering*, Vol. 16(3):187–

94.
Joshua,B.K.(1997). “Polymer-modified concrete review”. *Journal of Materials in Civil Engineering,* Vol.9 (5) : 85~92.
Li Zhe. (2012). “Study on self-compacting concrete with rubber aggregate*”*. Changsha: Central South University Thesis *(Chinese)*.
Liu Rixin, Hou Wenshun and Xu Yonghong, et al. (2009). “Effect of Crumb Rubber on the Mechanical Properties of Concrete.”*Journal of Building Materials*, Vol. 12(3):341-344. (*Chinese*)
Najim, K.B. and Hall, M.R.(2010). “A review of the fresh/hardened properties and applications for plain- (PRC) and self-compacting rubberized concrete (SCRC).” *Construction and Building Materials*, Vol. 24(11): 2043–2051.
Najim,K.B. and Hall Matthew,R. (2012). “Mechanical and dynamic properties of self-compacting crumb rubber modified concrete.” *Construction and Building Materials*, Vol. 27(1): 521–530.
Reda Taha,M.M., El-Dieb, A.S. and Abd El-Wahab, M.A. et al. (2008). “Mechanical, Fracture, and Microstructural Investigations of Rubber Concrete.” *Journal of Materials in Civil Engineering*, Vol. 20(10):640-648.
Segre, N. and Joekes I. (2000). “Use of tire rubber particles as addition to cement paste.”*Cement Concrete Research*, Vol. 30(9):1421–1425.
Turki,M., Bretagne,E. and Rouis,M.J., et al. (2009). “Microstructure, physical and mechanical properties of mortar–rubber aggregates mixtures.” *Construction and Building Materials*, Vol. 23(7): 2715–2722.
Turatsinze ,A. and Garros, M. (2008). “On the modulus of elasticity and strain capacity of self-compacting concrete incorporating rubber aggregates.” *Resour Conserv Recycl*, Vol. 52(10) :1209–1215.
Topcu, IB. and Bilir, T. (2009). “Experimental investigation of some fresh and hardened properties of rubberized self-compacting concrete.”*Mater Des,* Vol. 30(8):3056-3065.
Xu Shilang and Li Hedong. (2008). “A review on the development of research and application of ultra-high toughness cementitious composites.”*China Civil Engineering Journal*, Vol. 41(6):45~60. (*Chinese*).
Zheng, L., Sharon, H.X. and Yuan,Y. (2008). “Experimental investigation on dynamic properties of rubberized concrete.” *Construction and Building Materials*, Vol. 22(5):939–47.

Research on the Numerical Simulation Analysis ofSlope Stability under Rainfall Infiltration

Zhou Wei[1], Huang Xiaoming[2] and Xue Yanqing[3]

[1]Ph.D. Candidate, School of Transportation, Southeast University, Sipailou 2, Nanjing 210096, China; email: lygzhouw@126.com
[2]Professor, School of Transportation, Southeast University, Sipailou 2, Nanjing 210096, China; email: huangxm@seu.edu.cn
[3]Ph.D. Candidate, School of Transportation, Southeast University, Sipailou 2, Nanjing 210096, China; email: 494961575@qq.com

ABSTRACT: Based on the *FLAC*^{3D} software, this paper is devoted to researching on the numerical simulation analysis of slope stability under rainfall infiltration. Based on the shear strength and seepage of unsaturated soils, it should add matric suction and soil-water characteristic curve to *FLAC*^{3D}. So in this way *FLAC*^{3D} can be applied to the field of saturated-unsaturated seepage. Simulation analysis of the seepage of the slope and the change of security variation in the condition of rainfall can be done. It achieved the hazardous area of slope after rainfall and put forward the concept of "small slip failure occurred in the toe of slope". And in this paper, the relationship between coefficient of permeability, rainfall duration, rainfall intensity, slope height, slope and slope stability after the rainfall was researched by the written procedures l. This paper provides a basis for stability analysis of unsaturated soil slopes under rainfall infiltration.

INTRODUCTION

Our country has a vast territory and varied topography. During the process of highway construction there are a large quantity of slope engineering, which requires higher security and usability. However at present, the situations of highway slope disaster have become more and more serious. The slope deformation and instability caused by rainfall is a common geological disaster. It has been researched through experiments and theoretical analysis by many researchers (Brand, 1984; Ranardjo, 2007; Chen, 2009).

With the development of computer technology, more and more computer simulation softwares have been used in engineering. Because of the visualization technology used by modern simulation software, the result of the simulation is easy to be analyzed. Many researchers have used finite element software such as *ABAQUS*

or *ANASYS* to research on the slope stability and disaster simulation. $FLAC^{3D}$ is analysis software developed by ITASCA. It is good at simulating the mechanical characteristics of damage or plastic flow when the geological materials in the strength limit or yield limit. And it is adept at simulating instability and large deformation. So it is accomplished in analyzing the slope disaster. Based on the character of unsaturated soil, the percolation and slope safety models were modified to simulate slope stability under rainfall infiltration; and the relationship between coefficient of permeability, rainfall duration, rainfall intensity, slope height, slope and slope stability was researched.

THEORY AND METHOD

Slope Rainwater Infiltration

The percolation model should be used to simulate the slope rainwater infiltration. Unfortunately, two phase flow cannot be simulated in $FLAC^{3D}$. It is postulated that pore pressure above groundwater level is zero, and the function of gas is not be considered. The approximate method is only applicable to simulate the saturated material which capillarity is ignored. But the most of subgrade soil are unsaturated. Therefore, the percolation model in $FLAC^{3D}$ should be modified in order to be used in unsaturated soil.

In the classical saturated soil mechanics, the flow of water in a saturated soil is commonly described using Darcy' law. Darcy's law also applies for the flow of water through an unsaturated soil. However, the coefficient of permeability in an unsaturated soil cannot generally be assumed to be constant. Rather, the coefficient of permeability is a variable which is predominantly a function of the water content or the matric suction of the unsaturated soil (Fredlund, 1993).

The coefficient of permeability can be determined by direct or indirect ways. Direct measurements of permeability can be performed either in the laboratory or the in the field. The indirect method can be performed using either the matric suction versus degree of saturation curve or the soil-water characteristic curve.

Coefficient of permeability functions obtained from the matric suction versus degree of saturation curve have been proposed by Burdine (1952) and Brooks and Corey (1964). The most classical prediction function was proposed by Marshall (1958), Millington and Quirk (1959) based on the soil-water characteristic curve. The volumetric water content, θ_w, can be plotted as a function of matric suction, $(u_a - u_w)$, and the plot is called the soil-water characteristic curve as shown in Fig. 1. Therefore, the permeability function, $k_w(\theta_w)$, can also be expressed in terms of matric suction. In other words, the oil-water characteristics curve can be visualized as an indication of the conFig.uration of water-filled pores. The coefficient of permeability is obtained by dividing the soil-water characteristic curve into "m" equal intervals along the volumetric water content axis. The matric suction corresponding to the midpoint of each interval is used to calculate the coefficient of permeability.

$$k_w(\theta_w)_i = \frac{k_s}{k_{se}} \frac{T_s^2 \rho_w g}{2\mu_w} \frac{\theta_s^p}{N^2} \sum_{j=1}^{m} \left\{ (2j+1-2i)(u_a - u_w)_j^{-2} \right\} \qquad i = 1,2,\ldots, \mathrm{m} \quad (1)$$

Where:

$k_w(\theta_w)_i$: calculated water coefficient of permeability (m/s) for a specified volumetric water content, corresponding to the i th interval;

k_s : measured saturated coefficient of permeability (m/s);

k_{sc} : calculated saturated coefficient of permeability (m/s);

T_s : surface tension of water (kN/m);

ρ_w : water density (kg/m^3);

g : gravitational acceleration (m/s^2);

μ_w : absolute viscosity of water (N·s/m^2);

θ_s : volumetric water content at saturation;

p : a constant which accounts for the interaction of pores of various sizes, which can be assumed to be equal to 2.0;

$(u_a - u_w)_j$: matric suction (kPa) corresponding to the midpoint of the j th interval.

The coefficient of permeability, k_w, at a specific volumetric water content, θ_w, is computed directly from Formula 1. The permeability function, $k_w(\theta_w)$, can be written as follows:

$$k_w(\theta_w)_i = \frac{k_s}{k_{se}} A_d \sum_{j=1}^{m} \left\{ (2j+1-2i)(u_a - u_w)_j^{-2} \right\} \qquad i = 1,2,\ldots, \mathrm{m} \quad (2)$$

Where: A_d is adjusting constant.

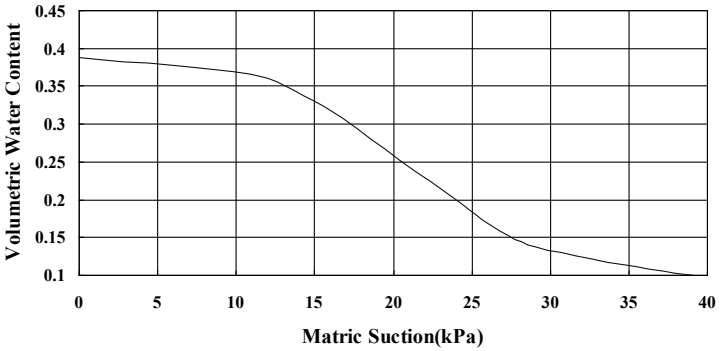

FIG. 1. Soil-water characteristic curve.

Darcy's law applied for the percolation model in *FLAC*^{3D} (2003). Therefore, the percolation model in *FLAC*^{3D} could be modified in order to be used in unsaturated soil by searching cell method. The procedure used in *FLAC*^{3D} based on FISH was as

follows. First, the pore pressure of every cell was gained by searching cell method and the matric suction could be calculated from pore pressure. Then, the coefficient of permeability could be calculated from prediction function (Formula 1) was proposed by Marshall, Millington and Quirk based on the soil-water characteristic curve. Finally, the new coefficient of permeability of each cell was assigned to each cell by searching cell method. The procedure was performed every time-step in order to modify the percolation mode constantly.

Fig. 2 showed the model and the initial pore pressure nephogram. The height was 10m and the slope was 1:1.5. It made up of 1312 nodes and 600 cells. The pore pressure under water table was shown as positive pressure gradient by hydrostatic pressure. The negative pore pressure from water table to 2m water table above was shown as a quadratic function. The negative pore pressure from 2m water table above to the top of the slope was -50kPa. Because of the pavement laid upon the top of the slope, the density of the pavement was 2500kg/m^3 and the thickness was 50cm. So, it was postulated that a uniform load about 12.5kPa loaded on the top of the slope. It was postulated that the pavement was impermeable; the rainwater fall on the road would flow away from the road to the bottom of the slope.

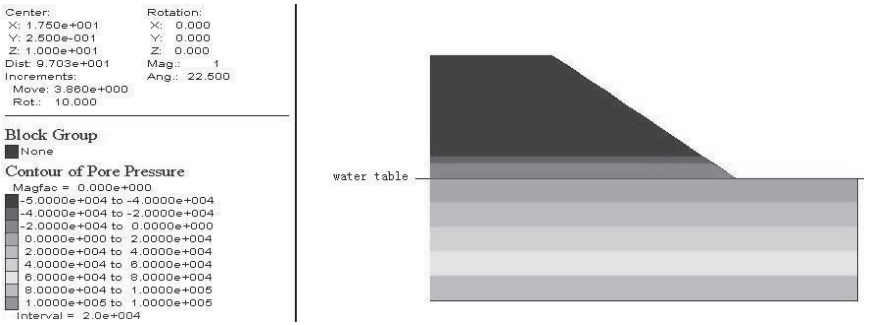

FIG.. 2. Model and the initial pore pressure nephogram.

In order to analyze the change law of seepage field under rainfall infiltration, the boundary condition was set as follows:

(1) The right and left sides of the model: leaky boundary was set bellow the water table, given pore pressure boundary was set above the water table;

(2) Slope and ground: the leaky or given pore pressure boundary was set on the slope and the ground. If the rainfall intensity was less than the permeability, the leaky boundary was set; the flow of infiltration was equal with rainfall intensity. Otherwise, a water film was formed on the slope and ground, then the given pore pressure was set.

(3) The bottom of the model: impermeable boundary

The annual rainfall of a region was about 1200mm/year. The relationship between rainfall duration and rainfall intensity at different repetition period of

rainfall are given in Table 1.

A hundred-year return period heavy rainfall was chosen to be simulated. The rainfall duration was 12h and the rainfall intensity was 23.7mm/h (6.58×10^{-6}m/s).

Table 1. Relationship Between Rainfall Duration and Rainfall Intensity at Different Repetition Period of Rainfall

	The Relationship Between Rainfall Duration(mm) and Rainfall Intensity(h)					
Repetition Period of Rainfall (year)	1	2	3	6	12	24
100	135.2	83.0	62.7	38.6	23.7	14.6
30	107.0	66.0	50.0	30.5	19.0	11.6
20	93.3	57.4	42.2	26.6	16.4	10.1

Slope Stability Under Rainfall

Base on the fluid-solid interaction theory, the rainwater infiltration and slope stability were simulated at the same time. The parameter of soil especially the density and total cohesion changed when the soil-slope under rainwater infiltration.

The water content was calculated from matric suction by soil-water characteristic curve. Then, the density of the soil in different water content was calculated by Formula 3:

$$\rho = \frac{G_s(1+\theta)}{1+e}\rho_w \tag{3}$$

Where:

ρ : the density of the soil at different water content, (1000kg/m^3);
G_s : specific gravity of soil particle;
θ : water content;
e : porous ratio;
ρ_w : water density (1000kg/m^3).

The shear strength of an unsaturated soil can be formulated in terms of independent stress state variables. The stress state variables, $(\sigma - u_a)$ and $(u_a - u_w)$, have been shown to be the most advantageous combination for practice. Using these stress variables, the shear strength equation is written as follows (Fredlund, 1982):

$$\tau_{ff} = c' + (\sigma_f - u_w)_f \tan\varphi' + (u_a - u_w)_f \tan\varphi^b = c + (\sigma_f - u_w)_f \tan\varphi' \tag{4}$$

Where:

u_{af} : pore-air pressure on the failure plane at failure;
ϕ' : angle of internal friction associated with the net normal stress state variable, ($(\sigma_f - u_w)_f$;

ϕ^b : angle indicating the rate of increase in shear strength relative to the matric suction, $(u_a - u_w)_f$;
c : total cohesion, $c = c' + (u_a - u_w)_f \tan\varphi^b$.

Therefore, strength reduction method used to simulate and analyze the safety of slope in $FLAC^{3D}$ should be modified in order to be used in slope safety simulation under rainfall by searching cell method. The procedure used in $FLAC^{3D}$ based on FISH was as follows. First, the pore pressure of every cell was gained by searching cell method and the matric suction could be calculated from pore pressure. Then, the density could be calculated from Formula 3 and the total cohesion could be calculated from Formula 4. Finally, the new density and total cohesion of each cell was assigned to each cell by searching cell method. The procedure was performed every time-step in order to modify the soil parameter constantly when the soil under rainfall infiltration.

Base on the fluid-solid interaction theory, the rainwater infiltration and slope stability were simulated in $FLAC^{3D}$ at the same time. The physical mechanics and permeability parameters of the slope are given in Table 2.

Table 2. The Physical Mechanics and Permeability Parameters of the Slope

Soil particle density ρ_s (kg/m^3)	2200	Elastic modulus E (MPa)	50
Poisson's ratio μ	0.3	Porosity n [%]	5
Cohesion c (kPa)	15	Angle of internal friction ϕ (°)	25
ϕ^b	20	Saturated permeability coefficient k (m/s)	1.0×10^{-9}
Fluid density ρ_c (kg/m^3)	1000	Fluid modulus (MPa)	2000

Sensitivity Analysis of Slope Failure

There are many influence factors for the slope failure under rainfall infiltration. In this paper, the relationship between coefficient of permeability, rainfall duration, rainfall intensity, slope height, slope and slope stability was researched.

In order to research the slope seepage field and stability at different slope and rainfall conditions, based on the model in the previous section, 10 different coefficients of permeability, 5 different rainfall durations, 6 different rainfall intensities, 5 different slopes and 5 different slope heights were simulated. The value selection of sensitive parameters is tabulated in table 3

Table 3. The value selection of sensitive parameters

Sensitive Parameters	Value									
Coefficient of permeability (m/s)	10^{-4}	5×10^{-4}	10^{-5}	5×10^{-5}	10^{-6}	5×10^{-6}	10^{-7}	5×10^{-7}	10^{-8}	10^{-9}
Rainfall intensity (mm/h)	10		20		30		40		50	60
Rainfall duration (h)	12		24		36		48		60	
Slope	1:1		1:1.25		1:1.5		1:1.75		1:2	
Slope height [m]	5		7.5		10		12.5		15	

RESULT AND DISCUSSION

Slope Stability under Rainfall

The factor of safety, F = 1.71 before rainfall was obtained by numerical simulation in $FLAC^{3D}$. Fig. 3 plots shear strain-rate contours and velocity vectors at last non-equilibrium state, which allows the potential failure surface to be identified, as shown in FIG.. 4. The connectivity of plastic zone can be identified. The velocity vector also proves the judgment. The speed of the node which is outside the potential failure surface is larger than others.

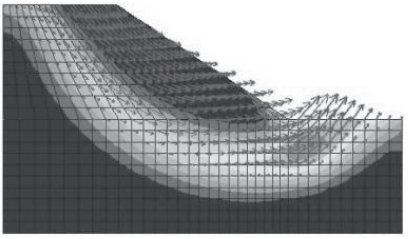

FIG.. 3. Shear strain-rate contours and chart velocity vectors.

Fig. 5 shows the pore pressure nephogram of slop after 12h rainfall. The figure shows that the water content of slop surface soil increases, the region of slope toe is saturation. The water content of the others little changes.

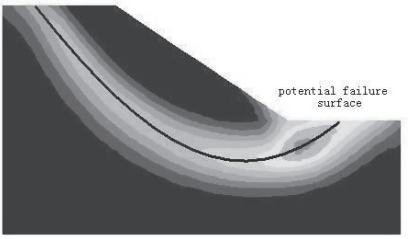

FIG.. 4. Potential failure surface before rainfall before rainfall.

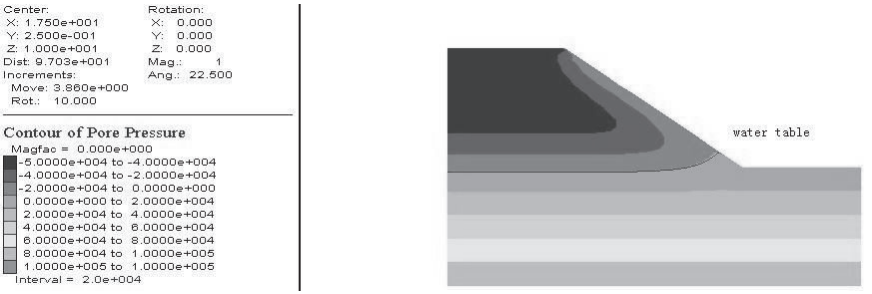

FIG.. 5. Pore pressure nephogram of slop after 12h rainfall.

It can be explained that: with the start of the rainfall, the rainwater flow into slop from the surface. The water content of slop surface soil increases. It is visualized that there is a micro "water channel" along the slope, from the top to the toe of the slope. Thus, the toe of the slope accumulates rainwater constantly and reaches saturation first. Then, the saturation surface at the toe of the slope rises and expands constantly. The infiltration of rainwater needs some time, the saturation of the inside region dose not change.

The factor of safety, $F = 1.72$ after 12h rainfall was obtained by numerical simulation using strength reduction method. Fig. 6 plots shear strain-rate contours and velocity vectors at last non-equilibrium state. Fig. 7 shows the potential failure surface which is identified from shear strain-rate and velocity vectors chart.

The numerical simulation result shows that the factor of safety decreased 0.16 after rainfall, which shows that the rainfall has a negative impact on slope stability. Shear strain-rate contours and velocity vectors and potential failure surface chart show that the toe of the slope becomes the weakest region after 12h rainfall. The most important factors for slope stability are no longer the whole slope stability, but the stability of the toe of the slope. The concept of "small slip failure occurred in the toe of slope" is put forward. The whole slope failure may happen due to the "small slip failure". "Small slip failure occurred in the toe of slope" was obtained by the numerical simulation can be explained by two reasons: (1) the density of the soil

increases as the water content of the slope surface increases, the load of the slope increases. (2) The rainwater flow into slop from the surface. The toe of the slope accumulates rainwater constantly and reaches saturation first. The shear strength decreases substantially as the saturation increases.

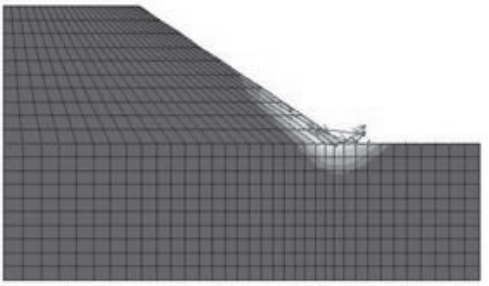

FIG. 6. Shear strain-rate contours and velocity surface vectors after 12h rainfall.

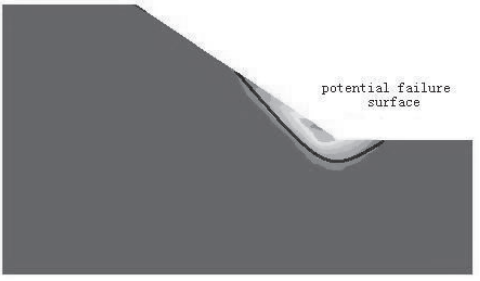

FIG. 7. Potential failure after 12h rainfall.

Sensitivity Analysis of Slope Failure

(1) Coefficient of permeability

Fig. 8 shows the slope seepage field at different coefficient of permeability. The saturated surface is marked by black line. The factors of safety at different coefficient of permeability are tabulated in Table 4.

As shown in the Table 4 and Fig. 8, when the coefficient of permeability is greater than 10^{-6}m/s, slope is very sensitive for rainfall, with the great rainwater infiltration capacity and dramatic reduction of the safety factor. On the other hand, when the coefficient of permeability is less than 10^{-9} m/s, the reduction of safety factor of the slope under rainfall reduces gradually. And the rainwater infiltration capacity is very little, the saturated surface and the water content of the inside region

of the slope almost unchanged.

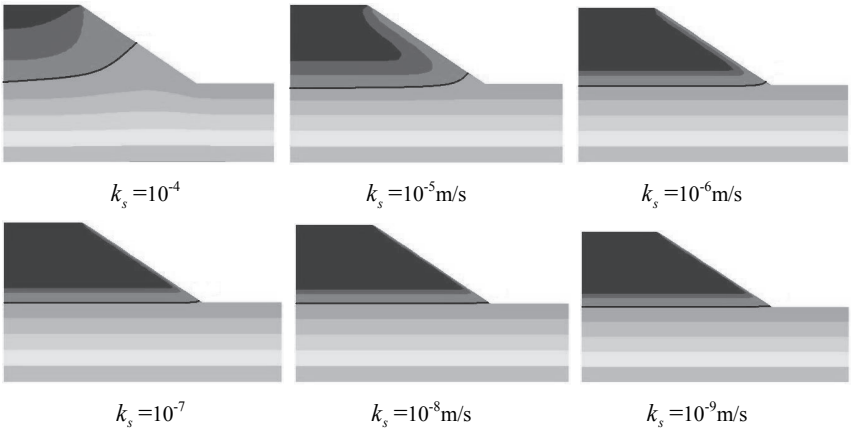

FIG.. 8. Slope seepage field after rainfall at different coefficient of permeability.

Table 4. Factor of Safety at Different Coefficient of Permeability

Coefficient of permeability (m/s)	Factor of safety after rainfall	Reduction	Coefficient of permeability (m/s)	Factor of safety after rainfall	Reduction
10^{-4}	0.69	1.19	5×10^{-6}	1.84	0.04
5×10^{-4}	1.31	0.57	10^{-7}	1.85	0.03
10^{-5}	1.72	0.16	5×10^{-7}	1.87	0.01
5×10^{-5}	1.79	0.10	10^{-8}	1.87	0.01
10^{-6}	1.82	0.06	10^{-9}	1.88	0.00

The coefficient of permeability is an important parameter for slope, the reference values of permeability coefficient of various types of soil are tabulated in Table 5.

Table 5. Reference Values of Permeability Coefficient

Types of soil	Coefficient of permeability (m/s)	Types of soil	Coefficient of permeability (m/s)
Gravel	10^{-2}~10^{-4}	Silt	10^{-5}~10^{-6}
Coarse sand	5×10^{-4}~10^{-4}	Silty clay	5×10^{-8}~10^{-6}
Fine sand	5×10^{-5}~10^{-5}	Clay	$<5\times10^{-8}$

Based on the reference values of permeability coefficient of clay soil and sandy soil, there is almost no effect on the clay soil slope under rainfall. So, the following sensitivity analysis of slope failure influence factors is only for the sandy soil. Anti-seepage and protective measure should be used on the sandy soil slope.

(2) Rainfall intensity

Fig. 9 shows the slope seepage field at different rainfall intensities. The saturated surface is marked by black line.

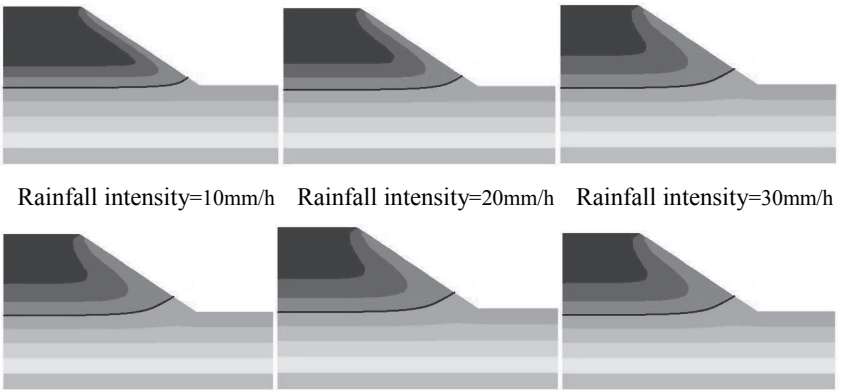

FIG.. 9. Slope seepage field at different rainfall intensities.

Fig. 9 shows that the saturation surface at the toe of the slope and water contents of the inside region of the slope are almost the same when the rainfall intensities are from 40mm/h to 60mm/h. But when the rainfall intensity are from 10mm/h to 30mm/h, the saturation surfaces at the toe of the slope low gradually, and water content of the inside region of the slope is less too.

The factor of safety at different rainfall intensities are tabulated in Table 6.

Table 6. Factor of Safety at Different Rainfall Intensities

Rainfall intensity (mm/h)	Factor of safety after rainfall	Reduction
Before rainfall	1.88	-
10	1.85	0.03
20	1.72	0.16
30	1.69	0.19
40	1.65	0.23
50	1.64	0.24
60	1.64	0.24

The coefficient of permeability of the slope soil is 10^{-5}m/s (36mm/h), Fig. 9 and Table 6 demonstrates the influence of the coefficient of permeability on the slope seepage field and stability. If the rainfall intensity is less than the permeability, the flow of infiltration is equal with rainfall intensity. Otherwise, a water film is formed on the slope and ground, and then the flow of infiltration does not increase as the rainfall intensity increases.

(3) Rainfall duration

Fig. 10 shows the slope seepage field at different rainfall durations. The saturated surface is marked by black line.

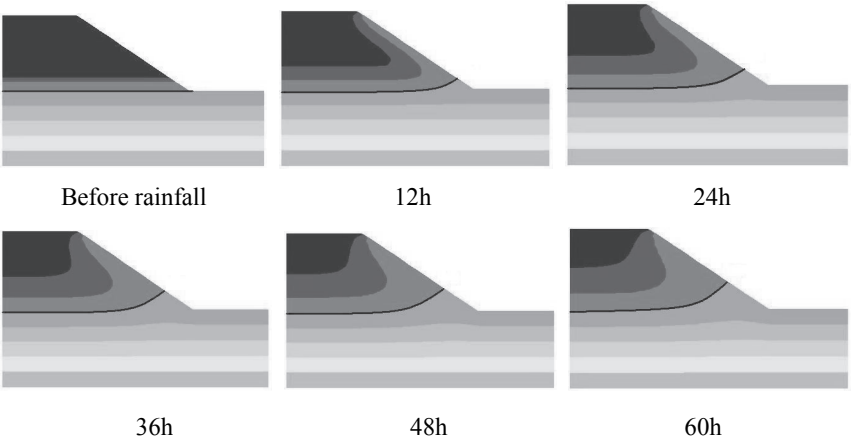

FIG. 10. Slope saturation surface at different rainfall durations.

Fig. 10 shows that the saturation surface at the toe of the slope rises and expands constantly as the rainfall duration increases.

The factor of safety at different rainfall durations are tabulated in Table 7. Fig. 11 shows the relationship between factor of safety and rainfall duration.

Table 7. Factor of Safety at Different Rainfall Durations

Rainfall duration (h)	Factor of safety after rainfall	Reduction
0	1.88	-
12	1.72	0.16
24	1.42	0.46
36	1.21	0.67
48	1.09	0.79
60	1.01	0.87

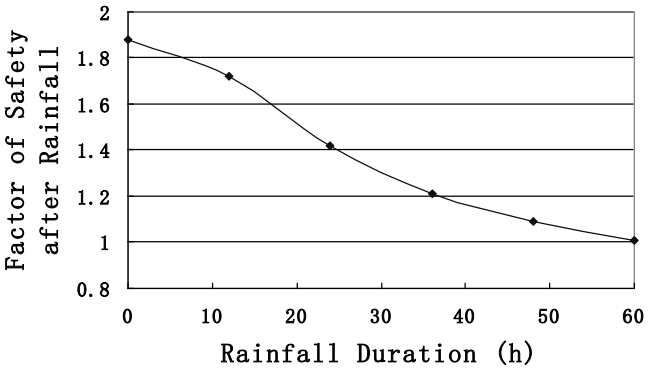

FIG.. 11. Relationship between factor of safety and rainfall duration.

Fig. 11 demonstrates the influence of the rainfall duration on the slope stability. With the rainfall duration increases, the factor of safety decreases constantly. But the rate of the reduction decreases gradually.

(4) Slope

The factors of safety of the slope with different slope are tabulated in Table 8. Fig. 12 shows the relationship between the factor of safety and slope.

Fig. 12 shows that the factor of safety increases constantly as the slope decreases before rainfall. In other words, with the slope decreases the slope stability improves gradually. The change law of the factor of safety after rainfall is the same, but the rate of change decreases. It can be interpreted that the slope surface increases as the slope decreases, the infiltration capacity of rainwater increases in the same time. Therefore, due to the slope decrease, the reduction of the factor of safety increases gradually.

Table 8. The Factors of Safety of the Slope with Different Slopes

Slope	Factor of safety before rainfall	Factor of safety after rainfall	Reduction	Rate of reduction (%)
1:1	1.66	1.61	0.05	3.01
1:1.25	1.79	1.66	0.13	5.59
1:1.5	1.88	1.72	0.16	8.51
1:1.75	1.98	1.79	0.19	9.60
1:2	2.07	1.86	0.21	10.14

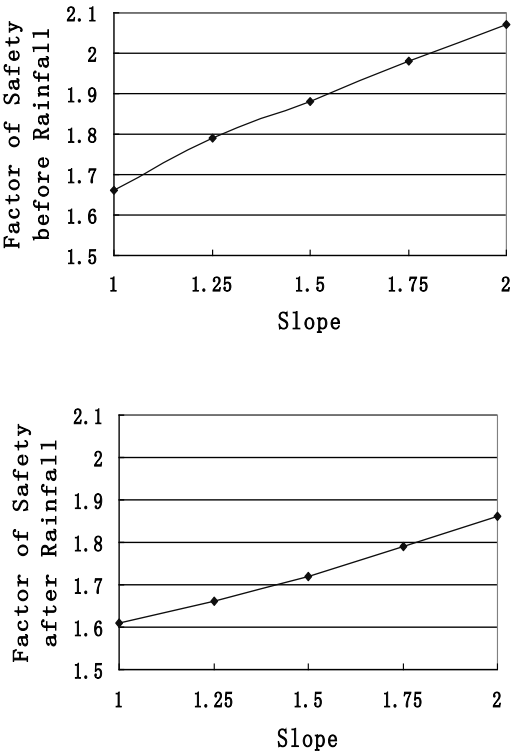

FIG..12. The relationship between the factor of safety and slope (upper: before rainfall; below: after rainfall)

(5) Slope height

The factors of safety of the slope with different height are tabulated in Table 9. Fig. 13 shows the relationship between the factor of safety and slope height.

Fig. 13 shows that the factor of safety decreases constantly as the slope height increases before rainfall. In other words, with the slope height decreases the slope stability improves gradually. The change law of the factor of safety after rainfall is the same, but the rate of change increases. It can be interpreted that the slope surface increases as the slope height increases, the infiltration capacity of rainwater increases in the same time. Therefore, with the slope height increases, the reduction of the factor of safety increases gradually. So, slope height is an important parameter of the slope, the slope height should not be too large.

Table 9. The Factor of Safety of the Slope with Different Height

Slope height(m)	Factor of safety before rainfall	Factor of safety after rainfall	Reduction	Rate of reduction (%)
5	2.41	2.35	0.06	3.01
7.5	2.07	1.97	0.10	3.35
10	1.88	1.72	0.16	8.51
12.5	1.71	1.47	0.24	31.31
15	1.64	1.30	0.34	43.96

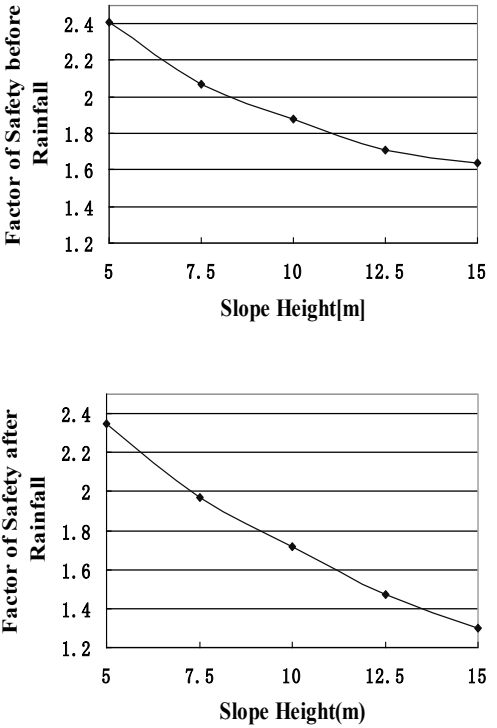

FIG..13. The relationship between the factor of safety and slope height(upper: before rainfall; below: after rainfall).

CONCLUSIONS

Based on the character of unsaturated soil, the percolation and slope safety models in *FLAC*^{3D} can be modified to simulate slope stability under rainfall

infiltration.

Toe of the slope becomes the weakest region after rainfall. The most important factors for slope stability are no longer the whole slope stability, but the stability of the toe of the slope. The concept of “small slip failure occurred in the toe of slope” is put forward.

Sandy soil slope is very sensitive for rainfall, but there is almost no effect on the clay soil slope under rainfall. Anti-seepage and protective measure should be used on the sandy soil slope.

With the rainfall intensity increases, the factor of safety decreases constantly. But when the rainfall intensity is greater than the permeability, a water film is formed on the slope, and then the influence degree does not increase as the rainfall intensity increases

With the rainfall duration increases, the factor of safety decreases constantly. But the rate of the reduction decreases gradually.

The factor of safety increases constantly as the slope decreases or slope height decreases before rainfall. The change law of the factor of safety after rainfall is the same, but the rate of change decreases.

REFERENCE

Brand,E.W. (1984). "State-of-the-art report of landslides in Southeast Asian." *Proc., 4th Int. Symp. on Landslides*, Toronto, pp. 17–37.

Brooks, H. and Corey, A.T. (1964). "Hydraulic Properties of Porous Media, Colorado State Univ. Hydrol. " Paper, No.3, pp. 27.

Burdine, N.T. (1952). "Relative Permeability Calculations from Pore-Size Distribution Data, " *Trans*. AIME.

Chen,R.H. et al. (2009). "Simulation of a slope failure induced by rainfall infiltration." *Environmental Geology*. Vol. 58:943–952.

Fredlund D G, Rahardjo H. Soil mechanics for unsaturated soils. New York: John Wiley& Sons, 1993.

Hod, Y. F. and Fredlund, D.G. (1982). "Increase in strength due to suction for two Hong Kong soils." In: *Proceedings of the ASCE specialty conference on engineering and construction in tropical and residual soils*, Hawaii, pp. 263–296.

Itasca Consulting Group. (2003).Inc. Fast Lagrangian analysis of continua in three dimensions user’s manual [M/CD]: Itasca Consulting Group, Inc.

Marshall, T. J. (1958). "A Relation between Permeability and Size Distribution of Pores. " *Soil Sci.*, Vol. 9, pp. 1-8.

Millington, R.J. and Quirk, J. P. (1959). "Permeability of Porous Media." *Nature*, Vol. 183:387-388.

Rahardjo, H. et al. (2007). "Factors controlling instability of homogeneous soil slopes under rainfall." *Journal of Geotechnical and Geoenvironmental Engineering*. Vol. 133(12):1532–1543.

Possible Acceptance of Small Recycled Aggregate Fractions for Concrete Production

Dubravka Bjegovic[1], Hrvoje Sironic[2] and Nina Stirmer[3]

[1]Full Professor, PhD, Faculty of civil engineering, University of Zagreb, Department of materials, Kaciceva 26, 10000 Zagreb, Croatia and Institute IGH, Janka Rakuše 1, 10000 Zagreb, Croatia; email: dubravka@grad.hr
[2]Director's Assistant, MSc, Institute for Materials and Structures, Institute IGH d.d., Zagreb, PC Rijeka, Rijeka, 51000, Croatia; email: hrvoje.sironic@igh.hr
[3]Associate Professor, PhD, Faculty of civil engineering, University of Zagreb, Department of materials, Kaciceva 26, 10000 Zagreb, Croatia; email: ninab@grad.hr

ABSTRACT: In western region of Croatia, small fractions of recycled aggregate have similar properties like small fractions of crushed natural aggregate regarding grain shape and fines content. The focus of this research was to analyze possibilities of using small fractions of recycled aggregate in the cases where only poor quality natural sand is available for production of concrete. The research is based on available data from concrete production in wider region of western Croatia and also on experimental research carried out on several series of mortar samples prepared with recycled and natural fine aggregate. Influence of two-phase mixing method on mortar properties in fresh and hardened state was analyzed. Based on the results of testing, it is concluded that small recycled concrete aggregate may be suitable for use in the concrete production. In concrete mix design, it is recommended to decrease absolute aggregate absorption determined according to HRN EN 1097 and to use double mixing method, due to its positive effect on the consistency and strength.

INTRODUCTION

Concrete produced with recycled aggregate will usually be of lower quality than ordinary concrete with same cement amount and produced with natural aggregate. It means that by using natural aggregate from a source of good quality, satisfactory concrete properties with acceptable price could be achieved. In that case, the production of concrete with the recycled aggregate, which would have approximately the same properties as concrete from natural aggregates will be economically infeasible.

In the concrete production, it is preferred to use small aggregates fractions (0-4 mm) from alluvial origin, in relation to the small crushed fractions. Comparing the properties of concrete mixtures produced with these two different natural aggregates, it is much possible to obtain a significant difference. With alluvial fraction can be produced concrete with excellent workability and good strength with lower cement quantity. On the other hand, use of crushed small fractions which often contains a large percentage of the fine particles (smaller than 0.063 mm), or even clay, is not nearly so desirable in concrete mixtures.

Tam et al., 2008 suggests that the traditional testing approach for water absorption cannot give accurate results for recycled aggregate, based upon which, errors in concrete mix designs may result. Solyman, 2006, paid attention on possible large variability of recycled aggregate absorption measured by standardized testing methods that use procedures for achieving saturated, surface dry condition of an aggregate. For that reason, Solyman is using specific term "water requirement" as a property that can more realistic characterize absorption. In the experimental research, Solyman measured mortar consistency by using flow table. For production of reference mortar, Solyman used standardized sand according to EN 196-3. In mortar mixtures produced with recycled aggregate, author added such amount of water as it was needed to achieve same consistency as for reference mortar. Initial absolute w/c was the same in all compared mixtures and before testing, recycled sand has been dried to a constant mass. Amount of water added to mortar with recycled sand, needed to achieve consistency of reference mortar, Solyman represents as absorption of the recycled sand. Based on the literature review (Solyman, 2006; Goncalves et al., 2004; Tam et al., 2008), conclusion is that prior to concrete mix design phase special testing of effective recycled aggregate absorption should be done.

It is so due to the fact that real absorption occurs in dense cement suspension in the concrete and it is often caused by increased content of fine particles. For that reason, recycled aggregate grains are not able to absorb all amount of water that is added to concrete for absorption correction (determined by one of the standardized procedures). Consequently, the amount of water that cannot be absorbed increases effective w/c and leads to additional decrease of recycled aggregate concrete quality. It is often misinterpreted and explained with poor quality of the recycled aggregate. This phenomenon can be easily observed in the case of double mixing method that results with additional absorption decrease (Ryu, 2002; Li et al., 2009; Tam et al., 2005, 2007, 2008, 2009). Furthermore, influence of particle shape should be considered as well (De Schutter and Poppe, 2004).

Reference concrete that has been used in most studies of the recycled aggregate concrete properties mainly consists of small fraction river sand. Properties of such concrete were usually better than properties of the obtained recycled aggregate concrete. The motivation for the research shown in the paper was the fact that in the western Croatia, properties of the small recycled aggregate fraction are similar to the properties of natural crushed fraction regarding shape and fine particles content. In such cases, when natural small fractions don't have significantly better properties, use of small recycled aggregate fraction should be considered and this could be an effective way to reduce concrete waste. The focus of this research was to analyze possibilities of using small fractions of recycled aggregate in the cases where only poor quality natural sand is available for production of concrete.

CONCRETE PRODUCTION IN THE WESTERN CROATIA

In the western Croatia, crushed limestone rock aggregates from local quarries are used in the concrete production (Fig. 1). Due to its poor quality (because of increased amount of fine particles smaller than 0.063 mm and less favorable particle shape), it requires a relatively large amount of cement than it is common in continental part of

Croatia and the rest of Europe.

FIG. 1. Local querries in western Croatia (Primorsko-goranska, Istarska and Licko-senjska county).

Cement quantity used for concrete production

From the majority of concrete producers in the western Croatia, data on the produced concrete types, its composition, i.e. used cement quantities for the production period since 2005. to 2008. were collected

The minimum cement quantity for concrete strength class C25/30 which is producing in 23 concrete plants in the analyzed area is 360 kg. This cement quantity was used in two concrete plants (8.7 %). Other minimum cement quantities for a specific strength class and associated number of concrete plants which use this cement content are shown in Table 1.

Data collected were used for analysis and better understanding of the available crushed stone aggregates quality and its influence on the concrete production costs.

Comparison with standard requirements

According to regulations, maximum cement content for concrete C25/30 is specified for environmental class XF2 and it is 300 kg/m3 while for class C30/37 and XF4 it is 340 kg/m^3.

From the data collected for the period since 2005. to 2008., it can be concluded that in this period, more than 90 % concrete plants used at least 380 kg/m3 of cement for production of strength class C25/30 or 36-43 % more than recommended minimum according to standard HRN EN 206-1. For strength class C30/37, even 12 concrete plants (54.5 %) used 440 kg/m^3 or more cement.

It should be mentioned that according to the new regulations, concrete producers have to establish their own quality control system which includes necessary test equipment and employment i.e. education of responsible staff. It resulted with a more strictly daily control and most producers reduced previously described cement quantities in concrete production.

Table 1. Minimum Cement Quantity and the Number of Observed Local Concrete Plants Which Use This Cement Content in the Production of Concrete Classes C25/30 and C30/37

Minimum cement content (kg/m^3) for concrete strength class	Number of concrete plants	
	C25/30	C30/37
360	2 (8,7%)	-
380	12 (52,2%)	-
390	5 (21,7%)	-
400	4 (17,4%)	2 (9,1%)
420	-	2 (9,1%)
430	-	6 (27,3%)
440	-	9 (40,91%)
460	-	2 (9,1%)
470	-	1 (4,6%)

MATERIALS

Recycled concrete aggregate

Concrete specimens (cubes of 15 cm), left after compressive strength testing during manufacturer's factory quality control were used for recycled concrete aggregate production. Specimens were tested at the age of 28 days and then left outside in environmental conditions for the period of 2 to 6 months. Specimens were taken from three different sources - plants which use crushed aggregates in concrete production. From the selected plants, original (natural) crushed aggregate was sampled and concrete specimens were produced with this aggregate. Accordingly, three pairs of recycled and natural aggregates of the same origin were obtained.

In the concrete production, plants V and I are using limestone, and plant D is using dolomite crushed aggregate fractions. All recycled aggregate is obtained from concrete specimens of approximately equal compressive strength (32.0 to 36.0 MPa). The original concrete from all three sources was produced with the same cement type: CEM II / BM (ST) 42.5 N and with the same maximum particle size Dmax = 16 mm. Obtained recycled concrete aggregate was sieved (separated by fractions) on the laboratory sieves, in fractions 0-4, 4-8, 8-16, and the fraction larger than 16 mm (Fig. 2).

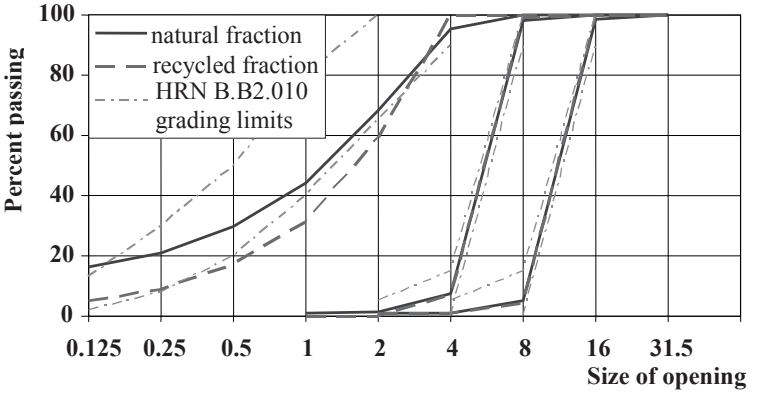

FIG. 2. Grading curves for aggregate from source V.

Fines content in the aggregate

Testing results for crushed naturally (original) aggregate from the production and recycled aggregates, and the results of testing density, absorption and content of fine particles (smaller than 0.063 mm) are shown in the Table 2.

From the results presented, significant reduction of fine particles can be observed at small fractions of recycled aggregates in relation to naturally crushed. Difference in the case of material from the source V is even 72 %. In the case of source D, difference in content of fine particles is 55 %, while in the case of source I, it is 25 %. For source I, difference in fines content of the fraction 8-16 mm is considerable, even 89 %.

From results obtained, it can be concluded that large part of dusty and clay particles smaller than 0.063 mm, that were present in the original crushed aggregate, remains trapped in the grains of free or bonded mortar in the recycled aggregate.

Absorption

As known from the literature, recycled aggregate has considerably higher absorption than natural aggregate. The resulting absorption is in the expected range between 3 and 12 %. Increase of absorption is 2.7 (small fraction of the source I) up to 25 times (small fraction of the source V). It is important to emphasize that aggregate absorption is determined according to HRN EN 1097-6. According to this standard, particles smaller than 0.063 mm were washed out from the aggregate sample prior to testing.

Absorption tests according to DIN 4226-100 showed that approximately 90 % of the total absorption is realized in the first 10 minutes of dry aggregates immersion in the water. Observing the sample during the test, it was found that the majority of absorption occurs in the first moments of aggregate contact with water, and after that, absorption slows down.

Table 2. Aggregate Testing Results

Aggregate property	Original (O) / Recycled (R)	Source V			Source D			Source I		
		0-4	4-8	8-16	0-4	4-8	8-16	0-4	4-8	8-16
Density (ρ_s) (dry condition) (kg/L)	O	2.68	2.69	2.69	2.79	2.80	2.80	2.64	2.66	2.69
	R	2.12	2.32	2.40	2.22	2.44	2.45	2.34	2.47	2.49
Absorption (%) HRN EN 1097-6 (24h) DIN 4226-100 (10 min)	O (24 h)	0.40	0.40	0.30	0.70	0.80	0.70	3.1	1.4	0.9
	R (24 h)	9.94	6.10	4.83	8.96	5.10	4.81	8.61	5.48	4.90
	R (10 min)	9.18	5.28	4.00	7.80	4.65	4.30	-	-	-
Fine particles ≤0.063 mm (%) HRN EN 933-1	O	11.33	3.63	1.18	8.48	2.31	0.81	10.14	2.30	2.06
	R	3.2	0.35	0.41	3.8	0.41	0.21	7.57	0.36	0.22

The values of absorption obtained by standardized procedures should be taken with certain precautions, as it is stated in the literature [1-3]. These test methods do not take into consideration significant effect of small particles, neither effect of slowing the absorption which does not occur in water but in a much denser cement suspension [2].

Different researchers stated that the major influence on consistency and compressive strength may have double mixing method [4-9], which can also be related with the influence of aggregate absorption and changes of the effective w/c ratio. But, double mixing method is usually applied in the case of recycled coarse aggregate.

Testing of mortar with recycled aggregate

In order to verify the suitability of the small recycled fractions for application in the concrete production, the influence of the double mixing method was analysed. Therefore, influence of the recycled aggregates absorption from a source V (which has a maximum absorption of the aggregates observed) was tested by measuring the change of consistency in the time of the recycled aggregate mortar, as well as compressive and bending strength. The results were compared with the results of testing reference mortar produced with natural aggregate from the same source.

Testing programme

Following properties of mortar with recycled and natural aggregates were tested:

1) change of consistency in time, measured in the period of 2 hours;
2) estimation of water requirement for recycled aggregate mortar to keep the same consistency as for reference mortar in the period of 2 hours;
3) testing of mortar bending and compressive strength after 7 and 28 days.

Specified period of 2 hours was chosen because it is usually applied in the practice as a maximum time allowed for concrete placing (without retarders) and it is specified

in the majority of the technical instructions of the local concrete producers as a maximum allowed time for concrete placing.

The above properties have been investigated in several mixtures and following cases were observed:

a. mortars with different w/c ratio (with the same cement paste volume);
b. agreggates with and without fine particles;
c. mixing method (one or two phases);
d. use of superplasticizer with extended workability;
e. time of taking the specimens for testing strength: immediately after mixing and after 2 hours.

All tests were conducted in the controlled conditions in the laboratory of the Institute IGH P.C. Rijeka, Croatia.

In all the mixtures, the same cement type was used: white cement CEM I 52.5 R. Cement properties testing results according to HRN EN 196-3 are shown in the Table 3.

Table 3. Cement Properties

Property	**Measured values**
Standard consistency (%)	30.5
Density (kg/m^3)	3160
Soundness - Le Chatelier method (mm)	1.0
Initial setting time (min)	195
Final setting time (min)	325

Natural and recycled aggregates from the source V have been used, since their characteristics have the largest differences.

In the mixtures for which was planned to add superplasticizer, it was used "Glenium Sky 510" manufactured by BASF, superplasticizer with extended workability, without delayed setting characteristics.

Change of consistency in time

Compositions were prepared for 1.0 L amount of mortar with different w/c ratios and in all mixtures with constant volume ratio of aggregates and cement paste. The compositions are shown in the Table 4.

Table 4: Mortars Compositions

	Proportion of components in mortar mixtures (kg)					
R (recycled) P (natural)	R	P	R	P	R	P
w/c	0.55		0.6		0.7	
Aggregate	0.824	1.049	0.824	1.049	0.824	1.049
Cement	0.644	0.644	0.609	0.609	0.549	0.549
Water	0.354	0.354	0.365	0.365	0.384	0.384

After weighing and dosing mortar components, mixing was performed in a laboratory mixer. Mixing was done in one or two phases. Reference mortar (consisting of natural crushed sand) was always mixed in one phase and it was always in approximately saturated surface dry condition (i.e. for a given case from 0.3 to 0.4 % - absorption of this aggregate is 0.4 %), to decrease the effect of absorption during the test.

Recycled aggregate mortar was mixed with aggregate that was always in completely dry condition, achieved by drying at 75 °C to constant weight. Temperature of 110 °C was not applied because at the higher temperature it is possible that crystallized water comes out from the old mortar, which can lead to unrealistic absorption values (Tam et al., 2008).

Mixing in one phase was performed in a way that in the mixer bowl were aggregate, cement and all necessary water dosed, and such a mixture was mixed for 60 seconds.

Double mixing method was done according to proposed modified mixing method (Li et al., 2009) in a way that in the mixer bowl was added cement and half of the required water, and mixing was performed for 30 s. After 30 s and when dense cement suspension appears, aggregate was added in the mixer and mixing continued for the next 60 s. At this phase of mixing, dense cement suspension covers recycled aggregate grains, and thanks to the large absorption capacity of the grain, it penetrates into the pores creating stronger and more dense interfacial zone. After this, in the mixture was added the remaining half of the water and mixing continued for additional 60 s (Fig. 3).

In this research, a slightly shorter time of mixing intervals was applied than it was proposed in the literature, because large difference in the mixing time after initial contact of aggregate and water can cause a big difference in the amount of absorbed water and thus affect the consistency, which will be shown below.

Dosing of mortar components

Mortar mixture after adding the aggregate in the cement paste and before the second phase of water dosing

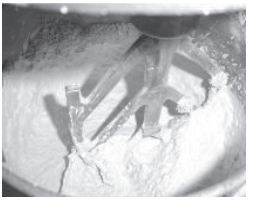

Mortar mixture after second phase of water dosing and mixing

FIG. 3. Preparation of mortar mixtures with recycled limestone aggregates: double mixing method.

After mixing is finished, mortar sample is taken to test consistency on the flow table. After testing, sample was returned into the mixer and covered with plastic foil to prevent drying (Fig. 4). The process of measuring the consistency was then repeated in the following intervals: 10, 30, 60, 90 and 120 minutes. Between each testing, mortar

was left in a covered mixer and before each measurement it was mixed for 60 s.

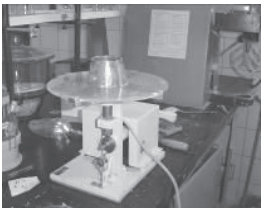

Flow-table with cone for a sample of the mortar

Mortar after consistency testing

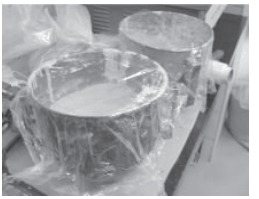

Samples of mortar between the two consistency tests

FIG. 4. Testing the consistency of mortar with natural and recycled limestone aggregate.

For double mixing method influence on the consistency analysis purpose, two variants were prepared, with a total w/c ratio of 0.7 and 0.6. As a reference mortar, mixture with natural aggregate was prepared. This part of the test was made with the fractions that were washed out before testing. i.e. small particles were removed.

Mortar mixtures were marked based on the used aggregate type: "R" for recycled and "P" for natural aggregate and based on mixing method: "F1" for mixing in one phase and "F2" for double mixing method. The results are shown in the diagrams, Fig. 5a and b.

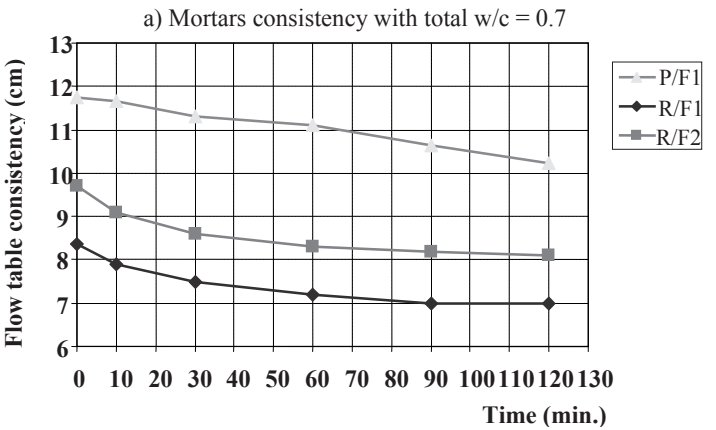

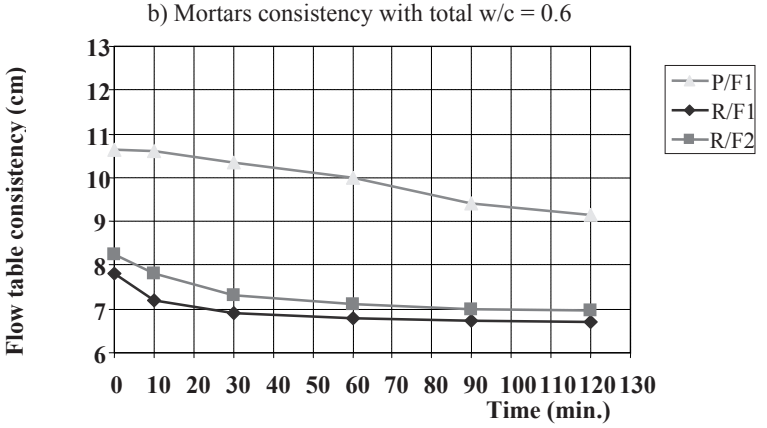

FIG. 5. Mortar consistency change in time of 120 min.

From diagrams, it can be seen that double mixing method has influence on the mortar consistency. i.e. it is effective as well in the case of recycled fine fractions application. This influence is more pronounced in the case of mortars with higher w/c ratio. During the test, it was observed that cement suspension with aggregate added should still have some minimal consistency to surround and cover entire aggregate. In the case of lower w/c ratio, mixture was too stiff to enable effective covering of the grains. Reason for that was because after adding the water in the second phase, aggregate mostly came into the contact with pure water. It is also significant that the initial difference in consistency between the recycled aggregate mortars mixed with different procedures during the test period of 2 hours was maintained. In other words, the most important factor for consistency is initial contact of aggregates and water which occurs already in the mixing phase.

The results obtained are in conformity with conclusions from different researchers which is that dense cement suspension slows or prevents further absorption of water. The loss of consistency after the first 10 or 30 minutes also occurs in the case of the reference mortar with natural aggregate which is in a saturated condition and its influence on absorption is minimized. It means that after 30 minutes, the loss of consistency is mainly caused by other factors such as cement hydration and partial evaporation which occurs during the test.

Estimation of water requirement in mortar

After 2 hours of making mixture and last consistency testing, assessment of recycled aggregates absorption in the mortar was conducted. This testing procedure can be summarized in the following steps:

1) The remaining sample was weighed to determine mass loss occurred due to testing.
2) Based on the obtained mass, quantity of cement was estimated in the

remaining sample according to the proportions in the initial composition

3) According to the estimated cement quantity, amount of water that will be added to the sample in steps of 0.05 w/c was determined. Mortar consistency was measured after each addition of water and mixing for 30 s.
4) Amount of water to be added to the mortar with recycled aggregate was determined by linear approximation (which is determined in relation to w/c ratio and flow-table consistency of mortar), to achieve mortar consistency as for mortar with natural aggregates measured after 2 hours of its preparation.
5) This amount of water is shown as the absorption of recycled aggregate, which occurred after 2 hours of sample preparation. Using the percentage of the total consistency loss determined from change of consistency in time (of the recycled mortar compared to the reference), equivalent percentages of absorption in these intervals were calculated.
6) As the starting point of absorption process, it is indicated the moment of first contact of the aggregate with the water, which occurred approximately 3-4 minutes before the first consistency measurement (on the diagrams marked as zero time).

The results are shown in the diagram in Fig. 6. This diagram shows that absorption of the mortar with lower w/c ratio is smaller than for the mortar with higher w/c ratio. For mortar with w/c=0.6 absorption was 5.9 %, while for the mortar with w/c=0.7 it was 7.2 %. It is 41 %, i.e. 27.6 % less than the measured absorption according to HRN EN 1097-6 which was 9.94 %. It also should be mentioned that the absorption measurement according to the standard is performed after 24 hours of the sample immersion in the water, and in our case, sample is mixing 2 hours in the cement paste. The difference of 18 % between absorption for mortar with w/c = 0.6 compared to mortar with w/c=0.7 can be explained with the assumption that in the denser cement suspension, it is more difficult to absorb than in cement suspension with more water. It should be also noted that more than 50 % absorption occurs in the first 4 minutes, that pass from the first contact with the water until completion of the first consistency measurement on the flow table. It should be emphasized that this is only assessment of absorption, and for determination of the necessary water for concrete mix design, the content of fine particles should be taken into account, which is not done in this work.

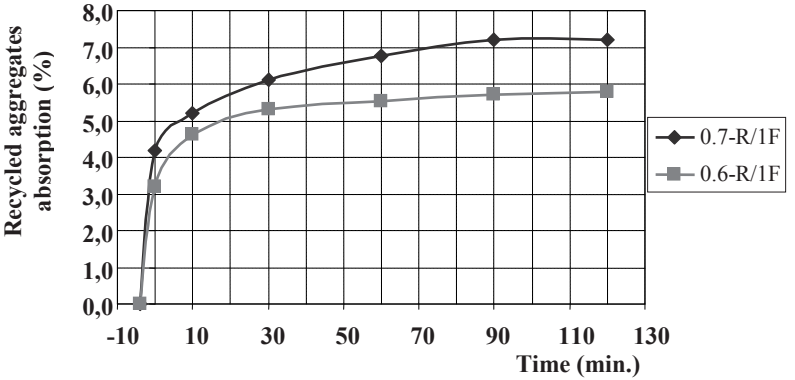

FIG. 6. Recycled aggregate absorption in mortar mixtures with total w/c = 0.6 and 0.7.

The next part of the test is performed on a mortar mixture with w/c = 0.55 and the following cases were analyzed:

a) regarding total w/c ratio:
   V0) assumption that the aggregate does not absorb water, the ratio of the total water amount and cement, "the absolute w/c" = 0.55
   V1) assumption that the aggregate will absorb all water measured according to HRN EN 1097-6 (as assumed in almost all the studies cited in the literature). In this case, the "effective w/c" = 0.55, and the total amount of added water is equal to the amount added in case V0 plus the amount required for the measured absorption.
   These two extreme cases were chosen because it is expected that consistency curve of the real reference mortar will be placed in the area between them.
b) regarding the fine particles content:
   M0) particles finer than 0.063 mm were removed from the aggregates before testing
   M1) aggregate is dosed in existing silty state. i.e. with fine particles
c) regarding mixing method:
   F1) mixing in one phase. i.e. with one water dosing
   F2) double mixing method. i.e. with two separate water dosing
d) regarding the addition of superplasticizer with extended workability:
   S1) mixing with the addition of superplasticizer in the amount of 0.6 % by weight of cement.
   Manufacturer's recommendations for dosing the superplasticizer are from 0.8 to 1.5% by binder weight, but in the practice it was shown that higher values (in case of dosing at once) may result with problems in concrete segregation.
   Mortar mixtures that do not contain the mark "S1" were made without addition

of superplasticizer.

Series of samples testing results as previously described and illustrated, are shown in the diagrams in Fig. 7-9.

Fig. 7 shows the results for mortars made with aggregate previously washed on 0.063 mm sieve (without fine particles), and Fig. 8 shows the results of testing mortar made with aggregates containing fine particles.

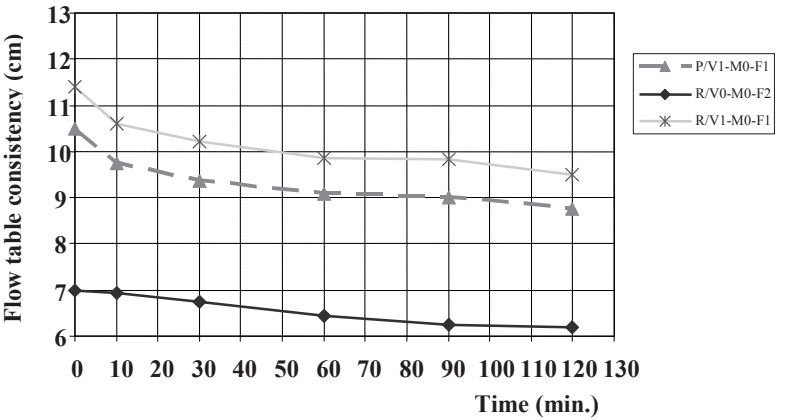

LEGEND:

P/V1-M0-F1: P - natural aggregate; V1 - mixture with additional water determined according to HRN EN 1097-6; M0 –mixture with washed aggregate; F1 - mixing in one phase

R/V0-M0-F2: R - recycled aggregate; V0 – same amount of water as for the reference mixture; M0 –mixture with washed aggregate; F1 - double mixing method

R/V1-M0-F1: R - recycled aggregate; V1 - mixture with additional water determined according to HRN EN 1097-6; M0 –mixture with washed aggregate; F1 - mixing in one phase

FIG. 7 Consistency of mortar made with washed aggregates (aggregate without fine particles), w/c=0.55 .

This diagram shows that mortar which contains recycled aggregate and all the water added for absorption has larger consistency than reference mortar made with natural, washed and saturated aggregate. It can be seen that there is a loss of consistency in the case of mortar without adding water for absorption. In this case, the loss of consistency occurred at the beginning of testing, i.e. although double mixing method was applied, aggregate absorbed larger amount of water in the moment of first contact with the water till beginning of the first consistency measurement (approx. 4 minutes).

From the results obtained, it is clear that it is necessary to add a certain amount of

water to correct consistency loss caused by absorption of recycled aggregates. Nevertheless not all amount of absorption measured according to HRN EN 1097-6, because consistency will be larger than consistency of the reference mixture and part of the added water will cause increase of the effective w/c ratio and thus reduce the quality.

From the consistency measurement after 2 hours of testing, it was obtained:

	P/V1-M0-F1	8.75 cm	(r_{ref})
	R/V1-M0-F1	9.50 cm	($r_{r.u}$)
and	cone radius	5.00 cm	(r_0),

with assumption of the linear relationship between the amount of water in the mixture and flow table consistency, absorption can be determined by linear approximation.

If the effective absorption is marked as $\mathbf{u_{ef}}$, and absolute absorption determined according to HRN EN 1097-6 marked as $\mathbf{U_{EN}}$, with rough approximation that dry sample immersed in the water for 2 hours will have same absorption as it was immersed into water for 24 hours, following formula could be established:

$$u_{ef} = U_{EN}* (r_{ref} - r_0) / (r_{r.u} - r_0) = 9.94* (8.75 - 5.00) / (9.50 - 5.00) = \\ = 9.94*3.75/4.50 = 8.28\% \quad (1)$$

In this way, the value of absorption after 2 hours can be obtained, and that is 8.28 % for mortar with effective w/c = 0.55, i.e. 17 % lower than value determined according to HRN EN 1097-6.

It should be mentioned that aggregate shape also has influence on the consistency, and that the real absorption of the sample immersed into water for 2 hours is a little bit less than absorption after 24 hours, which was not taken into account. But based on all the above, it can be concluded that the effective absorption in the period up to 2 hours is certainly less than the absolute absorption determined according to HRN EN 1097-6.

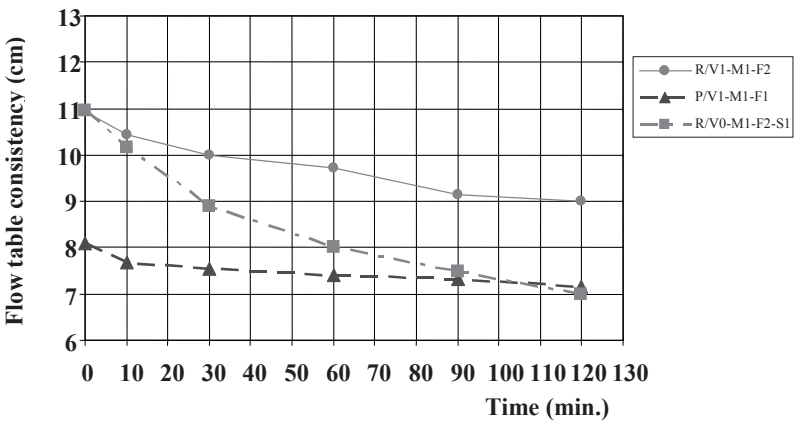

LEGEND:

R/V1-M1-F2: R - recycled aggregate; V1 - mixture with additional water determined according to HRN EN 1097-6; M1 –mixture with unwashed aggregate; F2 - double mixing method
P/V1-M1-F1: P - natural aggregate; V1 - mixture with additional water determined according to HRN EN 1097-6; M1 –mixture with unwashed aggregate; F1 - mixing in one phase
R/V0-M1-F2-S1: R - recycled aggregate; V0 – same amount of water as for the reference mixture; M1 –mixture with unwashed aggregate; F2 - double mixing method; S1 – mixture with superplasticizer

FIG. 8. Consistency of mortar made with aggregate that contains fine particles, w/c=0.55.

In this case, fine particles influence on consistency loss is obvious, both initial and final, comparing to the previous case. The consistency loss was more pronounced in the case of natural aggregate, which was expected because of the significantly higher content of fine particles in relation to recycled aggregate.

It is also significant that in the case of natural aggregate, difference between initial and final consistency is decreased, which can be explained by the influence of clay particles on the extension of the setting time, i.e. on slowing the hydration process.

It should be emphasized that addition of superplasticizer in the amount of 0.6 % by weight of cement significantly affects the initial consistency of the mixtures with recycled aggregates, i.e. it completely compensates water added for absorption correction. It is also obvious that there is a significant increase of consistency in relation to the reference mixture with silty natural aggregate, as for the mixtures with additive, and for the mixtures with added water.

After 2 hours (time needed for concrete placement), consistency of the mixtures with superplasticizer is significantly decreased compared to the initial value, but it is only slightly lower in relation to the value of the reference mixture. After addition of superplasticizer in the amount of additional 0.4 % by weight of cement (1 % of total), consistency of the sample after 2 hours increased to 12.1 cm. It means that by using the superplasticizer in quantity much lower than the maximum recommended value by the manufacturer (1.5 %), consistency of the mortar with recycled aggregates can be effectively corrected, not in any way by increasing the w/c ratio.

For better comparison of the mixtures with and without fine particles, results are summarized in the diagram shown in the Fig. 9.

From the results obtained, it can be concluded that the recycled aggregate (in the case of the conventional mixing method, and in the absence of the influence of fine particles) does not absorb all the water added to the mortar (and concrete) for absorption, thereby increasing the effective w/c ratio and consistency.

Bending and compressive strength of the mortar

For the mortar with the ratio w/c = 0.55 and composition indicated in Table 4, series of prisms 4x4x16 cm were made in order to test bending and compressive strength.

All composition materials aggregates, cement, superplasticizer and water were in the same condition as in the previous testing. Before making prisms, flow table consistency was tested. Two series were taken from the samples used for testing

change of consistency in time (after 2 hours). and these specimens were marked as „t2“. Other series were taken immediately after mixing, i.e. after initial consistency testing in zero time. Marks of the series were the same as for consistency testing with the addition of mark „t2“ for the series taken after 2 hours.

Mortars were placed into the molds, compacted and then stored in the climate chamber. After 24 hours, specimens were taken from the climate chamber, demolded and immersed into the water until test beginning. Bending and compressive strength testing results are shown in the Table 5.

All mixtures containing recycled aggregate have smaller bending strength after 7 days than mixtures with natural aggregate, even in the cases of smaller effective w/c ratio and in cases of superplasticizer addition. But for bending strength after 28-days, this is not the case. According to the results obtained, it can also be concluded that the compressive strength of the specimens with recycled aggregate is smaller compared to the reference mortar if all the water is added in the mixture according to absorption determined in HRN EN 1097-6. On the other hand, in that case consistency was increased in the whole observed time of two hours.

If the absolute w/c ratio is kept the same, consistency is reducing due to recycled aggregates absorption, and the effective w/c ratio is reducing as well. In the case of washed aggregate and double mixing method, it resulted with increased 7-day compressive strength by 5.5 % compared to the reference mortar.

In the case of the conventional mixing method, there is a slight decrease of the compressive strength by 0.9 %.

Testing after 28 days showed uniform compressive strength in the mixtures of the same absolute w/c ratio. The only decrease in strength in relation to the reference mixture is observed in the case of the specimen taken after 2 hours and with additional 0.4 % of superplasticizer added to the mixture immediately before this 2 hours.

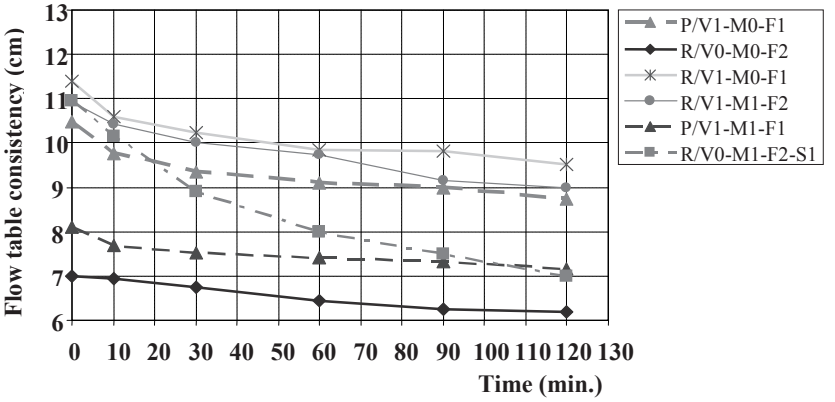

FIG. 9. Consistency of mortars (R and P), with and without fine particles, w/c=0.55

For the same pairs of specimens that differ only in mixing method, there is an evident increase of 7 - day compressive strength of all specimens mixed with double mixing method, compared to equivalent specimens prepared by using conventional (one phase) mixing method. Increase of compressive strength is 6.5% in the case of washed aggregates without water added for absorption, while in the case of added water it is 6.7%. In the case where aggregate consists of fine particles, compressive strength increase is 3.3 %, but with consistency increasing to 9.6 %. This trend is not confirmed in the case of 28 - day compressive strength. Increase of 28-day compressive strength of the specimens prepared by double mixing method is noticeable only in case of mortar with washed aggregate and with all water required for absolute absorption. In the case of mortar with unwashed aggregate and mortar with a clean aggregate without water added for absorption, when mixtures are made by double mixing method, there is very slightly compressive strength decrease.
In general, double mixing method should be certainly recommended for the production of mortar and concrete with recycled fine aggregates (besides its already confirmed positive effect in the case of recycled coarse aggregate). Double mixing method influences on the workability improvement, and therefore the less needed water and likely positive influence on the compressive strength.

Table 5. Results of Testing Mortar in Hardened State

Series	Mean compressive strength after7 days (N/mm^2)	Mean bending strength after7 days (N/mm^2)	Mean compressive strength after28 days (N/mm^2)	Mean bending strength after28 days (N/mm^2)	Flow table consistency (cm)
P/M0-V1-F1	51.4	7.8	60.6	6.2	9.9
R/M0-V0-F1	50.9	6.1	60.6	7.0	5.8
R/M0-V0-F2	54.4	7.1	59.4	6.5	6.8
R/M0-V1-F1	40.9	6.6	48.6	6.5	10.3
R/M0-V1-F2	43.8	6.1	51.0	5.2	11.3
P/M1-V1-F1	52.4	7.9	60.0	5.8	8.1
R/M1-V1-F1	39.3	6.3	46.9	5.9	10.3
R/M1-V1-F2	40.6	5.6	45.8	5.9	11.4
R/M1-V1-F2-t2	43.6	6.1	48.4	6.1	8.6
R/M1-V0-F2-S1	56.3	5.7	59.9	4.9	11.4
R/M1-V0-F2-S1-t2	52.0	6.4	54.3	6.3	12.1

LEGEND:
P - natural aggregate (reference mixture)
R - recycled aggregate
M0 –mixture with washed aggregate (without silty particles)
M1 - mixture with unwashed aggregate (with silty particles)

V0 –mixture with the same amount of water as for the reference mixture
V1 - mixture with additional of water (in relation to the reference mixture) determined according to HRN EN 1097-6
F1/F2 – mixing in one/two phases
S1 – mixture with superplasticizer
t2 – specimens taken after two hours of testing mortar consistency

Compressive strength is also increased in the case of using superplasticizer in recycled mortar in relation to reference mortar. Mixture with 0.6 % of admixture and with a specimen taken at zero time (after the first consistency testing, immediately after mixing) achieved compressive strength of 7.1 % larger than the reference mixture, while the mixture with the 1 % addition of superplasticizer, with the specimen taken after 2 hours achieved 0.7 % lower compressive strength. This slightly decrease can be explained by increased amount of superplasticizer, because in the case of mixtures without superplasticizer specimen taken after 2 hours reached 6.8 % higher compressive strength after 7 days than specimen taken immediately after mixing. That difference after 28 days is 5.7 %.

This increase in compressive strength of the specimen mixed for 2 hours can be explained by the fact that in the case of the specimen made immediately after mixing, an additional amount of water was not fully absorbed by the aggregate. It was partially involved in the hydration process, which started earlier, undisturbed by additional mixing of the mortar. It should be added that the water which still entered in the grain pores slowly extruded air bubbles. Due to the lack of additional mixing, they did not reach the surface, but remained trapped between the grains, thus having further influence on the compressive strength reduction. On the other hand, in the specimen that was mixed for 2 hours after preparation (with interruptions), the hydration process was slowed down due to mixing, there was more time for aggregate absorption and for air bubbles to come out on the surface. This probably led to a more compact mortar structure, with less air voids, but with a lower effective w/c ratio. To confirm these assumptions, a larger number of specimens should be tested.

CONCLUSION

Based on the results of consistency, bending and compressive strength mortars testing, it can be concluded that small recycled concrete aggregate may be suitable for use in the concrete production. It should be emphasized that this can be valid only for use in non-aggressive environment, and with stricter quality control than for natural aggregates. This control should, in the first place contain testing of the fine particles content, and control of the effective absorption.

Besides that, in production of the recycled aggregate concrete, following recommendations should be taken into consideration:

- In concrete mix design, correction of the water for absolute aggregate absorption determined according to HRN EN 1097 should be decreased. This reduction should be estimated based on the specific aggregate testing, taking into consideration the time required for concrete placing and methods of placing and compaction.
- In the production of concrete with the recycled concrete aggregate, it should be

recommended to use double mixing method, due to its positive effect on the consistency and strength.

- It is important to recommend the use of superplasticizer and to use it for necessary correction of consistency.

In further research, for much more precise analysis there should be observed influence of pore structure and interfacial transition zone of recycled aggregate concrete with scanning electron microscope (SEM).

ACKNOWLEDGMENTS

The authors appreciate the financial support from Croatian Ministry of Education. Science and Sport for two scientific projects “The Development of New Materials and Concrete Structure Protection Systems” 082-0822161-2159 and “From Nano - to Macro-structure of Concrete” 082-0822161-2990.

REFERENCES

De Schutter, G., and Poppe. A.M. (2004). "Quantification of the water demand of sand in mortar." *Construction and Building Materials 18*: 517–521.

Goncalves, A., Esteves, A. and Vieira, M. (2004). "Influence of recycled concrete aggregates on concrete durability." *International RILEM Conference on the Use of Recycled Materials in Buildings and Structures*

Li, J., Xiao, H., and Zhou, Y. (2009). "Influence of coating recycled aggregate surface with pozzolanic powder on properties of recycled aggregate concrete." *Construction and Building Materials.,* Vol. 23. Issue 3: 1287-1291.

Ryu. J. S. (2002). "Improvement on strength and impermeability of recycled concrete made from crushed concrete coarse aggregate". *Journal of Materials Science Letters 21*: 1565-1567.

Solyman. M. (2006). "Classification of Recycled Sands and their Application as Aggregates for Concrete and Bituminous Mixtures." *Kassel University Press GmbH*. Kassel.

Tam, V.W.Y., Gao, X.F., Tam, C.M., and Chan. C.H. (2008) "New approach in measuring water absorption of recycled aggregates." *Construction and Building Materials*. 22(3): 364-369.

Tam, V. W. Y., Gao, X. F., Tam, C. M., Ng, K. M. (2009) . “Physio-chemical reactions in recycle aggregate concrete.” *Journal of Hazardous Materials* 163(30): 823-828

Tam, V.W.Y., Gao, X. F., and Tam, C. M. (2005). "Microstructural analysis of recycled aggregate concrete produced from two-stage mixing approach." *Cement and Concrete Research.* 35(6): 1195-1203

Tam, V.W.Y., and Tam, C.M. (2008) "Diversifying two-stage mixing approach (TSMA) for recycled aggregate concrete: TSMAs and TSMAsc." *Construction and Building Materials* 22 (10): 2068-2077

Tam, V.W.Y., Tam, C.M., and Wang, Y. (2007). "Optimization on proportion for recycled aggregate in concrete using two-stage mixing approach." *Construction and Building Materials* 21(10):1928-1939

Analytical Solution of Displacement and Stress in CRCP under Thermal Load

Chen Xiaobing[1], Huang Xiaoming[2] and Tong Jinhu[3]

[1]Associate professor, School of Transportation, Southeast University, Jiangsu Nanjing, 210096, P. R. China; email: xbchen@seu.edu.cn
[2] Professor, School of Transportation, Southeast University, Jiangsu Nanjing, 210096, P. R. China; email: huangxm@seu.edu.cn
[3]Engineer, School of Transportation, Southeast University, Jiangsu Nanjing, 210096, P. R. China; email: 101010035@seu.edu.cn

ABSTRACT: Due to the relatively longer length of Continuously Reinforced Concrete Pavement (CRCP), CRCP can be regarded as a long slab on the elastic foundation. According to the slippage assumption of shearing stress and maximum principal stress theory, the analytical solutions of the displacement, tensile stress and shearing stress in CRCP under thermal load are deduced in this study. The following results are acquired from the analysis. Maximum thermal displacement, thermal tensile stress and shearing stress have relations with the temperature difference, resistance coefficient of friction between slab and base, the thickness, modulus and length of slab. And they are in proportion to temperature difference. The influence of resistance coefficient of friction is significant to maximum thermal displacement and stress. In conclusion, reducing the resistance coefficient of friction is a preferential choice to decrease the maximum thermal displacement and maximum thermal stress.

INTRODUCTION

Continuously Reinforced Concrete Pavement (CRCP) is a Portland cement concrete pavement structure with continuous longitudinal steel reinforcements but without any preventive measures for transverse expansion or contraction joints (Deng, 2007; Huang, 2000). The superiority of CRCP is exhibited under some special conditions (such as heavy traffic, uneven settlement and poor hydrogeological conditions).

It is believed that CRCP will crack naturally (Kohler, 2004). Repetitive loading and thermal load would lead the concrete to crack vertically. The closely spaced transverse and longitudinal cracks could cause punchouts (Che, 2005; Selezneva, 2003). Field investigations of CRCP indicate that spalling is another cause of damage of CRCP (Zollinger, 1994). Therefore, punchouts and smoothness are proposed as the basic design parameters in the Guide for Mechanistic-Empirical Design of CRCP (ARA, 2004). Therefore, it is practically significant to analyze the cracking of CRCP.

In this paper, based on slippage assumption of shearing stress (Zhu, 2006) and maximum principal stress theory (Jiang, 2009), the displacement and stress formulas of CRCP which is on an elastic foundation under thermal load are obtained. These analysis results are helpful in the study and design process of CRCP on an elastic foundation under thermal load.

BASIC THEORY AND DIFFERENTIAL EQUATIONS

Basic theory

After construction, the early transverse cracks of the slab are caused by the combined effects of decreasing temperature and dryness shrinkage. Slab thickness is far less than its length and width. The calculation model of CRCP under thermal load can be regarded as a longitudinal continuous elastic thin plate under the uniform stress on an elastic foundation(Fig. 1).

a)

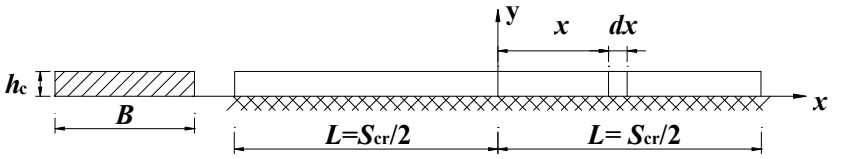

b)

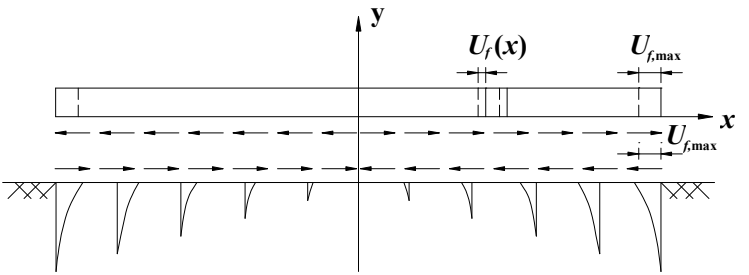

FIG. 1. Slab under thermal load: (a) size; (b) longitudinal displacement.

The differential equations of slab under the thermal load

According to slippage assumption of shearing stress, shearing stress between slab and base is proportional to the longitudinal displacement of slab.

$$\tau_c = k_{cb} u_f \tag{1}$$

Where,

τ_c : shearing stress between slab and base

k_{cb} : the resistance coefficient of friction between slab and base

u_f : the longitudinal displacement of slab

Based on the Saint-Venant's principle (Xu, 2009), the tensile stress of slab far away from the end can be regarded as uniform. Therefore, maximum principal stress theory is applicable in the analysis.

According to the basic assumptions of elastic thin plates (Deng, 2005) and the balance of internal forces and loads, the force differential equation of elastic thin plates in the horizontal direction is calculated as follows(Fig. 2).

$$N + dN - N + Q = 0 \tag{2}$$

$$h_c B d\sigma_x + \tau_c B d_x = 0 \tag{3}$$

$$\frac{d\sigma_c}{dx} + \frac{\tau_c}{h_c} = 0 \tag{4}$$

Where,

N: the composition of forces on the slab

Q: shearing force caused by base

h_c: slab thickness

B: slab width

σ_c : the tensile stress of slab

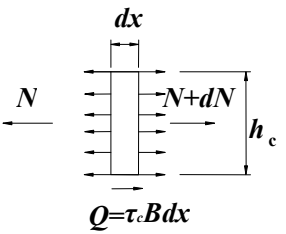

FIG. 2. Horizontal load action on the micro-unit slab.

THE DISPLACEMENT AND STRESS FORMULAS

The displacement of CRCP

The displacement of slab at any point can be divided into constrained displacement and free displacement. According to the Hooke's law (Sun, 2008), the equations of displacement and tensile stress of slab can be presented as

$$\begin{cases} u_\sigma = -u_f + \alpha \Delta T x \\ \sigma_c = E_c \dfrac{du_\sigma}{dx} \end{cases} \tag{5}$$

Where,

u_σ : constrained displacement

α : the coefficient of linear thermal expansion of concrete slab

ΔT : temperature difference

E_c: elastic modulus of slab

The first order derivative of the displacement and tensile stress can be presented as follows:

$$\frac{du_\sigma}{dx} = -\frac{du_f}{dx} + \alpha \Delta T \tag{6}$$

$$\frac{d\sigma_c}{dx} = E_c \frac{d^2 u_\sigma}{dx^2} = -E_c \frac{d^2 u_f}{dx^2} \tag{7}$$

By putting Eq. 1 and Eq. 7 into the elastic slab balance of Eq. 4, the new elastic thin plates' displacement differential equation on an elastic foundation under the thermal load is written as

$$E_c \frac{d^2 u_f}{dx^2} - \frac{k_{cb} u_f}{h_c} = 0 \tag{8}$$

$$\frac{d^2 u_f}{dx^2} - \beta^2 u_f = 0 \tag{9}$$

Where,

β : friction parameter of slab, $\beta = \sqrt{\dfrac{k_{cb}}{h_c E_c}}$

After successive integrals of Eq. 9, we can gain the general solution as follows:

$$u_f = C_1 \mathrm{ch}(\beta x) + C_2 \mathrm{sh}(\beta x) \tag{10}$$

Taking the boundary conditions into consideration, we can obtain integration constants. As x=0, $u_f(x)$=0, we get C_1=0. As $x=L=S_{cr}/2$, σ_c =0, we get $C_2 = \alpha \Delta T / (\beta \mathrm{ch} \beta L)$.

By putting the coefficients C_1 and C_2 into Eq. 10, the displacement formula is written as

$$u_f = \frac{\alpha \Delta T}{\beta \mathrm{ch} \beta L} \mathrm{sh} \beta x \tag{11}$$

As $x=L=S_{cr}/2$, maximum displacement could be obtained from

$$u_{f,\max} = \frac{\alpha \Delta T}{\beta} \mathrm{th} \beta L \tag{12}$$

Where,

S_{cr}: the crack spacing

The tensile stress

Substituting the displacement of Eq. 11 into Eq. 5, the longitudinal tensile stress formula is written as

$$\sigma_c = E_c(-\frac{du_f}{dx} + \alpha\Delta T) = E_c\alpha\Delta T\left(1-\frac{\mathrm{ch}\beta x}{\mathrm{ch}\beta L}\right) \tag{13}$$

As x=0, maximum tensile stress is obtained from

$$\sigma_{c,\max} = E_c\alpha\Delta T\left(1-\frac{1}{\mathrm{ch}\beta L}\right) \tag{14}$$

The shearing stress

Substituting the displacement of Eq. 11 into Eq. 1, the longitudinal shearing stress formula is written as

$$\tau_c = k_{cb}u_f = \frac{k_{cb}\alpha\Delta T}{\beta\mathrm{ch}\beta L}\mathrm{sh}\beta x \tag{15}$$

As x= L, maximum shearing stress is obtained from

$$\tau_{c,\max} = k_{cb}u_f = \frac{k_{cb}\alpha\Delta T}{\beta}\mathrm{th}\beta L \tag{16}$$

THE EFFECT ANALYSIS OF VARIOUS PARAMETERS

The effect of parameters on maximum displacement

As shown in Fig. 3, maximum displacement happens at the end of the slab. Temperature difference has a significant effect on the maximum displacement of the slab. The slab will expand as the rise of the temperature. Maximum displacement has relations with the temperature difference, resistance coefficient of friction, the elastic modulus of slab, slab thickness and slab length.

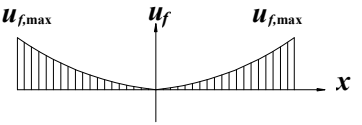

FIG. 3. Longitudinal displacement of slab.

The effect of parameters on maximum tensile stress

It is obvious from Fig. 4 that the maximum tensile stress is located in the middle of the slab. Similarly, the temperature difference has a significant effect on the maximum tensile stress of the slab. The effect of parameters on maximum tensile stress is just the

same as the parameters acting on maximum displacement.

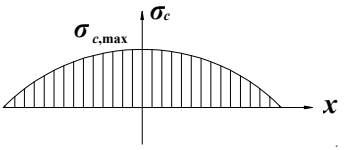

FIG. 4. Tensile stress of slab.

The effect of parameters on maximum shearing stress

Fig. 5 shows that the place of maximum shearing stress and the effect of parameters on maximum shearing stress are just the same as the parameters acting on maximum displacement too.

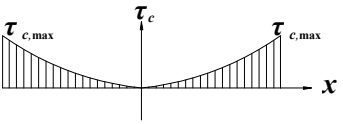

FIG. 5. Shearing stress of slab.

The variety of maximum displacement and tensile stress

When the temperature of slab decreases, the tensile stress appears. On the contrary, the compressive stress appears as the temperature of slab increase. If the tensile stress of slab is greater than tensile strength of slab, the crack appears in the middle of slab.

The dryness shrinkage of slab can be converted to equivalent temperature difference. After construction, the early transverse cracks of the slab are caused easily by the combined effects of decreasing temperature and dryness shrinkage. Therefore, CRCP constructed in summer is easier to crack than that constructed in autumn and winter.

CONCLUSIONS

Maximum displacement and stress have relations with the temperature difference, resistance coefficient of friction, elastic modulus of slab, slab thickness and slab length. Therefore, it is possible to decrease maximum displacement and maximum stress by reducing temperature difference and resistance coefficient of friction. The optimal construction seasons for CRCP are autumn and winter.

REFERENCES

Deng, X.J. and Huang, X.M. (2007). *Principles and Design Methods of Pavement*, 2nd Ed., China Communications Press, Beijing: 472-478.

Huang, W. and Qian, Z.D. (2000). *Theory and Methodology of High-Class Concrete Pavement Design*, 1st Ed., China Communications Publishers, Beijing: 206-212.

Kohler, E. and Roesler, J. (2004). "Active crack control for continuously reinforced concrete pavements". *Proceedings of Transportation Research Board 83rd Annual Meeting*, Washington, D.C.: 19-29.

Che, D.H., Scullion, T., Bilyeu, J., et al. (2005). "Detailed forensic investigation and rehabilitation recommendation on interstate highway-30." *Journal of Performance of* Constructed *Facilities*, Vol. 19 (2): 155-164.

Selezneva, O.I., Darter M.I., Zollinger D.G., et al. (2003). "Characterization of transverse cracking spatial variability: using of LTPP data for CRCP design." *Proceedings of Transportation Research Board 82nd Annual Meeting*. Washington, D.C.: 147-155.

Zollinger, D.G., Senadheera, S.P. and Tang, T.X. (1994). " Spalling of continuously reinforced concrete pavements." *Journal of Transportation Engineering*, Vol. 120 (3): 394-411.

ARA. (2004). "Guide for mechanistic-empirical design of new and rehabilitated pavement structures." Published by the ARA Inc.

Zhu, B.F. (2006). "Thermal stresses in concrete beams on elastic foundations." *China Civil Engineering Journal*, Vol. 39(8): 96-101.

Jiang, X.Y. and Gong, H. (2009). *Mechanics of materials*, 4th Ed., Xi'an Jiaotong University Press, Xi'an: 185-189.

Xu, Z.L. (2009). *Mechanics of elasticity,* 3rd Ed., Higher Education Press, Beijing: 21-23.

Deng, X.J. and Chen, R.S. (2005). *Rigid Pavement Design*, 2nd Ed., China Communications Press, Beijing: 10-11.

Sun, X.F., Fang, X.S. and Guan, T.L. (2008). *Mechanics of materials (Volume I),* 4th Ed., Higher Education Press, Beijing: 17-19.

A Method for Seeking the Domain of Chaboche Model of Cement Concrete Fatigue Damage under High Stress Ratio

Y.Q. Xue[1], X.M. Huang[2], W. Zhou[3], T. Ma[4] and S.Z. Qian[5]

[1] Ph.D. Candidate, School of Transportation, Southeast University, Nanjing, 210096, China; email: 494961575@qq.com.
[2]Professor, School of Transportation, Southeast University, Nanjing, 210096, China; email: huangxm@seu.edu.cn.
[3] School of Transportation, Southeast University, Nanjing, 210096, China;
[4]School of Transportation, Southeast University, Nanjing, 210096, China, E-mail: 784687597@qq.com, Phone: 0086 15805160021
[5] School of Transportation, Southeast University, Nanjing, 210096, China.

ABSTRACT: In order to determine the domains of Chaboche model of cement concrete fatigue damage under high stress ratios, first, the probability densities of general monotonic random variables including cement concrete fatigue life are deduced. And then, the probability density of Chaboche fatigue damage model is deduced. By virtue of laboratory fatigue test results, the fatigue damage probability density functions of Chaboche model can be obtained, considering different stress ratios. Substituting load cycles into the functions, the cement concrete fatigue reliabilities based on Chaboche model can be acquired through integral operation. Finally, on the basis of cement concrete fatigue reliability analysis, the critical values of load cycle of Chaboche model under different high stress ratios can be made certain and the model's domains corresponding to these stress ratios can be obtained. The obtained results also show that under the same stress ratio, with the increase in the load cycle, the fatigue reliability declines gradually from almost 100% to 0%. No matter under any stress ratio, in the initial stage of load action, there is always a relatively stable phase for fatigue reliability. With the increase in the stress ratio, the phase diminishes gradually and the load cycle corresponding to reliability of 0% also decreases. In descent phase of reliability, the higher stress ratio is, the lower cement concrete reliability is for the same load cycle.

INTRODUCTION

It is well known that, the phenomenon of vehicle overload is difficult to

effectively control in China. Although there are a lot of reasons for overload, for cement concrete pavement, the considerable vehicle overload will bring relatively high stress level to concrete slab undoubtedly. And then, the durability of pavement could be affected adversely. As a widely used building material, in many cases, cement concrete needs to undertake repeated loads practically, so its anti-fatigue property is vitally important. Obviously, for highways and urban roads paved with cement concrete surface course, the need of material's anti-fatigue property is quite high (Zhao, 1999; Sun, 2008). Moreover, because of the random fluctuations of load cases and the inherent heterogeneity of cement concrete, even under the same condition, the same concrete may perform differently. As a result, the fatigue life of cement concrete pavement will take on a certain degree of dispersion (Chaboche, 1988; Chandrakanth, 1995).

In terms of damage mechanics, no matter how many times of fatigue life is and no matter what change law of the load during entire fatigue life is, the essence of material's fatigue is nothing more than a gradual course of damage accumulation with the increase of load cycles. Therefore, based on damage mechanics, several fatigue damage models could be established (Zheng, 2010; Xu, 2010). Chaboche model is one of the cement concrete fatigue damage models generally accepted. However, there are some intrinsic defects about this model. The most important intrinsic defect is that Chaboche model can not describe the change law of fatigue damage at the beginning period of load cycle well. Therefore, to study certain the critical load cycle, a new proposed method is presented in this paper. This method is based on the cement concrete fatigue reliability analysis. By means of the analysis, the domains of Chaboche model under different high stress ratios can be obtained easily.

REVIEWS OF FATIGUE DAMAGE MODELS

In fatigue damage models, damage is generally defined as some certain functions of load cycles. The most simple and widely adopted fatigue damage model is Miner model. In Miner model, n/N is defined as fatigue damage D. For cement concrete, N is its fatigue life under some particular stress level and n is the load cycles having been exerted on it. Based on continuum damage mechanics, Chaboche and some other researchers proposed a new fatigue damage model taking dissipative structure theory of thermodynamics into account:

$$\frac{dD}{dn} = A\left(\frac{\sigma}{1-D}\right)^{p}(1-D)^{-q} \tag{1}$$

Where, A, p and q are test parameters. For the concrete material, q usually equal zero. Then, the model is simplified as follows:

$$\frac{dD}{dn} = A\left(\frac{\sigma}{1-D}\right)^{p} \tag{2}$$

The boundary conditions of the model is when $n = 0$, $D = 0$ and when $n = N$, $D = 1$. So, after carrying out integral operation to Eq.(2), a couple of equations can be obtained as follows:

$$N = \frac{1}{A}\left(\frac{1}{\sigma}\right)^{p}\int_0^1 (1-D)^{p}\,dD = \frac{1}{A(p+1)}\left(\frac{1}{\sigma}\right)^{p} \tag{3}$$

$$n = \frac{1}{A}\left(\frac{1}{\sigma}\right)^{p}\int_0^D (1-D)^{p}\,dD = \frac{1}{A(p+1)}\left(\frac{1}{\sigma}\right)^{p}(1-(1-D)^{p+1}) \tag{4}$$

Dividing Eq.(3) by Eq.(4), the fatigue damage D of Chaboche model can be obtained easily:

$$D = 1-\left(1-\frac{n}{N}\right)^{\frac{1}{1+p}} \tag{5}$$

Moreover, according to the concrete fatigue equation of Aas-Jakobsen, $R = 1-(1-\rho)\beta \lg N$, Zhao Yongli of Southeast University deduced another concrete fatigue damage model based on actual stress ratio change (Zhao, 1999):

$$D = 1-\frac{1}{1-\frac{(1-\rho)\beta}{R}\lg(1-\frac{n}{N})} \tag{6}$$

Where, R is the stress ratio; ρ is the characteristic value of the load cycles and equals to the ratio of minimum and maximum of cyclic load; β is the test parameter and according to Aas-Jakobsen's recommendation, β can be set as 0.0640; N is the fatigue life of cement concrete.

PROBABILITY DENSITY OF CEMENT CONCRETE CHABOCHE FATIGUE DAMAGE

Probability density of monotonic random variable

Setting the probability density function of random variable ξ is $f(x)$ and the probability density function of random variable η is $p(y)$. If η is monofonic function of ξ, $\eta = \phi(\xi)$, $p(y)$ can be obtained from $f(x)$.

The derivation process is as follows (Song, 2001; Cao, 2004):

1) $y = \phi(x)$ is monotonic function, so the single-valued inverse function $x = \psi(y)$ exists.

2) Can be proved in theory, if and only if $x < \xi < x + dx$ occurs, $y < \eta < y + dy$ would occur. That is to say, $P(y < \eta < y + dy) = P(x < \xi < x + dx)$ & $p(y)dy = f(x)dx$.

3) Substituting $x = \psi(y)$ & $dx = d\psi(y)$ into $p(y)dy = f(x)dx$, obviously, $p(y) = f[\psi(y)]\dfrac{d\psi(y)}{dy}$ (increasing function) or $p(y) = f[\psi(y)]\left|\dfrac{d\psi(y)}{dy}\right|$ (decreasing function).

Probability density of cement concrete fatigue life

As a kind of composite material, there are a lot of micro-pores and micro-cracks in cement concrete. Under repeated loads, the micro-pores will extend gradually, and finally forming the macro-cracks. The emergence of macro-cracks means that the fracture of concrete and this fracture is considered as the fatigue damage fracture. The load cycles before fatigue damage fracture is called the fatigue life of cement concrete.

Usually, after carrying out logarithmic transformation to fatigue life N_ξ, mathematical statistics and mechanical analysis are then executed. In general, the logarithm of fatigue life X is subject to normal distribution. That is to say, that the value of $X \sim N(\mu;\sigma)$ and its probability density function is $f(x) = \dfrac{1}{\sigma\sqrt{2\pi}} e^{-\frac{(x-\mu)^2}{2\sigma^2}}$. Where, μ and σ are the population mean and variance of logarithm of fatigue life respectively. If the value of $X = \lg N_\xi$, obviously, $N_\xi = 10^X$ and N_ξ is exponential function of X. Its probability density function can be set as $p(N)$.

Because $x = \lg N$, $dx = \dfrac{dN}{N \ln 10}$.

Besides, $P(N < N_\xi < N + dN) = P(x < X < x + dx)$ and $X \sim N(\mu;\sigma)$,

consequently,

$$P(x < X < x + dx) = f(x)dx = \frac{1}{\sigma\sqrt{2\pi}} e^{-\frac{(x-\mu)^2}{2\sigma^2}} dx$$

and $\frac{1}{\sigma\sqrt{2\pi}} e^{-\frac{(x-\mu)^2}{2\sigma^2}} dx = P(N < N_\xi < N + dN) = p(N)dN$.

Substituting $x = \lg N$ and $dx = \frac{dN}{N \ln 10}$ into it, the probability density function $p(N)$ of fatigue life N_ξ is obtained easily,

$$p(N) = \frac{1}{\sigma N\sqrt{2\pi}\ln 10} \exp\left[-\frac{(\lg N - \mu)^2}{2\sigma^2}\right] \tag{7}$$

Probability density function of Chaboche fatigue damage

Setting the probability density of Chaboche fatigue damage $D_\xi = 1 - \left(1 - \frac{n}{N_\xi}\right)^{\frac{1}{1+p}}$ is $q(D)$.

Evidently, D_ξ is a monotonic decreasing function of N_ξ. From $D = \phi(N) = 1 - \left(1 - \frac{n}{N}\right)^{\frac{1}{1+p}}$,

$N = \psi(D) = \frac{n}{1-(1-D)^{p+1}}$ and $\left|\frac{d\psi(D)}{dD}\right| = \frac{n(p+1)(1-D)^p}{[1-(1-D)^{p+1}]^2}$ can be acquired. Further, the following equation can be obtained according to the deducing process of probability density function mentioned above, as follows:

$$q(D) = \frac{1}{\sigma\sqrt{2\pi}\ln 10} \exp\left\{-\frac{\left[\lg n - \lg(1-(1-D)^{p+1}) - \mu\right]^2}{2\sigma^2}\right\} \times \frac{(p+1)(1-D)^p}{[1-(1-D)^{p+1}]} \tag{8}$$

According to statistics, using sub-sample mean $\bar{x}$ and sub-sample variance s^2 as the estimators of population mean μ and population variance σ^2 can meet the requirements of unbiasedness and consistency. So, the μ and σ in Eq.(8) can be gotten by the fatigue test of cement concrete. Beam-bent fatigue test is adopted here. The characteristic value ρ generally equals 0.1 (Li, 1998; Ministry of Transport of

China, 2002).

Table 1. Fatigue test results of cement concrete specimens

Specimen number	Stress ratio R					
	0.70		0.75		0.80	
	Fatigue life N	lg$N$	Fatigue life N	lg$N$	Fatigue life N	lg$N$
1	10184	4.008	10003	4.000	2110	3.324
2	11808	4.072	10943	4.039	2275	3.357
3	21684	4.336	11882	4.075	2659	3.425
4	21747	4.337	12413	4.094	3105	3.492
5	43683	4.640	14762	4.169	3758	3.575
6	49392	4.694	19048	4.280	4165	3.620
7	50997	4.708	20284	4.307	4749	3.677
8	70937	4.851	20328	4.308	5073	3.705
9	72266	4.859	23286	4.367	5981	3.777
10	77122	4.887	26291	4.420	6844	3.835
11	79778	4.902	26539	4.424	7161	3.855
12	82905	4.919	26561	4.424	8027	3.905
13	100411	5.002	40095	4.603	8345	3.921
14	101918	5.008	53683	4.730	8411	3.925
15	/	/	58835	4.770	/	/

Under ordinary traffic load, the stress ratio in cement concrete slab of pavement structure varies from 0.20 to 0.65 (Shi, 1990). However, heavy traffic is becoming more and more severe because of the temptation of economic interests. In traffic composition, the proportion of heavy vehicles and overload vehicles is increasing constantly. For the pavement structure designed under normal axle load and traffic composition conditions, its actual stress level is already in the high stress ratio range. A survey shows that under some certain traffic loads, the stress ratio may exceed 0.65 and even up to 1.00. According to a research of Key Laboratory of Highway Engineering in Special Region of Ministry of Education, Chang'an University, if the stress ratio R is more than 0.60, pavement structure will damage rapidly in a short time and the economical efficiency of that pavement thickness will be very poor (Jiang, 2005). On the basis of the above, the stress ratio R can be taken as 0.70, 0.75 and 0.80. The test data are displayed in Table 1.

According to Table 1, the mean $\bar{x}$, variance s^2 and standard deviation s of the logarithm of fatigue life from above-mentioned tests can be calculated. The statistical

results are shown in Table 2.

Table 2. Statistical analysis for fatigue test results

Stress ratio R	Sub-sample mean $\bar{x}$	Sub-sample variance s^2	Sub-sample standard deviation s
0.70	4.659	0.113	0.337
0.75	4.334	0.057	0.239
0.80	3.671	0.044	0.211

To ascertain the value of parameter p in Eq.(8), Eq.(6) is indispensable. Taking advantage of Eq.(6), the corresponding relations between n/N and D under the stress ratios of 0.70, 0.75 and 0.80 can all be obtained. In addition, according to Eq.(5), $\frac{1}{1+p}\ln(1-\frac{n}{N}) = \ln(1-D)$. Utilizing the corresponding relations between n/N and D mentioned above, regression models can be established so as to ascertain the value of p under different stress ratio, as shown in Table 3.

Table 3. Parameter p corresponding to different stress ratios

Load characteristic value ρ		0.1	
Stress ratio R	0.70	0.75	0.80
parameter p	31.362	33.364	35.364

Substituting the data of Table 2 and Table 3 into Eq.(8), the Chaboche fatigue damage probability density functions $q_1(D)$, $q_2(D)$ and $q_3(D)$ corresponding to the stress ratios of 0.70, 0.75 and 0.80 can be obtained as follows. Of course, respective characteristic values of load cycle are all 0.1 here.

$$q_1(D) = 0.514\exp\left\{-\frac{\left[\lg n - \lg(1-(1-D)^{32.362}) - 4.659\right]^2}{0.227}\right\} \times \frac{32.362(1-D)^{31.362}}{[1-(1-D)^{32.362}]};$$

$R = 0.70$.

$$q_2(D) = 0.726\exp\left\{-\frac{\left[\lg n - \lg(1-(1-D)^{34.364}) - 4.334\right]^2}{0.114}\right\} \times \frac{34.364(1-D)^{33.364}}{[1-(1-D)^{34.364}]};$$

$R = 0.75$.

$$q_3(D) = 0.821\exp\left\{-\frac{\left[\lg n - \lg(1-(1-D)^{36.364}) - 3.671\right]^2}{0.089}\right\} \times \frac{36.364(1-D)^{35.364}}{[1-(1-D)^{36.364}]};$$

$R = 0.80$.

Obviously, after been given n, the load cycles having been exerted on cement concrete, the form of probability density function of Chaboche fatigue damage can be entirely determined.

CALCULATIONS OF FATIGUE RELIABILITIES BASED ON CHABOCHE MODEL

Theoretically, D_c, defined as the critical value of fatigue damage may reach 1. However, a large number of tests show that the crack formation stage will generally end before fatigue damage achieving 1.

Table 4. The concrete fatigue reliability based on Chaboche model

Load characteristic value ρ		0.1		
Stress ratio R		0.70	0.75	0.80
Load cycles n	ln(n)	Reliability / Q_1	Reliability / Q_2	Reliability / Q_3
100	4.605	0.0004086249	0.0002807131	0.1733895614
200	5.298	0.0068353372	0.0136144710	0.6476503181
400	5.991	0.0559417670	0.1608595130	0.9540511106
800	6.685	0.2360122377	0.5783455491	0.9983225258
1600	7.378	0.5582723413	0.9156015448	0.9861658752
3200	8.071	0.8432426222	0.9950586859	0.7838170841
6400	8.764	0.9894254421	0.9868096496	0.2607187895
12800	9.457	0.9457216122	0.8292660482	0.0193202196
25600	10.150	0.7710948189	0.3780730366	0.0002370683
51200	10.843	0.4404520550	0.0580186527	0.0000004284
102400	11.537	0.1484522493	0.0023087255	0.0000000001

For most materials, $0.2 < D_c < 0.8$. In this article, as the material is cement concrete, its critical value of fatigue damage could be hypothetically set as 0.5. That is to say, when the fatigue damage is within 0 to 0.5, cement concrete is in the crack formation stage. Having been given n, the load cycles, in light of the above-mentioned range, definite integral operation on the probability density function of Chaboche fatigue damage can be carried out. In this way, the probability of cement concrete in crack formation stage can be calculated. The probability is none other than the fatigue reliability of cement concrete.

Hypothetically, the load cycles can be set as 100, 200, 400, 800, 1600, 3200, 6400, 12800, 25600, 51200 and 102400. Then, the concrete fatigue reliability based on Chaboche model, $Q_1 = \int_0^{0.5} q_1(D)dD$ (R = 0.70), $Q_2 = \int_0^{0.5} q_2(D)dD$ (R = 0.75) and $Q_3 = \int_0^{0.5} q_3(D)dD$ (R = 0.80) can be calculated. The calculation results are illustrated in Table 4.

DISCUSSION AND ASCERTAINMENT OF THE MODEL'S DOMAIN

Table 5. The domains of Chaboche model under different stress ratios

Domain	Stress ratio R		
	0.70	0.75	0.80
Critical values of load cycle (lower bounds of load cycle)	6400	3200	800
Upper bounds of load cycle	$(1-0.5^{p+1})N$		
The domains of Chaboche model	$[6400,(1-0.5^{p+1})N]$	$[3200,(1-0.5^{p+1})N]$	$[800,(1-0.5^{p+1})N]$

From Table 4, it is clearly that at the beginning period of load cycle, no matter under which stress ratio, there is always an abnormal and irrational phenomenon for the fatigue reliability (shaded portions). For the three stress ratios, at the beginning period of load cycle, the smaller load cycles is, the lower fatigue reliability of cement concrete is. So the data of shaded portions in Table 4 is invalid and they should be discarded. As mentioned above, one of the intrinsic defects of Chaboche model is it can not describe the change law of fatigue damage well at the beginning period of load cycle. This is the reason for that irrational phenomenon. Of course, after the critical load cycle, Chaboche model can describe the change law of material's fatigue damage relatively well. Based on the analysis mentioned above, the critical load cycles and the domains of Chaboche model of cement concrete fatigue damage under different high stress ratios can be obtained easily, shown in Table 5.

According to Table 4 and Table 5, it is clear that under the same stress ratio, the fatigue reliability of cement concrete decreases from almost 100% to 0% gradually with the increase in the natural logarithm of load cycle. No matter under which stress ratio, during the beginning period of load cycle, there is always a comparatively stable phase for the reliability of concrete. With the increase in stress ratio, the phase

diminishes and the natural logarithm of load cycle corresponding to the fatigue reliability just reducing to 0% also decreases. Accordingly, in the reduction stage of fatigue reliability, for the same load cycle, the higher stress ratio is, the lower fatigue reliability of cement concrete is.

Besides, the fatigue failure probability of cement concrete based on Chaboche model can be calculated easily, shown in Table 6.

Table 6. The concrete fatigue failure probability based on Chaboche model

Load characteristic value		0.1		
Stress ratio R		0.70	0.75	0.80
Load cycles n	ln(n)	failure probability	failure probability	failure probability
800	6.685	/	/	0.0016774742
1600	7.378	/	/	0.0138341248
3200	8.071	/	0.0049413141	0.2161829159
6400	8.764	0.0105745579	0.0131903504	0.7392812105
12800	9.457	0.0542783878	0.1707339518	0.9806797804
25600	10.150	0.2289051811	0.6219269634	0.9997629317
51200	10.843	0.5595479450	0.9419813473	0.9999995716
102400	11.537	0.8515477507	0.9976912745	0.9999999999

CONCLUSIONS

On the basis of cement concrete fatigue reliability analysis, a new method is developed to study the critical load cycle and obtain the domains of Chaboche model under different high stress ratios. The main findings are as follows:

(1) The obtained critical values of the load cycles of Chaboche model of cement concrete fatigue damage under high stress ratios of 0.70, 0.75 and 0.80 are 6400, 3200 and 800, respectively. The upper bounds of load cycles of Chaboche model of cement concrete under different high stress ratios are all in the form of $(1-0.5^{p+1})N$. The domains of Chaboche model of cement concrete fatigue damage under high stress ratios of 0.70, 0.75 and 0.80 are $[6400,(1-0.5^{p+1})N]$, $[3200,(1-0.5^{p+1})N]$ and $[800,(1-0.5^{p+1})N]$, respectively.

(2) No matter under which stress ratio, during the beginning period of load cycle, there is always a comparatively stable phase for the reliability of concrete. With the increase in the stress ratio, the phase diminishes and the natural logarithm of load

cycle corresponding to the fatigue reliability just reducing to 0% also decreases.

(3) Under the same stress ratio, the fatigue reliability of cement concrete decreases from almost 100% to 0% gradually with the increase in the natural logarithm of load cycle. In the reduction stage of fatigue reliability, for the same load cycle, the higher stress ratio is, the lower fatigue reliability of cement concrete is. After fatigue reliability analysis, the concrete fatigue failure probability based on Chaboche model can also be acquired.

REFERENCES

Cao, Z.H. and Zhao, P. (2004). "Probability and mathematical statistics." *Nanjing*: *Southeast University Press*.

Chaboche, J.L. and Lesne. P.M.A. (1988). "Linear continuous fatigue damage model." *Fatigue and Fracture of Engineering Materials Structure*, Vol. 11(1): 1-17.

Chandrakanth, S. and Pandey, P.C.(1995). "An isotropic damage model for ductile material." *Engineering Fracture Mechanics*, Vol. 50(4): 457-465.

Jiang,Y.J. and Dai, X.Z. (2005). "Study on mechanism of cement concrete pavement damage of heavy-duty traffic road and countermeasures." *Journal of Highway and Transportation Research and Development*, Vol. 22(7): 31-35.

Li, Y.Q. and Che, H.M. (1998). "A study on the cumulative damage to plain concrete due to flexural fatigue." *China Railway Science*, Vol. 19(2): 52-58.

Ministry of Transport of the People's Republic of China (2002). "JTG D40-2002 specifications of cement concrete pavement design for highway." *Beijing*: *China Communications Press*.

Song, B.S. and Luo. Q.L. (2001). "Advanced mathematics." *Beijing*: *Advanced Education Press*.

Shi, X.P., Yao, Z.K., Li, H., et al (1990). "Study on flexural fatigue behavior of cement concrete." *China Civil Engineering Journal*, Vol. 23(3): 11-21.

Sun, Z.L. (2008). "Research on fatigue damage of asphalt pavement based on damage mechanics." *Nanjing*: *School of Transportation of Southeast University*.

Xu, J.Q. and Guo, F.M.(2010). "Mechanism of fatigue damage evolution and the evolution law." *Journal of Mechanical Engineering*, Vol. 46(2): 40-46.

Zhao, Y.L. and Sun, W. (1999). "Establishment of the fatigue damage equation of the concrete material." *Journal of Chongqing Jiaotong Institute*, Vol. 18(1):17-22.

Zheng, Z.G., Cai, G.W. and Li Z.J. (2010). "A new model of fatigue damage evolution." *Engineering Mechanics*, Vol. 27(2): 37-40.

Carbonation Resistance of Concrete Containing $Mg(OH)_2$ as a Carbon Immobilizer

Wei Chen[1], Xiaoxing Chen[2] and Peiliang Shen[3]

[1]School of Materials Science and Engineering, Wuhan University of Technology, Luoshi Road 122, Wuhan, 430070, P.R. China; State Key Laboratory of Silicate Materials for Architectures (Wuhan University of Technology), Luoshi Road 122, Wuhan, 430070, China; email w.chen.whut@gmail.com.
[2] School of Materials Science and Engineering, Wuhan University of Technology, Luoshi Road 122, Wuhan, 430070, P.R. China.
[3] School of Materials Science and Engineering, Wuhan University of Technology, Luoshi Road 122, Wuhan, 430070, P.R. China.

ABSTRACT: The carbonation resistance of concrete with or without $Mg(OH)_2$ as a carbon immobilizer is investigated in this study. The carbonation rate of the concrete is evaluated with the accelerated carbonation tests. The results show that 4.8% of $Mg(OH)_2$ in the binder of concrete can reduce the carbonation depth to about 50%. Microstructural analysis show that the $Mg(OH)_2$ reacts with CO_2 and water to form the hydromagnesite, via which the CO_2 is immobilized.

INTRODUCTION

Carbonation is one of the major deterioration processes of concrete which lowers the alkalinity of the pore solution and de-stabilizes the passivated protective film on the steel rebars in structure (Monteiro, 2008). The carbonation reaction is the chemical reaction between CO_2 and hydration products (mainly C-S-H gel and Portlandite) (Chen, 2011). The carbonation rate of conventional concrete is mainly affected by the nature of hydration products and permeability of the hardened concrete. With the addition of large volume supplementary admixtures, the carbonation rate is greatly promoted (Sisomphon, 2007).

Magnesia is normally considered as a deteriorative agent to concrete due to the exchange of Mg^{2+} with Ca^{2+} and hence causing the decomposition of C-S-H gel (Bonen, 1999; Fernandez, 2005). The most common source of magnesia in concrete is that in the clinker packed in common clinker minerals. In the process of clinker hydration, the magnesia is released and reacts with water to form the potentially expansive periclase (Taylor, 1997).

The solubility of $Mg(OH)_2$ is low compared to that of portlandite, making it stable in a liquid environment (Vandeperre, 2008). But, it will react with CO_2 to form stable products. Hence, it is expected that the use of $Mg(OH)_2$ will enhance the carbonation resistance of concrete. In this paper, the carbonation behavior of concrete containing $Mg(OH)_2$ is investigated with the accelerated carbonation test, and the mechanisms of its effects are discussed.

EXPERIMENTAL

Materials

A Type P.I 52.5 Portland cement, Class I fly ash, ground granulated blastfurnace slag and reagent pure $Mg(OH)_2$ is used when preparing the concrete. The aggregates are 5-25mm crushed stone (986 kg/m^3) and a river sand (714 kg/m^3). Clean tap water (205.6 kg/m^3) is used in all mixes. Nowadays, most of concrete is adding large admixing amount of fly ash, the binder with 50% of fly ash replacement is utilized. Mix proportions of the concrete are listed in Table 1. In addition to the reference blank mix, 4.8% (by weight, referred to the mass of binder) $Mg(OH)_2$ is added in the mix M48. The water to binder ratio is 0.41, the concrete is belonged to C30 class.

Table 1. Mix proportions of concrete (kg/m^3)

Sample	Portland cement	Fly ash	$Mg(OH)_2$
M0	250	250	0
M48	250	250	23.92

Test methods

Concrete specimens of 100×100×100 mm^3 are prepared and curing at 20±3˚C, 60±5% RH for 24 hours. The demoulded specimens are then cured at 20±3^{o}C, RH>90%. The compressive strength of the concrete is tested at 28d and 84, respectively. Specimens for the carbonation tests are cured till 26d, and are then dried in a oven at 60^{o}C for 48h. Two opposite longitudinal faces of the samples are then sealed with wax and carbonated in a carbonation chamber (T = 20±3^{o}C, CO_2=20±3%, RH=70±5%). After being carbonated for 14d, 28d, 42d and 56d, the specimens are splitted and the cross section is sprayed with phenolphthalein solution to identify the carbonation depth. Paste samples for SEM, MIP, XRD, and FTIR tests are extracted from the intact and carbonated parts of the specimens at carbonation age of 48d.

RESULTS AND ANALYSIS

Compressive strength of concrete

The compressive strength of concrete with or without $Mg(OH)_2$ is shown in Table 2. The compressive strength increases slightly with the addition of $Mg(OH)_2$ in concrete. This is probably due to the super fine nature of the $Mg(OH)_2$ power that acts as nuclei for the formation of hydration products.

Table 2. Compressive strength of concrete (MPa)

Age	28d	84d
M0	35.2	41.8

Carbonation depth

Results of the carbonation depth tests are shown in Table 3. It is obvious that if $Mg(OH)_2$ is added, the carbonation depth is greatly reduced compared to the reference blank specimens. The reduction rate is 36%, 51%, 51%, 47% for carbonation age of 14d, 28d, 42d, 56d, respectively.

Table 3. Carbonation depth of concrete specimens (mm)

Age	14d	28d	42d	56d
M0	14.11	17.94	21.12	22.73
M48	9.04	8.83	10.28	12.10

XRD analysis

XRD patterns of samples in the carbonated and intact zones of the concrete specimens are plotted in FIG. 1. In the carbonated concrete (CM48), hydromagnesite is found via the XRD pattern, which is a major difference from the intact samples. With the presence of CO_2, the $Mg(OH)_2$ react with water to form the hydromagnesite ($4MgCO_3 \cdot Mg(OH)_2 \cdot 5H_2O$).

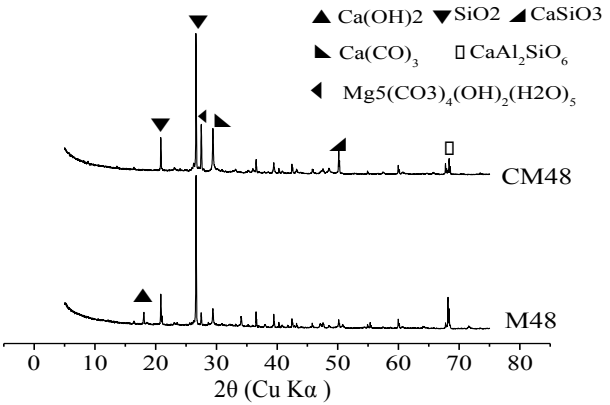

FIG. 1. XRD pattern of carbonated and intact concrete.

SEM observations

SEM images of the concrete before and after carbonation are shown in FIG. 2. Before the accelerated carbonation tests, the microstructure of concrete M48 is denser than the M0. Needle-like hydromagnesite crystals are observed in samples containing $Mg(OH)_2$, which is absent in the reference blank sample.

FTIR Analysis

The two groups of concrete are tested with FTIR tests (FIG. 3). The characteristic vibration wavenumber of CO_3^{2-} is about 1428cm^{-1}, and that of the Si-O bond is about 1080cm^{-1}, related to the polymerization degree. The relative intensity of the CO_3^{2-} vibration is compared to that of the Si-O intensity to give an index for the amount of CO_3^{2-} in the carbonated concrete. The index of carbonated concrete containing $Mg(OH)_2$ is 1.81, higher than that of the reference blank sample (1.60), indicating that more CO_2 is immobilized by the $Mg(OH)_2$.

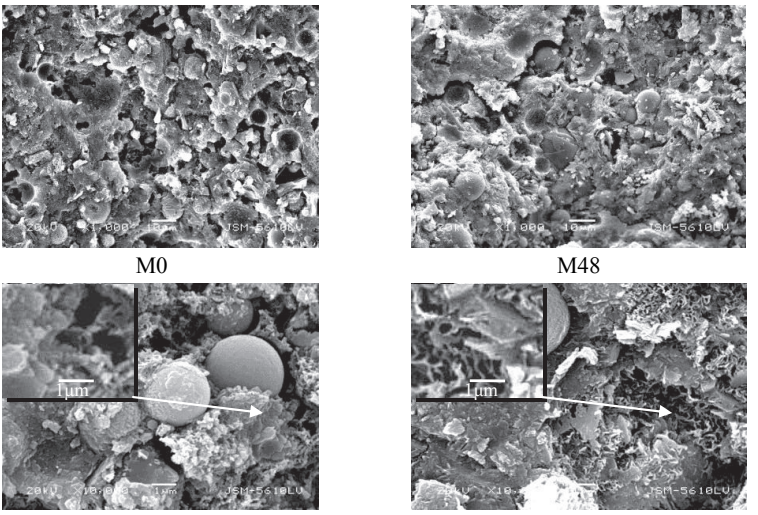

FIG. 2. SEM images of concrete.

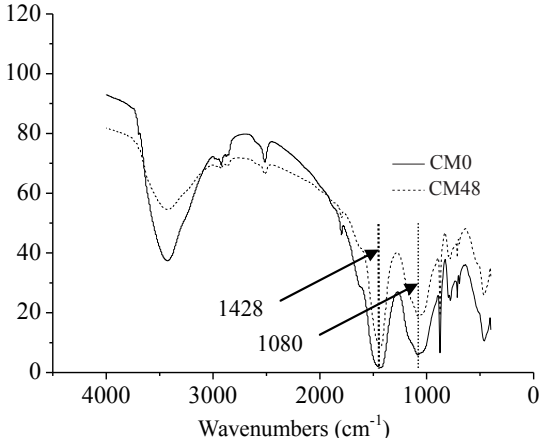

FIG. 3 FTIR pattern of concrete M0 and M48 after carbonation.

MIP test of concrete

The results of pore structure tests with MIP are shown in FIG. 4. Before the carbonation, the total porosity of concrete M0 is lower than the M48. The pore size distributions are similar. After carbonation, the total porosity of M48 is reduced, but the fine pores merge into large ones, which increases the proportion of large pores.

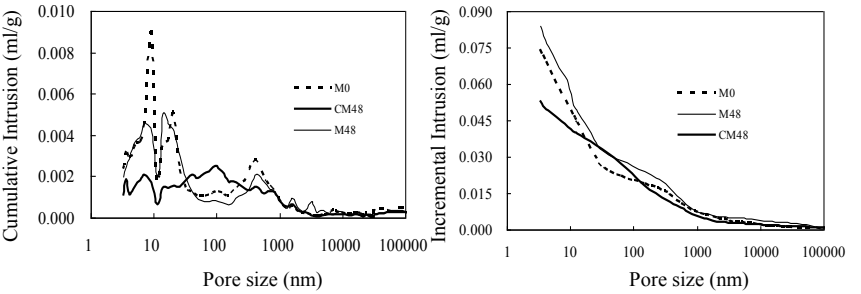

FIG. 4. Pore structure of concrete with or without $Mg(OH)_2$.

CONCLUSIONS

Carbonation behavior of concrete with or without $Mg(OH)_2$ is investigated in this study. Based on the results the following conclusions are drawn. The carbonation resistance of concrete is greatly enhanced when $Mg(OH)_2$ is added into the concrete indicated by the reduced carbonation depth in the accelerated tests. The $Mg(OH)_2$ is able to immobilize large amount of CO_2 to form the hydromagnesite.

ACKNOWLEDGEMENTS

This research is financially supported by the self-determined and innovative research funds of WUT (project 2012-IV-002) and the the Youth Chenguang Project of Science and Technology of Wuhan (project 201150431086).

REFERENCES

Bonen, D. and Cohen, M.D. (1992) “Magnesium sulfate attack on portland cement paste-I. Microstructural analysis.” *Cement and Concrete Research*. Vol. 22(1): pp. 169-180.

Chen, W., Xu, W., and Li, Y. (2011) “Microstructural Investigation of Carbonation of Calcium Silicate Hydrate in Hydrated Cement Paste.” *Advanced Materials Resear*. Vol. 261-263: pp. 601-605.

Fernandez, L., Alonso, C., Hidalgo, A., et al. (2005) “The role of magnesium during the hydration of C3S and C-S-H formation. Scanning electron microscopy and mid-infrared studies.” *Advances in Cement Research*. Vol. 17(1): 9-21.

Monteiro, P. (2008). “Advances in the Durability of Reinforced Concrete.”: Wuhan.

Sisomphon, K. and Franke, L. (2007) “Carbonation rates of concretes containing high volume of pozzolanic materials.” *Cement and Concrete Research*. Vol. 37(12): 1647-1653.

Taylor, H.F.W. (1997) *Cement chemistry*. 2nd ed. London: Thomas Telford Ltd. xviii, pp.459

Vandeperre, L.J., Liska, M., and Al-Tabbaa, A. (2008) “Microstructures of reactive magnesia cement blends.” *Cement and Concrete Composites*. Vol. 30(8): 706-714.

Performances of Electrically Conductive Concrete with Layered Stainless Steel Fibers

Wei Chen[1] and Ping Gao[2]

[1]School of Materials Science and Engineering, Wuhan University of Technology, Luoshi Road 122, Wuhan, 430070, China; State Key Laboratory of Silicate Materials for Architectures (Wuhan University of Technology), Luoshi Road 122, Wuhan, 430070, China; email: w.chen.whut@gmail.com
[2] School of Materials Science and Engineering, Wuhan University of Technology, Luoshi Road 122, Wuhan, 430070, China.

ABSTRACT: A new type of electrically conductive concrete with double-layered stainless steel fiber (DSSF) for deicing of pavements is developed in this study. The concrete is designed as a multi-layer structure with stainless steel fibers placed in two separate layers. The concrete matrix is modified with graphite particles or steel fibers. The mechanical properties and resistivity of the DSSF concrete are tested. The results have shown that the electrically conductive concrete with DSSF has low electric resistivity, making it suitable for the purpose of deicing.

INTRODUCTION

Development of deicing technologies has been a major interest in road engineering and materials science for the purpose of improving traffic safety during winter seasons. Deicing chemicals or salts are often used in most cases owing to the advantages of easy operation and cost benefits. However, these chemicals and salts are normally deteriorative to the concrete structure and are primarily responsible for the deterioration of the transportation infrastructure. Therefore, interests on seeking new technologies to replace the conventional deicing salts were rapidly growing during the recent decades. Advances in development of new deicing techniques were intensively reviewed in the work of Tuan (Tuan, 2008), including the use of electric cables, heated fluid in pipes, microwave heating and infrared heat lamps.

Electrically charged conductive concrete pavement is an emerging technology that combines the transportation supporting function of the pavement and the deicing demand perfectly. Conventional concrete is a non-conductive material itself. But, if steel fibers or graphite particles are added, the conductivity of the material is greatly enhanced and it is virtually conductive (Farrar, 1978). Heat is generated when the pavement is charged with AC or DC power, melting the snow or ice into dispatched water. This deicing system can operate continuously without interrupting the traffic. Furthermore, the steel fibers act as reinforcing materials in the concrete matrix and improve the load bearing capacity of the pavement. Yehia and Tuan have built a

complete system with electrically conductive cement concrete for deicing of pavement and validated it in a bridge construction project (Yehia, 1999; Yehia, 2000; Tuan, 2008; Tuan, 2008). Concrete mixes containing steel fibers and shaving were used to construction the test slab. Stable and uniform temperature distribution with gradual heating was achieved in their deicing experiments. An average power of about 590 W/m^2 was input into the conductive concrete overlay to prevent snow and ice accumulation. Performances of this type of steel fiber and shaving reinforced conductive concrete pavement was evaluated in other studies as well (Tang, 2006) and was extended for electrically conductive asphalt concrete (Wu, 2002).

Though the use of steel fiber (or shaving) reinforced concrete for the purpose of deicing has been proven effective in the lab and field tests, questions on the risk of tire punctuation in the long term service of the road due to the expose of steel fiber on the pavement surface are raised. Extra shield of the pavement may prevent the expose of steel fibers, but it impedes the heat conduction to the surface of the pavement as well.

Layered steel fiber reinforced concrete is a recent development in the field of road engineering. Instead of using steel fibers in the whole body of concrete, the fibers are layered in the pavement with a horizontal orientation (Lu, 2008; Ma 2010) in one or multiple layers. The surface layer concrete will not only prevent the steel fibers from corrosion, but also shield the fibers from expose. The layered fibers on the one hand enhance the mechanical properties of the pavement, and on the other hand reduce the amount of fibers in the concrete and thus lower the cost of the construction.

A type of electrically conductive concrete reinforced with double-layered steel fibers is developed and tested in this study. The steel fiber layers in the top and bottom of the pavement act as the main conductive phases for heat generation and conductivity of the concrete matrix is improved with graphite, silica fume or steel fibers. Properties and performances of the conductive concrete are tested in the lab in regard to its resistivity and ice removing capability.

EXPERIMENTAL

Materials

The electrically conductive concrete comprises Portland cement, sand, gravel, graphite, silica fume and a type of stainless steel fiber. The density of the stainless steel fiber is 7.8 g/cm^3, the length is 25 mm, the diameter is 0.2 mm and the resistivity is 30 $\mu\Omega \cdot m$. The fiber has a rectangular cross section with corrugated surface, which enhances the bond to the concrete matrix. The choice of a stainless steel fiber instead of normal carbon-steel fiber is intended to mitigate the formation of passive film on the surface of the fiber and the consequent increase of the resistivity. The cement used for preparing the conductive concrete is US Type I Portland cement produced by Huaxin Cement Co. LTD. The silica fume contains 89% amorphous silica by weight. Quartz sand with a fineness modulus of 2.3 and crushed limestone sizing between 5-16 mm are used as aggregates. Clean tap water is used in the mixtures.

Concrete design

Concrete mixtures are prepared with a water to cement ratio of 0.50. The detailed mix designs of concrete are listed in Table 1. Mix A is a Portland cement concrete containing 15% silica fume in binder. Mix B has the same design as Mix A. Mix C is steel fiber reinforced concrete. The volumetric fraction of steel fiber in concrete Mix C is 0.5%. Mix D is the graphite modified concrete containing 10% graphite particles referring to the mass of cement. All mixes contain 312 kg/m^3 water, 530.4 kg/m^3 Portland cement, 624 kg/m^3 sand, and 936 kg/m^3 coarse aggregates. Mix B, C and D are prepared together with double-layered stainless steel fibers (DSSF).

Table 1. Design of concrete (kg/m^3)

No.	Silica fume	Steel fiber	Graphite	DSSF
Mix A	93.6	0	0	No
Mix B	93.6	0	0	Yes
Mix C	93.6	40	0	Yes
Mix D	31.2	0	62.4	Yes

Structure of DSSF concrete and specimen fabrication

Structure of the DSSF concrete is shown in Fig. 1. The multi-layer structure consists of a bottom layer of concrete, a downward layer of stainless steel fiber, an intermediate layer of concrete, a upward layer of stainless steel fiber and a top layer of concrete. Each layer of concrete is 20 mm thick.

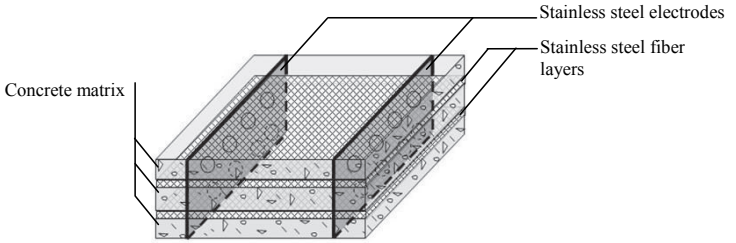

FIG. 1. Schematic illustration of the structure of electrically conductive concrete with double-layered stainless steel fiber.

Two slabs sizing 300×300×60 mm^3 are built as test specimens. Two stainless steel plates, 300 mm long, 60 mm wide and 0.6 mm thick, are firstly installed along the length of each slab as electrodes. The steel plates had perforations with a diameter of 20 mm, allowing the coarse aggregates to flow through and to ensure good contact between the electrodes and concrete. The bottom layer of concrete are then casted. Steel fibers are dispersed manually as even as possible with an amount of 2.4 kg/m^2 on the surface immediately after the casting and vibration of the bottom layer. The intermediate layer of concrete are then casted and vibrated, at the top of which another layer of steel fibers are dispersed. Finally, the top layer of concrete is casted and vibrated. Fox Mix A, no DSSF is added. The slab is cured at 23^{o}C, 60% RH for various ages, and a thermal couple for measuring the temperature of specimen is installed at the center of the up surface. A data logger is connected to the thermal couple and the output is recorded every 5 minutes. During all tests, the electrodes are connected to a DC power supply through an ammeter.

Testing

The temperature raise tests are conducted at room temperature (25 ^{o}C). The voltage of power supply (V), electric current (I) and temperature (T) are recorded every 5 minutes. The electric resistance (R) of the specimen is calculated from the voltage and electric current according to the Ohm's law as:

$$V = IR \tag{1}$$

and the resistivity (ρ) of the electrically conductive DSSF is calculated as:

$$\rho = \frac{RL}{A} \tag{2}$$

where L is the distance between the electrodes and A is the cross-sectional area of the slab parallel to the electrodes.

MECHANICAL AND CONDUCTIVE PROPERTITIES

Compressive strength of DSSF concrete

The compressive strength after 28 days are given in Table 2, it shows the influence of layered stainlee steel fiber on compressive strength.

Table 2. Compressive strength of DSSF concrete

No.	Compressive strength (MPa)	Increment of strength (%)	DSSF
Mix A	36.6	-	No
Mix B	41.1	12.30	Yes
Mix C	41.0	12.02	Yes
Mix D	33.4	-8.7	Yes

Because of DSSF, compressive strength can increase up to 41.1 MPa, compared to PC (Mix A), the increment of strength is 12.30%. For Mix C, adding fiber by 0.5%

volume content, the strength changes very little. In the test of mechanical properties of graphite conductive concrete, Zhao (Zhao, 2008) found that graphite increases per additional 5% by mass, the corresponding compressive strength of concrete reduces 50%, but For Mix D in this paper, adding graphite by 10% by mass, the compressive strength is decreased by only 8.7% compared to PC, it is clearly a enhanced result of DSSF.

In the process of experiment, the plain concrete presents bursting failure destruction and become inveted cone because of ring hoop effect, but DSSF concrete just appear some spalling in the area having no fiber distribution.

Flexural strength of DSSF concrete

The flexural strength after 28 days are given in Table 3, the change laws of flexural strength and compressive strength are basically similar. When compoisite with DSSF, flexural strength of concrete can increase up to 6.6 MPa, compared to PC (Mix A), the increment of flexural strength is 26.92%, it is twice as much as the increment of compressive strength, so the enhancement degree of DSSF on flexural strength is higher.

.

Table 3. Flexural strength of DSSF concrete

No.	Compressive strength (MPa)	Increment of strength (%)	DSSF
Mix A	5.2	-	No
Mix B	6.6	26.92	Yes
Mix C	6.6	26.92	Yes
Mix D	4.9	-5.77	Yes

In the process of experiment, the plain concrete is divided in two, but DSSF concrete just crack and still keep the integrity and can not be disconnected.

Conductivity of DSSF concrete

The resistivities of DSSF concrete are listed in Table 4, it can be seen that the resistivity of conventional concrete (Mix A) is the highest amongst the four recipes. It is greatly reduced when DSSF is built in the concrete. After adding conductive phases (steel fiber or graphite) into the matrix concrete, the resistivity decreases by order of magnitude compared to conventional concrete down to less than 1 Ω•m. The smallest conductivity is achieved with Mix D, indicating that the use graphite in the matrix concrete is the most effective for reducing the resistivity.

Table 4 Resistivity of DSSF concrete (kg/m^3)

Numbering	Resistivity (Ω•m)	DSSF
Mix A	2880	No
Mix B	265	Yes
Mix C	0.72	Yes
Mix D	0.40	Yes

The test results can be explained by the conductive model of concrete with double-layered steel fiber shown in Fig. 2. The steel fibers in the two layers overlap with each other and build a conductive route in each layer. These two layers act virtually as the electrodes, and the resistivity of the composite system is mainly controlled by the conductivity of the intermediate matrix concrete. If conductive particles or fibers like the steel fiber or graphite particles are added, they on the one hand build "bridges" between the two steel fiber layers and on the other hand compact the two conductive steel fiber layers. A skeleton of conductive routes is built and the resistivity is hence significantly reduced. The aspect ratio of graphite is far less than that of the steel fiber, building more contacts in the graphite modified matrix per unit volume.

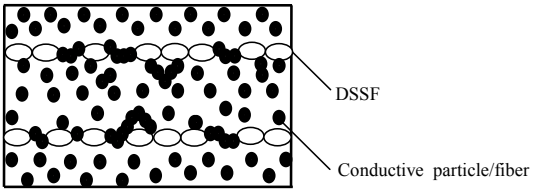

FIG. 2. Conductive model of DSSF concrete.

It is noteworthy that the resistivity of concrete Mix C and D measured in our experiments are far lower that those measured in the experiments of Yehia and Tuan (3.9 to 80.8 Ω·m) (Tuan, 2004), who uses carbon pellets or powder up to 30% in their study. Considering the low cost of steel fiber compared to the carbon products, the use of DSSF in electrically conductive concrete would not only be technically advantages, but also be economically attractive.

EXPERIMENTS ON DEICING EFFICIENCY

Experiments on deicing efficiency of the DSSF concrete are performed in a fridge. The power inputs (P) are 400 W/m^2 and 800W/m^2, respectively. The temperature in the fridge (ambient temperature, T_a) is set at -13^{o}C or -20 ^{o}C. The concrete slab built with Mix D (graphite modified concrete matrix) is placed in the fridge for 12 hours. It is taken out from the fridge and a thin layer of water is poured on the surface of the slab. The slab with water on the surface is then placed back into the fridge and is frozen for three hours. The thickness of the ice (D) is then measured. The DC power is switched on and the test starts. The parameters of the deicing efficiency tests are summarized in Table 5.

Effects of power inputs

The effects of power inputs on the deicing efficiency are plotted in Fig 3. With same ambient temperature and ice thickness, the whole process of de-icing takes 180

minutes with a power input of 400 W/m^2. Increasing the power input to 800 W/m^2 shortens the deicing process to 100 minutes. High power inputs can obviously reduce the deicing time and improve the efficiency.

Table 5. Parameters of the deicing efficiency tests

Power input (P, W/m^2)	Ambient temperature (T_a, ^{o}C)
800	-20
400	-20
400	-13

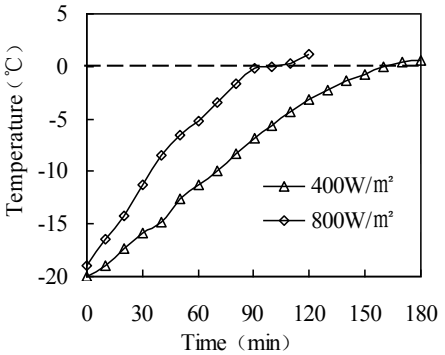

FIG. 3. Temperature raise of the concrete slab with different power inputs.

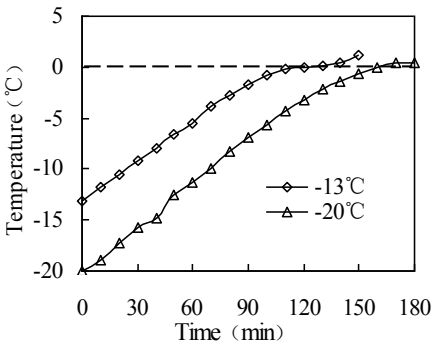

FIG. 4. Temperature raise of the concrete slab at different temperatures.

Effects of ambient temperatures

Results of the deicing tests at different ambient temperatures are plotted in Fig. 4. When ambient temperature decrease from -13^{o}C to -20^{o}C, the total time of melting the ice is prolonged from 120 minutes to 180 minutes. The deicing process takes obviously more time when the ambient temperature is lower. More energy is needed to heat the concrete specimen and the ice at a low ambient temperature. Furthermore, the tunnel effect is passivated at low temperatures, impeding the temperature raise as well.

CONCLUSIONS

We developed a new type of electrically conductive concrete with double-layered stainless steel fiber for deicing of pavement in this study and tested in different conditions. Based on the results of the experiments, the following conclusions can be drawn.

(1) The electrically conductive concrete with double-layered stainless steel fiber has low electric resistivity, making it suitable for the purpose of deicing. The steel fibers are horizontally layered in the concrete, preventing the risk of steel fiber expose. The stainless steel fibers do not form a passivated film on the surface and thus the resistivity is stable.

(2) By modifying the matrix concrete with steel fibers or graphite particles, the resistivity of the concrete is further lowered. The graphite particles are more efficient for reducing the resistivity than the steel fibers due to the tunnel effect and the small aspect ratio of the particle.

(3) The DSSF concrete is able to melt an ice layer of 6 mm thick within 100 minutes with a power input of 800 W/m^2 at -20 ^{o}C. Lowering the power input to 400 W/m^2 prolongs the deicing time, while the total energy consumptions are not significantly reduced.

(4) The ambient temperature is the most critical factor on the deicing time with the DSSF concrete. Further research on balancing the energy consumption and the deicing time is necessary for an optimal operation of the deicing operation with DSSF concrete.

ACKNOWLEDGMENTS

This research is supported by the Fundamental Practical Research Project on Transportation, Ministry of Transport, China.

REFERENCES

Anonymous (1963). “Electrical Properties of Concrete.” *Concrete and Constructional Engineering.* London**:** 195.

Farrar, J. J. (1978). "Electrically Conductive Concrete." *GEC Journal of Science and Technology* 45(1): 45-48.

Lu, Z., Fan, X., et al. (2008). “Mechanical properties of layered steel fiber and hybrid fiber reinforced concrete.” *Journal of Wuhan University of Technology-Mater. Sci.Ed.*23(5): 733-736.

Ma, G. and Fan ,X. (2010). "Experimental Research on Flexural Tensile Properties of Layer Steel Fiber Reinforced Rubber Concrete." *Proceedings of the 2010 International Conference on Mechanical, Industrial and Manufacturing Technologies.*

Tang, Z., Qian, J. et al. (2006). "Influential factors on deicing performance of electrically conductive concrete pavement " *Journal of Wuhan University of Technology-Mate. Sci. Ed.* 21(2): 123-127.

Tuan, C. Y. (2008). "Implementation of conductive concrete for deicing (Roca bridge): a final report." *University of Nebraska-Lincoln.* SPR-P1(04) P565.

Tuan, C. Y. (2008). "Roca Spur Bridge: The implementation of an innovative deicing technology." *Journal of Cold Regions Engineering* 22(1): 1-15.

Tuan, C. Y. and Yehia, S. (2004). "Evaluation of electrically conductive concrete containing carbon products for deicing." *ACI Materials Journal* 101(4): 287-293.

Wu, S.P., Mo L.T., et al. (2002). "An improvement in electrical properties of asphalt concrete." *Journal of Wuhan University of Technology- Mater. Sci.Ed* 17(4): 69-72.

Yehia, S. and Tuan, C. Y. (1999). "Conductive Concrete Overlay for Bridge Deck Deicing." *ACI Materials Journal* 96(3): 382-390.

Yehia, S., Tuan, C. Y., et al. (2000). "Conductive Concrete Overlay for Bridge Deck Deicing : Mixture Proportioning , Optimization , and Properties." *ACI Materials Journal* 97(2): 172-181.

Zhao, W.Y., Zhang, W.F., et al. (2008). "Mechanical and Thermoelectric Property of Graphite Electrically Conductive Concrete." *Journal of Daqing Petroleum Institute* 32(6): 83-92

Research on the Reactivity of Metakaolin with Different Grade

Jinlong Han[1], Zhonghe Shui[2] and Guiming Wang[3]

[1]PhD student, State Key Laboratory of Silicate Materials for Architectures, Wuhan University of Technology, Wuhan, 430070, P.R. China; email: hhjjllhjl@163.com
[2]Professor, State Key Laboratory of Silicate Materials for Architectures, Wuhan University of Technology, Wuhan, 430070, P.R. China; email: mre.shui@yahoo.com.cn
[3]Associate Professor, State Key Laboratory of Silicate Materials for Architectures, Wuhan University of Technology, Wuhan, 430070, P.R. China; email: guimingw@hotmail.com

ABSTRACT: The price of metakaolin is one of the constraining factors to large-scale applications in concrete. In this paper, 6 grade kaolins have been applied in the experiment to seek one that has high performance-cost ratio. All grade kaolins were treated by the same calcination system that heated treating of 750℃ for 4 hours to produce metakaolin. Techniques of X-ray diffraction (XRD) and scanning electron microscopy (SEM) were further employed to identify the composition and microstructure of metakaolin. Then mortar was prepared by replacing 10% Portland cement with different grade metakaolin to study the relative strength. The results show that all the compressive strength of mortar which contain metakaolin are higher than that of mortar without metakaolin, but the clay that the content of the particle size below 2 μm is 50% can be the best choice to use in concrete comprehensively considered from the strength enhancing efficiency and economic efficiency. The price of the clay is low and the intension rising rate is also high. The relative strength rising rate can be more than 20% at 7 day and 28 day.

INTRODUCTION

In recent years, metakaolin (MK), because of its high pozzolanic properties(Wild, 1996; Frias, 2000; Asbridge, 2002) due to its amorphous structure and high surfacearea, has been used as a highly active and effective pozzolan for the partial replacement of cement in concrete. Unlike other pozzolans, it is a primary product, not a by-product or secondary product, which is an ultrafine material produced by the dehydroxylation of kaolin precursor upon heating in the specific temperature range

of 700–800°C(Klimesch, 1997; Kakali, 2001).

Although the capability of metakaolin used as a mineral addition to improve mechanical and durability properties of cement and concrete is well noted in concrete science(Janotka, 2010; Hong-Sam, 2007; Fraire-Luna, 2006; Wong, 2005; Badogiannis, 2004), such as to produce high strength concrete (HSC) (YU, 2010), high and ultra high performance concrete(HPC, UHPC)(Eva Vejmelkova, 2010), etc. but until now its utilization in building industry was still limited mainly due to its high price. However, with the current shortage of mineral addition such as silica fume and high-quality slag in some countries, before long the attitude to metakaolin used in concrete may change. This change can be facilitated by making the price of metakaolin lower.

In this paper, 6 grade kaolins are studied. Special attention is paid to the effect of kaolinite content and distribution on the pozzolanic reactivity of the relative metakaolinite. Instrumental techniques, such as X-ray diffraction, scanning electron microscopy (SEM), are used for the characterization of raw materials. The pozzolanic activity is evaluated on the basis of relative strength. This research is aiming at the exploitation of kaolins in concrete technology.

EXPERIMENTAL PROGRAM

Materials

The following ingredients were used in this experiment: cement, standard sand and kaolin. The cement was P.O.42.5 cement from Huaxin cement Co. Ltd, China. The kaolin was supplied by Beihai kaolin Co. Ltd of Guangxi Province, China. There a-re 6 grade kaolin achieved from different production process and name them K1 to K6. The chemical composition of the cement and kaolin are given in Table 1.

Table 1. Chemical Composition of Cement and Kaolin(wt%)

	Cement	K1	K2	K3	K4	K5	K6
SiO_2	19.37	52.23	50.87	50.13	50.29	51.12	50.01
Al_2O_3	3.92	31.61	32.14	32.84	31.43	31.67	32.54
CaO	3.69	0.15	0.13	0.03	0.16	0.05	0.13
Fe_2O_3	68.3	0.84	1.18	1.25	1.67	1.86	1.15
MgO	1.61	0.29	0.418	0.4	0.45	0.41	0.34
Na_2O	0.13	0.13	0.19	0.12	0.22	0.17	0.28
K_2O	0.59	0.98	2.4	2.24	2.36	2.51	2.43
P_2O_5	<0.01	0.03	0.05	0.05	0.07	0.04	0.37
SO_3	0.81	1.06	0.5	0.3	0.13	0.16	0.29
LOI	1.09	12.1	11.97	12.4	13.1	11.92	12.02

The basic information of K1 to K6 as follow:

K1: In general , they are lager particles in pulp ,including the underflow pulp of mine pool, cyclone and horizontal screw, which had been bleached but not peeled, and the content of the particle size below 2 μm' is 50%.

K2: They are underflow pulp of cyclone, which had been bleached and compressed filtrated, and the content of the particle size below 2 μm' is 30%.

K3: They are overflow pulp of cyclone, which had been bleached and compressed filtrated, and the content of the particle size below 2 μm' is 60%.

K4: They are overflow pulp of cyclone, which had been peeled but not bleached, and the content of the particle size below2 μm' is 85%.

K5: They are overflow pulp of cyclone, which had been peeled but not bleached, and the content of the particle size below2 μm' is 90%.

K6:The finished product of kaolin, which had been compressed filtrated, peeled and bleached.

Metakaolin and motar preparation

The metakaolin was produced in laboratory by calcining kaolin in a muffle furnace.The muffle furnace is a programmable furnace. All grade kaolins were calcined by the same calcination system that heated at a constant heating rate of 5℃/min to 750℃,where they remained for 4h,then cooled down to atmospheric temperature rapidly. The details of the heating regime are showed in Fig.1. After all, the MK achieved was numbered in MK1 to MK6 correspond to K1 to K6.

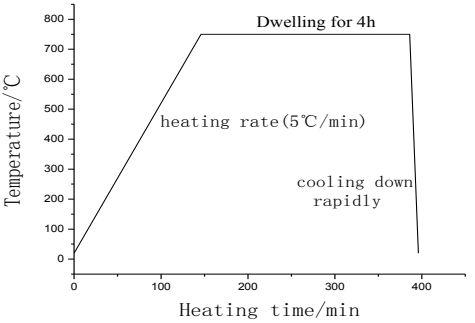

FIG. 1. Heating regime to produce MK.

The pozzolanic activity of metakaolins is evaluated on the basis of relative strength. The mortars tested in this study were designed with same replacement percentage(10 wt%) of Metakaolin into cement. They were prepared with the water/cement ratio of 0.5 and sand/cement ratio of 3. The mortar that without

metakaolin was named A0, the mortar that with MK1 A1 was named A1, with this analogize. Then the compression strength of mortars was tested after curing for 1 day, 3day, 7 day and 28 day.

Instrumental techniques

Mineralogical analyses in the raw and thermally treated samples were carried out by X-ray diffraction (XRD).

The microstructure of Metakaolin was observed on a JSM—5610LV Scanning Electron Microscope.

RESULTS AND DISCUSSION

Mineralogy

Fig. 2 presents the XRD patterns of the raw samples. According to the relative patterns, the samples mainly consist of kaolinite and muscovite, They also contain quartz and illite.

The semi-quantitative mineralogical estimation is presented in Table 2. The estimation is based on the characteristic XRD peaks of each mineral in combination with the bulk chemical analysis of the samples (Table 1).

The chemical formula of muscovite and illite are almost same ($KAl_2[Si_3AlO_{10}](OH)_2$), so they can be counted as one. The determination of them is based on the K_2O content of the samples, since there is no other detectable mineral which may contain K. The Al_2O_3 content, after extracting the Al_2O_3 in muscovite and illite is used for the determination of kaolinite since there is no other Al-containing mineral detected in the samples. The SiO_2 left is quartz.

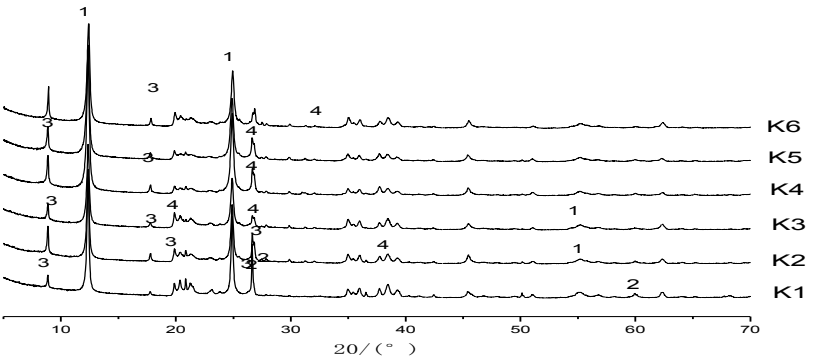

FIG. 2. XRD patterns of kaolins(1: kaolinite, 2: quartz, 3: muscovite, 4: illite).

Table 2. Mineralogical Composition of Kaolins (wt%)

	K1	K2	K3	K4	K5	K6
muscovite and illite	8.3	20.32	18.97	19.98	21.25	20.58
kaolinite	71.89	61.54	64.63	60.07	59.44	62.30
quart	14.80	13.05	11.49	13.31	13.86	11.72

The SEM images of MK are illustrated in Fig.3. After heating process, the structure of MK can be seen clearly, and the scale of the particle size of MK range from 1μm to 10 μm.

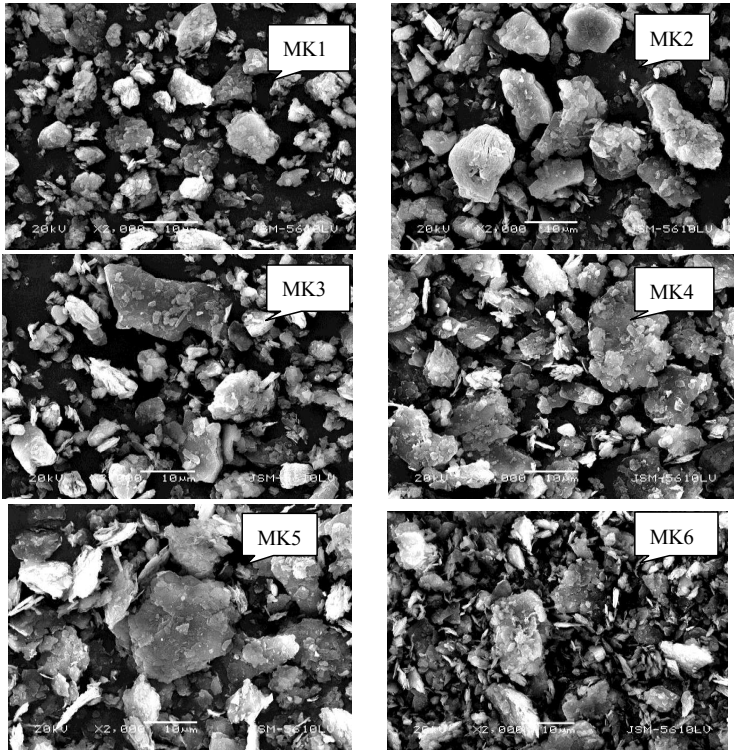

FIG. 3. SEM photograph of metakaolins.

The image of MK1 shows that MK1 particles appear as the shape of ball and distribute well, they also have good dispersion may be due to its high quart content. However, from the image of MK4, MK5 and MK6, the agglomerations of the MK particles are obvious. The scale of some MK particles are more than 10 μm and the laminated structure of MK can be seen clearly, which contain huge specific surface

and can absorb largely water.

Pozzolanic activity

The pozzolanic activity of metakaolin is evaluated on the basis of relative strength. Fig.4 shows the compressive strength of A0 to A6.

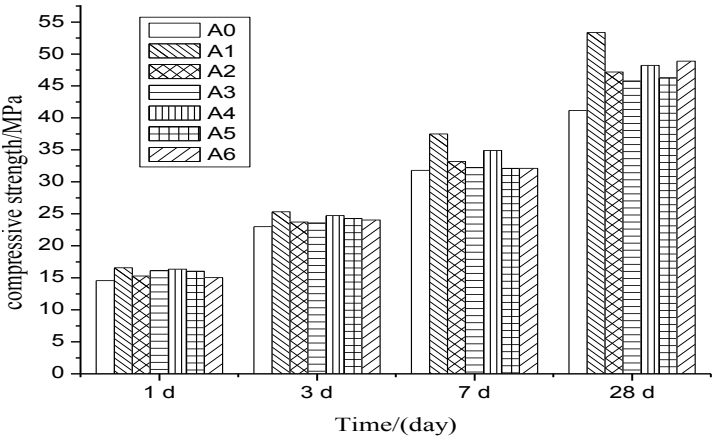

FIG. 4. The compressive strength of motar.

Comparing the difference of strength values under standard curing, we may see directly that the compressive strength of A1 to A6, which 10% cement were replaced by MK, are higher than A0' at 1 day, 3 day ,7 day and 28 day. The result shows the metakaolins have pozzolanic activity. We also can see that the compressive strength of A1 is always the highest after curing for 1 day, 3 day, 7 day and 28 day, it can arrive to 37.39 MPa at 7 day and 53.36 MPa at 28 day, the relative strength rising rate are more than 20% at 7 day and 28 day, due to the kaolinte content of K1 is highest of the 6 grade kaolins and MK1 has good dispersion. What's more, the price of K1 is less than 200 RMB per kilogram much less than the K6' price that about 2000 RMB per kilogram, which is very cost-effective.

CONCLUSIONS

The aim of this study was to seek one of 6 grade kaolins which has high performance-cost ratio used in cement and concrete. Based on a series of the performed tests, the following conclusions were drawn:

(1) The semi-quantitative mineralogical estimation shows that K1 has the highest

kaolinte content and quartz content, which leads to MK1 has good dispersion.

(2) Due to the high pozzolanic properties of MK, the compressive strength of motar contain MK is higher than that without MK, and A1 has the highest compressive strength.

(3) K1 would be the best choice in the 6 grade kaolins used in cement and concrete comprehensively considered from the strength enhancing efficiency and economic efficiency.

ACKNOWLEDGEMENTS

This work is financially supported by “Major scientific and technical Tackling key project of Hundred Bilion Industry of Guangxi Province No.11107016-4”, “Major scientific and technical project of Production, Study and Research Combination of Guangdong Province（NO.2011A090200070）”.

REFERENCES

Asbridge, A.H., Page, C.L. and Page, M.M. (2002). “Effects of metakaolin, water/binder ratio and interfacial transition zones on the micro hardness of cement mortars.” *Cement and Concrete Research*. Vol. 32(9):1365–1369.

Badogiannis, E., Papadakis, V.G. and Chaniotakis, E. (2004). “Exploitation of poor Greek kaolins: Strength development of metakaolin concrete and evaluation by means of k-value.” *Cement and Concrete Research*. Vol. 34:1035–1041.

Eva Vejmelkova, Milena Pavlikova and Martin Keppert. (2010). “High performance concrete with Czech metakaolin: Experimental analysis of strength, toughness and durability characteristics.” *Construction and Building Materials*. Vol. 24:1404–1411.

Frias, M. and Cabrera, J. (2000). “Pore size distribution and degree of hydration of metakaolin cement pastes.” *Cement and Concrete Research.* Vol. 30(4): 561–569.

Fraire-Luna, P.E., Escalante-Garcia, J.I. and Gorokhovsky, A. (2006). “Composite systems fluorgypsum blastfurnance slag metakaolin, strength and microstructures.” *Cement and Concrete Research*. Vol. 36:1048–1055.

Hong-Sam Kim, Sang-Ho Lee, Han-Young Moon. (2007). “Strength properties and durability aspects of high strength concrete using Korean metakaolin.” *Construction and Building Materials*.Vol. 21:1229–1237.

Janotka, I., Puertas, F. M. and Palacios, M.(2010). “Metakaolin sand–blended-cement pastes: Rheology, hydration process and mechanical properties.” *Construction and Building Materials*.Vol. 24:791–802.

Klimesch, D.S. and Ray, A. (1997). “Use of the second-derivative differential thermal curve in the evaluation of cement–quartz pastes with metakaolin

addition autoclaved at 180°C." *Thermochim Acta*. Vol. 307(2):167–76.

Kakali, G., Perraki, T. and Tsivilis, S. (2001). "Thermal treatment of kaolin: the effect of mineralogy on the pozzolanic activity." *Applied Clay Science*. Vol. 20:73–80.

Wong, H.S. and Abdul Razak, H. (2005). "Efficiency of calcined kaolin and silica fume as cement replacement material for strength performance." *Cement and Concrete Research,* Vol. 35:696– 702.

Wild, S., Khabit, J.M. and Jones, A. (1996). "Relative strength pozzolanic activity and cement hydration in uperplasticised metakaolin concrete." *Cement and Concrete Research*, Vol. 26(10):1537–1544.

Yu, R., Shui, Z.H. and Dong, J. (2010). "Preparation and Microstructure Analysis of High Strength Cementitious Materials Containing Metakaolin." *Journal of Wuhan University of Technology*, Vol. 32(17):117-136.

Misalignment of Dowel Bars in Rigid Pavement Joints

Hassan Mahdy[1]

[1]Associate professor, Highway and traffic engineering, public works department, faculty of engineering, Ain Shams University, Cairo, Egypt; email:Drhassanmahdy@gmail.com

ABSTRACT: The performance of concrete pavements depends to a large extent upon the satisfactory performance of the joints. Most jointed concrete pavement failures can be attributed to failures at the joint, as opposed to inadequate structural capacity (FHWA, November 30, 1990). Distresses that may result from joint failure include faulting, pumping, spalling, corner breaks, blow-ups, and mid-panel cracking. Characteristics that contribute to satisfactory joint performance, such as adequate load transfer and proper concrete consolidation have been identified through research and field experience. The incorporation of these characteristics into the design, construction, and maintenance of concrete pavements should result in joints capable of performing satisfactorily over the life of the pavement. Regardless of the joint sealant material used, periodic resealing will be required to ensure satisfactory joint performance throughout the life of the pavement. Satisfactory joint performance also depends on appropriate pavement design standards, quality construction materials and good construction and maintenance procedures. This research aims at structurally analyzing the effect of misalignment of dowel bars in rigid pavement joints on the joints performance and suggesting practical remediation.

COMMON TYPES OF RIGID PAVEMENT JOINTS

The most common types of pavement joints, defined by their function, are; (1) Transverse Contraction Joint - a sawed, formed, or tooled groove in a Concrete slab that creates a weakened vertical plane. It regulates the location of the cracking caused by dimensional changes in the slab, and is by far the most common type of joint in concrete pavements. (2) Longitudinal Joint - a joint between two slabs which allows slab warping without appreciable separation or cracking of the slabs. (3) Construction Joint - a joint between slabs that results when concrete is placed at different times. This type of joint can be further broken down into transverse and longitudinal joints. (4) Expansion Joint - a joint placed at a specific location to allow the pavement to expand without damaging adjacent structures or the pavement itself.

LOAD TRANSFER ACROSS JOINTS

The stress in the slab is determined by the truck axle load, the thermal gradient in the slab, slab thickness, slab length, subgrade support, and the edge support provided to the slab by load transfer devices (e.g., dowels, tied shoulders, and/or widened lanes) near the axle load (J. Harvey, J. Roesler, J. Farver, and L. Liang. 2000). A well-designed and constructed stabilized base layer increases the foundation support, helps reduce stresses and deflections from aircraft wheel loads, and improves load transfer across joints in the PCC slab (IPRF, 2005). Loads applied by traffic must be effectively transferred from one slab to the next in order to minimize vertical deflections at the joint. Reduced deflections decrease the potential for pumping of the base/subbase material and faulting. The two principal methods used to develop load transfer across a joint are: aggregate interlock; and load transfer devices such as dowel bars (FHWA, November 30, 1990).

It is recommended that smooth dowel bars be used as load transfer device and the joint is called dowelled joint (William R. HOOK 2001). The use of appropriately sized dowel bars is highly recommended for jointed concrete pavements that are subjected to high volumes of heavy truck traffic (FHWA 1989; AASHTO 1993). The purpose of dowels is to transfer loads across a joint without restricting joint movement due to thermal contraction and expansion of concrete. Studies have shown that larger dowels are more effective in transferring loads and in reducing faulting. It is recommended that the minimum dowel diameter be D/8, where D is the thickness of the concrete pavement. However, the dowel diameter should not be less than 1.50 inches. It is also recommended that 18-inch long dowels be used at 12-inches spacing. Dowels should be placed mid-depth in the concrete slab.

Dowels should be corrosion-resistant to pavement dowel seizure, which causes the joint to lock up. Epoxy-coated and stainless steel dowels have been shown to adequately prevent corrosion. For doweled JPCP pavements, dowel bars may be installed with basket assemblies or dowel bar inserters. Dowel baskets are heavy wire assemblies that are staked to the subgrade or base prior to paving. They must be rigidly staked so that they don't move during the paving. Fig.1 shows a dowel basket. The dowels must be lubricated with a thin film of grease to allow movement as the concrete slabs expand and contract (ACPA1996a:VI-31).When using dowel baskets, the baskets should be checked prior to placing the concrete to ensure that the dowels are properly aligned and that the dowel basket is securely anchored in the base. It is recommended that dowel baskets be secured to the base with steel stakes having a minimum diameter of 7.5 mm (0.3 inch). These stakes should be embedded into the base a minimum depth of 100 mm (4 inches) for stabilized dense bases, 150 mm (6 inches) for treated permeable bases, and 250 mm (10 inches) for untreated permeable bases, aggregate bases, or natural subgrade. A minimum of 8 stakes per basket is recommended. All temporary spacer wires extending across the joint should be removed from the basket. Securing the steel stakes to the top of dowel basket, as opposed to the bottom, should stabilize the dowel basket once these spacer wires are removed.

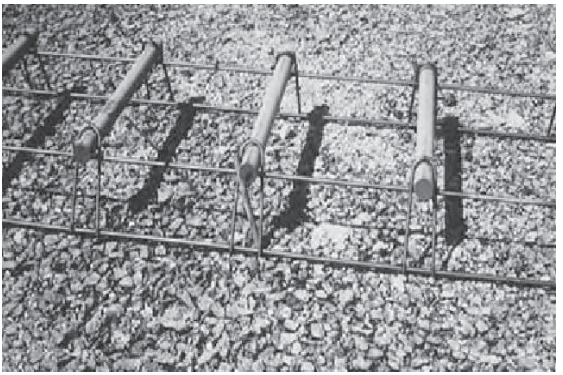

FIG.1. Dowel bar basket (FHWA 1990).

MISALIGNMENT OF DOWEL BARS

Recognizing the importance of good dowel alignment, most highway agencies have adopted requirements for dowel placement accuracy. These requirements, however, are not enforced rigorously by most highway agencies because there are no practical and quick means of measuring dowel alignment (FHWA June 2007). The difficulties in measuring dowel alignment have had at least two important consequences on concrete pavement construction:

• Dowel placement tolerances that may not reflect field experience. The existing specifications are based on limited laboratory testing and analytical investigations.

• Limited use of dowel bar inserters (DBIs). Because of the concern over dowel alignment, DBIs are not widely used in the United States. Many highway agencies specifically prohibit their use, even though DBIs may offer advantages in both speed and cost of construction.

In general, rotational misalignments (skew/tilt) impact the free joint movements, while translational misalignments (or misplacements) impact the effectiveness of individual dowel bars in performing the intended function (i.e., provide load transfer). The critical level of rotational misalignment is the level at which the joint may lock or the concrete around the bar may spall. The critical level of translational misalignment is the level at which the load transfer effectiveness of the dowel bar is adversely affected. In the case of depth error, the critical level is acceptable minimum cover. In general, the margin for placement error is much greater on translational misalignments than on rotational misalignments. For example, the typical specification in the United States for longitudinal translation (or side shift) and vertical translation is 25 mm (1 in.), whereas the requirement on horizontal skew or vertical tilt misalignments is 6 to 10 mm (0.25 to 0.375 in.) for 450- mm (18-in.) dowel bars.

With the availability of a practical, nondestructive means of measuring dowel alignment, questions are being raised as to the adequacy of the current standards on dowel placement tolerances. Recent investigations using MIT Scan-2 showed that many existing pavements contain at least a few significantly misaligned dowel bars, but with no apparent adverse effects on pavement performance. A national study is underway that is aimed at the determining the dowel placement tolerance needed to ensure good pavement performance. The current best practices on dowel placement tolerance, including the following key recent developments. (1) The Joint Score Rating system. (2) The percent-within-limit (PWL) specification for dowel bar tolerances developed by the Ministry of Transport, Ontario (MTO). (3) Acceptance criteria based on more in-depth consideration of pavement performance.

Types of Dowel Misalignment

Dowel bars need to be placed parallel to the pavement surface and to the longitudinal joint to enable free, uninhibited opening and closing of the joints. Temperature changes and initial drying shrinkage of concrete cause opening and closing of joints in jointed concrete pavements. The dowel bars should also be placed centered on the joint to ensure adequate embedment in both approach and leave slabs for load transfer. To ensure adequate concrete cover at slab (for both corrosion considerations and to avoid spalling), the bars should be placed near top and bottom of the mid-depth. The position of the bars along the joint is also important to ensure the bars are placed where they are needed to provide load transfer. Any deviations in dowel bar position from the ideal position may be defined as misplacement or misalignment. Fig.2 illustrates the possible types of dowel misalignments (Tayabji 1986).

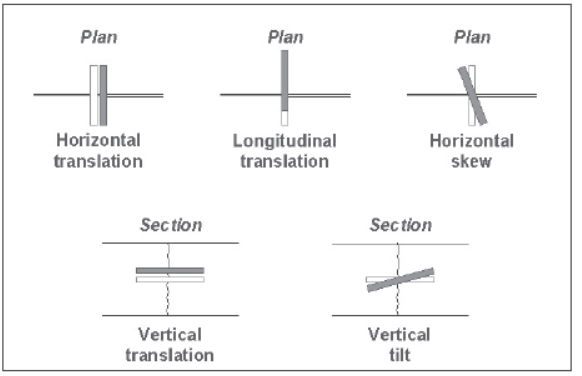

FIG.2. Types of Dowel Bars Misalignment (Tayabji 1986).

Effects of Dowel Misalignment

Dowel alignment has been of concern as early as the 1930s. During the late 1960s and 1970s, there was a moratorium on the use of the dowel bar implanters (an older version that used J-hooks) because of concern with excessive misalignment of dowel bars using these devices. The moratorium was exercised because of concerns with slab cracking as a result of misaligned dowels. During the mid-1980s, the new version of the implanters (now referred to as inserters) was introduced. Limited testing using the ground-penetrating radar device and coring at several projects during the late 1980s indicated that the inserters were capable of placing dowel bars generally within specified placement tolerances and that the inserter placement was comparable to basket placement.

Horizontal and vertical skew misalignments affect free joint movements. Consequently, dowel misalignment is often cited as the suspected cause when premature cracking or spalling occurs. While there are reported cases of extreme dowel misalignments causing failures shortly after construction, there are also many in-service pavements with poor dowel alignment that have not developed any visible distresses (Fowler and Gulden 1983; Yu 2005).

Joint locking is certainly not desirable, but the performance of in-service pavements indicates that the presence of occasional, isolated, locked joints does not have any adverse effects on pavement performance (Yu 2005). Field performance also indicates that one consequence of very poor dowel alignment can be poor faulting performance. Severe dowel misalignment can cause stress concentrations, which can lead to funneling with consequent loss in load transfer capacity.

Joint Score Rating of Misalignment

One limitation of existing specifications on dowel placement tolerances is that they do not fully consider the effects of dowel rotational misalignment on pavement behavior. The rotational misalignments govern joint movements. As such, a joint-by-joint evaluation is important in evaluating the potential impact of rotational misalignments on pavement performance. On short-jointed pavements, free joint movement is not necessary at every joint. In fact, pavement designs incorporating so-called “hinge joints” have been used on experimental pavements, with dowelled joints at every second or third transverse joint (Smith et al. 1997). Field studies have also shown that occasional locked joints have no adverse effects on pavement performance. However, many consecutive locked joints are not desirable, because of the potential for the buildup of restraint stresses in the locked group of slabs and excessive joint movements at the first working joint.

In (2005) Yu developed a simple weighted-score system was used to conduct a joint-by-joint evaluation of dowel alignments. The Joint Score, as defined in this evaluation, is a measure of the combined effects of misaligned dowel bars at a joint. Joint Score is determined by summing the product of the weights (given in Table 1) and the number of

bars in each misalignment category and adding 1. For example, if a joint has four misaligned bars in the range of 15 to 20 mm (0.6 to 0.8 in.), the Joint Score is 9; if a joint has one misaligned bar in the range of 15 to 20 mm (0.6 to 0.8 in.) and one bar in the range of 25 to 38 mm (1.0 to 1.5 in.), the score is 8. A Joint Score of 10 is the critical level, above which the risk of joint locking is considered high.

Table 1. Weighting factors used to determine joint score (YU 2005)

Range of misalignment*	Weight
10 mm <d< 15 mm (0.4 in.<d<0.6 in.)	0
15 mm <d< 20 mm (0.6 in.<d<0.8 in.)	2
20 mm <d< 25 mm (0.8 in.<d<1 in.)	4
25 mm <d< 38 mm (1.0 in.<d<1.5 in.)	5

d = deviation

*Resultant misalignment (square root of sum of squares of horizontal and vertical misalignments).

DOWEL MISALIGNMENT CASE STUDY

To determine the effect of dowel bars misalignment in rigid pavement design, EverFE2.24 rigid pavement design software is used. This software has a module for dowel misalignment. The designer can identify any expected dowel misalignment. Fig.3 shows snap shot of EVERFE2.24 and Fig.4 shows the dowel misalignment window in EVERFE2.24 software.

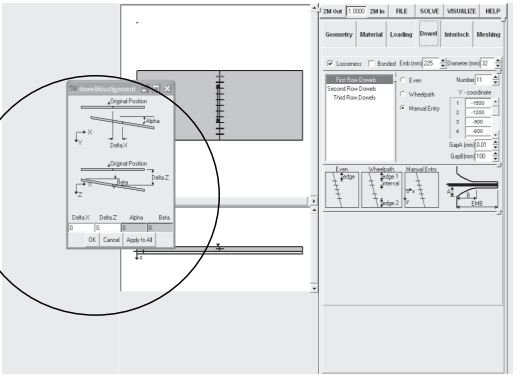

FIG.3. Snap shot of EverFE2.24 pavement design software.

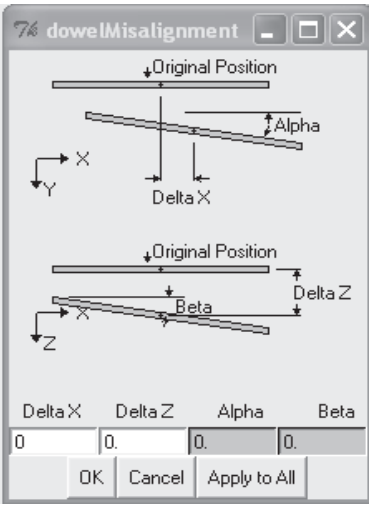

FIG.4. Dowel misalignment window in EverFE2.24 pavement design software.

To study the effect of dowel misalignment, a control slab design is done using EverFE2.24 rigid pavement design software in which the dowel bars are well aligned (no tilted or skewed dowels exist). The results of this control slab are used to compare the results of the misaligned dowel bars. The design data of the control slab are as follows:

- Slab length (X mm) 4600
- Slab width (Y mm) 3600
- Slab thickness (Z mm) 250
- Modulus of elasticity of concrete slab (E MPa) 28000
- Modulus of elasticity of base course underneath the slab (E MPa) 5000
- Depth of base course underneath the slab (Z mm) 150
- Temperature change 1 (deg C) -5
- Temperature change 2 (deg C) 5
- Dowel diameter (mm) 32
- Modulus of elasticity of dowels (E MPa) 200000
- Bonded embedded depth (mm) 225
- Dowel bar length (mm) 450, dowel spacing (mm) 300
- Dowel spacing (mm) 300
- Interlock; linear model

Figs. 5 to 7 show the design output of the control slab.

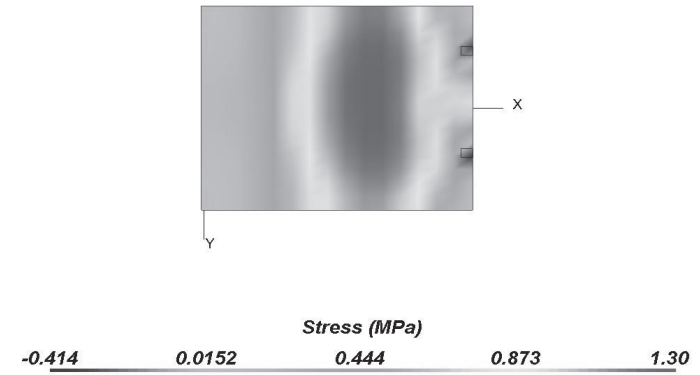

FIG.5. Stress diagram of the control slab in x-y plan from EverFE2.24.

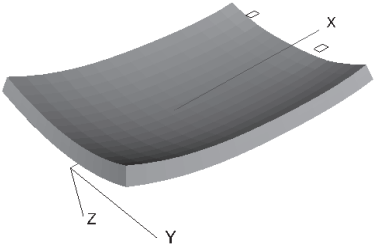

FIG.6. Displacement of the designed slab, displacement scale factor 500.

Slab with Dowel Misalignments

To determine the effect of dowel bar tilting, two cases for dowel misalignment are considered and analyzed using EverFE2.24 software as follows;

Case I: misalignment in X direction with a value of 100 mm for all dowel bars, as worst dowels misalignment in X direction.

Case II: misalignment in X direction with a value of 100 mm with misalignment in Z direction of a value of 5 mm, as worst dowels misalignment in X-Z plan.

The two above cases are analyzed using EverFE2.24 software an the resulted maximum moments as well as maximum shear forces are compared with the control case. The results are displayed in Figs.8 through 10.

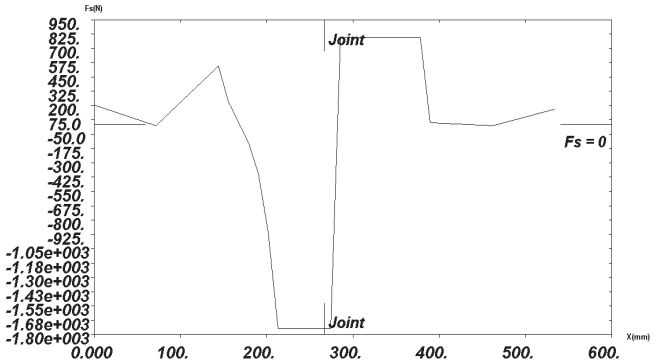

FIG.7. Shear force (N) on dowel bars.

INTERPRETATIONS OF RESULTS

Compared with the control case (well aligned dowel bars), Fig.8 shows that there are deviations in the resulted maximum moment due to the misalignment of dowel bars. These deviations increase as the dowels misalignment increase.

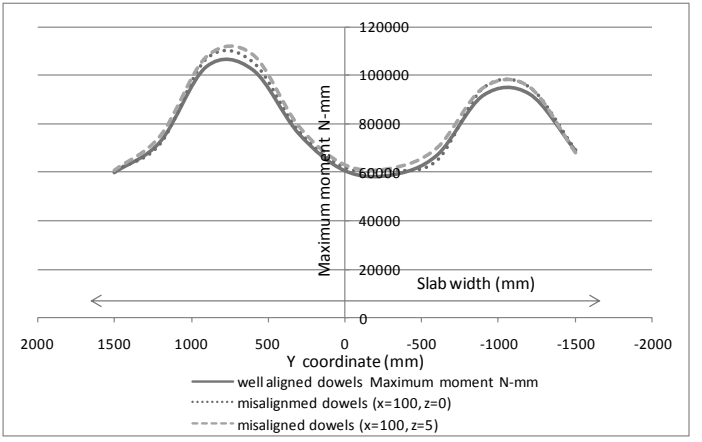

FIG.8. Resulted maximum moment in N-mm for control case and the two cases with dowel misalignment.

Similarly, compared with the control case Fig.9 shows that there are deviations in the resulted maximum shear forces due to the misalignment of dowel bars. These deviations increase as the dowels misalignment increase.

Compared with the control case (the well aligned dowel bars), Fig.10 shows that the increase of dowels misalignment resulted in significant increase/ and decrease in the resulted maximum moment and shear forces along the dowel length.

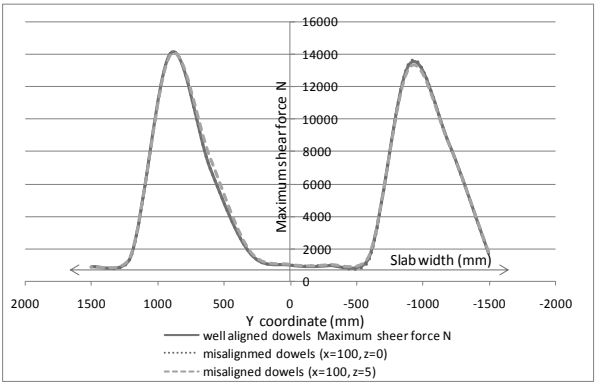

FIG.9. The resulted maximum shear force N for control case and the two cases with dowel misalignments.

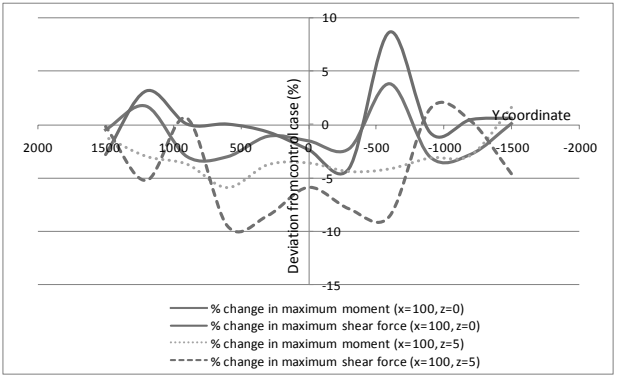

FIG.10. The variation (in percent) in both maximum resulted moment and maximum resulted shear forces of misalignment dowels compared to the control case.

CONCLUSIONS AND RECOMMENDATIONS

This paper showed the effect of dowel bar misalignments and presented resent research efforts studied the effect of misalignments of dowel bars in dowelled joint. Misalignments of dowel bars have negative influences on the resulted stresses and may lead to lock the joints.

A model is built using EverFE2.24 software to determine the effect of misalignments of dowel bars on the resulted stresses and displacements. The results showed that the increase of dowel bar misalignments (tilting) leads to higher stresses compared with the well aligned dowel bars (control case). Therefore, it is recommended that dowel bars placed in the corrected positions without any misalignments using either dowels basket shown in Fig.1 or any adopted method of construction that ensure a well alignment of dowels and prevent there misalignment during construction.

After analyzing different cases of dowel misalignments using EverFE2.24 software, it can concluded that the critical dowels misalignment, regarding the induced maximum moments and shear forces, are found to be approximately 28% of dowel bar length if the misalignment is in X direction and approximately 21% of dowel bar length if the misalignment is in X-Z plan. However, filed measurements using dowel bars misalignment testing devices such as MIT Scan-2 is recommended.

REFERENCES

AASHTO. (1993). Guide for Design of Pavement Structures. American Association of State Highway and Transportation Officials, Washington, DC.

FHWA. (1989). “Benefits of Using Dowel Bars.” Pavement Division Technical Paper 89-03. Federal Highway Administration, Washington, DC.

FHWA. (1990). “Chapter 3, Rigid pavement, Advisory comments”. Federal Highway Administration, Washington, DC.

FHWA. (2007). “Concrete Pavement Technology Program CPTP.” Pest Practice for Dowel Placement Tolerances.

Fowler, G. and Gulden,W. (1983). “Investigation of Location of Dowel Bars Placed by Mechanical Implantation.” *Report No. FHWA/RD-82/153.* Federal Highway Administration, Washington, DC.

Innovative Pavement Research Foundation IPRF report (2005). “Airport Pavement Technology Program. Stabilized and Drainable Base for Rigid Pavement.” A Design and Construction Guide. Report IPRF-01-G-002-021(G).

Harvey,J. J., Roesler, J. F. and Liang, L. (2000). “Preliminary Evaluation of Proposed LLPRS Rigid Pavement Structures and Design.” Inputs Report Prepared for California Department of Transportation.

Smith,K.D., H.T.Yu, Wade, M. J., Peshkin,D. G. and Darter.M.I.(1997). “Performance of Concrete Pavements: Volume I-Field Investigation”. *Report FHWA-RD-94-177.* Federal Highway Administration, Washington, DC.

Tayabji,S.D..(1986). “Dowel Placement Tolerances for Concrete Pavements.” Transportation Research Record 1062. Transportation Research Board, Washington, DC.

William R. H., et al. (2001). “Guide for Design and Construction of Concrete Parking Lots.” Reported by American Concrete Institute ACI Committee 330.

Yu, H. T. (2005). “Dowel Bar Alignments of Typical In-Service Pavements.” R&D Serial No. 2894. Portland Cement Association, Skokie, IL.

Traffic Capacity of Alps Car Tunnels

Hassan Mahdy

Associate professor, Public Works Department, Faculty of Engineering, Ain Shams University; Cairo, Egypt; email: Drhassanmahdy@gmail.com

ABSTRACT: Macroscopic traffic-flow models play an important role in the planning, design, and operation of transportation facilities (Easa, 1980). In the last decades, the Importance of highways as transportation facilities has been increased. However, there is lack of researches about the performance of traffic flow in tunnels. Furthermore, building and operating costs of tunnel segments are much expensive than free highway segments therefore, reliable realization of traffic performance in tunnels are of great importance for economical planning of tunnels. Moreover, speed-flow relationship has more gradual slope with constant speed for higher levels of flow (Singh, 1999). In the light of recent research dealing with speed-flow models, this research aims at: a) Investigation of speed-flow relationship in two-lane two-way Austrian tunnels during normal operating conditions, b) Investigation of the effects of heavy traffic on the rate of speed reduction with the increasing of traffic volume in tunnels and reviewing the passenger car equivalent factors that used to convert traffic volume to passenger car units, c) conducting of a speed-density relationship, and d) estimation of lane capacity by transforming speed-density model to speed-flow relationship.

INTRODUCTION

Since the middle of 50's the numbers of highway tunnels in many European countries have been increased. In some countries such as Germany, the numbers of highway tunnels in operation have been doubled only in the course of the last 10 years. Like highway bridges, construction of highway tunnels represent fastidious engineering work moreover, tunnel construction requires additional expensive equipment and special implementation. Thus the building, operation and maintenance costs of tunnel are much more expensive than normal highway segment. The selection of the cross-section and the method of construction are crucial cost factors, at the same time tunnel's cross-section affects the traffic capacity, quality and safety of traffic flow in tunnel. In most cases, due to local site constrains, the cost impacts of the selection of tunnel design elements specially cross-section, are not to be easily foreseen.

The objectives of the paper are to investigate traffic flow interaction inside two-way two-lane Austrian tunnels, to estimate the practical lane capacity which in turn will help in the selection of the most favorable and economical tunnel cross-section. Also the degree of homogeneity of traffic in tunnel is examined and speeds of both of passenger and non-passenger cars traffic are used to analyze the effect of non-passenger cars traffic on traffic stream in Austrian tunnels. This paper is done in a framework of study project sponsored by the Austrian highway financing and managing company (ASFINAG) in cooperation with the institute of transport studies BOKU, Vienna. The Author was one of the study team and used the collected data in the analyses presented in this paper.

FACTORS INFLUENCING KEY VARIABLES OF UNINTERRUPTED FLOW

Traffic composition, free flow speed, longitudinal slope, road surface conditions, lane width, horizontal alignment such as radii of horizontal curves, rate of superelevation, sight distance, shoulder width, weather conditions, etc. are the main factors influencing speed-flow relationship on normal freeway sections. In addition to these main factors, in tunnels there are some other factors influencing speed flow interaction such as: the length of the tunnel, the available side clearance, and emergency stop pockets, speed limit, ventilation and there effects on the temperature differences between in and outside the tunnel specially in winter, lighting inside tunnel as well in the tunnel approaches, which influencing the creation of black spot sections. All these factors are additional factors influencing traffic interaction in tunnels. Furthermore, for all of the examined Austrian tunnels, cross-section of the freeways are reduced in approaching tunnels to one lane per direction instead of the normal four lanes divided freeways cross-section.

THE EXAMINED AUSTRIAN TUNNELS

In this research, four two-way two-lane Austrian tunnels are examined, these tunnels are:

- Ambergtunnel, and Pfaendertunnel tunnels, both of them are on the A14 in Vorarlberg, the very west of Austria.
- Katschbergtunnel is on the A10 in Salzburg.
- Graeberntunnel on the A2 in Kaernten.

Traffic data are collected from these tunnels during the periods at which maximum traffic demand are expected to be occurred. The normal four lane divided freeway cross-section is reduced in approaching each of these tunnels to one lane per direction, (see Fig.1). The tunnel cross-section is a semicircular with one traffic lane of about 3.30 m width per direction. The side clearance is of about 0.5 m in each direction and the lengths of tunnels vary from 2.10 to about 3.50 km. There are an emergency telephones fixed on the tunnel walls.

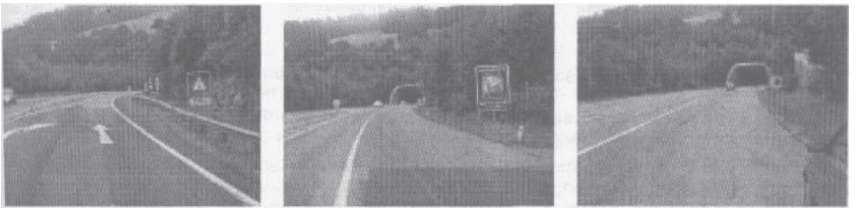

FIG. 1. The reduction of the normal four lane divided freeway cross section to one lane per direction, (Graeberntunnel on A2 in Kaernten)

Furthermore, Traffic flow inside and in approaching the examined tunnels are monitored using video cameras, these cameras are connected to an operating center. Also light traffic signals in approaching tunnels are existed and controlled by the operating center. These light signals are green for normal operating conditions and read in case of emergency, such as accidents, maintenance, or to avoid traffic congestion when unstable flow condition is expected due to the increase of traffic demand beyond the traffic capacity of the tunnel.

DATA ACQUISITION TECHNIQUES

Two different data acquisition techniques are used to collect traffic data from the examined Austrian tunnels. The first is the use of the automatic traffic count station, the second is the using of magnetic plates fixed on the pavement surface of each lane inside tunnel as well in tunnel approaches. In both cases the provided data are: the number, length, spot speed, and headway time for all vehicles traversing the count locations. Vehicles classification is done according to the vehicle's length, where vehicles' up to 6 meter length are passenger cars and vehicles of more than 6 meter length are non-passenger cars including trailers, trucks, light trucks, buses, recreational vehicles etc.

TRAFFIC FLOW INTERACTION INSIDE THE EXAMINED TUNNELS

Selection of the Optimum Observation Interval

It is necessary to identify the optimum observation interval that can be used to calculate the variables of interest such as spot speed, traffic volume and headway time. Although speed is expressed in kilometers per hour and volume is expressed in vehicles per hour, the observation intervals that used to calculate both of them are in fact, in the most of the traffic studies, less than one hour, whereas traffic characteristics are calculated for smaller time interval and converted to hour interval.

The question now is with which time interval can the speed flow data analyzed?

Some of the reviewed studies recommended that the minimum observation interval should be 15 minutes, others recommended five minutes as a minimum observation interval for traffic studies and none of them recommended time interval smaller than five minutes, they attributed that to the high fluctuation in both of speed and volume with smaller time intervals. In this research both of five minutes and one hour observation intervals are used to investigate traffic interaction and highlight the effect of time interval on the expected lane capacity in tunnels.

Influence of Non-Passenger Cars traffic

Non-passenger cars traffic especially heavy vehicles have great effects on the interaction between the main traffic variables. Some studies and international guidelines recommended weight /and or passenger cars equivalent factors according to the vehicle's type. The Austrian and German guidelines recommended a weight factor for non-passenger cars traffic, where each non-passenger car is considered as two passenger car units, in level terrain. In this research, the ratio between non-passenger and passenger cars traffic speeds is used as a measurement variable. Traffic volumes are analyzed against this variable to investigate the influence of non-passenger cars traffic on speed- flow interaction inside tunnels by performing nonlinear regression analysis on the following polynomial model:

$$\frac{V_{LKV}}{V_{PKV}} = A_1 * (Q_{PKW} + E*Q_{LKW})^2 + A_2 * (Q_{PKW} + E*Q_{LKW}) + A_3 \ldots\ldots\ldots (1)$$

Where:

$\frac{V_{LKV}}{V_{PKV}}$: Is the ratio of passenger and non-passenger cars traffic speeds.

Q_{PKW}, Q_{LKW} Are the corresponding traffic volumes of passenger and non-passenger cars respectively.

E: Is the passenger car equivalent factor for non-passenger cars from speed point of view only.

A_1, A_2, A_3 Are the model parameters.

It is recognized that the percentage of non-passenger cars traffic during normal working days are relatively higher than during holidays, therefore traffic data are classified into normal working days and holidays and each of them are analyzed the results are in Fig. 2.

The estimated speed based weight and / or passenger car equivalent factor (E) is less than the recommended weight factor in Austria guideline, that could be attributed to the existence of more degree of homogeneity in speed of passenger and non-passenger cars in tunnels than on normal freeway sections, in other words the lower non-passenger cars weight factor reflect the fact that, in these tunnels which have 80 km/h speed limit, there is no big difference in speeds between passenger and non-passenger cars traffic.

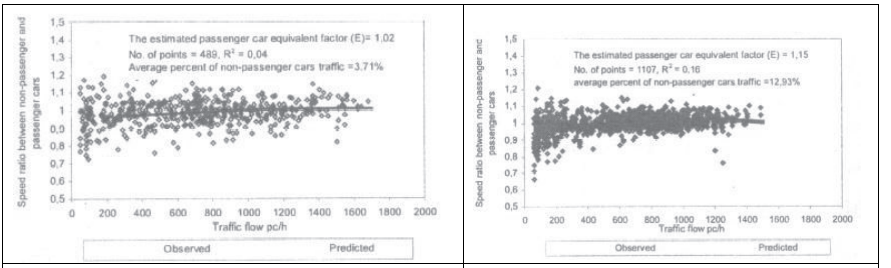

During holidays	During normal working days

FIG.2. Traffic flow versus speed ratio between non-passenger and passenger cars traffic with five minutes and one hour time intervals (Ambergtunnel on the A14 in Vorarlberg)

Relationship between Traffic Volume and the Percentage of Non-passenger Cars Traffic

Relationship between traffic volume and percentage of non-passenger cars traffic (trailers, trucks, light trucks, buses, and recreational vehicles) for different observation intervals are graphically represented in Fig.3. It is recognized that with lower volumes of traffic, in most cases evening traffic, the percentage of non-passenger cars is higher than those with higher traffic volumes, in most cases day traffic.

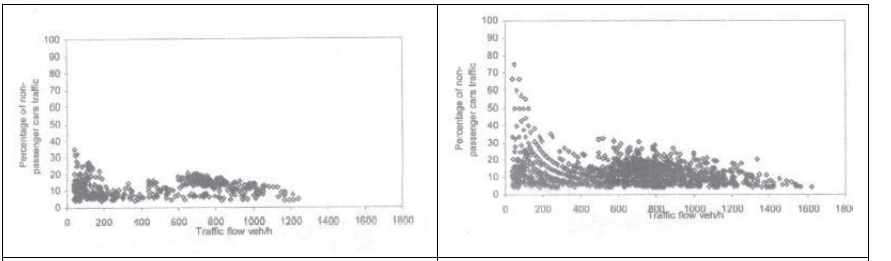

During holidays	During normal working days

FIG.3. Percentage of non-passenger cars traffic versus traffic volume with one hour time interval (Ambergtunnel on the A14 in Vorarlberg)

SPEED-DENSITY MODEL

Density, which is defined as vehicles per unit length, does not make sense for a point measurement, because no length is involved. Density can be calculated from point measurements when speed is available, but one would have to question the meaning of the calculation, as it would be density at a point (Fred L. HALL. 1992). Density is a typical variable from physics that was adopted by traffic science. (Immers, 2002) Also, (Banks 1989) has identified the condition more precisely as requiring both covariance of vehicle length with the inverse of vehicle speed and covariance of vehicle spacing with the inverse of vehicle speed to be zero. Speeds within a lane are relatively constant during uncongested flow.

To analyze the interaction between speed and density, two different groups of traffic data are used. The first group is based on five minutes observation interval and the second group are based on one hour observation interval are used. For each group of these traffic data, traffic volumes are first converted to passenger car units using weight factor of 2, then traffic density is calculated from the observed speed and volume. A continuous model is used in fitting speed-density data. The calibration of the model is done using nonlinear regression analysis with SPSS statistical software. The mathematical form of the model is given by:

$$S = S_F * e^{b*(\frac{D}{D_m})^c} \quad \text{.....(2)}$$

Where:

S	Is traffic speed km/h,
S_F	Is the free flow speed km/h, D is the traffic density pc/km,
D_m	Is the expected density at capacity and,
b, c	Are the model parameters.

Fig.4 shows the speed-density model with five minutes and one hour observation intervals

As graphically represented in Fig.4, it can be easily realized that all traffic data are in stable flow conditions and almost no traffic congestion inside tunnels are observed, that could be attributed to the fact that when the traffic demand approaching capacity congestion will be in tunnel approach, where freeway cross-section is reduced. The estimated traffic density at capacity vary from 34 to 36 passenger car units per kilometer per lane, accompanying with average passenger cars speed of about 49.50 to 51.17 km/h.

Taking into consideration the fact that, double transformation process in constructing speed-flow relationship leads to reduce the accuracy of the estimated speed-flow relationship, in other words minor changes in speed-density model lead to major changes in speed- flow relationship, more care is done in analyzing speed-density data.

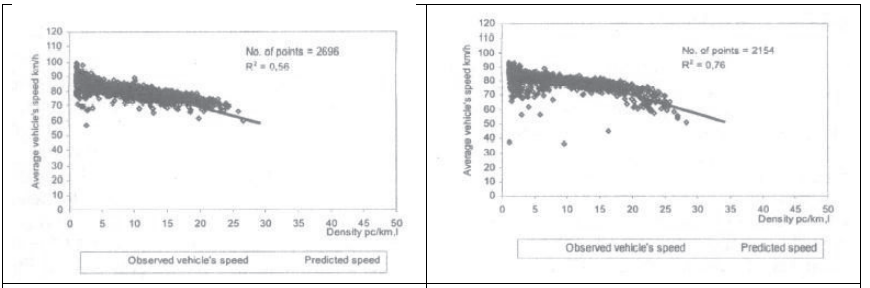

Five minutes observation interval | One hour observation interval

FIG. 4. Speed-density model with five minutes and one hour observation intervals (Ambergtunnel on the A14 in Vorarlberg)

SPEED-FLOW RELATIONSHIP

Speed-flow relationship is constructed by transforming the developed speed - density model using the fundamental relation between the main three key traffic variables, speed, density, and volume. The estimated speed-flow relationship with five minutes and one hour observation intervals are graphically represented in Fig. 5.

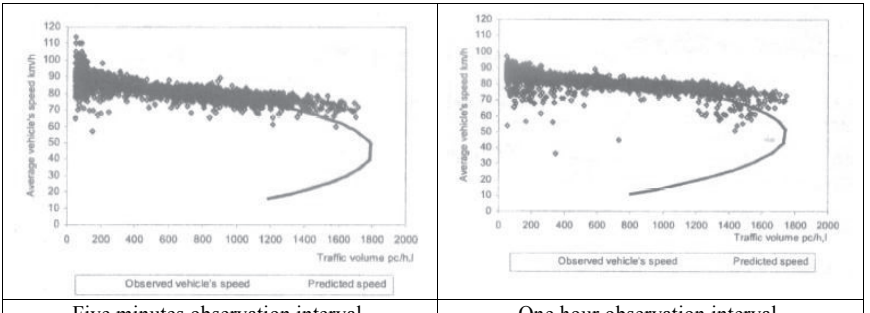

Five minutes observation interval | One hour observation interval

FIG. 5. Speed-flow relationship with five minutes and one hour observation intervals (Ambergtunnel on the A14 in Vorarlberg)

As graphically presented in Fig. 5, the estimated speed-flow relationship match to a good extent with the observed speed-flow data for both of five minutes as well one hour observation intervals, moreover the effect of 80 km/h speed limit can be recognized

although the predicted free flow speed is slightly higher. As mentioned before, almost all speed-flow data are for stable flow conditions and traffic congestion is only expected to be in the bottleneck segment where the freeway cross-section is reduced to one lane per direction. Furthermore traffic flow in these tunnels seems as a queue discharge flow. Taking into account all of these local conditions influencing traffic flow interaction, the expected range of lane capacity in two-lane two-way Austrian tunnels is 1740-1785 pc/h/l, where the lower limit is for one hour observation interval and the higher limit is for five minutes interval.

Highway Capacity Manual (HCM 2000) showed in Exhibit 8-19 of chapter 8- Traffic Characteristics Measured and Observed Values showed that traffic capacity of two-way two-lane long tunnels is about 1530 vehicle per hour per one lane. If this value is converted to passenger car unit per hour per lane, by considering the effect of traffic composition, the lane capacity will be almost close to the predicted values.

INTERPRETATION OF THE RESULTS

From the graphical and analytical analysis, it can be concluded that a) the estimated lane capacity with one hour interval is about 0,97 of that with five minutes interval, which confirm that five minutes observation interval can (with care) be used as in the estimation of the lane capacity and traffic interaction b) Although in calculating traffic volume in passenger car units a weight /and or passenger cars equivalent factor of 2 is used, but in tunnels this weight factor could be lower which could be attributed to the homogeneity in speed of passenger and non-passenger cars traffic inside tunnels, in other words non-passenger cars traffic does not constrain the movement of passenger cars to a great extent, c) because the bottleneck is in the weaving section (the tunnel approach), where freeway cross-section is reduced, therefore almost no traffic congestion is observed inside the tunnel, d) From the analysis, it can be concluded that traffic flow in tunnel is a queue discharge flow, after the bottleneck in the tunnel approach due to reduction of the freeway cross-section. Keeping that fact in mind, typical rang of lane capacity in tunnel, under these specific conditions, should be from 1740 to 1785 pc/h where the lower limit is for one hour time interval and the upper limit is for five minutes time interval e) compared with normal freeway cross section, it may be recognized that speed level in tunnel is relatively lower than normal freeway cross section moreover, the homogeneity between passenger cars and non-passenger cars speeds are relatively higher which may help in reducing the rate of accident inside tunnel comparing with the normal freeway section, f) Peak volumes inside tunnels are mainly due to passenger cars and the non-passenger cars represent a small portion of total traffic during peak periods, g) It may be important here to point out that Ambergtunnel was not the only examined tunnel but it was just one of a set of tunnels examined under a research project framework but it's results are here discussed as a representative example of the examined Austrian tunnels h) for all of the examined tunnels, under the same physical features and in level terrain, the expected lane capacity is approximately in the same range and in all cases lower than the proposed lane

capacity under ideal conditions.

CONCLUSIONS AND RECOMMENDATIONS

The conclusions of this research are:

a) With some care, can five minutes observation interval be used in investigating the lane capacity, where the predicted capacity can be transferred to that with one hour interval, b) with respect to vehicles speed, weight factor of non-passenger cars in tunnels is lower than two, which could be attributed to the higher degree of speed homogeneity between both of passenger and non-passenger cars traffic in tunnels, as well the used speed limit, c) no traffic congestion is observed in tunnels and the expected range of lane capacity of two-lane two-way Austrian tunnels is 1740-1785 pc/h/l, where the lower limit is for one hour observation interval and the higher limit is for five minutes observation intervals, 1) the expected range of lane traffic density at capacity is 34 - 36 pc/km/l, the lower limit is for one hour interval and the higher limit is for five minutes interval and, e) the expected range of speed at capacity is 19,50 - 51,17 km/h, the lower limit is for five minutes interval and the higher limit is for one hour interval.

The recommendations of this research are:

In analyzing traffic interaction in tunnels, the used passenger car equivalent factors should be lower than that in normal freeway sections b) In the selection of cross-section of two-lane two-way tunnels, which have the same criteria as the examined tunnels, lane capacity of not more than about 1700 > pcu/h/l should be used to ensure stable operating conditions and avoid traffic congestion in tunnels. As mentioned before, this lane capacity is close to that given by (HCM 2000) Chapter 18.

ACKNOWLEDGMENTS

This paper is sponsored by ASFINAG, Austria. The author wishes to express his deep thanks to ASFINAG, Austria for providing the data used in this paper.

REFERENCES

Banks, J.H. (1989). “Freeway Speed-Flow Concentration Relationships: More Evidence and Interpretations.” *Transportation Research Record* 1225, TRB, NCR, Washington, DC. Pp:53-60.

Easa, S.M. and May, A. D. (1980). “Generalized Procedures for Estimating Single and Two-Regime Traffic Flow Models.” *Transportation Research Record* 772, TRB, NCR, Washington, DC. Pp:24-37

Hall, F.L. (1992). “Traffic Stream Characteristics.” http://www.fhwa.dot.gov/publications/research/operations/tft/chap2.pdf

Highway Capacity Manual. (HCM 2000). “Chapter 8- Traffic Characteristics Measured

and Observed Values." *Transportation Research Board*, National Research Council.

Immers, L.H. and Logghe, S. (2002). "Traffic Flow Theory." Course H 111, Verkeerskunde Basis. Katholieke Universiteit LEVEN. http://www.kuleuven.be/traffic/dwn/H111part3.pdf

Singh, R. (1999). "Improved speed-flow relationships: Application to Transportation Planning Models." *7th TRB conference on Application on Transportation Planning Methods*. Boston Massachusetts, USA.

Influence of Microfiber Additive Effect on the Self-healing Behavior of Engineered Cementitious Composites

Shunzhi Qian[1], Zhigang Zhang[2], Eirini Tziviloglou[3], Sofia Antonopoulou[4], Jian Zhou[5] and Erik Schlangen[6]

[1]Institute of Highway and Railway Engineering, School of Transportation, Southeast University, P.O. Box 210096,Nanjing City, China; email: sqian@seu.edu.cn
[2] Institute of Highway and Railway Engineering, School of Transportation, Southeast University, P.O. Box 210096,Nanjing City, China.
[3] Microlab, CITG, Delft University of Technology, Delft, The Netherlands.
[4] Microlab, CITG, Delft University of Technology, Delft, The Netherlands.
[5] Sinoma Research Institute, Sinoma International Engineering Co., Ltd. Beijing 100102, China,
[6] Microlab, CITG, Delft University of Technology, Delft, The Netherlands

ABSTRACT: This paper investigates the self-healing behavior of Polyvinyl Alcohol Engineered Cementitious Composites (PVA-ECC) with the addition of other microfibers, including steel fiber and rock wool fiber. Four-point bending tests were used to precrack ECC beams at the age of 7 and 28 days, respectively. The precracked samples were then cured in water to promote the occurrence of self-healing and in air for control. The addition of microfibers help tighten the crack width greatly, resulting in enhanced flexural stiffness for the water cured samples. Furthermore, the additive effect also promotes larger extent restoration of deflection capacity, despite of much lower initial deflection capacity for the mixtures 2a and 3a. The self-healed samples were also examined under light microscope and environmental scanning electrical microscope (ESEM) to reveal the products of self-healing.

INTRODUCTION

Cracks are called as intrinsic material flaw, which are inevitable during the service life for concrete structure. Cracks can be caused by loading, volumetric change due to high temperatures, creep, plastic settlement, shrinkage, or deterioration mechanisms such as alkali-silicate reaction and freezing-and thawing cycles.

Therefore, concrete structures are always along with cracks during service life. Cracks lower the durability of concrete structure by providing paths for water or aggressive agent to go through and corrode concrete itself or reinforcing steel. Previous studies show that the crack width is the dominant factor for the water permeability as the flow rate is proportional to the width to the third powder(Massey, 1998).Therefore, the development of a new kind of cementitious material that can autogenouslycounter the effects of cracking by self-healing is highly desirable.

Edvardsen et al (1999) reported that self-healing behavior canoccur in concrete when crack width is controlled within a certain extent. Furthermore, tight crack width is beneficial to the self-healing behavior. Regardless of origin, self-healing leads to crack-closing, thus improving durability, permeability, and potentially mechanical properties. This is important for watertight structures (such as reservoirs and dams) and for prolonging the service life of infrastructure. While self-sealing is widely studied, the research on crack width control has received limited attention.

Polyvinyl Alcohol Engineered Cementitious Composites (PVA-ECC), a new class of ductile fiber reinforced concrete material designed base on micromechanics theory with self-controlled tight crack width (typically below 60 μm), making it suitable to develop robust self-healing material. Li and coworkers (Li, 2007; Yang, 2009; 2011)have investigated the self-healing behavior of ECC under a number of exposure conditions, including water submersion, wetting and drying cycles, etc for both early aged and matured ECC. Their results suggest that the mechanical properties can be largely recovered, especially for specimens preloaded to below 0.3% and 1% tensile strain for early aged and matured ECC, respectively.

While it is feasible to achieve self-healing for ECC, recent studies have indicated that it is desirable to have even tighter crack width than typically seen in ECC in order to achieve completely healing (Yang, 2009; Qian, 2009). Yang et al (2009) found that ECC at early age (3 days) recoverd with lesser stiffness compared with matured ECC (same mixture), which is due to increasing crack width with higher straining level for the early aged ECC, whereas more matured specimens maintain extremely tight crack width (15μm).

In an effort to develop green ECC with local waste materials, Zhou et al have developed a number of ECC mixtures with blast furnace slag (BFS) and limestone powder, all characterized with 2-3% tensile strain capacity and tight crack width (typically below 60μm) (Zhou, 2009). With these green ECC mixtures, Qian et al (2010) have demonstrated via four point bending test that it is possible to achieve self-healing behavior if the precracked samples were submerged in water for a certain period, while it is not the case for air cured samples.

This paper focuses on the enhancement of the two aforementioned aspects of ECC by adding microfibers, including steel-wool and rock-wool. The question that this research intends to answer is whether the addition of these extra microfibers can

help improve the ECC performance, by keeping the average crack width lower and increasing the degree of self-healing.

In order to study the behavior of ECC, several mixes with different additives were prepared. A displacement-controlled four-point-bending test was used in order to verify the initial bending strength/deflection capacity, and to pre-crack the cement specimens. Then, some of the pre-cracked specimens were cured under water and in air for 28 days to compare the healing effect of different curing conditions. Afterwards, the cured specimens were again tested in four-point-bending, and the results related to strength and stiffness, were compared to those of the virgin specimens. In addition, light-microscope was used for the measurement of crack width, and the detection of self-healing phenomena at preloaded samples. While light-microscope proved to be a functional tool, it could not provide information concerning the type of self-healing products that were formed in the cracks. For this purpose Environmental Scanning Electron Microscopy (ESEM) was used.

OUTLINE OF THE RESEARCH AND EXPERIMENTAL SET UP

Outline of the research

An overview of the experimental program is illustrated in Fig.1. As it is shown in the diagram the first step was the fabrication of the mixture. In total three different mixtures were prepared: one control mixture containing only 2% of PVA fibers, another two mixtures containing PVA (2%) together with steel fibers (0.5%) and rock-wool fibers (0.5%) respectively. The next step was the preparation of the specimens. The coupons were evenly cut into 4 species and then ground in order to obtain a smooth surface. Afterwards, the specimens were divided into 2 main categories: a) the specimens cured for 7 days and b) those cured for 28 days after casting under ambient conditions. Seven days after casting some of the specimens were tested until final failure while others were preloaded up to vertical deformation of 2 mm using the four point bending test in above mentioned cases. Some of the preloaded samples were then cured in water and the rest in air for 28 days. After the curing period, the air cured samples were put under the light microscope in order to ascertain the extent of healing as well as to measure the width of the formed cracks.

On the other hand, the water cured specimens were prepared for ESEM observation so as to determine the crystalline and chemical properties of the healing products. Finally, both the water and air cured specimens were then tested up to final failure by conducting a four point bending test. The same procedure was followed also for the samples that were cured for 28 days after casting.

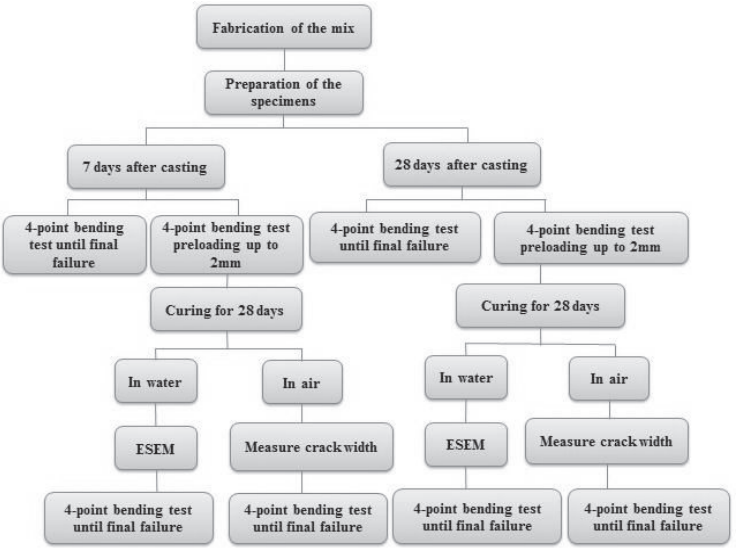

FIG.1. Experimental program.

Material design and preparation of the specimens

The mixture proportions of ECCs used in this investigation are presented in Table 1.The mix1is used as a reference in the ECC mix design. Steel fiber and rock wool fiber are mixed in a proportion of 0.5% of the total volume additionally besides PVA fiber in Mix2a and Mix3a, respectively. The dimensions of the fibers that were used for the three different mixtures are given in Table 2.

Table 1. Mix proportion of ECCs with different micro-fibers (Mix by weight (fiber by volume))

Mix No.	Cement	Fly ash	Limestone powder	Water	Super Plasticizer	PVA fiber	Steel fiber	Rock wool fiber
1	1.0	1.2	0.8	0.84	0.053	2%	0	0
2a	1.0	1.2	0.8	0.84	0.053	2%	0.5%	0
3a	1.0	1.2	0.8	0.84	0.053	2%	0	0.5%

Table 2. Dimensions of different micro-fibers

Additives	Length(mm)	Diameter(μm)
PVA Fibers (Kuralon K-II)	8	40
Steel Fibers (Frimeco F01)	1.8	100
Rockwool(Lapinus RBC300)	0.5-4	3-15

The solid materials, CEM I 42.5, fly ash and limestone powder were first mixed with aHOBART mixer for 2 minute thoroughly. Water and superplasticizer were then added and the mixture was mixed at low speed for 1 minute, followed by high speed for twominutes. Finally, the PVA fibers and additional fibers (steelwool, rockwool) were added at low speed,followed by high speed mixing for another twominutes. The fresh ECC was cast into moulds with the dimension of 240mm × 60mm × 10mm for the four-point bending test. After oneday of curing in moulds, covered with plastic sheet, the coupon specimens were evenly cut into four pieces with dimensions of 120 mm× 30mm × 10mm. Then, they were carefully ground on the middle-speed lap wheel with P220 and P500 sand papers.

Each grinding step lasted for 1 minute approximately. Afterwards, the samples were cured under room conditions for another 6 and 27 days respectively before testing. Especially, for the samples that had to be examined under the ESEM a particular preparation was followed. The specimens were cut into smaller pieces (approximately 50mm length) withonly the area of interest thatcontained the cracks. Then the samples were taken to the lap wheel where they were grounded with P320, P1200 and P4000 sand paper. For the grinding procedure, ethyl glycol was used instead of water in order to keep the existing healing products intact.

RESULTS AND DISCUSSION

Four point bending test

It includes two categories for each mixture: specimens that were tested seven days after casting, and those tested twenty-eight days after casting.Each category contains three basic schemes regarding the curing method as follows: 1) the virgin samples which were tested until final failure;2) the preloaded and then cured in water for 28 days;3) the preloaded and then cured in air for 28 days.The stress-deformation curves of Mix3a are presented in Fig.2.

From test results, it can be observed that the flexural strength of 28 daysspecimensunder three curing schemes (virgin, water cured, air cured) is higher than that of the 7 days specimens, which is what was expected considering the fact that the maturity of specimens was higher for 28 days case, and the material has fully developed its ultimate load capacityafter curingfor 56days.And the deformability of

Mix2a cured under all conditions is lower than Mix1, which may due to poor fiber distribution exhibited in the mixing caused by high water demand of the steel wool fibers. From Fig.2 (a) and (b), it can be observed that the deformability of Mix3a is relatively well after adding rock-wool fiber.The recovery ratio of deformability after pre-cracking is larger compared with that of the Mix1.

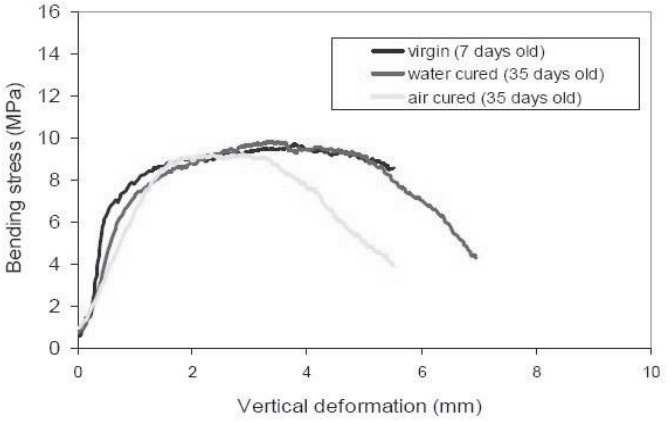

(a)

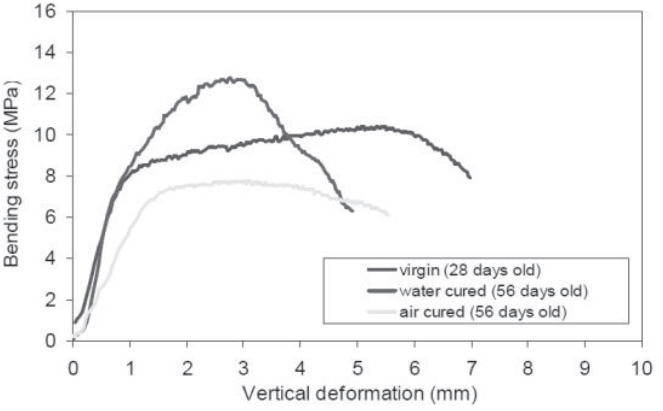

(b)

FIG.2. Comparison of typical bending behavior of Mix3.

The stiffness is defined as the slope of initial linear part of bending stress-deformation curves.As shown in Fig.3, the stiffness of the water cured specimens is higher than that of the air cured samples. It can be explained by the

strengthening effect of healing products which is more intense for specimens cured in water than that in air, so it is more difficult for the already existing crack to open for specimens cured in water.On the contrary, the stiffness of the water cured specimens has a lower value comparing with that of the virgin ones both in 7 and 28 days. This is expected, because calcium hydrates or calcium carbonates which are usually, as the ESEM observations will confirm later on, the main components of healing products, are weaker than CSH produced from cement hydration.

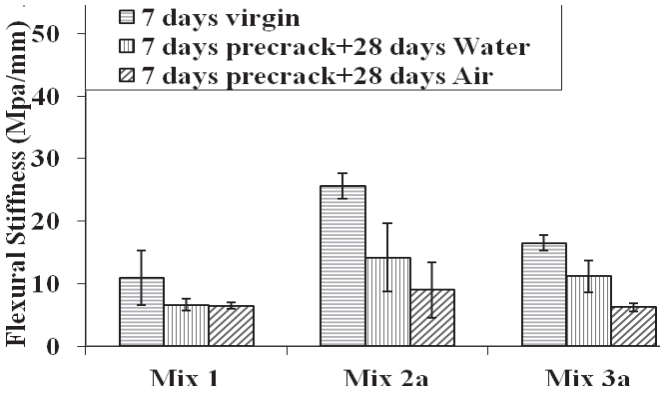

(a)

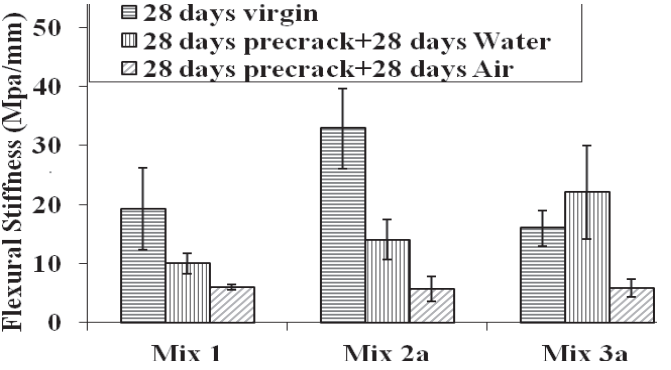

(b)

FIG.3. Comparison of flexural stiffness of different mixtures at different precracking time (a) 7 days and (b) 28 days.

Crack width

It is observed that specimens of all mixtures exhibit multiple micro-cracking behaviors under bending test, as is shown in Fig.4. The average crack width for each mixture is shown in Fig.5. It can be seen clearly that the crack width is much smaller for Mix2a and Mix3acompared with Mix1, which may be caused by the fiber hybriding effect. Tight crack width is beneficial to the self-healing behavior, especially for the recovery of flexural stiffness.

FIG.4. Multiple cracking along the length of the sample.

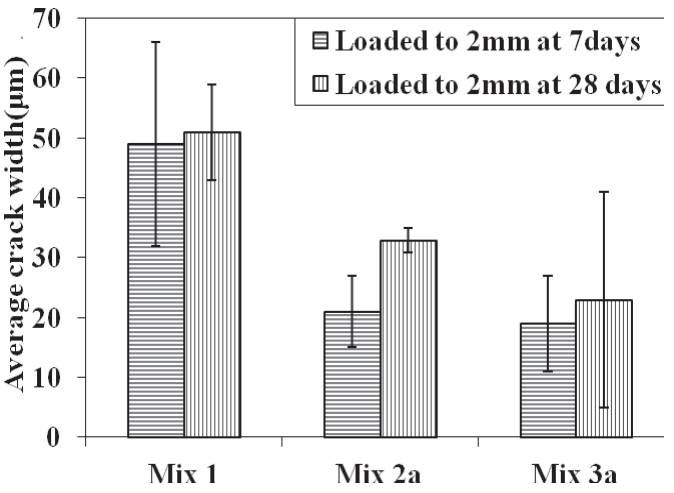

FIG.5. Comparison of average crack width.

Self-healing behavior

Fig.6 (a) and (b) show that self-healing behavior occurred in cracks of specimens cured in water, while it was not the case for specimens cured in air. White residue crystals emerged within cracks for specimens cured in water as shown in Fig.6 (a). All water cured specimens showed similar white residues inside the crack, while there are no signs of healing for specimens cured in air as shown in Fig.6 (b). Therefore, the curing condition after pre-cracking is critical to the self-healing behavior.

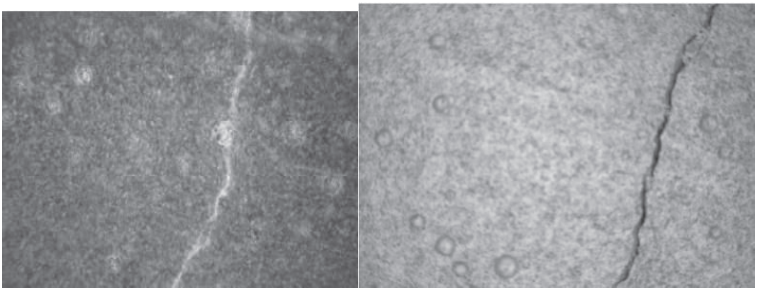

(a) **(b)**

FIG.6. (a) Healed specimen after water curing; (b) Unhealed sample after air curing.

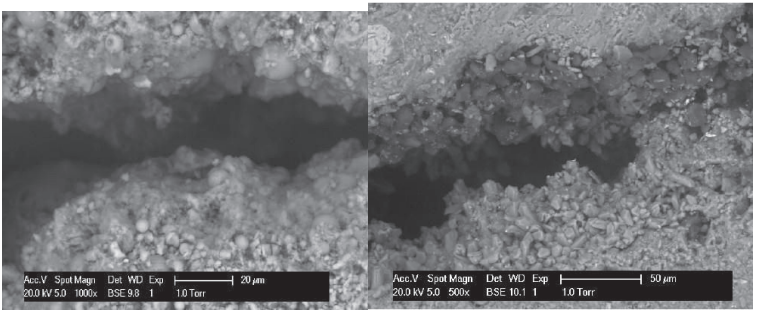

(a) **(b)**

FIG.7. (a) Air cured specimen shows no sign of healing; （b）Water cured specimen shows healing products inside crack.

Fig.7 (b) shows a typical pattern of a partially healed crack. In this picture one can observe that the healing products grow from both surfaces towards the middle of the crack. The products can be recognized by their morphology. For example, the crystals that are sticking out of the crack are met in various sizes and they are most probably calcium carbonate crystals generated by the carbonation of calcium hydroxide. This phenomenon appears in the presence of CO_2 dissolved in water and

the calcium met coming either form cement or limestone. In addition, between the crack surfaces there are thin hexagonal particles which seem to be calcium hydroxide and comprise a product of cement hydration. Apart from the two abovementioned forms of products; another formation of healing has been observed in Fig.8 (a). Very small amorphous clustered particles, most likely to be calcium silicate carbonate, appeared in a rather localized way. These clusters are possibly products of reaction between the anhydrous cement grains and water.

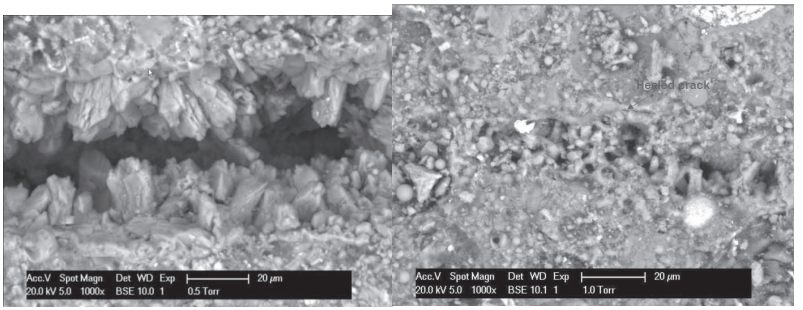

(a) **(b)**

FIG.8. (a) Partial crack healing (Mix1); (b) Saturated crack healing (Mix3).

The effect of crack width on self-healing was shown in Fig.9 (Qian, 2009).It can be observed that cracks fully healed when crack width is 15µm and 25µm, while it partially healed when crack width is 60µm. Similarly, Fig.10 shows that crack was partially healed for Mix1, while it was fully healed for Mix3a with a smaller crack width. It demonstrates that the crack width is critical factor to the degree of self-healing. Hence, self-healing is much easierto take placein Mix2a and 3a than Mix1 due to much tighter crack width control. The additive fibersin Mix2a and Mix3aare beneficial to self-healing behavior. It demonstrates the feasibility of mixing other fibers to enhance the capacity of self-healing.

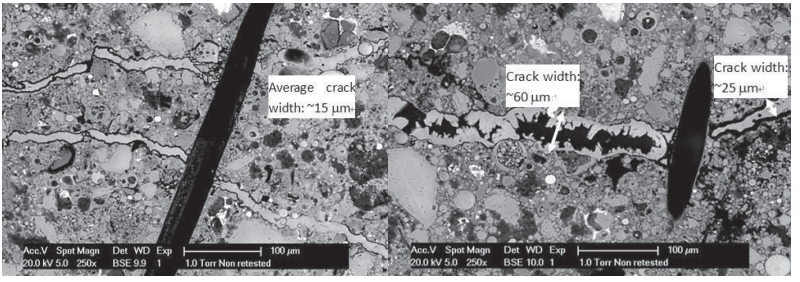

(a) **(b)**

FIG.9. (a) Fullcrack healing after water curing;(b) Partial crack healing after water curing.

CONCLUSIONS

Self-healing behavior of pre-cracked ECC with additives such as steel-wool and rock-wool with local waste materials (Fly ash and Limestone powder) is investigated in this paper. Four-point bending tests are used to pre-crack ECC beam specimens deflected up to 2.0 mm with subsequent curing in water and air for 28 days. The majority of the specimens cured in water showed greatly enhanced mechanical properties comparing with that cured in air. The observations using ESEM further confirmed the outcome from mechanical tests. The following conclusions can be drawn based on the investigation:

1. Crack self-healing behavior is only observed when the pre-cracked specimens are cured in water. Bending test results show specimens cured in water have a certain degree of recovery of the mechanical properties. On the other hand, specimens cured in air revealed no such effect. Furthermore, in many cases the performance after air curing even get worse, denoting that cracks exposed in air won't initiate self-healing behavior due to the lack of water which is necessary to self-healing behavior.

2. Mix additive microfibers into ECC can lower the crack width further, which is beneficial to the self-healing behavior; consequently, enhance the recovery of flexural stiffness. Specimens mixed with additive steel-wool fiber shows negative effect on deformability, possibly caused by poor fiber distribution.

3. The age of the pre-cracking influences the material's mechanical recovery. The recovery level after pre-cracking for 7days case is higher than that 28days case. This behavior may be attributed to the fact that at 7 days after casting, there remains much unhydrated cementitious material to initiate continuous reaction during the period of self-healing. On the other hand, the degree of hydration for 28days case is so high that there is little active material left.

ACKNOWLEDGEMENTS

The authors would like to graciously thank the Jiangsu Provincial and Chinese National Natural Science Foundation projects and Jiangsu Top Talents Program in Six Major Disciplines for partially funding this research under grant Nos.BK2010413, 51008071, and 2011-JZ-011, respectively. Furthermore, the authors also would like to thank Dutch Ministry of Economic Affairs for funding on IOP-SHM programs.

REFERENCES

Edvardsen, C. (1999). "Water permeability and autogenous healing of cracks in concrete." *ACI Materials J,* 96(4): 448-455.

Li, V.C., Yang, E. (2007). "Self healing in concrete materials." *In: van der Zwaag S, editor. Self Healing Materials.Dordrecht: Springer,* p:161-193.

Massey,B.S. (1998). “Mechanics of Fluids.” 3rd Edition, London, Van Nostrand Reinhold.

Qian, S.Z., Zhou, J., de Rooij, M., Ye, G., Schlangen, E. and van Breugel, K. (2009). “Self-healing Behavior of Strain Hardening Cementitious Composites incorporating Local Waste Materials.” *Cement and Concrete Composites,* 31(9):613-621.

Qian, S.Z., Zhou, J. and Schlangen, E. (2010). “Influence of Curing Condition and Precracking Time on the Self-healing Behavior of Engineered CementitiousCompositess.” *Cement and concrete composites*，Vol.32, No.9, pp:686-693,

Yang, Y., Yang, E.H. and Li, V.C. (2011). "Autogenous Healing of Engineered Cementitious Composites at Early Age." *Cement and Concrete Research,* 41:176-183.

Yang, Y.Z., Lepech, M.D., Yang, E.H. and. Li, V.C. (2009). "Autogenous Healing of Engineered Cementitious Composites under Wet-Dry Cycles." *Cement and Concrete Research,* Vol.39, pp:382-390.

Zhou, J., Qian, S.Z., Guadalupe Sierra Beltran, M., Ye, M., van Breugel, K. and Li, V.C. (2009). “Development of engineered cementitious compositeswith limestone powder and blast furnace slag.” *Materials and Structures*, DOI10.1617/s11527-009-9549-0

Influence of Rubber Powder on the Mechanical Behavior of Engineered Cementitious Composites

Zhigang Zhang[1] and Shunzhi Qian[2]

[1]Institute of Highway and Railway Engineering, School of Transportation, Southeast University, P.O. Box 210096, Nanjing City, China;
[2] Institute of Highway and Railway Engineering, School of Transportation, Southeast University, P.O. Box 210096, Nanjing City, China; email: sqian@seu.edu.cn

ABSTRACT: Engineered cementitious composite (ECC) is a kind of composites reinforced with moderate fiber volume fraction, typically 2% by volume. Of special interest is the capability of ECC material to deform to high tensile strains, commonly over 3%, while maintaining very tight crack width. In this study the rubber powder is used in ECC to partially replace fine silica sand, thus enhancing the greenness of ECC. Two particle size of rubber powder (450μm and 200μm in average) is used in this research. Furthermore, there are three different dosages (0, 10%, 15% by volume replacing silica sand) for each rubber powder size. The influence of rubber powder on the ECC mechanical properties is revealed via flexural deformation, crack width and compressive strength. In this paper, it is found that the addition of rubber powder into ECC decreases its first cracking strength with the trend of enhancingdeformation capacity. With the increasing volume of rubber powder, the crack width gets lower. The deformation capacity gets enhanced and compressive strength decreases when the dosage of rubber powder is 15%. The study results prove that it feasible to produce ECC by replacing silica sand partially with rubber powder, thus greatly promoting the greenness of ECC.

INTRODUCTION

With the development of the rubber and automobile industries, the growing amount of waste rubber, rubber products and angle scrap produced from scrap tires has raisedever-increasing environmental concern.In the past two decades, significant research work has been carried out to recycle the used tyres by grinding them into small particles (rubber powder) and to mix them into cement based materials like concrete (Garrick, 2005; Hernández-Olivares, 2007; Khatib, 1999; Sukontasukkul, 2006; Topcu, 1995; Donaldson, 2010).Results of various research studies indicate

that mixed rubber into concrete is beneficial to the deformability and durability (Turatsinze, 2005). A recent study by Ho et al. (2008) confirmed that rubber aggregate incorporation improves the strain capacity of concrete before macro-crack localization.

Although the utilization of rubber powder in concrete has attracted attention in the field of building materials in the past decades, the research on Engineered cementitious composite (ECC) mixed rubber powder is limited. ECCis a uniqueclass of the new generation high-performance fiber-reinforcedcementitious composites (HPFRCC) featuring high ductilityand medium fiber content, which designed based on micromechanics theory by Victor Li at 1990s. Tensile strain capacity at a rangeof 3 to 5% has been demonstrated in ECC materials usingpolyethylene fibers and polyvinyl alcohol (PVA) fibers withfiber volume fraction no greater than 2% (Li, 1998; 2002). Fig.1 shows a typical tensile stress–straincurve of ECC and its tight crack width (Li, 1998). The large straincapacity in ECC is contributed by sequential development of multiple cracks, instead of continuous widening of one localized crack in concrete. Theassociated high fracture toughness and controlled crackwidth (typically below 100 μm) make ECCs anideal material to improve serviceability and durability of the civil infrastructures.

ECC is called green material because of the constituents includes high volume of fly ash which is a by-product of coal burning power plants and usually considered a waste material. In an effort to develop green ECC with local waste materials, Zhou et alhave developeda number of ECC mixtures with blast furnace slag (BFS) and limestone powder successfully(Zhou, 2009). In this study, it is attempted to use rubber powder to replace silica sand partially. On one hand, it consumes the waste rubber reasonably; on the other hand, it reduces the consuming of silica sand, which would improve the greenness of ECC further.

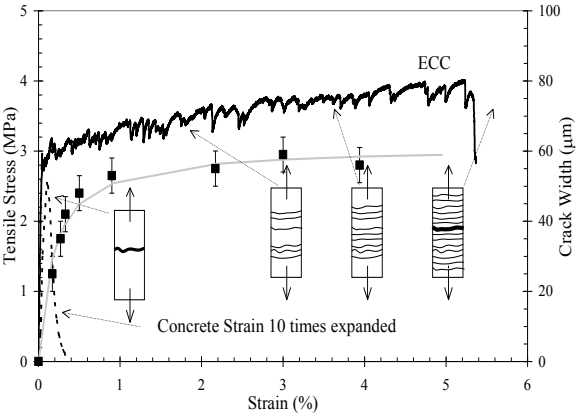

FIG .1. Tensile stress–strain curve and tight crack widthcontrol of ECC.

In this paper, it is attempted to do the researchbout the influence of rubber powder on ECC. Four-point bending and compressive tests were performed to investigate the effect of the addition of rubber powder on properties of ECC. Moreover, the influence on crack width and density were also highlighted.

EXPERIMENTAL PROGRAM

Materials

The mixtures are shown in Table 1, the ECC mixture includes Portland cement, fly ash, silica sand, rubber powder, and PVA fiber. Totally there are twoparticle sizes of rubber powder, including 450μm and 200μm in average. Thereare threemixtures which includedifferent dosages (0, 10%, 15% by volume replacing silica sand) for each rubber powder size.The properties of PVA fiber were revealed in Table 2.

Table 1. Mix proportion of ECC mixture (g/L)

Mix number	cement	Fly ash	Silica sand	Rubber powder/	Rubber particle size(μm)	water	Super-plasticizer	PVA fiber
Mix.1	395	868	459	0	--	312	8	216
Mix.2	395	868	413	21(10%)	200	312	8	216
Mix.3	395	868	390	31(15%)	200	312	8	216
Mix.4	395	868	413	21(10%)	450	312	8	216
Mix.5	395	868	390	31(15%)	450	312	8	216

Table 2. Properties of PVA fiber

Diameter (μm)	Length (mm)	Tensile strength (MPa)	Modulus (GPa)	Density (g/cm^3)
39	12	1620	42.8	1.2

Mixing and Testing

The matrix materials and rubber powder were first mixed with ahigh-shear mortar mixer for 1 min at low speed, followed by the addition of waterand superplasticizer. Mixing continued at low speed for 1 min and then athigh speed for 2 min. After fibers were added, the material was mixed at high speed for another 8

min.The fresh ECC was then cast into steel formwork and then demolded after 1 day curing. The specimens were then cured under standardcuring condition (20°C, 95% RH) until testing.All the specimens were cured for 14 days before testing. The bending specimens have dimensions of 400x70x16mm, while the compressive specimens with dimensions of 70x70x70mm.

After curing, the coupon specimens were used in four-pointbending test. The full span of the four-pointbending test was 300 mm with the middle span of 100 mm. The test was conducted under deformation control of 0.75 mm/min.Typically it takes about 20-30 minutes before the sample exhausts its deflection capacity and fails.

RESULTS AND DISCUSSION

Compressive strength

The material compressive properties for different mixtures can be found in Table 3.The compressive strength of mixtures which mix larger rubber powder particle is lower than that mix smaller rubber powder particle. That's because the larger particle increase the contact area between rubber powder and matrix. The compressive strength has a largely decrease after replacing silica sand by rubber powder with the ratio of 15% for Mix1, 3 and5 due to rubber powder reduce the toughness of matrix. However, it has negligible influence on compressive strength between Mix1, 2 and 4 with the ratio of 10%, which is not the same as literature referenced. It can be explained by the mechanism that compressive strength of ECC is controlled not only by toughness of matrix but also the fiber bridging restrain the horizontal deformation of specimen, consequently, increasing compressive strength. It demonstrates that the ratio of replacement by rubber powder with 10% cannot change the property of compressive strength.

Table 3. Compressive strength

Mix No.	Mix1	Mix2	Mix3	Mix4	Mix5
fc' (MPa)	43.43	43.50	31.33	38.10	28.35

Flexural performance

The flexural stress-load point deflection curves forall mixtureswere shown in Fig. 2. In theflexural stress–deflection curves, it defines the point of end of the linear stage as the first cracking strength, while the maximum flexuralstress is defined as the flexural strength, and thecorresponding deflection is defined as the flexuraldeflection capacity. The flexural specimen was first manually pre-loaded to

make sure four loading points were in full contact with the specimen, which explainsthat the flexural stress is not zero at the beginning of the curve.

Fig.2 (a), (b) and(c) show the curves for A case which mixed smaller rubber particle size. It can be seen from A case that the first cracking strength gets lower as the ratio of replacement of rubber powder increase, denoting that it lower the toughness of ECC for using rubber powder replace silica sand. It can be explained by the mechanism that the bonding between the matrix and rubber powder is much weaker than silica sand. In addition, the flexural stress between Mix1 and Mix2 shows negligible influence, while it decreases obviously between Mix1 and Mix3. The phenomenon can be reflected by that the influence on compressive strength is negligible after replacing silica sand by rubber powder with the ratio of 10%.

For the deformability, it has a slight decrease after using rubber powder replace silica sand for Mix1 and Mix2, but the deformability of Mix2 is within the range of variation of Mix1 due tothe variation for ECC is large. So the slight decrease can be negligible. On the other hand, the deformability of Mix3 gets larger than Mix1. And the curve for Mix3 is quite gentle which can be explained that the existing rubber powder act the inert filler filling well the flaw that is inevitable in concrete micro-structure, thus improved the inner structure which is beneficial to the multi-cracking behavior. Another alternative mechanism can explain the deformability gets larger for Mix3 is that the number of rubber powder for Mix3 offer the sufficientartificial flaws in matrix which is beneficial to achieve the saturated multiple cracking, thus improve the deformability of ECC(Wang, 2004).

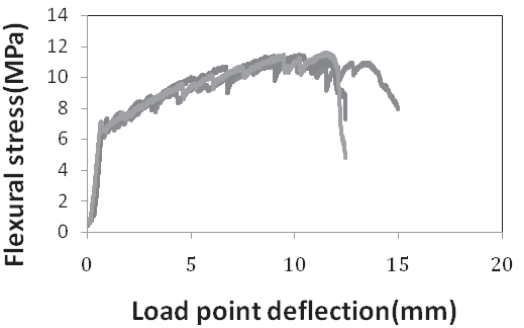

(a)

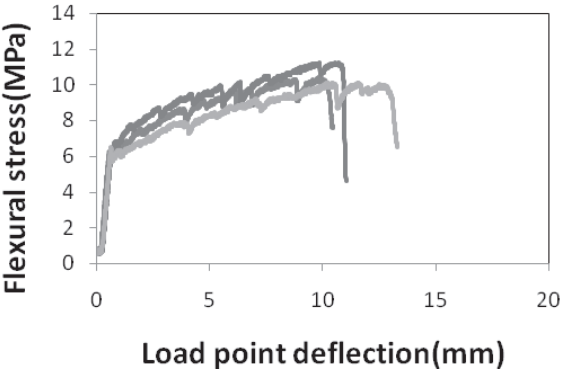
Flexural stress(MPa)
14
12
10
8
6
4
2
0
0
5
10
15
20
Load point deflection(mm)

(b)

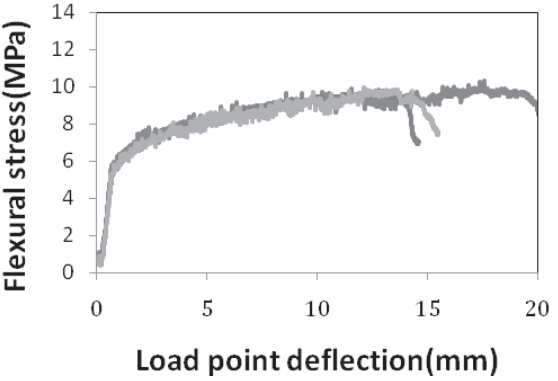
Flexural stress(MPa)
14
12
10
8
6
4
2
0
0
5
10
15
20
Load point deflection(mm)

(c)

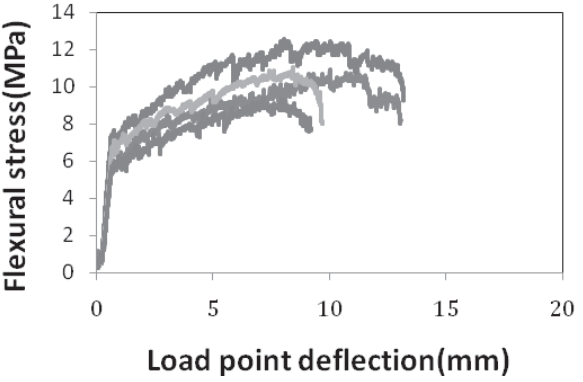
Flexural stress(MPa)
14
12
10
8
6
4
2
0
0
5
10
15
20
Load point deflection(mm)

(d)

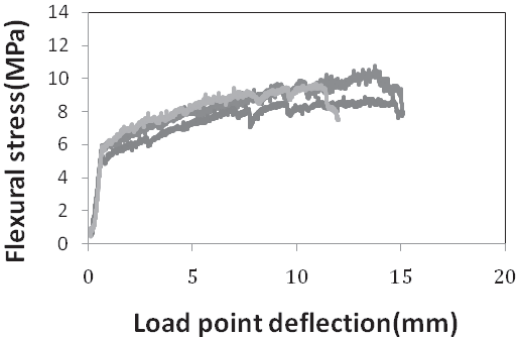

(e)

FIG. 2. Flexural stress – load point deflection relation from FPBT test for (a) Mix1,(b) Mix2, (c) Mix3, (d) Mix4, (e) Mix5.

Fig.2 (a), (d) and (e) show the curvesfor B case which mixed larger rubber particle size. Similar to A case, it shows the same change trend for B case.However, the variation for Mix 4 is larger than the other mixtures. And the deformability of Mix5 is lower than Mix3, although the ratios of replacement of rubber powder are both 15%. This can be explained that the size of rubber powder for 200μm is more suitable to act artificial flaw than 450μm. Wang and Li reported that controlling the size of the artificial flaw is essential to effectiveness of improving the ductility of ECC (Wang, 2004).

Crack width

It is observed that specimens of all mixtures exhibit multiple micro-cracking behaviors under bending test, as is shown in Fig.3. Crack width control many transport properties in cracked concrete material and has a direct impact on durability (Lepech, 2005).So it is necessary to investigate the crack width. The crack width in this paper is measured by optical microscope. The average of crack width for each mixture is shown in Table 4. It is seen obviously that the crack width get smaller with the increasing volume of rubber powder.The explained mechanism is that the rubber powder embeds in the matrix, and the surface of rubber powder is very rough; consequently, increase the interface frictional bond restrains the slippage of fiberwhich is responsible for the tight crack width.

The crack width of B case mix with lager rubber powder particle is tighter than that of A case. It demonstrates that it is beneficial to increase the interface frictional bond for the larger rubber powder particle.

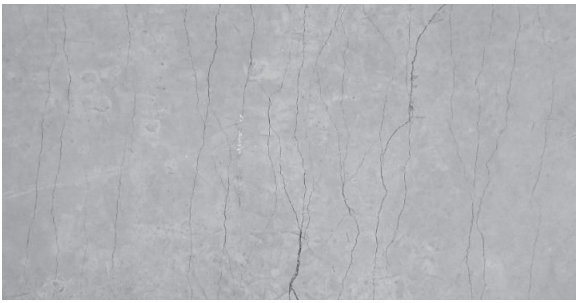

FIG. 3. Multiple cracking along the length of the specimen.

Table 4. Average crack width

Mix No.	Mix1	Mix2	Mix3	Mix4	Mix5
Average crack width(μm)	63	57	51	49	41

CONCLUSIONS

In this paper, it is attempted to develop ECC using rubber powder partially replace silica in order to improve the greenness of ECC and expects to enhance the deformation capacity of ECC.The influences of rubber powder on the mechanical behavior of ECC were studied. The following specific conclusions can be drawnfrom this study:

1. The influence on compressive strength of ECC is negligible when the dosage rubber powder is 10% which due to the fiber bridging restrain the horizontal deformation of specimen. While the compressive strength reduce greatly when the dosage rubber powder is 15% because of large the volume of rubber powder.
2. The deformation capacity gets improved when the dosage rubber powder is 15%, while it does not change when the dosage rubber powder is 10%. And, the first cracking strength decreases as the dosage of rubber powder increase, denoting the toughness of ECC decreases.To some degree, the rubber powder act as the artificial flaw making matrix easier to crack.

3. The addition of rubber powder increases the interface frictional bond restrains the slippage of fiber which contributes to tight crack width which is contributed to the increasing the interface frictional bond, consequently, improve its durability.

ACKNOWLEDGEMENTS

The authors would like to graciously thank the Jiangsu Provincial and Chinese National Natural Science Foundation projects and Jiangsu Top Talents Program in Six Major Disciplines for partially funding this research under grant Nos.BK2010413, 51008071, and 2011-JZ-011, respectively.

The authors also would like to graciously thank the Jiangsu provincial graduate student scientific research innovation plan projects for partially funding this research under grant No.CXLX_0136.

REFERENCES

Donaldson, L. (2010). "Research news; concrete revolutionises road construction." *Materials Today* 13, 10.

Garrick, G.M. (2005). "Analysis and testing of waste tire fiber modified concrete." Thesis (PhD), B.S., Louisiana State University.

Hernández-Olivares, F., Barluenga, G., Parga-Landa, B., Bollati, M. and Witoszek, B, (2007). "Fatigue behaviour of recycled tyre rubber-filled concrete and its implicationsin the design of rigid pavements." *Construction and Building Materials* 21:1918-1927.

Ho, A.C., Turatsinze, A. and Vu, D.C. (2008). In: Alexander, M.G., Beushausen, H.D,Dehn, F., Moyo, P. (Eds.), "On the Potential of Rubber Aggregates obtained byGrinding End-of-life Tyres to Improve the Strain Capacity of Concrete." *Taylor &Francis Group*, London, pp. 123-129.

Khatib, Z.K. and Bayomy, F.M. (1999). "Rubberized Portland cement concrete." *Journal of Materials in Civil Engineering* 11: 206-213.

Lepech, M. and Li, V.C. (2005). "Water Permeability of Cracked Cementitious Composites." *Proceeding of Eleventh International Conference on Fracture,* Turin, Italy.

Lepech, M., and Li, V.C. (2005). "Durability and Long Term Performanceof Engineered Cementitious Composites." *Proceedings of International RILEM Workshop on HPFRCC in Structural Applications,* Honolulu, HI.

Li, V.C. (1998). "Engineered Cementitious Composites—Tailored Composites Through Micromechanical Modeling." *Fiber Reinforced Concrete: Presentand the Future, N. Banthia, A. A. Bentur, and A. Mufti, eds., CanadianSociety for Civil Engineering,*Montreal, Quebec, Canada, 64-97.

Li, V. C., Wu, C., Wang, S., Ogawa, A. and Saito, T. (2002). “InterfaceTailoring for Strain-Hardening Polyvinyl Alcohol-Engineered CementitiousComposite (PVA-ECC),”*ACI Materials Journal*, 99(5) :463-472.

Sukontasukkul, P. and Chaikaew, C. (2006). “Properties of concrete pedestrian blockmixed with crumb rubber.” *Construction and Building Materials* 20: 450-457

Topcu, I.B. (1995). “The properties of rubberized concretes.” *Cement and Concrete Research* 25:304-310.

Turatsinze, A., Bonnet, S. and Granju, J.L., (2005). “Potential of rubber aggregates to modifyproperties of cement based-mortars: improvement in cracking shrinkageresistance.” *Construction and Building Materials* 21:176-181.

Wang, S. and Li, V. C. (2004)."Tailoring of Pre-existing Flaws in ECC Matrix for Saturated Strain Hardening," *Proceedings of FRAMCOS-5,* Vail, Colorado, USA, April, pp. 1005-1012.

Zhou, J., Qian, S.Z., Guadalupe Sierra Beltran, M., Ye, G., van Breugel, K. and Li, V.C. (2009). “Development of engineered cementitious composites with limestone powder and blast furnace slag.” *Materials and Structures*, DOI10.1617/s11527-009-9549-0

Effect of Limestone Powder on Microstructure of Ternary Cementitious System

Yong Zhang[1] and Guang Ye[2]

[1]Microlab, Civil Engineering and Geoscience, Delft University of Technology, 2628 CN Delft, The Netherlands; email: y.zhang-1@tudelft.nl
[2]Microlab, Civil Engineering and Geoscience, Delft University of Technology, 2628 CN Delft, The Netherlands

ABSTRACT: The pressure to reach sustainability favours the development of ternary composite cement. The synergistic effect on mechanical behaviour at 28 days between limestone powder (LP) and pozzolanic additives, i.e. fly ash (FA) and blast furnace slag (BFS), has been documented. In order to better understand the synergistic effect, this article investigated the effect of LP on the microstructure ofPC-FA and PC-BFScementitious system. The mineralogy and pore structure were determined after 28 days of curing at 20°C and 95% relative humidity. The mineralogy in pastes was identified by means of X-Ray diffraction (XRD) and thermogravimetry (TG). The pore structure was evaluated by Mercury intrusion porosimetry(MIP). The results showed that neither monosulfoaluminate nor ettringite was found in any of the XRD patterns,instead carboaluminate was observed.Hemicarboaluminate produced in FA-PC or BFS-PC system transformed into monocarboaluminate with the addition of LP. The porosity was enlarged compared with LP-free paste system. It seems that both the physical and chemical effect of LP contribute to the synergistic effect on mechanical behaviourof cementitious system hydrated up to 28 days.

INTRODUCTION

CO_2 emissions from concrete production accounts for around 8% man-made CO_2(Karen, 2012). The blending of cement clinker with supplementary cementitious materials (SCMs), such as blast furnace slag (BFS), fly ash (FA) and limestone powder (LP), has been the most promising route to increase the sustainability of construction engineering. Nowadays, Portland cement (PC) is still the essential component in cementitious system and blended cements are most often binary, e.g. FA-PC and BFS-PC. While at high replacement levels, the early age mechanical behaviour of binary cementitious system becomes an issue. An possible approach to improve early age mechanical behaviour is to develop ternary cement system, in which different SCMs can interact with each other and may enhance the performance of concrete. LP is a particularly interesting SCM, it can decrease the cost due to the less demand of gypsum content (Weerdt, 2011a) and produce almost zero associated

CO_2 emissions. Therefore, development of LP-filled ternary composite cement is meaningful.

Several series of experiments on mechanical behaviour of LP-filled ternary cementitious system have been performed. Replacing 5% of PC with LP in FA-blended ternary cement system resulted in no strength loss at the age of 28 days (Weerdt, 2011b). Katsioti(2009) also proved the compatible mechanical behaviour of 5% LP addition in pozzolanic mortar system at 28 days. While the effect of 5% LP addition on strength development of binary PC-LP samples appeared to be less pronounced than ternary PC-FA-LP and PC-BFS-LP samples (Seiichi 2006; Weerdt 2011a). In some cases, replacing PC by 5% LP in binary LP-PC concrete resulted in a reduction in both compressive strength and flexure strength at 28 days (Weerdt 2011b). It seems there is a synergistic effect on strength development when small amount of LP is combined with pozzolanic additives, i.e. FA and BFS.

Previous studies have documented the influence of LP on the hydration process of pozzolana-contained cement system. It is known that LP interacts with alumina-contained phases and leads to the formation of carboaluminate instead of monosulfoaluminate and thereby stabilizing the ettringite (Hoshino 2006; Kakali 2000; Lothenbach, 2008; Weerdt,2011a). Especially in high-alumina pozzolanic cement system, the effect of LP in stabilizing the ettringite would be more obvious, which is confirmed by Weerdt (2011b). However, the underlying reasons for the aforementioned synergistic effect on mechanical properties of hydrating cementitious system have not been investigated, except one assumption that the synergistic effect is most likely related to the interaction of LP with AFm and AFt phases (Weerdt 2010).

In order to better understand the synergistic effect, this paper investigated and compared the microstructure formed by pozzolana contained cementitious system with and without LP. To this end, experiments were carried out on a series of mixtures. In this study, 10% PC was replaced by LP. Two different pozzolanic additives were used, i.e. FA and BFS. The replacement level was 30%-50% for FA and 30%-70% for BFS. The mineralogy and associated pore structure were determined after hydration of 28 days. The synergistic effect on better mechanical behaviour of ternary cementitious system was eventually discussed.

EXPERIMENTS

Materials

Materials used for this work are Portland cement (PC), Fly ash (FA), ground granulated blast furnace slag (BFS), Limestone powder (LP). 10 mixtures were designed. The details of mixtures and chemical composition of each material are shown in Table 1. The CO_2 content in each mixture was obtained by thermogravimetric analysis. The mainly crystal phases in pozzolanic additives are quartz and mullite in FA , melilite and merwinite in BFS.

Sample preparation

For XRD, TGA and MIP measurements, the pastes were cast with constant water to binder ratio (W/B) 0.4. Each paste mixed with water in a HOBART mixer at low

speed for 1 minute and at high speed for 2 minutes. Then the fresh paste was poured into plastic bottles and shaken on the vibration table to remove big bubbles and then sealed with lids. In order to avoid bleeding, the samples were rotated almost one day and then placed in standard curing room with the condition of temperature 20°C and 95% RH. After 28 days curing, the samples were spitted into small pieces. Liquid nitrogen was used to stop the further hydration of the specimens (Ye, 2003). Then these small pieces were moved into a freeze-dryer with temperature of −24 °C and under vacuum at 0.1 Pa. Until the water loss was below 0.01% per day, the specimen then can be used for the XRD, TGA, MIP measurements.

Table 1 Mixture proportions (left) and chemical composition % (right)

	PC	FA	BFS	LP	W/B
M_1	100%				0.4
M_2	90%			10%	
M_3	70%	30%			0.4
M_4	50%	50%			0.4
M_5	70%		30%		0.4
M_6	30%		70%		0.4
M_7	60%	30%		10%	0.4
M_8	40%	50%		10%	0.4
M_9	60%		30%	10%	0.4
M_{10}	20%		70%	10%	0.4

	PC	BFS	FA	LP
CaO	64	42	5.8	-
SiO_2	19.9	33	54	0.34
Al_2O_3	4.5	12	23	0.2
SO_3	2.55	2.3	1.7	0.046
K_2O	0.42	0.46	1.9	0.011
Na_2O	0.4	0.28	1	0.017
MgO	2.2	7.5	1.4	0.27
Fe_2O_3	3.3	0.63	7.3	0.067
CO_2	0.52	0.07	0.66	99
Others	2.21	2.54	3.24	0.093

Measurements and methods

(1) Thermogravimetric analysis(TGA)

A STA(TG-DTA-DSC) 449 F3 Jupiter was used to measure the quantity of calcium hydroxide (CH) and assess the pozzolanic behaviour of additives in LP-filled cementitious system. The amount of CH is calculated from weight loss curve during thermal analysis (Bryan, 1988). The mass of sample was about 30-50 mg. The maximum heating temperature was 1100°Cwith the heating rate 10 °C/min. Argon was used for the protective gas.

(2) X-ray Powder diffraction(XRD)

XRD used in this work was mainly to study the mineralogy of cementitious system with and without LP. For mineralogical investigations, the powders were firstly mixed with standard crystal Al_2O_3 powders and thenpulverized to an average particle size of less than 10 micros with no particle feeling. After that, the pulverized powders were evaluated by X-Ray diffraction, operating at 40kV, 30mA, 2θ angle is from 5° to 70° with step size of 0.03°. A diffractometer was used to identify the crystalline phases. Cu $K\alpha$ radiation was used. The crystalline components of the powdered sample were identified by comparing with the standards established by the International Centre for Diffraction Data.

(3) Mercury intrusion porosimetry(MIP)

MIP was used to assess the influence of LP on pore structure of ternary cementitious paste system. With the assumption that pores are cylindrical and entirely and equally accessible to mercury, the applied pressure can be converted into the pore diameter by using the Washburn equation (Washburn, 1921)

$$D = \frac{-4\gamma \cos\theta}{p} \quad (1)$$

where, D is the equivalent pore diameter, P is the applied pressure, γ is the surface tension of mercury (485 dynes/cm) and θ is the contact angle between mercury and solids, in this study $\theta = 139°$ was used.

RESULTS

Mineralogy

The phases determined by XRD for the samples with and without LP were compared and shown in Fig. 1. The crystal phases were somewhat similar as expected, except the peaks lies at the low angles, where the hemicarboaluminate [$C_3A{\cdot}0.5CaCO_3{\cdot}0.5Ca(OH)_2{\cdot}11.5H_2O$] produced in PC-FA and PC-BFS samples disappeared (2Θ peak at 10.8°), and transformed into monocarboaluminate [$C_3A{\cdot}CaCO_3{\cdot}11H_2O$] (2Θ peak at 11.7°) in PC-FA-LP and PC-BFS-LP samples. This proved that LP did influence the chemical constitution of alumina-contained phase (AFm) in cementitious system. In addition, the products of carboaluminate would fill the capillary pores and the mechanical behaviour could be therefore enhanced. According to Kuzel (1991),

$C_3A + 1/2CH + 1/2\ CC + 11.5H_2O \rightarrow C_3A{\cdot}1/2CC{\cdot}1/2CH{\cdot}11.5H_2O$ (Hc) **(I)**

$C_3A{\cdot}1/2CC{\cdot}1/2CH{\cdot}11.5H_2O + 1/2CC \rightarrow C_3A{\cdot}CC{\cdot}11H_2O + 1/2CH + 1/2H$ **(II)**

$C_3A + CC + 11H_2O \rightarrow C_3A{\cdot}CC{\cdot}11H_2O$ (Mc) **(III)**

As shown in Fig.1, there was neither monosulfoaluminate (2Θ peak at 9.89° and 19.8°) nor ettringite (2Θ peak at 9.1° and 15.8°) in any of the cementitious systemsincluding pure PC system at 28 days, instead carboaluminate was observed. The absent of monosulfoaluminate was also found in literature (Ogawa, 2012). It can be ascribed to the presence of CO_3^{2-} in PC clinkers (from Table 1). Very small amount of CO_3^{2-} content could lead to the rapid consumption and decrease in the amount of monosulfoaluminate (Matschei, 2007). At 22°C and pH>12, the SO_4^{2-} groups in the interlayer region of monosulfoaluminate are easily substituted by CO_3^{2-}, therefore the crystallisation of Hc or Mc is observed (Kuzel, 1991). However, the sulfate released from monosulfoaluminate did not lead to the formation of gypsum (2Θ=20.7°) or anhydrite (2Θ=25.4°) or bassanite (2Θ=29.7°). Then it can be concluded that the absent 2Θ peak of ettringite was most probably due to its poorly crystalline and lower amount(<5%) in cementitious system.

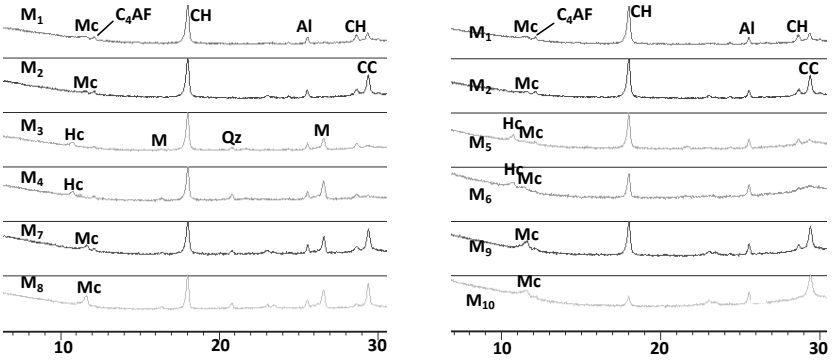

FIG. 1 XRD patterns (5°-30°) for pastes hydrated up to 28 days (Hc-hemicarboaluminate, Mc-monocarboaluminate, Qz-quartz, M-mullite, CH-calcium hydroxide, CC-$CaCO_3$, Al-Al_2O_3).

The 2θ peak at 11.7° is not so strong in mixture of pure PC and PC-LP system, which indicates that the chemical interaction (III) is not pronounced due to the limited aluminate content in anhydrous clinkers. Therefore, LP is often considered as inert filler in PC-LP cement system (Weerdt, 2011b). While pozzolanic additives (FA, BFS etc.) usually contain high amount of aluminate phases, thus additional calcium aluminate hydrates (Hc or Mc) may be produced, which is confirmed by the XRD patterns in this study. The strong chemical interaction between alumina phases of FA/BFS and LP may further account for the synergistic effect on strength development of cementitious system.

If looking into the patterns in detail, Mc is observed in PC system, both Mc and Hc are produced in BFS-PC system, while only Hc appears in FA-PC system. From chemical composition (as shown in Table 1), more aluminate phases contained in FA, followed by BFS and PC, the gradual transformation from Mc into Hc could indicate the reactivity of carbonate is highly dependent on the content of aluminate phases in cementitious system. While when 10% of LP is filled in FA-PC and BFS-PC system, all the Hc is transformed into Mc phase. Then it could be concluded that the occurrence of reaction (I) or (II) or (III) is determined by the ratio of weight percentage of CO_3^{2-}/Al_2O_3 in cementitious system. Due to the reaction between LP and alumina phases, the phases assemblage and stability in cementitious system were influenced with the addition of LP, which was confirmed by the patterns M_1-M_{10}. In addition, LP could react with CH(reaction I), with the hydration process, pozzolanic reaction would be significantly influenced. Hence, the chemical effect of LP is of great importance in high aluminate containing pozzolanic cement system and cannot be neglected. Nevertheless, its chemical benefit needs to be investigated in the long term standpoint and systematic studies are worthy to be carried out.

The CH content of each paste tested by TG was shown in Fig.2. As expected the CH content was decreased with the increase of replacement level of pozzolanic materials. This was mainly due to less amount of Portland cement in the mixture

meanwhile the CH was consumed by the pozzolanic reaction. It can be found that the CH content is less in BFS-filled system than that in FA-filled system when the same amount (30%) of PC is replaced. This proves that the pozzolanic behaviour of BFS is higher than that in FA at the early age. The presence of LP further reduced the CH content in all the ternary cementitious system and interestingly the reduction (1.74%-2.57%) is more than the dilution effect of 10% LP substitution (1.61%). The same phenomenon was also discovered in (Weerdt, 2010). As the formation of hemicarboaluminate (Hc) in both FA-PC and BFS-PC requires the consumption of CH, while the monocarboaluminate (Mc) produced in LP-FA-PC and LP-BFS-PC does not consume CH. Therefore the extra decrease of CH amount is most probably due to the enhancement of pozzolanic reaction, assuming the Ca/Si in C-S-H do not increase with the addition of LP (Locher, 1966; Stucke, 1976). It is well known in the presence of LP, cement hydration was highly accelerated in the first 7 hydration days, which involves a higher production rate of CH(Mounanga, 2011), and thus an increase in the pozzolanic behaviour at early age. In addition, the better phases assemblage with the addition of LP may also contribute to the progress of pozzolanic reaction. It should be noted that due to enhanced pozzolanic reaction CH (32.9cm^3/mol) transformed into C-S-H (almost 350 cm^3/mol) (Taylor, 1997) and the mechanical behaviour of cementitious system would be also enhanced.

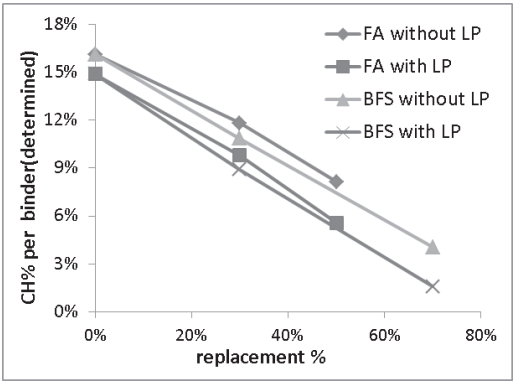

FIG. 2 CH content in pastes with and without LP at 28 days.

Pore structure

From Fig.3, as expected the porosity of FA-filled system increases with the increase of replacement levels (30% and 50%) at curing age of 28 days. However, lower amount of BFS substitution (30%) could decrease the porosity because of the intensive pozzolanic reaction at the early age, as indicated by the lower amount of CH in hydrated system (Fig.2). While the porosity increased when 70% of PC is replaced by BFS, this may be ascribed to the lower amount of CH content in the blended system that highly influenced the progress of pozzolanic reaction at the age

of 28 days. On the other hand, the rate of reaction of the slag decreases with the increase of replacement level of the slag (Escalante, 2001).

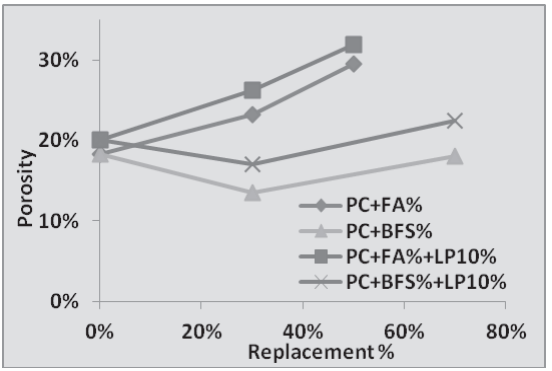

FIG. 3 Porosity of pastes at 28 days with and without LP.

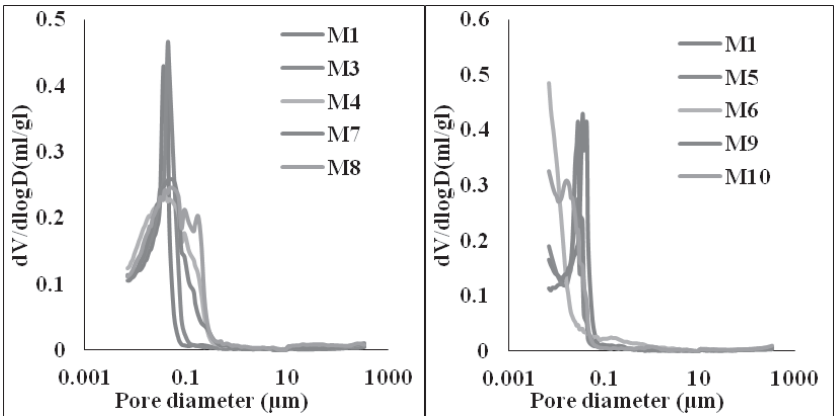

FIG. 4Pore size distribution of pastes at 28 days with and without LP.

In addition, from Fig.4 the critical pore size of reference Portland cement system is smaller than all the FA-filled cementitious system, while larger than all the BFS-filled cementitious system. The critical pore size in M_6 paste was even smaller than 0.01um, which revealed that the pore size was highly refined by BFS additives, this was also discovered by (Song, 2006). The denser microstructure in cement paste with BFS may also partly due to the optimal proportion match and particle size match. However, the data in Fig.4 should be treated with caution, as MIP is insufficient in determination of pore size distribution due to its accessibility problems (Sidney, 2000).

With the addition of LP, the porosity of all pozzolanic cement pastes increased and the pore size was also enlarged. When LP is introduced into pozzolanic cement system, the main phase change is the transformation of Hc (280 cm^3/mol) to Mc (262 cm^3/mol) (Taylor, 1997), which means there is a little bit increase of the pore volume percentage when this reaction happens. In addition, the stronger peak of pattern M_7-M_{10} in Fig. 1 at 29.4° and relatively weaker peak at 11.7° seemingly revealed that most of LP is still in the presence of unreacted calcium carbonate. Then it could be concluded that the dilution effect, combined with the chemical transformation, could account for the increment of porosity.

CONCLUSIONS AND DISCUSSIONS

This article investigated the effect of LP on the mineralogy and pore structure of PC-FA-LP and PC-BFS-LP system hydrated up to 28 days with cement substitution rates from 40%-80%. The results proved that LP reacts with aluminate contained phases and leads to the formation of carboaluminate in cementitious system, and monosulfoaluminate was not found as expected. The porosity and pore size of hydrated cement pastes were enlarged compared with LP-free cement pastes. In addition, the experimental results obtained also lead to the following conclusions:

(1) The reactivity of carbonate is highly dependent on the content of alumina phases in cementitious system and the phases assemblage of hydrated AFm (Hc or Mc) is determined by the weight ratio CO_3^{2-}/Al_2O_3 in cementitious system.
(2) The addition of LP may enhance pozzolanic reaction of additives due to the accelerated production of CH at early age and may also due to the better hydrates assemblage in ternary cementitious system.

Compared to FA-PC and BFS-PC system, the total porosity is increased with the addition of LP. Therefore, thebetter mechanical behaviourin the presence of LPat 28 days could be ascribed more to the filling effect of unreacted LP and reaction products of carboaluminate that fulfilled the big capillary pores of cementitious system, whereby the possibility of strength failure by big pores was reduced. Additionally, it seems due to filler effect, the addition of LP could enhance pozzolanic reaction at 28 days that contributes to the better mechanical behaviour. Thus, both the physical and chemical effect of LP could contribute to the synergistic effect on the mechanical behaviour of hydrating ternary cementitious system.Nevertheless, the chemical effect of LP needs to be investigated in the long term standpoint due to the probable transformation of carboaluminate into ettringite.
It is believed the phases assemblage in hydrating cementitious system is of paramount importance in mechanical behaviour of hydrating cement-based system. Therefore better understand the influence of LP on nucleation and formation of microstructure of hydrating ternary cementitious system would be helpful in better understanding of the synergistic effect. To this respect, further studies regarding to surface energy of unhydrated particles and hydrated particles should be performed.

ACKNOWLEDGEMENT

The authors would like to appreciate the financial support from China Scholarship Council (CSC). In addition, gratefully acknowledgment should be given to technicians in Microlab of Delft University of Technology.

REFERENCES

Bryan, K., Marsh and Robert, L. D. (1988).“Pozzolanic and cementitious reactions of fly ash in blended cement pastes.”*Cement and concrete research*. Vol. 8: 301-310.

Escalante, J.I., Go´mez, L.Y., Johal, K.K., Mendoza, G., Mancha, H. and Me´ndez, J. (2001).“Reactivity of blast-furnace slag in Portland cement blends hydrated under different conditions.”*Cement and Concrete Research* 31: 1403–1409.

Kakali, G., Tsivilis, S., Aggeli, E. and Bati, M. (2000).“Hydratccion products of C3A, C3S and Portland cement in the presence of CaCO3.”*Cement and Concrete Research* 30: 1073–1077.

Karen, L. S. (2012). “Impact of microstructure on the durability of concrete.”*Second International Conference on Microstructural-related Durability of Cementitious Composites*, 11-13 April 2012, Amsterdam, The Netherlands.

Katsioti, M., Gkanis, D., Pipilikaki, P., Sakellariou, A., Papathanasiou, A., Teas, Ch., Chaniotakis, E., Moundoulas, P. and Moropoulou, A. (2009).“Study of the substitution of limestone filler with pozzolanic additives in mortars.”*Construction and Building Materials* 23: 1960–1965

Kuzel, H. J. and Pollmann, H. (1991).“Hydration of C_3A in the presence of $Ca(OH)_2$, $CaSO_4 \cdot 2H_20$ and $CaCO_3$.”*Cement and Concrete Research*Vol. (21): 885-895.

Locher, F.W.(1966). ACI-SP 90, Washington, 300-308

Lothenbach, B., Le,Saout G. Gallucci, E. and Scrivener,K. (2008). “Influence of limestone on the hydration of Portland cements.”*Cement and Concrete Research* 38: 848–860.

Matschei, T., Lothenbach, B. and Glasser, F.P. (2007). “The role of calcium carbonate in cement hydration.”*Cement and Concrete Research* 37: 551–558.

Mounanga, P. et al. (2011).“Ahmed Loukili. Improvement of the early-age reactivity of fly ash and blast furnace slag cementitious systems using limestone filler.”*Materials and Structures* 44:437–453.

Ogawa, S., Nozaki, T., Yamada, K., Hirao, H. and Hooton, R.D.(2012). “Improvement on sulfate resistance of blended cement with high alumina slag.”*Cement and Concrete Research* 42: 244–251.

Seiichi, H. et al.(2006). “XRD/Rietveld Analysis of the hydration and strength development of slag and limestone blended cement.”*Journal of Advanced Technology*. Vol.(4): 357-367.

Diamond, S. (2000). “Mercury porosimetry An inappropriate method for the measurement of pore size distributions in cement-based materials.”*Cement and Concrete Research*. 30: 1517-1525.

Song,Ha-Won. andSaraswathy,V. (2006). "Studies on the corrosion resistance of reinforced steel in concrete with ground granulated blast-furnace slag—An overview."*Journal of Hazardous Materials* B138:226–233.

Stucke, M.S., et al.(1976).proc. CHCPSP., Sheffield, April, pp. 31-51.

Taylor, H.F.W.(1997). *Cement Chemistry*, 2nd edition, Thomas Telford Publishing, London.

Washburn, E.W. (1921)."Note on a method of determining the distribution of pore sizes in a porous material." *Porc. Natl. Acad. Sci.* USA 7 : 115–116.

Weerdt, K. De, Justnes, H., Kjellsen, K. O. and Sellevold, E. (2010)."Fly ash-limestone ternary composite cement: synergetic effect at 28 days."*Nordic Concrete Research*, Vol. 42: 51-70.

Weerdt, K. De, Haha, M. Ben., Saout, G. Le., Kjellsen, K.O., Justnes, H. and Lothenbach, B. (2011a)."Hydration mechanisms of ternary Portland cements containing limestone powder and fly ash."*Cement and Concrete Research* 41: 279–291.

Weerdt, K. De, Kjellsen, K.O., Sellevold, E. and Justnes, H. (2011b)."Synergy between fly ash and limestone powder in ternary cements."*Cement & Concrete Composites* 33:30–38.

Ye, G. (2003) Experimental Study and Numerical Simulation of the Development of the Microstructure and Permeability of Cementitious Materials, Ph.D. Thesis, Delft.

Evaluation of Crumb Tire Rubber Modified Hot Mix Asphalt Concrete in Sudan

S. A. Osman[1] and A. A. M Adam[2]

[1] Assistant professor, University of Dammam, College of engineering, P.O. Box 1982, Dammam 31451, Saudi Arabia, KSA, email:sakhair@ud.edu.sa

2 Lecturer, Gazera University, College of Engineering, Sudan, email: abdallaadam45@yahoo.com.

ABSTRACT: Scrap tires form a major part of the world's solid waste management problem. In recent years, the waste tire problem has become so acute that there is an urgent need to find an optimum and effective way to use scrap tires in asphalt mixtures. This paper investigates used tire rubber as an asphalt modifier and its potential prospects to enhance bitumen physical and asphalt mixture properties in hot climate like Sudan. Bitumen grade 60/70 blended with different percentage of crumb used tire rubber. Engineering and physical properties of bitumen and bitumen/rubber mortar were evaluated. Marshall Mix was designed and used to evaluate the bituminous mixtures properties. An extensive laboratory studies and tests have been done to evaluate the effect of crumb tire rubber on bitumen and bituminous mixture concrete. The laboratory results indicated that crumb rubber modifier provides better engineering properties in terms of rheological properties, penetration, softening point, specific gravity flash and fire point tests and indicated that crumb rubber modifier decrease the stability and density, increase the flow, and slightly increase the air voids and the voids of mineral aggregate. The study recommended that further studies should be conducted in mixing time and temperatures as well as a field test on rubberized constructed section.

INTRODUCTION

Waste material recycling into useful products has become a main solution to waste disposal problems. Many highway agencies are conducting wide variety of studies and research projects concerning the feasibility, environmental suitability, and performance of using recycled products in highway construction. The use of scrap tires in asphalt mixture applications is not a recent development with reclaimed tire crumb being used in the asphalt industry for over 50 years.

The use of crumb rubber in asphalt paving is gaining more attention in many parts of the world as this material gives better mechanical and functional performance of the mixture as well as being a proficient way of dealing with this waste product as explained by (Epps, 1994). Crumb rubber modified (CRM) asphalt is a general type of modified asphalt that contains scrap tire rubber. Modified asphalt paving products can be made with crumb rubber by several techniques, including a wet process and a dry process.

In Sudan asphalt rubber binders have been used for joint and crack sealers, in chip seals, and in hot paving mixes as thin overlays. Generally, the field performance of crumb rubber modifier (CRM) mixes have been positive but short comings due to poor performance have been reported which may be attributed in part to poor mix design practices, lack of performance based physical property tests and poor construction practices. In addition, the properties of CRM mixes have been found to vary with the rubber type and gradation, rubber concentration, asphalt type and concentration, cure time and reaction temperature and time. For these reasons this paper tries to answer some questions regarding the use of used tire in asphalt mix as a modifier in hot climate.

Different asphalt modifiers are proposed to improve the resistance of asphaltic mixtures to environmental changes in hot climate. Among these modifiers is crumb rubber that has been considered by many researchers to improve the performance of asphalt pavement mixtures (Epps, 1994). Another important objective of using crumb rubber as an asphalt modifier is to avoid environmental problems resulting from scrap tire disposal. Many studies have reported the improvement of properties of asphalt concrete mixtures when crumb rubber was used. Most of those studies were based on standard traditional tests like Marshall Stability, indirect tensile strength, and resilient modulus (Othamn, 2006).

Studies conducted by (Takallou and Sainton,1991) demonstrated that rubberized binder has to be used within 1 hour of its production as the interaction process continues after mixing while the mixture is at storage temperatures. The

viscosity reaches its maximum after approximately 45 minutes, remaining high for 1 to 2 hours and then decreases

A test conducted by the Alaska DOT showed that the wet process had the best thermal cracking resistance, compared to dry and control sections (saboundjian,1997). Both laboratory and field trials indicated that asphalt rubber mixtures are less temperature susceptible than conventional mixtures.

Generally, there are several researches which primarily focuses on the physical properties, chemical properties, engineering designs and constructability, has identified several promising uses for these wastes (Hamid,2008; Blow, 1971; green,1977;Harvey,2000; Heitzman,1992; Kaloush, 2003; Mohammad, 2000; Hozayen,2008).

Studies conducted in Texas and Nevada (Epps, 1994) suggests that mixtures containing crumb rubber and conventional mixtures have similar resistance to permanent deformation.

In Sudan asphalt rubber binders have been used for joint and crack sealers, in chip seals, and in hot paving mixes as thin overlays.

This research investigates properties of used tire rubber as an asphalt modifier and its potential prospects to enhance bitumen physical and asphalt mixture properties in hot climate like Sudan.

EXPERIMENTAL

Materials and Testing

Mixture composition, preparation and curing are significant elements in the production phase that affect mixture performance in service. Currently, no widely accepted mixture design method has been developed for rubber-modified asphalt mixtures in the Sudan. In this research, the mixture was designed as a binder course to avoid direct impact of mechanical wear and weathering. In addition, the mixture was designed using an existing Sudan gradation to minimize extra effort required in the material design stage. The coarse, fine and filler mineral aggregate fractions used in this investigation consisted of basalt stone obtained from Umdraman quarry, Sudan.

The Crumb Tire Rubber used was imported from Sarco Company for road and bridge at Khartoum District and graded according to ASTM C136-84. It has an

average specific gravity of 1.11.

The source and grade of the bitumen was Middle East grade 60/70 Pen as specified in BS EN 12591 from Petrodalta Company-Sudan- for road and bridge. The CRM mixtures were produced by adjusting the grading curve to incorporate different percentages of crumb rubber blended (0, 15, 20 and 25%by mass) at temperatures of 160˚C and 165˚C with mixing time of 2 and 4 hours. The bitumen/crumb rubber mix was examined microscopically to check homogeneity of the mixture as shown in Fig 1. Engineering and physical properties of bitumen and bitumen/rubber mortar were evaluated. Asphalt mixture was designed and used to evaluate the CRM bituminous properties by Marshall Test. An extensive laboratory studies and tests have been done to evaluate the effect of crumb tire rubber on bitumen and bituminous mixture concrete. Five specimens for each bitumen contents and more than 100 specimens have been tested. The presented results are average results of 5 tests except at mixture containing 15% it is an average of 3 tests.

The properties of Asphalt binder results were presented in Table 1. The laboratory tests performed for aggregates materials were: Los Angeles Abrasion (ASTM C131–81), Aggregate Impact Value, Aggregate Crushing Value, Sieve Analyses (ASTM C136-84), Specific Gravity and Water Absorption (ASTM C127–88), Fractured Faces of Aggregate and Angularity (BS 812) Flakiness and Elongation (BS 812 812:1989 Part 105 Section 105.1.). The tests for fine aggregates were: sieve Analyses (ASTM C117–87), Specific Gravity (ASTM C128–88) and Water Absorption. The tests for filler were Specific Gravity and Atterberge limits. The test results were presented in Table 2.

Table 1. Bitumen and Modified Bitumen Physical Properties Tests Results

Fire point (˚F)	Flash point (˚F)	Softening Point (˚C)	Ductility (cm)	Penetration (0.1mm)	Specific gravity	Rubber %
620	610	47.2	105	67	1.03	0
572	554	53.5	15	68	1.03	15
581	554	59	10	55	1.04	20
590	572	56.7	12	62	1.04	25

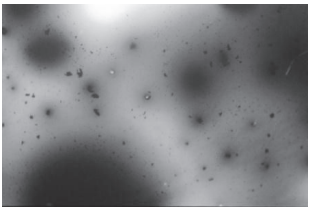
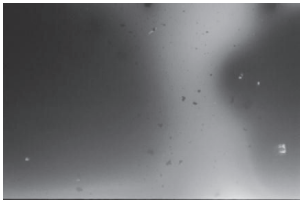

FIG.. 1. Microscopic Appearance of 15% Rubber Blended with Asphalt.

Table 2. Properties of used aggregate

Aggregate type	3/4″	3/8″	3/16″	Sand	Filler
Test					
Abrasion Value	11.1	12.6	-	-	-
Aggregate Crushing Value	10.2	-	-	-	-
Aggregate Impact Value	2.1	-	-	-	-
Specific gravity gm/cc (Bulk)	2.844	2.828	2.513	2.636	2.535
Specific gravity gm/cc (Apparent)	2.882	2.881	2.605	2.685	2.545
water absorption %	0.46	0.66	1.42	0.652	0.15
Flakiness index%	4.8	31	-	-	-
Elongation index%	15.1	21.3	-	-	-
Liquid Limit	-	-	-	-	N.L
Plastic Limit	-	-	-	-	N.P

RESULTS AND DISCUSSIONS

Evaluation of Effect of crumb rubber on Bitumen Properties

Grade bitumen 60/70 blended with three crumb rubber percentages to form modified asphalt which is evaluated by different tests: microscopic examination (morphological analysis), specific gravity, penetration, softening point, ductility, flash and fire points. The effect of crumb rubber percentages on the morphology, specific gravity, penetration, softening point, ductility, flash and fire points are

discussed and presented blow (see Fig 2).

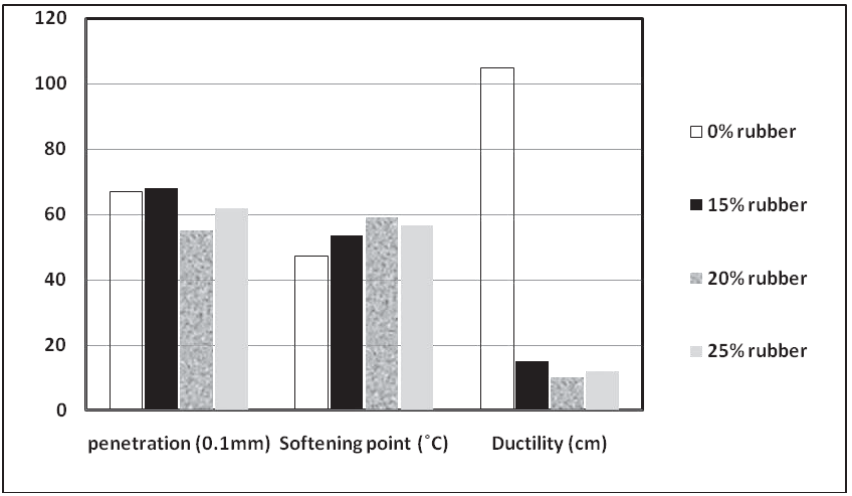

FIG.. 2. Effect of crumb rubber percentages in the bitumen properties.

Effect of Crumb Rubber Percentages on the Bitumen Specific Gravity

The specific gravity of the asphalt rubber and regardless of the rubber percentage is higher than the 60/70 asphalt. The difference in specific gravity values due to rubber percentage is marginal. The increasing in specific gravity may be attributed to the increasing in the Bulk Specific gravity of crumb rubber.

Effect of Crumb Rubber Percentages on the Bitumen Penetration Value

The penetration is a measure of hardness or softness of bitumen binder which shows an effect by adding crumb rubber to bitumen binder; it slightly decreases as rubber content is increased. The penetration shows lower values as tire rubber content increases at different mix conditions of rubberized bitumen binder, indicating that the binder becomes stiff and more viscous. These results indicate that the modified mixtures are stiffer than the conventional ones and therefore the rutting resistance of the modified mixtures is expected to be higher. This might be because of the primary mechanism of the interaction of crumb rubber with base binder is

swelling of the rubber particles caused by the absorption of light fractions into these particles and stiffening of the residual binder phase.

Effect of Crumb Rubber Percentages on the Bitumen Softening Point

The softening point refers to the temperature at which the bitumen attains a particular degree of softening. The use of crumb rubber in bitumen modification leads to an increase in the softening point by approximately 6 to 10˚ C as rubber crumb content increases. Others researchers also reported that the higher crumb rubber content leads to higher viscosity and softening point. The viscosity is a continuously increasing non linear function of rubber content and the relative increase is a factor related to the application of temperature (Bahia and Davies, 1995). Generally, the softening point of the modified asphalt is higher than the conventional asphalt binder. These results indicate the asphalt-rubber concrete pavements should be less susceptible to traffic –indicate deformation distress at high pavement temperatures compared to conventional asphalt pavements.

Effect of Crumb Rubber Percentages on the Bitumen Flash and Fire Points

The result shows that the flash point for asphalt rubber decreases by approximately 56 to 38˚ F by the addition of tire rubber percentage by weight to 60/70 asphalt grade. Also the fire point decreases by approximately 30 to 45˚ F by the addition of tire rubber. Generally, the flash and fire point of the modified asphalt and regardless of the rubber percentage is lower than the conventional asphalt. Asphalt-rubber for all percentages have lower flash point than the conventional asphalt 60/70. The decreases in flash point of modified asphalt may be attributed to the some fabric content in tire rubber.

Effect of Crumb Rubber Percentages on the Bitumen Ductility

The ductility is a distinct strength of bitumen, allowing it to undergo notable deformation or elongation. The ductility is defined as the distance in centimeter, to which a standard sample or briquette of bitumen material will be elongated without breaking. The ductility value of the modified asphalt and regardless of the rubber percentage is lower than the conventional asphalt. The reduction in ductility value of modified asphalt may be attributed to the some fabric content in tire rubber modifier

and may be due to non homogeneity of some crumb rubber particles which lead to decrease in adhesion. Furthermore, there are however, several practical and experimental issues, such as it requires an elevated composite of temperatures and extended digestion time during the mixing process for it to be diffused in the bitumen.

EVALUATION OF ASPHALT MIXTURE PERFORMANCE

A comparison between asphalt mixture performance due Percentage of the added Rubber is presented below. The comparison also includes the conventional asphalt mixture (No rubber), which acts as the control group.

Effect of Crumb Rubber of Mixture Stability

Stability of an HMA pavement, the most important property of the bitumen mixture in the wearing course design, is its ability to resist shoving and rutting under traffic. Therefore, stability should be high enough to handle traffic adequately, but not higher than the traffic conditions required. The lack of stability in an asphalt mixture causes unraveling and flow of the road surface. Fig 3 presents stability of the modified asphalt concrete mixtures is lower than the conventional asphalt concrete mixture. Fig 3 show the highest stability was reported for asphalt mixture that is treated with pure 60/70 asphalt grades, which is higher than mixture treated with the rubber modifier, stability of asphalt concrete mixture modified by using rubber is steadily increased by the decrease of the rubber content percentage. The decreases in stability while increasing rubber content may be attributed to the decreases in the adhesion.

Flow is the ability of an HMA pavement to adjust to gradual settlements and movements in the subgrade without cracking. The flow may be regarded as an opposite property to the stability, determining the reversible behavior of the wearing course under traffic loads and affecting plastic and elastic properties of the asphalt concrete, flow is an important factor in designing hot mix asphalt mixtures it is not desirable to have high flow values because the mix becomes more plastic and this tends to create stability problems, however low flow values may indicate mix with higher than normal voids and insufficient asphalt for durability which cause brittle mixes and therefore cracks can occur on the pavement surface under loads.

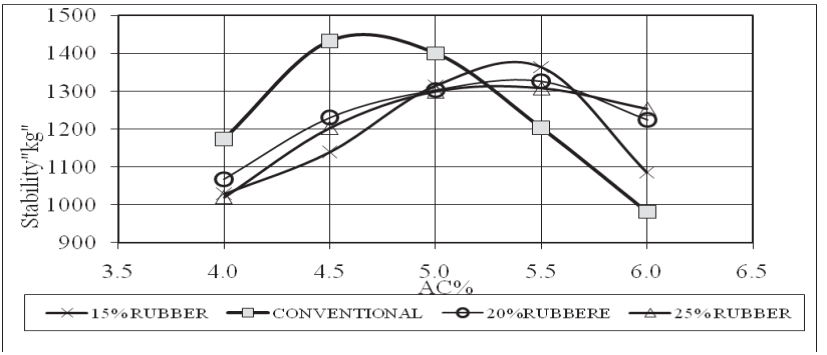

FIG.. 3. Stability of asphalt mixtures.

Effect of Crumb Rubber on Mixture Flow

The tests results show that flow of the modified asphalt concrete mixtures and regardless of the modified percentage is higher than the conventional asphalt concrete mixture. It shows that the flow increases continuously as the proportion of rubber modifier increases. The maximum flow (3.0 mm) was reported for asphalt mixture modified with rubber percentage at a proportion of 15% by weight of bitumen content, this indicates that modified mixtures are less stiff, flow values of unmodified mixtures fall within specification limits, and may imply that increase in the amount of rubber affects the interior friction of the mixture in a negative manner as presented in Fig 4.

Effect of Crumb Rubber on Mixture Density

The max mixture bulk density of the rubber modified asphalt concrete mixtures and regardless of the rubber percentage is lower than the conventional asphalt concrete mixture. Although the difference in bulk density due to rubber percentage is marginal, the general trend shows that the bulk density increases as the AC% increases until it reaches the peak that is associated with the highest bulk density, it started to decline significantly afterwards. Asphalt-rubber mixtures for all percentages are less dense than the conventional asphalt mixtures as the asphalt becomes softer and the asphalt content increases thicker films are produced around the aggregates thereby pushing the aggregate particles further apart and resulting in

lower density as presented in Fig 5.

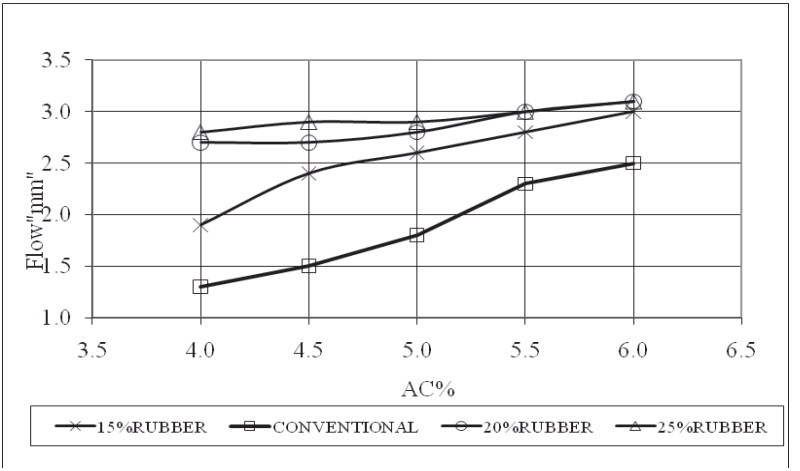

FIG.. 4. Flow of asphalt mixtures.

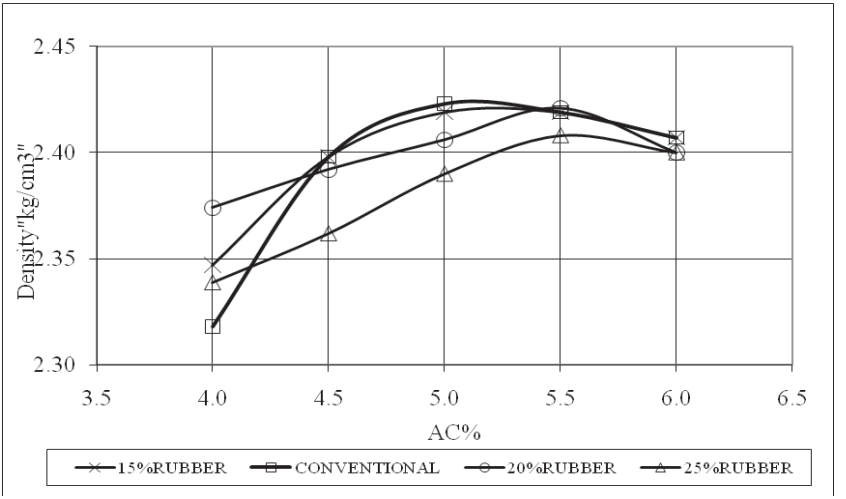

FIG. 5. Density of asphalt mixtures.

Effect of Crumb Rubber on Mixture Air voids

The results show that modified asphalt-rubber mixtures has lower air voids than conventional asphalt mixtures. The decreases in AV% while increasing rubber content may be attributed to the crumb rubber particle size fill the voids. All mixtures modified with rubber content have air voids within the specification as presented in Fig 6.

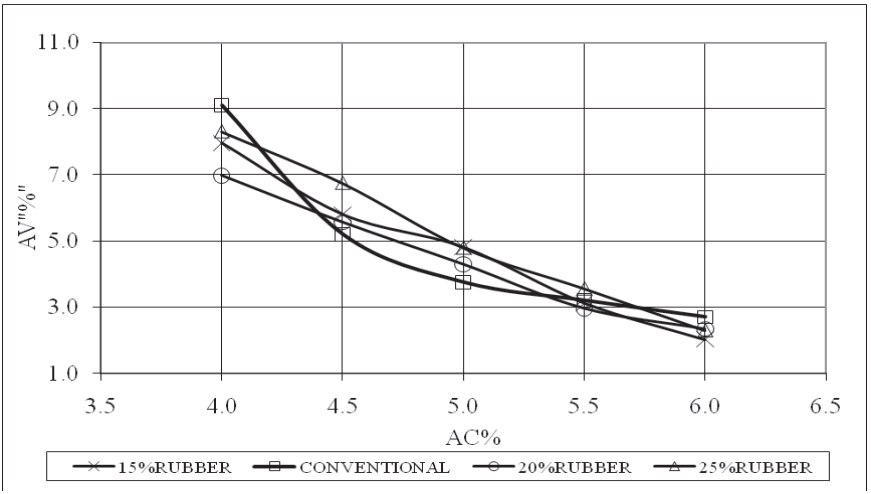

FIG. 6. Air voids in asphalt mixtures

Effect of Crumb Rubber on Void of Mineral Aggregate

The VMA percentage of the modified asphalt concrete mixtures is higher than the conventional asphalt concrete mixture. The VMA content of asphalt mixtures modified with 20% rubber are the lowest among other modified asphalt concrete mixtures. On the other hand, the VMA content of asphalt mixtures modified with 25% rubber are the highest among other modified asphalt concrete mixtures as presented in Fig 7.

Effect of Crumb Rubber on Void Filled with Bitumen (VFB)

The results shows that the asphalt-rubber mixtures have highest VFB% values

than conventional asphalt mixtures because VFB% is depend on the values of VMA % and VA %, all values fall within specification in the case of modified and unmodified asphalt are very close to each other all values fall within specification as presented in Fig 8.

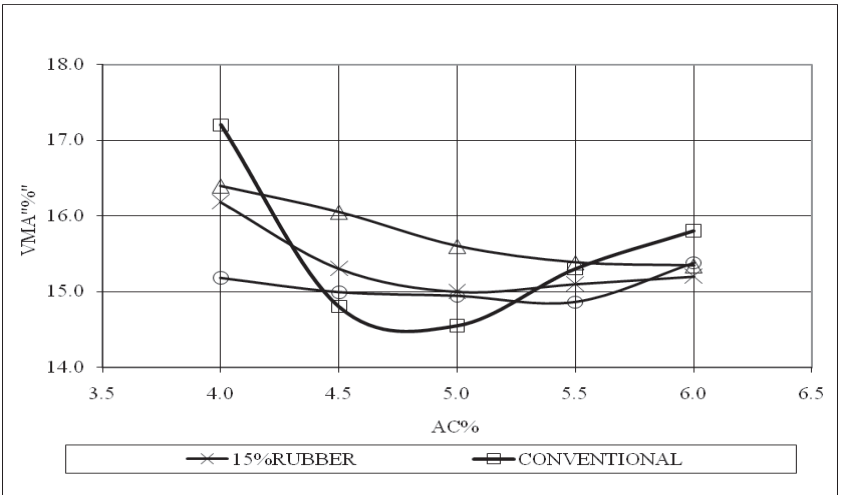

FIG. 7. Void in mineral aggregate of asphalt mixtures

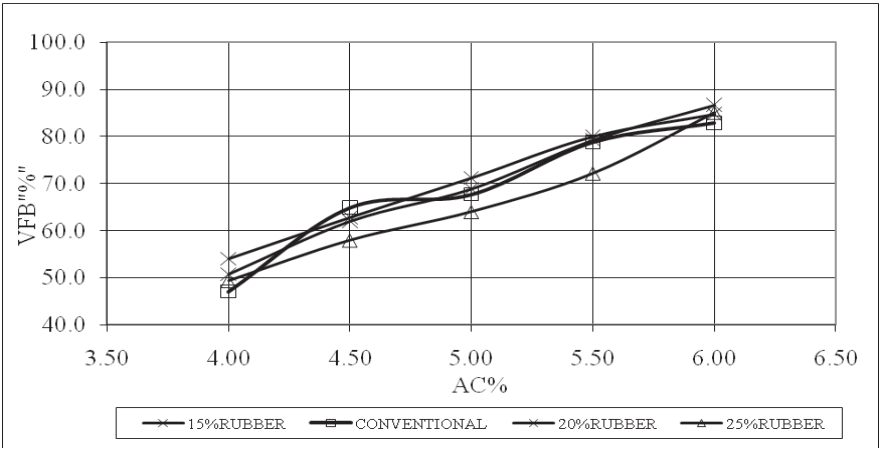

FIG. 8. Voids filled with bitumen of asphalt mixtures

CONCLUSIONS

The laboratory tests results indicated that crumb rubber modifier provides better engineering properties in terms of rheological properties such as penetration, softening point, specific gravity flash and fire point tests except ductility test attributed to some fabric content in tire, and indicated that crumb rubber modifier decrease the stability and density, increase the flow, and slightly increase the air voids and the voids of mineral aggregate. These results indicate the asphalt-rubber concrete pavements would be less susceptible to traffic –indicate deformation distress at high pavement temperatures compared to conventional asphalt pavements. The results are highly dependent on the input variables and testing conditions. The mixture with 20% rubber can represents the best mixture to be used. It could be used to enhance the properties of existing asphalt material. Bitumen modification can offer one solution to overcome some of the deficiencies of bitumen and thereby improve the performance of asphalt mixtures. It is recommended that a plan for laboratory testing, along with field validation to measure the performance of such mixes.

ACKNOWLEDGMENTS

The authors would like to thank ALL the people for their researching support, cooperation and encouragement

REFERNCES

Bahia, HU. and Davies, R. (1995). “Factors controlling the effect of crumb rubber on critical properties of asphalt binders.” *J. Assoc. Asphalt Paving. Technol.*, 64: 130-162.

Blow, C.M. (1971). “Rubber Technology and Manufacture.” *Institution of the Rubber Industry*, UK.

Epps, J. A. (1994). “Uses of recycled rubber tiers in highways.” *NCHRB synthesis of highway practice no. 198, Transportation Research Board*, Washington, DC.

Green, E.L. and Tolonen, W.J. (1977). “The Chemical and Physical Properties of Asphalt-Rubber Mixtures.” *Arizona Department of Transport*, Report ADOT-RS-14 (162).

Hamid, B., Hassan, Z. and Shams, N. (2008). "The Use of Polymer Modification of Bitumen for Durant Hot Asphalt Mixtures." *Journal of Applied Sciences Research*, 4(1): 96-102.

Harvey, J., Bejarano, M. and Popescu, L. (2000). "Accelerated Pavement Testing of Rutting and Cracking Performance of Asphalt –Rubber and Conventional Asphalt Concrete Overlay Strategies." *Conference on Asphalt Rubber*, Vilamoura, Portugal.

Heitzman, M.A. (1992). "State of the Practice for the Design and Construction of Asphalt Paving Materials with Crumb Rubber Additive." *Report No. FHWA-SA-92-022, Office of Engineering, Pavement Division,* Federal Highways Administration.

Hozayen, H.A. and Othman, A.M. (2008). "Improving mechanical prosperities of asphalt concrete mixers using thermoplastic polymer add datives." *Gulf conference of on transportation*, Dubai UAE. P 3-15.

Kaloush, K., Sotil, A. and Way, G. (2003). "Dynamic Modulus Properties of Asphalt Rubber Mixtures." *3rd International Symposium on Maintenance and Rehabilitation of Pavements and Technological Control*, The University of Minho, Guimaraes, Portugal, July 7-10.

Mohammad, L.N., Huang, B., Roberts, F. and Rasoulian, M. (2000). " Accelerated Loading Performance and Laboratory Characterisation of Crumb Rubber Asphalt Pavements." *Conference on Asphalt Rubber*, Vilamoura, Portugal.

Othman, A.M. (2006). "Fracture Resistance of Rubber-modified Asphaltic Mixtures Exposed to High-Temperature Cyclic Aging." Sage publishers, *Journal of Elastomers and Plastics*; 38; 19-32 available at http://jep.sagepub.com.

Saboundjian, S. and Raad, L. (1997). "Performance of Rubberised Asphalt Mixes in Alaska." *Transport Research Record 1583*, TRB, Washington, D.C, pp. 52-6.

Takallou, H.B. and Sainton, A. (1991). "Advances in Technology of Asphalt Paving Materials Containing Used Tire Rubber." *Transportation Research Record* 1339, Transportation Research Board, Washington, D.C.

Test methods on Binder Selection for Antiskid Surface Applications

Y. Xiao[1], M.F.C. van de Ven[2], A.A.A. Molenaar[3] and M.L. Li[4]

[1]PhD student, Section of Road and Railway Engineering, Faculty of Civil Engineering & Geosciences, Delft University of Technology, PO box 5048 2600 GA Delft, The Netherlands; email: Yue.Xiao@tudelft.nl
[2]Assoc. Professor, Section of Road and Railway Engineering, Faculty of Civil Engineering & Geosciences, Delft University of Technology, PO box 5048 2600 GA Delft, The Netherlands; email: M.F.C.vandeVen@tudelft.nl
[3]Professor, Section of Road and Railway Engineering, Faculty of Civil Engineering & Geosciences, Delft University of Technology, PO box 5048 2600 GA Delft, The Netherlands; email: A.A.A.Molenaar@tudelft.nl
[4]PhD student, Section of Road and Railway Engineering, Faculty of Civil Engineering & Geosciences, Delft University of Technology, PO box 5048 2600 GA Delft, The Netherlands; email: Mingliang.Li@tudelft.nl

ABSTRACT: Runway surfaces are optimally designed to meet specific mechanical requirements. These specific requirements mainly include surface friction, resistance to raveling and resistance to chemicals such as de-icing and fuel. Hence, in the Netherlands, Belgium, Germany and other countries, an additional antiskid thin surface layer is often applied to provide enough surface friction and avoid hydroplaning. These antiskid surfaces are specially designed to ensure high friction during a long service life. Until recently, tar-containing material was used as binder. Tar is toxic and not environmental friendly. For this reason it is necessary to develop new binders to replace these tar-containing binders.
This paper gives a brief introduction on the design approach that was developed to evaluate potential binders and to answer the question if they are qualified to be used for antiskid surfaces on runways. The test methods include Dynamic Shear Rheometer tests (DSR) and Dynamic Mechanical Analysis tests (DMA) on original binders, as well as weather aged and oxygen aged binders. Newly designed pull and shear tests were introduced to determine the bonding strength between antiskid layer and substrate layer.

INTRODUCTION

Runway pavement surfaces are prepared and maintained to maximize friction for

tire braking. The surface condition of runways has a significant influence on the braking effectiveness. Any failure at the surface will increase safety problems during takeoff and landing.

The runway surfaces that are currently used are mainly constructed by concrete and/or asphalt. There are many elements that can affect these pavement surfaces, including structure, the materials used, the surface type, de-icing chemicals and fuels, rubber deposits etc. Pavement grooving was the first major step to minimize hydroplaning following heavy rain and provides a rougher surface to achieve safer runway surfaces. The runway surface is usually transversely grooved (typically 6mm deep and 6mm wide spaced at 38 mm) so that the surface water film flows into the grooves while the peaks between grooves will still be in contact with the aircraft tires. Fig. 1 (left) shows a grooved surface on a runway. (Gransberg 2008)

FIG. 1. Grooved runway surface (left) and antiskid runway surface (right).

However, runway friction characteristics of a grooved asphalt mixture or cement concrete will change over time, depending upon the type and frequency of aircraft activities, the weather and environmental issues, together with other factors. Rubber deposits, dust particles, jet fuel, oil spillage, water, snow, ice and slush cause chipping, erosion, wearing away of the sharp grooved edges and resulting in friction loss of the surface. Furthermore, they are not easy to be repaired.

Another possibility is to use a high friction thin surface layer, also named antiskid layer, to provide sufficient friction on runways. The antiskid layer has advantages such as convenient application and easier for reconstruction. In European countries such as the Netherlands, Belgium, Spain and Germany, the POSSEHL antiskid surfacings are widely used on runways for its outstanding adhesion and fuel resistance properties. (Xiao 2012)

However, the POSSEHL antiskid surfacing has a tar-containing binder which makes it toxic and not environmental friendly. Hence, new binders are required to be developed to replace tar-containing binders for antiskid layers on airfield runways.

OBJECTIVES AND MATERIALS

The main objective of this research is to find suitable binders that can be used to replace the tar-containing binders for antiskid layers on runways. In order to achieve this goal, a list of test plans are introduced in this paper.

These test plans are based on one project of antiskid for airfield runways, which is carried on after a successful project on "Assessment Protocol for Tar-containing Antiskid Layers for Runways, Report No. 7-10-185-2. 2010, Delft University of Technology" (Xiao 2010). The surface characteristics, adhesion property and FEM simulation of tar-containing antiskid layers were introduced in Report No. 7-10-185-2. The aim of this research is to verify the conclusions from that project by testing several newly designed binders and antiskid layers, hence decide which one is qualify for antiskid surfacing.

The materials that mentioned in this paper are a tar-containing antiskid layer and an epoxy modified bitumen binder. Cylindrical samples with tar-antiskid layer on the surface were obtained from Dutch airfields. The epoxy modified bitumen binder is a two components thermosetting material, supplied by a Dutch company.

DESIGN APPROACH

Fig. 2 shows test program of the design approach. It includes tests on potential binders and on antiskid layers made from these.

Potential binders for antiskid surface applications need to have a good resistance to weather, UV light, oxygen and chemicals. Resistance to higher temperature and enough flexibility at lower temperature are also required. Furthermore, sufficient bonding strength at the interface is needed to transfer tire induced horizontal stresses into the asphalt layer and to prevent delamination due to low temperatures.

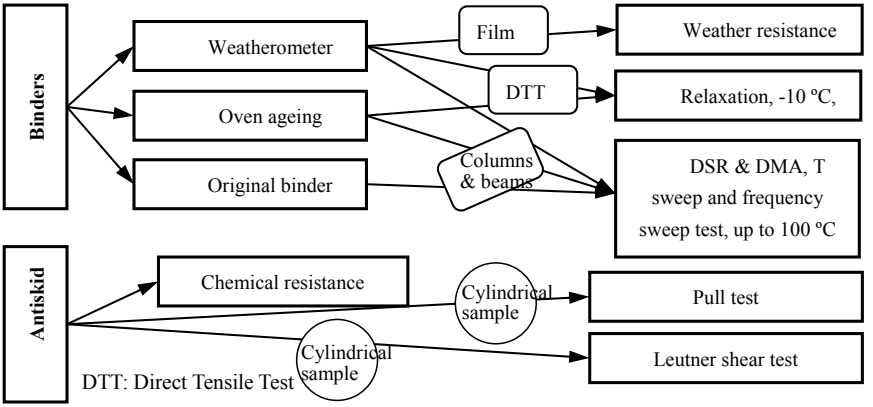

FIG. 2. Test program on binder selection for antiskid surface applications.

MACROTEXTURE AND FRICTION

Surface friction depends on the microtexture and macrotexture of the runway surface. The macrotexture has a wavelength from 0.5 mm up to 50 mm, while the microtexture has wavelengths below 0.5 mm.

The microtexture is associated with the surface of the aggregate and is controlled by the individual aggregate surface properties, such as shape and roughness. Microtexture has a large influence at speeds below 50 km/h, although it contributes to skid resistance at all speeds. On runways, macrotexture of runway surface has the major influence on surface friction.

Macrotexture refers to larger-scale irregularities of the pavement surface that are affected by aggregate orientation. It contributes to the speed-dependent part of friction and to wet surface friction. The primary function of the macrotexture is to help maintain adequate skid resistance to aircraft travelling at high speeds. It also provides paths for water to escape which helps to prevent aquaplaning. (Toan 2005; Nicholas 2009)

In the Netherlands, it is recommended to specify a texture depth ≥ 1.3 mm for new runway surface dressings at any location (CROW 2011). The sand patch test method (or laser measurement, such as CT (Computerized Tomography imaging) scan and Microscope) can be used to determine the macrotexture, while Continuous Friction Measuring Equipment can be employed to understand the surface friction both at dry and wet conditions.

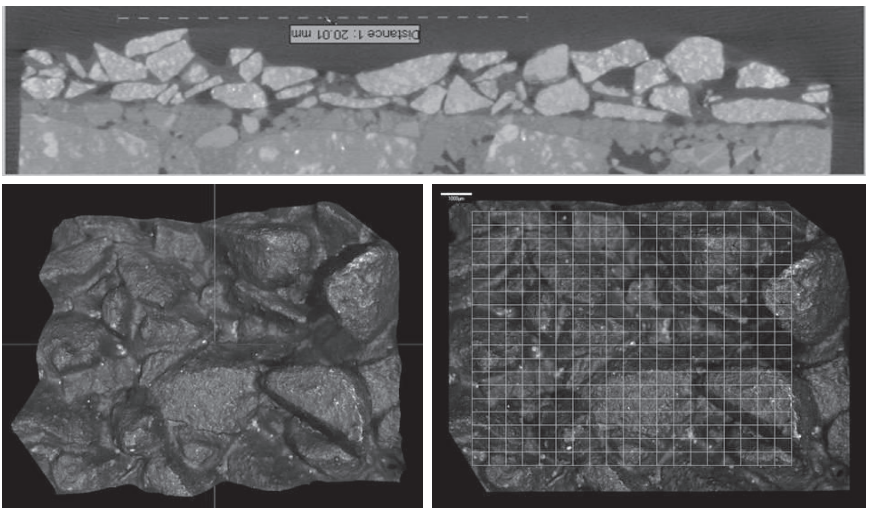

FIG. 3. CT scan and microscope on antiskid surface.

Fig. 3 shows results of CT scan and Microscope of tar-containing antiskid layer.

The surface characteristics and mean profile depth of the surface can be investigate from this results. Furthermore, the scan images can distinguish the individual stones, voids and mortar, which will be used for FEM (Finite Element Modeling) simulation.

FEM simulation can be used to study the stress and strain distributions under the wheel of airplane can be studied with in macro level (Xiao 2012). By changing the properties of the binder in the model, the FEM simulations will show the consequences. In this way, the stiffness, strength and fatigue properties of the binder can be predicated in the chose skeleton structure.

DURABILITY

The runway surface should have a long service life, which requires good resistance to weather, UV light, oxygen, and chemicals from outside.

Resistance to weathering

An antiskid surface is exposed to all kinds of outside activities. Climate induced impacts, including water flow, humidity, temperature changes, de-icing etc., have a significant influence on its performance. Hence, binders that used for antiskid surface applications should have a very good resistance to weathering.

The available laboratory equipment at Delft University of Technology to perform accelerated weathering tests is the SUNTETST XXL+ weatherometer from Atlas Materials. The testing instrument can simulate environmental parameters like sunlight, temperature, moisture and humidity. An artificial light source (Xenon arc lights) is used that closely simulates the UV and visible part of the solar radiation. This equipment is recommended to accelerate the aging of materials exposed to natural weather conditions during service. (Hagos 2008)

Thin films of binder with thickness between 1mm to 2mm can be placed in the weatherometer for a certain period of time under defined exposure conditions. After ageing, elasticity and relaxation properties can be determined.

Resistance to Ageing

The physical properties of the binder in antiskid layer change with service time. Generally, when an asphalt binder is used for a road pavement and it ages, its viscosity increases and therefore it becomes more stiff and brittle. On the pavement surface, the binder is closer to ageing factors as oxygen and UV light, causing it to age faster. So it is clear that the binder used for an antiskid surface should have extremely good ageing resistance. The service life of antiskid is in general much shorter than its structural design life. Previous research indicated that at low traffic condition, the 20 years old tar-containing antiskid surface remained its high texture value, which means that it can survive as long as more than 20 years (Xiao 2010).

Ageing resistance of binders is evaluated by fast ageing with standardized

equipment such as FTOR, RCAT etc. And then the changed properties are evaluated. Tests like DSR and DMA can be used to characterize the visco-elastic properties after ageing simulations.

Two-component epoxy modified bitumen was place in an oven for 7 days ageing at 85 °C. Relaxation properties were investigated by DTT test (Xiao 2011a). Maximum applied force is 40% of the maximum failure force that gained from DTT. Fig. 4 shows the difference of relaxation curve between original binder and aged binder. It clearly indicates that after ageing, the epoxy modified binder became harder and its relaxation property decreased from 74.3% to 38.3%. Relaxation property can be used to determine two crack resistance at lower temperature.

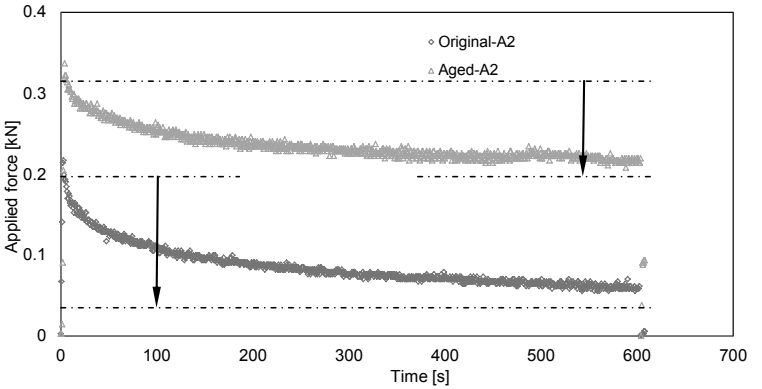

FIG. 4. Relaxation curves compared between original and aged binder

Chemical Resistance

Runways in airfields can be exposed to very intense jet fuel or oil spillage. Furthermore, de-icing chemicals are used quite often in winter time. This asks for outstanding chemical resistance of binders used for antiskid surface.

Resistance to de-icing fluids can be evaluated according to EN 12697-41. Specimens are stored in and not in de-icing fluid separately. A steel plate is bonded to the test surface of each specimen. During testing, the plate is pulled off with a tensile force with certain loading speed. The tensile force at failure load and the mode of failure are recorded. The results are compared with those for specimens which have not been stored in de-icing fluid. (CEN 2005a)

Fuel resistance can be tested with steel brush test standardized by EN 12697-43. A cylindrical test specimen with a known mass is immersed partly in a bath with the specified fuel for 72 hours. After removal from the bath, cleaning with water and drying for 24 h in a ventilated oven at 25 °C, the loss of mass of the specimen is measured and the immersed surface is visually inspected. The type of affection and the material loss of the immersed surface are also recorded. Then the test specimen is

put in a steel mould with the immersed surface up. At the bottom of the specimen a pneumatic cylinder pushes the immersed surface onto a steel brush, which is moving in epicycloids passages over the surface. After 30 s the brushing stops and the specimen is removed from the mould. Then the loss of mass is measured and the brushed surface is visually inspected. After that the specimen is put back in the mould and the same procedure is carried out again after 30 s and after 60 s, when the brushed surface is visually inspected again. The total brushing time is 120 s (two brushing periods of 30 s and one of 60 s). The material loss after the immersion and/or the brush test is a measure for the resistance to that fuel. (CEN 2005b)

Resistance to High Temperature

Taking off of aircrafts may cause for a short time very high temperature up to 100 ºC on the surface. As a consequence, the binders used for antiskid surface should have very good high temperature resistance. The DSR or DMA test can be employed to determine the high temperature properties. Modulus and phase angle of testing binders can give indications on high temperature resistance.

ELASTICITY AND RELAXATION

It is not possible to give a certain value for the stiffness or any other rheological parameters as requirement for potential antiskid binders. This is because the performance of antiskid is not just depending on binder properties; also the skeleton structure of the antiskid plays an important role. Results from previous antiskid projects indicate that the aggregate skeleton has a huge influence on the final antiskid performance. FEM is needed to combine the influence of rheological properties of binder and the structural characteristics of antiskid. (Xiao 2012)

Rheological properties can be evaluated by means of the DSR or DMA. Binder columns (approximately 6 mm diameter and 12 mm height) can be used for DSR testing as shown in Fig. 5 (1), while small beams can be used for DMA as shown in Fig. 5(2). (Mo 2011; Huurman 2010).

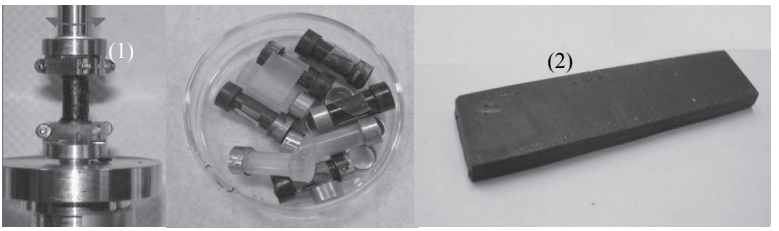

FIG. 5. DSR test on columns and DMA test on beams

With frequency/temperature sweeps in the linear viscoelastic range, the phase

angle and complex shear modulus of the binders can be determined. The test temperature range should at least go up to 100 °C for studying the high temperature resistance of binders.

In Fig. 6 and Fig. 7 results of modulus and phase angle of an epoxy modified bituminous binder with both the DMA and DSR tests are given. Temperature sweep tests from 10 to above 200 ºC were performed with the DMA at three frequencies. Frequency sweep tests at 60 °C, 70°C, 80 °C and 100 °C were carried out with DSR. The test results indicate that the DMA test and DSR test give similar information on temperature dependence about the stiffness modulus and phase angle for the same binder.

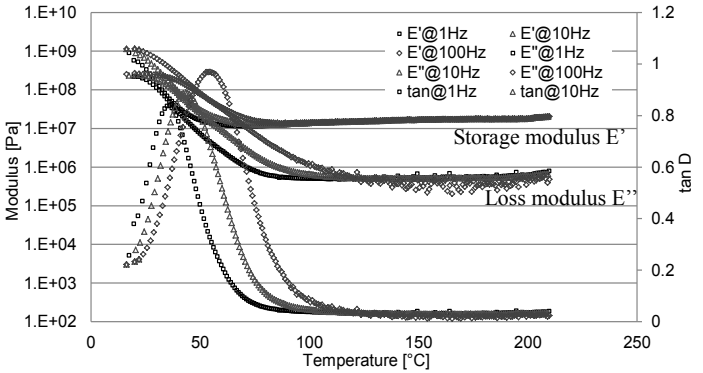

FIG. 6. DMA temperature sweep results for epoxy modified bitumen binder

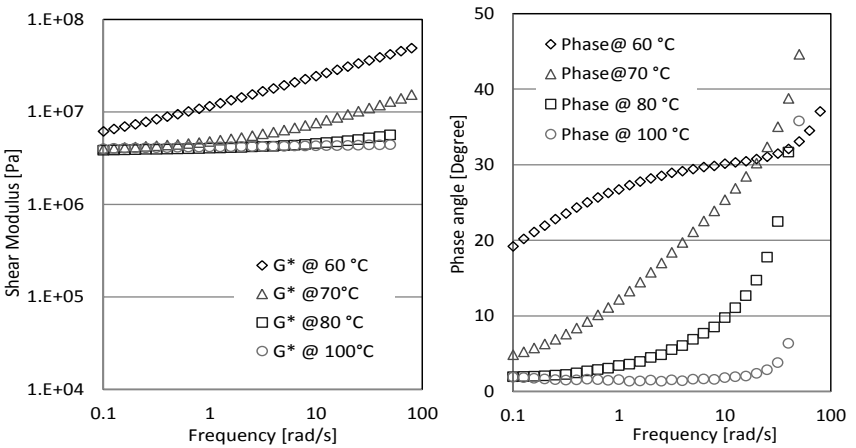

FIG. 7. DSR frequency sweep results for epoxy modified bitumen binder

The results show that at high temperatures (above 100 ºC), the epoxy modified bituminous binder behaves as a purely elastic material with a modulus close to 10 MPa while the phase angle is below 10 degree. The test results from the DSR test (see Fig. 7) confirm these values.

In order to reduce thermal cracking a relatively lower stiffness and a good relaxation behavior are required at low service temperatures. For this reason, a relaxation test at -10 ºC is added to the binder selection process.

BONDING OF THE UNDERLYING LAYER

A wide range of test methods, such as Pull tests and Shear tests, have been introduced to evaluate the bonding properties of surface layers in the field. However, the measured tensile strength by these tests gives only the adhesion property at the time of testing and cannot be used to predict the adhesion strength at other temperatures and environmental conditions. There is no temperature control when these tests are done at the runway. Although temperature control may be accomplished in the field using heat lamp, tests in the field are neither force nor displacement controlled. Stress versus strain curves cannot be obtained for further analysis. Therefore two new test methods were developed to determine the bonding strength between antiskid surface layer and substrate layer on cores for the runways.

Resistance to tensile forces

The direct tensile bonding strength was analyzed with a newly designed pull test. Cylindrical cuts with 50 mm diameter were cored on the samples to a depth of 10 mm to make sure that the drill passed the antiskid surface layer. A steel plate was then glued to the dry and clean surface with an X60 glue. After the glue was at full strength, the antiskid layer was pulled off and the tensile force was measured. Fig. 8 shows the sample preparation and setup for the pull test. (Xiao 2011b)

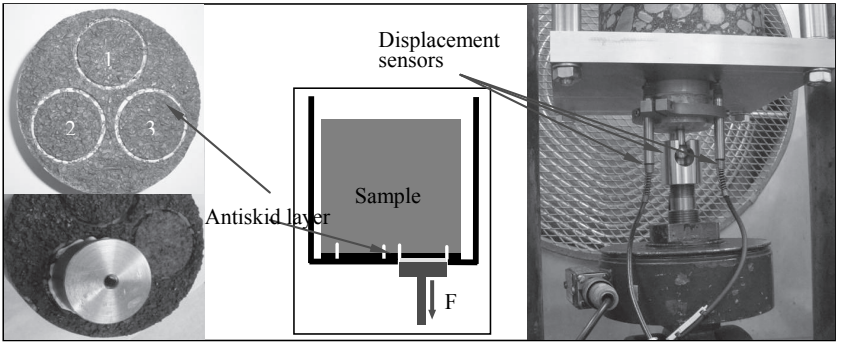

FIG. 8. Sample preparation and test setup for pull test

Any loading speed and test temperature can be applied in this pull test to study their influence on the results. The left graph in Fig. 9 shows the results of several pull tests on a tar-containing antiskid at speed of 0.025 N/mm2s. It illustrates that the tensile bonding strength increases with decreasing test temperature.

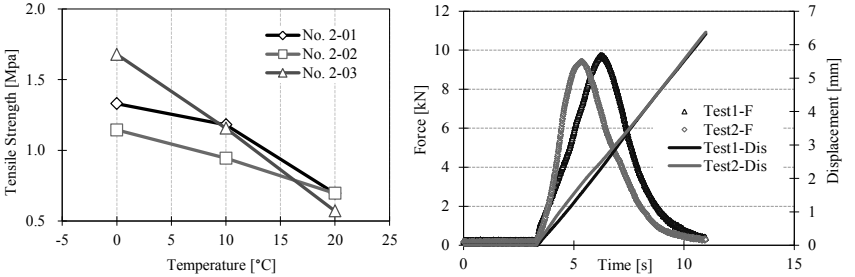

FIG. 9. Typical pull test results (left) and shear test results (right)

RESISTANCE TO HORIZONTAL FORCES

The Leutner shear test was employed in this research. The difference with the traditional Leutner shear test is the sample preparation process. The antiskid layer is too thin to test the shear strength in the interface by directly using the shear test setup as normally is done when testing a tack coat between two asphalt layers. Therefore, a strong glue and a steel cylinder are used to modify this test method.

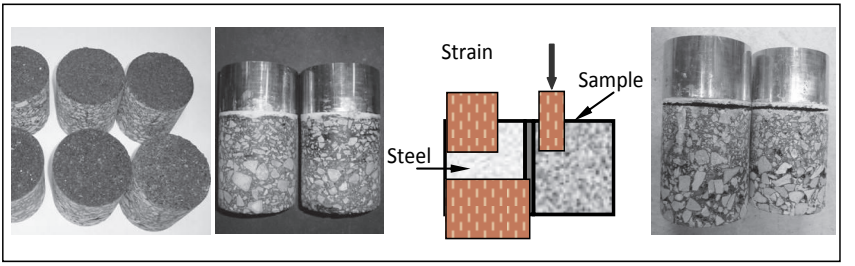

FIG. 10. Sample preparation and test setup for Leutner shear test

Fig. 10 shows the preparation process for shear test samples. First, the antiskid layer surface needs to be carefully cleaned and dried. Then a steel cylinder with 100 mm diameter and 40 mm thickness is glued onto the antiskid surface with X60 glue. In order to avoid the possible influence caused by penetration of the glue into the interface, the steel plate has to be placed at the bottom while the cylindrical sample is placed upside down on the steel plate. After the glue has reached its full strength, samples are placed into a temperature control cabinet for the shear test. (Xiao 2011b)

The test sample is loaded till failure with a constant displacement speed of 50 mm/min applied across the interface at 20 ºC of test temperature. The resulting shear force is measured. The effect of different displacement speeds and test temperatures can be evaluated with this test method. The right hand graph in Fig. 9 shows two typical shear test results for samples from same airfield and under same test conditions.

CONCLUSIONS

In this paper a brief introduction is given on the test methods proposed for binder selection for antiskid surface applications for runways in airfields. Based on this design approach, the followings can be concluded:

1. The surface macro texture of an antiskid layer on a runway is essentially important to ensure sufficient friction for aircrafts. The sand patch test (or laser measurement) and Continuous Friction Measuring Equipment can be used to test respectively macrotexture and surface friction.
2. Binders used for antiskid surfaces should have an excellent resistance to weather, ageing, chemicals and high temperatures. The weatherometer can be used to simulate the influence of environmental parameters, while oven aging can be used for oxygen ageing of thermosetting binders and traditional ageing method can be involved for bitumen based binders.
3. The elasticity properties of the binder are needed for further analysis such as FEM to simulate the binder performance by combining rheological properties of binder and structure characteristics of antiskid together in a realistic model.
4. High bonding strength between antiskid layer and substrate layer is required to carry tire induced stresses. The newly designed pull test and shear test are proposed to determine the tensile bonding strength and horizontal shear strength of the system.

REFERENCE

CEN, (2005a). EN 12697-41 Bituminous mixtures - Test methods for hot mix asphalt - Part 41: Resistance to de-icing fluids.

CEN, (2005b). EN 12697-43 Bituminous mixtures - Test methods for hot mix asphalt - Part 43: Resistance to fuel.

CROW, (2011). CROW (Center for Regulatory and Research in the Land Water and Road and Traffic Engineering)-Report D11-01 Specification for Runway Surface Dressings on Airfields.

Gransberg, D.D. (2008). “ACRP Synthesis11-Impact of Airport Rubber Removal Techniques on Runways.” *Transportation Research Board, Washington*, D.C. University of Oklahoma.

Hagos, E.T. (2008), "The Effect of Aging on Binder Properties of Porous Asphalt Concrete." PhD dissertation, in Section of Road and Railway Engineering. Delft University of Technology.

Huurman, R.M., Mo L.T., and Woldekidan M.F. (2010). "Unravelling porous asphalt concrete towards a mechanistic material design tool." *Road Materials and Pavement Design*, 11(3), 583-612.

Kim, K.G., Kim, J.H., Ryu, J.H. et al. (2007). "Nano X-ray Computed Tomography System." *World Congress on Medical Physics and Biomedical Engineering 2006*, R. Magjarevic and J.H. Nagel, Editors., Springer Berlin Heidelberg. p. 1417-1420.

Mo, L.T., Huurman, R.M., Wu, S.P., et al. (2011). "Research of Bituminous Mortar Fatigue Test Method Based on Dynamic Shear Rheometer." *Journal of Testing and Evaluation*, 40(1):73-84.

Nicholas, R.F. (2009), "Comparison of Macrotexture Measurement Methods." M.S. thesis, The Ohio State University.

Toan, D.V. (2005), "Runway friction performance in NZ." *International Conference on Surface Friction for Road and Runways*, Christchurch, New Zeland.

Xiao, Y., Molenaar A.A.A., van de Ven M.F.C., et al. (2011b), "Adhesion Properties of Tar-Containing Antiskid Surface Layers on Runways in Airfield." *Proceedings of the T&DI Congress 2011: Integrated Transportation and Development for a Better Tomorrow*, USA, ASCE.

Xiao, Y., van de Ven M.F.C., Molenaar A.A.A., et al. (2010). "Assessment Protocol for Tar-containing Antiskid Layers for Runways." 7-10-185-2, Delft University of Technology.

Xiao, Y., van de Ven M.F.C., Molenaar A.A.A., et al. (2012). "Stress and Strain Analysis in Tar-containing Antiskid Runways Using Finite Element Models." *Construction and Building Materials*, 27(1), 24-31.

Xiao, Y., van de Ven M.F.C., Molenaar A.A.A., et al. (2011a). "Characteristics of two-component epoxy modified bitumen." *Materials and Structures*, 44(3), 611-622.

Aging Behavior Characterization of SBS-modified Asphalt for Recycling Purpose

Tao Ma[1] and Hao Yuan[2]

[1]Lecture, School of Transportation, Southeast University, Nanjing 210096, PR China; email: mataoseu@163.com
[2]Engineerer, Engineer Division, Jiangsu Shanshui Co Ltd, Jurong 212400, PR China; email: yhaohao@163.com

ABSTRACT: To evaluate the recycling potentials of the aged styrene-butadiene-styrene (SBS)-modified asphalt binder, effects of the short-term and long-term oxidative aging on the physical properties, rheological properties and microstructure characteristics of the aged SBS-modified binder were investigated. Results showed that the aging of SBS-modified binder consists of two parts: i) the oxidative aging of the asphalt components and ii) the degradation of the SBS modifier. The aging inevitably leads to a hardening and brittle binder. By characterizing the aging behaviors of SBS-modified binder, the recycling of aged SBS-modified binder was conducted by adding a recycling agent and a modifying additive. The recycling agent is normally used in unmodified binder for rejuvenation. The modifying additive can benefit the asphalt mixture performance. Results indicated that the commonly used recycling agent may not enhance the performance of the recycled polymer modified asphalt when it is used alone. The rejuvenation of aged polymer modified asphalt requires new additive with well-balanced modification effect. It is found that the recycling agent together with a modifying additive MA^{TM} are proved to be capable of restoring the durability of SBS-modified binder and eventually satisfying the desired road performance. Therefore, compound rejuvenation method of polymer modified asphalt was recommended.

INTRODUCTION

Styrene-butadiene-styrene (SBS) triblock copolymer is one of the most widely used polymer modifiers for asphalt (Wen, 2001). Numerous researches to date concern the road performances of SBS-modified binder. Some reseraches focused on the stability improvement of the SBS-modified binder to ensure a good compatibility between SBS and asphalt (Sun, 2006; Wang, 2006). Other researches studied the rheological properties of storage-stable SBS-modified binder systematically and illustrated the influences of some important factors such as base asphalt property, structures and contents of SBS on the rheological behaviors of the modified binders (Wen, 2002; Wen 2002; Chen, 2007). Because aging is an inevitable process of asphalt binder during field use, some reasearches investigated the dynamic viscosity

change, rheological property change and morphological changes of the SBS-modified binder due to aging and suggested measures to improve the anti-aging performance of the SBS-modified binder (Zhang, 2010; Cortizo, 2004; Ruan, 2003).

Currently, many of the asphalt pavements using polymer modified binder reaches the end of their service life and need resurfacing. This will produce a lot of abandoned asphalt mixture materials with aged polymer modified asphalt. Those abandoned asphalt mixtures are huge pollution to the environment because the aged polymer modified binder is non-degradable. It not only pollutes the soil and underground water but also is hazardous to the whole enviroment and people. Therefore, recycling of pavements with polymer modified binder has become more and more important. Unfortunately, few studies have been conducted on the characterizations of aged polymer modified binder for recycling purposes.

The objectives of present work are: i) to analyze the evolution the microstructural degradation of SBS-modified binder due to short-term and long-term aging, and ii) to investigate the recycling potentials of the aged SBS-modified binder via recycling agent and new polymer additives.

EXPERIMENTAL PROGRAM

Materials

AH-90, that is a binder with penetration of 89 (0.1mm), was chosen as the base binder in this study. The modifier used in this study is SBS4303. It is a star-like polymer and contains 40 % (by weight) styrene. The average molecular weight of the SBS4303 is 350,000 g/mol. Two types of rejuvenator were employed for the aged SBS-modified binder: i) a recycling agent which is commonly used in the recycling of the aged unmodified binder and ii) a new-type modifying additive named MATM which is capable of modifying the asphalt mixtures during the producing process of the asphalt mixture.

The SBS-modified binder was prepared using the AH-90 binder and the SBS4303 modifier. The aged SBS-modified binder was prepared by carrying out laboratory short-term and long-term aging tests: rolling thin film oven test (RTFOT, standard ASTM D2872) and pressure aging vessel test (PAV, standard ASTM D6521). The recycling binder was obtained by using the recycling agent to rejuvenate the previous lab-aged SBS-modified binder. Then the modified recycling binder was obtained by adding the RATM additive to the recycling binder.

Testing Methods

Property Tests

The physical properties of binder, including penetration , softening point, ductility, and viscosity, were measured in accordance with ASTM D5, D36, D113 and D4402.

The rheological properties of binder were measured by using Dynamic Shear Rheometer (DSR) test and Bending Beam Rheometer (BBR) test in accordance with ASTM D7175 and D6648, respectively. The high-temperature viscoelastic parameters including complex modulus (G*), phase angle (δ) and rutting factor (G*/sinδ) were

measured by DSR test. The low-temperature creep parameters including creep stiffness (S) and creep rate (m) were measured by BBR test.

Micromechanism Analysis

Thin-Layer Chromatography with Flame Ionization Detection (TL-CFID) was used to conduct composition analysis for binder. During the TL-CFID test, binder were separated into four components including saturates, aromatics, resins and asphaltenes.

Fourier transform infrared (FTIR) spectrometer test was conducted to determine the functional characteristics of binder in wavenumbers range from 4000 to 400 cm^{-1}.

RESULTS AND DISCUSSIONS

Aging Behavior of SBS-modified Asphalt Binder

Physical Properties

Both chemical compositions and physical properties of the base binder (AH-90) were measured. As shown in Table 1, the four generic fractions were determined by using TLC-FID test. Then, the variations of different fractions due to aging were calculated through dividing the measured value of the aged binder by that of the unaged binder. The unaged and aged physical properties of the base binders were shown in Table 2. And, the variations of different physical properties due to aging were also calculated.

Table 1. Chemical Compositions of Base Binder (AH-90) Before and After Aging

Fractions	Unaged	RTFOT Aging		PAV Aging	
	Value	Value	Variation (RTFOT/Unaged)	Value	Variation (PAV/Unaged)
Saturates (%)	23.1	21.5	0.93	19.7	0.85
Aromatics (%)	45.9	41.9	0.91	36.1	0.79
Resins (%)	23.2	24.1	1.04	25.7	1.11
Asphaltenes (%)	7.8	12.5	1.60	18.5	2.37

Table 1 indicates that both short-term and long-term aging can increase the contents of asphaltenes and resins in asphalt. Especially, the content of asphaltenes increseas significantly. On the other side, the contents of saturates and aromatics decrease due to aging. Asphaltenes and resins are known as the hard components in asphalt. Especially, the asphaltenes is primarily responsible for the hardness of asphalt. Saturates and aromatics are known as the light components in asphalt. Therefore, it is believed that a componential transition occurred from the light components to the hard components in asphalt due to aging, resulting in a stiffer binder. The variation values in Table 1 indicate the change of chemical components due to aging. It is found that the variation becomes more significant for long-term aging than that in short-term aging. It means that the amount of the compenential

transistion increase as aging period increases.

Table 2. Physical Properties of Base Binder (AH-90) Before and After Aging

Parameters	Unaged	RTFOT Aging		PAV Aging	
	Value	Value	Variation (RTFOT/Unaged)	Value	Variation (PAV/Unaged)
Penetration (25°C, 0.1mm)	89	65	0.73	28	0.31
Softening point (°C)	44.9	50.1	1.12	59	1.31
Viscosity (135°C, Pa.s)	0.325	0.365	1.12	0.85	2.62
Ductility (5 °C, cm)	3.3	0	0	0	0

As shown in Table 2, the expected increase in softening point and viscosity are observed after aging. And the expected decrease in penetration and ductility are observed after aging. It is found that the variation becomes more significant for long-term aging than that in short-term aging. Take the viscosity for example, the viscosity of the unaged AH-90 was 0.325. It increased by 1.12 times after short-term aging and 2.62 times after long-term aging. This trend becomes very apparent with the increasing of the hard asphalt components. It indicates that the variation in the physical properties of the base binder after aging depends on the changes of the hard asphalt components.

As shown in Table 3, the physical properties of the SBS-modified binder before and after aging were also measured. And the variations of the physcial parameters due to aging were calculated. Compared with the physical properties of unaged base binder in Table 2, the softening point, viscosity and ductility increase while the penetration decreases with the appearance of SBS in binder. It is attributed to the crosslinked SBS network structure in the modified binder (Sengoz, 2008). Therefore, by adding SBS to asphalt, both the high- and low-temperature performances of binder are improved significantly.

In Table 3, similar changes of the physical parameters in the base binder were found for the SBS-modified binder. It clearly shows that the softening point and viscosity increase while the penetration declines with an increasing aging period. It indicates that aging improves the high-temperature performance of SBS-modified binder. Furthermore, by comparing the 5°C ductility data in Tables 2 and 3, it is noticed that the unaged base binder has a very poor deformability while the unaged SBS-modified binder has an excellent deformability at low temperature. However, the advantage of SBS-modified binder disappears with aggravated aging. Since the low-temperature ductility of binder is sensitive to the crosslinked network structure provided by SBS modifier, it is believed that aging may destroy the crosslinked SBS network structure and leads to a severe degradation of low-temperature deformablity. However, variations of all the parameters for SBS-modified binder due to aging, as shown in Table 3, are apparently relatively smaller than that of the base binder as shown in Table 2. It verifies that the SBS modifier can improve the anti-aging performance of binder.

Table 3. Physical Properties of SBS-modified Binder Before and After Aging

Parameters	Unaged	RTFOT Aging		PAV Aging	
	Value	Value	Variation (RTFOT/Unaged)	Value	Variation (PAV/Unaged)
Penetration (25 °C, 0.1mm)	69	57	0.83	42	0.61
Softening point (°C)	61	66	1.08	74	1.21
Viscosity (135°C, Pa.s)	1.225	1.362	1.11	1.64	1.34
Ductility (5 °C, cm)	37	25	0.68	2.6	0.07

Rheological Properties

The influences of short-term and long-term aging on the rheologcial behavior of the base binder and SBS-modified binder are shown in Table 4 and 5 respectively. In the DSR test, G* and δ are fundamental rheological parameters depicting the elastic and viscous behaviors of binder at high temperature condition like 64°C. It is considered that binder with high G* and low δ has high elasticity and low viscousity. The G*/sinδ, as a comprehensive rheological parameter, is often used to describe the contribution of the binder to permanent deformation. A high value of G*/sinδ indicates a good high-temperature performance of the binder. In the BBR test, the S and m can reveal the flexibility of binder at low temperature like -18°C. A low S as well as a high m represent good flexibility at low temperature. Tables 4 and 5 show the rheological properties of unaged base binder and SBS-modified binder, respectively. It is found that the SBS-modified binder apparently has higher G*, G*/sinδ and lower δ. It demonstrates that the SBS-modified binder has a better permanent deformation resistance than the base binder at high temperature. Meanwhile, SBS-modified binder has a lower S as well as a higher m. It indicates that it has better flexibility than the base binder at low temperature. It is proved again that the crosslinked SBS network structure can improve the high- and low-temperature performance of modified binder very well.

As shown ins Table 4 and 5, it is found that higher G*, G*/sinδ and S as well as lower m occur after aging for binder. It shows that aging results in a harder and more brittle binder with improved high-temperature performance but degraded low-temperature performance. PAV produces more birttle binder than the RTFOT due to a prolonged aging process in the PAV test. It is also clearly indicated that variations of the rheological parameters for the SBS-modified binder are apparently smaller than that of the base binder. It proves that the SBS modifier can act as an antioxidant in the modified binder.

It should be noted that the changing trends of δ due to aging for the base and the SBS-modified binder are different. The δ of base binder increases obviously with aggravated aging. However, a decrease trend of δ with aggravated aging is observed

for the SBS-modified binder. Measurements of δ are generally considered to be more sensitive to the chemical structure than complex modulus (Larsen, 2009). Thus, the most possible reason for the irregular changing trend of δ for SBS-modified binder is that the degradation of SBS polymer leads to the increase of the viscous behavior of binder.

Table 4. Rheological Properties of Base Binder Before and After Aging

Parameters	Unaged	RTFOT Aging		PAV Aging	
	Value	Value	Variation (RTFOT/Unaged)	Value	Variation (PAV/Unaged)
G* (64°C, kPa)	0.63	1.39	2.21	4.93	7.83
δ (64°C, Deg)	89.1	88.3	0.99	85.6	0.96
G*/sinδ (64°C, kPa)	0.63	1.39	2.21	4.94	7.84
S (-18°C, MPa)	314	378	1.20	470	1.50
m (-18°C)	0.309	0.278	0.90	0.246	0.80

Table 5. Rheological Properties of SBS-modified Binder Before and After Aging

Parameters	Unaged	RTFOT Aging		PAV Aging	
	Value	Value	Variation (RTFOT/Unaged)	Value	Variation (PAV/Unaged)
*G** (64°C, kPa)	2.42	4.27	1.76	9.43	3.90
δ (64°C,Deg)	69.2	69.3	1.00	70.3	1.02
G/sinδ* (64°C, kPa)	2.58	4.56	1.77	10.02	3.88
S (-18°C, MPa)	236	260	1.10	308	1.31
m (-18°C)	0.332	0.32	0.96	0.298	0.90

Microstructure Analysis

The FTIR spectrum of base binder is given in Fig. 1(a). The strong peaks within 2850-2960 cm^{-1} region are typical C-H stretching vibrations in aliphatic chains. The peak around 1603 cm-1 is attributed to C=C stretching vibrations in aromatics. The C-H asymmetric deforming in CH2 and CH3, and the C-H symmetric deforming in CH3 vibrations are observed around 1458 cm-1 and 1375 cm^{-1} respectively. The peak at 1030 cm^{-1} is ascribed to S=O stretching vibrations. The small peaks within 740-910 cm^{-1} region are typical C-H vibrations of benzene ring. The FTIR spectrum of SBS modifier, shown in Fig. 1(b), exhibits a similar set of hydrocarbon bands to the base binder, except one unique new peak around 966 cm^{-1} corresponding to the bending vibration of C-H in the butadiene double bonds -CH=CH-. Fig. 1(c) shows the FTIR spectrum of SBS-modified binder. Compared with the FTIR spectrum of base binder, the significant difference in the spectrum of SBS-modified binder is the new peak appeared around 966 cm^{-1}. It can be used to identify the existence of SBS in the

binder.

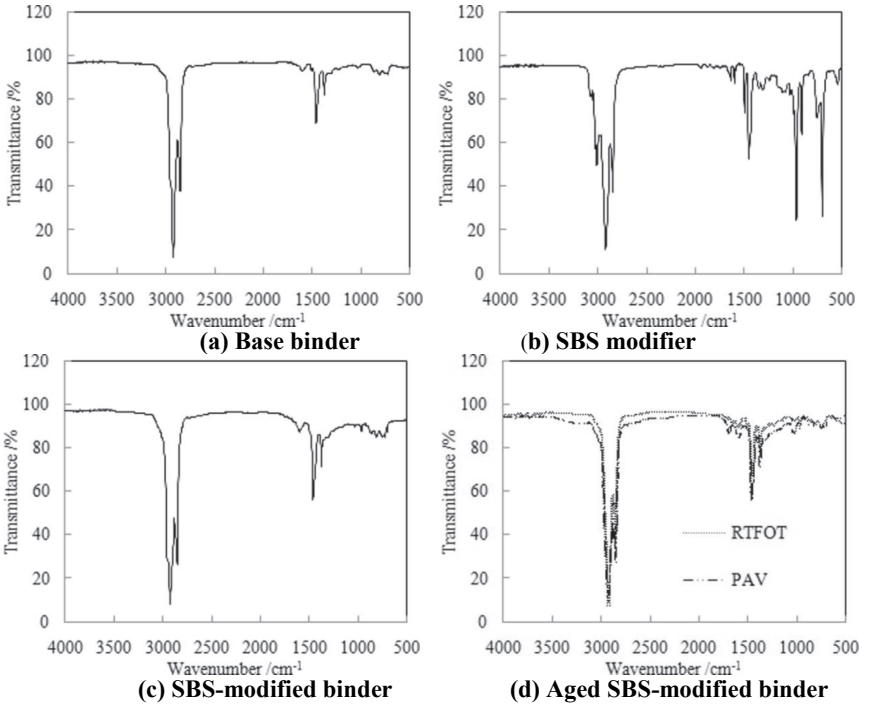

FIG. 1. FTIR spectra of different binders and SBS modifier.

The FTIR spectra of aged SBS-modified binder by RTFOT and PAV are shown in Fig. 1(d). The aging can be evaluated by studying the changes in the spectra. Specifically, two characteristic bands are monitored: i) the carbonyl functions C=O centered around 1700 cm^{-1} and ii) the butadiene double bonds CH=CH centered around 966 cm^{-1}). The C=O can provide the evidence of the oxidation of the base asphalt in the modified binder. The CH=CH can provide the monitoring of the deterioration of the SBS modifier as a result of the diminution of the double bond. The evaluation is performed by considering the area of the functional bands or by calculating structural indices based on the following Equations 1 and 2 (Daranga, 2005). The results of calculation are shown in Table 6.

$$CI_{C=O} = \frac{\text{Area of the carbonyl band centered around 1700 cm}^{-1}}{\sum\text{Area of the spectral bands between 2000 cm}^{-1}\text{ and 600 cm}^{-1}} \quad (1)$$

$$BI_{CH=CH} = \frac{\text{Area of the butadiene band centered around 966 cm}^{-1}}{\sum\text{Area of the spectral bands between 2000 cm}^{-1}\text{ and 600 cm}^{-1}} \quad (2)$$

Table 6 indicates that the carbonyl index (CI) increases with the aggravated aging. It means an increase in the content of the most polar components such as ketones and

carboxylic acids. It implies that the asphalt underwent a significant oxidation. It also confirms the conclusion obtained in the previous composition analysis that hard components in asphalt increase due to aging. Meanwhile, the butadiene index (BI) declines evidently with the aggravated aging. It indicates that the polybutadiene structure of SBS in the modified binder subjects to a sharp degradation. The less polybutadiene structure of SBS explains the degradation of low temperature ductility and the irregular changing trend of phase angle during aging process.

Table 6. Changes of Aging Indices Before and After Aging

SBS-modified binder samples	*CI*	*BI*
Unaged [-]	0	0.281
RTFOT aged [-]	0.149	0.192
PAV aged [-]	0.647	0.064

In sum, the influences of aging on the properties of SBS-modified binder are attributed to two major factors. One is the changing of chemical components in asphalt. Due to the effect of aging, the hard components such as asphaltenes are likely to increase in both the quantity and quality. It results in a more elastic asphalt. Another factor is the degradation of SBS polymer due to aging. The SBS may degrade into some chemical fragments with a lower molecular weight. It not only results in a loss of SBS network structure but also leads to a viscous behavior increase for the SBS-modified binder.

Recycling of Aged SBS-modified Asphalt Binder

Recycling Asphalt Binder

Recycling agent was used to rejuvenate the aged SBS-modified binder. Six different concentrations of recycling agent were selected as 2, 4, 6, 8, 10 and 12% by weight of binder. The physical and rheological properties of the recycled binder with different content of recycling agent are shown in Table 7 and Table 8 respectively.

As shown in Table 7 and 8, the expected rejuvenation of properties of aged binder is observed by adding recycling agent into the aged binder. It is clearly shown that the softening point, G*/sinδ and S decrease with the increasing concentration of recycling agent. The penetration, ductility and m increase with the increasing concentration of recycling agent. It means that the recycling agent decreases the high-temperature performance and improves the low-temperature performance of the aged binder. Results indicates that when 8% recycling agent is used, the properties of recycling binder are very similar to that of the unaged SBS-modified binder if considering the property parameters such as penetration, soften point, G*, G*/sinδ, S and m.

After a more careful examination on the testing results, it is noticed that the 5°C ductility of recycling binder with 8% recycling agent is still much smaller than that of the unaged SBS-modified binder. When the concentration of recycling agent reaches 12%, the recycling binder is already much softer than the SBS-modified binder because a much higher penetration and smaller G*/sinδ occur for the recycling binder.

The 5℃ ductility of the recycled binder still barely changes and significantly differs from the 5℃ ductility of the unaged SBS-modified binder. As discussed in the previous physical properties analysis in section 3.1.1, the 5°C ductility is sensitive to polymer microstructure of the asphalt. Although the recycling agent succeeds in composition recovery of the aged binder, it fails in the microstructure rebuilt of the aged SBS-modified binder because of degradation of the crosslinked SBS network structure. The testing data of δ reinforces this conclusion very well. It is indicated that, although the recycled binder has a similar G* to the unaged SBS-modified binder, the recycled binder has a much higher δ. As discussed in the previous rheological properties analysis in section 3.1.2, δ is more sensitive to the chemical structure than G*. Therefore, the much higher δ for the recycled binder than the unaged SBS-modified binder indicates a loss of the strong polymer modification structure in recycled binder. It may cause a severe temperature susceptibility and aging instability to the recycled binder.

Table 7. Physical Properties of Unaged, PAV Aged and Recycled SBS-Modified Binder

Asphalt samples	Recycling agent content (%)	Penetration (25°C, 0.1mm)	Softening point (°C)	Ductility (5°C, cm)
Unaged	0	69	61	37
PAV aged	0	42	74	2.6
Recycling	2	42	70	4.3
	4	49	67.5	6.5
	6	64	66	8.3
	8	70	63	10.6
	10	76	55	12.5
	12	90	50	14.2

Table 8. Rheological Properties of Unaged, PAV Aged and Recycling SBS-Modified Binder

Asphalt samples	Recycling agent content (%)	G^* (64°C, kPa)	δ (64°C, Deg)	$G^*/\sin\delta$ (64°C, kPa)	S (-18°C, MPa)	m (-18°C)
Unaged	0	2.42	69.2	2.58	236	0.332
PAV aged	0	9.43	70.3	10.02	308	0.291
Recycling	2	8.19	72.4	8.59	289	0.303
	4	5.88	75.9	6.06	269	0.312
	6	4.56	78.7	4.65	255	0.325
	8	2.63	79.9	2.67	219	0.344
	10	2.14	81.4	2.06	168	0.379
	12	1.01	82.5	1.01	110	0.396

To evaluate the aging properties of the recycled binder, RTFOT and PAV aging tests were conducted on the recycled binder with 8% recycling agent. The physical properties and rheological properties of the recycled binder before and after aging are shown in Tables 9 and 10 respectively. It is clearly shown that, similar to the base binder and SBS-modified binder, the physical and rheological properties of the recycled binder degrade with aggravated aging.

Table 9. Physical Properties of Recycled Binder Before and After Aging

Parameters	Unaged	RTFOT Aging		PAV Aging	
	Value	Value	Variation (RTFOT/Unaged)	Value	Variation (PAV/Unaged)
Penetration (25 °C, 0.1mm)	70	45	0.64	29	0.41
Softening point (°C)	63	73	1.16	81	1.29
Ductility (5 °C, cm)	10.6	1.5	0.14	0	0.00

Table 10. Rheological Properties of the Recycled Asphalt Before and After Aging

Parameters	Unaged	RTFOT Aging		PAV Aging	
	Value	Value	Variation (RTFOT/Unaged)	Value	Variation (PAV/Unaged)
G^* (64°C, kPa)	2.63	5.42	2.06	12.79	4.87
δ (64°C, Deg)	79.9	77.8	0.97	73.5	0.92
$G^*/sin\delta$(64°C, kPa)	2.67	5.55	2.08	13.34	5.00
S (-18°C, MPa)	219	275	1.26	348	1.59
m (-18°C)	0.34	0.305	0.90	0.267	0.79

Compared with the physical and rheological properties of SBS-modified binder before and after aging shown in Tables 3 and 5, it is evidently indicated that the aging speed of recycled binder is faster than that of SBS-modified binder. For example, the residual penetration ratios of SBS-modified binder after RTFOT and PAV aging are 0.84 and 0.56 respectively, while the residual penetration ratios of recycled binder after RTFOT and PAV aging decline to 0.64 and 0.41 respectively. The G*/sinδ of RTFOT aged and PAV aged SBS-modified binder are 1.77 and 3.88 times larger than that of the unaged SBS-modified binder, while the G*/sinδ of RTFOT aged and PAV aged recycled binder raise to 2.08 and 5 times larger than of the unaged recycling binder. In other words, aging causes more penetration loss and G*/sinδ increase to the recycled binder than the SBS-modified binder. It means the recycled binder is more easier to be aged and becomes a harder binder.

Special attentions are paid to the two important parameters, 5℃ ductility and δ, which are sensitive to the chemical structure of binder. The residual ductility ratios of

recycled binder after RTFOT and PAV aging are smaller than that of the SBS-modified binder after RTFOT and PAV aging. Meanwhile, the δ of recycled binder after RTFOT and PAV aging are much bigger than that of the SBS-modified binder. More importantly, the changing trend of δ of recycled binder with aggravated aging goes opposite direction from that of the SBS-modified binder. It evidently shows that the aging of recycled binder behaves more like the base binder. It validates previous conclusions that SBS modifier degrades due to aging and the recycling agent is not capable of re-building the SBS network structure.

Thus, it can be concluded that the aged SBS-modified binder can be rejuvenated by adding recycling agent. However, the road performance, particularly the durability of recycled binder cannot recover to the level of using original SBS-modified binder. The main reason is that most of the recycling agents being used recently are developed for unmodified binder and have no modification effect like polymer modifier on recycled binder. Therefore, a new recycling approach is needed to rejuvenate the aged SBS-modified binder.

Modified Recycled Asphalt Binder

To further improve the performance of recycled aged SBS-modified binder, a new-type additive MATM was used to modify the recycled binder. Based on previous analysis in section 3.2.1, recycled binder with 8% recycling agent was selected as a base to evaluate the modification effect of MATM. Five different concentrations of MA in the modified recycled binder were selected as 3, 6, 9, 12 and 15% by weight. The physical properties and rheological properties of the modified recycled binder with different contents of MATM are shown in Tables 11 and Table 12 respectively.

Table 11. Physical Properties of Recycling and Modified Recycled Aged SBS-Modified Binder

Asphalt samples	MA^{TM} content (%)	Penetration (25°C, 0.1mm)	Softening point (°C)	Ductility (5°C, cm）
Recycling	0	70	63	10.6
Modified recycling	3	66	66	16.5
	6	63	70	28.2
	9	59	78	34.1
	12	55	>80	37.6
	15	50	>80	35.5

As shown in Tables 11 and 12, compared to the properties of recycled binder without MATM, the penetrattion and δ of modified recycled binder decrease with the increasing addition of MATM. Meanwhile, the softening point, G* and G*/sinδ of modified recycled binder increase with the increasing addition of MATM. It means the MATM can improve the temperature sensitivity and high-temperature performance of recycling asphalt binder by improving the elastic behavior and lowering the viscous behavior of recycling asphalt binder at high temperature. The ductility data in Table 11 is illustrated to be increased and then decreased. It means MATM can improve the

low-temperature flexibility of the recycled binder when the content of MSTM reaches an optimum value. Meanwhile, the S decrasesd while the m decreased with the increasing content of MATM. It also indicates that optimum content of MATM needs to be determined to improve both the high-temperature and low-temperature performances of recycled ashphalt binder.

Based on the testing data of ductiltiy, S and m, 9% was selected as the optimum content of MATM in the modified recycled binder. Then, RTFOT and PAV aging tests were conducted to further evaluate the aging behavior of the modified recycling binder with 9% MATM. The physical and rheological properties of the modified recycled binder before and after aging are shown in Tables 13 and 14, respectively.

Table 12. Rheological Properties of Recycling and Modified Recycled aged SBS-Modified Binder

Asphalt samples	MA™ content (%)	G^* (64°C, kPa)	δ (64°C, Deg)	$G^*/sin\delta$ (64°C, kPa)	S (-18°C, MPa）	m (-18°C)
Recycling	0	2.63	79.9	2.67	219	0.344
Modified Recycling	3	3.11	77.5	3.19	208	0.335
	6	4.08	73.2	4.26	192	0.328
	9	5.48	68.9	5.87	185	0.320
	12	6.06	62.7	6.82	177	0.315
	15	8.58	49.2	11.17	196	0.298

Table 13. Physical Properties of Modified Recycled Binder Before and After Aging

Parameters	Unaged	RTFOT Aging		PAV Aging	
	Value	Value	Variation (RTFOT/Unaged)	Value	Variation (PAV/Unaged)
Penetration (25 °C, 0.1mm)	59	50	0.85	38	0.64
Softening point (°C)	78	82	1.05	88	1.13
Ductility (5 °C, cm)	34.1	22.3	0.65	5.8	0.17

It is clearly shown that, with the aggravated aging, high-temperature performance is significantly improved as shown by the decreasing penetration, increasing softening point, G* and G*/sinδ. Meanwhile, the low-temperature performance evidently degrades as indicated by the increasing S and the decreasing ductility and m. Although the initial low-temperature performance of modified recycling binder is lower than the SBS-modified binder, the resistance to low-temperature performance degradation of the modified recycling binder is even better than the SBS-modified binder during the long-term aging process. Furthermore, the modified recycled binder has a better high-temperature performance and durability than the original SBS-modified binder. As

shown by the variation index in Tables 3, 5, 9 and 14, it is evidently indicated that the aging speed of modified recycling binder is much lower than that of the recycled binder, but is similar to that of the SBS-modified binder.

Table 14. Rheological Properties of the Modified Recycled Binder Before and After Aging

Parameters	Unaged	RTFOT Aging		PAV Aging	
	Value	Value	Variation (RTFOT/Unaged)	Value	Variation (PAV/Unaged)
G^* (64°C, kPa)	5.48	7.79	1.42	11.96	2.18
δ (64°C, Deg)	68.9	69.2	1.00	70.5	1.02
$G^*/sin\delta$ (64°C, kPa)	5.87	8.33	1.42	12.69	2.16
S (-18°C, MPa)	185	211	1.14	266	1.44
m (-18°C)	0.32	0.313	0.98	0.295	0.92

Thus, the MATM modifying additive can promote the physical properties and durability of recycled binder. The modified recycled binder can reach the same performance level of original SBS modified binder. Therefore, the compound rejuvenation of aged SBS-modified binder by the combination of recycling agent and new additive is proved to be feasible and promising.

CONCLUSIONS

In this study, the aging behavior and recycling potentials of SBS-modified binder were investigated. The following conclusions can be drawn:

The elastic characteristics of binder at high temperature are enhanced significantly while the flexibility at low temperature is also evidently improved by adding SBS block copolymer. Therefore, the SBS polymer modifier can improve the resistance performance of binder to both rutting at high temperature and cracking at low temperature. Furthermore, the SBS modifier can improve the aging resistance of binder. However, the performance of SBS-modified binder will inevitably degrade with aggravated aging. The high-temperature phase angle in DSR test and the low-temperature ductility are proved to be sensitive to the colloidal structure of binder. The phase angle and ductility are considered to be capable of capturing the polymer modification effect and its loss due to aging of SBS-modified binder. The practicability of FTIR tests is also verified in characterizing the aging micromechanism of SBS-modified binder.

Aging has two major influences on the rheological behavior of SBS-modified binder. On one hand, the transition from light components to hard components in binder due to aging greatly contributes to the increase in the elastic behavior of modified binder. On the other hand, aging prompts the degradation of SBS polymer and leads to the increase in the viscous behavior of SBS-modified binder. Thus, the aging behavior of SBS-modified binder mainly consists of two parts, the aging of base binder and the degradation of SBS polymer network structure. It eventually leads to a brittle binder.

The complexity of aging behavior of SBS-modified binder makes it unreasonable to conduct the recycling procedure according to the standard methods developed for unmodified binder recycling. It is proved that the recycling agent in common use for unmodified binder can increase the flexibility of aged SBS-modified binder to some extent. However, it has no modification effect and cannot rebuilt the well-balanced network microstructure produced by polymer modifier in the asphalt matrix. Therefore, the recycling of aged SBS-modified binder requires new additives to fully restore the desired rheological properties. The combination of recycling agent and MATM additive is verified to be capable to achieve this objective. And the modified recycling binder by this combination is experimentally proved to have similar road performance and durability to the original SBS-modified binder. Therefore, compound rejuvenation of aged polymer modified binder is proved to be promising and recommended for further investigation.

The current research work satisfies the urgent need of recycling of polymer modified binder. However, more polymer modified binders, recycling agents and modifying additives are needed to be tested. Ongoing work includes the development of compound recycling agent specially used for polymer modified binder. The compound rejuvenation of aged polymer modified binder can be achieved by utilizing only one additive in the future.

ACKNOWLEDGMENTS

This paper is part of the research work of the National Natural Science Fund Project (51008075). The authors would like to thank for the financial support from the National Natural Science Foundation of China.

REFERENCES

Chen J. S. and C. C. Hang. (2007). “Fundamental characterization of SBS-modified asphalt mixed with sulfur.” *J. Appl. Polym. Sci*. 103: 2817-2825.

Cortizo, M.S., Larsen, H. and Bianchetto, J. L. (2004) “Effect of the thermal degradation of SBS copolymers during the ageing of modified asphalts.” *Polym. Deg. Stab.* 86: 275-282.

Daranga, C. (2005) “Characterization of aged polymer modified asphalt cements for recycling purposes.” Dissertation of Louisiana State University, USA.

Larsen, D. O., Alessandrini, J. L., Bosch, A. and Cortizo, M. S. (2009) “Micro-structural and rheological characteristics of SBS-asphalt blends during their manufacturing.” *Constr. Build. Mater.,* 23: 2769-2774.

Ruan, Y. H., Davison, R.R. and Glover, C.J. (2003) “The effect of long-term oxidation on the rheological properties of polymer modified asphalts”. *Fuel,* 82: 1763-1773.

Sengoz, B. and Isikyakar, G. (2008) “Analysis of styrene-butadiene-styrene polymer modified bitumen using fluorescent microscopy and conventional test methods.” J. Hazard. Mater. 50: 424-432.

Sun, D.Q., Ye, F., Shi F.Z. and Lu. W.M. (2006) “Storage stability of SBS-modified road asphalt: preparation, morphology, and rheological properties.” *Petrol. Sci. Technol.* 24: 1067-1077.

Wang, Y., P. D. J. Liu, Y. F. Li, Y. P. Wang and J. M. Gao. (2006) "Preparation and properties of asphalts modified with SBS/organobentonite blends." *Polym Compos*. 14: 403-12.

Wen, G.A., Y. Zhang, Y.X. Zhang, K. Sun and Z.Y. Chen. (2001) "Vulcanization characteristics of asphalt/SBS blends in the presence of sulfur." *J. Appl. Polym. Sci*. 82: 989-996.

Wen, G.A., Y. Zhang, Y.X. Zhang, K. Sun and Y.Z. Fan. (2002) "Rheological characterization of storage-stable SBS-modified asphalts." *Polym. Test.* 21: 295-302.

Wen, G.A., Y. Zhang, Y.X. Zhang. (2002) "Improved properties of SBS-modified asphalt with dynamic vulcanization." *Polym. Eng. Sci.* 42: 1070-1081.

Zhang, F., J. Y. Yu and S. P. Wu . (2010). "Effect of ageing on rheological properties of storage-stable SBS/sulfur-modified asphalts." *J. Hazard. Mater*. 182: 507-517.

Prediction of tensile strength of asphalt concrete

N. Li[1] and A.A.A. Molenaar[2]

[1]Ph.D. Candidate, Road and Railway Engineering, Faculty of Civil Engineering and Geosciences, Delft University of Technology, Stevinweg 1, 2628 CN Delft, The Netherlands; email: Ning.Li@tudelft.nl
[2]Professor, Road and Railway Engineering, Faculty of Civil Engineering and Geosciences, Delft University of Technology, Stevinweg 1, 2628 CN Delft, The Netherlands; email: A.A.A.Molenaar@tudelft.nl

ABSTRACT: Durable and sustainable asphalt pavements require high quality asphalt materials. In pavement design, the tensile strength of asphalt concrete is a fundamental engineering property. Due to the characteristics of bitumen, the tensile strength is a function of temperature and loading rate. In the past some regression equations were developed to predict the tensile strength of asphalt concrete. However, these equations are only valid for a narrow temperature and strain rate ranges and do not relate to the material properties. This paper proposes a new general equation for the prediction of the tensile strength, which is based on tension tests performed at different test conditions and relates to the complex modulus of the bitumen. By means of the Dynamic Shear Rheometer (DSR), frequency sweeps were done to obtain a master curve for the complex modulus of the bitumen. Uniaxial tensile strength (UTS) tests were conducted to get the tensile strength of the asphalt mixture at different temperatures and loading rates, respectively. In this paper, an S-shaped prediction curve is used to link the tensile strength of the mixture and complex modulus of the bitumen to each other. The test results indicate that the proposed prediction model has a low relative error, which means that it gives a realistic description for the tensile strength of an asphalt mixture.

INTRODUCTION

Cracking, including thermal and fatigue cracking, is one of the major damage modes in asphalt pavements. To build a durable and sustainable asphalt pavement, the tensile strength of the mixture is one of the essential indicators for pavement design. Numerous researches have been conducted relating the tensile strength of asphalt mixtures to the performance of asphalt pavements. Based on the fracture mechanics approach, Schapery (Schapery, 1975 and 1978) found a relationship between the tensile strength and the parameter A of Paris' law model, which is used to predict the crack propagation. Roque et al. (Roque, 1999) investigated the use of the tensile strength to determine the fracture properties of asphalt mixtures. Ning et al. (Ning 2010) calculated the fatigue endurance limit based on the tensile strength and the Four-point bending fatigue test results.

It is well known that the tensile strength of bituminous materials is related to the material properties and also strongly varies with temperature and loading speed. A number of prediction methods were proposed in the past to predict the tensile strength of asphalt mixtures. Heukelom (Heukelom, 1966) combined the influence of temperature and loading speed and related the relative tensile strength of bituminous materials to the bitumen stiffness S_{bit} at the considered temperature and loading speed. The curve was fitted by a regression equation was developed:

$$log\left(\frac{\sigma_m}{\sigma_{m,max}}\right) = a_0 + a_1 log\left(S_{bit}\right) + a_2 \left(log\left(S_{bit}\right)\right)^2 + a_3 \left(log\left(S_{bit}\right)\right)^3 \quad (1)$$

Where: σ_m is tensile strength [MPa]; $\sigma_{m,max}$ is maximum strength over all loading conditions [MPa]; $a_{0\text{-}3}$ are regression constants; S_{bit} is stiffness of bitumen [MPa].

In the asphalt concrete response (ACRe) project, Erkens (Erkens, 2002) conducted uniaxial tension tests on a fine grade mixture. A non-linear relation was used to describe the relation between tensile strength, temperature and strain rate, as shown in Equation 2. This general equation was also applied by Medani and Muraya in their PhD projects (Medani, 2006) (Muraya, 2007).

$$f_t = a\left[1 - \frac{1}{1 + \left[\dot{\varepsilon} e^{\left(b + \frac{c}{T}\right)}\right]^d}\right] \quad (2)$$

Where: a, b, c and d are regression constants; $\dot{\varepsilon}$ is strain rate [%/s]; T is temperature [K].

Due to the limitations of the test conditions, some of these models were developed in a relatively narrow range of temperatures and strain rates. At the extreme test conditions (low temperature and high strain rate or high temperature and low strain rate), the accuracy of these models will not be good. The objective of this paper is to develop a new prediction model for the tensile strength. As mentioned above, the tensile strength is simultaneously influenced by temperature and loading speed. The complex stiffness of the recovered bitumen was used to combine the influence of temperature and loading speed. In this paper, uniaxial tensile strength (UTS) tests were conducted over a wide range of test conditions and a frequency sweep was performed on the recovered bitumen extracted from the asphalt mixture. Based on the results of these tests, a new prediction model was proposed to express the relationship between tensile strength of the mixture, complex stiffness of bitumen and test conditions (temperature and strain rate). At the end, some additional uniaxial tensile strength tests were done for the model verification.

EXPERIMENTAL WORKS

Materials

A dense asphalt concrete DAC 0/8 with a maximum aggregate size of 8 mm was designed in accordance with the Dutch RAW specifications (CROW, 2005). The aggregate consists of Scottish crushed granite, Bestone and crushed sand. A 40/60 penetration grade bitumen was used at a design binder content by mass of total mixture of 6.5 %. The filler in the mixture is a kind of factory produced filler, Wigras 40K. The percentage passing of 0.063 mm is between 75 % and 85 %. Table 1 represents the mixture composition. The recovered bitumen extracted from the asphalt mixture was used for the frequency sweep by means of the DSR. The cylindrical specimens were cored horizontally and parallel from slabs with dimension of 150×185×450 mm, which were compacted with the PReSBOX compactor. After cored from the slabs, all samples were polished to make the two ends in parallel. The target air voids content was 3.5 %.

Table 1. Composition of the mixture DAC 0/8

Sieve (mm)	Scottish crushed granite		Norwegian Bestone	Crushed sand		Wigras 40K	Binder
	8-5.6	5.6-4	6-2	2-1	1-0.063	0.18-0.063	
Wt. %	11.2	19.6	21.5	16.8	16.4	7.9	6.5

Test methods

To obtain the complex modulus of the recovered bitumen and the tensile strength of the asphalt mixture, a frequency sweep test on the bitumen with a DSR and the uniaxial tensile strength tests on the mixture test were conducted. Fig. 1 shows the DSR equipment. Bitumen was sandwiched between a fixed plate and a plate that can oscillate to apply the shear strain during testing. The test was carried out in a temperature controlled chamber.

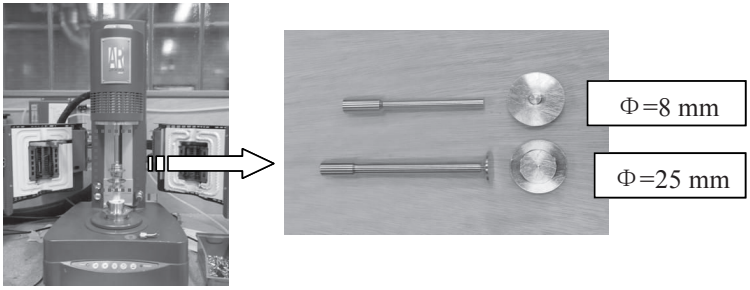

FIG. 1. DSR test set-up and parallel plates.

During the test, the bitumen sample was subjected to a sinusoidal loading of

constant strain at different loading frequencies (frequency sweep). The frequency sweep tests were conducted at eight temperatures from -10 °C and 60 °C. For each temperature, different frequencies between 0.3 ~ 400 rad/s were applied. The specimen size and plate diameter to be used depends on the test temperature. A specimen size of 2 mm thickness and 8 mm in diameter was used for the lower temperatures (≤ 30 °C). For the intermediate-to-high (40 ~ 60 ºC) temperatures, a specimen size of 1 mm thickness and 25 mm in diameter was used. After the test, the complex modulus and phase angle were automatically reported by the DSR software. Before conducting the frequency sweep tests, a strain sweep test was performed to determine the strain level at which the material response remains in the linear region. During the test, strain level varies from low to high gradually at a certain frequency. In the beginning, the complex modulus G^* keeps as a constant value. After the shear strain reaches a certain high level, the G^* will suddenly drop. The strain level used for frequency sweep can be calculated using Equation 3 (Peterson, 1994).

$$\gamma = \frac{12}{\left(G^*\right)^{0.29}} \tag{3}$$

Where: γ is shear strain used for frequency sweep [%], G^* is the constant value of complex modulus in the strain sweep test [kPa].

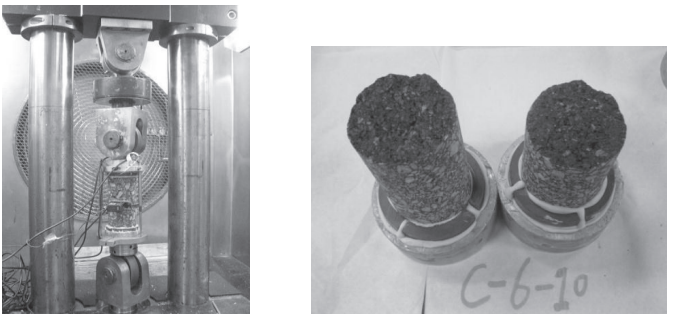

FIG. 2. UTS test set-up and a failure sample.

Fig. 2 gives the set-up of the uniaxial tensile strength (UTS) test. The UTS tests were performed on cylindrical specimens with a height of 125 mm and a diameter of 50 mm. The specimen, on which a bottom and top steel cap were glued, was placed between three hinges to ensure that the specimen was subjected to pure uniaxial tension. The axial deformation was measured by means of three displacement transducers (LVDT's). These LVDT's were fixed by two aluminium rings, which were placed around the steel caps. The tests were conducted at different strain rates ranging from 0.001 to 4 %/s and different temperatures ranging from 5 to 35 ºC. During the test, load and axial deformation data were captured electronically every 0.001 s.

TEST RESULTS AND DISCUSSION

DSR test results

Fig. 3 gives the results from the frequency sweep tests performed at various temperatures on the recovered bitumen. The rheological properties of bitumen can be described by a master curve using the time-temperature superposition principle. This principle allows shifting of the data obtained at various temperatures with respect to time or frequency to a selected reference temperature. The curve obtained in this way is plotted as a function of reduced time or frequency. The amount of shifting required at each temperature to the reference temperature is obtained using the Williams-Landel-Ferry (WLF) equation.

$$Loga_T = \frac{-C_1(T - T_0)}{C_2 + (T - T_0)} \tag{4}$$

Where: C_1 and C_2 are the constants; T and T_0 are the test and reference temperature respectively, ºC; a_T is the shift factor.

The resulting master curves for the complex shear modulus, G^*, are described using the Christensen Anderson (CA) model.

$$G^*(\omega) = G_g^* \left[1 + \left(\frac{\omega_c}{\omega'} \right)^{\frac{\log 2}{R}} \right]^{\frac{-R}{\log 2}}, \quad R = Log \frac{G_g^*}{G_c^*} \text{ and } \omega' = \omega \cdot a_T \tag{5}$$

Where: $G^*(\omega)$ is magnitude of the complex shear modulus [MPa]; G^*_g is the glassy modulus [MPa]; G^*_c is the cross modulus [MPa]; ω_c is the location parameter (cross over frequency) [rad /s]; ω' is reduced frequency [rad /s]; ω is frequency [rad /s]; R is rheological index.

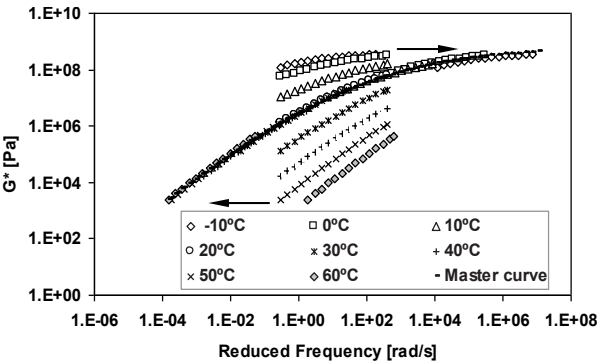

FIG. 3. Complex modulus of the recovered bitumen.

From Fig. 3, it can be seen that the prediction line does not fit the data obtained at -10 ºC very well. When the constants in the WLF equation are obtained with data at temperatures above the glass transition temperature (T_g), the WLF equation is only valid for the temperatures equal or higher than the glass transition temperature. In this case the temperature of -10 ºC might be much close to the glass transition temperature of the bitumen used in this paper.

In fact during the test the strain signal is a sine waveform, shown in Fig. 4. The strain rate of this alternating triangle signal is considered to be an acceptable approximation of the strain rate and can be computed as follows:

$$\dot{\varepsilon} = \frac{\varepsilon}{\frac{1}{4}t} = 4 \cdot \varepsilon \cdot \frac{\omega}{2\pi} = \frac{2\varepsilon\omega}{\pi} \tag{6}$$

Where: ε is strain amplitude, m/m; t is time duration in one cycle, s; ω is frequency, [rad/s].

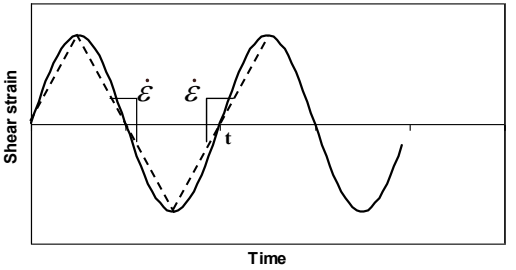

FIG. 4. Conversion from a sine signal to a triangle signal.

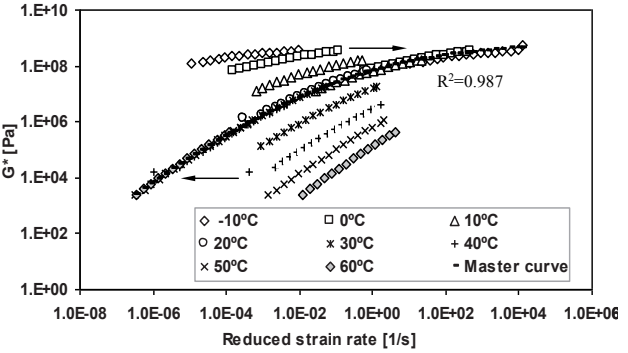

FIG. 5. Master curve for complex modulus vs. reduced strain rate at a reference temperature of 20ºC.

At a certain temperature, the maximum applied strain level is kept constant. So each frequency is corresponding to a different strain rate. Based on the results, the relationship between strain rate the complex modulus G^* can be obtained. From Fig. 5, we can see that the fit of the model is perfect with a high R^2 value of 0.987 at a reference temperature of 20 ºC.

$$G^*(\omega) = (7.16E+08)\cdot\left[1+\left(\frac{0.0583}{\dot{\varepsilon}\cdot 10^{\frac{18.4(T-20)}{122+(T-20)}}}\right)^{0.191}\right]^{-5.23} \tag{7}$$

UTS test results

Fig. 6 gives some of the stress-strain curves obtained from the UTS test. It is clear that the temperature and strain rate have a significant influence on the strength and brittleness of the material. In the uniaxial tensile strength test, the tensile strength of the asphalt mixture was obtained at certain strain rates and temperatures, as shown in Fig. 7. As expected, higher strain rates and/or lower temperatures result in a higher tensile strength.

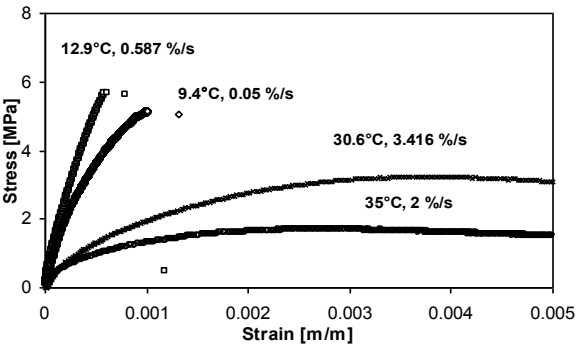

FIG. 6. Stress-strain curves at different strain rate and temperature.

Prediction function

Both the complex modulus G^* of the bitumen and the tensile strength f_t of the mixture relate to the strain rate and temperature. Therefore the relationship between G^* and the tensile strength of the asphalt mixture f_t could be found, as shown in Fig. 8. Taking into account the shape and the trend of the data points, the following S-shaped regression equation can be used to describe the relationship:

$$f_t = f_h + (f_l - f_h)\exp(-[\alpha\cdot G^*]^{\beta}) \tag{8}$$

Where: f_l is the tensile strength when $G^*\rightarrow 0$, MPa; f_h is the tensile strength when $G^*\rightarrow\infty$, MPa; α and β are the model parameters.

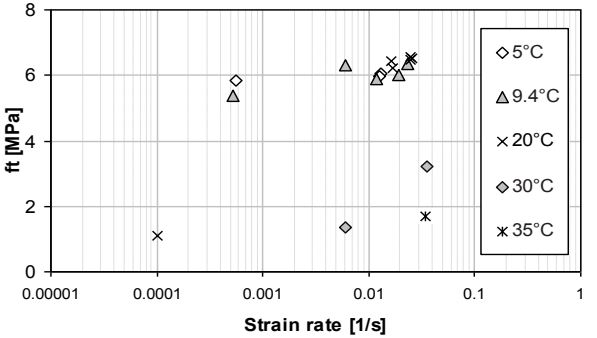

FIG. 7. Results of the UTS test.

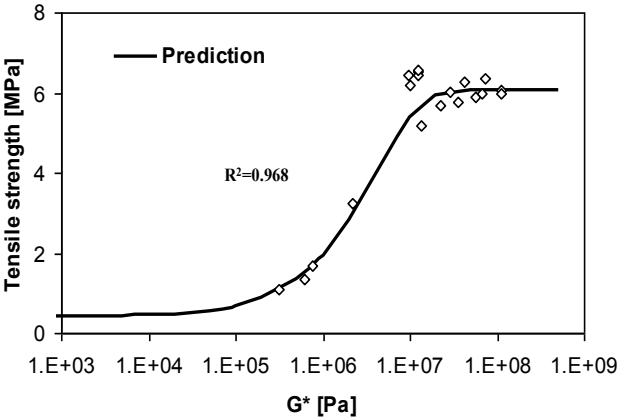

FIG. 8. Tensile strength vs. complex modulus of the recovered bitumen.

Based on the tensile strength test results, the parameters in this function can be simply found with the Solver function in Excel. Equation 9 gives the tensile strength function of the mixture DAC 0/8.

$$f_t = 6.05 + (0.414 - 6.05)\exp(-[(2.5E-07)\cdot G^*]^{0.829}) \quad (9)$$

When Equation 7 is substituted into Equation 9, the relation between tensile strength, strain rate and temperature can be given as Equation 10:

$$f_t = 6.05 - 5.636\exp\left(-73.7\left[1+\left(\frac{0.0583}{\dot{\varepsilon}\cdot 10^{-\frac{18.4\cdot(T-20)}{122+(T-20)}}}\right)^{0.19}\right]^{4.33}\right) \quad (10)$$

The comparison of the fitted tensile strength and the test results are presented in Fig. 9. In general, the tensile strength increases with the increase of the strain rate and the decrease of the temperature. For each temperature, the tendency of the prediction curve is similar. When the strain rate is too low or too high, the tensile strength of asphalt mixture does not change significantly. Only in a certain strain rate range, the tensile strength becomes much more sensitive. And this strain rate range increases with the temperature. The prediction lines show a good agreement with the measured results during the test. At 20 ºC and high strain rates (>1 %/s), the predicted values are a little lower than the test results. The mean percentage relative error (MPRE) of the model is calculated (Mo, 2010):

$$Error = \left|\frac{Measured\ value - Predicted\ value}{Measured\ value}\right| \times 100\%,\ MPRE = \frac{\sum_{1}^{n} Error}{n} \quad (11)$$

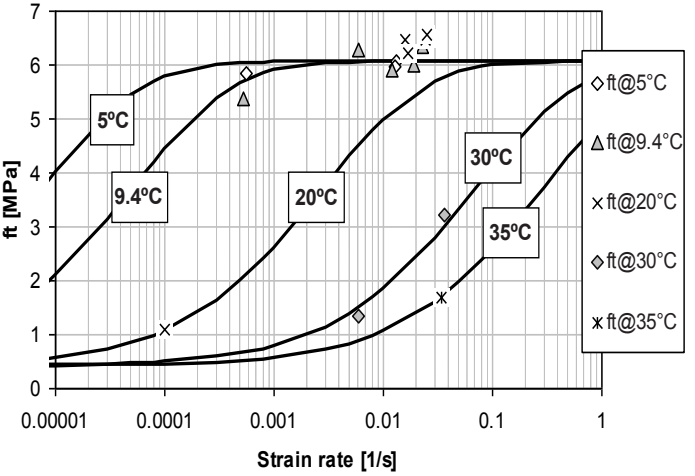

FIG. 9. Predicted tensile strength compared to the results.

Table 2. Tensile strength results and relative errors of the prediction model

Sample code	T [ºC]	$\dot{\varepsilon}$ [%/s]	f_t [MPa]	Predicted f_t [MPa]	Error [%]
C-8-4	5	0.056	5.84	6.04	4.99
C-6-5	5	1.318	6.05	6.05	0.00
C-6-9	5	1.274	5.97	6.05	1.28
C-8-7	9.4	0.052	5.17	5.67	9.80
C-8-10	9.4	0.592	6.29	6.05	3.84
C-8-5	9.4	1.196	5.89	6.05	2.66
C-7-7	9.4	1.93	6.00	6.05	0.85
C-6-7	9.4	2.3	6.36	6.05	4.81
C-6-10	20	0.01	1.08	1.06	2.01
C-8-2	20	1.607	6.45	5.34	17.32
C-7-1	20	1.74	6.20	5.37	13.42
C-6-2	20	2.56	6.51	5.61	13.77
C-7-10	20	2.46	6.46	5.59	13.40
C-6-4	20	2.501	6.56	5.60	14.67
C-8-1	30.6	0.595	1.35	1.49	10
C-6-8	30.6	3.579	3.23	2.97	8.07
C-6-6	35	3.38	1.68	1.68	0.00
				MPRE	7.1

The relative errors of each point and the mean relative error of all the data are listed in Table 2. The MPRE value is equal to 7.1 %, which means Equation 10 gives a good fit for the tensile strength.

Model verification

To verify the prediction model, additional uniaxial tensile strength tests were performed at the different temperatures and strain rates. For each temperature and strain rate, the predicted tensile strength could be calculated by Equation 10. Fig. 10 presents the test results and the prediction lines for each temperature. The comparison between measured and predicted data shows a satisfactory agreement. The relative error for each point and the mean percentage relative error are given in Table 3. The small MPRE value indicates that the tensile strength of the mixture can be predicted very well by the proposed model.

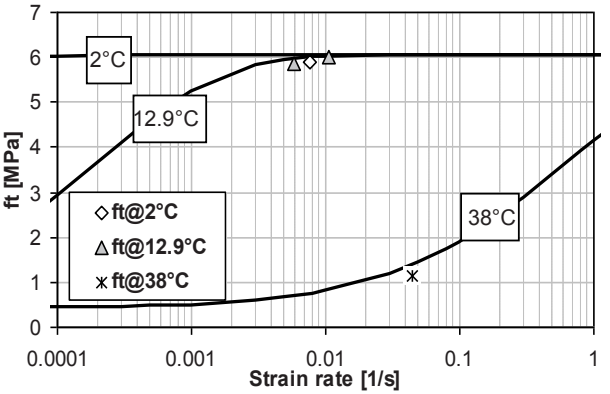

FIG. 10 Results of verification test.

Table 3. Results of the verification test

Sample code	T [ºC]	$\dot{\varepsilon}$ [%/s]	f_t [MPa]	Predicted f_t [MPa]	Error [%]
C-7-6	2	0.753	5.98	6.05	1.19
C-8-6	12.9	0.584	5.77	5.96	3.28
C-8-9	12.9	1.05	6.02	6.02	0.02
C-7-2	38	4.43	1.14	1.24	8.70
				MPRE	3.30

CONCLUSIONS

In this paper, a new prediction model for the tensile strength of an asphalt mixture has been presented. The model parameters were determined by uniaxial tensile strength tests on the asphalt mixture and the frequency sweep tests on the recovered bitumen using a DSR test machine. The tests have been performed at various test conditions. The following conclusions have been drawn:

In the frequency sweep on the DSR test machine, assuming the loading waveform as a triangle signal, the relationship between complex stiffness G^* and strain rate can be described by a master curve using the time-temperature superposition principle.

The tensile strength and the complex stiffness both change with temperature and loading rate. Based on the results, the tensile strength of the mixture has a unique relationship with the complex modulus G^* of the recovered bitumen from the mixture, which can be fitted very well by a S-shaped curve. This makes it possible to link the tensile strength to the test condition.

The small value of the mean percentage relative error indicates that the proposed model is able to predict the tensile strength of the asphalt mixture in a wide range of

temperatures and strain rates. This conclusion is also proved by the model verification.

ACKNOWLEDGEMENT

The scholarship from China Scholarship Council is gratefully acknowledged. The useful discussions and suggestions from M.F.C. van de Ven and A.C. Pronk are greatly appreciated. The authors also would like to thank Marco Poot and Jan Willem Bientjes who helped set up the experiment and prepare the specimens.

REFERENCES

CROW (2005). In: Standaard RAW Bepalingen, C.R.O.W., Ede (In Dutch).

Erkens, S.M.J.G. (2002) "Asphalt Concrete Response - Determination, Modeling and Prediction." PhD. thesis, Delft University of Technology, the Netherlands, 2002.

Heukelom, W. (1966). "Observations on the rheology and fracture of bitumens and asphalt mixes." *Asphalt Paving Technology* Vol. 35: 358-399.

Li, N., Molenaar A.A.A., van de Ven, M.F.C., and Wu, S.P. (2010) "Estimation of the Fatigue Endurance Limit of HMAC for Perpetual Pavements." *Journal of Wuhan University of Technology-Mater. Sci. Ed*. Vol.25(4): 645-649.

Medani, T.O. (2006). "Design Principles of Surfacings on Orthotropic Steel Bridge Decks." PhD. thesis, Delft University of Technology, the Netherlands, 2006.

Mo, L.T. (2010). "Damage Development in the Adhesive Zone and Mortar of Porous Asphalt Concrete." PhD. thesis, Delft University of Technology, the Netherlands,

Muraya, P.M. (2007). "Permanent Deformation of Asphalt Mixtures." PhD. thesis, Delft University of Technology, the Netherlands, 2007.

Schapery, R.A. (1975). "A Theory of Crack Initiation and Growth in Visco-Elastic Media; I: Theoretical Development." II: Approximate methods of analysis, III: Analysis of Continuous Growth. *International Journal of Fracture, Sijthoff and Noordhoff International Publishers,* Vol.11(1): 141-159; Vol.11(3): 369-388 and Vol.11(4): 549-562.

Peterson, J.C., Anderson, D.A. and et al. (1994). "Binder characterization and evaluation." Vol. 4: Test methods. SHRP-A-370, National Research Council, Washington, DC.

Schapery,R.A. (1978). "A Method for Predicting Crack Growth in Non-homogeneous Visco-Elastic Media." *International Journal of Fracture, Sijthoff and Noordhoff International Publishers,* Vol.14(3): 293-309.

Roque,R. Zhang,Z., and Sankar,B. (1999). "Determination of crack growth tate parameters of asphalt mixtures using the superpave IDT." *Journal of the Association of Asphalt Paving Technologists*, Vol. 68:404-433.

Evaluation of Properties of Aged and Recycled Mixture without Extraction and Recovery

Zhen Wang[1], Hao Liu[2] and Xiaoming Huang[3]

[1]Beijing Municipal Road and Bridge building Material Group Co.Ltd., Beijing 102600, China; email: wangzhen_seu2006@163.com
[2]Beijing Municipal Road and Bridge building Material Group Co.Ltd., Beijing 102600, China; email: liuhao19696@126.com
[3]School of Transportation, Southeast University, SipaiLou 2#, Nanjing 210096, China; email: huangxm@seu.edu.cn

ABSTRACT: Compared with the unmodified asphalt, aged SBS modified asphalt is harder to be extracted. It is difficult to completely remove the residual solvents and mineral powder in the recovery process. The objective of this research is to develop a procedure to evaluate the properties of aged and recycled binder without extraction and recovery, and to determine the species and amount of recycling agent. Properties of artificially aged mixture and asphalt were tested. Bending test of small beam was taken to evaluate the aged mixture and the regenerated mixture. The test data included limit flexural tensile strength and fracture energy. The test results showed that the aged mixture became more hard and brittle. The species and amount of recycling agent could be determined by fracture energy. The properties of regenerated mixture designed in the new way were better than those designed in the traditional way on high temperature and fatigue performances. The low temperature performances of regenerated mixtures designed in the two ways were both qualified.

INTRODUCTION

Polymer modified asphalt pavement shows a better performance than conventional non-modified asphalt pavement, such as rutting resistance, moisture damage resistance, etc. (Brule, 1996). Use of polymer modified asphalt binder has been increased steadily in the last decade. The highway agencies in China and United State both recommend that it should be given priority to use polymer modified asphalt binder in new highway construction, especially for the surface layer and the open grade friction course (OGFC) layer (Jinan Shen,2001; Codrin Daranga,2005).

There are two different stages during the bitumen aging in the field: The first stage is during the construction process. In this process, binder is exposed to rapid oxidation and volatilization resulting from high temperature and large surface area of the heated aggregates. The second stage is occurred during the service life of the pavement, when oxygen from the environment penetrates into the asphalt mixture and reacts with some components. Oxidation is known to be as the main hardening mechanism (Welborn,1984; Petersen,1984).

Extraction and recovery are used to estimate the aged binder properties in RAP as specified in the AASHTO T164 and ASTM D 2172 procedure. However, research studies (D. E. Carey,1982; G. Abson,1933; Imad L. Al-Qadi,2007) have consistently shown that this method is not accurate and has the following disadvantages:

(1) The binder content in the RAP cannot be accurately estimated, because the process of binder extracting from the aggregates might not be completed.

(2) Test results are sensitive to any residuals in the recovered binder. Small amount of residual filler or solvent can lead to a significant influence on the binder properties.

(3) Recycling agent blended with recovered asphalt completely, while the blending process can not be uniform practically.

Estimating the effect of RAP materials on performance of HMA requires an accurate evaluation of the RAP materials. As mentioned above, the extraction and recovery method poses a high variability as well as sensitivity to different variables. Therefore, a new procedure is needed to evaluate the property of RAP binder more accurately. An improved BBR test was developed to estimate the low temperature rheological properties of binders in the RAP without the damaging effects of solvent extractions (Emil G.,2008; Tao Ma,2010).

Recent research has usually focused on the intermediate fracture/cracking, low temperature cracking, and stiffness properties of the final asphalt mixture. Mechanical properties of recycled mixture for highways have been investigated (Ay¸se Edinçliler,2004; Blake Rubino,2010). As bitumen become harder and brittler after aging, dynamic shear modulus of SHRP test increases and phase angle decreases. These mean that the performances of aged mixture lost on anti-fatigue and low temperature cracking resistance. The use of the dynamic modulus test (E*) shows promise as it has been found to be sensitive to mixture volume properties, gradation, and asphalt binder stiffness, all of which are influenced by the inclusion of RAP (Thomas Bennert,2010; Robinette,2006). Li et al. (Li,2008;) conducted dynamic modulus and semi-circular bend (SCB) fracture testing to evaluate asphalt mixtures of varying RAP contents (0, 20, and 40%).

This paper introduces a procedure to estimate the properties of the aged and recycled mixture using the bending test of small beam.

OBJECTIVE

The objective of this research is to develop a procedure to evaluate the properties of aged and recycled binder without extraction and recovery, and to determine the species and amount of recycling agent. Bending test of small beam was taken to evaluate the properties of aged and regenerated mixture. The recycling agent was determined by fracture energy.

EXPERIMENTAL CONSIDERATIONS

Hypothesis

In the composite theory of material, the composite material is considered as a multiphase system. The performances of composite materials satisfy the following mixture equation (Hao Yuankai, 2004; Ma Tao, 2008):

$$K_c^{\ n} = \sum K_i^{\ n} \phi_i \tag{1}$$

where K_c is certain performance of composite material. K_i is corresponding performance of component material i relative to K_c, φ_i is volume fraction of component material i, and n is composite effect constant.

According to composite theory, the properties of aged asphalt and mixture change identically when the parameters of the mixture keep constant, such as aggregate gradation, binder content and air void. And regenerated asphalt and mixture share the same trend. As a result, the properties of aged asphalt could be obtained by testing mixture.

Material and Equipment

A standard cross link SBS modified asphalt binder (named original PMB) with penetration degree of 68 meeting the Chinese specification for SBS I-C with penetration grade 60-80 and SHRP specification for PG 76-22 was obtained. Artificial aging process was carried out using oven for SBS modified asphalt binder to prepare the aged binder. During the recycling process, two types of rejuvenators were selected. The gradation named AC13 is shown in Table 1. The aggregate was basalt. Bending test of Small Beam was taken by UTM. The dynamic stability test was taken by rutting test. The penetration grade Tests and SHRP binder tests were taken too in this paper. At least 3 samples were taken for every test in this study.

Table 1. Gradation

Sieve Size(mm)	19	16	13.2	9.5	4.75	2.36	1.18	0.6	0.3	0.15	0.075	BC
AC13	100	100	95.0	74	63	37	27	17	14	10	6	5%

Experimental Procedures

Preliminary Testing

The target of this phase is to prove that there are little difference between mixture aging and binder aging. In this phase, 3 kinds of samples were made to investigate the influence of aggregate on SBS modified asphalt binder when thermal and oxygen aging.

SBS modified asphalt were mixed with mineral powder passing #0.075mm Sieve. The weight of the binder and mineral powder were the same, and the mineral powder was heated to 160℃. This mixture named MA was cured in the oven at 80℃ for 24h. Then the MA samples were aged in oven (163℃) for 20h. The weight of SBS modified asphalt in each plate was 100g.

SBS modified asphalt was aged in the oven for 20h. The weight of SBS modified asphalt in each plate was 50g. Then the aged asphalt was mixed with heated mineral powder passing #0.075mm Sieve. The weight of the binder and mineral powder were the same, and the mineral powder was heated to 160℃. The mixture named AM1 was cured in the oven at 80℃ for 24h.

The process in this step was almost the same as step 2. And the weight of SBS modified asphalt in each plate was calculated as follows:

$$M_{asphalt} = \rho_{asphalt} \times (50/\rho_{asphalt} + 50/\rho_{mp}) \quad (2)$$

Where $M_{asphalt}$ is the weight of SBS modified asphalt in each plate. $\rho_{asphalt}$ is the density of SBS modified asphalt. ρ_{mp} is the density of mineral powder. After initial testing, it was decided that artificial aging could be adopted to prepare the aged mixture.

Evaluation of aged Mixture

The target of this phase is to prove that the properties of aged binder could be reflected by aged mixture when the parameters of the mixture keep constant. The performance of aged mixture whose aging time was different at different temperature could be reflected by one test.

Artificial aging process was carried out by using oven(165℃) for SBS modified asphalt binder to prepare aged binder. The thickness of the asphalt was 3mm. The pressure in the oven was standard atmospheric pressure. The size of the plate for aging was 30*50cm. The binders were aged for different time, such as 5, 10, 15, and 20 hours. The mixture was made by the aged binder and new aggregates. The content of binder and air void were the same for each kind of aged mixture. The penetration grade test and SHRP binder tests were taken. The test data contained penetration, softening point, ductility, phase angle and complex modulus. The high and low temperature performances were tested. The test data contained dynamic stability (60℃), limit flexural tensile strength (-10℃) and limit flexural strain (-10℃). The bending test of small beam at 20℃ was taken to reflect the degree of hardness and brittleness. The size of the beams which was cut by rutting samples was 35*30*200mm. The loading rate was 50mm/min. The test data contained limit

flexural tensile strength (20℃) and fracture energy.

Evaluation of Regenerated Mixture

The target of this phase is to prove that the new way of designing regenerated mixture was better than the traditional way. Designing regenerated mixture refer to determine the species and amount of recycling agent. The traditional way is to determine the species and amount of recycling agent by regenerated asphalt tests. The new way is to determine the species and amount of recycling agent by regenerated asphalt mixture tests.

Two kinds of rejuvenator whose properties were shown in Table 2 were taken in this phase. Aged mixture was made by the aged binder and new aggregates in the second phase whose aging time was 20h. Rejuvenator A was added to the aged mixture to produce regenerated mixture A, so as to regenerated mixture B. The content of binder and air void were the same for each kind of regenerated mixture. Rejuvenator A was added to the aged binder to produce regenerated SBS Modified Binder A (regenerated asphalt A), so as to regenerated SBS Modified Binder B(regenerated asphalt B). The penetration grade test and SHRP binder tests were taken to determine the species and amount of recycling agent (traditional way). The test data contained penetration, softening point, ductility, phase angle and complex modulus. The bending test of small beam at 20℃ was taken to determine the species and amount of recycling agent (new way). The high and low temperature performances of regenerated mixture designed by the two ways were tested for comparison.

Table 2. Properties of Rejuvenator

Rejuvenator		**A**	**B**
Viscosity(60℃,mPa.s)		90	512
Flash Point(℃)		208	227
TFOT Aging	Residual Viscosity Ratio(%)	1.28	1.16
	Quality Chang Fraction(%)	-1.6	-0.22
Density（15℃,g/cm^3）		0.91	0.97

Preliminary Testing

The purpose of this phase is to investigate the influence of aggregates on SBS modified asphalt binder during thermal and oxygen aging. If there is not great difference between mixture aging and asphalt aging, artificial aged asphalt would be prepared for the next phase. The test results were shown in Table 3.

The aging degrees of AM1 and MA were similar, while AM_2 was aged seriously. It can be concluded from Table 3 that the main factor of mixture aging was the

thickness of asphalt film. The polar component of aggregates might adsorb the polar component in asphalt, and this would protect asphalt from reacting with oxygen. The effects of mineral powder were not significant. After initial testing, it was decided to prepare aged mixture by artificially aged SBS modified asphalt.

Table 3. Test Results of Penetration Grade Test and SHRP Test

	penetration grade test		DSR		BBR	
	Penetration (0.1mm,25℃)	Softening Point(℃)	Dynamic Modulus(Pa)	Phase angle(°)	S(60) (MPa)	m(60)
AM_1	2.54	69.3	26500	73.2	81.8	0.503
AM_2	1.72	78.2	52959	63.8	146	0.439
MA	2.69	70.5	27658	72.8	86.5	0.506

Evaluation of Aged Mixture

Test results for artificially aged binder and mixture were shown in Table 4, 5. According to Table 4, penetration, softening point and ductility values for aged mixture with different aging time are showed in Fig. 1. The Penetration, softening point and ductility decrease linearly with the increasing of aging time. Viscosity, G*/sin δ , S, m values for aged mixture with different aging time are showed in Fig. 2. The Viscosity, G*/sin δ , and S increase linearly with the increasing of recycling agent content. The m value decreases linearly with the increasing of recycling agent content. Aged mixture becomes more hard and brittle. It is good for aged mixture becoming harder on high temperature performance. But it is bad for aged mixture becoming more brittle on low temperature performance. So the toughness is the focus of the evaluation and restoration.

Table 4. Results for Artificially Aged SBS Modified Binder

Aging Time(h)	Penetration Grade Tests			SHRP Binder Tests			
	Penetration 25℃ (0.1mm)	Softening Point(℃)	Ductility 5℃(cm)	Viscosity 135℃ (Pa • S)	G*/sin δ ,64℃ (MPa)	S,-12℃ (MPa)	M -12℃
0	65	63	37	1.21	3.52	36.1	0.519
5	49	68.2	15	1.71	9.85	68.6	0.471
10	42	70	7	2.16	12.4	79.6	0.449
15	35	71.5	2	2.49	14.6	88.3	0.417
20	30	72.1	0	2.87	16.7	95.6	0.396

Table 5. Results for Artificially Aged SBS Modified Binder Mixture

Aging Time(h)	Bending Test of Small Beam		High Temperature Performance	Low Temperature Performance	
	Limit Flexural Tensile Strength (MPa)	Fracture Energy(J)	Dynamic Stability(/times)	Limit Flexural Tensile Strength -10℃(MPa)	Limit Flexural Strain-10℃(μ ε)
0	3.436	2.365	2526	7	2232
5	4.21	1.96	3612	7.865	1980
10	5.22	1.81	4325	8.5	1710
15	6.33	1.542	4950	9.095	1642
20	7.033	1.242	5321	9.66	1520

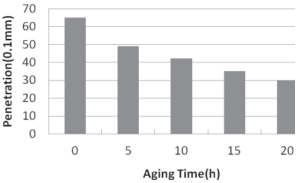

A Penetraion

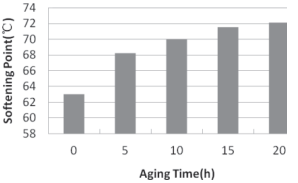

B Softening Point

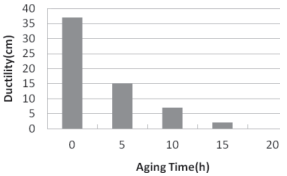

C Ductility

FIG. 1. Influence of Aging Time on Penetration Grade Tests.

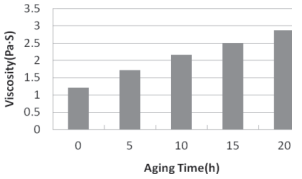

A Viscosity

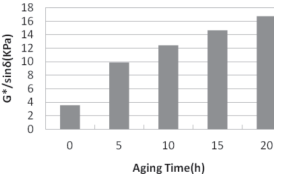

B G*/sinδ(KPa)

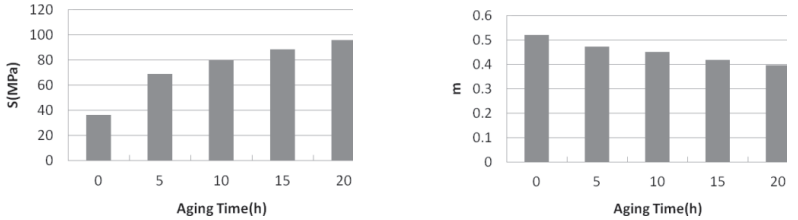

C S D m value

FIG. 2. Influence of Aging Time on SHRP Binder Tests.

Dynamic stability values for aged mixture with different aging time are showed in Fig. 3. The dynamic stability increases linearly with the increasing of aging time. Limit flexural tensile strength and limit flexural strain values for aged mixture with different aging time are showed in Fig. 4. The limit flexural tensile strength increases linearly with the increasing of aging time, and the limit flexural strain decreases linearly with the increasing of aging time. The property variations of aged mixture and binder are the same. The properties of aged binder could be reflected by aged mixture when the parameters of the mixture keep constant.

To evaluate the degree of hard and brittle of aged mixture, a destructive testing is needed. The asphalt mixture is a kind of viscoelastic material. There are not relationships on performances at different temperature for different materials, but for the same material. If the aged asphalt mixture is harder (aging seriously), it would be good at resistance to external loads than that whose aging time is different (the original mixture is the same), it's bad at resistance to deformation. So the properties at different temperature could be obtained by one test.

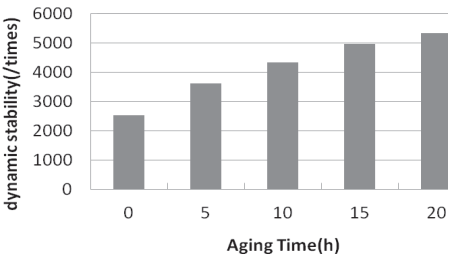

FIG. 3. Influence of Aging Time on High Temperature Performance(60℃).

The performances of aged mixture whose aging time was different at different temperature could be reflected by one test. Bending Test of Small Beam is taken, and the results are shown in Fig. 5~6. Limit flexural tensile strength values for aged mixture with different aging time are showed in Fig. 5. The limit flexural tensile

strength increases linearly with the increasing of aging time. Fracture energy values for aged mixture with different aging time are showed in Fig. 6. The fracture energy decreases linearly with the increasing of aging time.

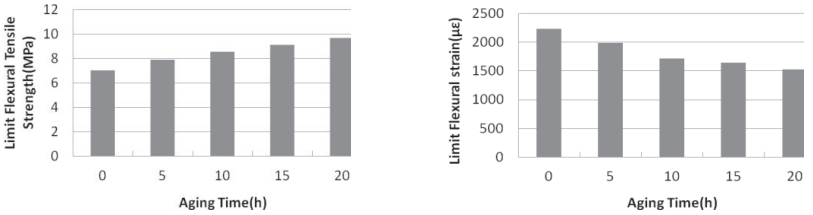

A Limit Flexural Tensile Sturngth B Limit Flexural Strain

FIG. 4. Influence of Aging Time on Low Temperature Performance (-10℃).

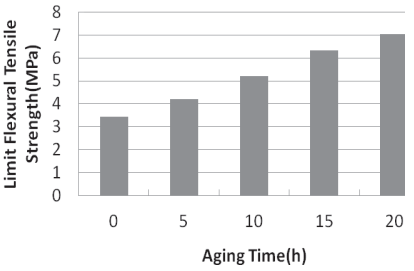

FIG. 5. Influence of Aging Time to Limit Flexural Tensile Strength

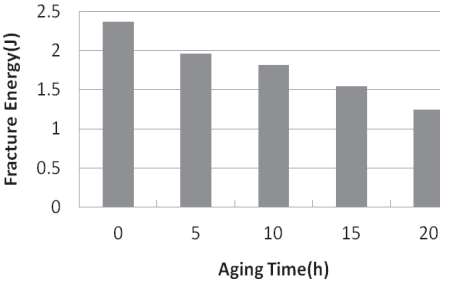

FIG. 6. Influence of Aging Time to Fractures Energy

Evaluation of Mixture Recycling

Test results for regenerated SBS modified binder and mixture were shown in Table 6~9. Limit flexural tensile strength and fracture energy curves for recycling mixture with different recycling agent percentage and types are showed in Fig. 7~8. The limit flexural tensile strength of recycling mixture increases linearly with the increasing of recycling agent content. The fracture energy of recycling mixture increases first and then decreases.

Different types of rejuvenator have different recycling effects on aged asphalt binder. However, the recycling targets to restore the pavement performances of different rejuvenators are basically the same. Toughness of the aged mixture is the most needed to restore. It is necessary to select a rejuvenator that can obtain the highest quality on crack resistance. So the fracture energy is an important index for regenerated mixture.

Table 6. Results for Regenerated SBS Modified Binder Mixture

Content of Recycling Agent(%)	Regenerated Mix A		Regenerated Mix B	
	Limit Flexural Tensile Strength (MPa)	Fracture Energy(J)	Limit Flexural Tensile Strength(MPa)	Fracture Energy(J)
0	7.033	1.242	7.033	1.242
3	5.103	1.613	5.415	1.721
6	3.742	1.621	4.056	1.956
9	3.125	1.432	3.674	1.685
12	2.901	1.293	3.265	1.418

Table 7. Results of Penetration Grade Tests for Regenerated Binder

Recycling Agent	Content of Recycling Agent (%)	Penetration Grade Tests		
		Penetration 25℃(0.1mm)	Softening Point(℃)	Ductility 5℃(cm)
A	**0**	27	72.1	0
	3	39.5	68.1	10.7
	6	48.9	63	12.2
	9	61.8	59.9	15.1
	12	73.6	56.8	17
B	**0**	27	72.1	0
	3	36.5	68.9	13.6
	6	45	66.1	17.2
	9	54	63	21.5
	12	63	59.9	25.8

Table 8. Results of SHRP Binder Tests for Regenerated Binder

Recycling Agent	Content of Recycling Agent (%)	SHRP Binder Tests			
		Viscosity,135℃ (Pa • S)	G*/sin δ ,64℃ (MPa)	S,-12℃ (MPa)	m,-12℃
A	**0**	2.87	16.7	95.6	0.396
	3	1.79	8.82	75	0.421
	6	1.43	5.92	59	0.439
	9	0.97	4.22	46	0.46
	12	0.51	3.78	35	0.483
B	**0**	2.87	16.7	95.6	0.396
	3	2.2	9.78	76	0.41
	6	1.96	7.8	62	0.429
	9	1.48	5.2	50.5	0.442
	12	1	4.5	38	0.461

Table 9. Results on Performances for Regenerated Mixture

Recycling Agent	Items	New Way	Traditional Way
Regenerated Mix A	Dynamic stability(/times)	2150	1642
Regenerated Mix B	Dynamic stability(/times)	2561	1892
Regenerated Mix A	Limit Flexural strain,-10℃(με)	2120	2812
Regenerated Mix B	Limit Flexural strain,-10℃(με)	2351	3036

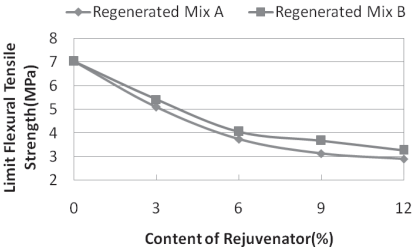

FIG. 7. Influence of Rejuvenator Content to Limit Flexural Tensile Strength.

The regression equation of fracture energy is showed in Table 10. With a content of 4.1% rejuvenator A, the regenerated mixture A gets the highest fracture energy, which means that it gets the highest toughness. With a content of 6.7% rejuvenator B, the regenerated mixture B gets the highest fracture energy, this means that it gets the highest toughness. The rejuvenator B is better than A on restoring the toughness of

regenerated mixture. So rejuvenator B is selected.

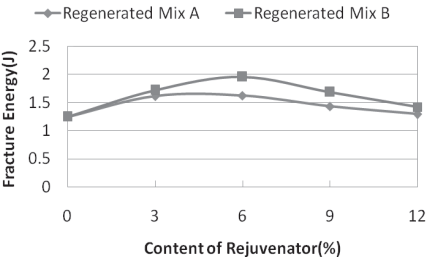

FIG. 8. Influence of Rejuvenator Content on Fracture Energy.

Table 10. Regression Equation of Fracture Energy

	Regression Equation	R^2
Regenerated Mix A	$y = 0.001x^3 - 0.032x^2 + 0.211x + 1.240$	0. 999
Regenerated Mix B	$y = -0.015x^2 + 0.200x + 1.255$	0. 952

Y-Fracture Energy, X-Content of Recycling Agent

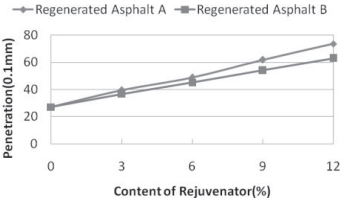

A Penetration

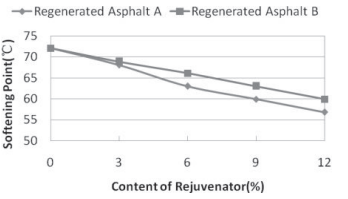

B Softening Point

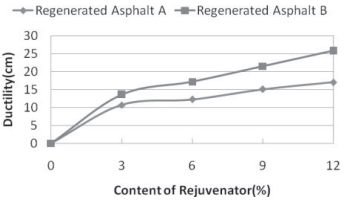

C Ductility

FIG. 9. Influence of Rejuvenator Content on Penetration Grade Tests.

Penetration, softening point and ductility curves for recycling mixture with different recycling agent percentage and types are showed in Fig. 9. The Penetration, softening point and ductility increases linearly with the increasing of recycling agent

content. According to the specification in China, the contents of rejuvenator A and B are 9% and 11% respectively.

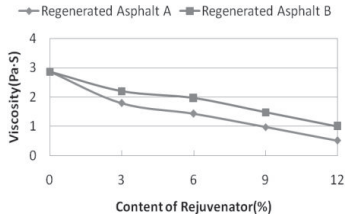

A Viscosity

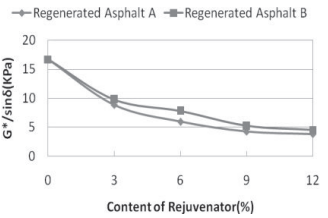

B G*/sinδ(64℃)

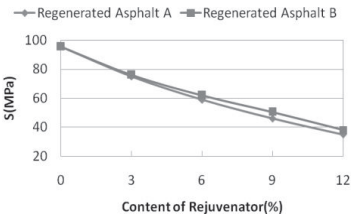

C S(-12℃)

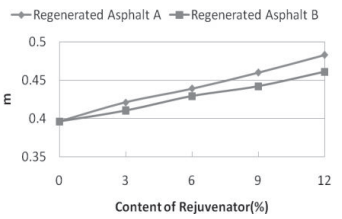

D m(-12℃)

FIG. 10. Influence of Rejuvenator Content on SHRP Binder Tests.

Viscosity, G*/sin δ, S, m curves for recycling mixture with different recycling agent percentage and types are showed in Fig. 10. The Viscosity, G*/sin δ, S decreases linearly with the increasing of recycling agent content. The m increases linearly with the increasing of recycling agent content. Although it could tell which rejuvenator is better on different performance of binder, it's different to regenerate mixture and binder. Because the regenerated binder is mixed uniformly, but regenerated mixture isn't. SHRP binder test couldn't be used to reflect the performances of regenerated mixture.

Comparison test results for different designing method are showed in Fig. 11~13. The properties of regenerated mixture designed by the new way are better than those designed by the traditional way on high temperature and fatigue performance according to Fig. 11, 13. The high temperature performance of regenerated mixture A and B don't meet the specification in China (>2000 times). The low temperature performances of regenerated mixture designed by the two ways are both qualified(>2000 με) as shown in Fig. 12. The reason is that there is too much rejuvenator in regenerated mixture designed by traditional method. The rejuvenator and the aged binder can't mix totally, so evaluation of regenerated mixture by testing mixture is necessary.

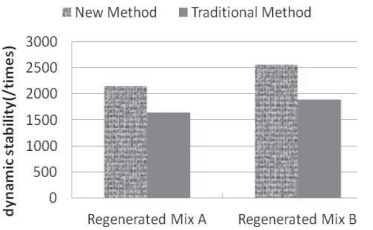

FIG. 11. Influence of Designing Methods on High Temperature Performance

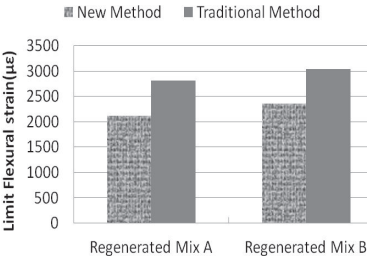

FIG. 12. Influence of Designing Methods on Low Temperature Performance

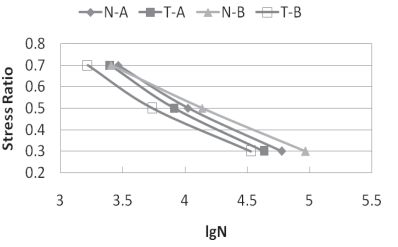

FIG. 13. Influence of Designing Methods on Fatigue Performance

Table 11. Fatigue Equations

Mixture	Regression Equation	R^2
NA	y = −0.302x + 1.734	0.992
TA	y = −0.320x + 1.775	0.99
NB	y = −0.256x + 1.568	0.998
TB	y = −0.300x + 1.650	0.985

NA-New Method, Recycling Agent A. TA-Traditional Method, Recycling Agent A. NB-New Method, Recycling Agent B
TB-Traditional Method, Recycling agent A

CONCLUDING REMARKS

In this study, a new procedure to estimate aging and recycling characteristics of SBS modified mixture without extraction and recovery was studied. Bending test of small beam was taken to evaluate the aged mixture. The conclusions were as follows: The main factor of mixture aging was the thickness of asphalt film. Aged mixture became much harder and brittler and the regenerated mixture became much softer and more flexible. The target of recycling is to make the regenerated mixture more flexible, but not much softer. Limit flexural tensile strength and fracture energy could reflect the degree of hardness and brittleness. The species and amount of recycling agent could be determined by fracture energy.

More work is needed to try other RAP sources and fresh binders. Low and high temperature properties should be considered for estimating aging and recycling properties of RAP.

REFERENCES

Al-Qadi, I.L.,Mostafa, E. and Carpenter, S.H. (2007). "Reclaimed asphalt pavement-a literature review." Illinois Center for Transportation Series No. 07-001

Abson, G. (1933). "Method and Apparatus for the Recovery of Asphalt." New Yorker: American Society for Testing and Materials Press.

Brule, B. (1996). "Polymer-Modified Asphalt Contents Used in the Road Construction Industry: Basic Principles." *Journal of the Transportation Research Board*, 1535:48–53.

Bautista, E.G. (2008). "Evaluation of Rheological Properties of Binders in RAP without Extraction and Recovery." Transportation Research Board 88th Annual Meeting.Paper No. 09-3076

Carey, D. E. and Paul, M. R. (1982). "Evaluation of Asphalt Cement Extraction and Recovery Methods." FHWA, U.S. Department of Transportation.

Codrin, Daranga. (2005). "Characteration of Aged Polymer Modified asphalt binders for Recycling Purposes." Doctor of Philosophy in Agricultural and Mechanical College, Louisiana State University, USA.

Edinçliler, A., and Baykal G. (2004). "Determination of static and dynamic behavior of recycled materials for highways." *Resources, Conservation and Recycling*.

Hao, Y.K. and Xiao, J.Y. (2004). "High Performance Composite Materials Science." Chemical Industry and Engineering Press, Beijing.Li, X., Marasteanu, M., Williams, R.C. and Clyne, T.R. (2008). "Effect of Reclaimed Asphalt Pavmeent (Proportion and Type) and Binder Grade on Asphalt Mixtures." *Journal of the Transportation Research Board,* 2051:90-97.

Ma, T., Huang, X.M. and Zhang J.P. (2008). "Recycling Law of Aged Asphalt Based

on Composite Theory of Material." *Journal of Southeast University,*.Vol. 38:520–524.

Ma, T., Mahmoud, E., and Bahia, H.U. (2010). "Development of Testing Procedure for the Estimation of RAP Binder Low-Temperature Properties without Extraction." Transportation Research Board 89th Annual Meeting

Petersen, J.C. (1984). "Chemical Composition of Asphalt as Related to Asphalt Durability: State of Art." *Transportation Research Record,* 999:13-30.

Rubino, B., and Ashlock J.C. (2010). " Effect of recycled asphalt shingles on mechanical properties of loess." TRB 2010 Annual Meeting CD-ROM.

Robinette, C. and Williams, R.C. (2006). "The Effects of the Testing History and Preparation Method on the Superpave Simple Performance Test." *Asphalt Paving Technology, Association of the Asphalt Paving Technologists*, Vol. 75:297 – 320.

Shen, J. (2001). "Road Performance of Asphalt and Asphalt mixture." China Communication Press, Beijing.

Thomas, B. and Dongré R. (2010). "A Backcalculation Method to Determine "Effective" Asphalt Binder Properties of RAP Mixtures." TRB 2010 Annual Meeting CD-ROM

Welborn, J.Y. (1984). "Physical Properties as Related to Asphalt Durability: State of the Art." *Transportation Research Record,* 999:31-36.

Ageing Prediction of Porous Asphalt

M.F.C. van de Ven[1], Y. Jemere[2], A.A.A. Molenaar[3] and M.M.J. Jacobs[4]

[1]Associate Professor, Faculty of Civil Engineering and Geosciences, Delft University of Technology, 2600 GA Delft, the Netherlands; email: m.f.c.vandeven@tudelft.nl
[2]Master Graduate, Faculty of Civil Engineering and Geosciences, Delft University of Technology, 2600 GA Delft, the Netherlands;
[3]Professor, Faculty of Civil Engineering and Geosciences, Delft University of Technology, 2600 GA Delft, the Netherlands; email:a.a.a.molenaar@tudelft.nl
[4]BAM Wegen, the Netherlands; email: m.jacobs@bamwegen.nl

ABSTRACT: In order to be able to make a realistic life cycle analysis for porous asphalt (PA) surface layers it is very important to be able to predict the PA surface layer properties during service life. As ageing of these very high voids content mixes will change properties dramatically and initiate ravelling as the major cause of failure, in depth knowledge of the field ageing of a PA layer is needed. In this paper a study is reported to develop a laboratory ageing procedure for PA mixtures. The aim was to realize approximately 10 years of field ageing in 10 days in a laboratory ageing procedure with standard laboratory equipment. Conventional empirical (penetration, softening point ring and ball), sophisticated fundamental rheological tests (DSR), chemical tests (FTIR) and adhesion tests (Wilhelmy plate) were conducted on binders recovered from field cores and on binders recovered from specimens aged in the laboratory. Several ageing methods were tried, resulting in two promising ageing procedures: one for the mortar in PA and one for the loose PA mix. To accomplish the same ageing of the bitumen as for a 10 year period in the field, the mortar has to be heated in an oven for 2 hours at 165°C and then be placed in a PAV at 90°C for 7 days under air pressure of 2.1 MPa. The loose PA mix was heated for 44 hours at 135ºC to accomplish the same degree of ageing.

INTRODUCTION

Since 1990 single-layer Porous Asphalt (thickness 50 mm) is applied on Dutch motorways as a standard wearing course for noise reduction. Generally PA has a lower service life in comparison with dense asphalt mixtures. Ravelling at the surface is the dominant damage determining the service life of PA. The ageing of the mortar is an important reason for ravelling.

During the design phase of a pavement structure, it is important to know

beforehand what the properties of the wearing course will be after field ageing. The structural design is important for the long term behaviour.

The service life of the wearing course can be predicted with an accelerated laboratory ageing procedure that can produce binder properties similar to field aged binder. In the literature only few researches are reported on ageing of PA mixtures (Khalid, H.A., 2002; Airey, G.D., 2003; ISAC, 2006; Hagos, E., 2008; Mo, L., 2010). In this study the objective was to develop a laboratory ageing procedure resulting in binder properties similar to 10 years field aged PA within 10 days in a lab using standard laboratory equipment.

In this paper first the research program is discussed (Jemere, Y., 2010). Then the characteristics of the reference material are discussed. The results of the various ageing procedures on bitumen, mortar and mix properties are analyzed and the conclusions and recommendations are given.

PROPERTIES OF THE REFERENCE AND LABORATORY MATERIALS

In order to compare accelerated laboratory ageing with field ageing, cores were taken from a 10 years old PA pavement taking into account the age or service period of the pavement. Specimens from a 10 year old PA pavement were cored and used as reference material. The cores were taken from the Motorway A4 near Burgerveen in the Netherlands. The cores were taken from the emergency lane of the pavement in order to avoid the effect of the traffic and noxious waste. The effect of clogging due to the absence of traffic of the emergency lane on the aging of the mortar is negligible, because the emergency lane is kept clean regularly with vacuum cleaners.

The field PA specimens were cut into two horizontal segments: the upper and lower part. The binder recovery process was conducted separately for these two parts. The properties of the recovered binder of the upper part of the PA layer are used as the reference.

From the 10 years old PA on the A4 motorway, the mix components are known. The same materials were used in the laboratory research. In Table 1 the mix composition of the PA is given.

Table 1. Mix composition of the PA on the A4 motorway near Burgerveen

Mix component	Mass percentage in the mix [%]	Density [kg/m^3]
Crushed gravel river Rhein 11/16	17.8	2650
Crushed gravel river Rhein 8/11	41.3	2659
Crushed gravel river Rhein 4/8	22.6	2665
Granite crusher sand	10.1	2650
Wigro 60K filler containing 25% $Ca(OH)_2$	3.9	2570
Pen grade bitumen 70/100	4.3	1035
Total	100.0	

A penetration grade bitumen 70/100 is commonly used in the Netherlands in a PA

mix. The properties of this bitumen are presented in Table 2.

Table 2. Properties of the used bitumen

Bitumen	Penetration [0.1 mm]	Softening Point [ºC]	Penetration Index [-]	Density [kg/m^3]
70/100	70	44.6	-1,9	1025

The material preparation can be broadly categorized into two main groups based on the type of specimens to be aged. In this research, both a mortar and a loose mixture were aged.

The mortar used in this study consisted of bitumen, filler and fine sand smaller than 0.5 mm, mixed at a mass ratio as shown in table 3. This mass ratio is based on the mass ratio in the PA mix from the A4 motorway given in Table 1. The reason for adding the fine sand fraction is that in previous research (Muraya, P.M., 2007) it was found that the aggregate skeleton of PA only consists of aggregates larger than 0.5 mm. This means that the mortar in PA can be defined as a mixture of bitumen and the fraction smaller than 0.5 mm. The sand percentage (m/m) in the mortar has been determined by using the total sand percentage in the asphalt mixture (see Table 1) and by multiplying this value with the percentage of the sand fraction less than 0.5 mm. The final mortar composition is shown in Table 3.

Table 3. Mortar composition of the Motorway A4 PA mixture

Mortar components	Mass percentage in the mortar [%]
Granite crushed sand (between 0.5 mm and 0.063 mm)	28.4
Filler (Wigro 60K) containing 25% $Ca(OH)_2$	34.1
Pen grade bitumen 70/100	37.5
Total	100.0

AGEING PROTOCOLS

In the Netherlands the filler part of a PA mixture has to contain at least 25% of hydrated lime, $Ca(OH)_2$. It is reported that hydrated lime in the PA mixture has influence on the rheological behaviour of the bitumen itself (ISAC, 2006; Johansson, L.S., 1995). So it is well known that hydrated lime has a strong influence on bitumen hardening and ageing. Based on this information it was decided to age the mortar and the mixture and not only the bitumen. In this way the influence of aggregate, sand and filler, or at least sand and filler on the ageing is included.

At the start three different ageing protocols were investigated in a first phase of the research program.

Ageing protocol 1: The mortar is short term aged and then long term aged in a pressure ageing vessel (PAV)

First bitumen, filler and sand were mixed at a temperature of 155 ºC for 3 minutes to make the mortar ready for short term ageing. After preparation of the mortar, 50 grams was poured on a circular steel plate with a diameter of 140 mm. The mortar was subjected to short term ageing (STA) at a temperature of 165ºC in an oven for two hours. After the short term ageing, long term ageing (LTA) was carried out in a PAV at a temperature of 80ºC and a pressure of 2.1 MPa (300 psi) for 7 days. After LTA the specimens were heated in an oven to 150ºC for 30 minutes to remove the aged samples from the circular plates for further testing.

Ageing protocol 2: The PA mixture is short term aged, then compacted and long term aged in a PAV.

After mixing the loose asphalt mixture was short term aged in an oven at 135 ºC for 4 hours. Every hour the mixture was turned and stirred similar to the SHRP studies. The short term aged mixture was heated to a temperature of 155ºC and compacted with a gyratory compactor to produce a cylindrical specimen of 100 mm diameter and a height of 50 mm. The compacted specimens were placed in a PAV at a pressure of 2.1 MPa for 7 days. During this period, the temperature was increased in two steps (70ºC for the first 3 days and 80ºC for the last 4 days).

Ageing protocol 3: The loose PA mixture is short term aged and then long term aged in an air forced ventilated oven.

In this protocol, a similar procedure like in RILEM TC-ATB-TG5 is used (De la Roche, C., 2009). 5 kg of loose PA mixture was placed in a steel box with dimensions 50×30×8 cm. The loose mix is placed in an air-draft ventilated oven for 4 hours at 135ºC to simulate short term ageing. Each hour the material is stirred for 1 minute and placed back into the oven. After this short term ageing, long term ageing of the loose mixture was performaed in an air ventilated oven at a temperature of 85ºC for 7 days.

The effect of these three ageing protocols has been examined (Jemere, Y., 2010). From the three preliminary proposed ageing protocols, protocol 2 failed already in the competition at the early stage due to the fact that the specimens were highly deformed/damaged and a lot of mortar/bitumen was drained to the bottom of the plate after 7 days. Recovery of the bitumen was not possible anymore so a comparison with field data was not an option. Therefore it was decided to delete protocol 2 as ageing protocol. The results from protocol 1 and protocol 3 are discussed further.

Based on the results protocol 1 and 3 were found to simulate the field ageing better.

TESTING PROGRAM

In order to compare field and laboratory ageing, rheological, chemical and adhesion tests were conducted on binders recovered from field cores and on binders recovered from specimens that were subjected to laboratory ageing.

The possibility that the use of a standard bitumen recovery process like soxhlett extraction may have influence on the recovered bitumen was also investigated. All the rheological and chemical tests mentioned in this part were also carried out on a bitumen sample which passed through the standard recovery process and on a bitumen sample not exposed to the recovery process.

The testing program consisted of the following tests for each group. Conventional empirical rheological tests: penetration (EN 1426) and softening point ring and ball (EN 1427);

Fundamental mechanical test: the complex shear modulus and phase angle determination of the binders were determined at different temperatures with the Dynamic Shear Rheometer (EN14470).

Frequency sweeps between 0.01-400 rad/s were conducted at seven temperatures (-10, 0, 10, 20, 30, 40 and 50ºC). For the lower temperatures (below and at 20ºC), an 8 mm diameter plate with a sample thickness of 2 mm was used and for higher temperatures (above 20ºC) a plate with a diameter of 25 mm and a sample thickness of 1 mm was used. Before starting the test and during a change in test temperature, the samples were first brought at the test temperature and conditioned for at least 10 minutes. The results of the DSR-tests in this paper are presented in the form of the master curve of the stiffness and the phase angle using the shift factors of the WLF-approach (Jemere, Y., 2010).

The chemical characterization of binders was conducted using Fourier Transform Infrared spectroscopy (FTIR). FTIR spectroscopy makes use of the Infrared part of the electromagnetic spectrum. The main reason for using FTIR was to follow the fact that it is believed that ageing affects the chemical composition of the bitumen during ageing. Infrared spectroscopy is a widely used technique to identify functional groups in organic compounds and to identify the chemical composition of materials at molecular level. Absorption of this lower energy radiation from infrared causes vibrational and rotational excitation of groups of atoms within the molecule. In analysing the FTIR-results, the procedure of De la Roche is used (De la Roche, C., 2009).

The surface energy determined with the Wilhelmy plate test was used as an indicator for the adhesion property of bitumen. The Wilhelmy plate test is based on kinetic force equilibrium when a thin plate, suspended from a highly accurate balance, is immersed or withdrawn from a liquid (water, glycerol and diiodomethane) at a very slow and constant speed (Bhasin, A., and Little, D.N., 2006). The dynamic contact angles that develop between the bitumen coated glass plates and liquids are obtained. The dynamic contact angle measured during the immersion process is called the advancing contact angle (a wetting process), while the dynamic contact angle measured during the withdrawal process is called the receding contact angle.

DISCUSSION OF TEST RESULTS

In this chapter the results and analysis of the test data on recovered bitumen after the ageing of the mortar and loose mixture are given. The results of the recovered bitumen test results for the three laboratory ageing methods are compared with the reference recovered field aged bitumen results. The effect of the binder recovery procedure on the properties of the binder was also investigated and no influence was reported (Jemere, Y., 2010).

Comparison of preliminary ageing protocols with field result

The field cores were horizontally cut into two segments both approximately 2.5 cm thick and the binder recovery were conducted separately for the upper and lower part. The upper part of the PA layer was considered the critical one, because ravelling takes place at the surface of the pavement.

The recovery method used was the same for the bitumen from specimens aged in the laboratory and bitumen from the field cores.

In Table 4, Figure 1 and Figure 2 some results of the ageing protocols 1 and 3 are given and compared to the 10 years field aged specimens.

Table 4. Test results field cores and ageing protocols 1 and 3

Property	Protocol 1	Protocol 3	Field aged upper part	Field aged lower part
Empirical tests				
Penetration [0.1 mm]	19	27	12	17
Softening Point [ºC]	60.0	55.2	67.6	63.0
Penetration Index [-]	-1.0	-1.3	-0.5	-0.6
WLF parameters DSR-test				
C1	11.6	17.8	28.7	20.4
C2	96.9	137.0	206.1	169.2
Wilhelmy Plate tests				
γ^{total} (advancing)	26.79	29.86	33.33	38.50
γ^{LW} (advancing)	24.89	29.86	33.33	37.04
γ^{+} (advancing)	6.90	4.79	3.75	1.13
γ^{-} (advancing)	0.13	0.00	0.00	0.47
γ^{total} (receding)	41.40	42.28	38.39	40.90
γ^{LW} (receding)	39.01	42.28	38.39	40.90
γ^{+} (receding)	0.04	0.00	0.00	0.00
γ^{-} (receding)	33.22	29.70	48.93	26.21
FTIR tests				
Ico	0.0382	0.0170	0.0462	0.0206
Iso	0.1307	0.1063	0.1867	0.1307

Property	Protocol 1	Protocol 3	Field aged upper part	Field aged lower part
1700 peak height	0.0078	0.0045	0.0099	0.0048
1030 peak height	0.0139	0.0136	0.0189	0.0141

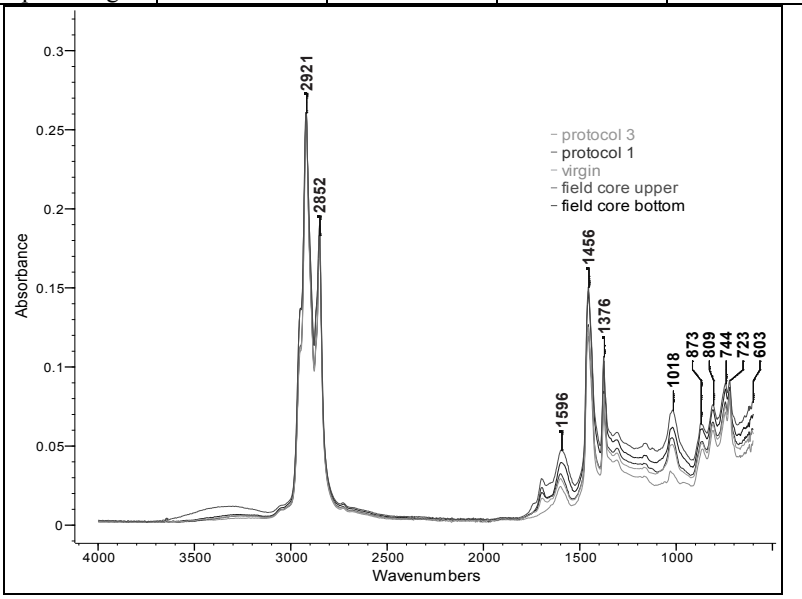

FIG. 1. Infrared spectra over large wavember region

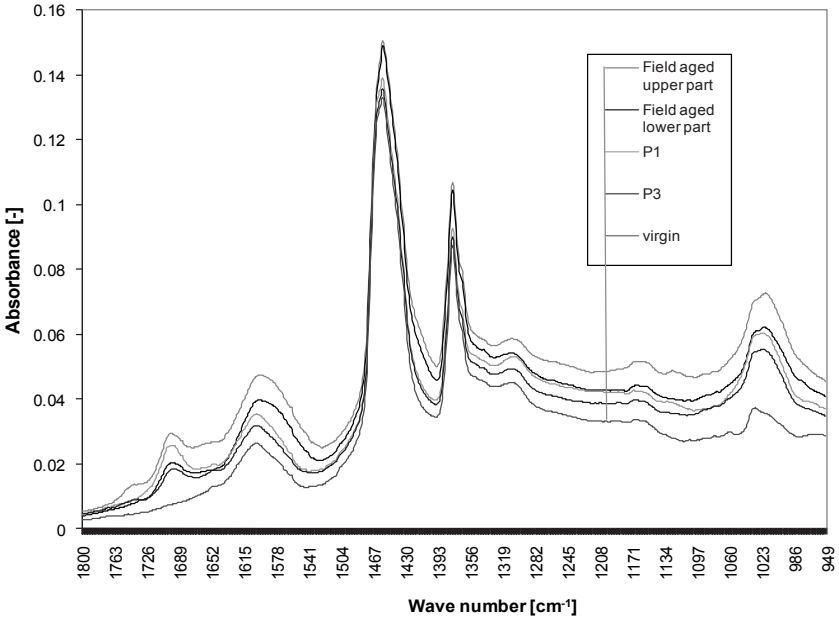

FIG. 2. Infrared spectra over 'finger-print' region

From the test results in Table 4 it was not possible to give a general trend for the surface energy in relation to the ageing of the bitumen for all the test samples. Since ageing leads to the formation of weak bases and acids such as ketones and sulfoxides, the net effect on the surface energy components due to ageing will depend on the initial chemical nature of the asphalt binder and the dynamics of various functional groups during the ageing process. Other possible reasons for this may be a difference in bitumen type (difference between bitumen used in the laboratory ageing protocols and the one used to build the pavement from which the field samples were cored). The purity of the chemicals (liquids) used for the test and the higher sensitivity of the test for the thickness and width measurement of the glass plate coated with bitumen might be additional reasons. The results in table 4 show that the total surface energy computed by using receding angles is higher compared to the advancing angles. The same trend has been reported by other researchers (Van Lent, D.Q., 2008; Little, D.N., 2005). The results also show that the LW component (free energy of Lifshitz-Van der Waals forces) is the most significant contributor to the total surface energy of the asphalt binders, while the magnitudes of acid and base components are very small. This is in line with the fact that most asphalt binders are weak polar materials.

From the test results in table 4 it can be seen that:

- The penetration and softening point for binder recovered from the upper and the lower part of the field cores are different. The upper part shows a higher degree of ageing compared to the lower part of PA;

– A comparison of the penetration and softening point values shows that the laboratory ageing protocol 1 and 3 were not severe enough to simulate the ageing of the top part of PA layer in the field. The results from ageing protocol 1 are close to the results from the lower part of PA from the field. The results from protocol 3 are far away from both the lower and upper part of PA from field;

From the spectra in Figure 1 and 2 and the computed indices and peak heights in Table 4 for C=O (wavenumber 1700 cm^{-1}) and S=O (wavenumber 1039 cm^{-1}) it can be seen that the material from the upper part of the 10 year old pavement has the highest peaks both at the C=O and S=O band. Protocol 1 gives the second highest peak and area at the C=O band. The lower part of the PA layer has a similar peak at the S=O band with Protocol 1. The binder from Protocol 3 has the lowest peak at 1030 cm^{-1} and 1700 cm^{-1} wave numbers of all aged bitumens. From the FTIR result, the change in C−C band (1600 cm^{-1}) is also apparent and field aged cores show the highest peaks. In general the spectrum line for field aged samples stays above the laboratory aged samples for the whole range of the finger print region except at 1700 cm^{-1} where Protocol 1 gives results above the lower part of field PA. These results are in full agreement with the empirical and fundamental rheological test results from the other tests

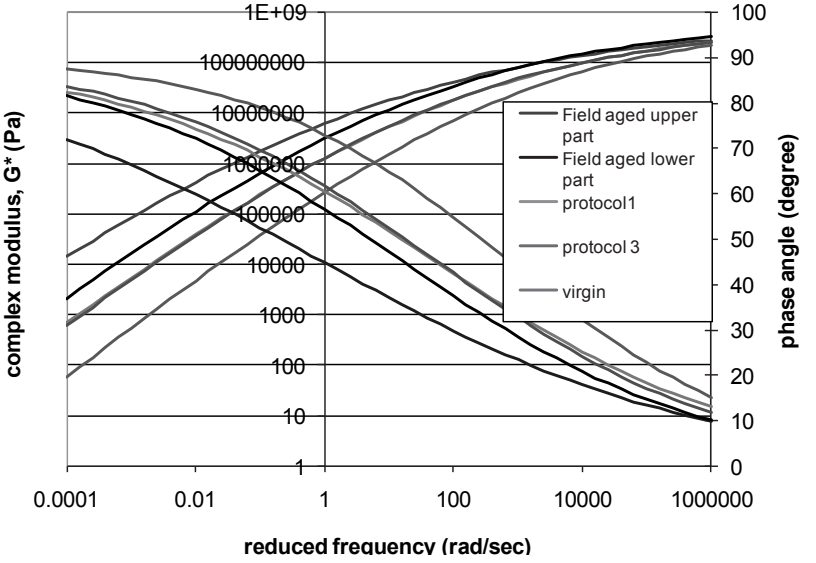

FIG. 3. Master curves for the recovered bitumen from field cores and specimens after ageing protocol 1 and 3 at a reference temperature of 20 °C

The DSR results are summarised in Figure 3 and they show similar trends as the penetration and softening point results. Bitumen recovered from the upper and lower part of field cores gives a higher complex modulus and lower phase angle compared

to the laboratory aged bitumen. The master curves of protocol 1 and protocol 3 give very similar results. The complex modulus for protocol 1 is positioned slightly above the curve for protocol 3 and the reverse is found for the phase angle curves. The comparison of complex modulus and phase angle test results of laboratory and field aged specimens confirm the fact that the laboratory ageing protocol 1 and 3 were not severe enough to simulate field ageing of PA.

In general the penetration, softening point, DSR and the FTIR test results for all the bitumen samples are in good agreement with each other. The analysis of the test results have shown clear differences in the rheological and chemical properties of the laboratory aged and field materials.

It can be seen from the results that protocol 1 and 3 are not severe enough to simulate 10 years of field ageing for the top part of the PA layer. Fortunately protocol 1 and 3 can be revised easily to provide higher ageing levels.

Revision of the ageing protocols 1 and 3

It was concluded that the used ageing protocols were not severe enough to get similar ageing in the lab similar to 10 years of ageing in the field. For this reason both protocols were changed:

- For protocol 1 the temperature for the long term ageing was raised from 80 to 90 (protocol 1B) and from 80 to 100ºC (protocol 1A);
- For protocol 3 the temperature of the long term ageing was raised to 135ºC and the period of long term ageing was shortened to 42 (protocol 3A) and 46,5 hours (protocol 3B);

In Table 5 the effect of the changed protocols on the various parameters are given.

Table 5. Test results field cores and ageing protocols 1A, 1B, 3A and 3B

Name	Protocol 1A (80→100ºC)	Protocol 1B (80→90ºC)	Protocol 3A (85→135ºC for 42 hours)	Protocol 3B (85→135ºC for 46,5hours)	Field aged upper part
Empirical tests					
Penetration [0.1 mm]	9	14	19	10	12
Softening Point [ºC]	73.6	65.4	63.4	76.4	67.6
Penetration Index [-]	0.0	-0.6	-0.4	0.5	-0.5
WLF parameters DSR					
C1	28.0	28.0	31.0	28.0	28.7
C2	213.0	205.0	220.0	219.0	206.1
Wilhelmy Plate tests					
γ^{total} (advancing)	37.75	32.70	n.a.	n.a.	33.33

Name	Protocol 1A (80→100ºC)	Protocol 1B (80→90ºC)	Protocol 3A (85→135ºC for 42 hours)	Protocol 3B (85→135ºC for 46,5hours)	Field aged upper part
γ^{LW} (advancing)	34.99	32.70	n.a.	n.a.	33.33
γ^{+} (advancing)	3.52	4.05	n.a.	n.a.	3.75
γ^{-} (advancing)	0.54	0.00	n.a.	n.a.	0.00
γ^{total} (receding)	43.06	45.48	n.a.	n.a.	38.39
γ^{LW} (receding)	39.58	42.85	n.a.	n.a.	38.39
γ^{+} (receding)	0.15	0.17	n.a.	n.a.	0.00
γ^{-} (receding)	19.65	13.00	n.a.	n.a.	48.93
FTIR tests					
Ico	0.096	0.064	0.0351	0.0646	0.0462
Iso	0.1370	0.1892	0.1285	0.1598	0.1867
1700 peak height	0.0175	0.0107	0.0069	0.0106	0.0099
1030 peak height	0.0147	0.0182	0.0137	0.0152	0.0189

Based on the results given in table 5 it can be concluded that the bitumen from the mortar in the upper part of a field aged PA specimen and bitumen from a laboratory aged mortar using protocol 1B are quite similar. The penetration, softening point, DSR and FTIR test results of protocol 1B show comparable results with the upper part of field aged PA cores. The bitumen recovered from protocol 1B exhibit similar rheological (both empirical and fundamental) and chemical characteristics compared to bitumen recovered from the upper part of 10 years field aged PA. Therefore, it can be concluded that ageing protocol 1B can reasonably predict binder properties from 10 years field aged PA.

The chemical test results show that protocol 3A with an ageing period of 46.5 hours gives higher ageing and with ageing duration of 42 hours gives less ageing, compared to the upper part of field aged PA,. This means that, in order to get an ageing result comparable to field ageing, the ageing period for protocol 3 should be approximately 44 hours. However, this procedure is only validated for a 70/100 bitumen. For other bitumen types the aging procedure can be different.

CONCLUSIONS AND RECOMMENDATIONS

Based on the findings of this research project some conclusions and recommendations were formulated.

Conclusions:

- From the field cores it is found that the binder in the top part showed higher ageing compared to the lower part. This is caused by the fact that the top part is exposed to UV light, direct air and other environmental factors.
- As ravelling (loss of stones) is a surface phenomenon, the laboratory simulation of ageing in this research has targeted the properties of the upper part of the PA core;
- It was not possible to find a general trend for the adhesive properties of bitumen related to ageing. The surface energy results determined with the Wilhelmy plate test for bitumen samples at different levels of ageing show no consistent trend. The reasons are not know at this time however it might be due to the sensitivity of the Wilhelmy plate test to the thickness measurement of the bitumen samples and/or may be due to the integrity of the test liquids used;
- Ageing protocol 1B on mortar (2 hours at 165ºC and 7 days in a PAV at 90ºC and 2.1 MPa pressure) and ageing protocol 3 on mortar (44 hours at 135ºC; during the first 4 hours the mortar is stirred manually each hour) can very well predict bitumen properties after 10 years of field ageing in PA. The penetration, softening point, DSR, FTIR and Wilhelmy plate tests on recovered bitumen from the lab and field aged PA specimens show comparable results. For these ageing protocols standard ageing laboratory equipment was used.

Recommendations:

- It should be emphasized that in the ageing protocol only one porous asphalt mixture from the road has been used as a reference. The validity of the ageing protocol has to be verified using samples from various pavements with porous asphalt top layers;
- The ageing protocols were developed for a PA with 4.3 % standard bitumen 70/100. In case more bitumen is used or a different type of bitumen (e.g. a PMB), the protocols must be reconsidered;
- Further studies need to be done to investigate the possible change in the adhesive properties of bitumen due to ageing. Surface energy using the Wilhelmy plate test has been used in this research to assess and compare the adhesive property of field and laboratory aged bitumen samples. As already mentioned, it was not possible to fully use the test results of the surface energy to compare laboratory and field aged samples. For future studies it is recommended to determine the surface energy with the sessile drop test method instead or in addition to Wilhelmy plate test;
- In this study the Infrared spectrum characteristic peak heights and peak areas were used as chemical test. In addition to this method, however, it is recommended in future studies to also perform SARA (saturates, aromatics, resins and asphaltenes) classification.

REFERENCES

Airey, G.D. (2003) “State of the Art Report on Ageing Test Methods for Bituminous Pavement Materials”, *International Journal of Pavement Engineering*, 165-176.

Bhasin, A., and Little, D.N. (2006). “Using Surface Energy Measurements to Select Materials for Asphalt Pavement”, *National Cooperative Highway Research Program*, Washington, DC.

De la Roche, C., Van de Ven, M., Van den Bergh, W., Gabet, T., Dubois, V., Grenfell, J. and Porot, L. (2009). Development of a laboratory bituminous mixtures ageing protocol.”, *7th international RILEM symposium - Advanced Testing and Characterization of Bituminous Materials*, Rhodes Island, Greece, 2009.

Hagos. E. (2008). “The Effect of Aging on Binder Properties of Porous Asphalt Concrete”, *PhD Dissertation*, Delft University of Technology, Delft, The Netherlands.

Institut für Straßenwesen (ISAC). (2006). “Learning of the road”, RWTH University in Aachen, Germany.

Jemere, Y. (2010). “Development of a laboratory aging method for bitumen in porous asphalt”, *MSc. Thesis,* Delft University of Technology, Faculty of Civil Engineering and Geosciences.

Johansson, L.S. (1995). ”Influence of hydrated lime on bitumen hardening”, *Licensiate Thesis*, KTH, Sweden.

Khalid, H.A. (2002). “A new approach to the accelerated ageing of porous asphalt mixtures”, *Proceedings of the Institution of civil engineers*, 171-181.

Little, D.N., and Hefer, A. (2005). “Adhesion in Bitumen-Aggregate Systems and Quantification of the Effects of Water on the Adhesive Bond”, Texas Transportation Institute, Texas.

Mo, L. (2010). “Damage Development in the Adhesive Zone and Mortar of Porous Asphalt Concrete”, *PhD Dissertation*, Delft University of Technology, Delft, The Netherlands.

Muraya, P.M. (2007). “Permanent Deformation of Asphalt Mixtures”, *PhD Dissertation*, Delft University of Technology, Delft, The Netherlands.

RWTH. (2006). “Learning of the road”, Institut für Straßenwesen (ISAC) of the RWTH University in Aachen, Germany.

Van Lent, D.Q. (2008). “Aggregate characterisation in relation to bitumen-aggregate adhesion”, *MSc. Thesis*, Delft University of Technology, Delft.

Increasing the Service Life of Porous Asphalt with Rejuvenators

Yuan Zhang[1], M.F.C. van de Ven[2], A.A.A. Molenaar[3] and S. Wu[4]

[1]PhD student, Road and railway engineering, Faculty of Civil Engineering and Geosciences, Delft University of Technology, Delft 2628 CN, the Netherlands; email: Y.Zhang-2@tudelft.nl
[2]Associate professor, Road and railway engineering, Faculty of Civil Engineering and Geosciences, Delft University of Technology, Delft 2628 CN, the Netherlands; email: M.F.C.vandeVen@tudelft.nl
[3]Professor, Road and railway engineering, Faculty of Civil Engineering and Geosciences, Delft University of Technology, Delft 2628 CN, the Netherlands; email: A.A.A.Molenaar@tudelft.nl
[4]Professor, State Key Laboratory of Silicate Materials for Architectures, Wuhan University of Technology, Wuhan, 430070, P.R. China; email: wusp@whut.edu.cn

ABSTRACT: The combination of load repetitions and severe environmental conditions (aging, moisture ingression, etc.) are causing ravelling (losing of the stones at the top) of porous asphalt. Ravelling has a strong influence on the service life, especially in the slow lane. The service life of porous asphalt can be extended by improving the self-healing capability in time. In this paper the rejuvenation approach is described to upgrade the self-healing capability during service life. With this approach, the porous asphalt is rejuvenated from outside at the top in order to regain the self-healing capability. Experience with some test trials is described. After the treatment with rejuvenators, the beams from the single-layer porous asphalt show a higher bending stiffness in the 3-point bending test. The beams from the two-layer porous asphalt show a lower bending stiffness after treatment. The results of Rotating Surface Abrasion Test (RSAT) indicate that the rejuvenators can improve the ravelling resistance of porous asphalt. The rejuvenation approach can be very cost-effective not only for porous asphalt but also for other (noise reducing) thin-surface layers and asphalt concrete containing highly aged reclaimed asphalt.

INTRODUCTION

Nowadays, porous asphalt concrete is widely used as wearing course on motorways in the Netherlands. A major advantage of traditional single-layer porous asphalt and two-layer porous asphalt is their noise reducing capacity. However, porous asphalt concrete is sensitive to ravelling (loss of the stones at the top) by the combination of traffic loading and severe climate conditions. Ravelling is the dominant damage of porous asphalt and has a strong influence on the service life (Molenaar, 2006; Hagos, 2008). In the Netherlands, the average service life of the

slow lane for single-layer porous asphalt is 12 years, for the fast lane it is 16 years (Voskuilen, 2004). The average service life of the slow lane for two-layer porous asphalt is 8 years (Hofman, 2005). If the service life of the slow lane can be increased to that of fast lane, this would be very beneficial, also from a sustainable point of view.

Preventive maintenance with rejuvenator is a possible method to extend the service life of an asphalt pavement. In recent years, research on preventive maintenance with rejuvenators for dense asphalt pavement have been reported frequently. The literature shows that a rejuvenator has the potential to reduce and reverse the aging of the asphalt surface. It seals the pavement surface against intrusion of air and water, thereby slowing oxidation, preventing stripping and ravelling and protects the pavement in-depth (Boyer, 2000; Prapaitrakul, 2005; Brownridge, 2010). Not much research has been carried out on preventive maintenance of porous asphalt with a rejuvenator. Because of the potential benefits of saving maintenance cost for porous asphalt, a fundamental research project "Lifetime Extension Maintenance of Porous Asphalt (LVO-ZOAB in Dutch)" for INFRAQUEST has been started at Delft University of Technology. In this project, the focus is on the development of a protocol to determine if these new products can be applied as rejuvenator in the upper part of the porous asphalt layer. A benchmark for new products coming into the market will be created in the near future. The research approach for the project is presented in Fig.1.

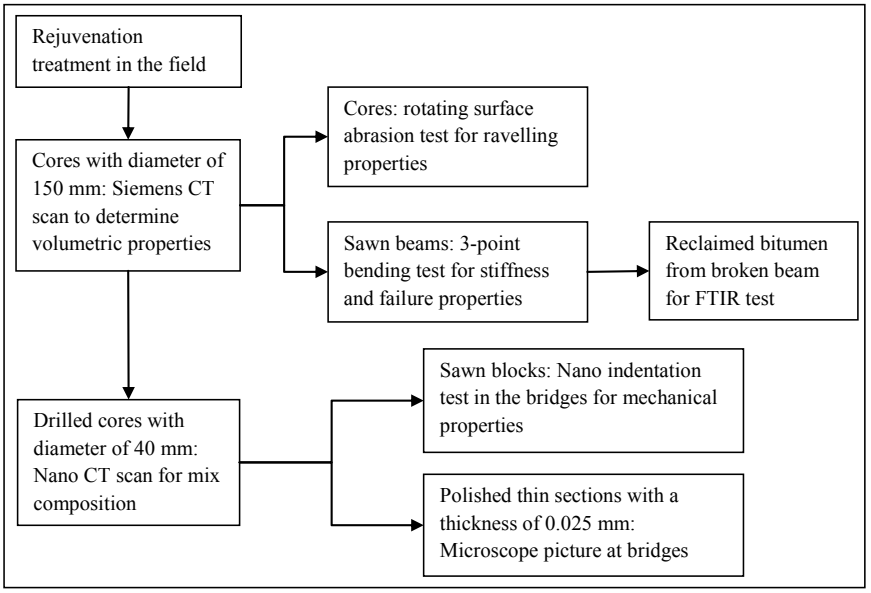

FIG. 1. Schematic diagram showing research approach for LVO-ZOAB project.

In the LVO-ZOAB project, rejuvenators supplied by contractors were applied in the test sections with porous asphalt surfacing. Porous asphalt cores will be taken from the test sections at 0, 1 and 3 years after the first application of rejuvenators. In the plan, the rejuvenation treatment will be implemented again in the same sections after 3 years. Then new cores will be drilled for research in the laboratory. As shown in Fig. 1, all the cores from the pavements are scanned to determine their volumetric properties using a Siemens CT Scanner (Verwaal, 2011). A number of the cores are used in the Rotating Surface Abrasion Test (RSAT) to investigate their ravelling properties. From other cores beams are sawn for mechanical characterization (Poot, 2011). Also small amounts of bitumen are reclaimed from the broken beams for Fourier Transform Infrared Spectroscopy (FTIR) test (Qiu, 2011; Zhang, 2011). In order to understand in more detail what happens in the bridges between two stones, small cores are scanned with a Nano CT Scanner with high resolution (Verwaal, 2011). After the scanning, Nano Indentation on the bridges is carried out in small porous asphalt blocks. Microscope pictures at the bridges are taken from thin sections (Schlangen, 2011; Zhang, 2011). The connection of these test results will be found in the research.

In this paper, the results from the bending beam tests and rotating surface abrasion tests are presented. The self-healing capability of porous asphalt concrete is investigated through mechanical properties of the beams and ravelling properties of the cores with and without rejuvenators. The work is still going on. More research results will be obtained in the future.

EXPERIMENTAL

Materials

Test sections in the A50 and A73 motorway in the Netherlands were selected for the application of rejuvenators. The wearing course of the A50 motorway is a Dutch single-layer porous asphalt 0/16+ (with higher binder content). The wearing course of the A73 motorway is two-layer porous asphalt, consisting of a 25 mm top layer of PA 4/8 and a 45 mm bottom layer of PA 11/16. Both test sections were 5 years in service at the moment of the treatment with rejuvenators.

The contractors supplied three rejuvenation products for the LVO project. Product 1, a type of bitumen emulsion, is sprayed on the surface at ambient temperature. Product 2, a bituminous binder, is sprayed at a temperature of 180 ^{o}C. Product 3, another bitumen emulsion, is sprayed on the pavement at a temperature of 70 ^{o}C. Small crushed sand particles were sprayed on the pavement after the rejuvenators in order to increase the skid resistance. Cores with a diameter of 150 mm were taken from reference and treated test sections of the A50 and A73 motorway, as listed in Table 1. Treated sites with rejuvenators are adjacent to the reference sites without rejuvenator.

Fig. 2 shows pictures of the test sections on the motorway A73 and porous asphalt cores from this section. Rejuvenators were only applied on the slow lane of the pavement. The difference between the reference and treated porous asphalt

surface can be seen clearly (in Fig. 2). Arrows are marked on cores to represent the traffic direction.

Table 1. Porous Asphalt Specimens from the Field

Test Sections		Ref.	Product 1	Ref.	Product 2	Ref.	Product 3
A50	location	192.7-192.5	192.5-191.9	191.9-191.7	191.7-191.3	191.3-191.2	191.2-190.7
	code	A50-R	A50-P1	A50-R	A50-P2	A50-R	A50-P3
	number	14	41	18	55	20	50
A73	location	100.1-100.2	100.2-100.6	100.6-100.8	100.8-101.0	101.0-101.1	101.1-101.5
	code	A73-R	A73-P1	A73-R	A73-P2	A73-R	A73-P3
	number	14	20	18	18	15	25

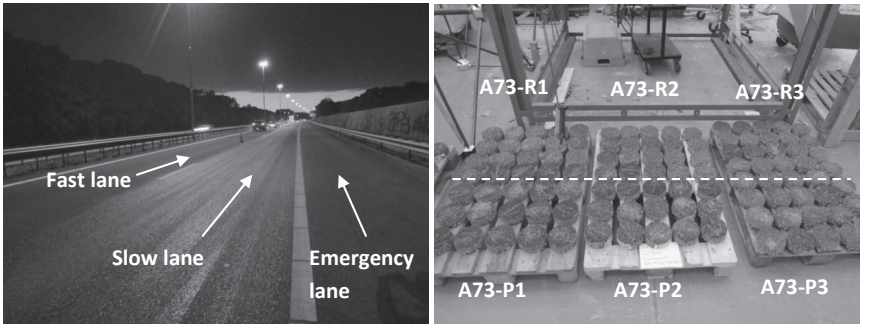

FIG. 2. Test section of porous asphalt pavement in the motorway A73 (left) and porous asphalt specimens from the motorway A73 (right).

Methods

The bending stiffness and failure properties are determined with a three-point bending test. Beams were sawn in the traffic direction from the center of cores. For the single-layer porous asphalt in A50, the dimensions (Length, Width and Height) of beams were 150 mm×50 mm×40 mm. Only the upper layer of the two-layer porous asphalt in A73 was tested in bending. The dimensions of those beams were 150 mm×50 mm×25 mm. Due to the penetration depth of rejuvenators, the texture on the surface, and the sawn surface, the stiffness of the top and bottom part of the beam are different. To determine this, two test configurations were used in the stiffness test.

As shown in Fig. 3, in one test the top part of the beam is in the compressive zone during loading. This test configuration is described as Surface-Up in this report. Another test configuration is with the top part of the beam in the tensile zone during loading. This is described as Surface-Down.

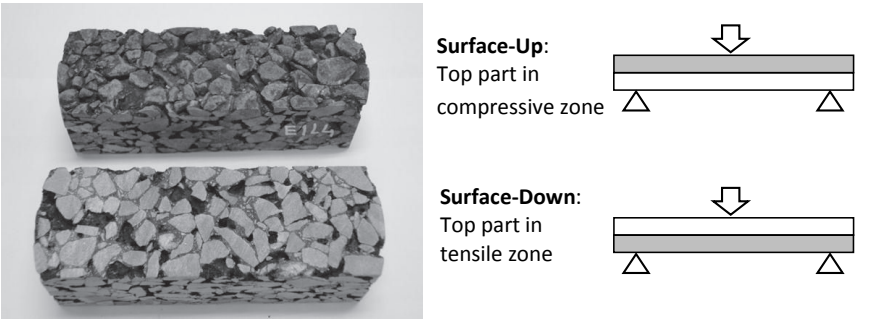

FIG. 3. Picture of the beams from the test section of A50 (left) and two configurations for the stiffness test in 3-point bending test (right).

Firstly, the stiffness of beams was tested with a haversine loading at the temperature of 5 ^{o}C. In order to avoid damage of the beams, the applied loads were 100 N for beams from A50 and 60 N for beams from A73. Six loading frequencies were used in this test: 0.1, 0.2, 0.5, 1, 2 and 4 Hz. After the stiffness test, failure tests were done in the Surface-Down mode at the temperature of 5 ^{o}C. A vertical displacement rate of 0.01 mm/s was used to control the loading. The failure loading curves can be used to calculate the maximum stress, initial modulus and failure energy.

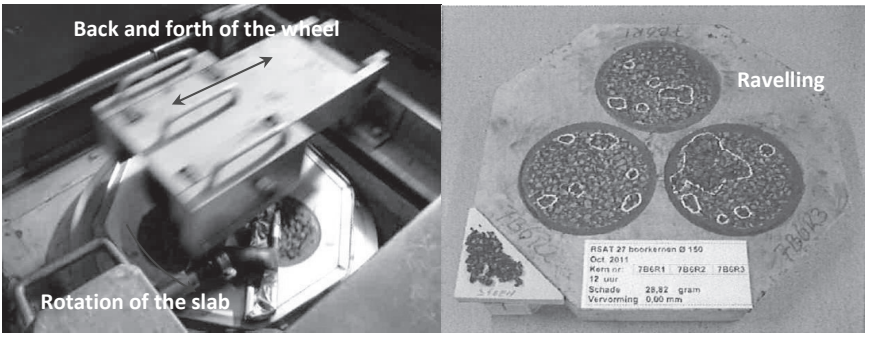

FIG. 4. Schematic of the rotating surface abrasion test (left) and picture of the specimens after RSAT from the test section of A73 (right).

The resistance to ravelling was measured with a test method developed by Dutch contractor Heijmans, the Rotating Surface Abrasion Test (RSAT). The RSAT

schematic and a picture of the test specimens are given in Fig.4. In the standard test, an octagonal plate of 50 cm in diameter is charged by a wheel with a solid rubber tire that is moved back and forth (3607 times per hour). The vertically loaded wheel (contact stress of 0.6 MPa) is tilted (33.7^{o}) with the direction of back and forth movement. So the horizontal forces occur on the surface. The entire surface of the test plate is uniformly loaded by rotating the test plate during the test (496 circles per hour). During the 24 hours test at a temperature of 20 ^{o}C, the loss of material from the surface is collected continuously with a vacuum cleaner. The mass consisting of stones with a grain diameter of more than 2 mm is reported as ravelling damage. In this research, three cores with a diameter of 150 mm from the road surface are glued in a multiplex plate with the same shape as the standard test plate. The rest of the test conditions are the same.

RESULTS AND DISCUSSION

Correction of the defection

When the length of structural element is considerably longer than the width and the thickness, the element is called a beam (at least one of its dimensions is small). The deflection of a beam due to shear can be neglected as small (less than 1%) compared to the deflection due to the moments when the length is much more than the height of the beam. According to classical beam theory, the bending formula for the maximum deflection of a beam loaded in the middle is as follows:

$$\delta_{max} = \frac{PL^3}{48EI} \tag{1}$$

Where, P is the concentrated load in the middle. L is the support span of the bending beam. I is the moment of inertia. E is the modulus of elasticity of the material.

When the length is much larger than the height, the calculation of the maximum deflection for a beam is based on the assumption that the deflection due to shear stresses is negligible. However, a certain percentage of the maximum deflection was caused by shear stresses in this stiffness test, because the support length of the beams is only 130 mm and the heights of the beams from A50 and A73 are 50 mm and 25 mm. In order to calculate the stiffness according to formula (1), the maximum deflection from the test results need to be corrected for the influence of the shear stresses. Therefore, the maximum deflections of an elastic beam model with the same dimensions as real samples were calculated using the formula and tested in a finite element model. The difference of the results between the modeling and the formula calculation represents the deflection caused by shear stresses. For the beam model with the same dimensions as samples from A50, the calculated deflection result is 66.1% of the modeling deflection result. For the beam model with the same dimensions as samples from A73, the calculated deflection result is 83.5% of the modeling deflection result. In this report, all test results of deflections from the stiffness tests are corrected for the calculation of the stiffness.

The bending stiffness

For the stiffness test, 10 test beams A50-R from the reference section of A50 were available. From the three rejuvenated sections 6 test beams A50-P1, 3 test beams A50-P2 and 5 test beams A50-P3 were available. The average values of their stiffness and standard deviations are given in Fig. 5 and Fig. 6. Obviously, the stiffness of all test beams increased with increasing loading frequency. Average values of the Surface-Down stiffness are always lower than the Surface-Up stiffness. The range of the Surface-Down stiffness of A50-R is between 3000 MPa and 5500 MPa (see Fig.5). The range of the Surface-Up stiffness of A50-R is between 4000 MPa and 6500 MPa (see Fig. 6).

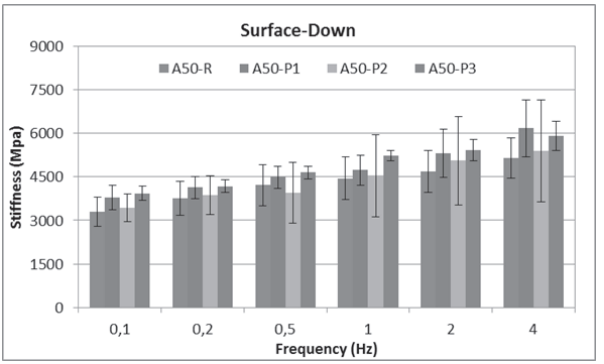

FIG. 5. Average values of Surface-Down stiffness for beams from A50 at 5 ^{o}C.

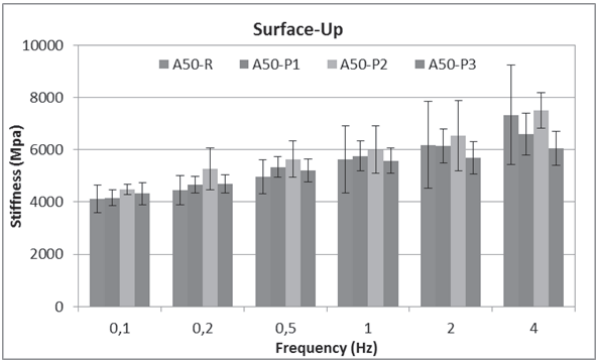

FIG. 6. Average values of Surface-Up stiffness for beams from A50 at 5 ^{o}C.

The Surface-Down stiffness of test beams from three rejuvenated sections is higher than that of the reference beams A50-R at most frequencies. The range of their average values is between 3500 MPa and 6000 MPa. A50-P3 shows the highest Surface-Down stiffness. A50-P2 shows the lowest Surface-Down stiffness. Fig. 6

reveals that the Surface-Up stiffness of test beams from three rejuvenated sections are higher than reference beams A50-R, except the stiffness of A50-R at frequencies of 2 and 4 Hz with high standard deviations. A50-P3 shows the lowest Surface-Up stiffness. A50-P2 shows the highest Surface-Up stiffness. Compared with the reference section of A50, the increased stiffness of the treated sections could be explained by the bonding effect of these rejuvenators to the single-layer porous asphalt. These rejuvenators provided extra binder to bond the stones in the single-layer porous asphalt.

From test sections of A73, 3 test beams A73-R of the reference section for the stiffness test were available. From the three rejuvenated sections 2 test beams A73-P1, 1 test beam A73-P2 and 3 test beams A73-P3 were available. The stiffness of all test beams increased with increasing loading frequency. The average values of the Surface-Down stiffness are always lower than the Surface-Up stiffness. They show the same tendency as the results from A50. The range of the Surface-Down and Surface-Up stiffness of A73-R are between 3000 MPa and 5500 MPa.

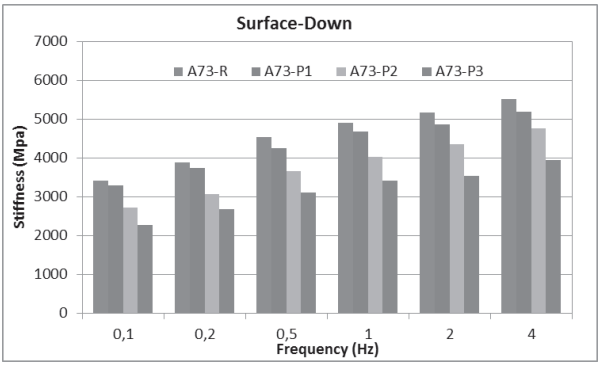

FIG. 7. Average values of Surface-Down stiffness for beams from A73 at 5 ^{o}C.

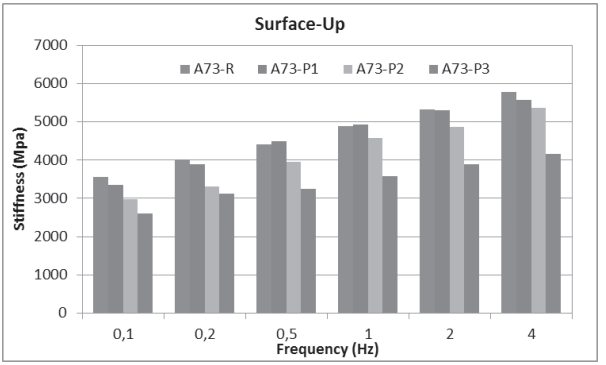

FIG. 8. Average values of Surface-Up stiffness for beams from A73 at 5 ^{o}C.

It is observed that the stiffness of the test beams of the three rejuvenated sections are lower than that of the reference section from A73. They are opposite to the results from A50. One possible reason could be that the polymer modified bitumen in the A73 ages different in time compared with the pen grade bitumen in the A50. Other factors also influence the results, such as different height of beams, different mixtures and different binder content. The reference sections of A73 and A50 show the same range of the Surface-Down stiffness.

The failure properties

After the stiffness tests, the failure properties of beams were tested in a vertical displacement rate control. The load versus deflection curves are used to calculate some properties. A typical loading curve is shown in Fig. 9.

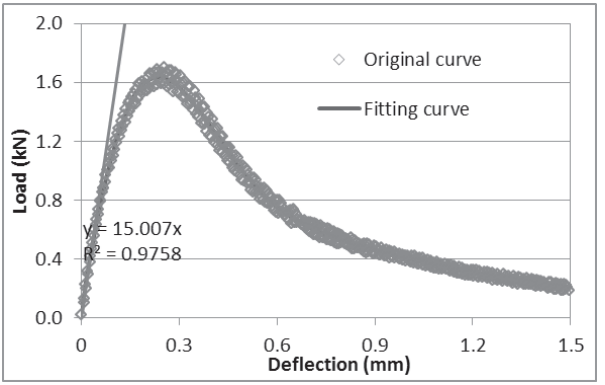

FIG. 9. Typical load deflection curve in the failure test.

As shown in Fig. 9, the original loading curve is fitted to get a smooth curve. The peak of the fitting curve is defined to calculate the failure stress at the bottom of the beam. The area under the curve of the load versus deflection figure represents the failure energy. During the initial loading period, the load and deflection show a linear behavior. It can be used to calculate the initial modulus of the beam. This initial modulus is not corrected for the shear stresses. The slope of the linear relationship between the load and deflection is used in the formula as follows:

$$E_{initial} = \frac{PL^3}{4\delta W H^3} \quad (2)$$

Where, Einitial is the initial modulus of test beam, P is the concentrated load, δ is the deflection, L is the support span of test beam, W is the with and H is the height.

Average values and a standard deviation of failure properties for the beams from A50 are listed in Table 2. The average value of the maximum stresses of all the beams is approximately 4 MPa. This means probably that single-layer porous asphalt

(A50) is still in good condition. The reference beams A50-R show similar average values of failure energy as A50-P1 and A50-P3. The beams of A50-P2 show the lowest failure energy. It's not possible to explain the difference of failure energy for the rejuvenation products. However, the initial modulus was tested with a small deflection of the beams. They can be used to represent the flexibility of the beams. The beams from rejuvenated sections show a lower initial modulus than the reference sections, which means they are more flexible than the reference beams.

Table 2. The Failure Properties for the Beams from A50 (5 ^{o}C, 0.01mm/s)

Section	Amount of specimens	Max stress (MPa)	Strain at max load	Initial modulus (MPa)	Energy until max load (mJ)	Energy until deflection-1.5mm (mJ)
A50-R	10	4.09 (0.56)	3.8E-03 (6.2E-04)	2675 (419)	318 (89)	1054 (229)
A50-P1	6	4.04 (0.33)	3.9E-03 (6.4E-04)	2438 (245)	310 (71)	1110 (132)
A50-P2	3	4.12 (0.13)	3.4E-03 (4.6E-04)	1986 (69)	261 (43)	911 (120)
A50-P3	5	4.10 (0.16)	4.0E-03 (4.2E-04)	2648 (216)	323 (43)	1120 (129)

For A73, it is notable that the average values of the failure energy of all test beams from rejuvenated sections are lower than reference beams. The reference beams A73-R show a higher average value of the initial modulus than A73-P1 and A73-P2, but lower initial modulus than A73-P3.

Table 3. The Failure Properties for Test Beams from A73 (5 ^{o}C, 0.01mm/s)

Section	Number of specimens	Max stress (MPa)	Strain at max load	Initial modulus (MPa)	Energy until max load (mJ)	Energy until deflection-1.5mm (mJ)
A73-R	3	3.09	6.7E-03	1.966	284	618
A73-P1	2	2.68	5.5E-03	1.580	202	504
A73-P2	1	2.22	8.3E-03	1.217	265	464
A73-P3	3	3.29	5.2E-03	2.347	233	610

Resistance to ravelling

The results of the RSAT for A50 are given in Table 4. Three specimens were tested for each sections, except the treated section A50-P2 with two specimens. All were tested for 24 hours. A large variation in individual results of cumulative loss of stones for test samples in the same section can be observed. Average values of cumulative loss of stones were calculated. A tendency can be observed that the treated sections (A50-P1, A50-P2 and A50-P3) show lower cumulative loss of stones than the reference sections (A50-R). So it seems that the rejuvenation sections have better ravelling resistance. More test results are needed to investigate the ravelling behavior of porous asphalt with the RSAT method.

Table 4. Results of RSAT for the Specimens from A50 at 20 °C

Section	A50-R			A50-P1			A50-P2		A50-P3		
Total test time (hour)	24	24	24	24	24	24	24	24	24	24	24
Cumulative loss of stone (g)	0.98	3.07	6.32	5.53	0.61	0.09	1.62	3.11	0.57	0.47	2.14
Average value of the loss (g)	3.46			2.08			2.37		1.06		

Table 5. Results of RSAT for the Specimens from A73 at 20 °C

Section	A73-R				A73-P1		A73-P2	A73-P3	
Total test time (hour)	5	24	24	24	24	17	24	24	24
Cumulative loss of stone (g)	57.05	64.51	22.80	28.50	12.29	41.54	34.63	6.93	29.47
Gradient loss of stone (g/h)	11.41	2.69	0.95	1.19	0.51	2.44	1.44	0.29	1.28
Average value of the loss per	4.06				1.48		1.44	0.79	

For the RSAT results of A73, more cumulative loss of stones was found than for the single-layer porous asphalt from A50. Sometimes the tests were terminated

before the 24 hours, because of strong damage of the surface during testing. One specimen of A73-R was tested for only 5 hours. The cumulative loss of stones of that specimen reached to 57.05 g. Another specimen of A73-P1 was tested for only 17 hours. Therefore, the gradient cumulative loss of stones was used to calculate the average values of test results. It is observed that the reference sections A73-R show a higher average value of gradient cumulative loss of stones. That tendency is the same as A50. Based on the RSAT result it is concluded that both the results from A50 and A73 show that the rejuvenators can improve the ravelling resistance of porous asphalt.

CONCLUSIONS

Sections of the porous asphalt surfacing of the motorways A50 and A73 in the Netherlands have been treated with rejuvenators. The performance and service life of porous asphalt sections with rejuvenators are monitored continuously. From the sections cores were taken for testing. In this paper results of a bending test and RSAT ravelling test are reported.

In the tree-point bending test, the bending stiffness increased with increasing loading frequency. Average values of the Surface-Down stiffness are always lower than the Surface-Up stiffness.

After treatment with rejuvenators, the single-layer porous asphalt A50 shows higher bending stiffness. The two-layer porous asphalt A73 with rejuvenators has lower bending stiffness than that without rejuvenators.

The failure test results show the same results for the reference and the treated beams from the single-layer porous asphalt A50. The failure stresses for all is approximately 4 MPa. For A73, it is found that the failure stress is lower than for A50.

Results of RSAT show that rejuvenators can improve the ravelling resistance of porous asphalt.

ACKNOWLEDGEMENTS

The authors acknowledge the financial support from the Center for Transport and Navigation (DVS) in the form of Infraquest Project LVO-ZOAB.

REFERENCES

Molenaar, A.A.A., Meekerk, A.J.J., et al (2006). "Performance of Porous Asphalt." *Journal of the Association of Asphalt Paving Technologists, CD*.

Hagos, E. T. (2008). "The Effect of Aging on Binder Properties of Porous Asphalt Concrete." PhD thesis, Civil Engineering & Geosciences, Delft University of Technology.

Voskuilen, J.L.M., Tolman, F., and Rutten, E. (2004). "Do Modified Porous Asphalt Mixtures have a longer service life?" *Proceedings of the 3rd Eurasphalt and Eurobitumen Congress*.

Hofman, R., van Wieringen, J.B.M. and Visser, J.C. (2005). "Noise Innovation Program IPG: Two Layer Porous Asphalt for use on the Dutch Main." *The 2005 Congress and Exposition on Noise Control Engineering*.

Boyer, R. E. (2000). "Asphalt Rejuvenators "Fact, or Fable"." *Transportation Systems 2000 Workshop*.

Prapaitrakul, N., Tom, F. and Gharles, J. G. (2005). "Analyze Existing Fog Seal Asphalts and Additives: Literature Rewiew." *FHWA Report*.

Brownridge, J. (2010). "The Role of an Asphalt Rejuvenator in Pavement Preservation: Use and Need for Asphalt Rejuvenation." *First International Conference on Pavement Preservation*.

Verwaal Wim, Zhang Yuan, Chen Feng (2011). "Field trial A50: Year 0 Results of CT Scans." *Report 7-11-185-1, Delft University of Technology*.

Schlangen Erik, Liu Quantao (2011). "Field trial A50: Year 0 Results of Optical Microscope Analysis." *Report 7-11-185-2, Delft University of Technology*.

Schlangen Erik, Liu Quantao (2011). "Field trial A50: Year 0 Results of Nano Indentation Test." *Report 7-11-185-3, Delft University of Technology*.

Poot Marco, Zhang Yuan, Chen Feng (2011). "Field trial A50: Year 0 Bending Beam Test." *Report 7-11-185-4, Delft University of Technology*.

Martin van de Ven, Zhang Yuan, Feng Chen (2011). "Field trial A50: Year 0 FTIR Test." *Report 7-11-185-5, Delft University of Technology*.

Verwaal Wim, Zhang Yuan (2011). "Field trial A73: Year 0 Results of CT Scans." *Report 7-11-185-7, Delft University of Technology*.

Zhang Yuan, Liu Quantao (2011). "Field trial A73: Year 0 Results of Optical Microscope Analysis." *Report 7-11-185-8, Delft University of Technology*.

Zhang Yuan, Liu Quantao (2011). "Field trial A73: Year 0 Results of Nano Indentation Test." *Report 7-11-185-9, Delft University of Technology*.

Zhang Yuan, Poot Marco (2011). "Field trial A73: Year 0 Bending Beam Test." *Report 7-11-185-10, Delft University of Technology*.

Qiu Jian, Zhang Yuan, Martin van de Ven (2011). "Field trial A73: Year 0 FTIR Test." *Report 7-11-185-11, Delft University of Technology*.

Prediction of Fatigue Life on Road System of Thermal Energy Collector and Release

Wang Hong[1], Wang Genyan[2] and Wu Shaopeng[3]

[1] Wuhan Sports University, Sports Information &Technology Department, 461 Luoyu Road. Wuhan. 430079. P. R. China; email: whtwanghong@163.com
[2] Wuhuan Engineering Co.Ltd. 1019 Minzu Avenue, East Lake Hi-tech Development Zone. Wuhan 430223. P. R. China;
[3] State Key Lab of Silicate Materials for Architectures, Wuhan university of Technology, Wuahn 430070, China.

ABSTRACT: The study is focused on the fatigue life prediction of RSTECR (Road System of Thermal Energy Collector and Release) using the finite element method. The pavement structure was modeled as two-dimensional four-layer stratum using ANSYS finite element soft. The maximum tensile strain or stress of asphalt layers was calculated in order to predict the fatigue life of the system. Especially, the different load position and installed tube's direction were considered. The results show that no matter where the traffic direction is vertical or parallel to the installed tube's direction, the tube must not be installed in the top layer. The most adverse load position is that the single wheel is upon the installed tube when the load direction is parallel to traffic direction. And the most adverse load position is that two wheels are upon the installed tube when the load direction is vertical to traffic direction. Finally, the simulating method of the system was put forward and the study is expected to be able to provide road engineers with some design basis.

INTRODUCTION

The air temperature in the center of a city is higher than that of surrounding areas. The center of the city resembles an island, a so-called "urban heat island" (Mallick, 2008). Heat islands are formed as vegetation is replaced by asphalt and concrete for roads, buildings, and other structures, which absorb - rather than reflect - the sun's heat, causing surface temperatures and overall ambient temperatures to rise. Asphalt pavements are one of the main contributors to this effect by altering land cover over significant portions of an urban area because of its materials properties.

On the contrary, freezing weather may affect the asphalt pavement's service

performance. On the one hand, asphalt mixture is easy to crack in low temperature. On the other hand, it is very difficult to remove the snow and ice of the road, which may cause the interruptive traffic and even serious economic loss. Therefore, it is of vital importance not only to cool pavement and mitigate the "urban heat island" effect, but also to heat pavement and remove the snow and ice of road for the preservation of existing road networks(Chen, 2011).

Asphalt pavement can heat up to 70°C during solar irradiation in summer times because of the excellent heat-absorbing property(Wu, 2008). Due to the enormous area of asphalt pavement, the thermal energy potential of asphalt collector may appear infinite. Therefore, it has become a newfashioned research task to make use of the asphalt pavement to collect solar energy just as solar cell. The idea of capturing energy from asphalt pavement does not only cool the surface asphalt pavement in summer avoiding some diseases (rutting, urban heat island effect etc.) caused by high temperature, but also could provide the thermal energy to neighboring building and melting the ice and snow of surface asphalt pavement in winter.

One new system - RSTECR (Road System of Thermal Energy Collector and Release) is shown in Fig. 1. The basic mechanism is that in summer asphalt pavement through a heat collection tube with water as a solar cell absorb thermal energy from the sun and is cooled, and in winter the snow and ice is removed over the road by the thermal energy from the pavement installed the heated tube with water.

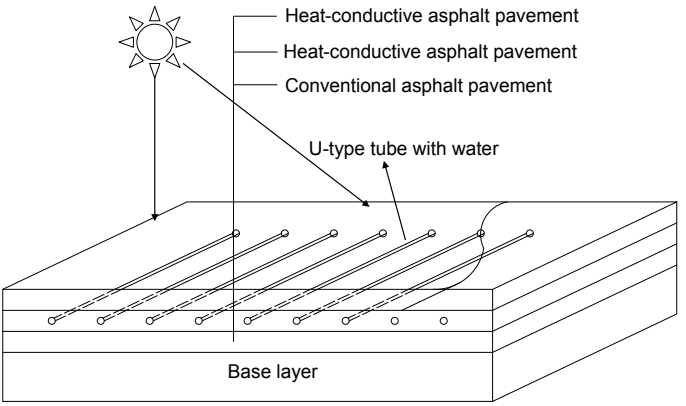

FIG.1. Sketch map of the asphalt pavement collector

In the study, the structural performance of RSTECR is evaluated using the finite element program ANSYS. The maximum tensile strain or stress of asphalt layers was calculated in order to predict the fatigue life of the system. Especially, the different

load position and installed tube's direction were considered. Finally, the simulating method of the system was put forward and the study is expected to be able to provide road engineers with some design basis.

THEORETICAL CONSIDERATIONS

A flexible pavement is a multilayer structure composed of asphalt surfacing layer and combined unbound aggregate roadbase, on a subgrade of natural soil. Under service conditions, the stress state is idealized as depicted in Fig. 2. Tyre loads cause the top and bottom of the pavement to shift rapidly from compression to tension, and fatigue cracks arise from the repeated tensile strains. According to elastic layer theory, the maximum strain is at the bottom of the asphalt surfacing layer. Most pavement design models are therefore based on straining at the bottom of the asphalt layer to predict performance with respect to fatigue cracking(Sheng, 2001; Owende, 2007).

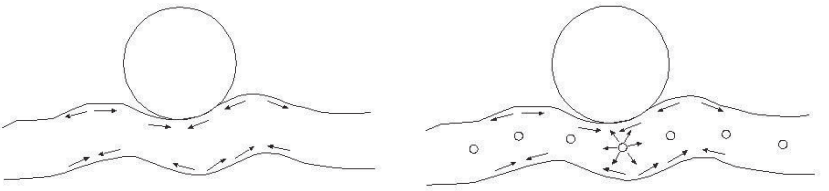

(a) Without tubes (b) With tubes

FIG. 2. Stress of asphalt layer at vehicle load

Pavement failure is determined by criteria based on longitudinal rutting or fatigue cracking in the wheel tracks. However, large elastic deflections on the pavements with weak foundations cause fatigue failure (cracking) before the appreciable rutting has occurred; hence, fatigue cracking is the limiting criterion. The failure criterion for fatigue cracking of the asphalt surfacing may be evaluated from the relationship(Mulungye, 2007):

$$\lg(N_f) = 16.664 - 3.291\lg(\frac{\varepsilon_t}{10^{-6}}) - 0.854\lg(E) \quad [1]$$

Where: N_f is the number of load applications to induce fatigue cracking over 10% of the wheel path area; ε_t is the horizontal tensile strain repeatedly applied at the bottom of the asphalt concrete layer; and E is the stiffness modulus for the

asphalt layer (MPa).

MATERIALS AND METHODS

Basic assumption

The 2D Finite-Element Method was used to simulate the mechanical behavior of RSTECR. Combined the actual situation, the model is simulated and is based on the following assumptions:

(1) Every layers of asphalt pavement, the semi-rigid base and the installed tube is uniform completely, isotropic and elastic.

(2) The interface between every asphalt layers, asphalt layer and base, and asphalt layer and installed tube is considered to be fully bonded (with no gaps).

(3) The bottom nodes of the base are fully constrained. In the transverse direction, all nodes are horizontally constrained along the line of symmetry, but are free to move in the vertical direction. In the longitudinal direction, all nodes in the edge of the pavement were fully constrained.

(4) The self weight of the road system is not considered.

Applied load

The standard dual-wheel single axle load 100kN – BZZ-100 is selected based on "Specifications for Design of Highway Asphalt Pavement". The tyre contact pressure is 0.7MPa. The virtual circle's diameter of single-wheel contact area is 21.3cm. The center distance between the two wheels is 31.95cm (Ministry of Transport of the People's Republic of China, 2006). The applied load's position was shown in Fig. 3.

Material model

Asphalt mixture is sensitive to environmental temperature. The elastic modulus is higher and the strain is lower in low temperature, hence, the fatigue performance is more excellent. In high temperature, asphalt mixture is just like rubbery and its flexibility is heightened, hence, the fatigue life is improved. However, in the normal temperature from 15-25℃, the asphalt mixture shows linear elastic, and its fatigue performance is worst. Therefore, in the study, the asphalt mixture's parameters are chosen in normal temperature. The high-density polyethylene(HDP) tube is elected as the installed tube. The corresponding parameters of RSTECR were shown in Table 1.

Finite element model

In the finite element model, the pavement layers, base and tube were considered as a solid continuum. In order to consider the most fatal stress of the pavement installed tube, only a tube was considered and the load is applied above the pavement installed the tube. Considering that the structure is full symmetrical, a 1/4 model with the layer profile was modeled. The layer is modeled in ANSYS/ED finite element suite, using PLANE42 elements with elastic capability(ANSYS Inc., 2010). The element is defined by eight nodes with two degrees of freedom at each node: translations in the nodal x, and z directions.

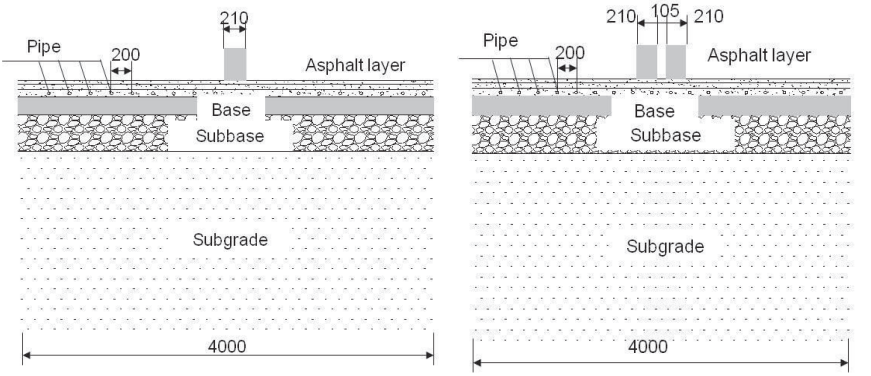

Installed tube is vertical to traffic direction (Case I)

Installed tube is parallel to traffic direction (Case II)

FIG.3. Two positions between installed tube and traffic direction

Table 1. The corresponding parameters of RSTECR

		Thickness(mm)	Elastic modulus(MPa)	Poisson's ratio
Top layer		40	2200	0.3
Middle layer		60	2000	0.3
Bottom layer		80	1500	0.3
Base		200	1000	0.35
Subbase		400	600	0.40
Soil		Infinite	200	0.45
Pipe	Inner diameter	10	1500	0.3
	Outer diameter	15		

RESULTS AND DISCUSSION

The peak longitudinal and lateral strains incurred by each wheel passage, i.e.,

wheel load and tyre pressure combinations, were used in estimating the associated number of load repetitions to failure (fatigue life) of the asphalt surfacing layer. Vertical stress influence which is the ratio of the normal stress on the subgrade to the tyre pavement contact pressure was used to compare the potential of the wheels to cause rutting. The number of load repetitions to failure, N_f, was calculated from Equation 1. When N_f can achieve 3×10^6-1.2×10^7, RSTECR can satisfy the medium traffic gradation(Ministry of Transport of the People's Republic of China, 2006). Table 2 showed the maximum tensile strain with the medium traffic gradation and the heavy traffic gradation. And different location of installed tube can affect the service performance of RSTECR. The different locations were shown in Table 3.

Table 2. The maximum tensile strain with different traffic gradation

	Top layer		Middle layer		Bottom layer	
	ε ($\mu\varepsilon$)	Fatigue life	ε ($\mu\varepsilon$)	Fatigue life	ε ($\mu\varepsilon$)	Fatigue life
Medium traffic gradation	≤169	$\geq3\times10^6$	≤173	$\geq3\times10^6$	≤186	$\geq3\times10^6$
Heavy traffic gradation	≤111	$\geq1.2\times10^7$	≤113	$\geq1.2\times10^7$	≤122	$\geq1.2\times10^7$

Table 3. Different location of installed tube

Location of installed pipe		
(a)	No pipe	-
(b)	Pipe installed in the bottom layer	z=14cm
(c)	Pipe installed between the bottom and middle layers	z=10cm
(d)	Pipe installed in the middle layer	z=7cm
(e)	Pipe installed between the middle and top layers	z=4cm
(f)	Pipe installed in the top layer	z=2cm

Especially, too many tubes may enhance the rigidity of RSTECR. In order to emphasize the worst case on load action, only an installed tube were considered.

Effect of different applied load's location in Case I

Fig. 4 gives the different load position when the installed tube is vertical to traffic direction (Case I), including that load is upon the installed tube, load position is just applied upon the edge of the installed tube, and the load position is far 5cm from the installed tube's position. And the maximum strain or stress action zone was shown of Case I in Table 4.

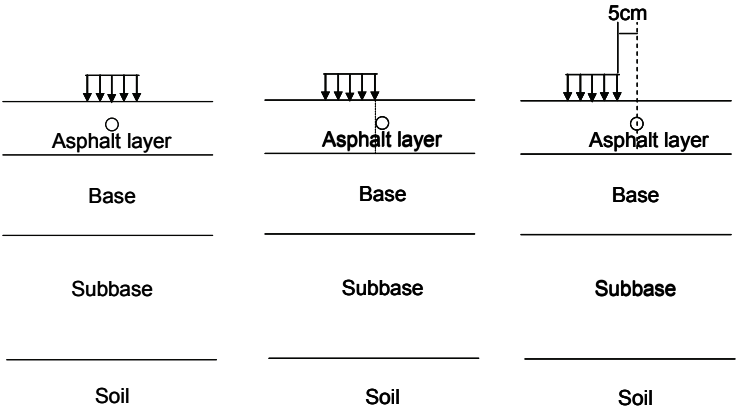

(a) Case I-1 (b) Case I-2 (c) Case I-3

FIG. 4. Different load position in Case I

Table 4. Maximum strain or stress zone in Case I

Zone I	Inside action zone of load	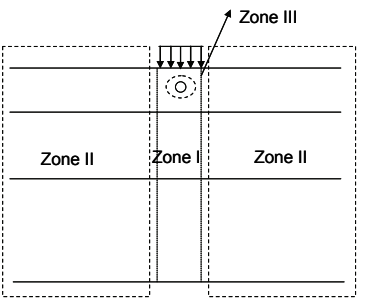
Zone II	Outside action zone of load	
Zone III	Around pipe	

The effects of different position of installed tube on the maximum tensile micro-strain were indicated respectively in Table 5, 6, 7. In Case I-1 the maximum tensile strain's change of asphalt layers was small with different position of installed

tube, except that the tube is installed in the bottom layer. And the maximum tensile strain of Case I-1 can meet the request of Table 2. The maximum tensile strain of top layer has exceeded the medium traffic's limited strain sharply in Case I-2 from Table 7. Therefore, it is very adverse to install the tube in the top layer when the installed tube is vertical to traffic direction (Case I).

Table 5. The maximum tensile micro-strain in Case I-1

	Top layer		Middle layer		Bottom layer		Base	
	ε_x	ε_z	ε_x	ε_z	ε_x	ε_z	ε_x	ε_z
(a)	11.3 Zone II	67.9 Zone II	7.36 Zone II	37.8 Zone II	123 Zone I	15.9 Zone II	189 Zone I	9.18 Zone II
	$\varepsilon_{max}=67.9$		$\varepsilon_{max}=37.8$		$\varepsilon_{max}=123$		$\varepsilon_{max}=189$	
(b)	11.2 Zone II	67.3 Zone II	10.8 Zone I	37.6 Zone II	144 Zone III	16.0 Zone II	188 Zone I	9.17 Zone II
	$\varepsilon_{max}=67.3$		$\varepsilon_{max}=37.6$		$\varepsilon_{max}=144$		$\varepsilon_{max}=188$	
(c)	11.3 Zone II	66.8 Zone II	14.6 Zone III	38.0 Zone II	114 Zone I	16.0 Zone II	188 Zone I	9.18 Zone II
	$\varepsilon_{max}=66.8$		$\varepsilon_{max}=38.0$		$\varepsilon_{max}=114$		$\varepsilon_{max}=188$	
(d)	11.3 Zone II	66.6 Zone II	14.2 Zone III	37.8 Zone II	118 Zone I	15.9 Zone II	188 Zone I	9.18 Zone II
	$\varepsilon_{max}=66.6$		$\varepsilon_{max}=37.8$		$\varepsilon_{max}=118$		$\varepsilon_{max}=188$	
(e)	11.3 Zone II	65.6 Zone II	7.40 Zone II	38.0 Zone II	121 Zone I	16.0 Zone II	189 Zone I	9.19 Zone II
	$\varepsilon_{max}=65.6$		$\varepsilon_{max}=38.0$		$\varepsilon_{max}=121$		$\varepsilon_{max}=189$	
(f)	11.4 Zone II	63.0 Zone II	7.44 Zone II	37.4 Zone II	124 Zone I	16.1 Zone II	190 Zone I	9.21 Zone II
	$\varepsilon_{max}=63.0$		$\varepsilon_{max}=37.4$		$\varepsilon_{max}=124$		$\varepsilon_{max}=190$	

Table 6. The maximal tensile stress in Case I-2

	Top layer		Middle layer		Bottom layer		Base	
	ε_x	ε_z	ε_x	ε_z	ε_x	ε_z	ε_x	ε_z
(a)	11.3 Zone II	67.9 Zone II	7.36 Zone II	37.8 Zone II	123 Zone I	15.9 Zone II	189 Zone I	9.18 Zone II
	$\varepsilon_{max}=67.9$		$\varepsilon_{max}=37.8$		$\varepsilon_{max}=123$		$\varepsilon_{max}=189$	
(b)	12.4 Zone II	68.4 Zone II	10.9 Zone I	37.0 Zone II	120 Zone I	15.8 Zone II	185 Zone I	9.25 Zone II
	$\varepsilon_{max}=68.4$		$\varepsilon_{max}=37.0$		$\varepsilon_{max}=120$		$\varepsilon_{max}=185$	
(c)	12.4 Zone II	69.4 Zone II	60.2 Zone III	39.6 Zone III	121 Zone I	26.2 Zone III	185 Zone I	9.25 Zone II
	$\varepsilon_{max}=69.4$		$\varepsilon_{max}=60.2$		$\varepsilon_{max}=121$		$\varepsilon_{max}=185$	
(d)	12.4 Zone II	72.4 Zone II	25.5 Zone III	50.9 Zone III	122 Zone I	15.4 Zone II	185 Zone I	9.26 Zone II
	$\varepsilon_{max}=72.4$		$\varepsilon_{max}=50.9$		$\varepsilon_{max}=122$		$\varepsilon_{max}=185$	
(e)	12.5 Zone II	87.3 Zone III	8.53 Zone II	83.5 Zone III	121 Zone I	15.4 Zone II	185 Zone I	9.26 Zone II
	$\varepsilon_{max}=87.3$		$\varepsilon_{max}=83.5$		$\varepsilon_{max}=121$		$\varepsilon_{max}=185$	
(f)	12.5 Zone II	201 Zone III	8.56 Zone II	84.5 Zone II	120 Zone I	16.2 Zone II	185 Zone I	9.27 Zone II
	$\varepsilon_{max}=201$		$\varepsilon_{max}=84.5$		$\varepsilon_{max}=120$		$\varepsilon_{max}=185$	

Fatigue life of every layer in different case is calculated by equation [1]. And the least fatigue life is regarded as the design fatigue life of RSTECR. Fig. 5 showed the corresponding fatigue life N_f at the different load position in Case I. The results indicated that no matter where the tube had been installed, and which case the load position was, the RSTECR could satisfy the fatigue design request in medium traffic; expect that the tube was installed in the top layer. However, the fatigue life is the shorter when the tube is installed in the bottom layer in Case I-1. Therefore, the most

adverse load position is in Case I-1 that the load position is upon the installed tube when the Installed tube is vertical to traffic direction.

Table 7. The maximal tensile stress in Case I-3

	Top layer		Middle layer		Bottom layer		Base	
	ε_x	ε_z	ε_x	ε_z	ε_x	ε_z	ε_x	ε_z
(a)	11.3 Zone II	67.9 Zone II	7.36 Zone II	37.8 Zone II	123 Zone I	15.9 Zone II	189 Zone I	9.18 Zone II
	$\varepsilon_{max}=67.9$		$\varepsilon_{max}=37.8$		$\varepsilon_{max}=123$		$\varepsilon_{max}=189$	
(b)	13.3 Zone II	69.2 Zone II	9.22 Zone II	37.5 Zone II	123 Zone I	45.2 Zone III	189 Zone I	9.54 Zone II
	$\varepsilon_{max}=69.2$		$\varepsilon_{max}=37.5$		$\varepsilon_{max}=123$		$\varepsilon_{max}=189$	
(c)	13.3 Zone II	70.7 Zone II	12.1 Zone III	81.9 Zone III	122 Zone I	60.2 Zone III	189 Zone I	9.55 Zone II
	$\varepsilon_{max}=70.7$		$\varepsilon_{max}=81.9$		$\varepsilon_{max}=122$		$\varepsilon_{max}=189$	
(d)	13.3 Zone II	73.3 Zone II	9.26 Zone II	95.2 Zone III	122 Zone I	15.6 Zone II	189 Zone I	9.55 Zone II
	$\varepsilon_{max}=73.3$		$\varepsilon_{max}=95.2$		$\varepsilon_{max}=122$		$\varepsilon_{max}=189$	
(e)	13.4 Zone II	121 Zone III	9.28 Zone II	97.2 Zone III	122 Zone I	15.6 Zone II	189 Zone I	9.55 Zone II
	$\varepsilon_{max}=121$		$\varepsilon_{max}=97.2$		$\varepsilon_{max}=122$		$\varepsilon_{max}=189$	
(f)	13.4 Zone II	104 Zone III	9.30 Zone II	81.8 Zone II	121 Zone I	16.9 Zone II	189 Zone I	9.56 Zone II
	$\varepsilon_{max}=104$		$\varepsilon_{max}=81.8$		$\varepsilon_{max}=121$		$\varepsilon_{max}=189$	

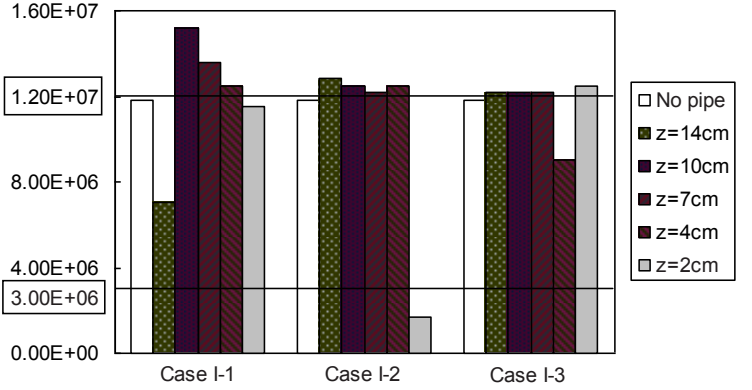

FIG. 5. Effect of different load position on the fatigue life in Case I

Effect of different applied load's location in Case II

Fig. 6 gives the different load position when the Installed tube is parallel to traffic direction (Case II), including that two wheels are upon the installed tube, load position is just applied upon the edge of the installed tube, and the single wheel is upon the installed tube's position. And the maximum strain or stress action zone is shown of Case I in Table 8.

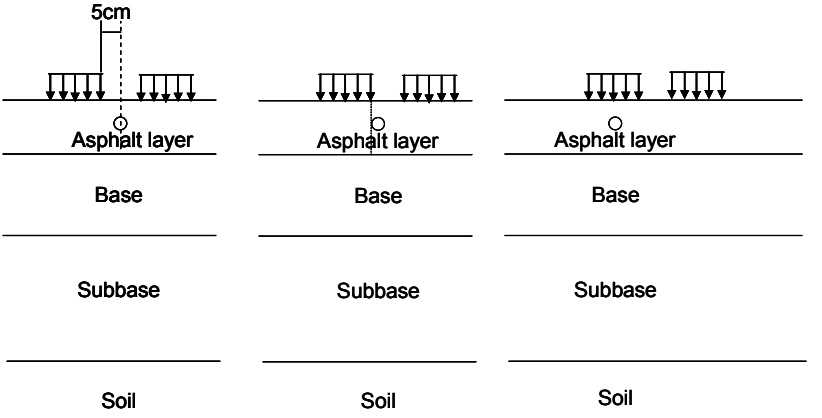

(a) Case II-1 (b) Case II-2 (c) Case II-3

FIG. 6. Different load position in Case II

Table 8. Maximum strain or stress zone in Case II

Zone I	Inside action zone of load	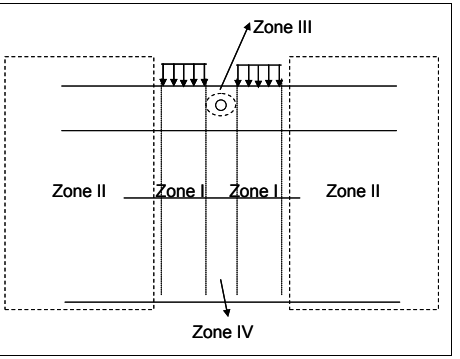
Zone II	Outside action zone of load	
Zone III	Around pipe	
Zone IV	Between two wheels	

The effects of different position of installed tube on the maximum tensile micro-strain are indicated respectively in Table 9, 10, 11 when the installed tube is parallel to the load's direction. In Case II-1 the maximum tensile strain's change of asphalt layers is very obvious with different position of installed tube. The results indicate that the lower the tube is installed, the higher the maximum tensile strain of asphalt layers in Case II-1 and Case II-2. However, the result is in contrary in Case II-3 because the tube plays a good role. The maximum tensile strain of top layer has exceeded the medium traffic's limited strain sharply in Case II-1 and Case II-2 from Table 6 when the tube is installed in the top layer. Therefore, it is very adverse to install the tube in the top layer when the Installed tube is parallel to traffic direction (Case II).

Fig. 7 showed the corresponding fatigue life N_f at the different load position in Case II. The results indicated that when the tube had been installed in the top layer, RSTECR couldn't satisfy the medium fatigue life. And RSTECR may hardly satisfy the medium fatigue life when the tube is installed between the top and middle layers. The most adverse load position is in Case II-1 that the load position is upon the installed tube when the Installed tube is vertical to traffic direction.

Table 9. The maximum tensile micro-strain in Case II-1

	Top layer		Middle layer		Bottom layer		Base	
	ε_x	ε_z	ε_x	ε_z	ε_x	ε_z	ε_x	ε_z
(a)	21.6 Zone II	102 Zone IV	14.0 Zone II	67.5 Zone IV	52.6 Zone I	23.1 Zone II	264 Zone IV	18.1 Zone II
	$\varepsilon_{max} = 102$		$\varepsilon_{max} = 67.5$		$\varepsilon_{max} = 52.6$		$\varepsilon_{max} = 264$	
(b)	21.6 Zone II	103 Zone IV	14.0 Zone II	69.6 Zone IV	53.3 Zone I	23.4 Zone II	263 Zone IV	18.1 Zone II
	$\varepsilon_{max} = 103$		$\varepsilon_{max} = 69.6$		$\varepsilon_{max} = 53.3$		$\varepsilon_{max} = 263$	
(c)	21.7 Zone II	104 Zone IV	14.0 Zone II	68.4 Zone IV	53.0 Zone I	23.0 Zone II	264 Zone IV	18.1 Zone II
	$\varepsilon_{max} = 104$		$\varepsilon_{max} = 68.4$		$\varepsilon_{max} = 53.0$		$\varepsilon_{max} = 264$	
(d)	21.7 Zone II	107 Zone IV	14.0 Zone II	86.9 Zone III	51.5 Zone I	23.0 Zone II	264 Zone IV	18.1 Zone II
	$\varepsilon_{max} = 107$		$\varepsilon_{max} = 86.9$		$\varepsilon_{max} = 51.5$		$\varepsilon_{max} = 264$	
(e)	21.7 Zone II	169 Zone III	14.1 Zone II	96.9 Zone III	49.5 Zone I	23.0 Zone II	265 Zone IV	18.1 Zone II
	$\varepsilon_{max} = 169$		$\varepsilon_{max} = 96.9$		$\varepsilon_{max} = 49.5$		$\varepsilon_{max} = 265$	
(f)	21.7 Zone II	186 Zone III	14.1 Zone II	112 Zone IV	47.9 Zone I	23.1 Zone II	265 Zone IV	18.1 Zone II
	$\varepsilon_{max} = 186$		$\varepsilon_{max} = 112$		$\varepsilon_{max} = 47.9$		$\varepsilon_{max} = 265$	

Table 10. The maximal tensile stress in Case II-2

	Top layer		Middle layer		Bottom layer		Base	
	ε_x	ε_z	ε_x	ε_z	ε_x	ε_z	ε_x	ε_z
(a)	21.6 Zone II	102 Zone IV	14.0 Zone II	67.5 Zone IV	52.6 Zone I	23.1 Zone II	264 Zone IV	18.1 Zone II
	$\varepsilon_{max} = 102$		$\varepsilon_{max} = 67.5$		$\varepsilon_{max} = 52.6$		$\varepsilon_{max} = 264$	
(b)	22.1 Zone II	101 Zone IV	14.6 Zone II	68.5 Zone IV	53.4 Zone I	22.5 Zone II	257 Zone IV	17.9 Zone II
	$\varepsilon_{max} = 101$		$\varepsilon_{max} = 68.5$		$\varepsilon_{max} = 53.4$		$\varepsilon_{max} = 257$	
(c)	22.2 Zone II	102 Zone IV	14.6 Zone II	89.1 Zone IV	54.0 Zone I	22.6 Zone II	257 Zone IV	17.9 Zone II
	$\varepsilon_{max} = 102$		$\varepsilon_{max} = 89.1$		$\varepsilon_{max} = 54.0$		$\varepsilon_{max} = 257$	
(d)	22.2 Zone II	103 Zone IV	14.6 Zone II	74.5 Zone III	53.5 Zone I	22.6 Zone II	258 Zone IV	17.9 Zone II
	$\varepsilon_{max} = 103$		$\varepsilon_{max} = 74.5$		$\varepsilon_{max} = 53.5$		$\varepsilon_{max} = 258$	
(e)	22.2 Zone II	131 Zone III	14.7 Zone II	96.8 Zone III	51.9 Zone I	22.7 Zone II	258 Zone IV	17.9 Zone II
	$\varepsilon_{max} = 131$		$\varepsilon_{max} = 96.8$		$\varepsilon_{max} = 51.9$		$\varepsilon_{max} = 258$	
(f)	22.3 Zone II	236 Zone III	14.7 Zone II	131 Zone IV	49.9 Zone I	22.7 Zone II	259 Zone IV	17.9 Zone II
	$\varepsilon_{max} = 236$		$\varepsilon_{max} = 131$		$\varepsilon_{max} = 49.9$		$\varepsilon_{max} = 259$	

Table 11. The maximal tensile stress in Case II-3

	Top layer		Middle layer		Bottom layer		Base	
	ε_x	ε_z	ε_x	ε_z	ε_x	ε_z	ε_x	ε_z
(a)	21.6 Zone II	102 Zone IV	14.0 Zone II	67.5 Zone IV	52.6 Zone I	23.1 Zone II	264 Zone IV	18.1 Zone II
	$\varepsilon_{max} = 102$		$\varepsilon_{max} = 67.5$		$\varepsilon_{max} = 52.6$		$\varepsilon_{max} = 264$	
(b)	25.6 Zone II	101 Zone IV	17.7 Zone II	66.5 Zone IV	77.9 Zone III	22.8 Zone II	265 Zone IV	18.7 Zone II
	$\varepsilon_{max} = 101$		$\varepsilon_{max} = 66.5$		$\varepsilon_{max} = 77.9$		$\varepsilon_{max} = 265$	
(c)	25.6 Zone II	101 Zone IV	17.7 Zone II	66.7 Zone IV	53.5 Zone I	22.8 Zone II	265 Zone IV	18.7 Zone II
	$\varepsilon_{max} = 101$		$\varepsilon_{max} = 66.7$		$\varepsilon_{max} = 53.5$		$\varepsilon_{max} = 265$	
(d)	25.7 Zone II	101 Zone IV	17.7 Zone II	66.1 Zone IV	53.5 Zone I	22.8 Zone II	265 Zone IV	18.7 Zone II
	$\varepsilon_{max} = 101$		$\varepsilon_{max} = 66.1$		$\varepsilon_{max} = 53.5$		$\varepsilon_{max} = 265$	
(e)	25.7 Zone II	100 Zone III	17.7 Zone II	67.6 Zone III	53.1 Zone I	23.0 Zone II	265 Zone IV	18.8 Zone II
	$\varepsilon_{max} = 100$		$\varepsilon_{max} = 67.6$		$\varepsilon_{max} = 53.1$		$\varepsilon_{max} = 265$	
(f)	25.8 Zone II	99.4 Zone IV	17.8 Zone II	66.7 Zone IV	54.7 Zone I	23.3 Zone II	264 Zone IV	18.8 Zone II
	$\varepsilon_{max} = 99.4$		$\varepsilon_{max} = 66.7$		$\varepsilon_{max} = 54.7$		$\varepsilon_{max} = 264$	

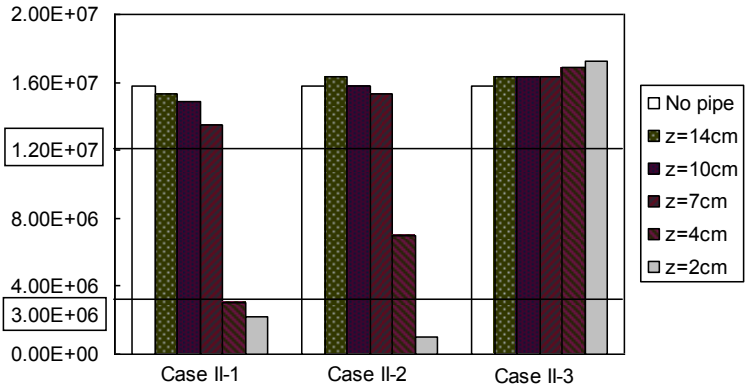

FIG. 7. Effect of different load position on the fatigue life in Case II

CONCLUSION

(1) No matter where the traffic direction is vertical or parallel to the installed tube's direction, the tube must not be installed in the top layer.

(2) When the load direction is parallel to traffic direction, RSTECR's fatigue performance can satisfy the medium traffic gradation and even the heavy traffic gradation, expect that the tube is installed in the top layer. The most adverse load position is that the single wheel is upon the installed tube.

(3) When the load direction is vertical to traffic direction, the most appropriate deepness of installed tube is z=10cm/z=7cm. The most adverse load position is that two wheels are upon the installed tube.

REFERENCES

ANSYS Inc. (2010). "ANSYS User's Manual".

Chen, M.Y., Wu, S.P., Wang, H. and Zhang， J.Z.(2011). "Study of ice and snow melting process on conductive asphalt solar collector". *Sol. Energy Mater. Sol. Cells*, Vol. 95: 3241-3250.

Ministry of Transport of the People's Republic of China. (JTG D50-2006). "Specifications for Design of Highway Asphalt Pavement", *Beijing: China Communications Press*.

Owende, P.M.O., Hartman, A.M. and Ward, S.M. (2001). "Minimizing distress on flexible pavements using variable tire pressure", *J. Transp. Eng.*: 254-262.

Mallick,R.B., Chen, B.L., Bhowmick, S. and Michael, S. Hulen(2008). "Capturing solar energy from asphalt pavements". *ISAP* :161-172.

Mulungye ,R.M., Owende,P.M.O. and Mellon K. (2007). "Finite element modeling of flexible pavements on soft soil subgrades". *Mater. Des.*, Vol. 28: 739-756.

Wu, S.P., Li, B., Xiao Y., Pang,L. and Mo, L.T.(2008). "The Effect of Thermal Conductive Fillers on Thermal Properties of Asphalt Mixtures". *ISAP* :153-160.

Sheng, J.N.(2001). "Asphalt and asphalt mixture's pavement performance", *Beijing: China Communications Press*.

Research on Low Temperature Rheological Behavior of Aging Resistant Bitumen and Mixture

Jun Han [1], Shaopeng Wu [2], Zhiyi Huang [3], Dehong Zhou [4] and Fujian Li [5]

[1] College of Civil Engineering and Architecture, Zhejiang University, Hangzhou 310058, China; Jiangsu Baoli Asphalt Co., Ltd, 214422, China; email: hanjun0309@163.com
[2] State Key Laboratory of Silicate Materials for Architectures, Wuhan University of Technology, 430070, China
[3] College of Civil Engineering and Architecture, Zhejiang University, Hangzhou 310058, China.
[4] Jiangsu Baoli Asphalt Co., Ltd, Wuxi 214422, China.
[5] Jiangsu Baoli Asphalt Co., Ltd, Wuxi 214422, China.

ABSTRACT: Bitumen is widely used in road construction, but it is an organic mixture with complex compounds and chemical structures which will change after exposed to heat, oxygen, and ultraviolet radiation (UV) and make the physical properties worse, especially at low temperature. In this paper, different aging levels (TFOT，UV-6days) of asphalt binders with various mass ratio of layer clay powder to asphalt (0,3%,5%) were considered to investigate the low temperature rheological properties of aged asphalt binders and low temperature strength as well as fatigue properties. Dynamic Shear Rheomoter (DSR) and Universal Testing Machine (UTM) were used to evaluate low temperature properties of bitumen and mixture. The ageing evaluation shows that the ageing resistance of bitumen and its mixture is improved and this improvement at low temperature properties can be better maintained compared to base asphalt.

INTRODUCTION

Oxidative aging of asphalt is a primary cause of binder hardening in pavements, thus contributing to various forms of pavement failures. An essential element of predicting long-term pavement performance is to understand binder oxidative aging and its effect on engineering properties (Wu, 2009; Lu, 1998). These aging processes

lead to decline of asphalt properties such as low temperature cracking and shorter lifespan of asphalt pavement (Ouyang, 2006; Durrieu, 2007). It is significant to explore an effective way to prevent the aging process. Recently, there are many researches on the anti-aging properties of the bitumen, which mainly focused on the ways to improve thermal-oxidative aging resistance (Yu, 2007; Airey, 2004). The Dynamic Shearing Rheology (DSR) and Universal Testing measuring system are used to evaluate the low-temperature properties of the modified bitumen and its mixture (Ouyang, 2006; Airey, 2004).

In this paper, the aged asphalt binders were prepared with different aging period and filler concentration. Related experiments were conducted to investigate the low temperature rheological properties of bitumen and its mixture. Except for maintaining good low-temperature properties, the aging resistant material has low cost, convenient and energy saving construction method while good dispersion in asphalt.

EXPERIMENTAL

Materials

SK-90# paving bitumen was supplied by SK Corp., Korea. Layer clay powder (Organic derivant of layered clay, White powder, Density 1.8 g/cm^3) was supplied by Fenghong Clay Chemical Factory, Zhejiang, China. The physical properties of bitumen before and after aging are shown in Table 1.

Table 1. Physical properties of bitumen before and after aging

Item	Penetration(25 °C,100g,5s)/0.1 mm	Softening point (R&B)/ °C	Ductility (5cm/min,15 °C)/cm
Base	83	45.1	＞120
Layer-3%	63	47	＞120
Layer-5%	58	49	99
Base-TFOT	39	53	74
Layer-3%-TFOT	43	52	80
Layer-5%-TFOT	41	50	76
Base-UV6 days	15	82	24
Layer-3%-UV6 days	22	75	42
Layer-5%-UV 6 days	25	69	50

Test method

The modified bitumens were prepared by using a lab high shear mixer. Bitumen was first heated until it becomes a well fluid at around 140°C in the mixer. Then layer clay powder was added into bitumen and then blended at 4000r/min rotation speed about 60 minutes to ensure the well dispersion. The pristine bitumen (SK-90) was also processed under the same conditions.

The asphalt mixture is AC16 gradation. The rutting samples were prepared firstly on wheel-roller machine at 140 ºC. After cooling down to the room temperature for 12 hours, the rutting samples were cut into the beam samples with the length of 380±2.0 mm, the breadth of 63.5±2.0 mm, and the thickness 50±2.0mm.

All bitumen samples were aged by thin film oven test (TFOT) in order to simulate the plant hot mixing process. The ultraviolet radiation aging (UV) was completed on self-made machine. The experimental conditions are showed in Table 2.

Table 2. UV Aging Parameters

Temperature	UV Strength	Film	Aging
50^{o}C	15,000 μW/cm^{2}	1250 μm	6 days

The physical properties of pristine asphalt and clay modified asphalts, including penetration, softening point and ductility, were tested according to Chinese standard test methodJTJ052 T0604-2000, JTJ052 T0604-2000 and JTJ052 T0605-1993, respectively.

Dynamic Shear Rheometer (DSR) MCR101 from Austria Anton Paar Company was used in this study for generating the dynamic data for the asphalts. The parameters are 10Hz with 2mm gap between 8mm rotor and bottom.

Three point bending test was done according to Chinese standard T07155-1993 at -10^{o}C and the loading rate is 50mm/min. The specimen is 250*30*35mm.

UTM-25 Universal Testing Machine was used to test the four point bending beam specimen according to AASHTO Designing Standard T321-03 at 0 ºC and 10 Hz while strain levels are 300, 400 and 500 μm.The mixture specimens were prepared through wheel-roller method at 140^{o}C and the dimension is 400mm×300mm×65mm which density met the Marshell standard attacking sample's 100±1%. And the rutting samples were put aside for more than12 hours then cut into beam which is length 380mm±2.0mm, width 63.5mm±2.0mm, height 50mm±2.0mm. All specimens were exposed into aging machine under UV light. Each test condition has three parallel experimentations to make it more accurate.

RESULTS AND DISCUSSION

DSR temperature sweep test

Dynamic Modulus and phase angle were tested by temperature sweep by DSR. Figs.1 and 2 are Complex Modulus and phase angle curve after UV aging 6 days.

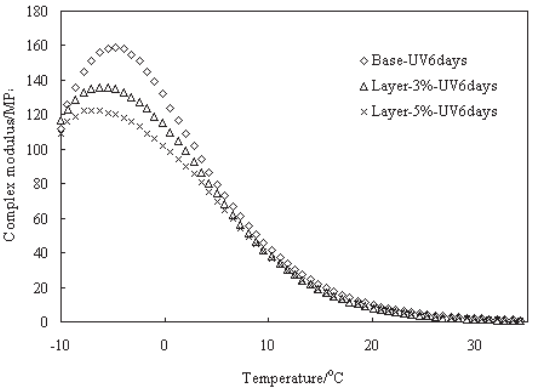

FIG. 1. Complex Modulus curve of bitumen after UV 6 days.

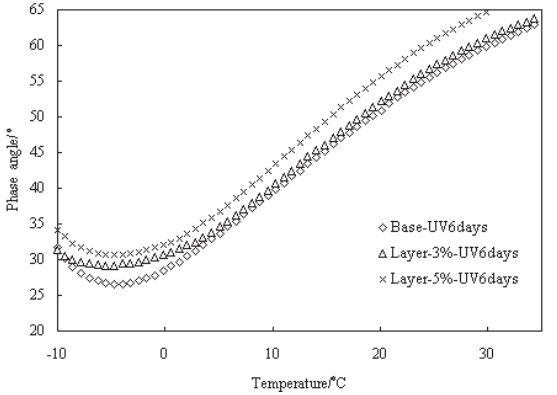

FIG. 2. Phase angle curve of bitumen after UV 6 days.

From Figs.1 and 2, it can be seen clearly that the complex modulus of base bitumen was bigger than that of modified bitumen, especially when 5 wt % additions after UV 6 days. And phase angle of base bitumen was smaller than modified bitumen. So the modified bitumen has more viscous part than base bitumen which means the aging degree was not as deep as base one. It implied better light-oxygen aging resistance of modified asphalts.

The reason for better light-oxygen aging resistance of layer clay modified asphalts is that the dispersing structures of the clay in bitumen. The dispersion of clay structures is well-ordered which lead to well protected bitumen body. The UV light was reflected back and stopped by the layer sheets and the between of the silicate layers. During the oxidation process, the infiltration of oxygen and UV light could be obstructed by the layers in modified bitumen and the energy of UV light is reduced. So the oxygen and UV light dispersion and penetration in modified asphalt was harder， and the aging extent in modified bitumen was reduced.

Three point bending test

Three point bending test was done at -10^{o}C to evaluate low temperature strength. Fig.3 is three point bending strength.

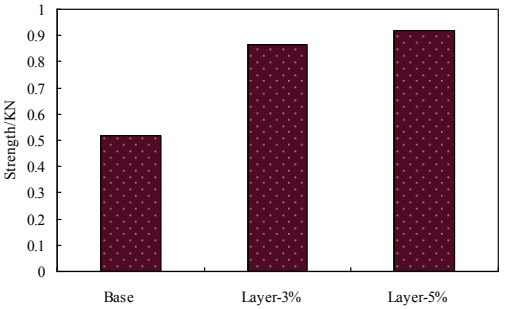

FIG. 3. Three point bending strength.

The strength of 3% and 5% layer clay powder modified asphalt after 6 days aging are 87% and 92% higher than base asphalt separately. The results are agreed with of low temperature sweep of bitumen.

Asphalt mixture fatigue

Four-point bending test was adopted to investigate the fatigue performance of aged mixtures at room temperature 10^{o}C. As shown in Fig.4, there is a good linear relationship between the strain level and the fatigue life after logarithm transformation at 0ºC. Due to the more loss of the dissipation energy at the low temperature, as the increase of the strain level, the fatigue life will decrease.

Fatigue damage of asphalt concrete is a type of unrecovery damage resulting from the repeated load on materials according to the theory of phenomenological fatigue methodology. In the way of strain control, fatigue life (N_f) was defined as the load number when the stiffness decreased to the half of its initial value. It also

satisfied the following formula:

$$N_f = \left(\frac{\varepsilon_{\max}}{\varepsilon_0}\right)^n = \varepsilon_{\max}^n \left(\frac{1}{\varepsilon_0}\right)^n = K\left(\frac{1}{\varepsilon_0}\right)^n \quad (1)$$

Where, ε_0 ——bending strain, $\varepsilon_{\max}$ ——maximal bending strain that beam sample can bear, also called limiting bending strain, K and n —— Regression coefficients.

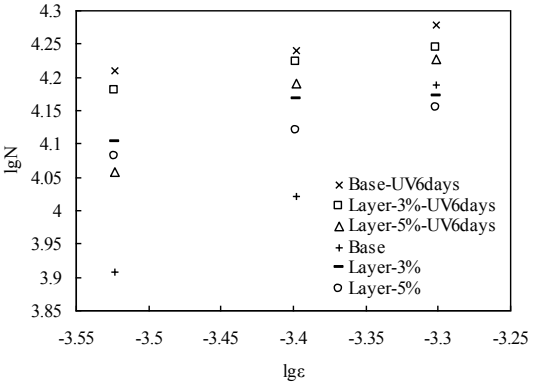

FIG. 4. Four point bending fatigue life before and after aging.

Table 3. Formulas of fatigue life and related parameters for each beam sample

Beam samples	Initial bending stiffness/MPa(300,400,500 μm)	Regression coefficient	
		K	N
Base	8090,10497,15410	2.35E+16	4.6650
Layer-3%	12699,14679, 14870	3.05E+16	4.9172
Layer-5%	13460,13200,14250	1.04E+17	5.0504
Base-UV6days	18722,17340,18957	1.8E+20	5.8339
Layer-3%-UV6 days	15100,16670,17590	1.2E+20	5.7155
Layer-5%-UV6 days	10405,15485,16852	3.8E+20	5.5635

Formulas of fatigue life and related parameters for each beam sample are given in Table 3. These formulas can be used to forecast the fatigue life for the different beam samples. Combining Fig. 3 and Table 3, it can be observed that, the layer 5% after UV 6 days aging beam exhibits much better fatigue resistance at the given strain level and temperature. Compared with the base beam samples, the layer 5% beam

samples behave better and the fatigue life can be 50% longer than base asphalt after aging. It means that the addition of layered clay powder improves UV aging resistance of asphalt effectively.

CONCLUSIONS

Laboratory tests were used to investigate the physical properties and the rheological properties of aged asphalt binders and its mixture. There is a significant influence of layer clay on rheological behaviors and basic physical properties of bitumen binders especially after UV aging. All the test results concluded that the layer clay could enhance the aging resistance of base bitumen and its mixture.

ACKNOWLEDGEMENTS

This work supported by “Research on key technology and industrialization for preparation of Ultra violate light resistant bitumen through super molecular structure Ultra violate light resistant material LDHs” which is the research Project of China Building Materials Academy (Pact No. SQ2010BAJY1169). The authors gratefully acknowledge its support.

REFERENCES

Airey, G. D. and Rahimzadeh, B. (2004). "Combined bituminous binder and mixture linear rheological properties." *Construction and Building Materials,* Vol. 18: 535-548.

Durrieu, F., Farcas, F. and Mouillet, V. (2007). "The influence of UV aging of a SBS modified bitumen: Comparison between laboratory and on site aging." *Fuel*, Vol. 86: 1446–1451.

Lu, X.H. and Isacsson, U. (1998). "Chemical and rheological evaluation of ageing properties of SBS polymer modified bitumens." *Fuel,* Vol. 77: 961-972.

Ouyang, C., Wang, S.F. and Zhang, Y. (2006). "Improving the aging resistance of asphalt by addition of Zinc dialkyldithiophosphate." *Fuel,* Vol. 85(7-8): 1060-1066.

Wu, S.P., Pang, L., Mo, L.T. et al. (2009). "Influence of aging on the evolution of structure, morphology and rheology of base and SBS modified bitumen." *Construction and Building Materials,* Vol. 23(2): 1005-1010.

Yu, J.Y., Zeng, X. and Wu, S.P. (2007). "Preparation and properties of montmorillonite modified asphalts." *Journal of Materials in Science and Engineering: A,* Vol. 447(1-2): 233–38.

Study on the Application of Coal Tar Pitch in Middle Asphalt Layer of Shanxi Highway Project

Fujian Li[1] , Jun Han[2] , Dehong.Zhou[3] and Hong Tao[4]

[1] Jiangsu Baoli Asphalt Co., Ltd, Wuxi 214422, China; Research Institute of Highway Ministry of Transport, Beijing 100088, China; email: fj.li@rioh.cn.
[2] Jiangsu Baoli Asphalt Co., Ltd, Wuxi 214422, China; Dept of Municipal Engineering, College of Civil Engineering and Architecture , Zhejiang University, Hangzhou 310058 ,China.
[3] Jiangsu Baoli Asphalt Co., Ltd, Wuxi 214422, China.
[4] Jiangsu Baoli Asphalt Co., Ltd, Wuxi 214422, China.

ABSTRACT: In this study, the objective was to dedicate to the application of coal tar pitch in road engineering construction. The present application situation of the coal pitch was discussed. The asphalt and the asphalt mix were designed: Appropriate adjustment of the proportion of coal pitch and petroleum asphalt improved the technical indexes of asphalt. The optimal bitumen-aggregate ratio based on the closest skeleton-interlocking dense condition principle is selected. Results indicated that the mix with modified coal tar pitch and the designed optimal bitumen-aggregate ratio had good performances, involving high temperature stability, low temperature cracking resistance and water stability. Besides，it was also found that the construction temperature can be reduced by the warm mix asphalt additive decreasing the volatile of polycyclic aromatic hydrocarbon which was a carcinogenic substance in coal pitch. The conclusion of this paper is valuable for the further application of coal tar pitch.

INTRODUCTION

Background

Coal pitch (whole name = coal tar pitch) is residue of coal tar. After being extracted the distillation fractions (such as light oil, phenol oil, naphthalene, etc.), it is the staple products of coal tar processing (Zielinski, 1987). The output rate is generally 50 to 60 per cent and the annual output is about 4 million tons. Although carbon products binder, carbon fiber and other products have been developed at

present, the effects are not nearly ideal. Due to the low value-added processing, the price of the coal pitch is usually less than that of coal tar, typically only 60 percent of petroleum pitch on the market. Improving the quality of coal tar and extending its scope of application will have enormous social and economic benefits. In China, the government and enterprises in the main coal industry provinces such as Inner Mongolia, Shanxi, Hubei have high expectations of increasing the application of coal tar pitch and seek to improve the efficiency of the industrial chain. So the new application way of coal pitch will be imperative.

For a long time, coal pitch has rarely been used in highway construction because coal pitch technology indexes are difficult to meet with road performance requirements. Practical experiences abroad have shown that modified coal tar pitch blending with petroleum pitch is a promising development (Li, 1999; Hong, 2006; Perez, 2001; Xue, 2004). On the other hand, it also has certain toxicity. The composition of the coal pitch is very complex according to statistics: it contains thousands of organic compounds of which only 500 kinds can be identified. Different gases compositions cause harm to human body in different degrees (Xiao, 2009; Wieslwa, 1998).

Parts of the toxic gases can be absorbed by the skin or through the respiratory tract; Breathing-in high concentrations of steam can cause headaches, blurred vision, pulmonary edema or lead to suppression of the central nervous system or liver or kidney damage as well as serious toxic black disease and cancer(Hossain, 2009; Zielinski, 1997). Therefore, content composition analysis for the coal tar pitch high temperature vapors is very necessary.

To reduce the sending out of harmful gas in the application of coal tar pitch, it is very important to reduce construction temperature by adding the WMA. In this paper, the coal tar pitch mix design which is used in the middle layer of the section asphalt pavement in Shanxi province in 2011 is tested and analyzed. The influences of a kind of WMA on the emission of harmful gases are studied. It can provide certain reference value for further application of coal tar pitch.

Mix design method

Because of the poor technology index of the coal pitch, it has been a major difficulty for road designers or research experts to resolve the shortage of high temperature stability and low temperature resistance of coal asphalt mixture. Asphalt mix with coarse-aggregate broken gradation has good performances and mechanical properties in current road applications. Therefore, this style gradation is used in this study.

In the design of mix, the key question is to explore the optimal bitumen-aggregate ratio through experiments. Currently, the compactness related with volume index has been widely accepted as the criterion to identify the optimal bitumen-aggregate ratio. In different projects, to a aggregate gradation of dense

graded mixture, dense agree varies with geometric shape and particle size; If the same design air void is applied, bitumen-aggregate ratio of the mixture will be higher due to focusing design air void of low compact degree mixture (e.g. 4%) and vice versa.

According to the research(Wang, 2009), Voids Mineral Aggregate (VMA), Void Coarse Aggregate (VCA) or mixture dry gravity ($G_{g,m}$) can correctly estimate the change regularity of mixture in various bitumen contents, the densest interlock condition can be identified with the optimal bitumen-aggregate ratio. In this paper, the optimal bitumen-aggregate ratio is chosen when the mixture is in the skeleton-interlocking dense condition (the densest condition).

EXPERIMENTAL

Raw material characteristics

The coarse aggregates and fine aggregates used in this test were limestone from Xibaqu, Shanxi. Stone technology indexes had been identified in accordance with "Test Method of Aggregate for Highway Engineering (JTG E42-2005)". AH-90, AH-70 and coal pitch were applied in the tests and main indicators were identified according to "Standard Test Methods of Bitumen and Hot Mix asphalt for Highway Engineering (JTJ052-2000)". All the materials quality indexes besides the coal pitch could meet the technical requirements for the highway asphalt pavement construction according to "Technical Specifications for Construction of Highway Asphalt Pavements (JTG F40-2004)".

The asphalt mixture Marshall test

In view of the design was for the middle layer of the highway, the nominal maximum aggregate size was 19 mm and selected 19 mm, 4.75 mm and 0.075 mm as the three control-points in accordance with skeleton-gap gradation. Therefore, the passage rates of the three control-points were estimated as 97.5%, 35% and 5% respectively. Coarse and fine aggregate gradation curves were achieved in power function. The gradations of all particle sizes are presented in Table1.

Table 1. Gradation in the experiment

Particle size [mm]	26.5	19	16	13.2	9.5	4.75	2.36	1.18	0.6	0.3	0.15	0.075
Passage rate [%]	100	97.5	85.9	74.5	58.4	35.0	25.2	18.2	13.3	9.6	6.9	5.0

To develop the technical index, the modified coal pitch was made up to coal tar pitch and petroleum pitch. Choose five bitumen-aggregate ratios in 0.4 percent

intervals: 3.4%, 3.8%, 4.2%, 4.6% and 5.0%. Four samples in each bitumen-aggregate ratio were formed by the 75 times Marshall Compactions. The theoretical mixture densities of various ratios were estimated by vacuum method. Bulk density can be identified by surface-dry condition method and estimation of ideal density can follow the "Standard Test Methods of Bitumen and Hot mix asphalt for Highway Engineering (JTJ 052-2000)". Table 2 illustrates all the results of the tests.

Table 2. Average of sample volume index

Bitumen-aggregate Ratio [%]	Bulk density [g/cm^3]	Dry density [g/cm^3]	Ideal density [g/cm^3]	V_V [%]
3.6	2.3334	2.2501	2.5383	8.1
4	2.3638	2.2729	2.5264	6.4
4.4	2.3937	2.2928	2.5132	4.8
4.8	2.3906	2.2811	2.4802	3.6
5.2	2.3775	2.2600	2.4575	3.3

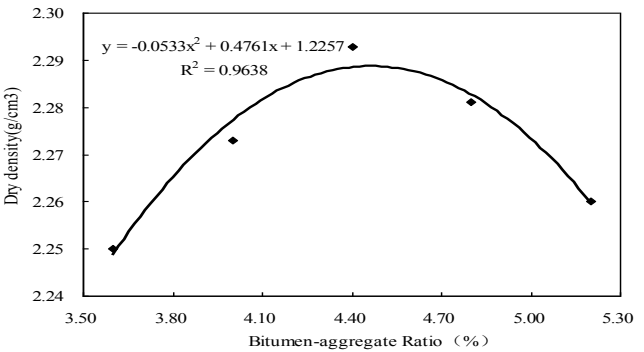

FIG. 1. Dry density versus bitumen-aggregate ratio.

Review the trend of dry density with bitumen-aggregate ratio, dry density increases with increasing bitumen-aggregate ratio at first, reaches a peak, then decreases. According to the optimal asphalt content design method based on the closest contact condition, the fitting function of the curve can get the inflection point value with 4.5% from the results showed by Fig. 1. Mix with this bitumen-aggregate ratio is in the densest condition with the minimum values of VMA or VCA_{mix}. The bulk density correspondingly is 2.394 g/cm^3 while the V_V is 4.4%.

Modified coal pitch design

Asphalt index

Coal tar pitch is also one kind of extremely complex colloidal dispersion as petroleum asphalt. According to colloid structure theory for petroleum asphalt, free carbon content is high in coal tar pitch; Colloidal nucleus is particularly large. On the other hand, the content of resin material as the dispersion medium is less. Compared with petroleum asphalt, performances like the resistant to high temperatures, low tensile strength are also very poor. By changing the relative content of each component in modified coal pitch, the colloid structure system in the disperse system is made in order to make the road properties reach the requirements quality index for road asphalt.

Table 3. Performances effect vary with the contents of coal tar pitch

Asphalt Type	Addition for coal tar pitch (%)	Penetration (25℃, 0.1mm)	Softening point (℃)	Ductility (15℃, cm)
AH-90	0	86	45.8	>150
	5	67	46.9	121.6
	10	56	48.6	85.9
	20	50	49.3	66.4
AH-70	0	67	52.8	>100
	15	51	53.1	66
	20	40	53.1	50.6
	30	38	54.9	26.4

As shown in Table 3, with the increase of the content of coal pitch, two blended asphalt become harden as the softening point rises, the penetration is reduced, and ductility is descended. As is analyzed, with coal pitch and petroleum asphalt blended, the content of saturate and aromatic are reduced. Viscosity in the system is increased so that the penetration becomes lessen. Because of the insoluble dispersing in the asphalt, the frictional resistance in the movement process of asphalt molecular chain gets bigger. Thus, the softening point is increased while the ductility reduced significantly.

Mixture performance

According to the bulk density parameter from the Marshall test, the wheel rutting test samples were formed according to 98% compaction degree level then carried out the rutting test according to “Standard Test Methods of Bitumen and Hot mix asphalt for Highway Engineering (JTJ052-2000)”. The results are presented as in Table4.

Table 4 shows that the coal pitch mix does not have good high temperature performance as the dynamic stability lower than 1500 times / mm which is the

designed value. Therefore, it is necessary to use the content of the modified coal tar pitch by necessary.

Table 4. High temperature stability test results for coal pitch mixture

Asphalt type	E_1 [mm]	E_{45} [mm]	E_{60} [mm]	Dynamic Stability [times/mm]	Relative deformation [%]
Coal pitch	2.39	6.38	7.23	735	9.7
	1.98	5.87	6.61	851	9.26
	2.45	6.27	6.98	887	9.06
AH-70	0.97	2.703	2.931	2763	3.9
	1.25	2.85	3.08	2739	3.66
	1.22	2.93	3.15	2864	3.86
AH-90	0.62	2.524	2.891	1717	4.5
	0.74	2.638	2.994	1770	4.51
	1.276	2.943	3.28	1869	4.01

This research discussed the effect of components changes in coal pitch on the stability of mixture at high temperature through a variety of programs. First of all, verified the high temperature stability of the asphalt mixture used respectively AH-70 and AH-90 while the bitumen-aggregate was fixed 4.5%.

Table 5 shows that the high temperature stability of the asphalt mixture used respectively the AH-70 and AH-90 can meet the design requirement. The high temperature of AH-70 is superior to that of AH-90 while dynamic stability increased by 56.2% and the relative deformation was reduced by 12.3%.

Table 5. High temperature stability test results of the matrix asphalt

Asphalt type	E_1	E_{45}	E_{60}	Dynamic Stability	Relative deformation
	[mm]	[mm]	[mm]	[times/mm]	[%]
AH-70	0.97	2.703	2.931	2763	3.9
	1.25	2.85	3.08	2739	3.66
	1.22	2.93	3.15	2864	3.86
AH-90	0.62	2.524	2.891	1717	4.5
	0.74	2.638	2.994	1770	4.51
	1.276	2.943	3.28	1869	4.01

This paper improved the high temperature stability of the asphalt mixture through four test plans as follows. Scheme1: kept the content of AH-90 was 70 percent; Scheme2: replaced AH-90 by AH-70 while kept the content still at 70 percent;

Scheme3: adjusted the content of AH-70 to 80 percent. Scheme4: added the anti-rutting agent into the coal tar pitch (0.4 percent by weight of mixture). The bitumen-aggregates were fixed 4.5% in the four cases.

Fig. 2 shows that the dynamic stability index could not meet the requirement when the content of AH-90 at 70 percent; But when AH-90 was replaced to AH-70, the index get better and it could meet the requirement. When the content was increased to 80 percent, there was only a certain degree increase as to the dynamic stability index, the range was limited. Scheme4 indicated that anti-rutting agent could significantly improve the high temperature stability of asphalt mixture. The dynamic stability index improved by 4.5 times and relative deformation reduced to 34.3% than before; At last, scheme2 was selected as the optimal scheme considered the test index cases and the engineering cost as to dedicating to promoting coal pitch.

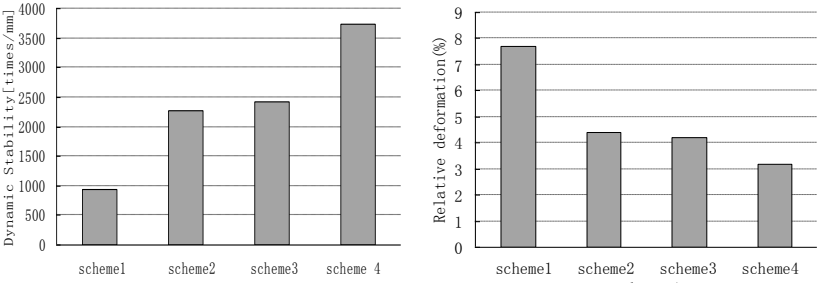

(a) Dynamic stability **(b) Relative deformation**

FIG. 2. High temperature stability test results.

RESULTS AND DISCUSSION

Mixture of coal tar pitch is also a typical visco-elastic material. With repeated traffic load in hot season, the strength and stiffness of the asphalt mixture will be significantly decreased, resulting in the rutting, hugging and other damages, which have serious impact on road-driving comfort and safety. In this study, the road performance tests included the high temperature stability test, the low temperature crack resistance test and the water stability test. The asphalt mixture samples were taken from the road construction site and the laboratory hot-mixed.

Performance test

In the Rutting test, the weight of samples was calculated based on the standard density got from indoor Marshall Test considered the compaction of 98 percent. The results are showed in table 6.

Table 6. High temperature stability test results

Different sits	E1 [mm]	E45 [mm]	E60 [mm]	Dynamic Stability [times/mm]	Relative deformation [%]
Indoor test	2.39	3.859	4.136	2273	3.5
on-site test	1.534	3.379	3.645	2368	4.2

Meanwhile, the Low temperature bending test was conducted by the mixture samples from the construction site and the indoor hot-mixed. In the test, the temperature was kept 10 degrees centigrade below zero and the loading rate was 50 mm / min. Test parameters were included damage strength, failure strain and failure stiffness modulus. Water stability tests included Remnants stability test and Freeze-thaw splitting test. Test results are shown in table 7.

Table 7. Road performance test results

Different sits	Flexural strain ($\mu\varepsilon$)	Remnants stability (%)	Tensile Strength Ratio (%)
Indoor test	2390	90.4	85.8
on-site test	2452	88.8	85.4

Test results show that the asphalt mixture samples taken from different sites have similar road performance. The high temperature stability index of the mixture of coal tar pitch is extremely important in design. As showed in the table, the dynamic stability which about 2300 times / mm were greater than the designed value (1500 times / mm); In the low temperature crack resistance test, the flexural strain was about 2400, which basically met the design requirements; As to the water stability, remr $\mu\varepsilon$ s stability and freeze-thaw splitting tensile strength were more than 80% of the design requirements. The test results indicated that coal tar pitch mixture designed in this study could meet the designed documents and have good road performances.

Thus, it can be concluded that blending the coal pitch with matrix can have very good cross-linking reaction, which bring about good performance to road. It can provide reference value for the further application of coal tar pitch.

Environment detection

Coal tar pitch, the staple product of coal tar separation process is a component of highly complex organic compounds. It is found that most of the compounds are at least 3 rings polycyclic aromatic hydrocarbons among more than 70 identified compounds (Arthur, 1995). The pollution that is produced by the asphalt smoke in the construction is drawn more and more attention. By adding warm mix asphalt

additive not only can it reduce the temperatures in mixing and compaction, reducing the energy consumption, but also effectively reduce the emission of harmful gas (Wieslwa, 1998).

In order to fully understand the harmful gas components in the construction of coal tar pitch and the different content of emission gas in different construction conditions, the warm mix asphalt additive was added in a section of the asphalt pavement. From the experiment and engineering practice, the construction temperature could be decreased by 30℃. The Ministry of Environmental Protection authority was commissioned in the test section to monitor and quantitatively analyze the components of the harmful gases in the construction, the test results are as follows:

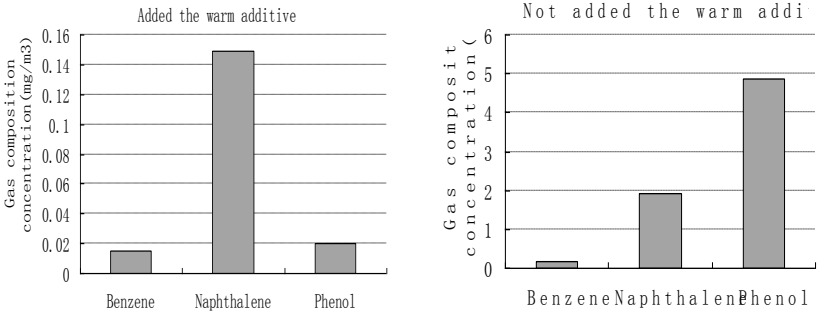

(a) Added the warm additive **(b) Not added the warm additive**

FIG. 3. Influences of harmful gas emission with different construction techniques.

The result shows that appropriately reducing construction temperature can effectively restrain the emission of toxic gases in asphalt smoke. The benzene concentration in the gas was reduced by 11.7 % from 0.017 mg/m^3 to 0.015 mg/m^3 while the naphthalene concentration was reduced by 92.2% from 1.915 mg/m^3 to 0.149 mg/m^3. In particular, the phenol concentration was reduced by 99.8% from 4.875 mg/m^3 to 0.02 mg/m^3. Therefore, the phenol and the naphthalene were influenced greatly by addition of the warm mix asphalt additive, but it was not so much as to the benzene. Overall, the addition of the warm mix asphalt additive to the coal tar pitch could greatly reduce harmful gas emissions to environment.

CONCLUSIONS

Based on the data collected and its analysis, the following conclusions can be made:

Firstly, the findings suggest that blending coal tar pitch and petroleum pitch is an important way of engineering application for coal pitch bitumen. Besides, the performance increase level is not so much obvious as the constant content increase of the matrix bitumen in some extent.

Secondly, it is indicated that the mixture designed in the densest condition can have good road performance no matter whether the mixture samples were taken from road construction site or the indoor hot-mixed. It can provide reference value for the further application of coal tar pitch.

Thirdly, it can be concluded that blending the coal pitch with matrix can have very good cross-linking reaction, which bring about good performance to road. It can provide reference value for the further application of coal tar pitch.

The last, the construction temperature can be decreased by adding WMA in coal pitch. It can effectively influence the emission of the harmful gas in fumes from bitumen in high temperature. The phenol is decreased by 99.8% while the naphthalene is decreased by 99.2%.

ACKNOWLEDGEMENTS

The authors appreciate the financial support from the Research Institute of Highway Ministry of Transport (RIOH) and also thank ZhiFeng.Yang(director in highway research centre), Prof. XuDong.Wang and Ph.D. Lei. Zhang. All of them gave their self-giving guidance and support in this project.

REFERENCES

Arthur, M.U. and William, B.G. (1995). "SBS-modified asphalt-based material with resistance to cross linking." USA, US5451621:125-128.

Deng, X.L. and Gao, J.S. (1999). "Progress in upgrading coal tar pitch for paving materials." *Journal of Coal Chemical Industry*, Vol. 13 (11): 87-92.

Dou, H.B. (1999). "Discussion of Actuality and Development Tendency of Coal Tar Processing Home and Abroad." *Journal of Henan Metallurgy*, Vol. 5 (51): 37-42.

Hossain, Z.A. and Bhudhala, M. (2009). "Evaluation of the use of warm mix asphalt as a viable paving material in the united states." *Final Report No.DTFH61-06-H-00044: Task 3*, Federal Highway Administration, McLean, Virginia.

Perez, M. and Granda, M. (2001). "Preparation of binder pitches by blending coal-tar and petroleum pitches." *Journal of Light Metals*, Vol. 55 (48): 573-579.

Wang, X.D. and Zhang, L. (2009). "Optimal bitumen-aggregate ratio selection method of hot mix asphalt based on closest compaction condition." *Journal of Testing and Evaluation*, Vol. 37(5): 490-493.

Wieslwa, A. and Stanislaw, B. (1998). "Modyfikae jaw laseiwosei fizykoe chemiezn

yehpakow weglo ehpolimernaji." *Journal of Korbo Energoehemia Ekologia,* Vol. 43(11): 372-375.

Xiao, Y.H. and Hu, R. (2009). "Effects of five dangerous chemicals in coal tar to workers and preventions." *Journal of Guangzhou Chemical Industry*, Vol. 37(4): 17-19.

Xue, Y.B., Yang, J.L. and Liu, Z.Y. (2004). "Paving asphalt modifier from co-processing of FCC slurry with coal." *Journal of Catalysis Today*, Vol. 98(2): 333- 338.

Xue, Y.B., Yang J.L. and Wang, Z.Y. (2004). "Heavy products from coprocessing of FCC slurry and coal as bitumen modifier." *Journal of Fuel Chemistry Division*, Vol. 49(1): 24-25.

Zielinski, J. (1987). "Coal tar pitch has a high boiling solvent for polymers." *Fuel*, Vol. 66 (11): 1556-1557.

Zielinski, J. (1997). "Pirenu wsubstanej bitmuieznyeh." *Journal of Karbo Energoehmai aEkologia*, Vol. 42(4): 162-164.

Study of the Thermal Regeneration Process of Ready Mixed Hot Asphalt Mixture Based on Diffusion Theory

Honghai Liu [1], Dengcheng Ma [2], Xireng Wang [3] and Daile Gao [4]

[1] Key Laboratory for Highway Construction Technology and Equipment of Ministry of Education, Chang'an University, Xi'an 710064, China; email: liuhonghai@chd.edu.cn
[2] Key Laboratory for Highway Construction Technology and Equipment of Ministry of Education, Chang'an University, Xi'an 710064, China.
[3] Fujian rail extension machinery limited company
[4] Fujian rail extension machinery limited company

ABSTRACT: When using the batch asphalt mixing plant for thermal regeneration of RAP, to a certain extent, the performance of the recycling mixture depends on the degree of diffusion permeation of the regeneration agent in the aging asphalt. Based on the analysis of the structure and working principle of mixer, the mathematical model was established, which is related with the use parameters and operating parameters of stirrer, and the time that the recycling agent uniformly distributed required was determined. Based on solute solvent diffusion theory, the time that regeneration agent diffusion penetration required was identified by test, and last, the thermal regeneration process of ready mixed hot asphalt mixture was obtained.

INTRODUCTION

In road construction, after heating, storage, transportation, construction and service process, and by the atmosphere, external environment and the long-term effects of traffic load, evaporation, deoxygenating, oxidation, condensation, and a series of physical and chemical reaction occurs, the asphalt will produce hardening, brittleness, this phenomenon is known as aging. On the physical properties of asphalt, penetration and extension reduced, softening point and viscosity increased. In order to restore the original performance of aging asphalt, the regeneration is needed.

The regeneration of old asphalt is the reverse process of the aging process. According to the component adjustment theory, if you want the aging asphalt to restore its original performance, you need to add the missing component of a reasonable allocation. Or according to the compatibility theory, put recycling agent into aging asphalt can reduce the solubility parameter difference value between asphaltenes and soft asphaltenes. This will make asphalt has good compatibility, form a stable solution, and to restore its good rheological properties.

It can be seen from the above analysis, in the whole process of the asphalt mixture regeneration, the regeneration and recovery performance of aging asphalt is important. For batch mixing plant thermal regeneration of industrial production, whether the regeneration agent is evenly distributed at the surface of the particles of recycled materials, and full penetration and fusion is the important factor for Impact renewable Mixture Performance degree of recovery.

Therefore, how to arrange the mixing process of the mixing equipment is a key part of aging asphalt recycling technology. For the problem, the aging of asphalt to the aggregate transfer law was studied by Ling DIN and Xiaomin HUANG, they think that the best way to increase the amount of asphalt transfer is to add recycling agent, increase the temperature of recycled material (RAP), and extend the mixing time (Ding, 2009).The regeneration mechanism of the asphalt pavement and regeneration agents was studied by Chongli LIU, the aging mechanism of asphalt, composition of recycling agent were analyzed and the technical requirements of regeneration agents was proposed (Liu, 2010).The harmony of old and new asphalt regeneration was studied ,and the Performance variation of harmonic process was analyzed (Hou, 2006).

The contents of this article is based on diffusion theory, Analysis of the using parameter of stirrer impact on recycling agent dispersed and infiltrated to the aging of asphalt in the industrial production process. And determine to improve the quality of regeneration of the mixture mixing process.

THE BLACK ROCK STUDY OF RAP AND REENTRANT DIFFUSION THEORY

The black rock study of RAP

When the RAP in the thermal regeneration, if the aging asphalt and new asphalt integration is? What the degree of integration? This will have a major impact on the quality of the mixture of renewable. When the aging asphalt and new asphalt is complete segregation, it can be seen as overall aggregate; when the aging asphalt with new asphalt integration, you should consider the degree of integration of recycled asphalt mixture. To solve the above problems, the United States conducted a special study, namely, Black Rock study. The test is divided into three cases: The first case is the new asphalt, new aggregate and the old aggregate of RAP mixed and then made into the specimen; The second case is the aging asphalt of RAP with new asphalt mixed in proportion, and then mixed with new aggregate and the old aggregate of RAP made into the specimen; The third case is the new asphalt and new aggregate and RAP mixed with by a certain percentage made into the specimen.

The high temperature stability, low temperature cracking and intermediate temperature fatigue resistance of the comprehensive test of the three specimens, the conclusions as follows:

When the RAP content is low (less than 15%), the sample has almost the same

performance in three conditions; When the RAP content is high, the performance of the sample is different in three conditions, the performance of the third specimen took place a significant change; This suggests that only the aging asphalt of RAP fusion, regeneration mixture can play its due performance. The NCHRP study also proves this conclusion (McDaniel, 2000), thermal regeneration mixture of the RAP not only act as the aggregate, but also the old asphalt played a role in the regeneration process, regeneration performance of the mixture depends on the new, the old asphalt mixing of the degree. Therefore, when RAP content is high (greater than 15%), we need to adopt renewable agent adequate penetration and regeneration of aging asphalt.

Diffusion penetration theory

The diffusion is that, when the concentration is not the same between the different components of the mixture, the high concentrations of material molecules to the low concentration of the material in the migration process. Through research, the description of diffusion process equation was given by Fick, when a certain pressure and temperature, and its expression can be written as Eq. (1).

$$C = \int_0^t D \cdot \left(\frac{\partial^2 C}{\partial Z^2} + \frac{1}{A} \cdot \frac{\partial A}{\partial Z} \cdot \frac{\partial C}{\partial Z} \right) \cdot dt \tag{1}$$

Where Z is the position, C is the concentration at position Z, D is diffusion coefficient, A is diffusion area, t is diffusion duration time.

When the diffusion occurs in a certain section, the concentration of a point Z depends on the diffusion coefficient D and the diffusion duration time *t*. Stoke-Einstein formula shows that the diffusion coefficient can be estimated by the Eq. (2) (Zheng, 1996):

$$D = \frac{K \cdot T}{6\pi\mu R_0} \tag{2}$$

Where K is the Boltzmann constant, T is thermodynamic temperature, R_0 is Solute molecular radius, μ is Solvent viscosity.

From Eq. (1) and Eq. (2), for the given section, the regeneration agent in the bitumen solution of a point spread function can be expressed by Eq. (3).

$$C = f(K, T, \mu, R_0, t) \tag{3}$$

Where the parameters in the regeneration effect can be explained as follows: ① The solvent viscosity μ has a significant impact on the proliferation of materials, the occurrence of diffusion can be considered as the results of molecular Brownian motion, the greater the solvent viscosity, the greater the diffusion resistance at the same temperature, and the longer the molecular concentration to balance need. ② The temperature *T* on the proliferation of materials is reflected in two aspects: First of all, because the asphalt is the temperature materials, to some extent, its viscosity is determined by temperature, when the temperature is low, the viscosity of bitumen is

high, when the temperature is high, the viscosity of bitumen is low; On the other hand, with temperature increasing, the energy of the molecules Brownian motion increases, the diffusion speed is accelerate. ③To some extent, the size of the solute molecular radius R_0 determine the friction of the solute movement, the average radius is proportional to the diffusion ability of molecules, the larger the radius, the slower rate of diffusion. ④The proliferation of duration t is the key factor in the process of diffusion occurs, the longer the t the more fully the diffusion occurs.

THE TIME OF RECYCLING AGENT DIFFUSION AND PENETRATION REQUIRED

Regeneration of mixing technology of the batch asphalt mixing plant

The stirrer is the core of the batch asphalt mixing plant. The feature is to carry out mixing a batch cycle in the compulsory mixer on the aggregates and asphalt, slag, and RAP. Its function is mixing the aggregate, the powder and asphalt binder into a homogeneous mixture at a certain temperature according to the ratio of mixture. The forced mixing after the material discharged into the blender, the mixing time is determined by the time required for uniform wrapped cover a layer of asphalt film to the surface of aggregate particles. For the original raw material, the mixing time is usually divided into without asphalt stirring time, asphalt stirring time, discharge time and cycle time. The time without asphalt stirring is the mixing time before asphalt added to the stirrer, from discharged the aggregate into the stirrer to the asphalt began to spray; The asphalt stirring time is the mixing time after asphalt added to the blender, from the asphalt spray to the blender began to discharge; The time stirrer discharge the mixture spent was called discharge time. Various aspects of the mixing length of time depends on the design parameters of the agitator, the ease of material mixing, the material in a stirrer full of rate and other factors. Generally speaking, the time without asphalt stirring is between 3-5s, The time with asphalt stirring is between 25 ~ 35s, the time stirrer discharge the mixture is 9s and the cycle time is between 36 ~ 50s.

When the regeneration of recycled materials, the stirrer mixing time allocation has become complex and sensitive, and generally the feeding sequence is as follows: First join the recycled materials, after a period of without asphalt mixing adding the recycling agent mixing, then add the overheating of the new aggregate, after a certain time mixing, join asphalt continue mixing, to complete the process of mixing of the batch of material to be uniform mixing

In the mixing process of the renewable mixture, the interaction between the materials can be described as follows: The first process is the regeneration process of the regeneration agent on the recovery of compound aging asphalt, including the regeneration agent dispersed in the particle surface of the old material and the

regeneration agent diffusion and penetration in asphalt. If the regeneration agent is dispersed unevenly or infiltration is not sufficient, this will reduce the reduction effect of the aging asphalt, affecting the regeneration performance of the mixture. Therefore, it needs to have sufficient duration of action. The second stage is the old asphalt, new asphalt uniformly mixed and mingled with stage, at this stage, if the aging asphalt has been renewable，its mixing process is the same as the original raw material. If the aging asphalt have not been fully renewable, it is necessary to increase the mixing time. Therefore, when the regeneration of the RAP must determine the mixing time, That is, the RAP and recycling agents dispersed required time, the recycling agents penetration required time, and recycled asphalt and new asphalt distributed to old and new aggregate surface required time。

Determine the time required for uniform mixing materials

In order to determine the material uniformly distributed in the stirrer needed time, according to Fig. 1 shows the agitator structure and working principle to establish a mathematical model, which is associated with the mixing uniformity, motion parameters, and using parameters.

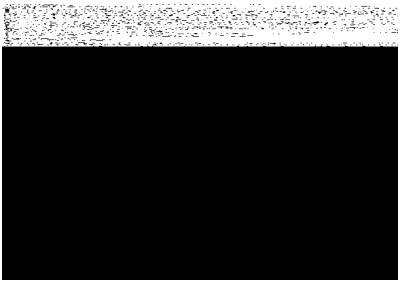

FIG. 1. Schematic diagram of mixer.

Fig. 1 shows schematic diagram of mixer. Where Ⅰ is mineral powder or asphalt concentrated cutting area, Ⅱ is blade overlap area, Ⅲ is aggregate concentrated cutting area. In Fig. 1, the asphalt content of area Ⅰ is i_1', area Ⅱ is i_2', and area Ⅲ is i_3'. When i_a is the average of i_1' and i_3', then the asphalt content of area Ⅱ can be expressed using Eq: $i_2' = (i_1' + i_3')/2 = i_a$. To facilitate the analysis and calculation, define the ratio of i_1, i_2, i_3 and i_a is relative asphalt content, and it can be expressed using Eqs.(1)-(3). Thus Eq.(4) can be obtained.

$i_1 = i_1'/i_a$ (1); $i_2 = i_2'/i_a$ (2); $i_3 = i_3'/i_a$ (3); $i_2 = (i_1 + i_3)/2 = 1$ (4)

In the stirring process, when the shaft rotates one lap, the exchange coefficient between the materials section can be expressed using Eq.(5).

$$k = N \cdot \Delta m / m = N \cdot \Delta m / (m_0 \cdot \eta) = N \cdot k_B / \eta \quad (5)$$

Where k is the exchange coefficient between the materials section when the shaft

rotates a lap, N is the number of blades which are installed on the same cross-section, $\triangle m$ is the exchange capacity of a single blade, the unit is kg; m is the amount of actual material of area Ⅰ or area Ⅲ, the unit is kg; η is the mixer filling rate, the unit is %; m_0 is the amount of material of area Ⅰ or area Ⅲ as $\eta=1$, the unit is kg; k_B is the exchange coefficient between the materials section of every blade as $\eta=1$.

As shown in Fig. 1, with area Ⅱ and area Ⅲ as the research object, $N\triangle m_3\times i_3$ is the amount of asphalt material from area Ⅲ into area Ⅱ, $N\triangle m_2\times i_2$ is the amount of asphalt material from area Ⅱ into area Ⅲ. So the amount of asphalt material of area Ⅲ can be expressed using Eq. (6), when the shaft rotates a lap.

$$m \times i_{3.1} = m \times i_3 - N\Delta m_3 \times i_3 + N\Delta m_2 \times i_2 \tag{6}$$

Where m is the amount of actual material of area III, the unit is kg; $i_{3.1}$ is relative content of asphalt, shaft per revolution, the unit is %; $\triangle m_3$ is the amount of asphalt material from area III into area II, when a single blade rotates a lap, the unit is kg; $\triangle m_2$ is the amount of asphalt material from area II into area III, when a single blade rotates a lap, the unit is kg.

Because the total material in each section is unchanged, Eq.(7) can be obtained. Put Eq.(7) and Eq.(4) into Eq.(6), Eq.(8) can be obtained.

$$\Delta m_3 = \Delta m_2 = k \cdot m / N \tag{7}$$

$$i_{3.1} = i_3 - k\times i_3 + k\times i_2 = i_3 + k(1 - i_3) \tag{8}$$

When the shaft rotates two laps, the relative content of asphalt of area Ⅲ can be expressed using Eq.(9). So when the shaft rotates n laps, the relative content of asphalt of area Ⅲ can be expressed using Eq.(10). In Eq. (10), the expression within the braces is the infinite series, the first item is 1, and the series ratio range is from1 to k. Because when $n\to\infty$, $(1-k)^n\to 0$, the series converges. Eq.(11) is the sum of the value of the n items. When $n\to\infty$, the limit of Sn can be expressed using Eq.(12) .Then the relative content of asphalt of area Ⅲ can be expressed using Eq.(13).

$$i_{3.2} = i_{3.1} + k(1-i_{3.1}) = i_3 + k(1-i_3) + k(1-i_3)(1-k) \tag{9}$$

$$i_{3.n} = i_3 + k(1-i_3)[1 + (1-k) + (1-k)^2 + (1-k)^3 + \cdots + (1-k)^{n-1}] \tag{10}$$

$$S_n = \frac{1-(1-k)^n}{k} \tag{11}$$

$$\lim_{n\to\infty} Sn = \lim\left(\frac{1}{k} - \frac{1-(1-k)^n}{k}\right) = \frac{1}{k} \tag{12}$$

$$i_{3.\infty} = i_3 + k(1-i_3)/k = 1 \tag{13}$$

The provisions for asphalt allow deviation, and the value of n_0 and Sn_0 can be obtained. Put the value of Sn_0 into Eq. (10), Eq.(14) and Eq.(15) can be obtained.

$$i_{3.n_0} = i_3 + k(1-i_3)[1-(1-k)^{n_0}]/k \tag{14}$$

$$n_0 = \frac{\log(1 - i_{3.n_0} + i_3) - \log(1 - i_3)}{\log(1 - k)} = \log(1 - i_{3.n_0}) / \log(1 - k) \quad (15)$$

Set the blender mixing shaft speed is n, put i_3=0(The most unfavorable initial relative asphalt content is 0 in area Ⅲ) and k=$N\ k_B/\eta$ into Eq.(15), Eq.(16) can be obtained.

$$t = n \cdot \log(1 - i_{3.n_0}) / \log(1 - N \cdot k_B / \eta) \quad (16)$$

For the formed mixer, the mixing time is determined by the uniform mixing of the mixture i_{3n0}, agitator speed n and material fill rate η together.

For the stirrer, its fill rate is 65%, speed is 52rpm, N is 2, and k_B is 0.04, when the requirements of the asphalt content is 5%, and the content of error is less than 0.3%(relative deviation is 0.06, asphalt content is 0.94), according to Eq. (16), the mixing time is not less than 26*s*. If without asphalt mixing time is 5*s*, the sum of without asphalt mixing time and asphalt mixing time is not less than 31*s*. When RAP stirring is 40%, the fill rate is 26%, If the incorporation of the recycling agent is 5%, and the content of error of less than 0.3%, according to Eq. (16), the uniform mixing time of recycling agent required is less than 8*s*.

The diffusion and penetration time of regeneration agent

Material diffusion theory suggests that, the basic factors that determine the recycling agent diffusion and penetration effects are solvent viscosity, material temperature, the solute molecular radius and diffusion time, as shown in Eq.(3).Because it is difficult to determine diffusion time required for recycling agent in the asphalt film from the theoretical derivation. In this study, the determination of the regeneration mixture of physical indicators indirectly reflects the penetration time of the recycling agent. In order to simulate actual working conditions, the RAP heating temperature is 140^{o}C.The aging asphalt, recycling agent and new asphalt performance are shown in Table 1, Table 2 and Table 3. Mixing the mixture of RAP Blending ratio of 40%, the recycled mixture has the same gradation and asphalt content, the RAP mixing diffusion and penetration time was set: 10*s*, 20*s*, 30*s*, And then mixing with new asphalt, aggregate, determination of the stability of the mixture, the results were shown in Table 4.

Eq. (17) and Fig. 2 can be obtained by fitting the stability data in the table, derivative of Eq. (17) to obtain the extreme value of time is 27.5s, extreme value 15.1KN. Therefore, we can determine the 95% extreme value of the diffusion and penetration is less than 20S, reaching 85% extreme value of the diffusion penetration is less than 15s.

$$y = 0.014x^2 + 0.77x + 4.5 \quad (17)$$

Table 1. Aging Asphalt properties

Items	Test values
Penetration at 25 °C/0.1mm	32
Ductility at 15 °C /cm	13.5
Softening point / °C	58.1
Rotary viscometer at 60 °C /Pa.S	＞1000

Table 2. Recycling agent performance

Items	Test values
flash point / °C	240
density /g/cm^3	0.925
Rotary viscometer / Pa.S	0.08
Aromatic content /%	61

Table 3. Asphalt performance of 70#

Items	Test values
Penetration at 25 °C /0.1mm	72
Ductility at15 °C /cm	＞150
Softening point / °C	48
Rotary viscometer at 60 °C /Pa‖ S	225

Table 4. Recycling Mixture Marshall experimental parameter values

Items		Diffusion time/S		
		10	20	30
Degree of stability /kN	1	11.4	14.1	15.1
	2	9.9	14.5	15.1
	3	11.0	13.7	14.7
	Mean value	10.8	14.3	15.0

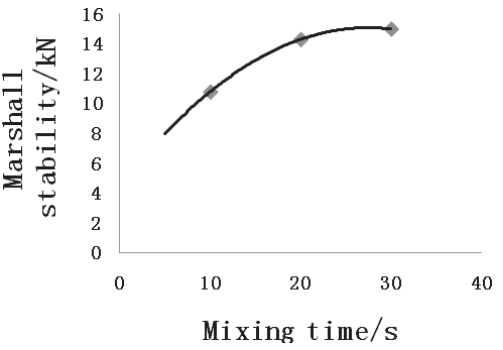

FIG. 2. Stability with the mixing time curve.

CONCLUCSIONS

When the RAP content is high (>15%), the RAP not only act as aggregate in the recycled mixture, the aging asphalt also play an important role, the different degree of mixing of the new and old materials have a significant impact on the performance of the recycled mixture.

Adding recycling agent is an important measure to recovery the performance of aging asphalt. In order to make recycling agent to fully diffusion and penetration, In the regeneration mixture production process should have enough ready-mixed time, RAP and recycling agent uniform mixing time required to less than 8*s*, the time recycling agent diffusion and penetration required to less than 15s.

ACKNOWLEDGMENTS

The authors appreciate the support of the special fund for basic scientific research of central colleges, chang'an university and basic research support program of chang'an university (CHD2011SY005)

REFERENCES

Ding, L.L. and Huang, X.M. (2009). "Diffusion mechanism of asphalt rejuvenation agent and research on diffusion simulation test." *Transportation Science & Technology.*

Hou, R. and Huang, X.M. (2006). "Study of recycling aged asphalt by new asphalt." *Petroleum Asphalt*.

Karlsson, R. and Isacsson U. (2003). "Laboratory studies of diffusion in bitumen Using markers." *Journal of materials science*, Vol. 38(7):2835-2844.

Liu, C.L. (2010). "Study of asphalt pavement regeneration mechanism and regenerating agent." *Northern Communications*.

McDaniel, R.S., Soleymani, H. and Anderson, R.M. (2000). "Recommended 21se of reclaimed asphalt pavement in the superpave.mix design method." *NCHRP Web Daument 30(project D9-12)*.

Zheng, S.L. and Huang, E.C. (1996). "Application of colloid chemistry." *Shanghai East China University of Science and Technology*.

Influence of Volatile Organic Compounds Emission under Different Conditions on Performances of Asphalt

Man Yu [1], Shaopeng Wu [2], Juntao Lin [3]and Honghua Zhang [4]

[1] Master student, State Key laboratory of Silicate Materials for Architectures, Wuhan University of Technology, Wuhan 430070, China, email: yuman@whut.edu.cn
[2]Ph.D, Professor, State Key laboratory of Silicate Materials for Architectures, Wuhan University of Technology, Wuhan 430070, China, email: wusp@whut.edu.cn
[3]Ph.D candidate, State Key laboratory of Silicate Materials for Architectures, Wuhan University of Technology, Wuhan 430070, China, email: linjt1004@gmail.com
[4]Master student, State Key laboratory of Silicate Materials for Architectures, Wuhan University of Technology, Wuhan 430070, China. email: honghuazhang@126.com

ABSTRACT: During application process of the bitumen, along with aging, there also exists the volatile phenomenon at the non-high temperature condition. This paper simulated different circumstances in the laboratory-based environment, Infrared (IR), Ultraviolet Radiation (UV) and Vacuum (Va), to investigate the effects of volatile organic compounds (VOC) emission from different asphalts on the performances of the bitumen. Mass changes, chemical compositions, soften point as well as penetration test were conducted to analyze the experimental results. Basic tests were used to evaluate the colloidal structure and temperature-sensitive property of the bitumen. Temperature sweep, frequency sweep tests as well as stress and strain scanning test were introduced in this paper to investigate the effects on rheological properties by *Dynamic Shear Rheomoter (DSR).*Results in this paper show that asphalt can volatile at the non-high temperature circumstance and performances of the asphalt are influenced by VOC emission conditions.

INTRODUCTION

Asphalt binder, mainly used in the asphalt pavement, is an extremely complex mixture of more than one thousand of different types of hydrocarbons consisting of high molecular weight of asphaltee micelles dispersed or dissolved in a lower molecular weight oily medium. During heating, mixing, transfer, and application of asphalt binders, some odor often is perceived in relation to the emission of volatile organic compounds (VOCs), leading to the deteriorate of asphalt pavement.There

were many reported researches on the asphalt fumes, produced at the high temperatures, mainly concerning about the hazardous of the environment and human. In addition to mucosal irritation, workers with differing occupational exposures to asphalt fumes also reported skin irritation, rash, nausea, stomach pain, decreased appetite, headaches, and fatigue. However, there is little research about the volatilization during service process; neither is about the research on the influences of VOC emission on the performance of asphalt. Researches concerning about the service process of the asphalt pavement were referring to aging phenomenon, which can induce the performances of the asphalt, such as the changes of mass, chemical composition or rheological properties and so on. However, VOC emission from the asphalt binder, whether it happens at high temperature or during the service process, is harmful to human health and the air quality which also affects the performances of the asphalt leading to the deterioration of the asphalt pavement. The objective of this research is to study the influences of VOC emission during service process on the asphalt performances by simulating different conditions in the laboratory-based environment. Basic tests, such as mass changes, chemical compositions, soften point as well as penetration test and so on were conducted to evaluate the colloidal structure and temperature-sensitive of the bitumen. In additional, rheological properties by DSR were also investigated in this paper through temperature sweep, frequency sweep and stress and strain scanning. And investigate the changes of the maximum strain limit through stress and strain scanning by Box-Lucas model.

EXPERIMENTAL

Materials

These asphalts chosen for the experiments were SK-70 and PJ-90 provided by KOCH Asphalt Co. Ltd (Hubei Province, China). As previous research, asphalt can also volatile even if under non-high conditions. This research emphasizes on the influences of VOC emission under different conditions simulated in the laboratory-based environment at a non-high temperature.

Experiments

VOC emission of the asphalt in laboratory–based environment

Based on the laboratory environment, conditions of Infrared (IR) and Ultraviolet Radiation (UV) in the presence of the oxygen were simulated, and the non-oxygen environment of Vacuum (Va) was also simulated to investigate the influences on the asphalt's performances. In additional, the strength of UV and IR is 100W/m^2 and not less than 700 W/m^2, respectively. The temperature of all the conditions in this research was 70℃, a non-high temperature environment. Air compressor was used in

this experiment to ensure that the ambient temperature was 70. Thickness of all specimens was 1250 μm. After the release for 48h, properties of the asphalts released or unreleased were investigated.

Mass change with VOC emission

Analytical balance was used in this experiment to weight mass of all the specimens and mass accuracy was 0.001g. Rates of mass change with the release time were studied to investigate asphalt mass changes under different conditions. The reduction of the specimen's mass can be directly representative of the volatilization of the asphalt.

Component analysis

Thin-layer chromatography with flame ionization detection (TLC-FID) was used in the paper to detect four components of the asphalt. 2%(w/v)solutions of three asphalts were prepared in dichloromethane, and 1 μl sample solution spotted on chromarods using a spotter. The separation of asphalt into four generic fractions (saturates, aromatics, resins and asphaltenes) was performed by a three-stage development using n-heptane, toluene and dichloromethane/methanol (95/5 by volume), respectively. The fractions were determined by means of Iatroscan MK-6 analyzer (Iatron Laboratories Inc., Tokyo, Japan). While saturates and aromatics are the smaller molecular composition in the asphalt, the changes of these two components were investigated in this research.

Physical properties Test

Physical properties tests, such as soften point and penetration, were carried out according to Chinese standard test method JTJ052 (T0604-2000 and T0605-1993), respectively. The increment of soften point was investigated and penetration index was performed to evaluate the temperature-sensitive of the asphalt. Results of soften point and penetration index were studied in this research to evaluate the colloidal structure of the released asphalt.

Dynamic Rheological Characterization

Dynamic Shear Rheometer (DSR) MCR101 from Austria Anton Paar Company was used in this study for generating the dynamic data for the asphalt. The parameters for the DSR were in following Table1-2. Stress and strain scanning was conducted at 20^{o}C with 8mm plate and the result of this experiment was to fit curve between stress and strain according to Box-Lucas model. Relationship between stress and strain meets the following formula: $\sigma=a(1-b^{\gamma})$. Parameters of "a" and "b" were deduced by the fitting curve. In additional, maximum limit strain of the asphalt could also be inferred through stress and strain scanning.

Table 1. Parameters for Frequency Sweep

Temperature(°C)	[a]D(mm)	[b]h(mm)	[c]Fre. (rad/s)
-10, 0, 10, 20	8	2	0.1~400
30, 40, 50, 60	25	1	
[a] is the diameter of the plate; [b] is the gap between the plates; [c] is sweep frequency			

Table 2. Parameters for Temperature Sweep Test

Temperature	-10 °C~35 °C
D(mm)	8 mm
h(mm)	2 mm
Fre.(rad/s)	10rad/s
Strain (%)	0.2%
Temperature rise rate	2 °C /min

RESULTS AND DISCUSSION

Mass change with the release time

Rates of mass change with the release time were presented in Fig.1. As shown in the figure, Both two asphalts show the decreasing tendency under different conditions. The decrement of Va is smaller than that of UV and IR, which can also demonstrate that the asphalt can volatile at the non-high temperature and indicate that the oxygen at 70 °C may promote VOC emission from the asphalt. Both the two asphalts of SK-70 and PJ-90, mass loss in UV is the largest in the three conditions. In additional, mass loss of PJ-90 is larger than that of SK-70 in Va condition while smaller in UV and IR conditions, which may due to the oxidation of PJ-90 asphalt with a more light components in UV and IR conditions with a more light components.

Chemical components before and after VOC emission

While saturates and aromatics are the smaller molecular composition in the asphalt, the changes of these two components were investigated in this research. The total content of saturates and aromatics and rate of the content change were shown in Fig.2-Fig.3. Negative value of saturates and aromatics contents change rate demonstrates that the released specimen presented a smaller content of saturates and aromatics and a bigger content of asphaltee and resin compared to the unreleased

asphalt and the figures also show the different decreasing tendencies of saturates and aromatics with different asphalts and different release conditions. PJ-90 asphalt shows a smallest loss of saturates and aromatics in Va condition while a biggest loss in UV condition. However, SK-70 shows a smallest loss in UV while a biggest in IR. The cause of the decreasing tendency in Va condition may be partly that saturates and aromatics could be vaporization into the air. Different tendencies with different conditions may be due to the different mechanism of IR and UV to the bitumen.

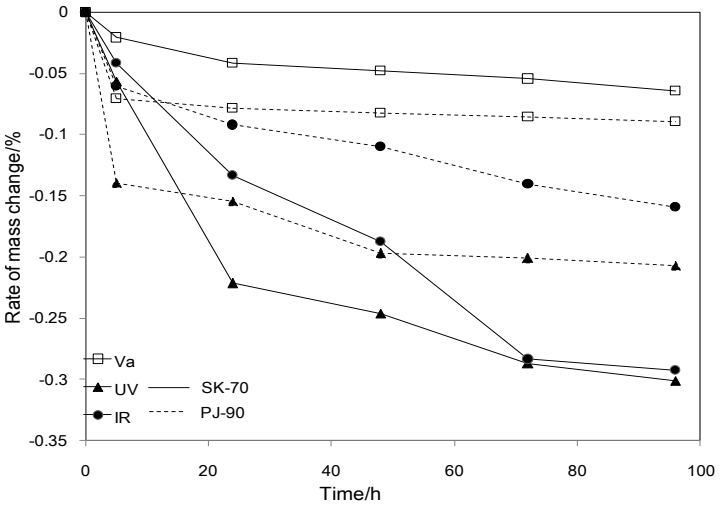

FIG.1. Rate of mass change with time in different conditions.

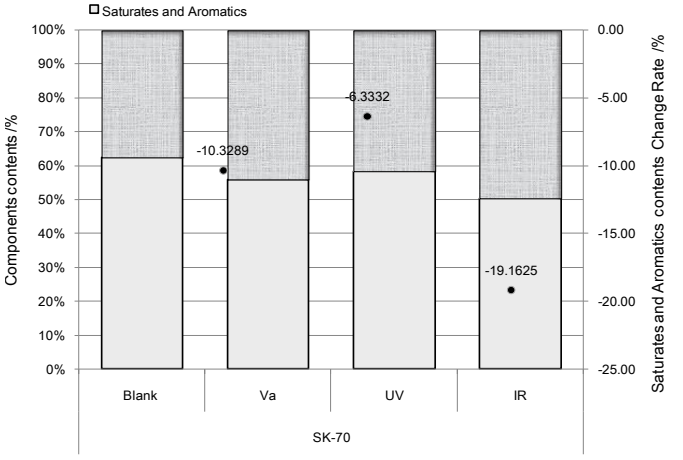

FIG.2. Components contents change of SK-70.

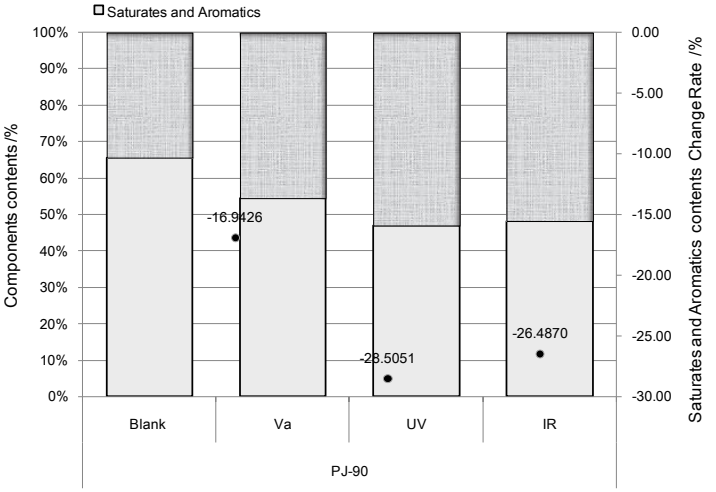

FIG.3. Components contents change of PJ-90.

Basic Physical properties

The increment of soften point, may be due to the ease of the large molecular chains in the asphalt, is usually used as the indicator to measure the aging of asphalt while a larger increment shows a more serious aging. During VOC emission process, light volatile components in the asphalt may vapor into the air, leading to the condensation of short molecular chains into a larger molecular structure. In additional, the unsaturated bonds in the asphalt will condense or be oxidized into the larger molecular structure because of the role of ultraviolet and infrared, leading to the increment of soften point. Soften point increment is shown in Fig.4. As shown in the figure, soften point of the two asphalts increased in Va condition, demonstrating a growth of molecular chains in the asphalt after VOC emission, while smaller than that in conditions of IR and UV. PJ-90 shows a larger increment in UV and Va conditions while smaller in IR condition. According to the results of 3.1 and 3.2 above, all the outcomes of mass loss, the decreasing of saturates and aromatics and the increment of soften point in Va condition can demonstrate that the asphalt would be volatile at the non-high temperature and PJ-90 observe a greater potential for volatiles than SK-70. In the condition of UV and IR, under the circumstance in the presence of the oxygen, light molecular components can volatile accompanied with the polycondensation and oxidation. Different tendencies may be due to the different mechanism of ultraviolet and infrared to the asphalt in different conditions.

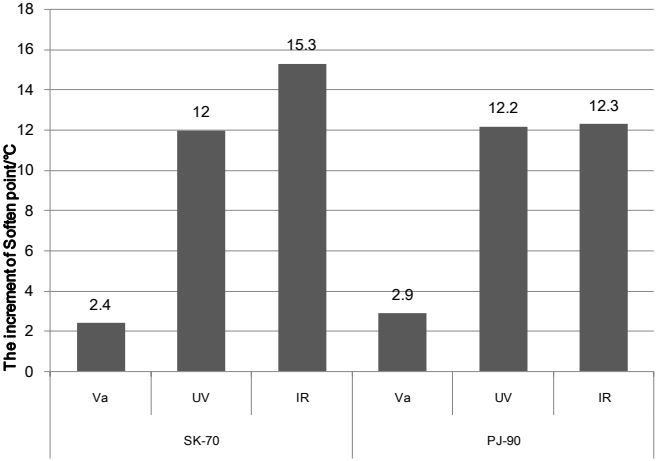

FIG.4. The increment of soften point in different conditions.

As we all known, penetration and temperature shows a good relationship. The formula to calculate the penetration index is as follows: LogP=A*T+K. Fig.5 and Fig.6 show the relationship between penetration and temperature of different asphalts in different conditions. The formula to calculate penetration index is shown below. Results are shown in Table 3 too.

$$PI = \frac{30}{1+50\dfrac{\lg 800 - \lg P_{(25,100g,5s)}}{T_{R\&B}-25}} - 1 \tag{1}$$

Table 3. Results of temperature susceptibility experiments

Bitumen	Conditions	PI value	A	K	Correlation coefficient R^2
SK70	Blank	-2.11	0.04453	0.6574	0.9943
	Va	-2.11	0.04023	0.6182	0.9966
	UV	-1.17	0.03762	0.3655	0.9944
	IR	-0.46	0.03183	0.4608	0.9946
PJ90	Blank	-2.35	0.04695	0.5562	0.9875
	Va	-2.31	0.04258	0.5351	0.9931
	UV	-1.41	0.03477	0.4608	0.9961
	IR	-1.54	0.03399	0.4608	0.9921

As shown in the figures, the penetration at the same temperature was larger compared to unreleased asphalt. Penetration of the two asphalts showed the

maximum in Va condition and different tendencies in UV and IR conditions. The slope of the line, A value shown in the figures and the Table, reduced with the minimal decrement in Va condition and the maximum in IR condition. The decreasing tendency of A value can indicate that released asphalt showed a good temperature-sensitive property accompanied with the harden phenomenon of the e asphalt. PI value, representative of the colloidal structure of the asphalt, increased after VOC emission. The increment of PI value can indicate that the transition of colloidal structure is into the gel colloidal structure. As shown in the Table, PI value in Va condition didn't change and increment in UV and IR conditions showing the tendency to the gel colloidal one.

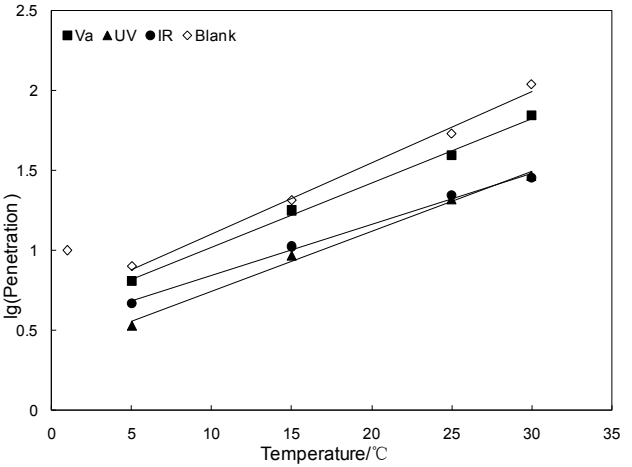

FIG.5. Linear Relationship of SK-70.

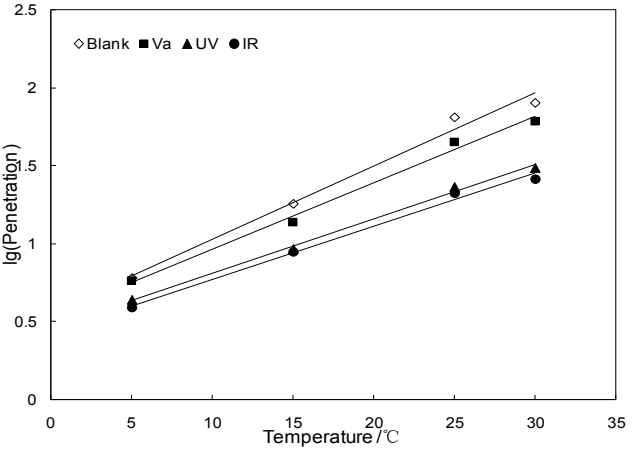

FIG.6. Linear Relationship of PJ-90.

Dynamic rheological characterization

Temperature sweep

This experiment investigated the ratio of loss modulus and storage modulus which can attribute the relationship between the viscous and the elastic of asphalt at the certain temperature, especially at low temperatures. Smaller damping factor (the ratio of G" and G') indicates bigger storage modulus at the same temperature. Curves in Fig 7, Fig 8 show the damping factors of SK-70 and PJ-90. Compared to the blank condition representative of the unreleased asphalt, damping factor reduced indicating the increase of elastic part in the asphalt and showed a different variation of different asphalts in different conditions. Larger elastic part shows a more complex molecular chains structure in the bitumen. Results in this experiment can indicate a larger elastic part after VOC emission from the asphalt and be influenced by the conditions.

Frequency sweep

The mechanical properties which obtained at different temperature and loading frequency of these materials can be parallel moved at a certain temperature to a smooth curve which called Master Curve. After frequency sweep to samples, complex modulus Master Curve was confirmed according to time-temperature equivalent principle to analysis dynamic mechanical properties of asphalt in wider loading frequency. This experiment fits Master Curve according to Time-temperature equivalent principle, results of which were presented in Figs.9 and 10.

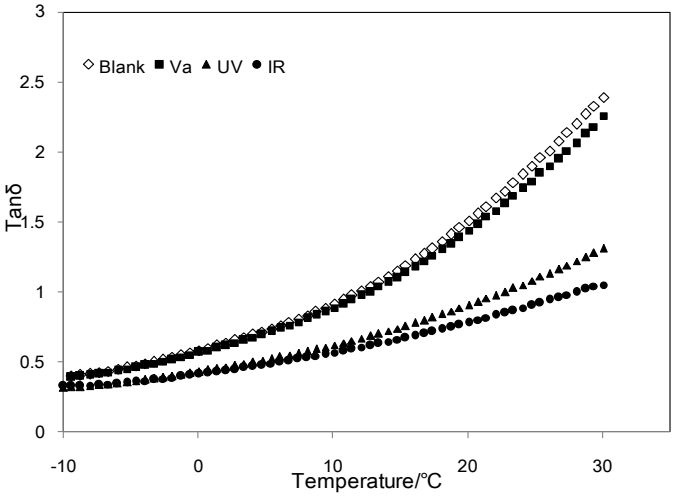

FIG.7. Damping factor with temperature of SK-70.

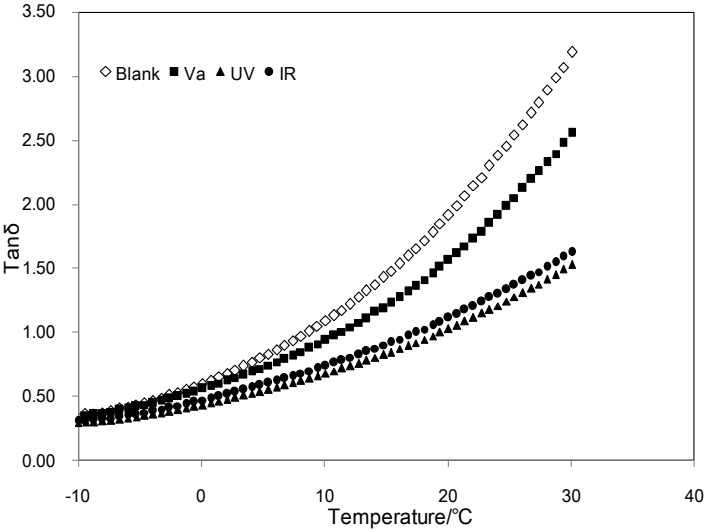

FIG.8. Damping factor with temperature of PJ-90.

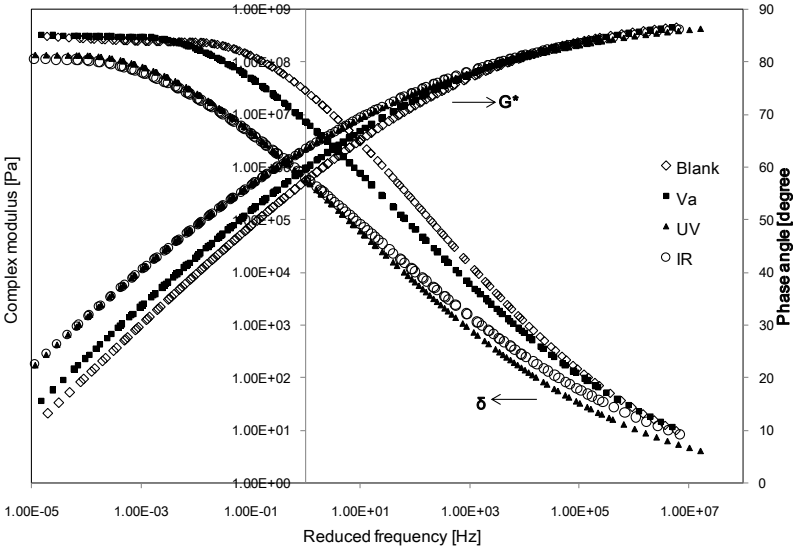

FIG.9. Master curve of SK-70 in different conditions.

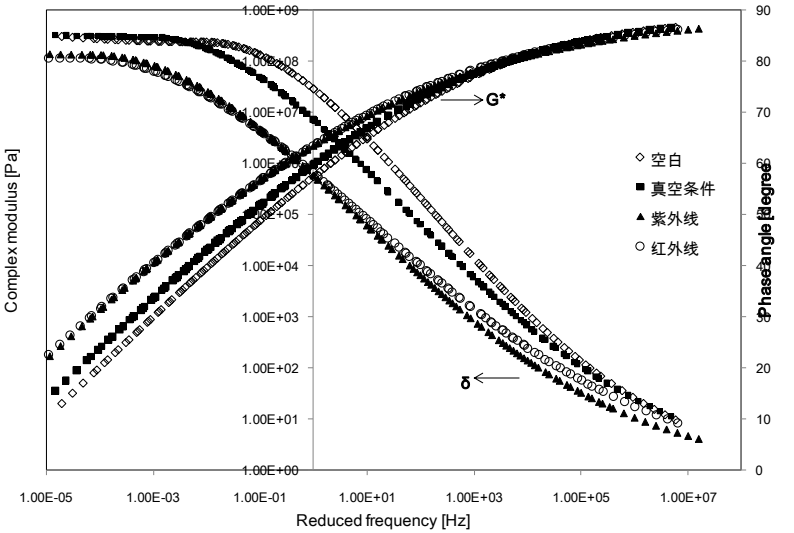

FIG.10. Master curve of PJ-90 in different conditions.

As shown in the figures, complex modulus increased and phase angle decreased with the increased frequency. Compared to blank condition, complex modulus increased and phase angle decreased after VOC emission in different condition. Different variations were showed in the figures with different asphalts in different conditions which may be due to the different mechanism of UV and IR to the asphalt.

Stress and Strain scanning

Based on the data set of stresses and strains in DSR testing, a typical distribution state of data can be plotted as the curve, It is clearly shown that the distribution of stress-strain data is very similar to the constitutive curve represented by the Box-Lucas model， which is shown in Fig 11. The Box-Lucas model is expressed as the following from,

$$\sigma=a(1-b^{\gamma}) \quad (3)$$

where, γ is tγhe variable respective for the shear strain and γ>0 , “a”，”b” are constants and 0<b<1. σ is stress and “$\sigma=a_0$” is the asymptote equation of the Box-Lucas model.

The meaning of this asymptote equation is that when the shear strain $\gamma\rightarrow\infty$,the shear stress tends towards a constant. And when σ tends to the constant “ a_0”, there will be correspond with the γ_{max}, which represents the maximum strain limit. Table 5 shows the different γ_{max} values in different conditions. As shown in the Table 5， γ_{max}

decreased after VOC emission compared to blank asphalt. Both of Sk-70 and PJ-90, the variation tendency in different conditions is the same and the descending of γ_{max} in different conditions was: blank condition, Va, UV and IR. All the results demonstrate that the maximum strain limit is significantly influenced by VOC emission.

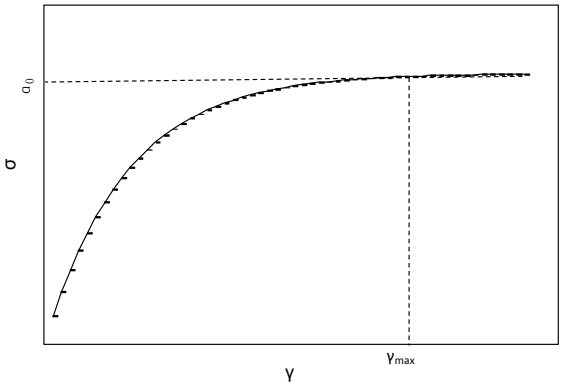

FIG.11. Relationship between γ and σ by Box-Lucas model.

Table 4 .γ_{max} value in different conditions

Asphalt	Blank	Va	UV	IR
SK70	1000%	700%	350%	10%
PJ90	3000%	2000%	400%	20%

CONCLUSIONS

Different conditions of VOC emission from the asphalt was simulated in the laboratory-based environment at a non-high temperature. Performances of the asphalt were influenced by VOC emission under different conditions. The conclusions are as follows:

- VOC emission can change the basic physical properties of asphalt. Compared to unreleased asphalt, both of asphalt mass and the contents of saturates and aromatics reduced while soften point increased in all conditions. Changes in Va condition is the smallest and different tendencies of SK-70 and PJ-90 in UV and IR conditions which may be due to different mechanism of ultraviolet and infrared to the asphalt. In additional, results in this experiment can also show that PJ-90 observe a greater potential for volatiles than SK-70.
- Basic physical test also show that PI value, representative of the colloidal structure in the asphalt, increased after VOC emission indicating that the asphalt

structure is of the transition into the gel colloidal structure. In additional, the slope of the relationship between penetration and temperature decreased after VOC emission which can indicate that released asphalt showed a good temperature-sensitive property accompanied with the harden phenomenon of the asphalt

- Damping factor from temperature sweep test decreased after VOC emission indicating the increase of elastic part in the asphalt. Larger elastic part shows a more complex molecular chains structure in the asphalt. Results in this experiment can also indicate a more complex molecular chains structure after VOC emission and be influenced by the conditions.
- Complex modulus increased and phase angle decreased after VOC emission according to the master curve through frequency sweep test.
- Through Stress and strain scanning test, the maximum limit strain γ_{max} was investigated by Box-Lucas model. γ_{max} reduced and is significantly influenced by different VOC emission conditions .

REFERENCE

Gu, G.F. and Pu ,H.D. (2000) "The basis of polymer rheology." Tongji University Press.

Mary, A.B., Gregory, B., David,D., et al. (2001) "Health Effects of Occupational Exposure to Asphalt. " *Hazard Review*. NIOSH.

Qiu, J. (2008) "Self Healing of Asphalt Mixes: Literature Review". *Delft University of Technology*.

Ratkowsky, D.A. (1990) "Handbook of non-linear regression models." New York: M. Dekker,:75-98.

Shell, B. (1995). *The shell bitumen Industrial Handbook*, Surrey, U.K.

Wong, W.G., H.F Han, G.P He, et al. (2004) "rutting response of hot-mix asphalt to generalized dynamic shear moduli of asphalt binder."*Construction and Building Materials*.18:399-408.

Yang, L. (2009) "Properties of the asphalt on long-term oxidative aging." *Northern Communi Cations*.2:53-57.

Yu, M., Wu,S.P. and Chen, M.Z. (2012) "Experimental investigation of the volatilization of asphalts under different conditions." *Advanced Materials Research.* Vols.463-464:69-75.

Yu, M., Wu, S.P., Chen, M.Z., et al. (2012) "Evaluation of Volatile organic compounds from asphalt using UV-visible spectrometer." *Advanced Materials Research*. Vols.473-475:432-436.

Zhang,Q., Zhao,J., Shi ,M.Q., et al. (2004) "Analysis on chemical aging mechanism of asphalt under effect of natural environment." *Journal. Xi'an University of Architecture and Technology (Natural Science Edition)*. 6:23-28.

A Sustainable Maintenance Solution for Porous Asphalt Pavements via Rejuvenation Technology

Zhao Su

Icopal Group R&D, Hoendiep 316, 9744 TC Groningen, the Netherlands; email: zhaosu53@gmail.com

Abstract: The paper presents the research results and discussions of a sustainable maintenance solution for porous asphalt (PA) pavements through a rejuvenation technology. A specially designed rejuvenator (as a form of emulsion) is developed and applied by means of a spraying truck on the asphalt pavement surface. The rejuvenator is able to drain via the voids and migrate into the aged bitumen, and eventually to activate and restore the flexibility of old asphalt pavements. This paper firstly gives a brief introduction to the theoretical background and research approach. Then a theoretical model has been proposed to predict the lifetime of the treated asphalt pavement. Afterwards some laboratory and field test results and the LCA investigation results are presented and discussed. The results of the rejuvenation treatment do not only show the improvement in the mechanical performance and functional requirements, but also exhibit an environmental benefit (LCA analysis) as compared with the current maintenance option. Finally, the conclusions have been drawn, followed by the recommendation for a sustainable pavement maintenance strategy based on this rejuvenation technology.

INTRODUCTION

The performance of asphalt pavements decreases with service time due to ageing of bitumen, influence of rainwater and de-icing salt, as well as dynamic loads of traffic in service. The deterioration of asphalt pavements is manifested in the form of pitting and ravelling of the surface, brittle cracking, spalling, or combinations thereof. The damage of the pavement network does not only imply high maintenance costs, but also temporary closure of traffic and hence increased road congestion. Given the high costs for the road authorities and the inconvenience for the road users, it is greatly desired to shift the solution from a repair to a preventive philosophy. Therefore, it will be of great economic benefit for road authorities if it is possible to slow down, stop or even reverse the ageing process, in situ, by adding appropriate

asphalt components, lost during the service period at the right time. Based on this idea, a great effort has been made to try to develop a new solution for asphalt maintenance, particularly for porous asphalt (PA).

PA, with an open-graded asphalt mixture, consists of a large amount of course aggregates in combination with a relatively small amount of fine fractions resulting in a very open structure (20-25% of voids by volume). As a result, PA shows various functional advantages over traditional dense asphalt, such as driving comfort, noise reduction, water drainage as well as improvement of skid resistance in wet weather (Elvik, 2005; Nielsen, 2006). Due to these undeniable advantages, PA has become very popular as a wearing course in the Netherlands, Japan and Southeast Asia countries. PA was first applied on the Dutch road network in the early of 80's and accepted as a wearing course in 1987. Since then the application has been rapidly increased and nowadays ca. 90% of the primary road network has been surfaced with this type of wearing course.

Despite the various advantages of PA, a fatal problem is its durability, manifested in the form of premature damage - ravelling, i.e. early stone loss. This type of damage mostly occurs after a severe winter. Every year ca.10-15% of PA surface layer has to be maintained or re-surfaced. In order to improve the quality and extend the lifetime of PA pavements, the Dutch Ministry of Infrastructure and Environment (RWS) has launched several huge research projects (Morgen, 2008; Hagos, 2008; Mo, 2010; RWS, 2010). One of PhD investigations at TU Delft was carried out into the effect of ageing on binder properties of porous asphalt concrete (Hagos, 2008). It was found out that the ageing process of PA took place much faster than that of dense asphalt. Furthermore the ageing degree of the binder from the top to the bottom layer is almost identical due to its high voids content. As a result, the ageing process significantly increases the "critical" temperature, at which the binder starts to behave brittle. On the other hand, the ageing also reduces the strain level and stress relaxation behaviour, which thus results in the accumulation of micro damages (defects) in PA pavements during the service period by traffic loading and climate variation. This could be the major reason for PA ravelling, particularly after a severe winter. Another PhD work looked into the damage development in the adhesive zone and the mortar of PA mixture. A theoretical model to predict the lifetime of PA pavements was established, indicating when the maintenance of the PA pavements should be carried out (Mo, 2010). It could be concluded that the ageing of the binder is the major cause of the premature damage (ravelling) of PA pavements. If this is the case, then the rejuvenation technology could be a right solution for the maintenance of PA pavements.

In 2010, the Dutch Ministry of Infrastructure and Environment (RWS) initiated a project -"The lifetime of PA pavements and maintenance strategy (LVO)", including field practical tests and laboratory theoretical investigations (RWS 2010). The aim of this project is to encourage the material suppliers and contractors to come up with

new ideas, new materials and new technology to extend the lifetime of PA pavements. Icopal/Esha Infra Solutions is one of four industrial participants with her sustainable maintenance solution - rejuvenation technology – a cold-applied product in the form of a special bituminous emulsion mixture by a spraying truck. The rejuvenator is firstly able to drain into the aged asphalt, then to migrate into the aged binder and further activate the binder, and eventually to restore the original flexibility of asphalt. As a result, new bonds are established between aggregate particles through the activated bitumen phase, so that the lifetime of the asphalt pavement can be extended, the performance of the road will be improved, and the disintegration (ravelling and cracking) will be prevented (Su, 2006; Su, 2000; Su, 2002; Su, 2005; Su, 1999; Su, 2007).

For a successful research and development, two requirements must be fulfilled: one is the high rejuvenation power of the rejuvenator to the aged binder of PA mixture; the other is the structural and functional requirements, such as the pavement stability, skid resistance, acoustic (noise) effect and water drainage power of PA pavements as compared with the untreated one.

This paper firstly gives a brief introduction to the theoretical background, research approach, followed by an example, showing how to predict the lifetime of the asphalt pavement. Then laboratory and field test results of porous asphalt pavement and the LCA analysis results are presented and discussed. Finally, the conclusions have been drawn, followed by the recommendation for a sustainable pavement maintenance strategy based on this rejuvenation technology.

MATERIALS AND TEST METHODS

Materials

The rejuvenator: A specially designed bitumen emulsion mixture.
Asphalt cores: Taken out of roads.
Broken sand: 0-2mm fraction of broken sand.

Test Methods:

Reactivity of Rejuvenator: The reactivity of the rejuvenator with bitumen is determined by means of a modified penetration test (EN-1426) at the ambient temperature (in air instead of in water). The reactivity is expressed as a migration depth of the rejuvenator into the bitumen at certain time. The migration depth of the rejuvenator into the bitumen is calculated by the penetration depth difference between 2 samples with and without rejuvenator at the same time and same condition minus the thickness of rejuvenator film left on the bitumen surface. The higher the migration depth, the more reactive the rejuvenator will be. The test method is

described elsewhere (Su, 2000; Su, 1999).

Extraction and recovery of the binder: The asphalt cores were taken out of the roads. The extraction test was done in accordance with Test Method NEN-EN 12697-1 B.1.3 at KOAC-NPC Laboratory in Groningen, the Netherlands. The reactivity of the rejuvenator with the extracted bitumen was determined (Su, 2000; Su, 1999) by applying the rejuvenator on the surface of extracted binder in a penetration cup.

Field skid resistance test: Standaard RAW Bepalingen 2010 – Proef 72.

Field brake deceleration rate test: See www.koac-npc.com.

Field PA drainage test: See www.koac-npc.com/Flex/Site/Download.aspx?ID.

Life cycle assessment (LCA): Done according to NEN 8006 by TNO.

Dynamic creep test: A dynamic axial stress is applied to a specimen (Ø = 100mm) for a specified number of load cycles (otherwise up to 10% of deformation) while axial strain is monitored. The samples are pretreated to be sure the top surface is parallel to the bottom surface. Before the test, the specimen is preconditioned at 50°C till reaching the constant temperature. The test conditions are listed in Table 1. The test method was also described in (Su, 2007).

Table 1. Parameters for dynamic creep test

Parameter	Value	Parameter	Value
Temperature	50°C	Test loading stress	250 kPa
Pulse width	200 *ms*	Conditioning time	10 minutes
Pulse Period	1000 *ms*	Preload rest time	1 minutes
Conditioning	25 kPa	Recovery time	1 minutes

THEORETICAL MODEL AND PREDICTION

Theoretical consideration

The viscosity of oil-bitumen blends follows the mixing rule. Various models have been used to predict the viscosity of the oil-bitumen blends (Jian, 2006).
Theoretically the penetration of bitumen binder can be expressed as a function of its viscosity at a given temperature as shown in equation (1):

$$P = F(\eta) \quad (1)$$

Where: P - Penetration of bitumen
η - Viscosity of bitumen at a given temperature

Fig. 1 presents the test results of the penetration against the viscosity of various types of bitumen in a logarithmic scale. The penetration grade of bitumen is in a range of 20-100 pen (at 25°C, x0.1mm); whereas the viscosity varies from 100 to 1000 Pa.s at 60°C. Therefore, the current research approach is to determine the viscosity, which has a much wider range and more accuracy in the measurement over the penetration measurement in practice. Afterwards, the viscosity is able to be correlated back to the penetration grade, which is used to specify the stiffness of the bitumen in asphalt. The results in Fig. 1 also show the higher the penetration, the lower the viscosity will be, but there is no linear relationship between the penetration and viscosity. By a regression analysis, the relationship between the penetration (at 25°C, x0.1mm) and viscosity (at 60°C) could be expressed by equation (2):

$$P = 5367.4*\eta^{-0.7711} \qquad (R^2 = 0.9956) \tag{2}$$

In practice, the dosage (g/m^2) and viscosity of the rejuvenator are known. On the other hand, it is also possible to know the ageing degree of the binder in the existing asphalt pavement to be treated (by means of extraction and recovery method) and the penetration depth of the rejuvenator into asphalt (by means of adding a trace amount of lightening agent, viewed under a UV light). Thus, it is also possible to know the amount of the aged binder (g/m^2) in the pavement to be rejuvenated.

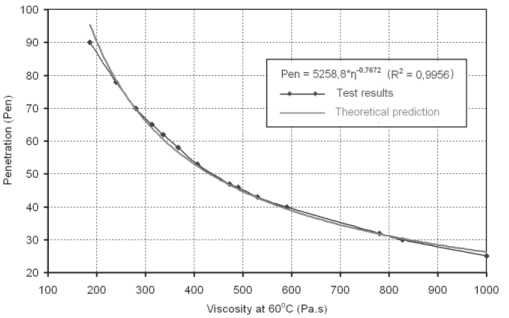

FIG. 1. Penetration of bitumen as a function of viscosity.

Theoretically the rejuvenating effect (the end viscosity) of asphalt pavement can be predicted by equation 3. Conversely, the end viscosity of the treated binder can also be correlated back to the penetration.

$$\eta_R = G(\eta_1, V_1, \eta_2, V_2) \tag{3}$$

Where: η_R : End viscosity of the treated bitumen in asphalt (after treatment)
η_1, V_1 :Viscosity & volume fraction of the rejuvenator
η_2, V_2 :Viscosity & volume fraction of aged bitumen (before treatment)

$$V_1 + V_2 = 1$$

Based on Equation 2, the predicted penetration values of the rejuvenated binders are presented in Table 2, in which the measured results are also given for a comparison purpose. The predicted values are in a good agreement with the measured ones as shown in the Table. The results further confirm the validation of the model developed.

Table 2. Model predicted penetration values vs test results for different types of bitumen

Viscosity at 60°C (Pa.s)		1000	780	590	490	367	280	186
Penetration (at 60°C,	Test results	25	32	40	46	58	70	90
	Prediction	26	31	38	44	55	68	93

Lifetime prediction

The method of the lifetime prediction of the treated asphalt pavement can be demonstrated by using the results, obtained in at Ribe Pavement Laboratory, Denmark (Su, 2008). Table 3 presents the penetration, softening point, penetration index and binder content of the asphalt before and after the treatment in this investigation. The results show that the penetration of the recovered binder increases from 43 pen to 68 pen, whereas the softening point decreases from 54.4 to 49.9^{0}C. As can be seen from Table 3, the penetration index also increases from -0.52 to -0.46, meaning that the binder becomes less susceptible to temperature. Furthermore, the binder content increases ca 0.4% due to the contribution of the new binder in the rejuvenator, which compensates the binder lost during the passed years in the service.

The test results in Table 3 show the treatment brings the penetration from 43 pen up to 68 pen, whereas the model prediction is 62 pen, only 6 pen difference, which implies that the model prediction is in a good agreement with the measurement. The results further confirm the validation of the model prediction

Table 3. Properties of the recovered binder (Done in by Ribe Pavement aboratory)

Properties	Before treatment	After treatment
Penetration	43 x0.1mm	68 x0.1mm
Softening point	54.4°C	49.9°C
Penetration index	-0.52	-0.46
Binder content	4.94%	5.33%

Based on the viscosity or penetration of the recovered binders, the lifetime of the

treated asphalt pavement can be predicted. Fig. 2 presents 2 curves, of which one is the viscosity of the recovered binder at 60°C against its corresponding penetration (the dash line); the other is the service time (in year) of the asphalt pavement against the penetration of the binder in the asphalt due to the ageing (the solid line), which is provided by Ribe County road authority. As can be seen in the Figure, the treatment brings the viscosity from 530 Pa.s down to 336 Pa.s, which corresponds to the penetration from 43 pen up to 62 Pen. If this is the case, then one single treatment brings this piece of asphalt pavement age from 8th year back to 2nd year, meaning the extension of the pavement lifetime for 6 years.

RESULTS AND DISCUSSIONS

In this section, the laboratory and field test results, including LCA results of porous asphalt pavements are presented and discussed. Some results are from the LVO project.

Laboratory test results

The principle of the rejuvenation technology was described in a previous contribution (Su, 2008). An investigation showed a good reactivity of the rejuvenator with hard-type of fresh bitumen and aged bitumen in dense asphalt as described. In order to understand the reactivity of rejuvenator with aged binder in PA pavements, the binder was extracted and recovered from asphalt cores taken out of PA pavement. The same dosage of the rejuvenator (ca. 1mm thick layer) is applied on the surface of extracted binder from PA cores in a penetration cup. The reactivity of the rejuvenator is determined by means of a modified penetration method described elsewhere (Su, 1999 & 2008).

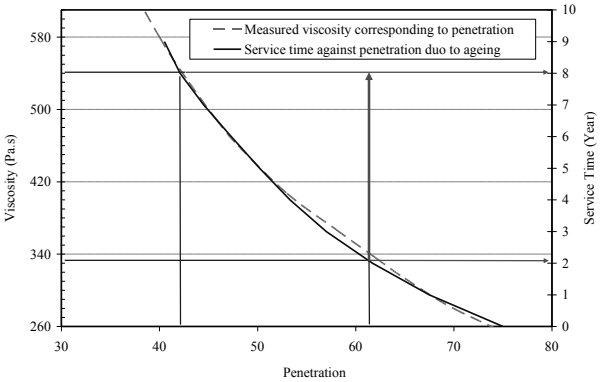

FIG. 2. Model-prediction of the lifetime of the treated pavement (extension of 6 years).

Fig. 3 shows the reactivity of 2 types of rejuvenators with the aged bitumen out of asphalt cores taken from the PA pavement. The results demonstrate that the reacted depth is ca 0,5mm in the first 24 hours, reaches a maximum value (0.8mm) at 3 days. Afterwards, the reacted depth of Rejuvenator-1 reduces to 0,4mm at 7 days, then it appears to be stabilised at ca. 0,4mm. In contrary, the reacted depth of rejuvenator 2 remains at the same level of ca. 0,8mm after 3 days. The test results also demonstrate that the thickness of the rejuvenator applied is initially ca. 1mm thick. Then around 50% of it (in fact water from the emulsion) is evaporated within the first 24 hours, eventually the remained rejuvenator film on the bitumen surface is 0,5mm, meaning that the rejuvenator has ca. 50% of residual binder in it. From the rejuvenation point of view, the rejuvenator 2 is better than Rejuvenator 1.

It is well known that the thickness of bitumen film around minerals in PA is 10 to 15 μm maximum. The reaction speed of the rejuvenator with bitumen is obviously quick enough to activate the aged binder in PA within a short period of time. The point is how to bring the rejuvenator homogeneously into a PA mixture, instead of remaining on the surface of the pavement. Fig. 4 demonstrates the penetration pattern of the rejuvenator into the PA mixture (indicated by green-yellowish colour). The rejuvenator was treated with a trace amount of fluorescent dye, which emits a distinguished colour under a UV light. The test result shows that the rejuvenator penetrates homogeneously throughout the PA mixture via voids. The ageing process just happens in the same way through the whole PA mixture layer in practice (Hagos, 2008). This means that the rejuvenation of the aged binder at the bottom of PA layer is also required.

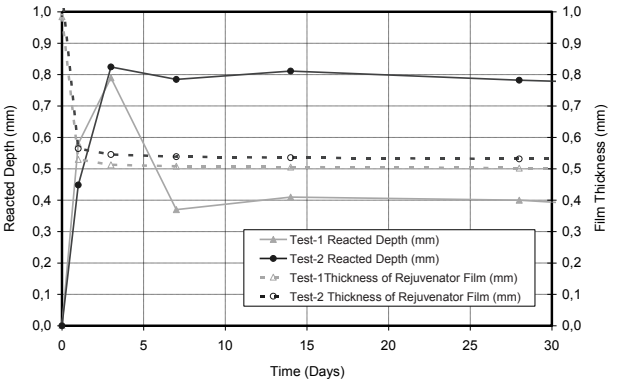

FIG. 3. Reacted depth (blue curve) of the rejuvenator with the recovered bitumen vs time.

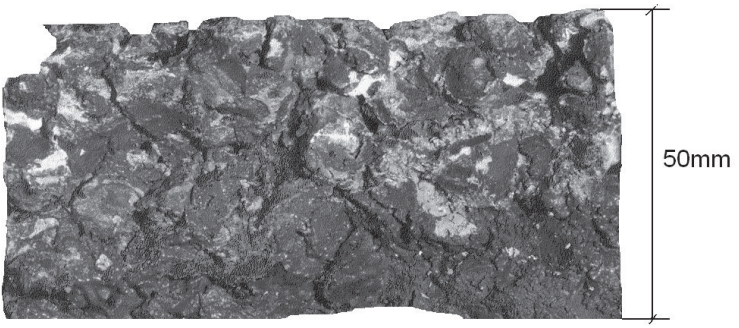

FIG. 4. Penetration of the rejuvenator in PA mixture (shown by green-yellowish colour).

The test results reveal that the rejuvenation effect of the rejuvenator is remarkable. A question may be proposed whether the treated PA mixture is still stable enough to bear the traffic loading in the service period of time, particularly in hot summer days, in case the rejuvenation degree is too high. The treated and untreated porous asphalt cores were taken out of the pavement for mechanical tests. For a relevant comparison purpose, the attention was paid to take each pair of cores as close as possible to have identical structure, composition, as well as the similar traffic experience in service time.

Figs 5 and 6 present the dynamic creep test results, i.e. the resilient modulus and permanent deformation against a number of loading repetition, respectively. Fig. 5 (I) shows the treated core with a lower resilient modulus than the untreated one, meaning rejuvenating or softening effect on the aged binder in PA mixtures, particularly in the first 2000 loading repetitions. Furthermore, the modulus of the untreated core decreases more remarkably against the loading repetitions than that of the treated one, meaning that the micro defects in PA starts growing, coupled with the stress accumulating and dissipating under the dynamic loading pulses. Fig. 5 (II) demonstrates that there is no much difference in the permanent deformation in the first 3000 loading repetitions; afterwards the permanent deformation increases much faster than that of the treated cores, implying that the micro-damage in it starts growing more rapidly and the pavement lost its bearing capacity. On the other hand, the treatment has also a healing effect on the micro-cracks in the PA pavement. Fig. 6 presents the dynamic test results of the second pair of cores from the same piece of pavement. Fig. 6 (I) shows that there is not much difference in the modulus between the treated and untreated cores in the first 2000 loading repetitions, then the modulus decreases very rapidly in a form of saw-tooth (the force cumulated and released alternatively). Fig. 6 (II) clearly demonstrates that the permanent deformation develops much quicker than that of the treated core from the beginning of the test. It could be concluded that the rejuvenation treatment helps to soften the aged asphalt,

heal the micro-defects in PA mixtures, thus to improve the stability and bearing capacity of the PA pavement.

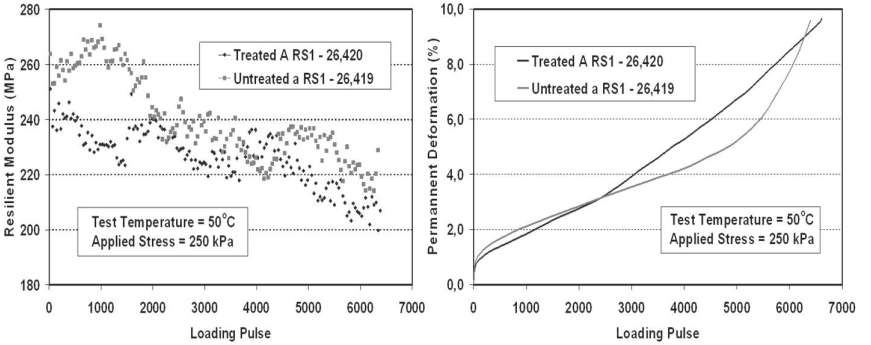

(I) Resilient modulus (II) Permanent deformation

FIG. 5. Dynamic creep test results of 1e pair of PA cores out of Dutch Motorway A12.

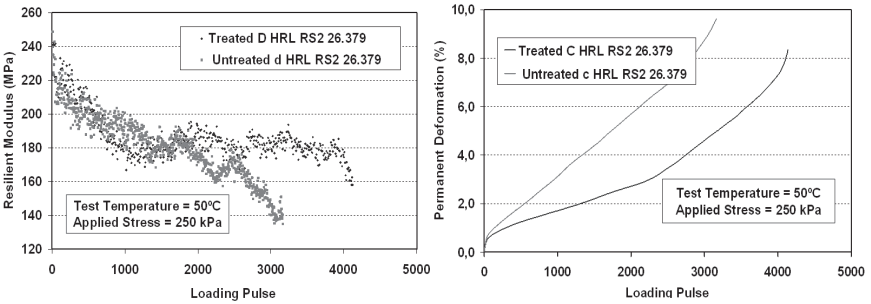

(I) Resilient modulus (II) Permanent deformation

FIG. 6. Dynamic creep test results of 2e pair of PA cores out of Dutch Motorway A12.

Field test results

It remains a major goal for road authorities and engineers to find a sustainable solution for the extension the lifetime of PA pavements. A large scale field test was carried out, for example on Dutch highways A6, A50 and A73 in 2010 and 2011, aiming at finding out a practical and efficient way to do the maintenance of porous asphalt. Some of the test results will be presented and discussed.

Fig. 7 presents 2 photos, showing the application of the rejuvenator at night (see Photo A) and immediately open to the traffic next morning after the treatment. The advantage of the night maintenance is to avoid traffic congestion during the day, particularly in the rush hours. Photo (B) shows the rejuvenator migrates into porous asphalt, no binder smeared to the untreated section. This ensures the early skid resistance.

(A) Application of the rejuvenator at night (B) Open to traffic next morning

FIG. 7. Application of the rejuvenator at night and open to traffic next morning.

Fig. 8 shows the surface characteristics of the treated and untreated porous asphalt. Compared with the untreated PA surface texture, the rejuvenator appears to penetrate (or run) homogeneously into PA mixture through the voids, with only a very thin film on top of the stone aggregates.

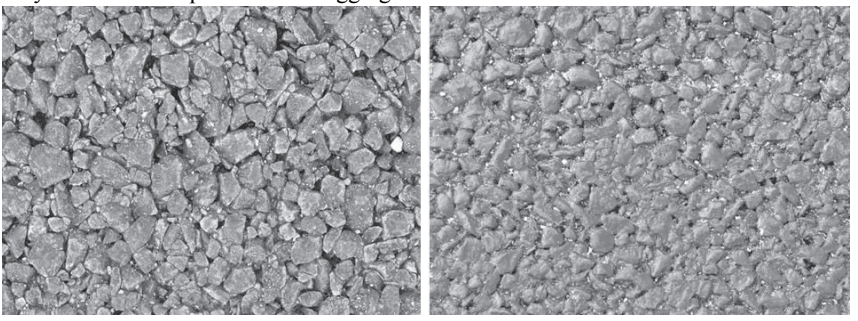

(A) Before the treatment (B) A few hours after the treatment

FIG. 8. Surface structure of porous asphalt pavement before and after the treatment

The laboratory test results reveal that the rejuvenation treatment does rejuvenate the aged binder, but does not influence the stability of PA pavements. The question is whether the treatment has any influence on the functional requirements of PA

pavements, particularly concerning the initial skid resistance due to the presence of a very thin film on the top of the aggregate surface shown in Fig. 8 (B).

Table 4 presents the field test results - effect of the rejuvenation treatment on the functional properties of PA pavement. The test results include brake deceleration rate, skid resistance and water drainage properties. For porous asphalt pavements, the brake deceleration rate and skid resistance should be above 5.2 m/s² and 0.38, respectively.

Table 4. Effect of the rejuvenation treatment on the functional properties of PA

Test section	Test Length	Brake deceleration rate	Skid resistance	Water drainage (Bekerproef)		
				Test -1	Test - 2	Test -3
Reference	100m	6,99 m/s²	0.45	32 sec	>180 sec	65 sec
Treatment - 1				72 sec	58 sec	>180 sec
Treatment - 2		5.22 m/s²	0.36			
Treatment - 3				100 sec	>180 sec	>180 sec
Treatment - 4		5.31 m/s²	0.38			
Treatment - 5				71 sec	50 sec	48 sec
Treatment - 6		5.24 m/s²	0.38			

Notes: Brake deceleration rate and skid resistance done directly after the treatment; Water drainage test done 14 days after the treatment

The brake deceleration rate is most important concerning the safety, since it can be correlated to the travelled distance of a vehicle as it travels with a certain speed (for instance 80km/hour) after it is braked. As shown in the Table, the brake deceleration rate and skid resistance of the test section are indeed lower than that of the reference (the untreated section), but almost meet the minimum requirements (with the exception of the skid resistance of treatment-2). The initial low skid resistance appears to be associated with the presence of a very thin film on the top of aggregates. 90% of the skid resistance of treated section will come back after 1 day under the traffic, as a result of gradual removal of the biner film from the top of the aggregates. Therefore, a speed limit sign (long brake distance) is normally erected on the side of the pavement in the first a few days after the treatment. The results also show that the water drainage power is only slightly influenced by the treatment, meaning no significant clogging of the open structure by sprayed materials during the treatment. The PA pavement keeps its original open structure; this means that the treatment has no influence on the noise level.

LCA investigation results

In recent years, there has been increasing attention to environmental impact and sustainability of asphalt pavements. As a result, the government encourages and awards industrial enterprises to purchase and use environmental friendly and sustainable raw materials, as well as reduce emissions and energy. The environmental performance is measured using an environmental life cycle assessment (LCA). The purpose of the LCA is to establish a reliable, accurate and quantitative environmental profile which includes all environmental interventions (raw materials, emissions and energies) during the total life cycle of the product, so-called from cradle to grave. Referring to this development, the LCA profile of porous asphalt pavement maintenance solution with the rejuvenation technology was studied in accordance with LCA NEN 8006:2004 by Netherlands Organization for Applied Scientific Research (TNO). The calculation was carried out in accordance with the framework of NEN-EN-ISO 14040, based on a planned lifetime of 32 years (Head , 2010, NEN, 2004).

Fig. 9 presents a comparison of environmental profile of the rejuvenation maintenance system over a conventional maintenance system used intensively nowadays for PA pavement maintenance. The result shows that the rejuvenation maintenance system has a more favorable environmental profile over the conventional one, for instance, nine of ten environmental impact categories of the rejuvenator are about 10 to 30% lower. The less frequency to replace asphalt involves less maintenance work, so does the less consumption of the energy and raw materials for bitumen and asphalt production and construction.

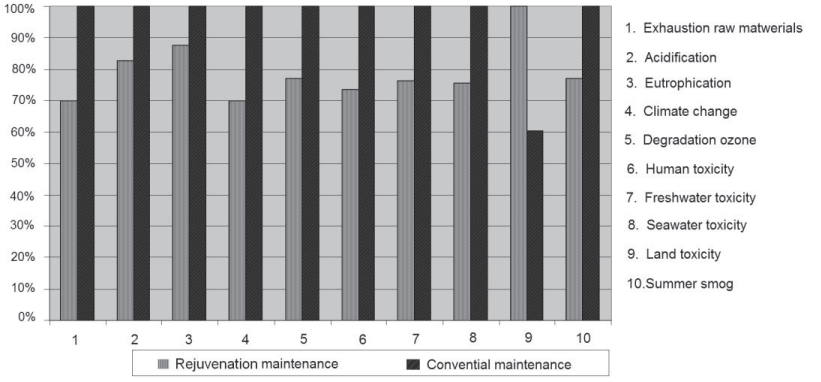

FIG. 9. A comparison of environmental profile of the rejuvenation maintenance system over a conventional maintenance system used intensively nowadays for PA pavement maintenance

Fig. 10 demonstrates a comparison of total environmental impact of porous asphalt with the rejuvenation system versus conventional system in terms of shadow costs, which estimates the damage to society caused by the environmental inputs. It

is clear that porous asphalt with the rejuvenation maintenance solution has an average about 25% lower environmental impact than that with the conventional maintenance system. The difference is mainly due to the larger contributions of the climate change and human toxicity due to a fact that the rejuvenation maintenance has a lower environmental score for most environmental items. It is sure that the choice for organic vegetable oils gives an environmental improvement.

It is concluded that the rejuvenation maintenance solution of PA pavement has a better profile than that of the current maintenance system on all environmental issues, except land ecotoxicity.

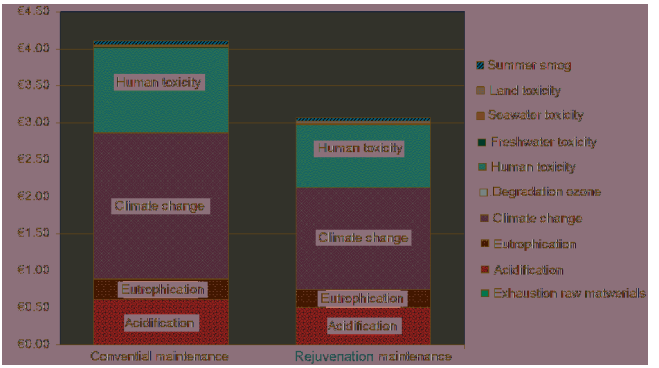

FIG. 10. A comparison of environmental impact in terms of shadow costs of the rejuvenation maintenance system with conventional maintenance system applied widely for PA pavements.

MAINTENACE STRATEGY

It is far less expensive to keep a road in good condition than it is to be replaced once it has deteriorated. This is why some road authorities place the priority on preventive maintenance of their roads in good condition, rather than reconstructing roads in poor condition. In terms of lifetime cost and long term pavement conditions, this will result in better system performance.

Fig. 11 presents a strategy of the road maintenance program. As the road is newly laid, the performance of the road is in an ideal situation (100% satisfaction). However, the performance will decrease in practice with the time. In order to keep the road in the good condition, the maintenance at the right time is essential. For example, if the road performance should be above a certain level, for example above 90% of satisfaction, then the advice is to take maintenance Option II, which will not only result in a satisfaction of the road performance, but also relatively low maintenance costs involved. If the right time for the maintenance is missed, for

instance 3-4 years later, then the pavement performance will decline rapidly, and the maintenance will also involve a high cost (see Option-III). Furthermore the road users drive on a poor road condition road for many years (see the shadow area in Fig. 11) and reclaim more damages to their automobiles. If there is no any measure to do the maintenance, the road performance will decrease dramatically after a few years in service, and eventually the road has to be removed and a new top layer has to be laid. Of course, the costs are much higher then.

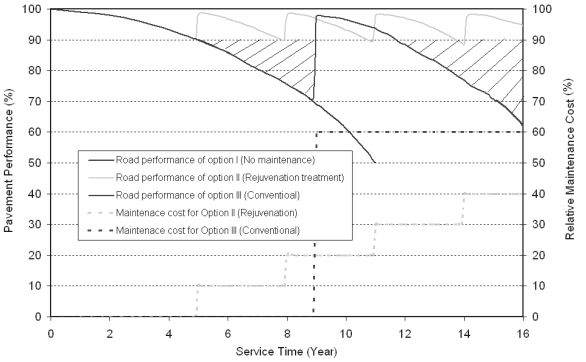

FIG. 11. A strategic maintenance of asphalt pavements.

CONCLUSIONS

Based on the test results and LCA calculations presented in this paper, the following conclusions can be drawn:

1. The rejuvenator shows a clear rejuvenation effect on the aged binder, extracted out of PA pavement.
2. The present treatment not only shows a rejuvenation effect on porous asphalt, but also improves the integral stability, probably due to the rejuvenation effect in combination with healing effect as suggested by the dynamic creep test results.
3. The rejuvenation treatment does not virtually influence functional properties of porous asphalt. The initial skid resistance and brake deceleration rate are just above the limit requirement concerning the safety issue, but the skid resistance will come back shortly after opening the road to traffic. The drainage effect of porous asphalt is almost not affected by the treatment.
4. LCA study shows that the rejuvenation maintenance system has a more favorable environmental profile over the conventional system. This is associated with the use of organic vegetable additives, which contribute to an environmental improvement.
5. As a preventive maintenance solution of the pavement, the rejuvenation

technology offers a sustainable maintenance with respect to the mechanical performance and functional requirements, as well as social benefits, environmental and cost-saving considerations.

6. Prevention is better than cure. It is commended that the maintenance should be done in right time with a right solution.

REFERENCES

An ongoing research project by Dutch Ministry (RWS). (2010). "InfraQuest project – Levensduurverlenging ZOAB m.b.v. verjongingsmiddelen (LVO)."

Elvik, R., et al. (2005)."Road safety effects of porous asphalt: a systematic review evaluation studies." *Accident Analysis & Prevention,* 37(3): 515-522

Head, M.E.(2010)."LCA van zeer open asfaltbeton (ZOAB) met PenTack onderhoudssysteem", TNO Research Report.

Hagos, E.T. (2008). "The effect of Aging on binder properties of Porous Asphalt concrete." PhD dissertation, TU Delft, ISBN: 978-90-8570-331-0

Morgen, P.A. (2008). "Innovatieprogramma geluid – Scientific strategy document and end report ." DVS-2008-16

Mo, L.T. (2010). "Damage development in the adhesive zone and mortar of Porous Asphalt concrete." PhD dissertation, TU Delft, ISBN: 978-90-8570-444-7

Nederlands Normalisatie-Instituut (NEN). (2004). NEN 8006 - Environmental data of building materials, building products and building elements for application in environmental product declarations – Assessment according to the Life Cycle Assessment (LCA) methodology.

Nielsen, C.B. (2006). "Durability of porous asphalt – international experience." Danish Road Institute Technical Note 41, Road Ministry of Transport and Energy. Denmark

Qian, J.H. et al. (2006). "SPECIAL REPORT: Study evaluates viscosity prediction of crude blends." Oil & Gas Journal, Vol.104(39).

Su, Z., et al. (2008). "Major life-cycle Costing Reduction and Environmental Benefits of an Innovative Preventive Maintenance Strategy for Dense Asphalt Pavements." 300-015, *Proceedings of EE Congress*, May 21-23. Copenhagen, DK.

Su, Z., et al. (2000). "Strategic Maintenance by Sealing: Application of PenTack and Its Effect on Asphalt Properties." *Proceedings of EE Conference*, Sept. 20-22, Barcelona, Spain, pp. 568-575 in Book II

Su, Z., et al. (2002). "Strategic Maintenance of Pavement by Sealing with a Special Mixture of Bituminous Emulsions." *Proceedings of 3rd Intern. Conference on Bitumen Mixture and Pavements*, Nov. Thessaloniki, Greece, pp. 91-100 in Volume I

Su, Z., et al. (2005). "10 Years Experience with Airport Pavement Maintenance using a Special Sealing Technique" *1st European Airport Pavement Workshop*, May Dorint Sofitel Amsterdam Airport, the Netherlands

Su, Z., et al. (1999). "PenTack – An Ideal Product for Asphalt Road Maintenance" *Proceedings of ISAET 99*, Nov. 11-14, Washington D.C. USA, P195-208.

Su, Z., et al.(2007). "Effect of PenTack Treatment on the Properties of Dense Asphalt Pavements." ESHA Internal Research Report.

Development of a New Type of Prediction Model for Predicting Tyre/Road Noise

Mingliang Li [1], Wim van Keulen [2], M.F.C. van de Ven[3] and A.A.A. Molenaar[4]

[1]PhD student, Section of Road and Railway Engineering, Faculty of Civil Engineering & Geosciences, Delft University of Technology, PO box 5048 2600 GA Delft, The Netherlands; email: Mingliang.Li@tudelft.nl
[2]Consultant, VANKEULEN advies bv, Multatulistraat 5, 5251WV Vlijmen, The Netherlands; email: wim@vankeulenadvies.nl
[3]Assoc. Professor, Section of Road and Railway Engineering, Faculty of Civil Engineering & Geosciences, Delft University of Technology, PO box 5048 2600 GA Delft, The Netherlands; email: M.F.C.vandeVen@tudelft.nl
[4]Professor, Section of Road and Railway Engineering, Faculty of Civil Engineering & Geosciences, Delft University of Technology, PO box 5048 2600 GA Delft, The Netherlands; email: A.A.A.Molenaar@tudelft.nl

ABSTRACT: In this study, the importance of reducing tyre/road noise is stated. Different types of noise reducing pavement and prediction models are introduced. A new method of modeling is forwarded which links the difference of the tyre/road noise level to the variation of the mixture properties. The model concentrates on certain type of road surface. In the current research, thin layer surface layers are taken into account. Measurements are carried out to collect data of material properties and road surface characteristics. A modeling process is also shown using the existing database. The result model is closely related to practical engineering and can be easily used for estimating the tyre/road noise level changes.

INTRODUCTION

Road traffic is the predominant source of environmental noise. In European Union countries, more than 44% of the population (about 210 million people) are regularly exposed to over 55 dB of road traffic noise, a level potentially dangerous to health (Boer 2007). In cities of developing countries, the noise pollution caused by traffic and the densely travelled road is more severe and the equivalent sound pressure levels for 24 hours can reach 75-80 dB (A) (Berglund 1999). In China, with the great development of road traffic and increase of passenger cars in recent years, the traffic noise has already been an important consideration for well-being and health of citizens living in and around urban area. In big cities of China, such as Beijing and Chongqing, noise levels higher than the required level 70dB are observed on more than 35% of the road network (Qiao 2003; Han 2002). In some cities, this percentage is even up to 90% (Xie 2007).

The World Health Organisation (WHO) pointed out that environmental noise, including traffic noise, has direct as well as cumulative adverse effects on the health and/or well-being of exposed people on following aspects:

- Annoyance;
- Sleep disturbance;
- Interference with communication and intellectual performance;
- Cardiovascular disease;
- Adverse effects on mental health.

In addition, noise also affects future generations, socio-cultural, aesthetic and economic aspects. The problem is therefore accompanied by the increasing complaints from people who are influenced.

In general, road traffic noise is generated from three sources: the propulsion (power train) noise, aerodynamic noise and tyre/road interaction noise. As illustrated in Fig.1, noise generated from interaction between tyre and road surface is the dominant source at speeds above 50km/h. Reduction of noise level from this interface is thus an effective way to eliminate the overall traffic noise and has caught attention of most road authorities (Donavan 2007).

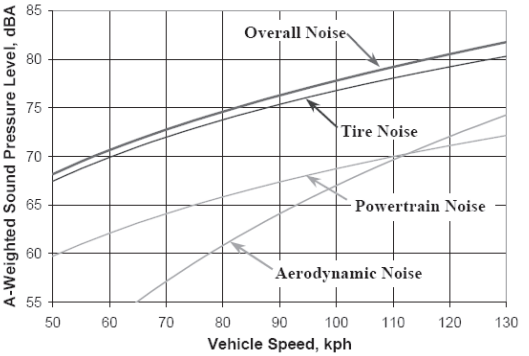

FIG.1. Contributions of various sub-sources to the overall road traffic noise .(Donavan 2007).

In the following sections, the factors influencing tyre/road noise, different type of noise reducing pavement used in Europe and the existing models for tyre/road noise prediction are introduced in detail. In order to develop a model which can be easily and directly used by road engineer, a new modeling method is proposed by the author. The modeling process and results from the undergoing work are also presented. The model is considered to be used as correction or complementary for existing models, and makes accurate evaluation possible for certain types of surface.

NOISE REDUCING SURFACES AND PREDICTION MODELS

Influencing parameters

Tyre/road noise generation is an extremely complicated process which depends on various mechanisms and influencing parameters. FIG.2 gives an overview of these noise related parameters. It can be seen that the road surface characteristics, vehicle properties and environmental factors work cooperatively on the tyre/road noise production through different mechanisms. From current research, it is known that the surface texture, sound absorption and mechanical impedance are the three main factors of the road surface which play an important role in the tyre/road noise generation. These surface characteristics are also determined by basic material properties, including air voids, aggregate size, stone gradation and binder content. These factors are of importance for road engineering since they can be controlled by road engineers when designing the surface mixture.

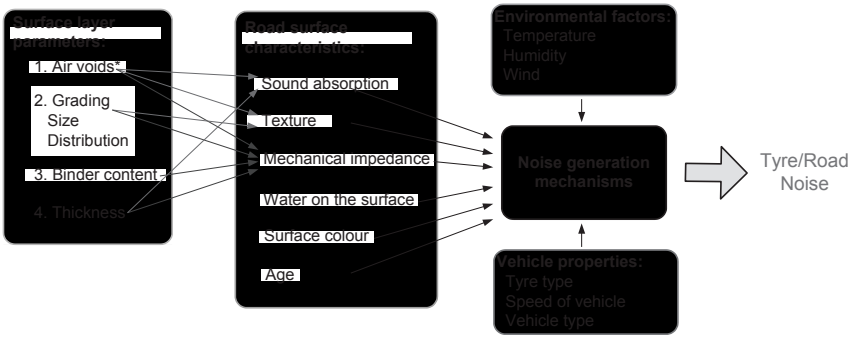

*refers to residual air void content, and clogging effect is included;

FIG. 2. Major influencing factors on tyre/road noise.

Noise reducing surfaces

Development and application of noise reducing pavements can be regarded as the most direct way to attenuate the tyre/road noise from the source and it is cost-effective when considering other technologies available to road authorities to reduce traffic noise (Boer 2007). Currently, the most effective and commonly used low noise road surfaces in Europe are porous asphalt and thin layer surfaces (Nilsson 2005).

Porous asphalt is a wearing course with a high stone content (typically 81-85%) and a small proportion of sand and filler, providing a high air voids content (usually > 20%) (COWI 2006; Huurman 2010). Sound energy at the source as well as in propagation can be partly absorbed due to the porosity. One of the problems for using porous asphalt is the clogging of the pores by dirt and dust, which results in decreasing the acoustical performance of the porous surface (Tan 2000). In order to counter the clogging effect, two-layer porous asphalt (TLPA) is developed. The TLPA is made up of a bottom layer of porous asphalt with a coarse grading (typically 0/14, 0/16, 11/16) and a thin top layer of fine graded aggregate (typically 4/8, but sometimes 2/4 or 2/6). The initial noise reduction is excellent: 4-6 dB (A) for passenger cars at 50 km/h. It is one of the quietest road surfaces which are actually in use (Abbott 2010).

Thin layer noise reducing surfacings are a commonly technique in the Netherlands and some other European countries at present. It is a top layer with a thickness of about 25 mm. The tyre/road noise is reduced mainly by two properties:

1) Small maximum size aggregates are used in order to increase the smoothness of the road surface and reduce the noise generated by tire vibration.

2) An open surface structure is created by high air voids aiming for reducing the noise generated from air pumping (van Keulen 2005).

The third generation silent pavement such as Poro-Elastic Road Surfaces (PERS) (Sandberg 2010) and roll pave (Morgan 2008) are also under investigation. These surfaces provide both a low texture and high air voids for noise reduction. The rubber is used for decreasing the stiffness of the surface, which is also considered as a way to reduce the vibration generated noise. However, the durability and the mechanical properties of this type of surface still need to be improved.

Prediction models

As noise reducing surfacings are commonly developed and built in Europe, there is increasing need for prediction models which provide information of noise generation before the road is constructed. Such models play an important role in detecting tyre/road noise, optimizing the pavement design and improving the materials and building technology (Beckenbauer 2006).

Tyre/road noise models can be classified into three categories: statistical models, physical models and hybrid models. The statistical models usually characterize the relationship between noise level and the influencing parameters by regression equations. For example, the models developed respectively by Sandberg and Klein evaluate the tyre/road noise level from the surface texture levels and sound absorption coefficient of porous asphalt (Sandberg 1987; Klein 2007). Physical models focus on specific noise production mechanisms. In current studies, the vibration mechanism is widely simulated by mechanical models or finite element method (FEM). A great deal of work has been done and is still going on at Chalmers University for developing such a physical model (Larsson 2002). The hybrid models combine both the statistical and physical elements in the framework. The structure is complicated but it gives an overall simulation on the emission and propagation of tyre/road noise. Two typical examples of hybrid models are the so-called Acoustic Optimization Tool (AOT) and Tyre Road Interaction Acoustic Simulation (Trias) model. These models have already been applied for noise prediction in road engineering.

Further consideration of modeling

At present stage, defects still exist in the models, and attention needs to be paid to the following aspects for further model development:

Physical models describe part of the noise generation process, and cannot work independently for predicting the noise level. A big amount of data, such as original surface profile, needs to be collected to run the contact model. For certain models, the tyre indexes should also be given, and this makes no sense for road engineers. It can be concluded that the physical model is essential for describing the tyre/road noise generation in a theoretical way, but long term effort still needs to be put into it.

Statistical models can give good predictions for pavements with similar properties as the surfaces used for the development of the regression model. These models however have difficulties in providing a general rule for all types of surfacings. Therefore, for developing a statistical model, one has to develop specific models for different types of surfacings.

The mixture properties are directly related to the design of the road surface and are of interest for road engineers. However, the road parameters in most of the existing models are normally parameters of the surface layer, such as texture spectrum, surface profile, absorption coefficient; such parameters however are not yet linked to the mixture composition parameters. For road engineers, a model linking the noise level to the material properties and composition of the road surface mixture is quite essential for designing and constructing noise reducing surfacings. Parameters are preferred which are directly related to road design and which can be easily obtained, such as air voids content, gradation, binder content and MPD of the surface. In addition, the road surface characteristics change with service time, and an age based correction is important for long term evaluation of the tyre/road noise.

Most of the current modeling work focuses on dense and porous asphalt road surfaces. However, there is less research done on thin layer surfacings, which also produce a quiet pavement. As the mixture composition and surface layer characteristics are different from those of the dense and porous layers, the acoustical performance is also different. Special investigation and modeling and improvement of the existing acoustic models are necessary for an accurate prediction of tyre/road noise from thin layer surfacings.

NEW TYPE OF PREDICTION MODEL

Consideration of change

Aiming for improving the tyre/road noise model for accurate prediction, a new type of statistical model was proposed (Li 2009). Different from the conventional models, it evaluates the differences of tyre/road noise level caused by surface characteristics or material changes; it does not predict the global noise level from a certain surface.

“Change” exists in each step of road design, construction and application. It can imply: different designs of the road mixture composition; changes in road surface characteristics during the lifetime of the surface layer; different surface properties between two sections. For tyre/road noise, the “change” expresses the increase or decrease of the noise level, and can be used directly as an indication of noise reduction. Thus, the concept of “change” is introduced in developing the model.

Fig.3 gives an example of the influence of material changes on surface characteristics and tyre/road noise level. The data are from thin layer surfaces of trial sections in Kloosterzande. The thickness of the surface is equally 25mm but with different material compositions. It can be seen that mixtures with a higher content of coarse aggregates, namely thin layer 4/8, SMA 0/8 and PCA 4/8 (as shown in Fig.3 (a)), have a higher texture level (as shown in Fig.3 (b)), while the ones with more fine aggregates possess relatively lower texture levels. Similarly, surfacings with highest air voids content, PCA 4/8, 24%, show a much greater absorption coefficient around

2000 Hz; this is shown in Fig.3 (c). Fig.3 (d) illustrates the noise levels from CPX measurements performed at a speed of 70 km/h. It can be found that in the low and medium frequency range, the sequence of the noise levels just follows the order of the texture. In high frequency range, there are great drops of the noise curve for those layers with higher absorption coefficients.

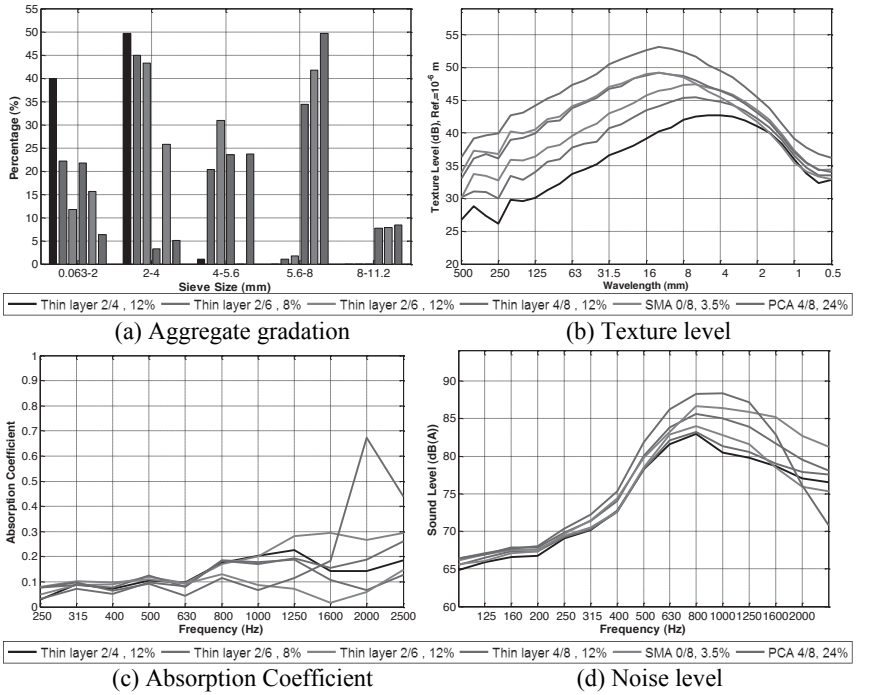

(a) Aggregate gradation (b) Texture level

(c) Absorption Coefficient (d) Noise level

FIG. 3. Investigation of surface properties and noise level of thin layer surfacing.

It is clear that variation of the mixture composition leads to a corresponding change in the surface characteristics, such as texture and absorption coefficient. As a result, a change appears in the generated tyre/road noise level.

Framework of the model

Fig.4 shows the framework of the target model. Two models are to be established. Model I relates the change of surface characteristics to the variation of the material properties, while Model II deduces the variation of the noise level from the change of the surface characteristics. The input parameters for prediction can be either the change of material properties or the change of surface characteristics. The result achieved is the change of tyre/road noise level ΔL. The tyre properties and other influencing factors are of no interest because the model concentrates on the noise

emission from the road point of view. In this research, small changes of the influencing parameters are supposed to occur in a relatively stable system. Averaged noise levels generated from different tyres are used and the environmental condition is considered to be fixed.

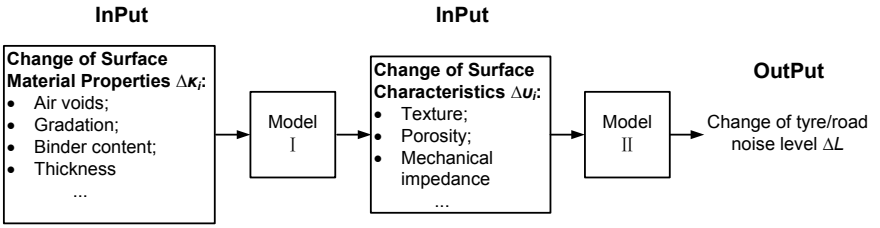

FIG. 4. Framework of the model.

Another key point is that the model concentrates on a certain type of road surface. In the current study, only thin layer surfacings are included for model development. Therefore the resulting model is mainly applicable for such thin layer surfacings. For a certain type of road surface, one can assume that the changes in characteristics do only occur in a small range, and the relationship between the input and output can be considered to be linear. The Model I and Model II can then be developed by linear regression respectively:

Model I: $$\Delta \upsilon_i = \sum_{j=1}^{m} \beta_j \Delta \kappa_j \quad (1)$$

Model II: $$\Delta L(f) = \sum_{i=1}^{n} \alpha_i \Delta \upsilon_i \quad (2)$$

where $\Delta \upsilon_i$ denotes the change of a certain surface characteristic, which can be the surface texture, sound absorption or mechanical impedance. $\Delta \kappa_j$ presents the change of individual mixture properties (design parameters), such as air void content, binder content, aggregate size and gradation. α_i and β_j are the coefficients to be identified by regression.

REALIZATION OF THE MODEL

The model development was realized by data collection and data analysis. The data collection refers to using an existing database and obtaining data from measurements. The Dutch Ministry of Infrastructure and the Environment has provided a database containing information of thin layer surfacings in The Netherlands. Related measurements are done in the Road and Raiway Engineering lab of TU Delft.

Laboratory test

Laboratory measurements were carried out aiming to investigate the relationship between the material properties and the surface characteristics; this is called Model I in the framework. An overview of the measured properties, the corresponding test methods and required sample type are listed in Table 1.

Table 1. Test Properties and Methods

Item	Test Methods	Sample Type
Mixture composition	CT Scan	core
Surface Texture	Laser profilometer	slab and core
Sound absorption	Microflown surface impedance	slab and core
Airflow resistance	Direct airflow	core
Mechanical impedance	Impedance hammer	slab
	Direct compression	block
Airflow resistivity	Direct airflow	core

The mixture composition is investigated by CT scan. The connected air voids content and the aggregate gradation were calculated from the image. It is known that the surface texture and sound absorption are the most important factors related to tyre/road noise level. A 2D laser profilometer is developed for the test according to the specification ISO 13473 (2002). As to sound absorption, the surface impedance setup based on P-U technology is introduced (Bree 2008). As it is a new approach, the test method of using the device on asphalt mixture samples needed to be explored. The measurements of surface texture and sound absorption on slab samples are illustrated in Fig.5. The mechanical impedance has received increasing attention as a parameter for influencing tyre/road noise emission in medium range (630-1600 Hz) and there is no standard for the measurement (Kuijpers 2005). The impedance hammer which is commonly used for detecting the dynamic response of railways and the repeated load direct compression test are two alternatives. Details of mechanical impedance measurement are discussed in another paper. The airflow resistivity, which presents the resistance to air flow encountering through a structure, is an influencing parameter on sound absorption. Measurement of this factor is for better understanding of the effect of material properties on sound absorption. The direct airflow method is used according to ISO9053 (1991). The results achieved from the measurement are then used for regression to develop the Model I.

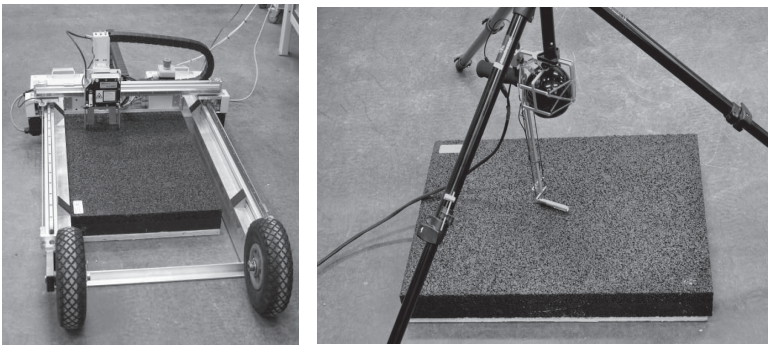

(a) Texture measurement (b) Sound absorption measurement

FIG. 5. Laboratory measurement of surface texture and sound absorption.

Data analysis

In the current study, a model describing the relationship between the change of the tyre/road noise and variations of road surface characteristics, texture and sound absorption, is developed based on a regression analysis performed on the data of thin layer surface sections. These data were measured on trial sections some years ago and were provided by the Ministry of Infrastucture and the Environment. Fig.6 shows the process of the data analysis.

Firstly a pre-treatment on the datasets was performed and the data were processed such that they were in the right form to be used in the regression analyses. The change of the A-weighted equivalent sound level $L_{A,eq}$ from the Close Proximity (CPX) tests was taken as the dependent variable. Surface characteristics involved are the texture and acoustic absorption. Indexes like the MPD, texture level and absorption coefficient are selected to characterize the surface and were used as the explanatory variables for the model. The difference values of the noise level, texture level, MPD and sound absorption coefficient are calculated between each two of the surface in the database.

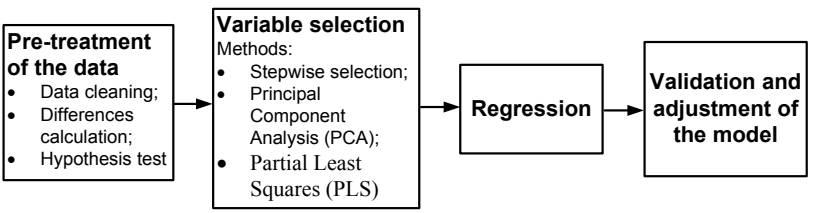

FIG. 6. Process of data analysis.

Multivariate regressions were then carried out on the processed data based on Eq.(2). It should be noticed that the multi-collinearity exists between the explanatory variables. In the regression analysis, different algorithms were employed for lowering

the multicollinearity, i.e. stepwise regression, principal component analysis (PCA) and partial least squares (PLS) regression. The results showed that the multicollinearity could be effectively reduced by these methods, and the regression coefficients clearly reflected the influence of the explanatory variables.

Results from different variable selection and regression methods are obtained. Examples of the resulting models are given below.

For stepwise regression, the number of explanatory variables was reduced by removing those variables which were irrelevant to the output or redundant. In this study, only three variables were retained. The regression equations could be written as:

$$\Delta L_{aeq} = 0.17\Delta TL_{63} - 5.13\Delta AL_{1250} + 2.65\Delta AL_{2000},\ R^2=0.948 \quad (3)$$

$$\text{or } \Delta L_{aeq} = 4.27\Delta MPD - 4.27\Delta AL_{1250} + 1.475\Delta AL_{2000},\ R^2=0.975 \quad (4)$$

where ΔL_{aeq} – Change of the overall noise level, dB (A);

ΔTL_{63} – Change of the texture level at the 63 mm octave band, dB, ref 10^{-6}m;

ΔAL_{1250} – Variation of the sound absorption coefficient curve at 1250 Hz;

ΔAL_{2000} – Variation of the sound absorption coefficient curve at 2000 Hz.

It can be seen that the effect of surface texture on noise difference can be expressed by the change of MPD or the representative texture level with wavelength 63mm. The parameters of sound absorption ΔAL_{1250} and ΔAL_{2000} show an adverse influence for noise level on medium (1000 Hz and 1250 Hz) and high (2000 Hz and 2500 Hz) frequency.

In addition, the noise level difference at certain frequency can also be described with a high fit by the selected parameters, for instance:

$$\Delta L_{1250} = 0.31\Delta TL_{63} - 11.35\Delta AL_{1250} + 7.10\Delta AL_{2000},\ R^2=0.965 \quad (5)$$

$$\text{or } \Delta L_{1250} = 7.80\Delta MPD - 9.84\Delta AL_{1250} + 5.05\Delta AL_{2000},\ R^2=0.979 \quad (6)$$

where ΔL_{1250} is the change of noise level at 1250 Hz.

The model achieved from stepwise regression has a simple structure. The prediction can be performed with a small number of input variables. Thus the model can be easily used as an estimation tool for engineering purposes.

The PCA and PLS algorithms distribute the regression coefficients to each explanatory variables and the influence of individual variables is reflected in the derived functions. Examples of PLS regression results are as follows:

$$\Delta L_{aeq} = -0.075 + 0.033\Delta TL_{250} + 0.041\Delta TL_{125} + 0.046\Delta TL_{63} + 0.040\Delta TL_{32} + 0.020\Delta TL_{16} - 3.396\Delta AL_{1000} - 2.947\Delta AL_{1250} - 0.642\Delta AL_{1600} + 1.313\Delta AL_{2000} + 1.569\Delta AL_{2500},\ R^2=0.822 \quad (7)$$

$$\Delta L_{1250} = -0.016 + 0.054\Delta TL_{250} + 0.083\Delta TL_{125} + 0.080\Delta TL_{63} + 0.069\Delta TL_{32} + 0.037\Delta TL_{16} - 8.904\Delta AL_{1000} - 5.878\Delta AL_{1250} - 0.293\Delta AL_{1600} + 3.017\Delta AL_{2000} + 3.081\Delta AL_{2500},\ R^2=0.846 \quad (8)$$

where ΔTL_i denotes the change of texture level with wavelength i mm, and ΔAL_j is the change of sound absorption at frequency j Hz.

Eq. (7) and (8) show that the change of the overall noise level is mainly affected by the texture level; the contribution of ΔTL_{63} is prominent. The noise is significantly reduced by the sound absorption at 1000 Hz and 1250 Hz. The regression results show that the influence of the sound absorption at high frequency (2000 Hz and 2500 Hz) is different from that of in medium frequency range (1000 Hz and 1250 Hz).

With this method, a number of variables are incorporated in the regression equation, and the resulting model relates the change of noise level to individual explanatory variables. It helps to understand the effect of texture levels with different wavelengths and absorption coefficients at different frequencies on the tyre/road noise change.

The model still needs to be validated by using additional data. Adjustments and modifications are to be made according to the test results. The final mode is a group of individual regression functions.

CONCLUSION

A new method of modeling the tyre/road noise is proposed. The model evaluates the difference of the noise based on the change of material properties and the corresponding change of surface characteristics. The basic indexes related to engineering are involved, which facilitates the use of the model in practice. In the current study, the model is developed based on data obtained on thin layer surfacings. Two types of model were achieved from the various regression approaches. One contains only three inputs of surface characters, and it can be used as a simple tool for evaluating the tyre/road noise change. In the other model, more explanatory variables are included, and it shows specific relations between the tyre/road noise change and individual factors. This model also provides information for further study and understanding of the tyre/road noise emission mechanisms.

REFERENCES

Abbott, P.G., Morgan, P.A. and McKell, B. (2010). "A Review of Current Research on Road Surface Noise Reduction Techniques." *Transport Research Laboratory report for the Rural and Environment Research Analysis Directorate of the Scottish Government*.

Beckenbauer, T. and Kropp, W. (2006). "A hybrid model for analysis and design of low noise road surfaces." *EuroNoise 2006 conference*, Tampere, Finland.

Berglund, B., Lindvall, T. and Schwela, D.H. (1999). "Guidelines for Community Noise." *World Health Organization*, Geneva.

Boer, L.C.d. and Schroten, A. (2007). "Traffic noise reduction in Europe - Health effects, social costs and technical and policy options to reduce road and rail traffic noise." in CE Delft.

Bree, H.E.d., Nosko, M. and Tijs. E. (2008). "A handheld device to measure the acoustic absorption in situ." *NVH GRAZ*.

COWI (2006). "Noise classification of road pavements :Task 1: Technical background information." *European Commission - DG Environment*, Brussels, Belgium.

Donavan, P.R. (2007). "Handbook of Noise and Vibration Control." Malcolm Crocker, John Wiley and Sons.

Han, M. and Ma, C. (2002). "Noise control in the planning of urban roads (in Chinese)." *Journal of Xi'an University of Architecture & Technology*.Vol. 34(1): 96-98.

Huurman, R.M., Mo, L. and Woldekidan, M.F. (2010). "Unravelling porous asphalt concrete towards a mechanistic material design tool." *Road Materials and Pavement Design*. Vol. 11(3): 583-612.

ISO9053 (1991). "Acoustics — Materials for acoustical applications — Determination of airflow resistance."

ISO13473-3 (2002). "Characterization of pavement texture by use of surface profiles -- Part 3: Specification and classification of profilometers." *International Organisation for Standardization (ISO)*, Geneva, Switzerland.

Klein, P. and Hamet, J.F. (2007). "Tyre/road noise prediction with the HyRoNE model." *Proceedings of INTER-NOISE conference*, Istanbul, Turkey.

Larsson, K., Barrelet, S. and Kropp, W. (2002). "The modelling of the dynamic behaviour of tyre tread blocks." *Applied Acoustics*, Vol. (6): 659-677.

Li, M., van Keulen, W., Molenaar, A.A.A. and van de Ven. M. (2009). "New approach for modelling tyre/road noise." *Proceedings of INTER-NOISE Conference*, Ottawa, Canada.

Morgan, P.A. (2008). "IPG Research Report - Innovative mitigation measures for road traffic noise." *Report DVS-2008-018*, Road and Hydraulic Engineering Division of Rijkswaterstaat: Delft, the Netherlands.

Nilsson, R., Nordlander, J. and Silwa, N. (2005). "Design guidelines for durable, noise-reducing pavements." *SILVIA Project Report* SILVIA-SKANSKA-018-01-WP4-231105.

Qiao, S. (2003). "The Solutions on Controlling Beijing City's Traffic Noise (in Chinese)." *Urban Management Science & Technology*. Vol. 5(3): 111-116.

Sandberg, U. (1987). "Road traffic noise—The influence of the road surface and its characterization." *Applied Acoustics*. Vol. 21(2): 97-118.

Sandberg, U., et al. (2010) "State-of-the-art regarding poroelastic road surfaces." *Deliverable* D8.1.

Schwanen, W. and Kuijpers A.H.W.M. (2005). "Development of a measurement system for mechanical impedance." *SILVIA Project Report* SILVIA-M+P-013-01-WP2-230605.

Tan, S.A., Fwa, T.F. and Guwe, Y.K. (2000). "Laboratory Measurements and analysis of clogging mechanism of porous asphalt mixes." *Journal of testing and evaluation*, Vol. 28(3): 207-216.

van Keulen, W. and Duškov, M. (2005). "Inventory study of basic knowledge on tyre/road noise." *IPG Report DWW-2005-022*, Delft, the Netherlands.

Xie, J. (2007). "The evaluation about traffic noise of central roads in Harbin (in Chinese)." Northeast Forestry University, Harbin.

Characteristic Behavior of Asphalt with SBS and PE

Yang Peng[1], Ren Ruibo[2], Wang Lizhi[3] and Zhang Xiaoning[4]

[1]Lecturer, Shandong Provincial Key Laboratory of Road and Traffic Engineering in Colleges and Universities, Shandong Jianzhu University, Jinan 250101, China; School of Civil Engineering and Transportation, South China University of Technology, Guangzhou, 510640, China; email: peng.y@mail.scut.edu.cn.
[2] Professor; Shandong Provincial Key Laboratory of Road and Traffic Engineering in Colleges and Universities, Shandong Jianzhu University, Jinan 250101, China.
[3]Associate Professor; Shandong Provincial Key Laboratory of Road and Traffic Engineering in Colleges and Universities, Shandong Jianzhu University, Jinan 250101, China.
[4] Professor,School of Civil Engineering and Transportation, South China University of Technology, Guangzhou, 510640, China.

ABSTRACT: Styrene-butadiene-styrene tri-block copolymer (SBS) and waste polyethylene (WPE) were combined to modify the base asphalt in order to improve the performance of asphalt. In the presence of special stabilizer (mainly sulfur), SBS/PE combined asphalts showed much better storage stability at high temperature and no visible phase separation was observed under optical microscope observation. The physical properties and dynamic mechanical properties (including viscosity change and rheological characteristics) of SBS/PE combined asphalt with and without sulfur were studied respectively. SBS/WPE combined asphalt with sulfur should be recommended to be used and was a member in high modulus asphalt.

INTRODUCTION

Improving the properties of asphalt has been a subject of particular concern due to the importance of this constituent of road pavement materials. Many methods have been utilized to improve the properties of asphalt as a pavement binder. Polymeric materials are often considered as the most important family of asphalt modifiers. Depending on their excellent properties, polymers are able to impart higher viscosity at high temperatures to asphalt binders and ductility at low temperatures. Lack of these properties leads to two types of distress in pavement: rutting at high temperature and cracking at low temperature (Ait-Kadi, 1996; Airey, 2002).

As common polymer, styrene-butadiene-styrene (SBS) is often used in modification of asphalts (Lu, 1997; UIsacsson, 1999; William,1997; AG William,1997; Shingo, 2001;Vargas,2005). SBS enhances the asphalt with elastic recovery capacities, therefore, its resistance to permanent deformations. However, SBS polymers become quite expensive along with the rising prices of petroleum products and subjected to degradation when exposed to atmospheric agents and

mechanical stress. Therefore, SBS has to be added as virgin polymers and even if used in small percentages it can double the price of the binders. This is the reason why researchers have focused on cheaper materials for modification of asphalt for example waste polyethylene (WPE) (Giavarini, 1996; Yousefy, 2000; Panda, 2002). As a recycled material, WPE can bring a high rigidity to the materials and significantly reduce deformation under traffic load. Unfortunately, asphalt with higher quantity (6-30% by weight) WPE was very poor in low temperature properties (easy to wheel rutted, oiled and cracked) (Stock, 1995; Nolank, 1995). Therefore, maybe combined modification of asphalt by SBS and WPE was best technical method for solving the problems. Some research work had been carried out presently, and more and more research begin to focus on polyethylene related asphalts (Morrison, 1994).

The purpose of this study is to prepare high performance asphalt modified by SBS and WPE, and identify the favorable rheological and physical characteristics and morphology of the asphalts with addition of sulfur, to compare the asphalts without sulfur. It can not only improve the performance of asphalts, but also is beneficial to solve the waste PE related materials “white pollution”.

MATERIAL and MEASUREMENTS

Material

AH-70 paving asphalt was obtained from Zhong-hai Petroleum Asphalt Factory in Jiangsu province of China. The physical properties of this asphalt were as follows: penetration, 63 dmm,(25℃, ASTM D5); softening point, 47.9(ASTM D36); viscosity, 0.442Pa.s (135℃,ASTM D4402); flash point , 235℃ (ASTM D92); and solubility in trichloroethylene, 99.3% (ASTM D2042). SBS D1101AT with MW 100,000(linear polymer containing 40 wt% of styrene) was produced by Kraton Co., Ltd, in America. PE was produced by Liaoning Ai-pu Co., Ltd. in China, density, 95g/cm3; softening point, 175℃. A special stabilizer (mainly sulfur) was used.

Preparation of samples

The modified asphalts were prepared by applying high speed shear mixer (made by FLUKE Shanghai Co., Ltd, China) at 180 to 185℃ and a shear speed of 10000rpm.Firstly, asphalt was heated until it became a fluid in a steel container at 135 to 140℃,then, the SBS and PE (wt.(SBS):wt.(PE)=1:1, based on 100 parts of asphalt) were added slowly; when temperature reached to 175 to 180℃ and the asphalt and polymers were stirred at 12000rpm, the shearing time was 1h. After presence of stabilizer (a special sulfur, 2.5% wt of asphalt), a storage-stable SBS and PE combined modified asphalt was obtained and the stirring was continued for another 1h at 180 to 185℃ with shear speed of 10000rpm.

Storage Stability Test

The storage stability of asphalt was carried out as follows. The sample was poured into a glass toothpaste tube (32mm in diameter and 160mm in height). The tube was sealed and stored vertically at 163±0.5℃ for 48h, and then it was taken out and cooled at room temperature. Before being cut horizontally into three equal sections, the samples taken from the top and bottom sections were used to evaluated the storage stability of the SBS and PE modified asphalts by measuring their softening points. If the difference between the softening point of the top and bottom sections was less than

2.5℃, the samples were considered to be good in high temperature storage stability. Similarly, if the softening points differed by more than 2.5℃, the SBS and PE modified asphalt was considered unstable.

Morphology Observation

The sample morphology was observed using an optical microscope made by OLYMPUS (CX21). Squashed slides of modified binders were prepared by utilizing small amounts of heated sample and viewed under the microscope at a magnification of 400.

Physical Properties Test

The physical properties of asphalts, including softening point, penetration and ductility, were tested according to ASTM D36, ASTM D5, and Chinese specification GB/T 4508.

Viscosity Measurement

The flow properties of asphalt samples were determined by a rotational viscometer (made by Brook-field Engineering Inc, USA) at given temperatures, 135℃,140℃,150℃,160℃,170℃ and 180℃ according to ASTM D4402.

Rheological Characterization

A strain-controlled dynamic shear rheolometer (DSR, AR2000, American) with parallel plate geometry (25 mm in diameter) was applied to determine the rheological behavior of the asphalts before and after modification. Temperature sweeps (from 40 to 90℃) with 2℃ increments were applied at a fixed frequency of 10rad/s and variable strain. During the test, about 1.0g sample was placed on the bottom plate, covering the entire surface, and the palate was then mounted in the rh0eometer. After the sample was heated to melt condition, the top plate was brought into contact with the sample, and the sample was trimmed. The actual strain was measured to calculate various visco-elastic parameters such as anti-rutting factor $G^*/\sin\delta$ and phase angle (δ) and creep property (the strain at 30pa, 100pa and 300pa and applied stress pattern circle 1s load and 9s unload).

RESULTS and DISCUSSION

Storage stability of SBS and PE combined asphalt

Due to the difference in solubility parameters, phase separation among SBS, PE and asphalt would take place in SBS and PE combined asphalt. Droplets of the SBS and PE melt dispersed in asphalt will be accumulated and appear on the top of asphalt at high temperature. The results of high-temperature storage stability of SBS and PE combined asphalt are shown in Fig 1 (a). For asphalts modified by SBS and PE, the difference of softening points between top and bottom sections are very large and this differences become apparent with increasing SBS and PE contents. When the SBS and PE content reaches to 5.5wt.%, the difference in softening point is 39℃,which indicates the phase separation of SBS and PE combined asphalts is very serious. Storage-stable SBS and PE combined asphalt was prepared by adding sulfur at high temperature with high speed mixing. The sulfur dosage was 2.5wt% based on the

asphalt and high-temperature storage stability was shown in Fig.1(b).It can be seen that the asphalt containing 4.5wt.% SBS and PE shows better storage stability after adding sulfur. It indicates that the active groups of SBS can react with the sulfur and keep stable after reaction. On the other hand, the absence of active groups in PE causes the accumulation and serous phase separation. It is the reason why the difference of softening point increases with increasing PE content.

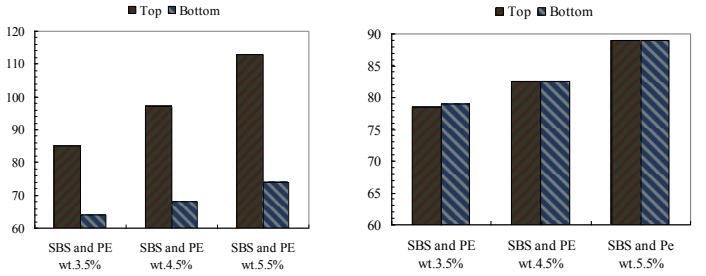

(a) without sulfur (b) with 2.5wt.% sulfur

FIG.1. High-temperature storage stability of SBS and PE.

Morphology analysis

The results of morphology of asphalt were shown in Fig.2. The change of SBS and PE combined asphalt without sulfur was shown in Fig.2 (a) and (b). SBS (darker color section) and PE (lighter color section) in larger matrix were dispersed in asphalt system unevenly. After 0.5h (163℃), SBS and PE particles got together seriously and the size of particles began larger and larger. From Fig.3 (a) and (b), after adding sulfur, the size of PE was decreased obviously, and the size of SBS particles began smaller and almost reached to the size of the optical microscope resolution. After introduction of small amount of sulfur, a three-dimensional steric stabilization layer appeared on the surface of PE particles. So, the polyolefin particles could not collide with each other and reduced the occurrence of possibility of phase separation effectively. As a result, the SBS and PE achieved stabilization state in asphalt system.

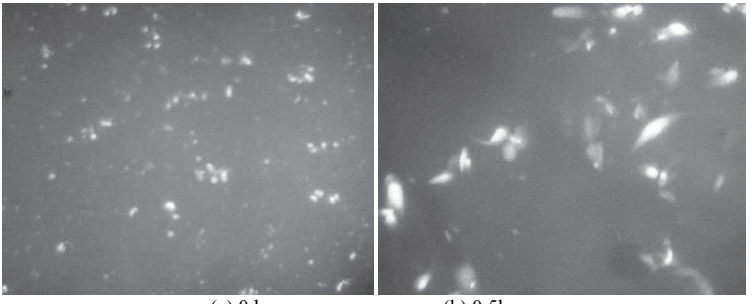

(a) 0 h (b) 0.5h

FIG.2. Morphology development of SBS and PE combined asphalt without sulfur.

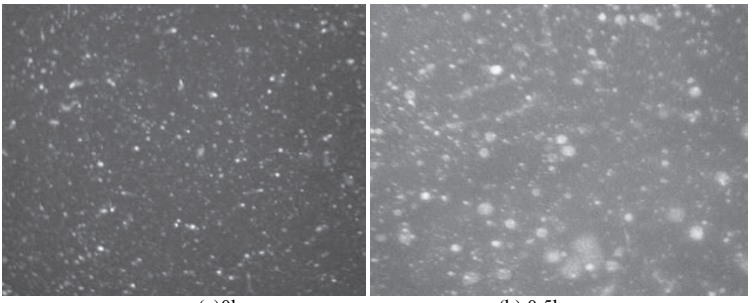

(a)0h (b) 0.5h

FIG.3. Morphology development of SBS and PE combined asphalt with sulfur.

Physical Properties

The effect of sulfur on the physical properties of SBS and PE modified asphalt was shown in Table 1. It could be seen from Table 1,with the SBS and PE increasing, the softening point, T800, and ductility were increased and the penetration was decreased correspondingly. It implied that high and low temperature properties of asphalts were strengthened significantly by increasing SBS and PE content and the susceptibility of asphalts to temperature was also improved. Compared to the asphalt without sulfur, when 2.5wt.% sulfur was added, the susceptibility to temperature were raised further. However, the low temperature index ductility declined, this phenomenon implied that the anti-crack property was influenced negatively because of the gelation of asphalts structure. Fortunately, the loss of ductility was very slight for the asphalt. Asphalt with SBS and PE content 4.5wt.% and 2.5wt.% sulfur was considered best choice. Note: T800 (℃) is the temperature when the penetration was 800dmm.

Table 1. Physical properties of asphalts

Sulfur content (wt.%)	0			2.5		
SBS and PE content (wt.%)	3.5	4.5	5.5	3.5	4.5	5.5
Softening point（℃）	65	69	76	78	82	89
Penetration (dmm/25℃)	45	44	42	31	33	32
Ductility (cm/5℃)	9.5	13.6	13.4	10.2	10.6	10.2
Penetration index	1.2	1.4	2.1	2.6	3.5	3.9
T_{800} (℃)	63.9	66.1	69.5	77.2	83.1	89

Viscosity Behavior

The effects of SBS and PE on the viscosity of asphalts were shown in Fig.4.The effect of temperature on asphalt viscosity could be described by Arrhenius equation:

$$\eta(T) = Ke^{E\eta/RT}$$

where η is the viscosity (Pa.s), K the material coefficient, R the gas constant, $E\eta$ the activation energy (kJ/mol). By plotting versus $1/T$, the activation energy of asphalts could be calculated from the slope of plots, and listed in Table 2. Obviously,

after adding sulfur, a somewhat the shift of asphalt structure from sol to gel, and the activation was increased. For base asphalt, after adding SBS and PE the viscosity was increased, but the activation energy was decreased, it was shown that the activation energy is a important factor affecting the viscosity. Compared to the SBS and PE without sulfur, the slope if logn~1/T×1000 curve of asphalt with sulfur was much steeper, it indicated the SBS and PE without sulfur was more sensitive to the change of temperature.

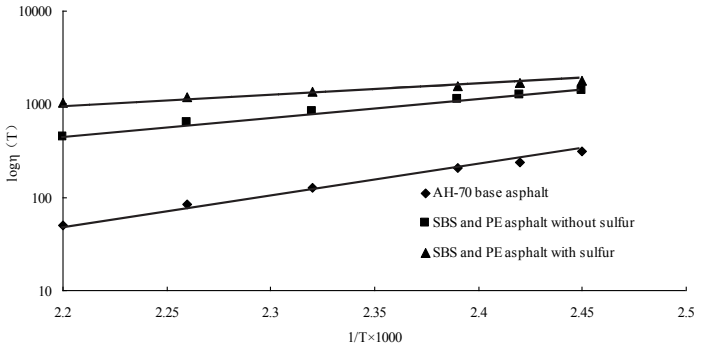

FIG.4. Effect of SBS and PE and sulfur on the viscosity of asphalt.

Table 2. Effect of sulfur on activation energy of asphalts

Sample	$E\eta$ (kJ/mol)
AH-70	70.2
SBS and PE asphalt without sulfur	66.2
SBS and PE asphalt with sulfur	65.4

Visco-elasticity of SBS and PE asphalt with and without sulfur agents

The results of temperature scanning by dynamic shear rheometer were shown in Fig.5. With the temperature increasing, the anti-rutting factor $G^*/\sin\delta$ was slowed down (from 51.64 kPa(40℃) to 0,08945kPa (90℃)) significantly, and the phase angle was increased from 83.45° to 89.5° and reached the viscous state basically. Although $G^*/\sin\delta$ of the combined asphalts with and without sulfur were also decreased, the values were 12.1 and 10.8kPa at 60℃ and phase angles were 65.6° and 66.2°. According to the criteria of defining the high modulus asphalt (Liu, 2010) (i.e. $G^*/\sin\delta$ is over 10kPa at 60℃ and phase angle is less than 70°), SBS and PE combined asphalt was a member of high modulus asphalts. Seen from Fig.5, the effect of sulfur on the $G^*/\sin\delta$ was more sensitive than phase angle.

The creep properties of asphalts were shown in Fig.6, Fig.7 and Fig.8. For AH-70 base asphalt, the strain was almost kept unchanged after 1s load function and the deformation of the sample could not be recovered, which was the characteristic of base asphalt in creep property. From Fig.7 and Fig.8, the creep recovery property of

SBS and PE asphalt was very satisfactory. At 30Pa stress level, the strain of the asphalt without sulfur was observed to be 0.042788 and recovered to 0.014419 after the second load function, the strain recovery ratio was 33.7%; the strain of the asphalt with sulfur was observed to be 0.027019 and recovered to 0.01235 after the second load function, the strain recovery ratio was 45.7%. It implied that SBS and PE combined asphalt was excellent in creep recovery property and could be used to withstand the rutting damages in the road pavement (Silvino, 2006; Hyun, 2007).

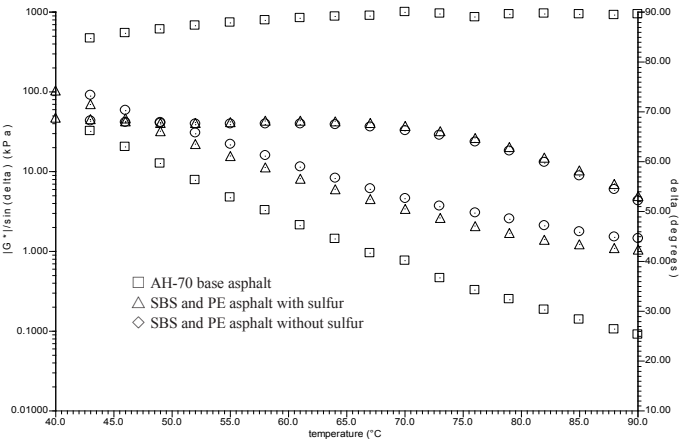

FIG.5. Results of temperature scanning of asphalts.

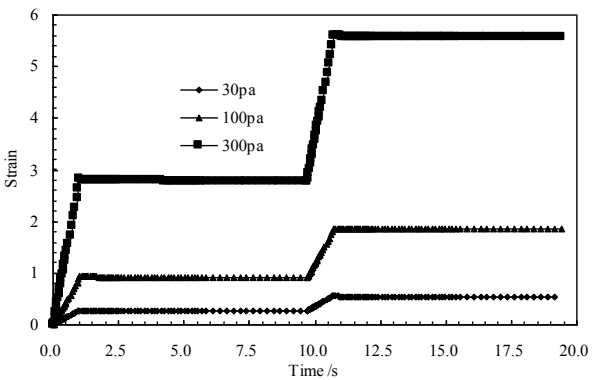

FIG.6. Results of creep test of AH-70 base asphalt.

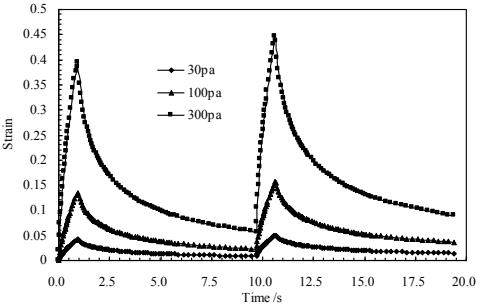

FIG.7. Results of creep test of SBS and PE asphalt without sulfur.

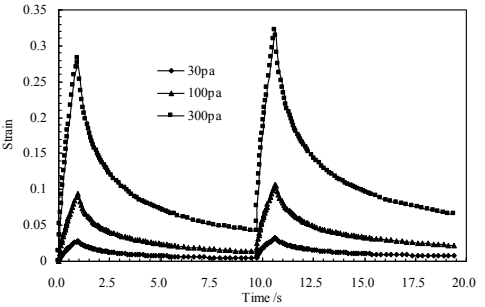

FIG.8. Results of creep test of SBS and PE asphalt with sulfur.

CONCLUSIONS

For base asphalt, the addition of SBS and PE can improve the storage stability, rheological and physical properties of modified asphalt. The active groups of SBS can react with the sulfur and keep stable after reaction. The absence of active groups in PE causes the accumulation and serous phase separation. After introduction of small amount of sulfur, a three-dimensional steric stabilization layer appeared on the surface of PE particles. The polyolefin particles could not collide with each other and reduced the occurrence of possibility of phase separation effectively. SBS and PE combined asphalt was excellent in creep recovery property and could be used to withstand the rutting damages in the road pavement.

ACKNOWLEDGMENTS

Financial support of scientific research foundation of the national natural science foundation of China (NO.50808087,50878090) are gratefully acknowledged. The authors are also heartily grateful to Li Hongjie and Hu Meijuan for providing help in experiments.

REFERENCES

Airey, G.D. (2002). "Rheological evaluation of ethylene vinyl acetate polymer modified bitumens." *Constr. Build. Mater*. Vol.16(8):473–87,

Ait-Kadi, A., Brahimi, B., and Bousmina, M. (1996). "Polymer blends for enhanced asphalt binders." *Polym Eng Sci*. Vol.36:1724–1733

Giavarini, C., De Filippis, P., Santarelli, M.L. and Scarsella, M. (1996). "Production of stable polypropylene-modified bitumens."*Fuel*. Vol.75(6):681–686.

Hyun, J. L., Jung, H. L. and Hee, M. P. (2007). "Performance Evaluation of High Modulus Asphalt Mixtures for Long Life Asphalt Pavements." *Constr. Build. Mater*. Vol.21: 1079-1087.

Isacsson, U. and Lu, X. (1999). "Characterization of Bitumens Modified with SEBS, EVA and EBA Polymers ." *J. Materi. Sci*. Vol.34: 3737-3745.

Liu, Y., Fan, X.H. and Zhang, H.Z., (2010). "Development and Evaluation of the Hard-grade Asphalt."*J. Materi. Civi.Eng*. Vol.22:800-805,

Lu, X., Isacsson, U. (1997). "Characterization of Styrene-butadiene-styrene Polymer Modified Bitumens-comparison of Conventional Methods and Dynamic Mechanical Anaysis." *J. Testing. Evaluation*. Vol.25:383-390,

Morrison, G., Hedmarks, A.H.A. and Hesp, S. (1994). "Elastic steric stabilization of polyethylene-asphalt emulsion. " *Colloid Polym Sci.*, Vol.272:375-384.

Nolank L. (1995). "Low temperature nature of PE modified binder and asphalt concrete mix ."AAPT. No.64.

Panda, M. and Mazumdar, M. (2002). "Utilization of reclaimed polyethylene in bituminous paving mixes." *J. Materi. Civil.Eng*. Vol.14(6):527–530.

Shingo, K.,et al. (2001). "Compatibilizer role of Styne Butadiene Styrene triblock copolymer in asphalt." *Journal of Polymer*. Vol.33:209-210,

Silvino, D. Capitão. and Luís, P.S. (2006). "Assessing Permanent Deformation Resistance of High Modulus Asphalt Mixtures." *J.Transportation.Eng*. Vol.5:394-401.

Stock, A.F. (1995). "The use of Fracture mechanics for the evaluation of Asphalt Mixes." AAPT.No.64.

Vargas, M.A., et al. (2005). "Asphalt modified by partially hydrogenated SBS triblock copolymers." *Rubber Chem Technol*. Vol.78:620-643,

William, A.G. and Baton, L. R. (1997). "Compatible Asphalt-polymer Blends." US Patent 5672642.

William, G. E. (1997). "Polymer Enhances Asphalt." WO Patent 9745488.

Yousefy, A.A., Ait-Kadi, A. and Roy, C. (2000). "Composite asphalt binders: effect of modified RPE on asphalt." *J. Materi. Civil.Eng*. Vol.12(2):113–123,

The Influence of Climate on Libyan Roads Deterioration

Ahmed .A Othman Roffa[1] and Farhat Agribi Farhat[2]

[1] PhD, Organization for development Administration Centers (Odac), Houn, Libya; email: ahmed_roffa@odac-libya.com
[2] PhD, Faculty of Engineering Technology, Houn, Libya; email: Farhat84@hotmail.com

ABSTRACT: The Libyan climate which, characterized by hot arid climatic region (high variation in daily temperatures, high solar radiation, low humidity, low rainfall intensity, wind and dust storms), lies between 15° and 45° both north and south. Asphalt pavement roads are the main and only source of the Libyan overland transportation system for most passengers and goods. Most of Libyan deteriorated roads are passing through a hot arid climatic region (Libyan Desert); Libyan roads expected design life is 20 years, but these roads do not last so longer due to aging rapid deterioration and cut down of service life. The tendency for the asphalt binder to harden and aging under atmospheric influences has been known and studied for many years, Therefore, high solar radiation in hot arid climate region in Libya with presence of oxygen accelerate and increase the physical, chemical, and photochemical process in the asphalt binder, while, the pavement in mid day of summer season can be heated by the solar radiation to more than 70 °C, it may be cooled down in some extreme cases to freezing temperatures during night. These swinging and fluctuation of solar radiation and temperatures induces thermal stresses and cause fast aging in the asphalt pavement layers, therefore, the deterioration in the form of thermal cracking became a problem in cold regions as well as in hot arid climate region with great variation in daily temperatures. The aim of this paper was to estimate the solar radiation energy and present the influences of Libyan climate conditions on roads deterioration.

INTRODUCTION

The hot-arid climate is characteristic of regions lying mostly between 15° and 45° both north and south. The severe conditions of hot dry climates markedly complicate construction and call for special architectural treatments, design approaches, and construction practices to make durable buildings and other structures (Stoll and Evstratov 1987). Asphalt pavement roads are the main and only source of the Libyan overland transportation system for most passengers and goods. These roads are without of traffic control system or limitations to the loading. There is also lack of exact and accurate traffic information relating to axle loads and traffic growth trends

In Libya. The estimated number of equivalent standard axle load (8.2 tons), the repetition reaches or exceeds 2 500 000 EAL, medium to heavy traffic (Roffa 2000).

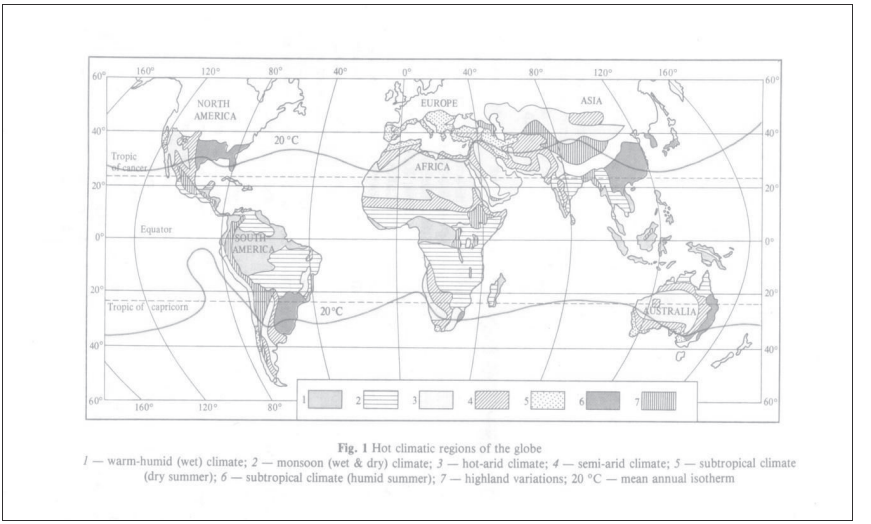

Fig. 1 Hot climatic regions of the globe
1 — warm-humid (wet) climate; *2* — monsoon (wet & dry) climate; *3* — hot-arid climate; *4* — semi-arid climate; *5* — subtropical climate (dry summer); *6* — subtropical climate (humid summer); *7* — highland variations; 20 °C — mean annual isotherm

FIG.1. Geographic and climatic location of Libya.

Most of Libyan main the roads are passing through different geological formations, and located between 27° and 29°, the most deteriorated roads are passing through a hot arid climatic region (Libyan Desert), which characterized by hot arid climatic region (high variation in daily temperatures, high solar radiation, low humidity, low rainfall intensity, wind and dust storms). Although in this geographical location the usual mode of failure expected is deformation (rutting), but it has been seen that the main mode of pavement deterioration was cracking failure. This type of pavement failure is seen in many highways in Libyan Desert, i.e. (Waddan-Sebha highway, Brak bête-Brak, Waddan-Zellah, and Ajdabiya-AlKufra highway).
The asphalt cement (bitumen) binder used in Libyan roads is semi – solid asphalt (AC 60/70), which is recommended by general road department, Libya and produced by Azzawia Oil Refining Company in Libya. Bituminous mixture pavement regarded as linear visco-elastic materials, where the bitumen plays the major part for the viscous properties, while, the mineral substances are responsible for the elastic properties[4]. The viscous property plays a large part in the asphalt pavement performance and deterioration, the cracking and deterioration of asphalt pavement layers due to the consequence of several causes like, material fatigue, shrinkage, sub grade rutting, ageing due to environment influences and poor construction quality, etc.

Particularly, for Libyan roads deterioration, we expect that, the hot arid climate (high temperature, high solar radiation, and low humidity) play a predominant role, leads to a much faster ageing process in the bituminous binder than usually observed in other regions. The high solar radiation in hot arid climate region with presence of

oxygen accelerates and increases the asphalt binder physical, chemical, and photochemical process. In the mid day of summer season, the pavement in this region can be heated by the solar radiation to more than 70 °C, and at night, it may be cooled down in some extreme cases to about freezing temperatures[3]. In addition to hardening and aging, these swinging and fluctuation of solar radiation and temperatures induce thermal stresses, which accumulated in the pavement. As the accumulated thermal stresses exceeds the pavement strength, the thermal cracks in the pavement surface started, and by the time deterioration in the pavement initiated. The observed cracks closely representing the thermal cracking pattern of cement concrete pavements

CLIMATE CONDITIONS

The Libyan climate condition located in the hot-arid climate region, which mostly lies between 15° and 45° both north and south respectively; the Libyan climate condition is hot arid dry, with high temperature, , and low humidity in summer. The desert climatic is extremely severe in summer and winter, especially in the desert; where the mean annual duration of the sunshine is about 11 hours daily, high solar radiation, and the temperature is over 25 °C, continue about 7 months a year (Roffa 2005). The ambient temperature, (the absolute temperature) is being in excess of 40 °C, the daily average temperature in hottest month being over 20 °C. The extreme max temperature in summer exceeds 52 ^{0}C, and extreme min temperature in winter reaches below freezing (-6 °C). The hottest world recorded temperature ever on earth was in Libya on September 13, 1922, which was 58 °C. Azizia is which lies at about 32.53 °N 13.02 °E, and a height above sea level about 112 m / 367 feet, and only about 50 km far from the seaside. The rain fall in Libyan Desert is not uniform natural phenomenon, the rain fall storm in the desert did not last longer, which can be considered as negligible, its annual intensity as low as 0 -10 mm in the desert.

Mean annual relative humidity of about 30 to 50 %. The dry wind and dust storms are very severe and has its impact and effect on the structures and human (Roffa 2002). The well known scorching wind called the "gibli"(a hot, very dry, sand laden wind) can raise the temperatures in a matter of hours to between 40 °C and 50 °C. The under study road sections are passing through hot-arid climatic region, subjected to long hot summer (over 100 days a year). The above-mentioned climate not only causes human discomfort but also building materials deterioration. This hot arid environmental condition has its hard impact and influences on the asphalt pavement mixtures, leading to fast and rapid hardening and aging. Fig.2. shows the temperature variation along the months of the year. As the asphalt pavement binder aged (oxidation of the organic materials and sublimation of volatile fractions), due to the repeated cycles of temperatures, then, the pavement loses its durability, and became intolerant, and behave as rigid pavement and owes its strength to friction between the mineral component alone. The rapid aging of asphalt pavement due to daily temperatures and solar radiation swinging lead to low temperature thermal cracking in hot arid climate region, which subjected to high variation in daily temperatures, as that observed in cold regions. The deterioration and cracks start to be initiated and later propagated down wards to the full depth of the pavement. This deterioration and failure of Libyan roads, due to cracking, an even and roughness led

to make the asphalt pavement structures unable to carry out its intended function and became no longer capable of carrying the applied loads, without causing discomfort for both users and vehicles, which result in hazardous, unsafe, and unpleasant riding.

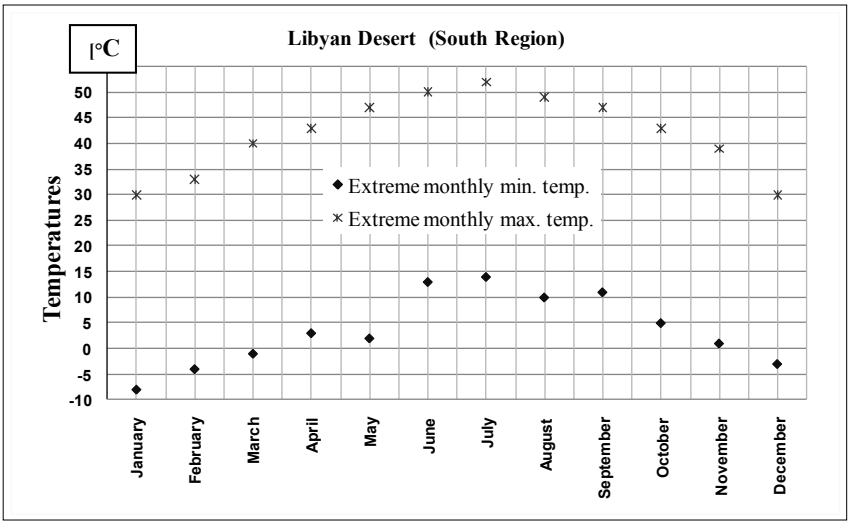

FIG.2. Temperature variations in south region in Libya.

SOLAR RADIATION

The solar radiation going through the atmosphere is partially absorbed by its constituents, partially reflected back to space and partially diffused, with the remaining reaching the ground as direct solar radiation. On a planetary scale, 17% of solar radiation is absorbed by the atmosphere, 30% is reflected by the constituents of the atmosphere, and 53% reaches the surface of the earth, 31% of it as direct solar radiation and 22% as diffuse radiation (Shaltout, Hassan and Fathy 2001). Libya is laying between subtropical of high pressure cell and the equatorial of low pressure cell. We have mentioned that, its climate located in (harsh region), hot arid and dry region, where, about 88% of Libyan area is considered to be desert areas, The daily average of solar radiation on a horizontal plane is 7.1 kWh/m^2/day in the coastal region, and 8.1 kWh/m^2/day in the southern region, with average sun duration of more than 3500 hours per year (Saleh 2001). The Libyan climate (sky) mostly clear and no clouds, where there is a high potential of solar energy. The intensity of the incoming solar energy varies widely and significantly over the 24-hour period and as well as over the course of the year. As we see from the Fig.3, the solar radiation is ranging from about zero solar radiation during night to its maximum of about 450 joules per second (watts per square meter W/$m^{2)}$ in the (middle of the day), September. It is kwon that, the solar radiation can be transmitted through empty space. The above-mentioned fluctuations of incoming solar energy, between day and

night, and course of the year, which causing the daily air temperatures rhythm of rising and falling in addition to the high absorption coefficient of asphalt binder to solar radiation, leads the upper layers of the pavement to be rapidly effected and deteriorated. Therefore, prior to introduce the influence of the solar radiation on asphalt pavement layers, we introduce hereafter, the solar radiation simulation for Libyan roads pavement and climate conditions.

PAVEMENT SOLAR RADIATION SIMULATION

Heat is transferred from one point to the other in the following forms; conduction, convention, and radiation. Conduction is the mode of heat transfer through solids, liquids, and gases, by which the heat energy is transferred in the direction of the fall of temperature (from region of high temperature to the region of low temperature) due to vibration and collision of molecules. In asphalt pavement the heat is transferred by conduction phenomenon, The Fourier Law, (heat equation, Equation 1), which mathematically describes this phenomenon, was applied to compute and simulate, the variation of temperatures in asphalt pavement layers in Libya, Schmidt procedure were used. The real air and pavement temperatures (experimental result) were compared with the simulation results, the temperatures at different depths of the asphalt pavement layers were evaluated (Roffa 2003). The same data, in Table 1., which was used for the estimation and simulation of temperatures in different asphalt pavement layers, were used to simulate and estimate the solar radiation on asphalt pavement for Libyan climate condition, The reader may refer to Ref.((Roffa 2005 and 2003), for more information.

$$\lambda \frac{d^2T}{dZ^2} = \rho c \frac{dT}{dt} \qquad (1)$$

Where,

λ : Thermal conductivity (W/m.k)
ρ : Material density (kg/m^3)
C: Heat capacity (J/kg.k)
T: Temperature (^{0}C)
t: Time in (s)
Z: Depth (m).

Table 1. Thermodynamic Parameters

Number of solving elements No.	Depth (d) (m)	Thermal cond. (λ) (W/m.K)	Heat capacity (c) (J/kg.K)	Density (ρ) (kg/m^3)
20	0.1	2.0	870	2200
3	0.2	2.1	840	1800
3	0.5	2.0	840	1800
1	5.0	2.0	840	2000

The thermodynamic parameters used for the estimation and simulation solar radiation intensity, is given in Table 1. were used. These parameters depend largely on many factors, and may differ for different geographical locations, conditions and mixture properties and compositions, and accordingly the estimation results.
For simulation the following variables were used,

Newton condition α = 19 W/m^2.k on the road surface, while, for numerical solution use (unreal) α = 999 W/m^2.k. Time interval for numerical solution of the problem $\Delta\tau$ = 0.25 hr. Number of time interval n = 960.

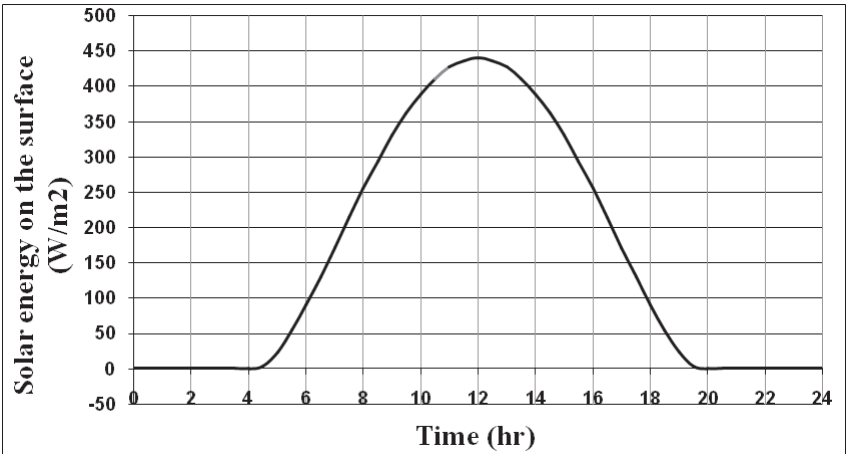

FIG.3. Libyan climate solar radiation simulation, Month September.

AGING DUE TEMPERATURES AND SOLAR RADIATION

The ageing of bitumen is a process of change in the bitumen properties due to hardening and changes in the bitumen structure and composition. The presence of oxygen, ultra-violet, and temperature, in addition to dry wind storms, lead to rapid loss of the volatile material in the bitumen resulting in decreasing the penetration and increasing the softening point, and increasing in the penetration index (PI). The short-term aging is influenced by the source of the bitumen used, the chemical composition, type of mixture, mixing process temperature and time. The long term aging is related mainly to the bitumen hardening due to the effect of the environmental condition on the road pavement, which known as on road hardening.
The long - term aging happened more in the surface of the pavement due to the presence of oxygen and the temperatures variation is more likely to occur at the surface, the aging decreases as the depth of the pavement increases. In-service aging, which occurs when the asphalt (bitumen) reacts with the oxygen in the atmosphere by oxidation, is also affected by the air voids, bitumen content and bitumen type or source of bitumen.

Aging of bitumen is one of the major factors influencing the performance of the pavement, where the bitumen is subjected to a wide range of temperatures; during storage, mixing, and laying process, which is known as short-term aging, and in service life, which is known as long-term aging.

FIG.4. The Effects of temperature and solar radiation on pavement.

FUNCTIONAL TESTING

COMPLEX MODULUS TESTING

Field samples were tested for complex modulus (stiffness) and resistance to permanent deformation evaluation, according to prEN 12697-26 standard. The test pieces were taken from the existing road section. The test pieces are in the shape of trapezoidal truncated wedge of height of 300 mm and variable lower and upper bases. The specimen is loaded by variable harmonic force at its free end corresponding to the load speed or to common travels of vehicles occurred (6 - 25 Hz) in the road[4].

EXPERIMENTAL DEVICE

The samples were tested in two point bending (2PB) arrangement governed by the provision of ČSN 73 6160, which in compliance with prEN 12697-26. The test pieces are placed and fixed to the main frame of the air-conditioned chamber, which provided by forced air circulation unit. By controlling the forced air circulation, the temperature of the test piece and the chamber are kept constant with accuracy of ± 0.5 ºC, by the help of computer unit and sensor fixed to the lateral surface of the

specimen. The frequencies of cyclic loading used were 1,2,5,10,15, and 20 Hz. The temperatures applied for the asphalt mixture were –5, 0, 15, 30, and 45 ºC. Reader/readers may refer to ref. 1 and 4, for more information.

TESTING RESULTS

During the testing, and by the help of the computer unit, the amplitude of the applied force, phase angle of a shift in deformation lagging behind the variation of the applied force, and the deflection of the specimen at the frequency set up are measured. The evaluation results are presented in Fig.5.

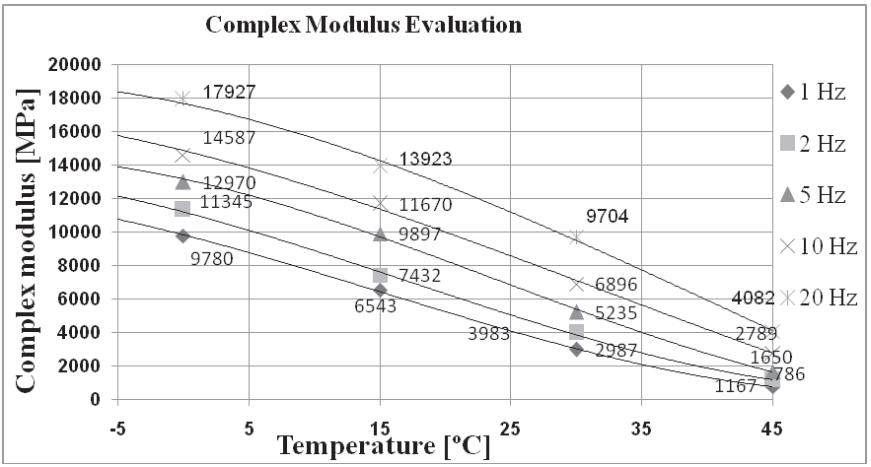

FIG.5. the Complex modulus evaluation.

PERMANENT DEFORMATION EVALUATION

For the determination of the resistance to permanent deformation, a plate sample of thickness 50 mm was prepared and tested in accordance with prEN 12697-22. The testing temperature was 50 ºC (water tempered). The samples could be taken them from the road pavement or could be prepared in the mould under standard conditions.

EXPERIMENTAL DEVICE

The wheel tracking test equipment used is a device for testing bituminous mixture resistance to permanent deformation (rutting) caused by wheel loading). The device consists of main frame, loading units, water bath for the sample (water tempered 50 °C), metal plates, moulds for fixation of the samples, wheel (s) having certain specification and dimensions. In this equipment the wheels used of 47 mm width and having hardness of 80 IRDH. After the specimens are prepared, they are put into the

mould and fixed tightly. The mould with the test specimen is mounted to the testing device frame. The above-mentioned wheel is passing horizontally; to and fro, and accordingly, the specimens are subjected to vertical stress, there are no horizontal stress as the rolling of wheel are free.

TESTING RESULTS

The samples are prepared in laboratory in any proportional bituminous mixture compositions, the mixture slabs are compacted by kneading action of metal plates, according to prEN 12697-33.
The test pieces are maintained horizontally in the water bath (water tempered) so that the water just covering the top surface of the test pieces. The Prepared test slabs of a certain compaction value are tracked cyclically with a loaded wheel at a temperature of 50 °C. During the testing the temperature, number of cycles and the rut depth are measured and recorded by the help of computer unit connected to the equipment. The evaluation of the resistance to permanent deformation is represented graphically by plotting the number of cycles and the rut depth, as shown in Fig.6.

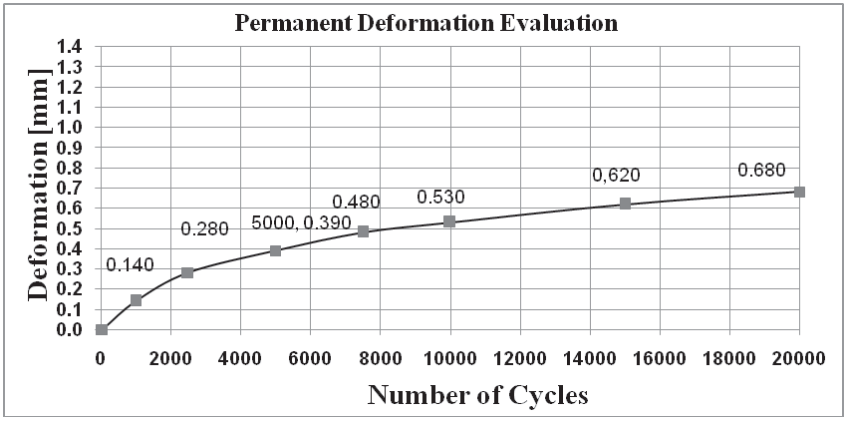

FIG.5. The Permanent deformation evaluation.

RESULTS DISCUSSION

The traffic volume on Libyan roads is relatively low, although, in some cases we observe that, there is overweight traffic loading; therefore, we think that, the hot arid climatic impact in the desert region play a predominant role in asphalt pavement deterioration. Asphalt binder has tendency to harden under influence of climate conditions, therefore, we expect the high solar radiation (UV-Ultra Violet), in excess of Oxygen and very low humidity is very tough on Libyan roads pavement surfaces, causing rapid ageing process, destruction, and oxidation. ,

The Libyan hot arid climate (temperature, solar radiation, dry weather, etc.) condition has its hard impact on the asphalt pavement mixtures, leading to fast and rapid hardening and aging, which results in increased in asphalt mix stiffness, and high resistance to rutting (permanent deformation) of the asphalt mixture. Although, the high resistance to permanent deformation may be considered as benefit of aging, on the other hand, as the bitumen aged then it becomes less ductile, and limiting the flexibility of the mixture, and can result in the development and / or acceleration of several distress types, such as disintegration and fracture from both fatigue and thermal cracking distress which; may lead to the deterioration and failure of the pavement structure. As the asphalt mixture aged the strain in turn became intolerant, and the pavement became very sensitive to temperature variations. The asphalt mixture aging process leads to slow the relaxation of the stresses, and accordingly the bituminous mix starts to behave as rigid layer, and the observed cracks closely representing the thermal cracking pattern of concrete pavements[1]. Therefore, the rapid ageing of asphalt binder in hot arid dry region where, subjected to great variation in daily temperatures, and sun ultraviolet radiation has introduced the pattern of pavement low temperatures cracking as those seen in cold regions, and created huge deterioration in the roads pavement. As the temperature drop even by a single shock, the cracks in the asphalt pavement surface start to be initiated. As the low temperature cycles repeated, the accumulated thermal stress reaches or may exceed the tensile strength of the asphalt pavement, and accordingly the cracks started to propagate down wards to the full depth of the pavement.

In order to minimize the Libyan roads pavement deterioration, we propose the following recommendations, which, may help and prolong the Libya roads service life.

CONCLUSIONS

Since there exist different types of pavement failure and deterioration in Libyan roads that means, there are different causes and sources of cracking, and for the above presented climate condition which has large impact and influences on the Libyan asphalt pavement, the following recommendation may help to minimize the problem:

The rapid increase in traffic volume and loading on Libyan roads speeds up the wearing and deterioration of the roads, the lack and shortage (no accurate data) of traffic studies and information leads to the need for considerable work for traffic studies in Libya and became essential for both volume and loading.

The fatigue cracking and deterioration due to traffic loading can be controlled by installation of weighting stations to control excess loading for heavy vehicles.

The roads department is using single grade asphalt bitumen binder (60//70) for all geographical Libyan roads, therefore, due to the large Libyan land, we think that it is important to study and re-evaluate the Libyan road specifications, and may need to categorize the country in to sectors each of special specification with different asphalt bitumen binder grade.

The asphalt binder grade could be improved and upgraded to softer grade, and/or modified using suitable types of modifiers such as; (SBS, styrene-butadiene-styrene).

The so-called semi-hard bitumen (less temperature susceptible) which is stiffer at high temperature and less brittle at low temperature could be another solution.

More studies and evaluation for the performance of asphalt pavement under the influence hot arid climate condition is recommended and essential.

REFERENCES

Ahmed, A. and Othman, R. (2000). "The Evaluation of Pavement in Desert Region in Libya", *2nd Eurasphalt&Eurobitume Congress 2000, (The World Road Association, PIARC),* Barcelona, Spain:500-502.

Ahmed, A. and Othman, R. (2005). "Roads Construction in Libya", *Asfaltove Vozovky*, (Q-2005), Zilna, Slovak Republic:53-58.

Ahmed, A. and Othman, R. (2003). "Temperature Variation in Asphalt Pavement Layers in Libya", *Asfaltove Vozovky,* (Q-2003), Zilna, Slovak Republic:46-51.

Ahmed, A. and Othman, R. (2002). "The Evaluation of Pavement in Desert Region in Libya", PhD, thesis, Brno, Czech Republic:90-96.

Ibrahim M. S. (2001), "Prospects of Renewable Energy in Libya", *International Symposium on Solar Physics and Solar Eclipses* (SPSE):153.

Moslam, M.A. Shaltout, Hassan, A.H., Fathy, M.A. (2001). "Total Suspended Particles and Solar Radiation over Cairo and Aswan", *National Research Institute of Astronomy and Geophysics, Renewable Energy 23*, Helwan, Cairo, Egypt:605.

Stoll, T. M. and Evstratov, G.I. (1987). "Building in hot climate", *Mir Publishers,* Moscow:9-13.

Rut Resistance of Foamed Warm Mix Asphalt Containing RAP

Jianlong Zheng[1], Sheng Zhao[2], and Baoshan Huang[3], M. ASCE

[1]Professor, Key Laboratory of Highway Engineering of China Ministry of Education, Changsha University of Science and Technology, Changsha, Hunan Province, China, 410004; csust.zheng@gmail.com

2Graduate Research Assistant, 223 Perkins Hall, Department of Civil and Environmental Engineering, The University of Tennessee, Knoxville, TN, 37996; szhao2@utk.edu

[3]Associate Professor, 223 Perkins Hall, Department of Civil and Environmental Engineering, The University of Tennessee, Knoxville, TN, 37996; bhuang@utk.edu

ABSTRACT: This paper evaluated the stiffness characteristic and rutting resistance of warm-mix asphalt (WMA) mixtures containing different percentages of reclaimed asphalt pavement (RAP) through laboratory performance tests. The WMA mixtures were plant produced with a commonly-used foaming technology in the U.S. RAP content ranged from 15 up to 40%. Laboratory performance tests included resilient modulus test, dynamic modulus test, and asphalt pavement analyzer (APA) rutting test. For comparison purpose, HMA mixtures containing 15% and 30% RAP were also evaluated and compared to WMA. Based on the laboratory test results, WMA mixtures with RAP showed high rut resistance and were expected to perform satisfactorily in terms of rutting.

INTRODUCTION

Warm mix asphalt (WMA) has been used by asphalt industry to deal with concerns about global warming and energy consumption. WMA may be produced by adding additives while mixing or introducing water to produce foamed warm mix asphalt resulting in good workability at lower temperatures. The lower temperatures, however, could lead to a less oxidative hardening of the binder, which may contribute to loss of stability in hot weather and lead to increased rutting (Newcomb 2007). Studies conducted to address the rutting concern with WMA technologies indicate that WMA mixes exhibit a lower or similar rutting performance to HMA mixes (Hurley et al. 2005a, Hurley et al. 2005b, Xiao et al. 2010). However, this shortcoming of WMA may be overcome by use of another increasingly popular technology in asphalt industry – recycled asphalt pavement (RAP). The aged binder in RAP might help improve the hardening of the soft binder due to lower temperatures in WMA, resulting in a better stability of asphalt mixtures. Limited studies have been conducted to

explore the possibility of adding RAP to improve the rut-resistance of WMA mixtures (Copeland 2011; Willis et al. 2011; Nordcbeck et al. 2012; Zhao et al. 2012).

OBJECTIVE AND SCOPE

The objective of the laboratory study is to evaluate the stiffness characteristics and rut resistance of plant-produced foamed WMA containing different contents of RAP (Table 1). WMA was produced with a commonly-used foaming procedure in the U.S. WMA and HMA mixtures for a surface layer of a pavement project in Tennessee, USA were evaluated in the study. Resilient modulus and dynamic modulus tests were conducted to characterize stiffness, while Asphalt pavement analyzer (APA) rutting test for rut resistance evaluation.

Table 1. WMA and HMA evaluated in the study

Mix	WMA				HMA	
RAP content (%)	15	20	30	40	15	30

LABORATORY EXPERIMENTS

Materials

Six plant-produced surface mixtures (called "411-D" mixture in Tennessee) were selected in this study with one asphalt binder, PG 64–22. The virgin aggregates selected in this study consisted of limestone (called "D rock" in Tennessee) with a nominal maximum size of 12.5 mm, No. 10 screenings and natural sand. All mixtures include a combination of two fractionated RAP to keep the mixture gradations close to each other with the addition of RAP. All the aggregate properties meet the specification of Tennessee Department of Transportation (TDOT) (TDOT 1995).

Mix Design

The Marshall mix design procedure was employed to design mixture. Materials meet the gradation specification of TDOT and all the mixtures were adjusted to keep the similar aggregate structures after RAP was added. Table 2 presents the different asphalt contribution from RAP and virgin asphalt. The optimum asphalt content for each mix was 5.3%, namely asphalt from RAP together with the virgin asphalt was 5.3% by the weight of the mix. Anti-strip additive was added in the mixture with a dosage of 0.3%, which is determined based on TDOT construction experience.

Sample Preparation

HMA and WMA mixtures were collected at plant site and kept in Oven for 2 hours for short-aging prior to compaction. Cylindrical WMA samples were fabricated on site with the Superpave gyratory compactor (SGC) to avoid reheating and further loss of moisture. HMA mixtures were shipped to the laboratory in University of Tennessee and cylindrical samples were compacted with SGC. 7% was selected as the target air

void to simulate a properly designed and constructed mixture immediately after construction, while 4% was selected for mixture after two or three years of traffic. The sample dimensions and the target air voids are presented in Table 3.

Table 2. Composition of each mix

RAP content	Virgin Binder	RAP Binder	D Rock (Limestone)	No 10	Natural sand	RAP-I	RAP-II
15	4.66	0.64	47.350	9.470	25.675	4.907	10.068
20	4.41	0.89	42.615	9.470	23.675	9.813	10.021
30	3.96	1.34	37.880	9.470	18.940	14.720	15.032
40	3.41	1.89	37.880	0	18.940	14.720	25.053

Table 3. Laboratory percentage of material for each mix

Performance test	Dimension	Target air void
Resilient Modulus test	150 mm in diameter, 50 mm in thickness	4± 0.5%
Dynamic Modulus test	100 mm in diameter, 150 mm in thickness	4± 0.5%
APA rutting test	150 mm in diameter, 75 mm in thickness	7± 0.5%
Hamburg wheel-track test	150 mm in diameter, 75 mm in thickness	7± 0.5%

Resilient Modulus Test

In the resilient modulus test, a specimen is subjected to multiple cycles of repeated load. Each load cycle consists of a 0.1-s load application and a 0.9-s rest period. The indirect tensile stress calculated from the applied load and the measured vertical and horizontal strains were used to calculate the resilient modulus M_R. The test was conducted at 25°C.

Dynamic Modulus Test

In the dynamic modulus test, a continuous uniaxial sinusoidal compressive stress is applied to a specimen at a specified test frequency, which induces a sinusoidally changing compressive strain. The dynamic modulus is defined as the ratio of the stress amplitude to the strain amplitude. In this study, the dynamic modulus test was conducted at 25°C and at the loading frequencies ranging from 0.1 Hz to 25 Hz.

APA Rutting Test

The Asphalt Pavement Analyzer (APA) was tested at a temperature of 64°C. Rut depths at 8,000 cycles were recorded for comparison in this study. The APA rut test was conducted in accordance with the AASHTO T340 procedures.

RESULTS AND DISCUSSION

Resilient Modulus Test Results

Fig. 1 compares the resilient modulus (M_R) results of the WMA and HMA mixtures containing different contents of RAP. It can be seen that the M_R results of HMA and WMA mixtures increased with the increase in RAP content, indicating an improvement in rut resistance of the mixtures. The resilient modulus results of the WMA and HMA mixtures were similar with low RAP addition (15%) but a lower modulus of WMA with high RAP content was observed compared to corresponding HMA, which indicates that the rut resistance of WMA high-RAP mixtures may be slightly lower than that of HMA mixtures.

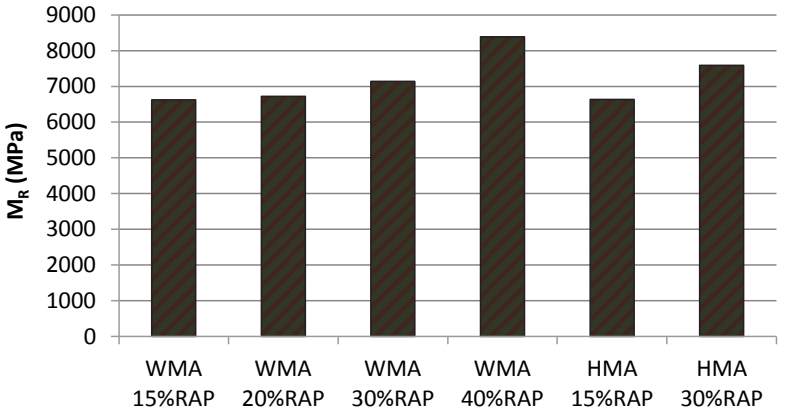

FIG. 1. M_R Results

Dynamic Modulus Test Results

Fig. 2 compares the dynamic modulus results of the WMA and HMA mixtures containing different percentages of RAP at 25°C and at different loading frequencies. It is clear that the dynamic moduli of both WMA and HMA mixtures follow the general trend of dynamic modulus, i.e. dynamic modulus increases with the increase in loading frequency.

Addition of RAP into WMA mixtures increased their dynamic moduli. The higher the RAP content, the higher the dynamic modulus of asphalt mixture containing RAP. This means that incorporation of RAP into asphalt mixtures resulted in the improvement in rut resistance of asphalt mixtures. Higher RAP contents leaded to larger increases in rut resistance of WMA mixtures. The dynamic modulus of WMA mixtures containing 30% RAP was slightly lower than that of corresponding HMA

mixtures, which indicates that WMA-high RAP might have a slightly lower rut resistance than HMA-high RAP mixtures. The results of dynamic modulus were consistent with those obtained in resilient modulus test.

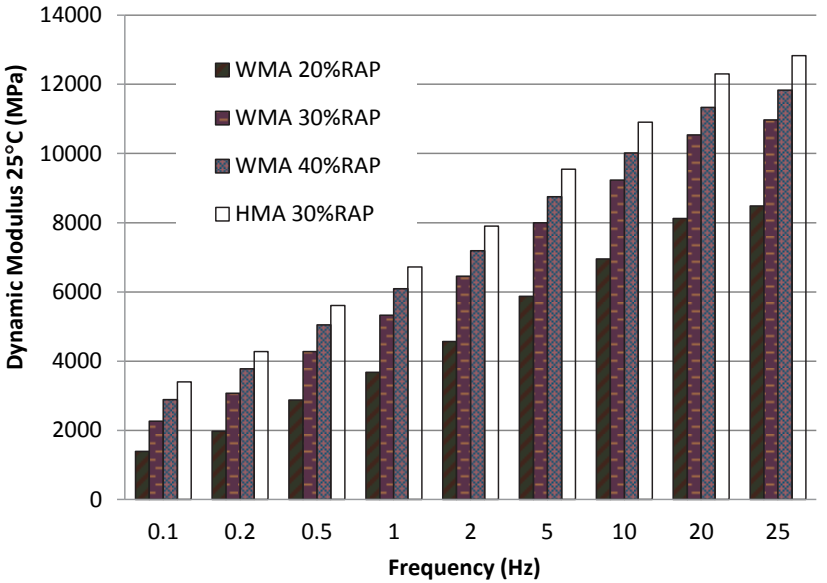

FIG. 2. Dynamic Modulus Results

APA Rutting Test Results

Fig. 3 shows the rut depths from the APA rutting test for the WMA and HMA mixtures containing different percentages of RAP. Generally, excluding WMA containing 15% RAP, it is expected that the WMA and HMA mixtures containing high RAP exhibited lower rut depths than those mixtures with low RAP, which confirmed that addition of RAP increased the rut resistance of both WMA and HMA mixtures.

The rut depths of the WMA mixtures were slightly higher than those of the corresponding HMA mixture, which was consistent with the results from the dynamic modulus and resilient modulus. Those tests showed similar or slightly lower dynamic modulus and resilient modulus, which would result in slightly lower rut resistance and subsequently was confirmed by the rut depth results.

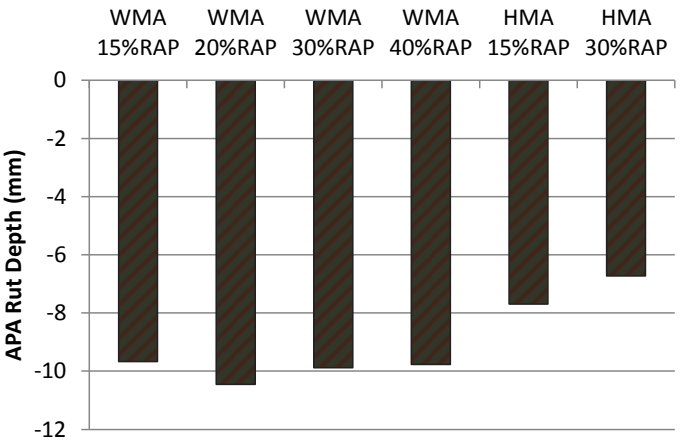

FIG. 3. APA Rutting Test Results

CONCLUSIONS

Multiple laboratory tests were conducted to evaluate the rutting related performance of WMA surface mixtures with different percentages of RAP produced with a plant foaming technology. Based on the test results, conclusions can be summarized as follows:

1. Addition of RAP into HMA and WMA mixtures increased resilient modulus as well as dynamic modulus while decreased APA rut depth, indicating that incorporation of RAP could increase the rut resistance of WMA and HMA mixtures. The higher the RAP content, the higher the improvement.
2. The WMA mixtures with low RAP showed slightly lower or comparable resilient modulus, higher APA rut depth than the HMA mixtures containing low RAP. This indicates that WMA containing low content of RAP may have slighter lower or equal rut-resistance than HMA-low RAP mixtures.
3. Generally, the WMA mixtures containing high percentages of RAP showed improved resistance to rutting that was similar to the HMA mixtures containing low percentage of RAP. This indicates in combination with high percentage of RAP (equal to or more than 30%), WMA mixtures were expected to perform well in terms of rut resistance.
4. The results from different laboratory performance tests were generally consistent in the characterization of rut resistance of WMA and HMA mixtures.

ACKNOWLEDGMENTS

This study was funded by the Key International Collaborative Research Program of Hunan Province, China.

REFERENCES

Copeland, A. (2011). "Reclaimed asphalt pavement in asphalt mixtures: state of the practice." *Report No. FHWA-HRT-11-021*, Federal Highway Administration, McLean, Virginia.

Hurley, G.C. and Prowell, B.D. (2005a). "Evaluation of Aspha-Min zeolite for use in warm mix asphalt." *NCAT Report 05-04*, National Center for Asphalt Technology, Auburn University.

Hurley, G.C. and Prowell, B.D. (2005b). "Evaluation of Sasobit for use in warm mix asphalt." *NCAT Report 05-06*, National Center for Asphalt Technology, Auburn University.

Newcomb, D. (2007). "An introduction to warm mix asphalt." National Asphalt Pavement Association (NAPA). http://fs1.hotmix.org/mbc/Introduction_to_Warm-mix_Asphalt.pdf, accessed August 8, 2007.

TDOT. (1995). "Standard specification for road and bridge construction." the Tennessee Department of Transportation, Nashville, TN, March 1995.

Vargas-Nordcbeck, A. and Timm, D.H. (2012). "Rutting characterization of warm mix asphalt and high RAP mixtures. Road Materials and Pavement Design." Road Materials and Pavement Design, iFirst, 1-20.

Willis, J.R., West, R., Nelson, J., Taylor, A. and Leatherman, K. (2011) "Combining Warm Mix Asphalt Technologies with Mixtures Containing Reclaimed Asphalt Pavement. " Presented at 2nd International Warm-mix Conference. St. Louis, Missouri. October 11-13.

Witczak, M. (2005). "Simple Performance Tests: Summary of Recommended Methods and Database." *NCHRP Report 547*, 2005.

Xiao, F., Amirkhanian, F.S. and Putman, B.J. (2010). "Evaluation of rutting resistance in warm-mix asphalts containing moist aggregates." *Journal of the Transportation Research Board*, No. 2180, National Academies, Washington, DC, 75 – 84.

Zhao, S., Huang, B., Shu, X., Jia, X., and Woods, M. (2012) "Laboratory performance evaluation of warm mix asphalt containing high percentages of RAP. " Presented at the 91th Transportation Research Board Annual Meeting, Paper No. 12-4542, Washington, D.C.